

# **ANN BASED SPATIO-TEMPORAL MORPHOLOGICAL MODEL OF THE RIVER BRAHMAPUTRA**

## **A THESIS**

*Submitted in partial fulfilment of the  
requirements for the award of the degree*

*of*

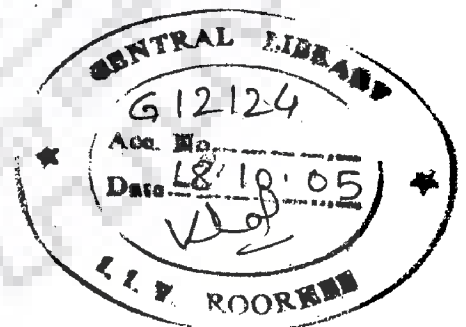
**DOCTOR OF PHILOSOPHY**

*in*

**WATER RESOURCES DEVELOPMENT**

*By*

**RABINDRANATH SANKHUA**

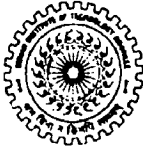


**WATER RESOURCES DEVELOPMENT & MANAGEMENT  
INDIAN INSTITUTE OF TECHNOLOGY ROORKEE  
ROORKEE-247 667 (INDIA)**

**JULY, 2005**



© INDIAN INSTITUTE OF TECHNOLOGY ROORKEE, ROORKEE, 2005  
ALL RIGHTS RESERVED.



INDIAN INSTITUTE OF TECHNOLOGY ROORKEE, ROORKEE

**CANDIDATE'S DECLARATION**

I hereby certify that the work which is being presented in the thesis entitled "ANN BASED SPATIO-TEMPORAL MORPHOLOGICAL MODEL OF THE RIVER BRAHMAPUTRA" in partial fulfilment of the requirement for the award of the Degree of Doctor of Philosophy and submitted in the Department of Water Resources Development and Management (WRD&M), Indian Institute of Technology Roorkee, Roorkee is an authentic record of my own work carried out during the period from July 2003 to July 2005 under the supervision of Prof. Nayan Sharma, Prof. A .D. Pandey and Prof. P.K. Garg, IIT Roorkee, Roorkee (India).

The matter presented in this thesis has not been submitted by me for the award of any other degree of this or any other institute.

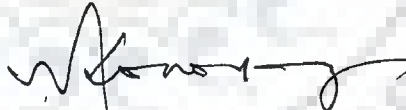
  
(R N SANKHUA)

This is to certify that that the above statement made by the candidate is correct to the best of our knowledge.



(NAYAN SHARMA)

Professor  
WRD&M



(A. D. PANDEY)

Asst. Professor  
Earthquake Engg. Deptt.




(P.K. GARG)

Professor  
Civil Engg. Deptt.

Indian Institute of Technology Roorkee, Roorkee

Date: 29.07.2005.

The Ph.D. Viva-Voce examination of Mr R N SANKHUA, Research Scholar, has been held on 18.9.2005

  
Signature of Supervisor (S)

  
Signature of External Examiner

# SYNOPSIS

---

## INTRODUCTION

The channel geometry of a large braided river like the Brahmaputra in India with energy environment and complex adaptive process response system, displays variable and intricate fluvio-geomorphologic characteristics with rapid significant changes in planform. The limited width of the Brahmaputra valley coupled with the abruptly flattened gradient, leads to tremendous drainage congestion and resultant flooding, bank erosion and channel instability.

The channel geometry attributes at many discrete spatial points emerging out of the post-flood phase represent the footprints left behind by the river hydrodynamic action, and a careful analysis of these for a longer period provide the clue for understanding the future river behaviour with the help of a spatio-temporal morphological model. The conventional mathematical means for idealization of the intricate morphological attributes of the river Brahmaputra fail to accrue desired results for developing a spatio-temporal model. From a review of the literature, hardly any significant studies on spatio-temporal morphology of the highly braided river Brahmaputra could be found. Thus, for idealisation of intricate braided geometry to evolve desired spatio-temporal morphological models, powerful tools of artificial intelligence (AI) have been employed in making optimum use of the available hydrographic, hydraulic and topographic data so as to extract information on the prognosis of complex river behaviour. Monitoring and bringing about a paradigm shift in the management strategy of the Brahmaputra with complex and diverse behaviour is a formidable task by all measures. Thus, a systematic analysis of the river dynamics using

robust ANN modelling approach does have many potential avenues of practical applications for monitoring and management of the Brahmaputra river system.

## **2. THE STUDY AREA**

The study area comprised of 64 pre-defined cross-sections, from Kobo (cross-section 65 at chainage 640.07 km) at the upstream side to Dhubri (cross-section 2 at chainage 17.34 km from Bangladesh border) at the downstream side, spanning over about 622.73 km length in Assam province of India. Considering the river flow, the confluence of river tributaries and gradient, the study area has been divided into 7 reaches.

## **3. DATA COLLECTED AND USED**

The digital satellite data comprising of 32 scenes of Indian Remote Sensing (IRS) Linear Imaging Self Scanner-I (LISS-I) & LISS-III sensors for the years 1990, 1997, 2000 and 2002 along with that of National Oceanographic & Atmospheric Administration (NOAA) for August 2002 and Radarsat data of February, 2002 have been used. During the process of geo-referencing the images, 39 numbers of Survey of India (SOI) toposheets were used. Cross-section data for years 1957, 1971, 1977, 1981, 1988, 1993 and 1997 were used. Stage, discharge and sediment data of the river Brahmaputra and important tributaries during 1990-2002 have been used in the study.

## **4. METHODOLOGY**

The intense variability and complexity of the fluvio-morphologic features of the river were captured in sufficient details to elicit meaningful abstraction of channel processes and morphology using remote sensing, Geographic Information System (GIS) and neuromorphic techniques. ANN technique has been applied to circumvent the difficulty in meaningful processing of huge hydrographic data by conventional means, where the

relationship between parameters are not easily discernible, because the physics of the complex phenomena of formation of braided channels. Fuzzy logic system has been used in developing stage-discharge relationships, which deals with explicit knowledge that could be explained and understood. Comparison of the stage-discharge relationships yielded by ANN, fuzzy, neuro-fuzzy was made with the observed stage-discharge data of the river.

## 5. VALIDATION OF RESULTS

The available data sets for all the models were randomly partitioned into training sets and a test set. The training set was further partitioned into two disjointed subsets; (i) estimation set, used to select the model; (ii) validation set, used to validate the model. Some portion of data was withheld for validation. To assess the validity of the models, all the ANN generated outputs were compared with the observed data of the river Brahmaputra. The goodness-of-fit of statistical criteria like root mean square error (*rmse*), Nash-Sutcliffe coefficients were evaluated for each model. The efficiency has also been tested for each model.

## 6. SALIENT CONTRIBUTIONS OF THE PRESENT RESEARCH

This research endeavour encompasses the development of a number of ANN-based spatio-temporal morphological models of the river resulting in significant findings, important observations and the right provoking predictions as briefly narrated below:

### **Stream bank migration models**

The stream bank migration ANN models, so developed, have simulated the desired information on erosion and deposition patterns, stream bank migration at discrete points with respect to space and time. What-if-then ANN models have also been developed

## Prediction of sediment load concentration

A sediment concentration ANN model was constituted to estimate the natural sediment discharge of the river in terms of sediment concentration at Pancharatna using sediment variables based on the dynamic laws of flow and sediment.

## 3.4. Morphology

Changes in Normalised Difference Vegetation Indices (NDVI) for the Assam Brahmaputra basin were found out reach-wise, for different years to infer trends in morphological variability response in the basin due to presence of forest cover in the flood-plain. Furthermore, digital satellite data of NOAA for the year 2002 have been used for deriving the Digital Elevation Model (DEM) and shallow to deep flooding phenomena in the valley.

The average northing for right bank line of the Brahmaputra river moved about 0.47 km to the north between 1990 and 2002, while that for the left moved about 0.48 km to the south. The river has avulsed just upstream side of the Dibrugarh town and excised areas of floodplain to create new bars. The river mean width has increased from 7.99 km to 8.94 km in the study reach. The study further revealed that the total area within the stream banks increased by 12.10% between 1990 and 2002 due to erosion process causing channel widening. Expansion of the river had taken place primarily through floodplain erosion and excision coupled with bar or island growth.

For morphological processes fraught with great deal of uncertainty in temporal and spatial variability, displaying nonlinearity of physical phenomena, ANNs could be seen to have provided fairly rational answers by mapping pertinent functional relationships of river behaviour. The signal contribution that emerged from the present study focuses on use of neuromorphic techniques for gainful planning and management of intricate river systems like the Brahmaputra.

## ACKNOWLEDGEMENT

---

I wish to record my sincere thanks with profound sense of respect and gratitude for my supervisors Prof. Nayan Sharma, Prof. A D Pandey and Prof. P K Garg. The words prove to be insufficient to express my deep feelings for their high benevolence and un-hesitated guidance throughout the study period. Without their enthusiasm and determination, the study would not have seen the light of the day.

I am grateful to Prof. S.K. Tripathi, Professor and Head, WRD&M. I express my heartfelt thanks and gratitude to Prof. Devadutta Das, Prof. Gopal Chauhan, Dr. M.L. Kansal and all the faculty members of WRD&M for their help and encouragement during the course of the study.

I do acknowledge Er. C.K. Agrawal, Director, Remote Sensing, CWC, Government of India, for his co-operation to do my Ph.D. at IIT Roorkee. I am deeply indebted to the Central Water Commission, Ministry of Water Resources, Government of India, for permitting me to complete this Ph.D. work. I also gratefully acknowledge the various authors and publications from where relevant references have been drawn in this thesis. I express my sincere thanks and compliments to Er. Ambuj Dwivedi, Er G D Singhal and Mr. Neeraj Kumar for their help.

Especially, I acknowledge the utmost co-operation rendered by Kshanaprava during the thesis preparation. Finally, I heartily acknowledge the utmost co-operation, forbearance and persistent encouragement shown by my wife Bhargabi and my daughter Lisna throughout the study.

29<sup>th</sup> July, 2005

  
(R N SANKHUA)



# CONTENTS

---

<b>COPYRIGHT CERTIFICATE</b>	ii
<b>CANDIDATE'S DECLARATION</b>	iii
<b>SYNOPSIS</b>	iv
<b>ACKNOWLEDGEMENT</b>	x
<b>CONTENTS</b>	xi
<b>NOTATIONS</b>	xx
<b>LIST OF FIGURES</b>	xxv
<b>LIST OF TABLES</b>	xxxiii
<b>SYMBOL OF UNITS</b>	xxxv
<b>ABBREVIATIONS</b>	xxxv
<b>CHAPTER - 1 INTRODUCTION</b>	
1.1 GENERAL	1
1.2 EARLIER RESEARCH	2
1.3 THE PROBLEM IDENTIFICATION	4
1.4 OBJECTIVES	7
1.5 THE STUDY AREA	8
1.6 DATA COLLECTED AND USED	8
1.7 THE METHODOLOGY	8
1.8 VALIDATION OF RESULTS	9
1.9 SALIENT CONTRIBUTIONS OF THE PRESENT RESEARCH	9
1.9.1 Stream Bank Migration Models	10
1.9.2 Flow Characteristic Models	10
1.9.3 Hydrographic Characteristic Models	11
1.9.4 Erosion Model for Majuli Island	11
1.9.5 Evolution of New Fluvial Landform Indicators	11
1.9.6 Prediction of Sediment Load Concentration	12
1.9.7 Planform Morphology	13
1.10 ORGANISATION OF THESIS	14

## **CHAPTER - 2 REVIEW OF LITERATURE**

2.1 INTRODUCTION	15
2.2 MODELLING OF BRAIDED RIVERS	16
2.2.1 General Characteristics of Braided Streams	17
2.3 MEANDERING PARAMETER (SINUOSITY)	18
2.4 EXISTING BRAIDING INDICES	18
2.4.1 Braiding Index (BI)	18
2.4.2 Braid Channel Ratio (BCR)	20
2.4.3 Planform Index (PFI)	21
2.5 DEPOSITIONAL STREAM CHANNEL FEATURES	23
2.6 CLASSIFICATION OF THE BRAIDED PATTERN	24
2.7 CLASSIFICATION OF RIVER CHANNEL PATTERN	25
2.8 THE DISTINCTION BETWEEN BARS AND ISLANDS	27
2.9 INFLUENCE OF FLOW STAGE ON CHANNEL PATTERN CLASSIFICATION AND BRAIDING	28
2.10 CHANNEL HIERARCHY AND BRAIDED CLASSIFICATION	29
2.11 CHARACTERISTICS OF BRAIDED AND ANASTOMOSED PATTERNS	31
2.12 CONFLUENCE-DIFLUENCE MECHANICS	32
2.12.1 Channel Confluence	33
2.12.2 Flow Difluence	34
2.13 BED MATERIAL INFLUENCES UPON RIVER BRAIDING	36
2.14 CHANNEL SCALE AND THE BRAIDED PATTERN	36
2.15 INFLUENCE OF SECONDARY CURRENTS IN BRAIDED CHANNELS	36
2.16 RIVER MORPHOLOGY USING REMOTE SENSING DATA	39
2.16.1 Application of Remote Sensing to River Engineering	40
2.16.2 Earlier Works	41
2.16.3 Digital Image Processing	42
2.16.3.1 Geo-referencing	42
2.16.4 Normalized Difference Vegetation Index (NDVI)	43
2.16.5 Digital Image Classification	44
2.16.6 Supervised and Unsupervised Classification	44
2.17 NEUROMORPHIC SYSTEMS	45

2.17.1 Artificial Neural Networks	47
2.17.2 Neural Network Topology	50
2.17.3 Model of Neural Networks	51
2.17.4 ANN Modelling Processes	52
2.17.5 Representing the Variables	53
2.17.6 Summation and Transformation Function	53
2.17.6.1 Sigmoid function	54
2.17.7 Initial Weights	55
2.17.8 Number of Neurons in the Hidden Layer	55
2.17.9 Weights and Biases	56
2.17.10 Training and Generalization	57
2.17.10.1 Methods of training	60
2.17.10.1.1 <i>Supervised training</i>	61
2.17.10.1.2 <i>Unsupervised training</i>	62
2.17.10.2 Learning factors of back propagation	62
2.17.10.2.1 <i>Learning rate (<math>\eta</math>)</i>	62
2.17.10.2.2 <i>Momentum</i>	64
2.17.10.2.3 <i>Gradient descent learning algorithm</i>	65
2.17.11 Back-propagation Training Algorithm and Generalized Delta Rule (GDR)	65
2.17.11.1 Feed forward back-propagation network	70
2.17.12 Criteria for Stopping Training	71
2.17.13 Testing and Validation	71
2.17.14 Strength of ANN	72
2.17.15 The Problem of Explanation	73
2.17.16 Applications of ANN Technique in River Morphology	74
2.18 FUZZY LOGIC SYSTEM	74
2.18.1 Membership Functions	75
2.18.2 Rule Definition	76
2.18.3 Implication and Aggregation	77
2.18.4 Defuzzification	78
2.19 HYDROLOGIC ENGINEERING CENTER (HEC-6) SOFTWARE	79

2.19.1 Theoretical Basis for Hydraulic Calculations	79
2.19.2 Hydraulic Losses	80
2.19.2.1 Friction losses	80
2.19.2.2 Other losses	81
2.19.3 Theoretical Basis for Sediment Calculations	81
2.20 REVIEW OF SEDIMENT DISCHARGE PREDICTORS	83
2.20.1 Ackers and White Method	83
2.20.2 Yang's Model (1973 & 1979)	85
2.20.3 Yang's Model of 1973	85
2.20.4 Yang's Model of 1979	86
2.20.5 Engelund and Hansen Model (1967)	86
2.20.6 Swamee and Ojha Formulations	87
2.21 CONCLUDING REMARKS	88
<b>CHAPTER - 3 DESCRIPTION OF STUDY AREA</b>	
3.1 INTRODUCTION	90
3.2 LONGITUDINAL SECTION OF THE BRAHMAPUTRA RIVER	92
3.3 THE BRAHMAPUTRA BASIN	93
3.4 THE BRAHMAPUTRA RIVER SYSTEM	96
3.5 THE TRIBUTARIES OF THE BRAHMAPUTRA RIVER	98
3.5.1 The North Bank Tributaries	99
3.5.2 The South Bank Tributaries	100
3.6 HYDROLOGICAL CHARACTERISTICS OF SOME MAJOR TRIBUTARIES	101
3.7 HYDROLOGIC AND PHYSIOGRAPHIC CHARACTERISTICS OF THE BRAHMAPUTRA	104
3.8 GEOLOGY AND GEOMORPHOLOGY	106
3.9 BRIEF DESCRIPTION ON ORIGIN OF MAJULI ISLAND	109
3.10 CHANNEL PROCESSES	109
3.11 THE STUDY AREA	113

## CHAPTER - 4 DEVELOPMENT OF SPATIO-TEMPORAL MORPHOLOGICAL MODEL

4.1	INTRODUCTION	115
4.2	DATA SOURCES AND DATA TYPES	117
4.2.1	Topographical Maps	117
4.2.2	Digital Satellite Images	119
4.2.3	Collateral Data (Published)	122
4.2.4	Observed Hydrographic and Hydraulic Data	122
4.2.4.1	Hydrographic data	122
4.2.4.2	Discharge and stage data	123
4.2.4.3	Sediment data	124
4.3	PROCESSING OF HYDROGRAPHIC DATA	126
4.3.1	Generation of Hydraulic/Hydrologic Data	126
4.3.2	Generation of Discharge and Stage Data	127
4.3.3	Generation of Sediment Data	127
4.3.4	Normalisation of the Generated Data	129
4.4	PROCESSING OF REMOTE SENSING DATA	129
4.4.1	Data Base Geo-referencing	130
4.4.2	Extraction of Channel Forms	131
4.4.3	Preparation of Normalized Difference Vegetation Index (NDVI) Layer	134
4.4.4	Preparation of Theme Layers	135
4.4.5	Digital Elevation Model (DEM)	148
4.5	GIS ANALYSIS	148
4.5.1	Mapping of River Configuration Changes	152
4.5.2	River Behaviour and Configurations from 1990 to 2002	153
4.5.2.1	Reach - I (from Fakirganj to Goalpara)	153
4.5.2.2	Reach -II (from Goalpara to Palasbari)	155
4.5.2.3	Reach -III (from Palasbari to Tongani)	160
4.5.2.4	Reach-IV (From Tongani to Behali)	162
4.5.2.5	Reach -V (from Behali to Jhanjimukh)	164
4.5.2.6	Reach -VI (From Jhanjimukh to Kahai Spur, Dibrugarh)	171
4.5.2.7	Reach-VII (From Kahai Spur, Dibrugarh to Dighaltarang (Kobo)	172
4.5.2.8	Tributaries	177

4.6	MONITORING OF EROSION	178
4.6.1	Erosion Status and Response	178
4.7	NEUROMORPHIC MODELLING	182
4.7.1	Data Division	182
4.7.2	Selection of Input and Output Variables and Hidden Neuron	182
4.7.3	Normalisation of the Data	183
4.7.4	Validation and Evaluation of Predictive Capability	184
4.8	MORPHOLOGICAL CHARACTERISTICS	188
4.8.1	Stream Bank Migration Models	188
4.8.1.1	Model 1	189
4.8.1.2	Model 2	193
4.8.1.3	Model 3	197
4.8.1.3.1	<i>Validation and Evaluation of Predictive Capability</i>	198
4.8.1.4	Model 4	198
4.8.1.5	Models 5, 6, 7 and 8	200
4.8.1.5.1	<i>Data Preparation and Selection of Input and Output Variables</i>	200
4.8.1.5.2	<i>Results and Model Validation</i>	201
4.8.1.6	Model 9 and 10 (scenario analysis)	205
4.8.2	Hydrographic Models	214
4.8.2.1	Model 11	214
4.9	FLOW CHARACTERISTIC MODELS	216
4.9.1	Predictive Models	216
4.9.1.1	Model 12, 13 and 14	216
4.9.2	What-If-Then Model	221
4.9.2.1	Model 15 (composite model for missing & imperfect data)	221
4.10	MAJULI RIVER ISLAND EROSION MODEL	223
4.10.1	GIS Analysis	223
4.10.2	Erosion Process of the Island	223
4.10.2.1	Model 16	229
4.10.2.1.1	<i>Neural network modelling for future trend prediction of Majuli</i>	229
4.10.2.1.2	<i>Ground truth verification</i>	231

4.11 ANN-BASED STAGE - DISCHARGE RATING CURVES AT DIBRUGARH, PANCHARATNA AND DHUBRI	232
4.11.1 Model 17, 18 and 19	233
4.11.2 Validation of Models	234
4.12 FUZZY AND NEURO-FUZZY MODELS	238
4.12.1 Models 20, 21, 22, 23, 24 and 25	238
4.12.2 Fuzzy Expert System Design	239
4.12.3 Rule Definition	239
4.12.4 Model Construction	240
4.12.5 Sensitivity Analysis	240
4.13 ANFIS (ADAPTIVE NEURO-FUZZY INFERENCE SYSTEM) MODELS	242
4.13.1 Validation and Comparison of Results	243
4.14 REAL-TIME FLOOD FORECASTING	246
4.14.1 Models 26, 27 and 28	246
4.14.1.1 Input and Output Data	246
4.14.1.2 Network Setup and Adjustment	247
4.14.1.3 Validation of Results	248
4.15 NEURAL NETWORK IN PREDICTION OF SEDIMENT LOAD CONCENTRATION	255
4.15.1 Selecting Sediment Discharge Parameters	255
4.15.2 Training the Network and Verification of Results	258
4.15.3 Calibration of Flow and Sediment Parameters	259
4.16 APPRAISAL OF PLANFORM MORPHOLOGICAL CHANGES	260
4.16.1 Stream Bank Migration	260
4.16.2 River Width	261
4.16.3 Within-bank Morpho-dynamics	261
4.16.4 River Braiding	262
4.17 ANALYSIS OF EROSION COUPLED WITH GROUND TRUTH	263
4.18 CONCLUDING REMARKS	266
<b>CHAPTER - 5 FLUVIAL LANDFORM INDICATORS</b>	
5.1 GENERAL	268
5.2 EXISTING BRAIDING INDICATORS	269
5.2.1 Topological Analysis of the Brahmaputra River	273

5.3	INTERPRETATION OF THE TOPOLOGICAL INDICES	275
5.4	FORMULATION OF FLUVIAL LANDFORM INDICES	279
5.4.1	Hydraulic Geometry	279
5.4.2	Hydraulic Geometry Index (HGI)	280
5.4.3	Fluvial Landform Index (FLI)	282
5.5	THRESHOLDS OF THE INDICES	282
5.6	DETERMINATION OF FUNCTIONAL RELATIONSHIP	287
5.7	CONCLUDING REMARKS	289
<b>CHAPTER - 6 RESULTS AND DISCUSSIONS</b>		
6.1	CHANGES IN THE BRAHMAPUTRA RIVER CONFIGURATION	301
6.2	DISCUSSION ON DEVELOPMENT OF CHANNEL AVULSION IN THE BRAHMAPUTRA - THE RATIONALE	304
6.3	INFERENCE ON DOMINANT CHANGE IN SEDIMENT LOAD	306
6.4	CHANGES IN FLUVIAL PLANFORM	306
6.5	NEUROMORPHIC MODELLING	308
6.5.1	Stream bank Migration Models	308
6.5.2	Hydrographic Models	309
6.5.3	Flow Characteristic Models	310
6.5.4	Composite Model for Missing and Imperfect Data	310
6.6	MAJULI RIVER ISLAND EROSION MODEL	311
6.7	STAGE - DISCHARGE RATING CURVES	312
6.8	REAL-TIME STAGE FORECASTING	313
6.9	PREDICTION OF SEDIMENT LOAD CONCENTRATION	313
6.10	TOPOLOGICAL ANALYSIS OF THE RIVER BRAHMAPUTRA	313
6.11	FORMULATION OF NEW FLUVIAL LANDFORM INDICES	315
6.11.1	Thresholding of the Indices	316
6.11.2	Functional Relationship of HGI with B/D Ratio and Energy Slope	316
6.12	CONCLUDING REMARKS	317
<b>CHAPTER -7 CONCLUSIONS AND FUTURE SCOPE OF WORK</b>		319
<b>BIBLIOGRAPHY</b>		325



## ANNEXURE-I LIST OF COMPUTER PROGRAMS

### FORTRAN 90

- |         |     |   |
|---------|-----|---|
| Program | - 1 | Program for normalisation of data                     |
| Program | - 2 | Spatio-temporal idealisation of the Brahmaputra river |
| Program | - 3 | Ackers and White model (1973)                         |
| Program | - 4 | Engelund and Hansen's model (1967)                    |
| Program | - 5 | Swamee et al. model (1991)                            |
| Program | - 6 | Yang's model (1973) & (1979)                          |
| Program | - 7 | Computation of geometry of a river cross-section      |

### MATLAB 6.5

- |         |      |   |
|---------|------|---|
| Program | - 8  | Program for simulation of the river data training |
| Program | - 9  | Program for testing of the river data             |
| Program | - 10 | Program for validation of the river data          |
| Program | - 11 | Nash and RMSE                                     |

### ANNEXURE - II

### Publications

## NOTATIONS

Symbol	Description
$\tau$	= bed shear stress;
$\tau_c$	= critical bed shear stress;
$\psi_c$	= critical dimensionless shear stress;
$\psi$	= dimensionless tractive shear stress;
$\delta_{np}$	= error signal of neuron p in the hidden layer;
$\frac{B}{D}$	= form ratio;
$\sigma_g$	= geometric standard deviation of the grain size;
$\bar{d}$	= mean of the desired output;
$\tau'$	= shear stress due to grains;
$\sigma$	= statistical standard deviation;
$\alpha_1$	= velocity distribution for flow at d/s end of reach;
$\alpha_2$	= velocity distribution for flow at u/s end of reach;
$\alpha_1 \dots \alpha_{100}$	= Area of a strip / Sum of areas of all strips;
$\frac{VS}{w}$	= non-dimensional unit stream power;
$\phi$	= velocity ratio;
$\nu$	= kinematic viscosity of fluid;
$\gamma_w$	= specific weight of water;
$\sigma_{y_j}$	= standard deviation of the model output $y_j$ ;
$\bar{y}$	= mean of the model output;
$\sigma_{d_j}$	= standard deviation of the model output $d_j$ ;
$f$	= Darcy-Weisbach friction factor;
$\rho$	= density of any fluid;
$\nu$	= kinematic viscosity;
$\alpha$	= momentum factor;
$\omega_o$	= sediment particle fall velocity in water;

$\phi$  = sigmoidal activation function;

$\alpha$  = slope parameter;

$\gamma$  = unit weight of fluid;

$$\beta \text{ index} = \frac{t}{n+e};$$

$$\gamma \text{ index} = \frac{t}{3(n+e-2)};$$

$\eta$  = learning rate

$\tau$  = dimensionless shear stress;

$\tau_0$  = shear stress;

$\Delta E$  = change in error function;

$\Sigma L_i$  = the length of all islands or bars in the reach;

$\gamma_s$  = unit weight of sediment;

$\tau^*$  = non-dimensional grain shear stress;

$A$  = cross sectional area of the channel;

$a$  = value of  $F$  at nominal initial motion;

$A_1$  = downstream area;

$A_2$  = upstream area;

$\rho_s$  and  $\rho$  = sediment and fluid density;

$B$  = over all river width;

$B_0$  = width of movable bed;

$B_c$  = percentage of silty clay content in the bank material;

$B_L$  = transect length;

$c$  = coefficient in sediment transport function, total number of entire segments;

$C_L$  = loss coefficient for contraction and expansion;

$C_s$  = sediment concentration by weight / parts per million by weight;

$C_t$  = total sediment concentration in parts per million by weight.;

$C_{y_j d_j}$  = covariance between the model output ( $y_j$ ) and desired output ( $d_j$ );

$d$  = diameter of bed material representative size of sediment;

$D$  = mean depth of flow at the cross section;

$d_{50}$  = median grain size of bed material;

$DD$  = duration of time step;

$dh/dQ$  = rate of change of surface-water level;

$d_i$  = depth of submerged sub-channel;

- $d_j$  = model (<sup>desired</sup> output,  $d_j = d_1, d_2, d_3 \dots d_n$ );  
 $d_o$  = object output;  
 $e$  = number of bisected segments;  
 $f$  = activation function;  
 $F$  = Froude number;  
 $F_{gr}$  = mobility number;  
 $F_r$  = Froude number;  
 $g$  = acceleration due to gravity;  
 $G$  = sediment discharge  
 $G_s$  = sediment specific gravity = 2.65;  
 $h$  = elevation above a common datum of water surface;  
 $h$  = water depth;  
 $h/B$  = width scale ratio;  
 $h/d_{50}$  = water depth ratio;  
 $h_e$  = energy loss;  
 $h_f$  = friction loss;  
 $h_o$  = form loss;  
 $i$  = total number of unbisected islands within the section; is the index;  
 $\alpha$  index =  $\frac{t - (n + e) + 1}{2(n + e) - 5}$ ;  
 $J$  = total number of subsections;  
 $k$  = number of neurons in the single hidden layer;  
 $k_i$  = of neurons that feed forward to neuron  $i$ ;  
 $L_{ctot}$  = Sum of total channel lengths of all segments of primary channels;  
 $L_{cmax}$  = mid channel length of the widest channel through the reach;  
 $L_d$  = length of the down stream reach used in control volume computation;  
 $L_j$  = length of the  $j^{th}$  strip between subsections;  
 $L_m$  = thalweg length of channel;  
 $L_r$  = length of the reach measured midway between the banks of the channel belt  
 $L_R$  = overall length of the meander belt reach measured along a straight line;  
 $L_s$  = valley length;  
 $L_u$  = length of the upstream reach used in control volume computation;  
 $m$  = Exponent in sediment transport function;  
 $M_2, N_2$  = parameters related to flow and sediment characteristics;

$n$  = Manning's rugosity coefficient; number of nodes;  
 $N$  = Number of braid channels;  
 $n$  = number of data;  
 $\phi_B$  = bed load parameter;  
 $\phi_s$  = suspended load parameter;  
 $P$  = modified sinuosity parameter, wetted perimeter;  
 $p$  = total number of islands bisected by the bounding lines;  
 $P_c$  = channel sinuosity;  
 $q$  = water discharge per unit width;  
 $Q$  = water discharge;  
 $Q_b$  = bank full discharge;  
 $Q_{ci}$  = Computed sediment load;  
 $Q_m$  = mean annual discharge;  
 $Q_{mi}$  = Measured sediment load;  
 $Q_s$  = sediment discharge;  
 $q_t$  = sediment discharge per unit width;  
 $R$  = hydraulic radius;  
 $r$  = correlation co-efficient;  
 $R_s$  = shear velocity Reynolds number;  
 $R_1, R_2$  = down stream and upstream hydraulic radius;  
 $Re$  = Reynold's number;  
 $R_i$  = Discrepancy ratio;  
 $S$  = longitudinal bed slope;  
 $SF$  = scaling factor;  
 $S_f$  = slope of energy grade line;  
 $SR_{max}$  = upper scaling range limit;  
 $SR_{min}$  = lower scaling range limit;  
 $t$  = total number of segments;  
 $T$  = flow top width;  
 $T_e$  = end heights;  
 $T_i$  = height maxima between hollows;  
 $t_i$  = minima between peaks;  
 $u^*$  = shear velocity;  
 $u'*$  = grain shear velocity;  
 $u_c$  = average velocity of incipient sediment motion;

$u_m$  = mean velocity of flow;  
 $\nu$  = kinematic viscosity;  
 $V_{cr}$  = average flow velocity at incipient motion;  
 $U_{*S}$  = unit stream power;  
 $V_{sed}$  = volume sediment in control volume;  
 $W$  = water surface width of stream / channel;  
 $w_0$  = particles fall velocity;  
 $w_0/u_*$  = dimensionless suspended sediment parameter;  
 $W_h$  = weights of the  $h^{th}$  input node and  $p^{th}$  hidden layer neuron;  
 $w_{ij}$  = weight of the network;  
 $W_o$  = weights of the connection between  $p^{th}$  hidden layer neuron and  $q^{th}$  output neuron;  
 $WS_1$  = water surface elevations at reach 1;  
 $WS_2$  = water surface elevations at reach 2;  
 $X$  = actual value of a numeric column, rate of sediment transport in terms of mass flow per unit mass flow rate;  
 $x$  = distance along channel;  
 $x_i$  = top lateral distance of submerged sub-channel;  
 $X_{max}$  = maximum actual value of the column;  
 $X_{min}$  = minimum actual value of the column;  
 $X_p$  = pre-processed value;  
 $y$  = depth of flow distance from boundary;  
 $y_j$  = model (predicted output,  $y_j = y_1, y_2, y_3 \dots y_n$ )  
 $Y_o$  = observed value;  
 $Y_p$  = predicted value;  
 $y_q$  = output;  
 $Y_s$  = depth of sediment in control volume;  
 $\lambda_1 \dots \lambda_{100}$  = length of arc of a strip/ total length of stream bank;

## LIST OF FIGURES

FIGURE	DESCRIPTION	PAGE NO.
Figure 1.1(a):	Satellite image near the peak of monsoon flood of the Brahmaputra river	3
Figure 1.1(b):	Satellite image showing the braided pattern of the Brahmaputra river	3
Figure 2.1:	Schematic diagram representing the computation of sinuosity for single channel and multi channel rivers	18
Figure 2.2:	Schematic diagram representing the computation of the Braiding Index (Brice, 1964)	20
Figure 2.3:	Schematic diagram representing the computation of the braid channel ratio, (Friend and Sinha, 1993)	21
Figure 2.4:	Planform Index (Sharma, 1995)	22
Figure 2.5:	Plan view of the depositional features in a typical straight channel	24
Figure 2.6:	Function distinguishing between meanders and braided channels on the basis of slope and discharge (Leopold and Wolman, 1957)	26
Figure 2.7:	Channel and bar ordering schemes of (a) Williams and Rust (1969), and (b) Bristow (1987)	31
Figure 2.8:	Alternative channel and bar ordering scheme, (Bridge, 1993)	31
Figure 2.9:	Various kinds of channel pattern as defined by Bridge (1993), adapted from 1994 Landsat-TM image of the Brahmaputra in the region of Bahadurabad	33
Figure 2.10:	Ashworth's (1996) model of mid-channel bar growth downstream of a junction scour	35
Figure 2.11:	Flow in a bifurcated channel as mirror image meanders (Ashworth et al., 1992)	39

<b>Figure 2.12:</b>	Linear regression and data driven model (ANN)	46
<b>Figure 2.13:</b>	The building blocks of ANN	48
<b>Figure 2.14:</b>	Simple illustration of biological and artificial neuron	51
<b>Figure 2.15:</b>	Activation function (Rajasekharan, 2001)	54
<b>Figure 2.16:</b>	Gradient descent in one dimension	65
<b>Figure 2.17:</b>	Two layered back-propagation network (Umamahesh and Rao, 2001)	67
<b>Figure 2.18:</b>	Representation of terms in energy equation	79
<b>Figure 2.19:</b>	Deformed control volume for bed deposits	82
<b>Figure 3.1:</b>	Longitudinal section of the Brahmaputra river	92
<b>Figure 3.2:</b>	Average annual runoff of the Brahmaputra	105
<b>Figure 3.3:</b>	Seven reaches of the study area	114
<b>Figure 4.1:</b>	Index to IRS 1A coverage	120
<b>Figure 4.2:</b>	Index to IRS 1C/1D coverage	121
<b>Figure 4.3:</b>	Flow chart showing the methodology of image processing and GIS analysis	132
<b>Figure 4.4:</b>	False Colour Composite of the mosaic image frame of LISS III, 2000	133
<b>Figure 4.5:</b>	NDVI image of the Brahmaputra basin, 1997	136
<b>Figure 4.6:</b>	NDVI image of the Brahmaputra basin, 2000	137
<b>Figure 4.7:</b>	NDVI image of reach number 1 of the study area	138
<b>Figure 4.8:</b>	Trends of vegetation cover	139
<b>Figure 4.9(a):</b>	Trends of low vegetation cover change in the basin	139
<b>Figure 4.9(b):</b>	Trends of high vegetation cover change in the basin	140
<b>Figure 4.10:</b>	Trends of observed total sediment load at Pancharatna	140
<b>Figure 4.11:</b>	Embankment locations in Reach I along the Brahmaputra, before 1990	141



<b>Figure 4.12:</b>	Embankment locations in Reach II along the Brahmaputra, before 1990	142
<b>Figure 4.13:</b>	Embankment locations in Reach III along the Brahmaputra, before 1990	143
<b>Figure 4.14:</b>	Embankment locations in Reach IV along the Brahmaputra, before 1990	144
<b>Figure 4.15:</b>	Embankment locations in Reach V along the Brahmaputra, before 1990	145
<b>Figure 4.16:</b>	Embankment locations in Reach VI along the Brahmaputra, before 1990	146
<b>Figure 4.17:</b>	Embankment locations in Reach VII along the Brahmaputra, before 1990	147
<b>Figure 4.18:</b>	FCC image of NOAA, August , 2002	149
<b>Figure 4.19:</b>	DEM of Assam valley, NOAA, August , 2002	150
<b>Figure 4.20:</b>	Deep and shallow flooding map of Assam valley, NOAA, August , 2002	151
<b>Figure 4.21:</b>	Avulsion by Jinjiram river near Dhubri, 2002	154
<b>Figure 4.22:</b>	River configurations in Reach I of the Brahmaputra	157
<b>Figure 4.23:</b>	Radarsat image (FCC) at d/s of Guwahati	158
<b>Figure 4.24:</b>	River configurations in Reach II of the Brahmaputra	159
<b>Figure 4.25:</b>	River configurations in Reach III of the Brahmaputra	161
<b>Figure 4.26:</b>	Radarsat image near Tezpur, 2002	163
<b>Figure 4.27:</b>	River configurations in Reach IV of the Brahmaputra	166
<b>Figure 4.28(a):</b>	Radarsat image of Majuli, 2002	168
<b>Figure 4.28(b):</b>	Location of Majuli, 1990	169
<b>Figure 4.29:</b>	Radarsat image of Kaziranga Reserve Forest, 2002	170
<b>Figure 4.30:</b>	River configurations in Reach V of the Brahmaputra	173
<b>Figure 4.31:</b>	River configurations in Reach VI of the Brahmaputra	174

<b>Figure 4.32:</b>	IRS ID, LISS III image showing braiding near Dibrugarh, 2002	175
<b>Figure 4.33:</b>	IRS ID, LISS III image showing avulsion near Saikhowa, 2002	176
<b>Figure 4.34:</b>	River configurations in Reach VII of the Brahmaputra	179
<b>Figure 4.35:</b>	Radarsat image of the Brahmaputra, 2002	180
<b>Figure 4.36:</b>	Stream bank migration of the river Brahmaputra	181
<b>Figure 4.37:</b>	The Brahmaputra river divided into 100 equal strips	189
<b>Figure 4.38:</b>	The Brahmaputra river divided into 100 arcs	189
<b>Figure 4.39:</b>	Architecture of the ANN Model 1	190
<b>Figure 4.40:</b>	Plot of observed and ANN predicted left bank co-ordinates (2002)	193
<b>Figure 4.41:</b>	Plot of probable changes of left bank co-ordinates in 2006 (ANN) with respect to 2002 (observed)	193
<b>Figure 4.42:</b>	Plot of observed and ANN predicted left bank co-ordinates (2002)	194
<b>Figure 4.43:</b>	Plot of observed, ANN predicted and data computed from spatio-temporal idealisation programme for left bank co-ordinates (1996)	195
<b>Figure 4.44:</b>	Plot of probable changes of right bank co-ordinates in 2006 (ANN) with respect to 2002 (observed)	197
<b>Figure 4.45:</b>	Plot of observed and ANN predicted data for right bank co-ordinates (2002)	199
<b>Figure 4.46:</b>	Plot of observed, ANN predicted for right bank co-ordinates (2001)	199
<b>Figure 4.47:</b>	Plot of observed, ANN predicted and data computed from spatio-temporal idealisation programme for right bank co-ordinates (1996)	200

<b>Figure 4.48:</b>	Architecture of ANN Models 5, 6, 7 & 8	201
<b>Figure 4.49:</b>	Plot of observed, ANN predicted area of strips for left bank	202
<b>Figure 4.50:</b>	Plot of observed, ANN predicted area of strips for right bank (2002)	202
<b>Figure 4.51:</b>	Plot of observed, ANN predicted strip arc length of for left bank (2002)	203
<b>Figure 4.52:</b>	Plot of observed, ANN predicted strip arc length for right bank (2002)	203
<b>Figure 4.53:</b>	Change in strip area and arc length	204
<b>Figure 4.54:</b>	Plot of right bank migration due to flash flood at Jia Bhareli - section 53	214
<b>Figure 4.55:</b>	Plot of observed and predicted reduced level data for Pancharatna	215
<b>Figure 4.56:</b>	Observed v/s ANN predicted water level for August, 2001 (Model 12)	218
<b>Figure 4.57:</b>	Observed v/s ANN predicted sediment discharges for July, 2001 (Model 12)	219
<b>Figure 4.58:</b>	Observed v/s ANN predicted sediment discharge for June, 2001 (Model 13)	219
<b>Figure 4.59:</b>	Observed v/s ANN predicted water level for Sept, 2001 (Model 13)	220
<b>Figure 4.60:</b>	Plot of observed v/s ANN predicted water levels from Model 12 & 13 for Sept, 2001	220
<b>Figure 4.61:</b>	Plot of observed v/s ANN predicted discharge from Model 14 for June, 2001	221
<b>Figure 4.62:</b>	Plot of observed v/s ANN predicted sediment discharge from Model 14 for August, 2001	221
<b>Figure 4.63:</b>	Plot of observed v/s ANN predicted water levels for October, 2001	222

<b>Figure 4.64:</b>	Plot of observed v/s ANN predicted sediment discharge for October, 2001	222
<b>Figure 4.65:</b>	Eight sectors of Majuli island, 2002	224
<b>Figure 4.66:</b>	Superimposed areas of Majuli in different years	225
<b>Figure 4.67:</b>	Area of Majuli island in different years	226
<b>Figure 4.68:</b>	Variation of sector-wise area of Majuli	227
<b>Figure 4.69:</b>	Typical landmass slide (Indian Express, 23 <sup>rd</sup> July, 2004)	228
<b>Figure 4.70:</b>	Architecture of neural net of model 16	230
<b>Figure 4.71:</b>	Observed and ANN predicted area, 2002	231
<b>Figure 4.72:</b>	Plot of <i>root mean square error</i> v/s iterations	231
<b>Figure 4.73:</b>	Validation of output model of model 17 (Dibrugarh)	234
<b>Figure 4.74:</b>	Validation of output model of model 18 (Pancharatna)	235
<b>Figure 4.75:</b>	Validation of output model of model 19 (Dhubri)	235
<b>Figure 4.76:</b>	Plot of target and output data in model 17 training (Dibrugarh)	235
<b>Figure 4.77:</b>	Plot of target and output data in model 18 training (Pancharatna)	236
<b>Figure 4.78:</b>	Plot of target and output data in model 19 training (Dhubri)	236
<b>Figure 4.79:</b>	Gaussian membership functions for the input and output variable	239
<b>Figure 4.80:</b>	Defuzzification methods	241
<b>Figure 4.81:</b>	Rule viewer of model 21 ( Pancharatna)	241
<b>Figure 4.82:</b>	Learning rate control by fuzzy logic	242
<b>Figure 4.83:</b>	Architecture of the neuro-fuzzy models	243
<b>Figure 4.84:</b>	Plot of target and out put data of the ANFIS model 24	244
<b>Figure 4.85:</b>	Validation and comparison of models 17, 20, 23 and observed data (Dibrugarh)	244

<b>Figure 4.86:</b>	Validation and comparison of models 18, 21, 24 and observed data (Pancharatna)	245
<b>Figure 4.87:</b>	Validation and comparison of models 19, 22, 25 and observed data (Dhubri)	245
<b>Figure 4.88:</b>	Plan of the study reach showing the gauging stations Pandu, Pancharatna and Dhubri	246
<b>Figure 4.89:</b>	Architecture of the ANN models 26, 27 and 28	248
<b>Figure 4.90:</b>	Characteristics of stage data at Pandu, Pancharatna and Dhubri (May-Oct, 2002)	249
<b>Figure 4.91:</b>	Plot of observed data and ANN forecasted data for Pandu	251
<b>Figure 4.92:</b>	Plot of observed data and ANN forecasted data for Pancharatna	252
<b>Figure 4.93:</b>	Plot of observed data and ANN forecasted data for Dhubri	252
<b>Figure 4.94:</b>	Comparison between measured and estimated concentration	259
<b>Figure 4.95:</b>	Validation of observed and ANN predicted concentration	259
<b>Figure 4.96:</b>	Erosion at u/s of Dibru Reserve Forest	262
<b>Figure 4.97:</b>	A view of erosion at Dibru Reserve Forest	262
<b>Figure 4.98:</b>	Erosion due to bowled shaped failure at d/s of Neamatighat	266
<b>Figure 4.99:</b>	Flow failure triggered by adjacent waterlogged areas, d/s Neamatighat	266
<b>Figure 4.100:</b>	Shear failure of bank near spur no 2 Neamatighat	266
<b>Figure 4.101:</b>	Shear failure of bank near spur no 5 Neamatighat	266
<b>Figure 5.1:</b>	A typical definition sketch of the topological parameters (February, 1990)	273

<b>Figure 5.2:</b>	Variation of $t$ in different blocks	276
<b>Figure 5.3:</b>	Variation of $c$ in different blocks	277
<b>Figure 5.4:</b>	Variation of $e$ in different blocks	277
<b>Figure 5.5:</b>	Variation of $n$ in different blocks	277
<b>Figure 5.6:</b>	Variation of $i$ in different blocks	278
<b>Figure 5.7:</b>	Variation of alpha index in different blocks	278
<b>Figure 5.8:</b>	Variation of beta index in different blocks	278
<b>Figure 5.9:</b>	Variation of gamma index in different blocks	279
<b>Figure 5.10:</b>	Suspended sediment in relation to water discharge for the Brahmaputra at Pancharatna	280
<b>Figure 5.11:</b>	Sediment concentration in relation to water discharge for the Brahmaputra at Pancharatna	280
<b>Figure 5.12:</b>	Plot of Energy slope $S_f / F_R$ v/s B/D	287
<b>Figure 5.13:</b>	Plot of HGI v/s B/D	288
<b>Figure 5.14:</b>	Plot of HGI v/s energy slope $\frac{S_f}{F_r}$	288
<b>Figure 5.15(a) to 5.15 (h):</b>	Topologic condition of blocks of the Brahmaputra river	291 -300

## LIST OF TABLES

TABLES	DESCRIPTION	PAGE NO.
Table 3.1:	The Brahmaputra river: Country and Indian state-wise break-up of basin area and channel length	92
Table 3.2:	Hydrological characteristics of some major tributaries	101
Table 3.3:	Tributary distances measured from Indo-Bangladesh border (from Dhubri along the upstream)	103
Table 3.4:	Details of study reaches	113
Table 4.1:	Survey of India toposheets used in the study	117
Table 4.2:	Digital satellite data used in this study	122
Table 4.3:	Discharge and stage data	124
Table 4.4:	Sediment data of the Brahmaputra	125
Table 4.5:	Discharge and sediment data of tributaries	125
Table 4.6:	Comparisons of sediment load by different predictors (Pancharatna)	129
Table 4.7:	Classes in NDVI analysis	135
Table 4.8:	Major fluvial hazard points of river Brahmaputra	178
Table 4.9:	Classes of erosional response	181
Table 4.10:	Description of neuromorphic models	187
Table 4.11:	Comparison of ANN predicted co-ordinates in metre from 25 <sup>o</sup> Latitude for 2006 with 2002 (left bank)	191
Table 4.12:	Comparison of ANN predicted co-ordinates for 2006 & 2002 (right bank)	195
Table 4.13:	Performance indicators of the models 1, 2, 3 and 4	200
Table 4.14:	Performance indicators of the models 5, 6, 7 and 8	204
Table 4.15:	Sample erosion and deposition pattern analysis for left bank	206
Table 4.16:	Performance analyses for observed and ANN predicted data for Models 12, 13 and 14	218
Table 4.17:	Sector and year wise area of Majuli island	226

<b>Table 4.18:</b>	Categories of bank erosion in Majuli island	229
<b>Table 4.19:</b>	ANN predicted values of sector areas for 2004	230
<b>Table 4.20:</b>	Performance indicators for Model 17 (Dibrugarh)	236
<b>Table 4.21:</b>	Performance indicators for Model 18 (Pancharatna)	237
<b>Table 4.22:</b>	Performance indicators for Model 17 (Dhubri)	238
<b>Table 4.23:</b>	Statistical measures of goodness-of-fit for models	238
<b>Table 4.24:</b>	Network input and output data of three stations	247
<b>Table 4.25(a):</b>	Performance indices based on data from test set at Pandu	250
<b>Table 4.25(b):</b>	Statistical parameters for Model 26 (Pandu)	250
<b>Table 4.26(a):</b>	Performance indices based on data from test set at Pancharatna	250
<b>Table 4.26(b):</b>	Statistical parameters for Model 27 (Pancharatna)	250
<b>Table 4.27(a):</b>	Performance indices based on data from test set at Dhubri	251
<b>Table 4.27(b):</b>	Statistical parameters for Model 28 (Dhubri)	251
<b>Table 4.28:</b>	Observed and ANN forecasted stages at Pandu	253
<b>Table 4.29:</b>	Observed and ANN forecasted stages at Pancharatna	253
<b>Table 4.30:</b>	Observed and ANN forecasted stages at Dhubri	254
<b>Table 4.31:</b>	Total load discharge approaches and relevant variables	257
<b>Table 4.32:</b>	Range of data used in learning and verification of sediment concentration model	259
<b>Table 5.1:</b>	Different types of indices	272
<b>Table 5.2:</b>	Model variables for Hydraulic Geometry Index	281
<b>Table 5.3:</b>	Values of Alpha ( $\alpha$ ), Beta ( $\beta$ ) and Gamma ( $\gamma$ ) Index for different years for the Brahmaputra river (Howard et al. 1970)	283
<b>Table 5.4:</b>	Fluvial Landform Index (FLI) for different years	285
<b>Table 5.5:</b>	Thresholds for the indices for the Brahmaputra river	286
<b>Table 5.6:</b>	Comparison of Hydraulic Geometry Index, Alpha Index, Beta Index and Gamma Index (Year - 2002)	286



## SYMBOLS FOR UNITS

Cumec	Cubic metre per second
ha. m.	Hectare-meter
Kg	Kilogram
Km	Kilometre
km <sup>2</sup>	Square kilometre
m	Meter
MCM	Million cubic meter

## ABBREVIATIONS

ANFIS	:	Adaptive Neuro-Fuzzy Inference System
BRI	:	Bed Relief Index
CSI	:	Cross Slope Index
CWC	:	Central Water Commission
DEM	:	Digital Elevation Model
FGI	:	Flow Geometry Index
FLI	:	Fluvial Landform Index
FLS	:	Fuzzy logic system
FORTTRAN	:	Formula Translation
GIS	:	Geographic Information System
HEC	:	Hydrologic Engineering Center
HGI	:	Hydraulic Geometry Index
IRS	:	Indian Remote Sensing
LISS	:	Linear Imaging Self Scanner
MATLAB	:	Mathematics Laboratory
NDVI	:	Normalised Difference Vegetation Indices
NOAA	:	National Oceanographic & Atmospheric Administration
NRSA	:	National Remote Sensing Agency
PFI	:	Planform Index
<i>rmse</i>	:	Root mean square error
WRD&M	:	Water Resources Development and Management

## INTRODUCTION

---

### 1.1 GENERAL

India is endowed with one of the largest river networks in the world with highly diverse and intricate fluvio-geomorphologic characteristics. The channel geometry of a large braided river like the Brahmaputra in India with a mega energy environment and a complex adaptive process response system, displays highly variable and intricate fluvio-geomorphologic characteristics with significantly rapid changes in planform. The nature of variability of channel geometry and fluvial planform of the river are fraught with great deal of uncertainties and complexities. The channel geometry of such a river reflects the end result of complex interaction between environmental features and hydrodynamics of water and sediment flow over its erodible bed and banks.

The braided streams are associated with high stream power and unstable braid bars formed of sediments, which are often unvegetated. Braiding is basically the division of a single channel into two or more anastomosing channel ways. Braided rivers may be envisioned as a series of channel segments, which divide and rejoin around bars in a regular or repetitive pattern as could be seen from the satellite image of the river Brahmaputra in Bangladesh vide Figures 1.1 (a & b). Generally, braiding is favoured by high-energy fluvial environments with steep valley gradients, large and variable discharges, dominant bed load transport and non-cohesive banks lacking stabilisation by vegetation.

Monitoring and bringing about a paradigm shift in the management strategy of such a large braided river with complex and diverse behaviour is a formidable task by all

measures. Thus, a systematic study of the river dynamics of the Brahmaputra is a pre-requisite for sound planning of its management programme. The imperative need for systematic taming of the river system and harnessing its huge untapped water resources have the latent potential for making a massive leap forward in the national economic growth and warrants application of modern techniques of Artificial Neural Network (ANN), fuzzy logic and remote sensing in synergy.

The channel geometry attributes emerging out in the post flood phase are in fact the footprints left behind by the river hydrodynamic action. Careful analysis of these river footprints for a long period provides the valuable clue for understanding the future river behaviour. As a result, the conventional mathematical means for idealization of the morphological attributes, such as channel geometry of the river Brahmaputra do not accrue desired results for developing a spatio-temporal model for interpolation and extrapolation with respect to time and space. The river cross-sections along with planform configuration provided by the satellite data represent footprints of the river at the end of flood season; and using these hydrographic, hydrologic, hydraulic and satellite data, ANN models have been developed for morphology of the river.

## **1.2 EARLIER RESEARCH**

World-wide, earlier research by Leopold and Wolman, 1957; Lane, 1957; Brice, 1964; Coleman, 1969; Howard et al., 1970; Schumm and Khan, 1972; Parker, 1976; Miall, 1977; Hong and Davies, 1979; Mosley, 1981; Richards et al., 1982; Ashmore, 1991a; 1992; Friend and Sinha, 1993; Bristow and Best, 1993; Thorne et al., 1993; Ashworth et al., 1996; and Richardson and Thorne, 2001 on braided rivers has been devoted towards the development of braid indicators and understanding the processes responsible for the occurrence of braiding.

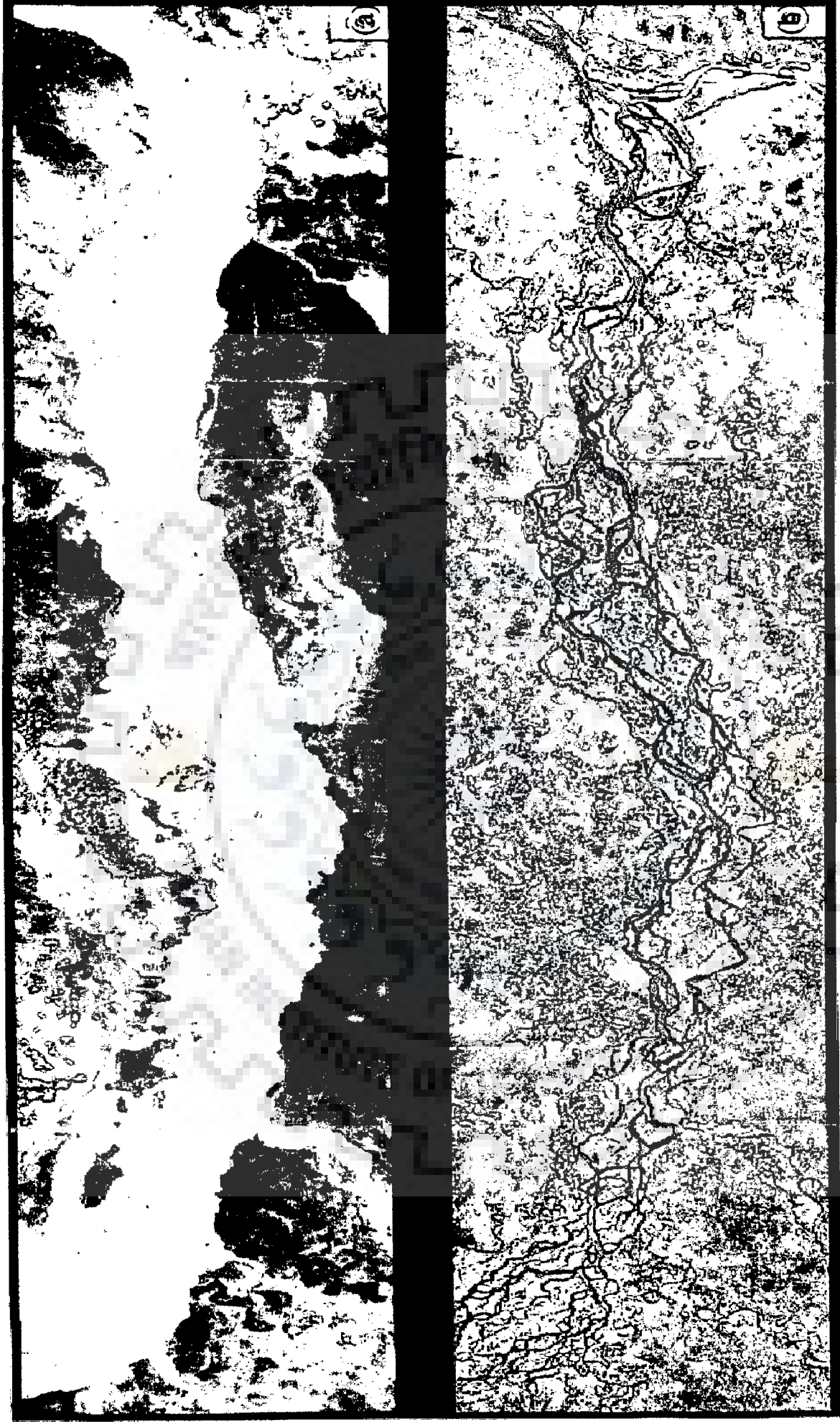


Figure 1.1 (a) Satellite image near the peak of monsoon flood of the Brahmaputra River (17/8/1987)  
(b) Satellite image showing the braided pattern of the Brahmaputra River (7/2/1987)  
(Best and Bristow, 1993; Images collected from ISPAN, FAP-19 Dhaka, Bangladesh)

Off late, ANN has become an attractive technique for solving many hydrologic problems, as established by Daniel (1991), Karunanithi et al. (1994), Zhu and Futija (1994) and Smith and Eli (1995). According to several authors, such as Bastarache et al. (1997), Muttiah et al. (1997), Clair and Ehrman (1998) and Wen and Lee (1998), multilayer perceptrons are powerful tools in solving non-linear water resources problems. Hsu et al. (1995), Minns and Hall (1996), Dawson and Wilby (1998), and Tokar and Johnson (1999) used multilayer perceptron to process rainfall-runoff relationships. Bhattacharya and Solomatine (2000), Raman and Sunilkumar (1995) and Thirumalaiah and Deo (1998) applied ANN to develop stage-discharge relationships and river stage forecasting respectively.

### **1.3 THE PROBLEM IDENTIFICATION**

The river Brahmaputra is seized with spells of severe spate, attendant deluge and sediment deposition and erosion. The Brahmaputra valley represents an acutely flood-prone region characterized by awesome hazards of flood and erosion that create an annual mayhem of devastation. The limited width of the valley and abruptly flattened gradient leads to tremendous drainage congestion and resultant flooding, bank erosion and channel instability.

Although occurrence of flood has been an age-old phenomenon in the riverine areas of this region, yet the extent of damage caused by the hazard has increased significantly in recent years, particularly after the great Assam earthquake of 1950, which recorded 8.7 on the Richter scale. The Brahmaputra valley has experienced major floods in 1954, 1962, 1966, 1972, 1974, 1978, 1983, 1986, 1988, 1996, 1998, 2000 and 2004. With more than 40% of its land surface susceptible to flood damage, the total

flood-prone area in the Brahmaputra valley is 3.2 million hectares, which accounts for 9.6% of the country's total flood prone area (60).

The unique environmental setting of the basin vis-à-vis the eastern Himalayas, highly potent monsoon regime, weak geological formations, active seismicity, accelerated rates of erosion, rapid channel aggradation, massive deforestation, intense land use pressure and high population growth in the floodplain belt and adhoc temporary measures of flood control are some of the dominant factors that caused and/or intensify floods in Assam (61). However, the single most important cause for frequent occurrence of flood in this region is the extremely dynamic monsoon rainfall regime in the backdrop of unique physiographic setting. The scenario is further exacerbated by a myriad of social, economic and environmental factors causing increased vulnerability of people to the flood hazard. The flood problem has three main facets as far as the river Brahmaputra is concerned. First, the problem of inundation of riverine areas is due to overtopping of banks by the Brahmaputra and tributaries. Second, the problem of drainage congestion especially near the outfalls of the tributaries during high flood stages of the river. Third, the problem is mainly due to bank erosion and channel instability.

The behaviour of the river is highly unpredictable and erratic; it shifts its course abruptly during monsoon season causing erosion and deposition at various locations leading to immense loss of property. While the river Brahmaputra is the life-line of the North-East India, it is also its sorrow during high floods. The maximum flood discharge observed is of the order of 48,060 m<sup>3</sup>/sec (Pancharatna) in the month of August, 1998. Discharge of this magnitude is capable of submerging a large number of villages in the plains of Assam valley.

The problem of erosion and flood in Assam is fast assuming frightening dimensions, rapidly heading for an irreversible state. Unless urgent remedial steps are implemented, Assam would have to endure a much enlarged flood plain with higher flood levels, great loss of prime land to stream-bank erosion, severe drainage congestion, recurrent urban flood events and flood devastation of agriculture, which is the backbone of Assam's economy.

Frequent and unpredictable stream bank migration of the Brahmaputra, noticed on both banks, results in erosion and accretion. This response of fluvial morphology deserves attention because of its large impacts on important landscapes like the Ramsay Heritage site (Kaziranga National Park), Numaligarh Oil Refinery, National Highway as well as important towns such as Dhubri, Guwahati, Tezpur, Jorhat and Dibrugarh.

The river Brahmaputra, which happens to be a highly braided river with complex fluvial planform changes, suitable morphological indicators do not exist. From a review of the literature, hardly any significant studies on spatio-temporal morphology of the highly braided river Brahmaputra could be found. Thus, for idealisation of intricate braided geometry to evolve desired spatio-temporal morphological models, powerful tools of artificial intelligence (AI) have been employed in making optimum use of the available hydrographic, hydraulic and topographic data so as to extract information on the prognosis of complex river behaviour. Thus, a systematic analysis of the river dynamics using robust ANN modelling approach does have many potential avenues of practical applications for monitoring and management of the Brahmaputra river system.

## 1.4 OBJECTIVES

Based on the review of literature, the following objectives were set for the present study:

- (i) Study of stream bank migration patterns of river Brahmaputra with respect to space and time using digital satellite data and ANN.
- (ii) Study of erosion and deposition patterns at different locations of the river Brahmaputra using digital satellite data and ANN.
- (iii) Establish a correlation of river discharge, water level and sediment discharge at a point of river cross-section with respect to space and time using ANN.
- (iv) Formulation of stage-discharge relationship models for Dibrugarh, Pandu and Pancharatna sections of the river Brahmaputra using ANN.
- (v) Real-time one-day-ahead stage forecast at Pandu, Pancharatna and Dhubri sections of the river Brahmaputra using ANN.
- (vi) Generation of reduced levels with respect to space and time using input from satellite and hydrographic survey data and employing ANN.
- (vii) Study of the erosional activity of the Brahmaputra in the Majuli island digital satellite data and ANN.
- (viii) Development of fluvial landform indicators to identify severity and intensity of braiding.
- (ix) Prediction of sediment load concentration at Pancharatna using ANN.
- (x) Appraisal of planform morphological changes of the river Brahmaputra.



## **1.5 THE STUDY AREA**

The study area comprised of 64 pre-defined cross-sections, from Kobo at the upstream side to Dhubri at the downstream side, spanning over about 622.73 km length in Assam province of India. Considering the river flow, the confluence of river tributaries and gradient, the study area from Dhubri (cross-section 2 at chainage 17.34 km from Bangladesh border) to Kobo (cross-section 65 at chainage 640.07 km) has been divided into 7 reaches.

## **1.6 DATA COLLECTED AND USED**

The digital satellite data comprising of 32 scenes of Indian Remote Sensing (IRS) Linear Imaging Self Scanner-I (LISS-I) & LISS-III sensors for the years 1990, 1997, 2000 and 2002 along with that of National Oceanographic & Atmospheric Administration (NOAA) for August 2002 and Radarsat data of February, 2002 have been used. During the process of geo-referencing the images, 39 numbers of Survey of India (SOI) toposheets were used. Cross-section data for years 1957, 1971, 1977, 1981, 1988, 1993 and 1997 were used. Stage, discharge and sediment data of the river Brahmaputra and important tributaries during 1990-2002 were used in the study (Central Water Commission and Brahmaputra Board).

## **1.7 THE METHODOLOGY**

The intense variability and complexity of the fluvio-morphologic features of the river were captured in sufficient details to elicit meaningful abstraction of channel processes and morphology using remote sensing, Geographic Information System (GIS) and neuromorphic techniques. ANN technique has been applied to circumvent the difficulty in meaningful processing of huge hydrographic data by conventional means,

where the relationship between parameters are not easily discernible, because the physics of the complex phenomena of formation of braided channels. Fuzzy logic system has been used in developing stage-discharge relationships, which deals with explicit knowledge that could be explained and understood. Comparison of the stage-discharge relationships yielded by ANN, fuzzy, neuro-fuzzy was made with the observed stage-discharge data of the river. The intense variability and complexity of the fluvio-morphologic features of the river Brahmaputra were captured in sufficient details to elicit meaningful abstraction of channel processes and morphology using remote sensing, Geographic Information System (GIS) and neuromorphic techniques. ANN technique has been applied to circumvent the difficulty in meaningful processing of huge hydrographic data by conventional means, where the relationship between parameters were not easily discernible, because the physics of the complex phenomena of formation of braided channels are not yet adequately understood. In addition, there is no distinct mathematical relationship between the pertinent parameters with respect to space and time. Neural networks deals with the generalized implicit knowledge acquisition learning process. Fuzzy logic system has been used in comparing stage-discharge relationships, which deals with explicit knowledge that could be explained and understood. Comparison of the stage-discharge relationships yielded by ANN, fuzzy, neuro-fuzzy was made with the observed stage-discharge data of the river.

## **1.8 VALIDATION OF RESULTS**

The available data sets for all the models were randomly partitioned into training sets and a test set. The training set was further partitioned into two disjointed subsets; (i) estimation set, used to select the model; (ii) validation set, used to validate the model. Some portion of data was withheld for validation. To assess the validity of the models, all

the ANN generated outputs were compared with the observed data of the river Brahmaputra. The goodness-of-fit of statistical criteria like root mean square error (rmse) <sup>and</sup> Nash-Sutcliffe coefficients were evaluated for each model. The efficiency has also been tested for each model.

## **1.9 SALIENT CONTRIBUTIONS OF THE PRESENT RESEARCH**

This research endeavour encompasses the development of a number of ANN-based spatio-temporal morphological models of the river Brahmaputra resulting in significant findings, important observations and the thought provoking predictions as briefly narrated below:

### **1.9.1 Stream Bank Migration Models**

The stream bank migration ANN models, so developed, have simulated the desired information on erosion and deposition patterns, lateral migration at discrete points with respect to space and time. What-if-then ANN models have also been developed to predict the scenario of the river pertaining to lateral migration, if a flash flood was impinged at the confluence of the tributary with the main stem of the river Brahmaputra.

### **1.9.2 Flow Characteristic Models**

The ANN models developed have simulated the river flow characteristic variables, which profoundly influenced morphological variability, such as discharge, water level, sediment at discrete points of river cross section with respect to space and time. The stage-discharge relationship models evolved for important stations at Dibrugarh, Pandu and Pancharatna of the river Brahmaputra have been used to predict the discharge at these points for a given stage. Real-time one-day-ahead stage forecasts at three

stations, namely Pandu, Pancharatna and Dhubri have been made through another set of neuromorphic models.

### **1.9.3 Hydrographic Characteristic Models**

The research contributed the development of ANN models capable of predicting reduced levels of the river cross-sections profile in the past, present and the future to investigate the morphological changes of the river Brahmaputra from spatial as well as temporal standpoints.

### **1.9.4 Erosion Model for Majuli Island**

The erosion process in Majuli island of the Brahmaputra, the world's largest river island, has also been investigated deploying remote sensing and ANN techniques, which captured the trend of erosion in the island, qualitatively and quantitatively. The area of the Majuli river island has evidently decreased by 39.30 km<sup>2</sup> over a period of 12 years from 416.23 km<sup>2</sup> in 1990 to 376.93 km<sup>2</sup> in 2002. The study has revealed that the loss of land area has been 4.94% in 1997 and 9.44% in year 2002 with reference to the area of Majuli island in the year 1990.

### **1.9.5 Evolution of New Fluvial Landform Indicators**

For appraisal of degree and intensity of braiding appropriately by duly reflecting the influence of pertinent hydraulic variables, fluvial landform index (FLI) and hydraulic geometry index (HGI) were evolved in this work making conjunctive use of field and remote sensing data. The empirical topological indices alpha ( $\alpha$ ), beta ( $\beta$ ) and gamma ( $\gamma$ ) have been found out block-wise for the river, for different years to investigate the braiding pattern.

The performance evaluation of the newly developed hydraulic geometry index with topological indices, like the alpha ( $\alpha$ ), beta ( $\beta$ ) and gamma ( $\gamma$ ) with respect to intensity of braiding clearly demonstrated the usefulness and relevance for applying these indices in the Brahmaputra for a measure of the fluvial landform. The newly developed indices FLI and HGI were designed to rationally classify the degree as well as intensity of braiding for the Brahmaputra by accounting for the pertinent fluvial variables. These indices logically reflected the effect of planform changes on channel migration, island formation and resultant braiding, which wielded significant influence on river morphology.

Furthermore, on the basis of a critical analysis of the trends of the variation of HGI, FLI, form ratio,  $\alpha$ ,  $\beta$  and  $\gamma$  indices in the study area of the river Brahmaputra, the thresholds were determined for all the aforesaid indices to provide an objective basis for classification of the braiding phenomenon as well as to make them useful for practical applications subsequently. Generalised functional relationships of the hydraulic geometry index with form ratio and energy slope were also worked out.

#### **1.9.6 Prediction of Sediment Load Concentration**

A sediment concentration ANN model was constituted to estimate the natural sediment discharge of the river Brahmaputra in terms of sediment concentration at Pancharatna using water and sediment variables based on the dynamic laws of flow and sediment. The variables used to predict were tractive shear stress  $\psi$ , velocity ratio  $\varphi$ , longitudinal slope  $S$ , suspension parameter  $w_0/u$ , water depth ratio  $h/d_{50}$ , Froude number  $Fr$ , Reynold's number  $R$ , width scale ratio  $h/B$ . The model efficiency is 62%. The mean of the discrepancy ratio between obtained and measured values was 0.961 and the standard deviation for the mean was 0.156.

### 1.9.7 Planform Morphology

Digital satellite data of National Oceanographic & Atmospheric Administration (NOAA) for the year 2002 have been used for deriving the Digital Elevation Model (DEM) and shallow and deep flooding phenomena in the Brahmaputra valley. Furthermore, the variation in Normalised Difference Vegetation Indices (NDVI) for the Assam part of Brahmaputra basin were found out reach-wise, for different years to infer dominant trends in morphological variability response in the basin due to presence of vegetative cover in the flood-plain.

The average northing for right bank line of the river Brahmaputra moved about 0.47 km to the north between 1990 and 2002, while that for the left moved about 0.48 km to the south. The river has avulsed just upstream side of the Dibrugarh town and excised areas of floodplain to create new bars. The study showed that the mean annual discharge at Pancharatna for 1990 - 2002 is 13,714 m<sup>3</sup>/s. Average monthly discharge was highest in July (19.23%) and lowest in February (1.55%). The mean annual suspended sediment load was 440.8 million tons and average monthly sediment discharge was highest in July (25.36%) and lowest in January (0.35%). The river mean width has increased from 7.99 km to 8.94 km in the total length of the river, where as the minimum width at Pandu is slightly constricted due to hard geological formations. There was no radical change in the maximum width of 18.13 km just downstream side of Pandu at cross-section 17 near Gumi. The study further revealed that the total area within the stream banks increased by 12.10% between 1990 and 2002 due to erosion process causing channel widening. Expansion of the river had taken place primarily through floodplain erosion and excision coupled with bar or island growth. Trends of expansion showed no sign of slacking and the expansion process appears to continue.

The degree of braiding of individual reaches fluctuates in the short-term due to morphological response to the magnitude and duration of monsoon runoff events.

For morphological processes fraught with great deal of uncertainty in temporal and spatial variability, displaying nonlinearity of physical phenomena, ANNs could be seen to have provided fairly rational answers by mapping pertinent functional relationships of river behaviour. The signal contribution that emerged from the present study focuses on use of neuromorphic techniques for gainful planning and management of intricate river systems like the Brahmaputra.

## **1.10 ORGANISATION OF THESIS**

The chapters are organized in the following way:

**Chapter -1-** Description of introductory aspects of the topic studied, underlying objectives and the layout of the thesis.

**Chapter -2-** Presentation of a comprehensive review of literature

**Chapter -3-** Description of the study area

**Chapter - 4-** Presentation of the development of spatio-temporal morphological models

**Chapter - 5-** Description of the study and analysis of fluvial landform indicators

**Chapter - 6 -** Presentation of results and discussions

**Chapter - 7-** Presentation of conclusions and scope for future work

**Bibliography**

Furthermore, at the end of the thesis two annexures are placed for the purpose of ready reference. These are:

**Annexure I -** Computer programmes used in the thesis

**Annexure II -** List of research papers published/accepted/communicated

## REVIEW OF LITERATURE

---

### 2.1 INTRODUCTION

River morphology has long been recognized as a diagnostic tool in evaluating the fluvial landforms. It can be considered to include aspects of the shape of a river channel in profile, in cross-section, which includes fluvial landforms and channel patterns. Cross-sectional characteristics include channel width and depth, and features, such as the bed bars, banks, floodplains and terraces. River morphology can be used in combination with other attributes of the river system, such as riparian vegetation and character of the boundary sediments to infer the dominant trends in channel processes and response (42). Fluvial geomorphic processes and landforms normally exert a profound influence on the vegetation patterns.

The study of alluvial river attempts to explain and describe the typical features of the river. These features appear as a result of complex dynamics of flow over a mobile bed. Channel morphology changes with time and is affected by water and sediment discharge including sediment characteristics, composition of bed and bank materials, and vegetation (152). The prediction and post-diction of fluvial system behaviour is greatly complicated by the variability of fluvial system morphology and dynamics through time. Channels change in different ways through the process of erosion and deposition. Almost in all cases, river bed profiles are irregular in shape and size. For representing these profiles, mathematical functions are generally used in the conventional methods of idealization. But, the representation becomes difficult when the river geometry exhibits significant variability and complex patterns. The complexity in representing this



information is made somewhat easier and quick by application of artificial neural network and remote sensing technique. A thorough understanding of the morphology of alluvial streams presupposes detailed knowledge of their planform characteristics (152). The planform of alluvial streams can be classified into the following three categories:

(a) **Braided stream:** A braided stream can be defined as one which flows in two or more channels around alluvial islands. Leopold and Wolman (1957) stated that braided pattern in alluvial stream develops after local deposition of coarse material, which cannot be transported under local conditions of flow existing within the reach. This coarse material becomes the nucleus for a bar formation, and subsequently grows into an island made up of coarse as well as fine material. The formation of the bar deflects the main stream towards the banks and may cause bank erosion (134).

(b) **Meandering streams:** A sinuous channel is called meandering stream. It consists of regular or irregular pattern of loops and a distinct sinuous plan-form. A meandering river has a single flow channel, while a braided river has a number of channels (134).

(c) **Straight stream:** A stream in this classification refers to one that does not have a distinct meandering pattern. It is extremely difficult to find straight reach of stream over large lengths. Straight reach implies neither constant depth of the channel nor a straight thalweg. Even though the channel is straight, the line of maximum depth commonly known as thalweg moves from one bank to another bank (134).

## 2.2 MODELLING OF BRAIDED RIVERS

Braided rivers are characterized by wide, shallow channels which during low discharges split into multiple smaller channels that repeatedly branch off and rejoin around alluvial islands. The sediment transport rate in these rivers is often relatively

high, causing them to be morphologically very active which leads to rapid planform changes. The limited understanding of the behaviour of these rivers becomes clear when dealing with rivers, like the braided, 18.13 km wide river Brahmaputra in India. The channels of this river can migrate several hundreds of meters in only a few months time. Reliable predictions for these channel migrations are often crucial for construction activities on the river.

### **2.2.1 General Characteristics of Braided Streams**

Braided streams occur in high energy environments of large and variable discharges, heavy sediment load and steeper gradients with erodible banks. Braided streams are characterized by wide and shallow cross-sections with random bar formations creating flow divisions. Flume experiments by Leopold and Wolman (1957) suggest that a bar of coarse sand diverts flow to cause channel widening and positive feedback, which then accentuates bar development, resulting in braided channel pattern. Sediment transport takes place over the bar surface while incision in the lateral channels lowers the water surface to expose the bar which then becomes dissected. The complex of islands is stabilized by vegetation in natural streams and experiences further high stage sedimentation (134).

The distributary channels formed by braiding are less hydraulically efficient than a single parent channel. Braided reaches are characterized by steeper slopes for maintenance of stream power necessary for sediment transport. Braided reaches show greater complexity, that is, more bars and distributaries in the highest energy environments (81). This observation confirms that the braided channel pattern is optimal for the dissipation of excess energy in high energy streams, since the enhanced total flow resistance of the multi-thread channel results in rapid energy loss (134).

## 2.3 MEANDERING PARAMETER (Sinuosity)

Leopold and Wolman (1957) have defined sinuosity of a stream as the ratio of the thalweg length to the valley length (Figure 2.1). They have arbitrarily classified streams with sinuosity greater than 1.5 as meandering streams. Friend and Sinha (1993) defined the meandering parameter (Sinuosity) as modified sinuosity parameter, and presented as

$$P = L_{cmax} / L_R \quad (2.1)$$

Where,  $P$  = Modified Sinuosity Parameter,  $L_{cmax}$  = mid channel of the widest channel

Where, there is more than one channel and  $L_R$  = overall length of the meander belt reach measured along a straight line.

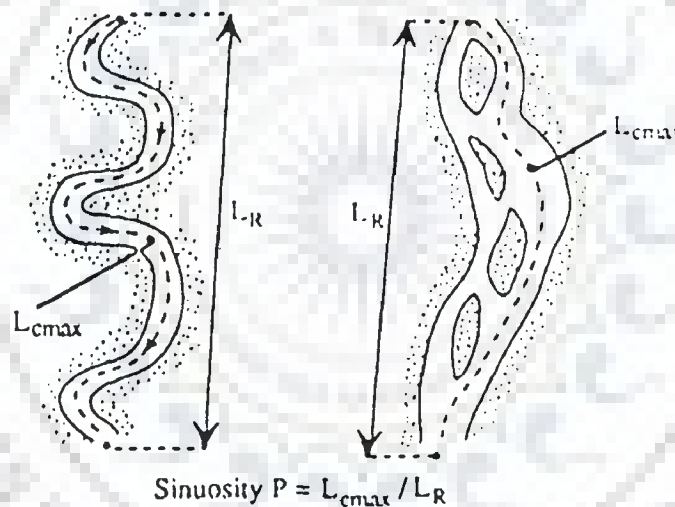


Figure 2.1: Schematic diagram representing the computation of sinuosity for single channel and multi-channel rivers

## 2.4 EXISTING BRAIDING INDICES

### 2.4.1 Braiding Index (BI)

For measuring channel multiplicity, Brice (1964) has introduced a braiding index parameter, which is defined as follows:

$$\text{Braiding index (BI)} = 2 * (\sum L_i) / L_r \quad (2.2)$$

Where,  $\Sigma L_i$  = the length of all islands or bars in the reach,  $L_r$  = the length of the reach measured midway between the banks of the channel belt

Brice (1964) rationalized this parameter as a measure of the total amount of bank length (Figure 2.2), where most island significantly have a greater length than width, so that the total bank length is approximated by doubling the island or bar length. Its higher value shows the higher degree of braiding.

Howard et al. (1970) proposed three different topological indices namely alpha ( $\alpha$ ) index, beta ( $\beta$ ) index and gamma ( $\gamma$ ) index

$$\text{Alpha } (\alpha) \text{ Index} = \frac{t - (n + e) + 1}{2(n + e) - 5} \quad (2.3)$$

Where,  $t$  = total number of segments,  $e$  = number of bisected segments and  $n$  = number of nodes.

Alpha Index is a measure of connectivity, which assesses the number of cycles in a network in comparison with the maximum number of cycles. The higher the alpha index, the more a network is connected. Trees and simple networks will have a value of 0. A value of 1 indicates a completely connected network.

$$\text{Beta } (\beta) \text{ Index} = \frac{t}{n + e} \quad (2.4)$$

This measures of the level of connectivity and is expressed by the relationship between the number of links ( $e$ ) over the number of nodes ( $n$ ). More complex networks have a value greater than 1. In a network with a fixed number of nodes, the higher the number of links, the higher the number of paths possible in the network. Complex networks have a high value of Beta.

$$\text{Gamma } (\gamma) \text{ Index} = \frac{l}{3(n+e-2)} \quad (2.5)$$

Gamma Index is a measure of connectivity that considers the relationship between the number of observed links and the number of possible links. The value of gamma is between 0 and 1, where a value of 1 indicates a completely connected network.



**Figure 2.2:** Schematic diagram representing the computation of the Braiding Index (Brice, 1964)

#### 2.4.2 Braid Channel Ratio (BCR)

Friend and Sinha (1993) have proposed the braid channel ratio (BCR) to define the braiding parameter of a braided river. It has also been used for total sinuosity, as developed by Richards (1982), to measure the braiding in gravel bed river. It measures the tendency of a channel belt to develop multiple channels in any reach. BCR can be computed by

$$BCR = L_{ctot} / L_{cmax} \quad (2.6)$$

Where,  $L_{ctot}$  = Sum of total channel lengths of all segments of primary channels, and  $L_{cmax}$  = the mid channel length of the widest channel through the reach.

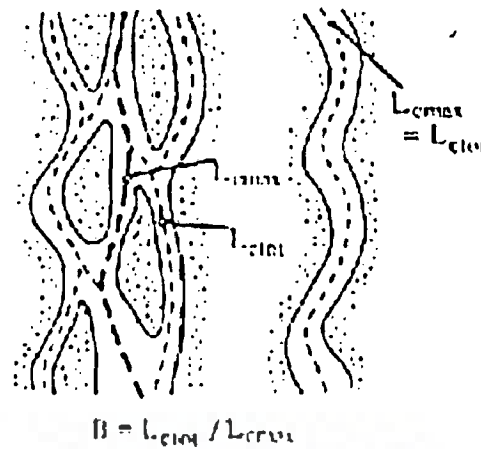


Figure 2.3 Schematic diagram representing the computation of the braid channel ratio, (Friend and Sinha, 1993)

### 2.4.3 Plan Form Index (PFI)

The braiding indicators, explained above, are inadequate, as these are not related to hydraulic efficiencies of the stream.

Sharma (1995) formulated a new braiding index to describe the braiding phenomenon and fluvial landform pattern in quantitative terms. He mentioned that the braided channels are hydraulically less efficient. Also, the formation of braid bars plays an important role in the modification of the energy losses due to friction. With a view to incorporating the effect of the above hydraulic variables, he proposed a new index as follows:

$$PFI = T/B * 100/N, \quad (2.7)$$

Where, T = flow top width, B = over all river width and N = Number of braid channels

It is expressed in percentage, which shows the fluvial landform disposition with respect to a given water level and its lower value indicates higher degree of braiding. Figure 2.4 shows the measurement of planform index.

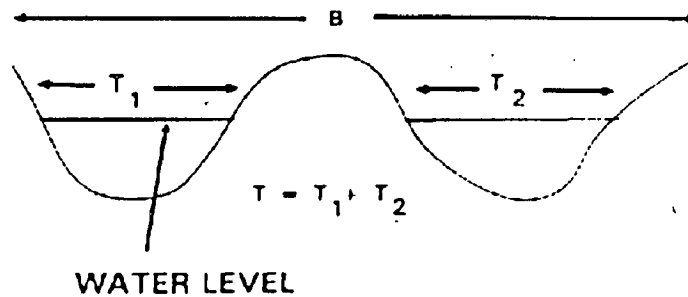


Figure 2.4 Planform Index (Sharma, 1995)

Braided river reaches and alluvial systems are abundant in many areas. They are characterized by their multi-threaded plan-form, and are agents of substantial sediment transport, erosion and deposition. The high rates of sediment transport, erosion and deposition, and the frequent shifting of river channel positions in braided rivers pose many problems to a whole range of disciplines. Despite this importance, they have been relatively neglected in academic study when compared with the wealth of material on meandering rivers (25). The majority of studies to-date have been qualitative in nature, with Howard et al. (1970) and Murray and Paola (1994) being notable exceptions.

The neglect of braided river study is partly due to the difficulty of undertaking field work and characterizing complex features. Although, advances have been made in the qualitative understanding of flow and sediment processes in braided systems, Bristow and Best (1993) have identified several key issues that remain to be addressed, such as (a) the mechanisms of braid bar genesis and evolution, (b) flow and sediment dynamics at bifurcations and confluences, (c) the influence of flow stage on planform development, (d) the implications of a channel hierarchy system found over a range of channel scales and (e) the influence of secondary currents on the morphological development of braid bars.

A number of indicators and hydraulic controls for channel pattern have been proposed in the past as a measure of classifying streams in braiding category or as a measure of degree of braiding. Leopold and Wolman (1957) gave a functional relationship between the bed slope and discharge to identify braided reaches. Lane (1957), Henderson (1961) and Antropovskiy (1972) developed similar functions relating slope with discharge to predict braids at higher slope and discharge. Smith (1970) formulated bed relief index to account for bar type and bed relief to implicitly characterize braids. Schumm and Khan (1972) plotted sinuosity as a function of experimental flume slope to provide the threshold when braiding begins. Brice (1964), Howard et al. (1970), and Rust (1978)<sup>(a)</sup> have emphasized the role of sinuosity as well as braiding indicators in characterizing the braided streams.

Many of the existing braid indicators do not adequately account for the hydraulic parameters and the underwater bars, both of which are seen to have a close relationship with the braiding process. Hence, it can be concluded that there is a need to formulate new braid indicators by incorporating the above indicators to have a more rational description of the braiding phenomenon. A variety of braid indicators are described in Chapter - 5.

## **2.5 DEPOSITIONAL STREAM CHANNEL FEATURES**

Point bars develop where stream flow is locally reduced because of friction and reduced water depth. In a meandering stream, point bars tend to be common on the inside of a channel bend. In straight streams, bar-like deposits can form in response to the thalweg and helical flow. Figure 2.5 shows a plan view of these deposits and related features.



Top-Down View of Stream Channel

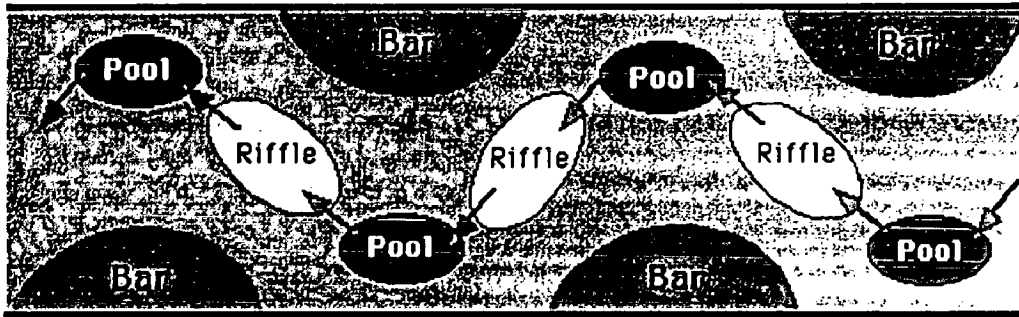


**Figure 2.5** Plan view of the depositional features in a typical straight channel (Source: Natural Resources Canada terrain sciences division-Canadian landscapes)

## 2.6 CLASSIFICATION OF THE BRAIDED PATTERN

A natural river adjusts its channel pattern in space along with its channel network and in time at a given point to accommodate imposed flow and sediment regimes. The forms of natural channels when viewed in plan fall within a continuum of channel patterns that is traditionally sub-divided into straight, meandering, braided and anastomosed. The term 'braided' has been given several definitions in literature (23). Leopold and Wolman (1957) described the braided river as 'one which flows in two or more anastomosing channels around alluvial islands', while Lane (1957) reported that a braided stream is characterized by having a number of alluvial channels with bars or islands between meeting and dividing again. Brice (1964) recognized the importance of defining the difference between mid-channel bars or islands within braided rivers and portions of the floodplain excised by channel diversions and avulsions. Schumm (1977) made the distinction between braided rivers that at low stages have islands of sediment or islands of semi-permanent vegetation, and multiple-thread rivers or anastomosing channels that have branches with individual channel patterns.

Bridge (1993) concluded that these conflicting definitions of the braided pattern raise the issues concerning; (a) the difference between mid-channel bars and islands,

(b) the precise nature of the interaction between flow stage and bars or islands and (c) the differences between the mechanisms of channel divergence that lead to river patterns termed as 'braided' and those defined as 'anastomosing'.

## **2.7 CLASSIFICATION OF RIVER CHANNEL PATTERN**

Bridge (1993) found that Leopold and Wolman's (1957) classification system for river pattern was inappropriate. Leopold and Wolman (1957) classified river pattern to be either straight, meandering or braided; each class being separated by threshold values of river discharge and channel slope (Figure 2.6). They regarded a single channel division around a bar or island as a braid, and showed that hydraulic factors, such as slope adjusted to the presence of braids. Meandering channels have been defined as having a sinuosity greater than or equal to 1.5, whereas channel multiplicity defined the braided pattern. Bridge (1993) stated that this is unsatisfactory because the classes are not mutually exclusive and different parameters are used to define the different patterns. As a result, a channel may contain characteristics of both channel patterns.

Robertson-Rintoul and Richards (1993) stated that classification systems similar to that developed by Leopold and Wolman (1957) which separated meandering and braided channel patterns based on threshold values of discharge ( $Q$ ) and slope ( $S$ ) are flawed. Because, both the coefficient and constant in the power relationship between

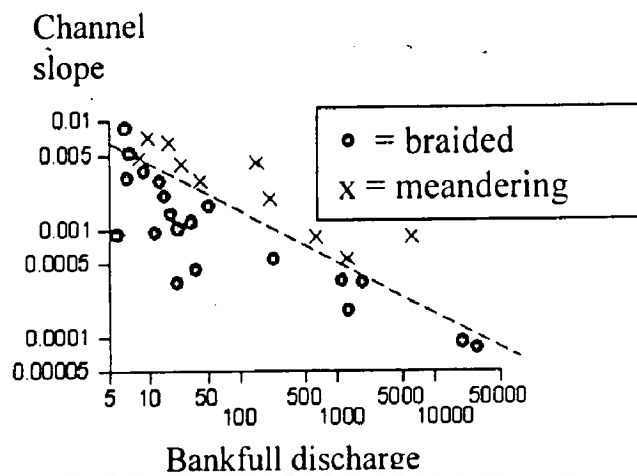


**Figure 2.6** Function distinguishing between meanders and braided channels on the basis of slope and discharge (Leopold and Wolman, 1957)

discharge and slope vary with bed material size (69), bank sediment (47) and the discharge criterion employed (4). They also commented that assigning a nominal planform class to a river system, such as 'meandering' or 'braided', implied that there is a greater uniformity of morphology within a class than is the case in reality. Robertson-Rintoul and Richards proposed a classification system based on an index of total sinuosity, based on earlier work by Richards (1982). Their approach involves the quantitative evaluation of parameters directly related to meandering and braided patterns and the description of how they vary with controlling variables, such as stream power.

Rust (1978) proposed a system of alluvial channel classification based on two parameters: the braiding index and sinuosity. The braiding index is defined by the number of bars per mean meander wavelength with single and multi-channel systems having a braiding index of less than and greater than one, respectively. The channels are then divided further into two categories of high and low sinuosity, with the distinction made at a sinuosity of 1.5. This classification lead to four channel types: (i) single-channel high-sinuosity (meandering); (ii) single-channel low-sinuosity (straight); (iii)

multi-channel high-sinuosity (anastomosing) and (iv) multi-channel low-sinuosity (braided).

To identify more clearly the anastomosing channel pattern, Knighton and Nanson (1993) suggested a classification system for channel pattern that did not include sinuosity as a parameter. Their classification system is based on a continuum concept using three variables; flow strength, bank erodibility and relative sediment supply. Straight reaches are represented by low values of flow strength, bank erodibility and sediment supply. Meandering reaches are represented by medium values of flow strength and low to medium values of bank erodibility and sediment supply. Braided reaches are defined as those in which there is a high flow strength, high bank erodibility and medium to high sediment supply, as opposed to anastomosed reaches which are defined as having low flow strength, low bank erodibility and medium to high sediment supply. Knighton and Nanson (1993) stated that sinuosity is probably not a sufficiently discriminatory characteristic for classifying any channel pattern, but particularly anastomosed channels, because it can vary widely not only between anastomosing rivers, but also between different channels within a given anastomosing reach.

Bridge (1993), also recognized the shortfalls of previous attempts at a universal classification system for channel pattern and suggested that any descriptive classification system should first incorporate the nature of channel splitting around bars or islands and then the degree of sinuosity in channels.

## **2.8 THE DISTINCTION BETWEEN BARS AND ISLANDS**

Brice (1964) defined bars as transient features that are submerged at bank full stage and are un-vegetated, whereas islands are stabilized features that are vegetated

and are not submerged at bank full stage. Bridge (1993) stated that the difficulty with the definition of bars and islands put forward by Brice (1964) is that the degree of vegetation that exists on a mid-channel feature is dependent on the length of time that feature remains emergent above the flow stage, the type of vegetation that is available for colonization, the nature of available sediment and the climate. Bridge (1993) further suggested that in order to overcome the subjective nature of terms such as 'transient', 'stable' and 'unstable', they should be replaced by quantitative measures of bar persistence, rates of deposition, migration and erosion.

## **2.9 INFLUENCE OF FLOW STAGE ON CHANNEL PATTERN CLASSIFICATION AND BRAIDING**

The form of bars is controlled by high in-bank flows, although some features such as cross-bar channels are controlled by falling stages (26). Bridge (1993) recommended that the braided channel pattern should ideally be observed and characterized at formative high discharges when falling stage features are not present. A further problem in defining river channel pattern examined by Bridge (1993) was which of the channel segments should be used to define channel sinuosity and which of the bars should be used to define channel splitting. This problem is highlighted when cross-bar channels are considered as it is debatable whether these low-stage features should be ignored when defining channel pattern although they may well evolve into major channels. Bridge (1993) noted that this problem has led to the development of a system that assigns orders to channels and bars in multiple channel rivers, and then each order of channel is described by a particular flow pattern (177; 143; 26; 167). Kellerhals et al. (1976) and Rust (1978) recommended the definition of channel patterns at mid-way or mean channel stages that have a high frequency of occurrence.

The fluvial planform of many braided rivers change dramatically with changes in flow stage. Bristow and Best (1993) noted that these fluctuations in flow stage or discharge are a pre-requisite for river braiding (40; 112). This hypothesis has been discounted in many cases by the physical modelling of braided river planform in steady discharge flume experiments (6). Further work has shown that bars may disappear at high flow stages, the implication being that some braided systems act as single channels at bank full stage and only adopt the characteristic braided pattern on the falling stage (159; 31).

Carson (1984), in a study of a mechanistic approach to the classification of channel pattern in relation to a variety of river types in the Canterbury Plains, New Zealand, found that many large bars were in fact merely exposed tracts of the flat bed, dissected into lower order bed features, rather than a cluster of small genuine medial bars, and as a result at bank full stages the channels revert to acting as single channels. Many of the other braided features of the rivers observed by Carson (1984) were in fact formed by low flow channels dissecting large point bars during flood events. The channels slowly revert back to their meandering pattern through gradual accretion of sediment in the ruts.

Bristow and Best (1993) stated that these observations appear to be a typical and the majority of braided river systems, including the river Brahmaputra, which have been observed to maintain their bars at both high and low flow stages (33; 158; 24; 26).

## **2.10 CHANNEL HIERARCHY AND BRAIDED CLASSIFICATION**

Williams and Rust (1969) proposed a system of braided channel classification that incorporated three levels of channels and bars (Figure 2.7a). Their first order

channels formed the main anabranches of a braided system that flow around first order islands or bars. Second and third order channels in the Williams and Rust approach dissect these first order bars to form second and third order segments of bars. The distinction between the second and third order channels is unclear, the second and third order bars that they form are actually only dissected segments of first order bars, and these second and third order channels may well contain mid-channel bars of their own (23).

In a study of channel migration and deposition on the river Brahmaputra, Bangladesh, Bristow (1987)<sup>(a)</sup> defined a three level channel hierarchy system (Figure 2.7b). The entire river system makes up the first order channel, with the channel margin being defined by the outermost river banks. First order channels may be comprised of several second order channels that form the main anabranches of the system, and have been observed on the Brahmaputra to display a variety of channel patterns. These second order channels may themselves contain third order channels such as cross-bar channels. Bristow (1987)<sup>(a)</sup> found that the bars around which the channels divide and rejoin, scale with the bank full depth and width of each channel. Further work on the river Brahmaputra by Thorne et al. (1993) confirmed the existence of Bristow's channel hierarchy system. Thorne et al. (1993) went on to describe in more detail the nature of the hierarchy system and the way in which islands, bars and various bed features were scaled by the various channel orders.

Bridge (1993) put forward a two level channel and bar hierarchy system, in which the largest scale of bars or islands in a system and their adjacent channels are first order, but unlike Williams and Rust's scheme, all of the channels cutting across first

order bars are second order. However, the dissected segments that the second order channels form are not themselves second order bars.

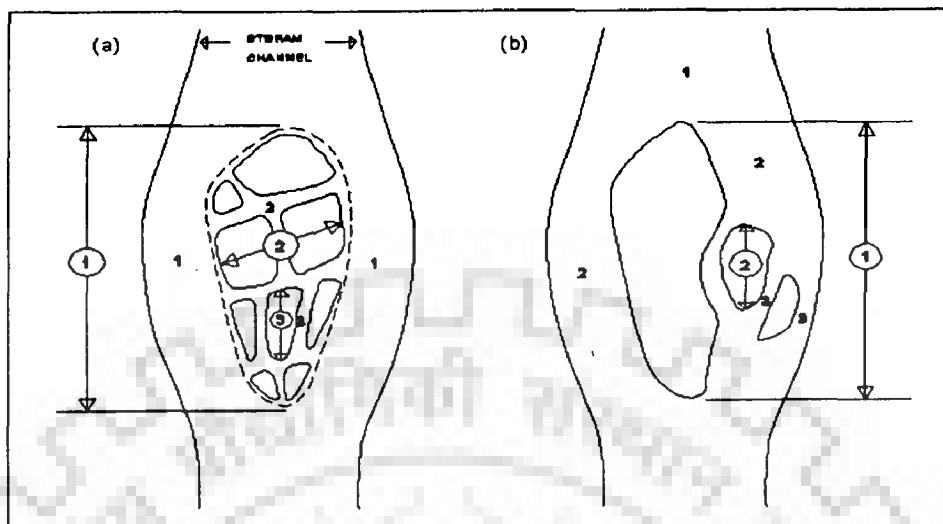


**Figure 2.7** Channel and bar ordering schemes of (a) Williams and Rust (1969), and (b) Bristow (1987). Numbers in circles refer to bars, other numbers refer to channels

Second order bars are defined as those which form in and at the termination of second order channels (Figure 2.8).

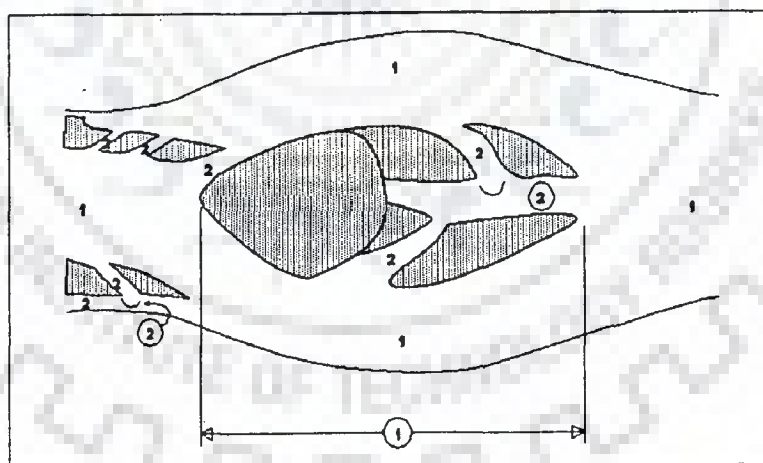


**Figure 2.8** Alternative channel and bar ordering scheme, (Bridge, 1993).

## 2.11 CHARACTERISTICS OF BRAIDED AND ANASTOMOSED PATTERNS

Generally, the term braided when applied to river channel pattern is taken to mean the splitting of flow around an island or bar (23). However, there is another mechanism of flow divergence widely recognized that of anastomosing (96; 155; 93). An



anastomosing river consists of multiple channels separated by islands which are usually excised from the continuous floodplain and which are large relative to the size of the channel (93). The principal characteristic of an anastomosing system is that each channel segment behaves significantly different from adjacent segments, having its own channel pattern with an independent sinuosity or braiding index (23) and the distance between channel junctions is independent of channel width (167).

However, in many multi-thread rivers the distinction between braided and anastomosed channel reaches is unclear (26). For example, for Brahmaputra river, Bristow (1987) found that some second order channels (defined using Bristow's classification scheme) contained many features characteristic of anastomosed channel reaches. Bridge (1993) proposed a solution to this problem by defining anastomosed reaches as those where the length of channel segments exceeds the length of first order channels around individual first order bars (Figure 2.9).

## 2.12 CONFLUENCE-DIFLUENCE MECHANICS

Lane (1957) described braided rivers as, 'having a number of alluvial channels with bars and islands between meeting and dividing again'. The continual coming together and diverging of channels is inherent in the nature of braided systems (25). The flow dynamics and morphology of regions of channel convergence have been studied by Mosley (1982)<sup>(a)</sup>, Best (1988) and Best and Roy (1991). However, the connection between flow convergence and the subsequent downstream divergence of flow has often been disregarded (25), Ashworth (1996) being a recent exception.

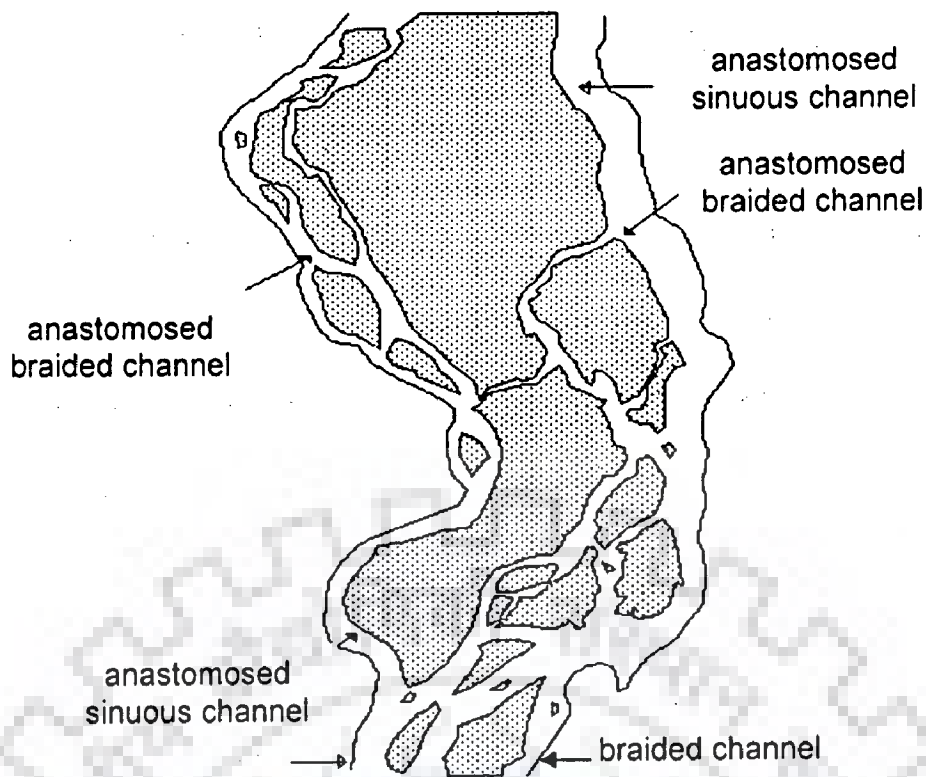


**Figure 2.9** Various kinds of channel pattern as defined by Bridge (1993), adapted from 1994 Landsat TM image of the Brahmaputra in the region of Bahadurabad

Ashmore (1991), Ashworth et al. (1992) and Bristow and Best (1993) have all commented that the region of flow divergence is the area that may well be fundamental to the development of braid bars.

### 2.12.1 Channel Confluences

The morphology and flow dynamics of channel confluences have received considerable attention recently in geomorphology, sedimentology and hydraulic literature (5; 17). Where channels converge in a braided system, rapid changes occur in the velocity and sediment distributions that result in rapid shifting of the channel geometry (134).

Confluence channel morphology is widely accepted as being typically composed of three distinct elements that are controlled by the confluence angle and the ratio of discharges. These are; (i) avalanche faces at the mouth of each channel, (ii) a deep

confluence scour and (iii) a bar formed in the separation zone at the downstream junction corner (17). Best (1988) found that increases in the confluence angle or discharge ratio resulted in greater confluence scour, deflection of sediment around the increased zone of turbulence and flow separation at the confluence centre. Best and Roy (1991) suggested that a depth differential in two converging channels has a significant effect on the three-dimensional flow structures at the channel confluence and on the downstream mixing of the flows.

### **2.12.2 Flow Diffuence**

Anabranches of braided river systems shift rapidly across their braid belt, constantly producing new channel junctions, sediment erosion through confluence scour, subsequent mid-channel bar formation and growth downstream (8).

In general, areas of flow divergence within a fluvial system are associated with flow deceleration and sediment deposition. Once sediment deposition has been initiated, the sediment accumulation promotes further flow divergence, additional flow deceleration and sediment deposition and finally bar formation (27). Flow being diverted around mid-channel sediment deposits impinges on the channel boundaries at an increased angle of attack. This results in bank erosion, widening of the braid belt and localized increases in the amount of sediment available for transport. All of these conditions are liable to lead to the development of a new braid bar (31; 167). Bristow and Best (1993) commented that there is a clear need for a better understanding of the fluid dynamics and their effect on braid bar initiation in areas of flow bifurcation.

Ashworth (1996) used a generic-scale flume study of mid-channel bar growth of a fixed junction scour (Figure 2.10). Ashworth's flume experiments differed from previous

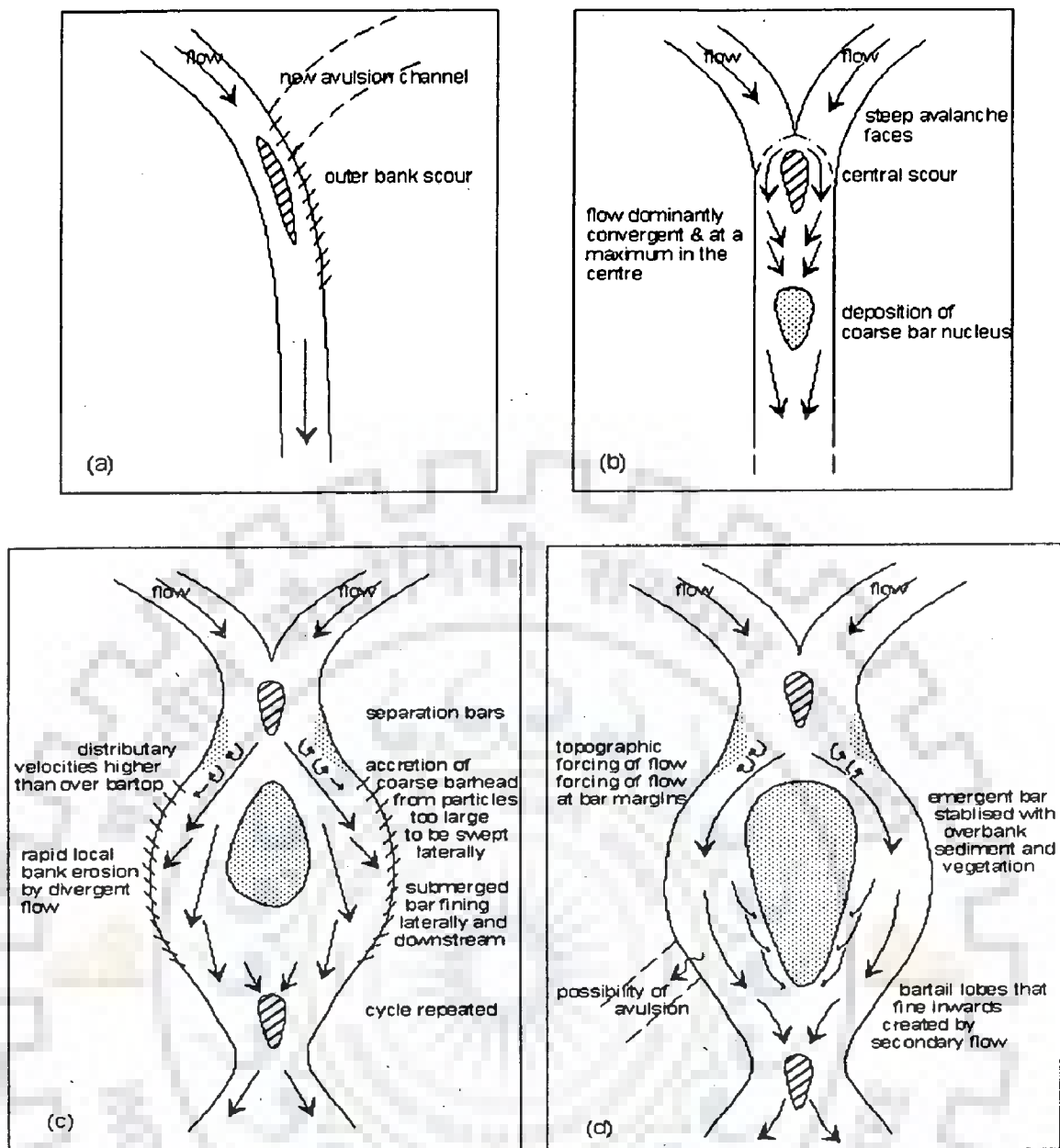


Figure 2.10 Ashworth's (1996) model of mid-channel bar growth downstream of a junction scour

work by Leopold and Wolman (1957) and Ashmore (1991)<sup>(a)</sup> in two respects; first, the channel junction was fixed and not allowed to develop naturally, Ashworth concluded that this probably had the effect of increasing the rate of morphological change; second, previous studies have involved 'before and after' type observation, whilst Ashworth continually monitored both flow structures and sediment transport.

## **2.13 BED MATERIAL INFLUENCES UPON RIVER BRAIDING**

Bristow and Best (1993) in their recent review of braided river issues and problems concluded that although there is an apparent differentiation necessary when calculating sediment transport parameters and considering sedimentary structures and detailed bar features, there would seem to be more gross channel morphological similarities between sand-bed and gravel-bed rivers than differences.

In geomorphologic and sedimentologic literature, the distinction between gravel-bed and sand-bed rivers has been long established, despite the fact that it is unusual for a particular river to have a homogenous bed material. Though the apparent similarities between planform characteristics in gravel-bed rivers with that of sand-bed rivers suggest that they may share many important common processes, Bristow and Best (1993) found that little quantitative data exists to enable the comparison.

## **2.14 CHANNEL SCALE AND THE BRAIDED PATTERN**

Bristow and Best (1993) commented that investigations into braided channel morphology and dynamics have covered the entire scale of braided river size from micro-scale physical models of braided systems in the laboratory through small upland braided drainage channels (159; 48) to meso-scale rivers with braid belts several kilometre in width (9) to the largest macro-scale alluvial rivers such as the Brahmaputra (33; 28; 167).

## **2.15 INFLUENCE OF SECONDARY CURRENTS IN BRAIDED CHANNELS**

Secondary currents have originally been defined by Prandtl (1952) as currents, which occur in the plane normal to the axis of the primary flow, they originate from interactions between the primary flow and gross channel features. Two types of

secondary currents have long been recognized; skew induced and stress induced secondary currents.

There have been few field and laboratory investigations of flow structures in braided rivers and as a consequence their link to braided morphology is little understood. Unlike meandering single-thread rivers, in which observations of key flow processes can be undertaken over a range of flow stages, in braided rivers most channel changes are associated with changes in bed morphology, which occur at high discharges when observation is very difficult (159; 144). Any mention of secondary currents in braided systems has been restricted to areas of channel confluence, and the effect of secondary currents in bifurcations and around braid bars has been largely neglected.

Mosley (1976) reported the presence of helical flow at channel confluences in a general flume experiment of confluence behaviour. Using dye injection to visualize flow patterns, He observed that the pattern of secondary flow at channel confluences consisted of a pair of helical cells, converging in the channel centre over the point of maximum scour and diverging at the bed. He concluded that the observed helical flow pattern resulted in steepening of the scour walls beyond their natural angle of repose, giving rise to their characteristic avalanche faces. Mosley further stated that the helical flow structure resulted in most of the sediment transport in the confluence occurring at the channel fringes away from the area of maximum scour. There is also evidence found for smaller cells of reverse rotation further downstream from the channel confluence, resulting in elevated portions of the bed flanking the channel centre line. Mosely observed that this secondary flow pattern resulted in high rates of sediment transport restricted to the zones between opposing cells.

Best and Roy (1991) proposed that these secondary flow patterns are the result of horizontal separation vortices formed in the lee of the avalanche faces at the entrance to the confluence, particularly when the converging channels are of unequal depth. Another probable cause of the helical circulation is the same mechanism that causes helical flow in meander bends, i.e. the relationship between the outwardly directed centrifugal force and the inwardly directed pressure gradient force caused by super-elevation. In the case of channel confluences the centrifugal force would be acting towards the confluence centre and the pressure gradient force would be acting towards the confluence fringes. Mosley (1976) observed a degree of super-elevation in the centre of their model confluences. Ashmore et al. (1992) proposed that the flow separation at the confluence entrance probably reinforced, rather than replaced, the circulation due to channel curvature.

Ashmore et al. (1992) carried out a field investigation of secondary flow patterns in river confluences on the gravelly Sunwapta River, Alberta. They confirmed for the first time in a real river the existence of the secondary flow patterns observed in laboratory experiments by Mosley (1976). Ashmore et al. made measurements in two Y shaped anabranch confluences at relatively high discharge levels and found that the pattern of secondary flow observed in laboratory experiments existed in both of the surveyed cross-sections, although the pattern was much stronger in one of the confluences. In both confluences, the larger of the two helical cells tended to dominant the other in the downstream direction. They conceded that the methods employed to correct velocities in meandering rivers were inappropriate for braided rivers and as a result the flow patterns reported may be susceptible to small errors.

Ashworth et al. (1992) in a descriptive model for bed load transport and sorting around a braid bar proposed a secondary flow structure similar to that found in meandering channels. They suggested that the actual pattern of secondary flow in the two anabranch channels around a braid bar would mirror the pattern in two 'back-to-back' meanders (Figure 2.11). This system of flow structure in anabranches around braid bars taken together with the observed patterns of secondary flow in channel confluences (114; 9) would lead to the following impact of secondary flow on the morphology of braid bars.

In braided rivers, the width to depth ratio tends to be higher than for single thread meandering river and the secondary flow patterns for bed load transport and sorting around a braid bar may only develop above average discharges (9).

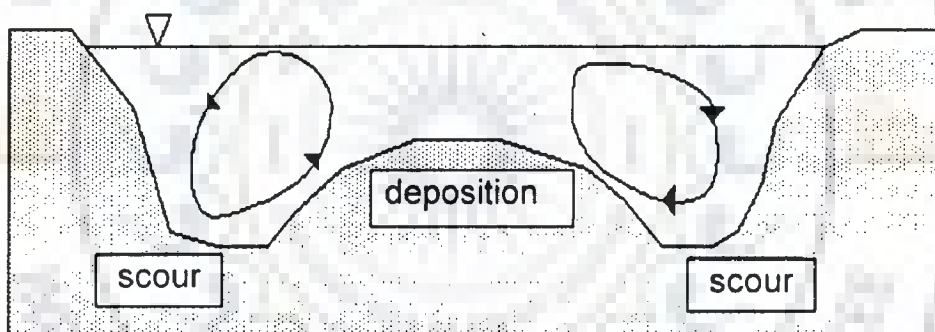


Figure 2.11 Flow in a bifurcated channel as mirror image meanders (Ashworth et al., 1992)

## 2.16 RIVER MORPHOLOGY USING REMOTE SENSING DATA

Remote Sensing (RS) and Geographical Information System (GIS) play a rapidly increasing role in the field of water resources development. Remotely sensed based information is of great value since many hydrologically relevant data can be derived from it. One of the greatest advantages of using RS data for hydrological modelling and monitoring is its ability to generate information in spatial and temporal domain, which is



very crucial for successful model analysis, prediction and validation. However, the use of RS technology involves large amount of spatial data management, and requires an efficient system to handle such data. The GIS technology provides suitable alternatives for efficient management of large and complex databases. The remote sensing data provides synoptic view of a fairly large area in the narrow and discrete bands of the electromagnetic spectrum. The space borne multi-spectral data enable generating timely, reliable and cost effective information on various natural resources, namely surface water, land-use and land-cover, soil and environmental hazards.

### **2.16.1 Application of Remote Sensing to River Engineering**

Changes in the river channel alignment and size, development of bars, islands take place during floods, time dependant changes can be monitored in the specific river reach using remote sensing. Depending on the resolution of the imageries, accurate and dependable predictions can be made covering long reaches.

Changes in the river channel monitoring include the aspects, like changes in the location, size and alignment. In case of rivers with multiple channel system or braided rivers, these could be the important aspects resulting in bank erosion. This can also be important while considering the development of inland navigation system, locating riverine ports and other structures, design of anti-erosion works, etc. These aspects are generally affected by the development of islands, bars in the channel, changes in the orientation of channel etc. Monitoring of temporal changes in the river channel with the help of satellite imageries would highlight on these aspects.

Other information, like existence of paleo channels, low lying areas, reaches under active erosion, damages due to over bank flows, breaches in the embankments,

damages to the existing hydraulics structures can be identified using satellite imageries. In spite of the fact that normally the changes in a braided channel are sudden and unpredictable, efforts have been made with the help of satellite imageries to identify any cyclic behaviour observed in the past. Efforts are also made to identify physical limits of such changes, if any, observed earlier. Co-relating these observations with other information can give fairly good idea of the river behaviour in a specific reach and likely behaviour in the immediate future.

### **2.16.2 Earlier Works**

The study on river morphology with the use of remote sensing data is a relatively new development, and has been in practice for not more than the last 20 to 25 years in India. Murthy (1990) has studied the flood plain of Brahmaputra river using satellite imageries. Hussain (1992) has carried out morphological studies of river Brahmaputra with the help of satellite imageries. Morphological studies of the river Brahmaputra has been undertaken by Brahmaputra Board, Government of India in 1993. Best and Bristow (1993) studied the braiding pattern of Brahmaputra in Bangladesh using satellite data. Arshad (1996) through satellite imageries has done morphological analysis for identification of river training sites in a stretch of the river Ganga. Oak (1998) worked on the prediction of bank erosion of bank of the Brahmaputra river on Gumi-Alikash reach (down stream of Pandu). Some erosion studies using satellite imageries in the vicinity of Majuli island and Kaziranga National Park had been studied by Space Application Centre, Ahmedabad.

### 2.16.3 Digital Image Processing

The term digital image processing generally refers to processing of two – dimensional picture by a digital computer. A digital image is an array of real or complex numbers represented by finite number of bits. The processes are described in brief:

#### 2.16.3.1 Geo-referencing

The image is assumed to be available as a matrix of M rows and N columns, with each element of the matrix being a vector of K components, each component representing the measurement in a particular wavelength band of electromagnetic spectrum. Each element of the image matrix is referred to as pixel (picture element). There are several processing operations, where each band of the data is processed separately. In such a case a single band image can be viewed as a black and white image and the value at each pixel may be viewed as shade of gray ranging from black to white. Thus, the pixel values are also referred to as gray levels (102). Geo-referencing the image to standard cartographic reference involves two major steps.

##### *a) Transformation of pixel co-ordinates*

The procedure requires that polynomial equation be fitted to the Ground Control Points (GCP) using least squares criteria to model the corrections in the domain without identifying the source of distortion. The image points are mapped from the distorted frame to the reference frame. An example of such a map can be represented by a polynomial in two dimensions as

$$x' = a_1x^2 + b_1y^2 + c_1xy + d_1x + e_1y + f_1 \quad (2.8)$$

$$y' = a_2x^2 + b_2y^2 + c_2xy + d_2x + e_2y + f_2 \quad (2.9)$$

where, x & y positions represent the coordinate positions in the distorted frame and x', y' the points in the reference frame.

Determination of the gray level values of the pixel mapped to the reference frame. This step is necessary because integer co-ordinate locations in the distorted frame do not map to integer location in the reference frame. This process is more commonly known as re-sampling or registration.

#### **b) Registration**

This involves extraction and interpolation of gray level from pixel location in the original distorted image and their re-location to the appropriate matrix coordinate locations in the rectified image. Methods of interpolating gray level include nearest neighbourhood, bilinear interpolation and cubic-spline interpolation. These methods produce increasingly better interpolated images, while consuming more computer time.

#### **2.16.4 Normalized Difference Vegetation Index (NDVI)**

Ratio images are enhancements resulting from the division of pixel values in one spectral band by the pixel values in another spectral band. These are computed and appropriately stretched to an output range. NDVI is a simple ratio that is transformed to reduce range of ratio values from -1 to 1. NDVI is defined as the ratio of difference in the reflectance in the infrared (IR) and red (R) bands to their sum.

$$NDVI = \frac{(IR - R)}{(IR + R)} \quad (2.10)$$

Healthy vegetation possesses high digital numbers in infrared band and low digital numbers in red band. Other land use classes, e.g. bare soil possesses high values in both bands. Near infrared (NIR) band is highly useful for land and water

discrimination. Water possesses very low value in infrared band and low value in red band. Thus, a ratio of values in infrared band to that in red band is large for healthy vegetation and small for other features. Two bands are thus used for a simple two class (vegetation and non-vegetation) classification. For the vegetation class, NDVI is small positive number. For water stressed and deceased vegetation the NDVI is small positive number.

Advantage of using ratio is that it is not affected by geometry of sun-sensor-object. That is, the NDVI conveys the spectral or colour characteristics of the image features, regardless of the variation in scene illumination condition. The resultant image shows better spectral features which are masked in the usual intensity images by the variations in the brightness. Digital numbers are affected more in visible bands than infrared bands by atmospheric attenuation. Thus, the use of absolute value of NDVI to indicate vegetation state is hindered by radiometric distortions.

#### **2.16.5 Digital Image Classification**

Image classification refers to the process of assigning the pixels in the image to various classes or categories based on measurements in various bands of the electromagnetic spectrum. In the context of remote sensing, the various land use or land cover categories include, such as water, vegetation cover, crop land, sand and open areas. A classifier assigns to every pixel a level from the predefined categories so that the classified image can be displayed for visualisation purposes.

#### **2.16.6 Supervised and Unsupervised Classification**

Classifiers can be broadly grouped into two major types - supervised and unsupervised. Supervised classifiers make use of any a priori information available with

the user pertaining to the terrain so that the characteristics of each class can be accurately inferred before classifying all the pixels. The information enables the user to identify with high degree of confidence a small number of pixels to derive estimates of the statistical parameters for each of the classes, which are subsequently used in the classification. Every pixel is assigned to a class for which its likelihood of belonging is highest compared to other classes (169). Generally, three algorithms are used for supervised classifications: minimum distance to means, parallelepiped and Gaussian maximum likelihood.

The unsupervised classifiers do not employ any training data. These methods try to extract inherent natural groupings within the data, under the premise that pixels belonging to a class will have very similar gray levels or feature values, and those belonging to different class will have widely differing values. In the present study, minimum distance to means technique has been used for the classification of Indian Remote Sensing (IRS) images.

## **2.17 NEUROMORPHIC SYSTEMS**

Numerical modelling techniques are now well established methods for describing the physical processes occurring in the aquatic environment. The development in information technology over the last decade has presented opportunities of extended computational ability together with the improved data manipulation, storage and retrieval. As a result, the numerical models are now being used more extensively in the management of water resources. The reason behind this is that in many areas of applications to complex flow systems the demand on computing time are of a magnitude that is far from acceptable.

Traditional modelling of physical processes is often named physically-based modelling, because it tries to explain the underlying processes. The data-driven models, borrowing heavily from artificial intelligence (AI) techniques are based on a limited knowledge of the modelling process and rely on the data describing input and output characteristics. These methods, however, are able to make abstractions and generalizations of the process, and play often a complementary role to physically-based models. Data-driven modelling uses results from such overlapping fields as artificial neural networks (ANN), rule-based approaches like fuzzy logic concepts. Sometimes "hybrid models" are built combining both types of models. More complex data-driven models are highly non-linear, allowing to have many inputs and many outputs (Figure. 2.12). The neural models are different from the regression models in the sense that the former gives output from memorisation and the latter by generalisation. ANN is resorted to when the dimension of input space is high, where regression analysis becomes ineffective in delivering a solution. They need a considerable amount of historical data to be trained, and if this is done properly, they are able not only to approximate practically any given function, but also to generalize, providing correct output for the previously unseen inputs.

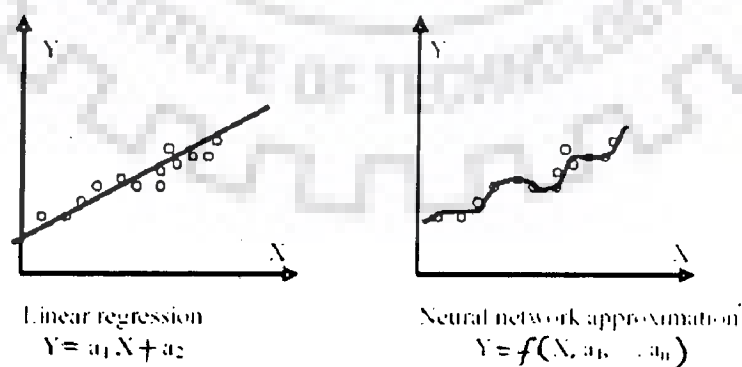


**Figure 2.12** Linear regression and data driven model (ANN)

The origin of fuzzy logic approach dates back to 1965, since Zadeh's introduction of fuzzy-set theory and its applications. Since that period, fuzzy logic concept has found a very wide range of applications especially in the systems that are very complex, uncertain and cannot be modelled precisely, even under various assumptions and approximations.

Neural network and fuzzy logic have been successfully applied to a wide range of problems covering a variety of sectors. Their practical applications, especially of neural networks expanded enormously, starting from mid 80s till 90s partly due to a spectacular increase in computing power. During the last decade ANN evolved from being only a research tool that is applied to many real-world engineering problems.

Neuro-fuzzy approach is comparatively new, and is a growing area of research. Neuro-fuzzy systems combine the advantage of fuzzy logic system, which deal with explicit knowledge that can be explained and understood, and neural networks, which deal with implicit knowledge, which can be acquired by learning. A faster rate of convergence by controlling the learning rate parameter with fuzzy rules can be obtained.

### **2.17.1 Artificial Neural Networks**

An artificial neural network (ANN) is a computing paradigm designed to mimic the human brain and nervous system. Neural network (NN) has a big role to play in the field of hydrology where complex natural processes dominate. The high degree of empiricism and approximation in the analysis of hydrologic systems make the use of NN highly suitable. In other words, when the possibility of representing the complex relationships between various aspects of the processes in terms of physical or conceptual modelling is very remote, the NN plays an important role.



ANN is an information processing system that uses an approach entirely different from conventional algorithmic programming and roughly replicates the behaviour of a human brain by emulating the operations and connectivity of biological neurons. From a mathematical point of view, it is a complex non-linear function with many parameters that are trained in such a way that the ANN output becomes similar to the measured output on a known data set. ANNs are highly distributed interconnections of adaptive nonlinear processing-elements (PEs) (Figure 2.13). When implemented in digital hardware, the PE is a simple sum of products followed by non-linearity. The connection strengths, also called the network weights, can be adapted such that the network's output matches a desired response.

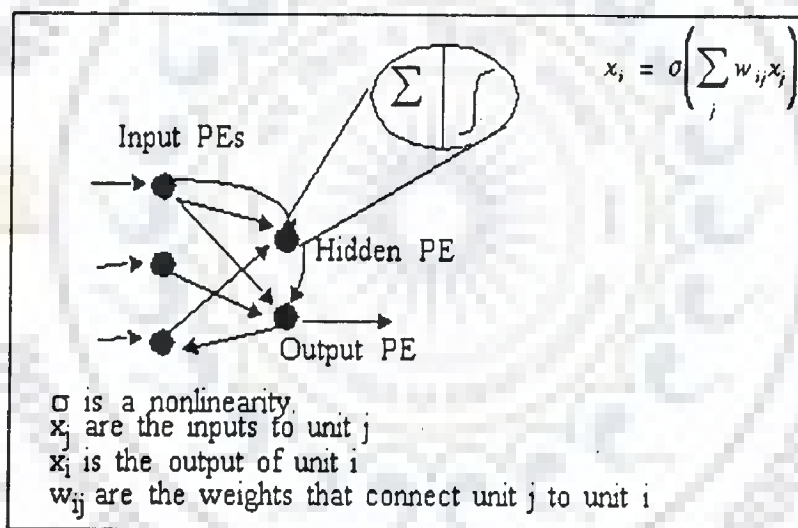


**Figure 2.13** The building blocks of ANN

In multi-layered perceptron, hidden layer means a third layer of processing elements or units in between the input and output layers that increases computational power. In principle, the hidden layer can be more than one layer. In practice, the number of neurons in this layer is evaluated by trial and error. Hornik et al. (1989) proved that a single hidden layer containing a sufficient number of neurons could be used to approximate any measurable functional relationship between the input data and the

output variable to any desired accuracy. In addition, De Villars and Barnard (1993) showed that an ANN comprising of two hidden layers tends to be less accurate than its single hidden layer counterpart.

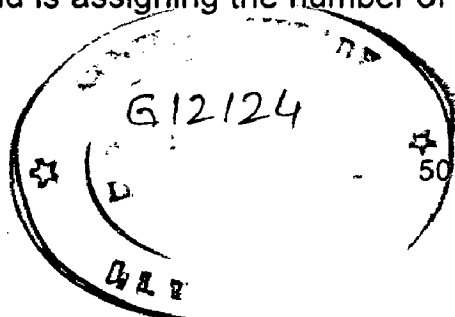
The ANNs are not exactly the substitute to regression. General regression can not solve the problems where the input dimension space is high and there is restriction on the number of input data. Regression imposes a priori variable selection, with all the inherent pitfalls, where one is limited to a few inputs among hundreds available. Regressions are performed using simple dependency functions that are not very realistic. In regression there is only one dependency function over the whole data set, instead of many distinct niches, which is taken care of by ANNs. Where dependency between the input variables and the output are not well-defined, ANNs solve it better. The most important difference between ANN and regression is that the former maps the output by generalization where as the later by memorization. Generalization refers to the neural network producing reasonable outputs for inputs not encountered during learning. To oversimplify, if an object is represented in a network as a pattern of activation of several units, and if a unit or two responds incorrectly, the overall pattern remains pretty well the same, and the network will still respond correctly to stimuli.

In 1943, McCulloch and Pitts studied the finest element of the brain, the neuron, with its cell body, axon, and synapses to create the perceptron. ANNs have become an attractive technique for approaching many hydrologic problems as established by Daniel (1991), Hall et al. (1993), Karunanithi et al. (1994), Zhu and Futija (1994) and Smith and Eli (1995). According to Bastarache et al. (1997), Muttiah et al. (1997), Clair and Ehrman (1998) and Wen and Lee (1998), multilayer perceptrons are powerful tools in solving non-linear water resources problems. Zealand et al. (1999) worked on short-term stream

flow forecasting using ANN. Dastorani et al. (2002) used ANN for real time river flow prediction. Bhattacharya et al. (2000) used ANN to predict stage and discharge relationship. Kumar et al. (2004) forecasted the river flow using recurrent neural network. In general, neural networks offer viable solutions when there are large volumes of data to train the neural network. When a problem is difficult (or impossible) to formulate analytically and experimental data can be obtained, a neural network solution is normally appropriate.

### 2.17.2 Neural Network Topology

The arrangement of the processing units, connections, pattern input and output is referred to as topology. The processing units are arranged in three layers as input, hidden and output. The units of a layer are similar in the sense that they all have the same activation dynamics and output function. The number of input and the number of output are problem specific. There are no fixed rules as to the how many units should be included in the hidden layer. If there are too less units in the hidden layer, the network may have difficulty in generalizing the problem. On the other hand, if there are too many units in the hidden layer, the network may take an unacceptably long time to learn. On the basis of direction of information flow and processing, the ANNs are classified as feed forward and feed backward network. The manner in which the neurons of a neural network are structured and intimately linked with learning algorithm ceased to train the network. The optimal architecture is one, which yields the best performance in terms of error minimization, while training simple and compact structure. The numbers of input and output nodes are problem dependent. The flexibility lies in selecting the number of hidden layers and is assigning the number of nodes to each of these layers.



### 2.17.3 Model of Neural Networks

The human nervous system may be viewed as a three-stage system. The forward and feedback arrows are shown for the movement of information. The neural (nerves) net continually receives information, perceives it, and makes appropriate decision. The receptors convert stimuli from the human body or the external environment into electric impulses that convey information to the neural net (brain). The effectors convert electrical impulses generated by the neural net into discernible responses as system outputs. The operation of brain is believed to be based on simple basic elements called neurons, which are connected to each other with transmission lines, called axons and receptive lines, called dendrites (67). A simple illustration of biological and artificial neuron is shown in Figure 2.14(a) to (c).

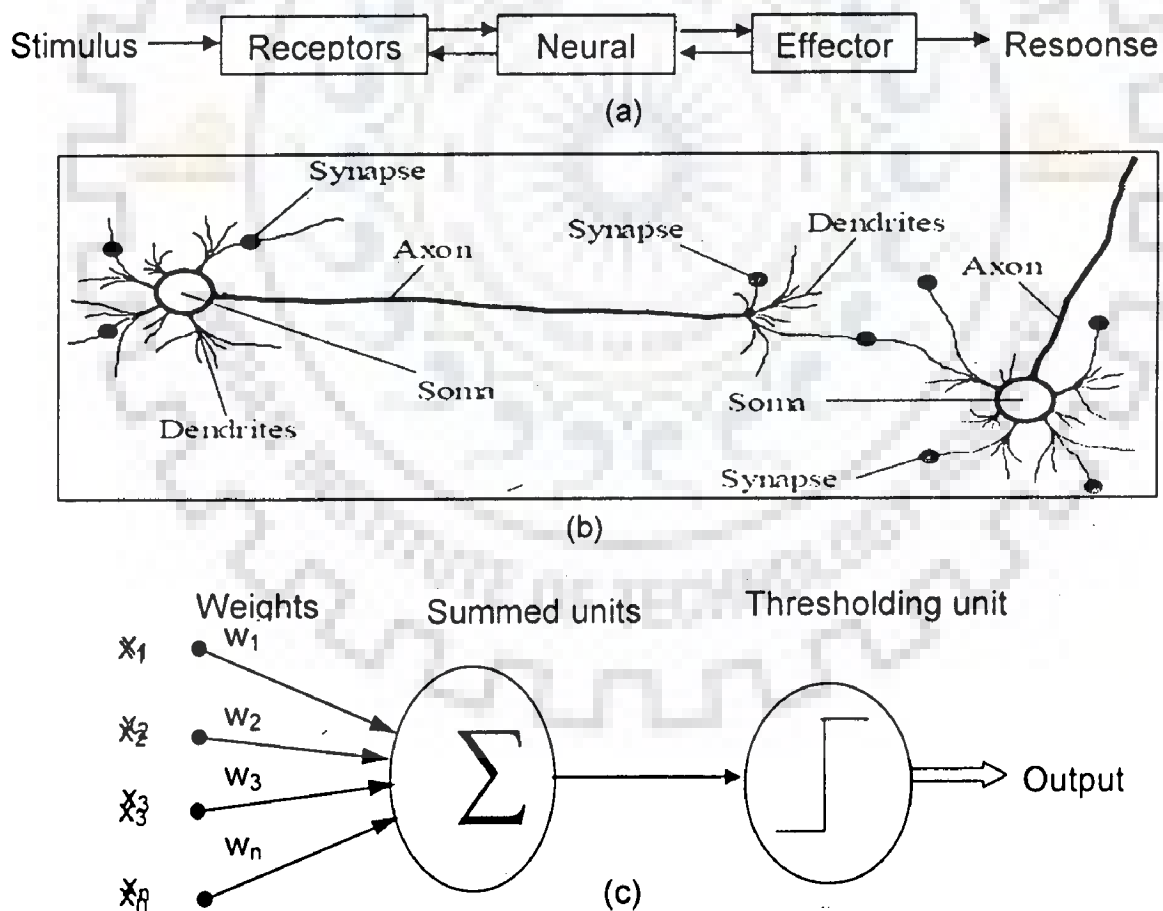


Figure 2.14 Simple illustration of biological and artificial neuron

Each input  $x_i$  ( $i = 1, \dots, n$ ) is attenuated by a factor  $w_{ij}$ , more commonly called a weight of the network, which is associated with the connection linking input  $x_i$  to hidden neuron  $j$  ( $j = 1, \dots, k$ ), where  $k$  is the number of neurons in the single hidden layer. The weighted sum of the incoming signals entering a neuron is fed via an activation function, which is non-linear, producing a value that in turn acts as an input signal sent to the output layer. This is repeated for the output weights. The following expression gives the output value of the network:

$$y = \phi \left[ \sum_{j=1}^N \phi \left\{ \sum_{i=1}^N x_i w_{ij} \right\} a_j \right] \quad (2.11)$$

Where  $\phi$  is a sigmoidal activation function (described at para 2.17.5.1)

To obtain the best approximations, it is needed to determine the optimum set of weights  $w_{ij}$  and  $a_j$  that will yield the least mean square value of the desired response. Thus, the following performance criterion needs to be satisfied.

$$\min_{a, w} \frac{1}{2} E[(y - y_D)^2] \quad (2.12)$$

Where,  $E$  is the statistical expectation operator, the factor  $\frac{1}{2}$  is included for convenience of presentation.

#### 2.17.4 ANN Modelling Processes

Neural networks concentrate on machine learning which is based on the concept of self-adjustment of internal control parameters. The ANN environment consists of five primary components; learning domain, neural nets, learning strategies, learning process and analysis process (2). Accordingly, neural network based modelling process involves five main aspects which are: (i) data acquisition, analysis and problem representation, (ii) architecture determination, (iii) learning process determination, (iv) training of the

network and (v) testing of the trained network for generalization evaluation (178). Elazouni et al. (1997) classified ANN modelling into three main phases: (a) design, (b) implementation and (c) use for problem solving. The design phase consists of two tasks - problem analysis and problem structuring. The implementation consists of three main aspects: (1) acquiring the knowledge (including data collection); (2) selecting the network configuration; and (3) training and testing the network.

#### **2.17.5 Representing the Variables**

Smith (1993) explained that the way independent variables are represented by input nodes of the network has a major impact on the training of the network and on the performance of resulting model. The ability of the network is mainly referred to as its effectiveness in generalizing. The amount of computation and the time required for learning are both greatly influenced by the form of representation used. There are two types of independent and dependent variables: (1) quantitative; and (2) class variables. The quantitative or continuous valued variable can be any number. It is not necessary to fall within the bounds of the applied sigmoid function. It also is possible to normalize the quantitative variables to some standard range such as 0 to 1, -1 to 1, or none (157; 41). Elazouni et al. (1997) opined that the networks usually provide improved performance when the data are normalized. When the variables fall in the range, it smoothes the solution space and averages out some of the noise effects.

#### **2.17.6 Summation and Transformation Function**

Summation function is a function which finds the weighted average of all inputs elements to each processing elements. It simply multiplies the input values by the weights and totals them up for a weighted sum. The transformation function (or transfer function or local memory) is a relationship between the internal activation level ( $N$ ) of the

neuron (called activation function) and the outputs. The transformation function is a kind of sigmoid function. A function  $f(N)$  will be a sigmoid function if it has two certain characteristics: (1) it is bounded; and (2) the value of a sigmoid function always increases as  $N$  increases (157). A number of different functions have these characteristics, and thus qualify as sigmoid functions. Any of them may be used in the neural network.

### 2.17.6.1 Sigmoid function

This function is a continuous function (Figure 2.15) that varies gradually between asymptotic values 0 and 1 or  $-1$  and  $+1$  and is given by:

$$\phi(l) = 1 / (1 + e^{-\alpha l}) \tag{2.13}$$

Where,  $\alpha$  is the slope parameter, which adjusts the abruptness of the function as it changes between the two asymptotic values. Sigmoid functions are differentiable, which is an important feature of neural network theory. Experimentally, observations of biological neurons demonstrate that the firing is roughly sigmoid, when plotted.

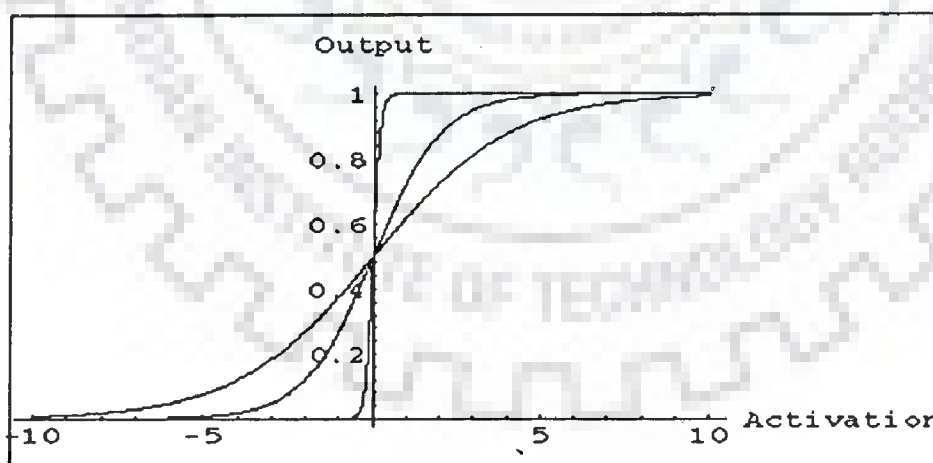


Figure 2.15 Activation function (Rajasekharan, 1996, 2004)

The problem with linear type processing elements is that their transfer functions are not differentiable (111). Because of this fact, networks using linear type processing

elements are difficult to train. To overcome the linear behaviour of networks using linear-threshold type transfer functions, smooth nonlinear transfer functions, which are continuous and differentiable everywhere, i.e. the sigmoidal type has been used. The output of a sigmoidal unit asymptotically goes to 1 as the weighted sum of its inputs approaches positive infinity, and to 0 as the weighted sum of its inputs approaches negative infinity. This function is defined as:  $f(x) = 1/(1 + e^{-x})$ , where  $x$  is the net input to the unit. Sigmoid units bear a greater resemblance to real neurons than do linear or threshold units, but all three must be considered as rough approximations (74).

### 2.17.7 Initial Weights

The initial weights of a multilayer feed forward network strongly affect the ultimate solution. They are typically initialized by small random values. Equal weights values cannot train the network properly if the solution requires unequal weights to be developed. The initial weights cannot be large, otherwise the sigmoid will saturate from the beginning, and the system will <sup>get</sup> stuck at a local minimum. The saturation is avoided by choosing the initial values of the synaptic weights to be uniformly distributed inside a small range of values. The range should not be too small as it can cause the learning to be very small. The range of initial weight  $w_{ij}$  is  $(-3/\sqrt{k_i}$  to  $3/\sqrt{k_i})$ , where,  $k_i$  is the number of neurons that feed forward to neuron  $i$  (170).

### 2.17.8 Number of Neurons in the Hidden Layer

In multi-layered perceptron, hidden layer means a third layer of processing elements or units in between the input and output layers that increase computational power. In principle, the hidden layer can be more than one layer. The network can approximate a target function of any complexity, if it has enough hidden nodes. The



output of hidden nodes can be considered as a new variable, i.e. an input to the nodes on the next layer or the nodes on the output layer. They contain interesting information about the relationship being modelled.

Too few hidden nodes for a given problem will cause back-propagation not to converge to a solution (87). However, many hidden nodes cause a much longer learning period. At some point, increasing the number of hidden nodes does not greatly increase the ability of the neural network to classify (176). On the other hand, too many units on a layer can make a network to become over specific, particularly on the extreme case where the number of units on the first processing layer is equal to the number of examples in the training set (141). Too many hidden nodes can over fit, such that the network can model the accidental structure of the noise in the sample as well as the inherent structure of the target function (157). Therefore, minimum sized network which uses as few hidden units as possible is important for efficient classification and good generalization (89). Berke and Hajela (1991) suggested that the number of hidden nodes should lie between the average and sum of nodes on the input and output layers. Rogers and Lamarsh (1992) suggested that a good initial guess for hidden nodes is to take the sum of nodes on the input and output layers. Soemardi (1996) suggested that the number of hidden nodes should be 75% of the input nodes. Thus, experience shows that the number of hidden nodes has a maximum limit of the sum of the input and output nodes but the minimum could be either 75% of the input nodes or the average of the input and output nodes. The size of a hidden layer is usually determined experimentally.

#### **2.17.9 Weights and Biases**

Weights are defined as the strength of input connections which are expressed by a real number. The processing nodes receive inputs through links. Each link has a

weight attached to it. The sum of the weights make up a value that updates the processing nodes, the output excitation to get either on or off. The weights are the relative strength (mathematical value) of the initial entering data that transfer data from layer to layer. They are the relative importance of each input to a processing element (110). In practice, the weights would be initiated and assigned to the network prior to the start of training. The weights initiation techniques are also important in order to control and obtain the convergence of training and training time. For each network, the number of unknowns is equal to the sum of the weights and biases. For a given network, the number of weights is the product of the number of nodes on all links, and the number of biases is the sum of numbers of all the nodes.

#### **2.17.10 Training and Generalization**

Network training means adjusting neural network weights. The weights and biases are initialized randomly. During training, the network analyzes the data provided and changes weights between network units to reflect dependencies found in the data. Training is the process whereby it (1) computes outputs, (2) compare outputs with desired outputs, and (3) adjusts the weights and repeats the process (110). The main purpose of training is to determine the set of connection weights that cause the neural network to estimate outputs that are sufficiently close to target values.

A good subset of input variables can substantially improve model performance. Presenting as large a number of input variables as possible to ANN models usually increases network size, resulting in a decrease in processing speed and a reduction in the efficiency of the network. An approach is that appropriate input variables can be selected in advance based on a priori knowledge (105). Another approach used by some researchers (171) is to train many neural networks with different combinations of

input variables and to select the network that has the best performance. A step-wise technique described by Maier and Dandy (2000) can also be used, in which separate networks are trained, each using only one of the available variables as model inputs. The network that performs the best is then retained, combining the variable that resulted in the best performance with each of the remaining variables. This process is repeated for an increasing number of input variables, until the addition of any extra variables results in no improvement in model performance.

ANNs perform best when they do not extrapolate beyond the range of the data used for calibration (49; 113). Therefore, the purpose of ANNs is to non-linearly interpolate (generalize) in high-dimensional space between the data used for calibration. Unlike conventional statistical models, ANN models generally have a large number of connection weights and can therefore over fit the training data, especially if the training data are noisy. In other words, if the number of degrees of freedom of the model is large compared with the number of data points used for calibration, the model might no longer fit the general trend, as desired, but might learn the idiosyncrasies of the particular data points used for calibration leading to 'memorisation', rather than 'generalisation'. Consequently, a separate validation set is needed to ensure that the model can generalise within the range of the data used for calibration. It is common practice to divide the available data into two subsets; a training set, to construct the neural network model, and an independent validation set to estimate the model performance in a deployed environment (105). A modification of the above data division method is cross-validation (164), in which the data are divided into three sets: training, testing and validation. The training set is used to adjust the connection weights, whereas the testing set is used to check the performance of the model at various stages of training and to

determine when to stop training to avoid over fitting. The validation set is used to estimate the performance of the trained network in the deployed environment. There are no guidelines in the literature for the optimal proportion of the data to use for training, testing and validation. In many situations, the available data are small enough to be solely devoted to model training and collecting any more data for validation is difficult. In this situation, the *leave-k-out* method can be used (106), which involves holding back a small fraction of the data for validation and the rest of the data for training. After training, the performance of the trained network has to be estimated with the aid of the validation set. A different small subset of data is held back and the network is trained and tested again. This process is repeated many times with different subsets until an optimal model can be obtained from the use of all of the available data.

As ANNs have difficulty extrapolating beyond the range of the data used for calibration, in order to develop the best ANN model, given the available data, all of the patterns that are contained in the data need to be included in the calibration set. For example, if the available data contain extreme data points that were excluded from the calibration data set, the model cannot be expected to perform well, as the validation data will test the model's extrapolation ability, and not its interpolation ability. If all of the patterns that are contained in the available data are contained in the calibration set, the toughest evaluation of the generalisation ability of the model is if all the patterns are contained in the validation data. In addition, if cross-validation is used as the stopping criterion, the results obtained using the testing set have to be representative of those obtained using the training set, as the testing set is used to decide when to stop training or, for example, which model architecture or learning rate is optimal. Consequently, the statistical properties (e.g. mean and standard deviation) of the various data subsets (e.g.

training, testing and validation) need to be similar to ensure that each subset represents the same statistical population (106). However, it was not until recently that systematic approaches for data division have been proposed in the literature.

The available data set is randomly partitioned into a training set and a test set. The training set is further partitioned into two disjointed subsets:

- (i) Estimation set used to select the model
- (ii) Validation set used to validate the model

The training data submitted to the network for it to learn and generalize the relation between input and output should be sufficient and proper. There is no rule for choosing the training data. Networks with too many trainable parameters for a given amount of training data learn well but do not generalize well. This phenomena is called over fitting with too few trainable parameter, the network fails to learn the training data. Once a network has been structured for a particular application, that network is ready to be trained. To start this process, the initial weights are chosen randomly, and then the training or learning begins. Supervised and unsupervised are two methods used to train the neural network.

#### ***2.17.10.1 Methods of training***

Training is a process of adjusting the connection weights in the network so that the network's response best matches the desired response. Although, this can be addressed as an optimization method, the back-propagation methods avoid this costly exercise by using an approximation to a gradient descent method. A network learns because the strength of the connections between neurons changes. The efficiency of a neuron in exciting or inhibiting another is not constant. Specifically, at each setting of the

connection weights, it calculates the error committed by the network simply by taking the difference between the desired and the actual response determined by the network. In training a network, error is used to modify the weights so that next time the network gives a more correct answer. It may increase or decrease over time, depending systematically on experience. There are two categories of training (157), i.e. supervised and unsupervised.

#### **2.17.10.1.1 Supervised training**

The learning is said to be supervised, when the performance function is based on the definition of an error measure. Normally, the error is defined as the difference of the output of the ANN and a pre-specified external desired signal. In engineering applications, where the desired performance is known, supervised learning paradigms become very important.

In supervised training, both the inputs and the outputs are provided. The networks then process the inputs and compare its resulting outputs against the desired outputs. Errors are then propagated back through the system, causing the system to adjust the weights, which control the network. This process occurs over and over as the weights are continually tweaked. During the training of a network, the training data set is processed many times as the connection weights are ever refined.

For supervised learning, there are three basic decisions that need to be made: choice of the error criterion, how the error is propagated through the network, and what constraints one imposes on the network output. The first issue is related to the formula that computes the error. The second aspect is associated with the mechanisms that modify the network parameters in an automated fashion. The gradient descent learning is the most common in supervised learning schemes. The third aspect is associated with

to constrain the network output with respect to the desired signal. One can specify only the behaviour at the final time (fixed point learning). A feed forward network, since it is an instantaneous mapper (the response is obtained in one time step), can only be trained by fixed-point learning.

### **2.17.10.1.2 Unsupervised training**

The unsupervised training has been introduced by Kohonen (1988) and is a far more plausible model of training in biological systems. Target vector is not required for the outputs. The training process extracts the statistical properties of the training set and groups similar vectors into classes, applying a vector from a given class to the input will produce a specific output vector. There is no way to determine prior to training which specific output pattern will be produced by a given input vector class. Hence, the outputs of such a network must generally be transformed into a comprehensible form subsequent to the training process.

### **2.17.10.2 Learning factors of back propagation**

One of the major issues concerning back-propagation algorithm is its convergence. The convergence of back-propagation is based on some important learning factors, such as the initial weights, the learning rate, the nature of training set and the architecture of the network.

#### **2.17.10.2.1 Learning rate ( $\eta$ )**

Back-propagation is a time consuming algorithm when either the size of the net is large or the number of the training patterns is large (89). Back-propagation has some limitations. There is no guarantee that the network can be trained in a finite amount of time. It employs gradient descent, i.e. follows the slope of the error surface downward

and constantly adjusts the weights towards minimum. Therefore, it has the danger of getting trapped in a local minimum before achieving the global minimum. It is important to select the correct learning rate and momentum term when using back propagation. Unfortunately, there is little guidance available other than experience, which is based on trial-and-error (3; 89).

Learning rate  $\eta$  is the constant of proportionality which provides dynamic access to the rate at which weights may be changed. A high learning rate corresponds to rapid learning which may push the training towards a local minimum or cause oscillation. In turn, when applying small learning rates, the time to reach a global minimum will considerably be increased (89). Learning rates for each layer of the same network can be different.

The remedy for problems of choosing learning rate is to apply a momentum factor, which is multiplied by the previous weight change so that while the learning rate is controlled the changes are still rapid (89). The role of the momentum term is to smooth out the weight changes, which helps to protect network learning from oscillation (3). A rule of thumb is that the learning rate for the last hidden layer should be twice that of the output layer.

- The values of learning rate ( $\eta$ ) ranges between  $10^{-3}$  to 10 (Umamahesh and Rao, 2001).
- The best value of the learning rate of the beginning of training may not as good in later training.
- A more efficient approach is to vary the learning rate as the training progresses.



- The effectiveness of the learning rate may be checked as the training progresses, and the value of the learning rate can be changed based on the change function.

If after a particular weight update, the error function has increased, then  $\eta$  can be increased.

$$\Delta\eta = \begin{cases} +a & \text{if } \Delta E < 0 \text{ consistently} \\ -b\eta & \text{if } \Delta E > 0 \\ 0 & \text{otherwise} \end{cases} \quad (2.14)$$

where,  $\Delta E$  is the change in error function, and  $a$  &  $b$  are positive constant.

#### 2.17.10.2.2 Momentum

A simple method of increasing the rate of learning and yet avoiding the danger of instability is to include a momentum term to the normal gradient descent method. The greater the momentum, the more the current weight change is affected by the weight change that took place during the previous iteration. The remedy for problems of choosing learning rate is to apply a momentum factor, which is multiplied by the previous weight change so that while the learning rate is controlled the changes are still rapid. The role of the momentum term is to smooth out the weight changes, which helps to protect network learning from oscillation. The scheme is implemented by giving a contribution from the previous step to each weight change.

$$\Delta w_{ij}(n) = \eta \delta l x_j + \alpha \eta w_{ij}(n-1) \quad (2.15)$$

Where,  $\alpha$  is usually a positive number, in the range (0, 1) called the momentum factor. A value of 0.9 is generally used for momentum factor.

### 2.17.10.2.3 Gradient descent learning algorithm

Gradient descent learning is the most widely used principle for ANN training. The reason is that trivial computation is required to implement this method, and the fact that the gradient can be computed with local information. The principle of gradient descent learning is very simple. The weights are moved in a direction opposite to the direction of the gradient. The gradient of a surface indicates to the direction of the maximum rate of change (Figure 2.16). Therefore, if the weights are moved in the opposite direction of the gradient, the system state will approach points where the surface is flatter (123)

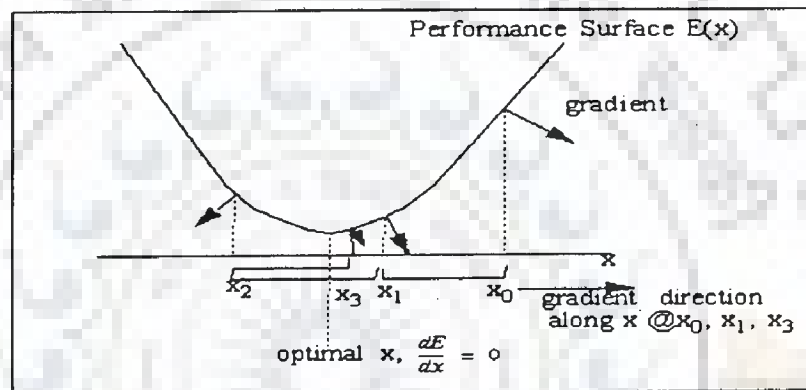


Figure 2.16 Gradient descent in one dimension

### 2.17.11 Back-propagation Training Algorithm and Generalized Delta Rule (GDR)

In the mid 1950's, Rosenblatt proposed a neural net model, called perceptron. Widrow and Hoff established an algorithm that can be expressed in terms of the delta rule for learning the value of weights and known as Widrow-Hoff Rule (103). In 1986, Rumelhart, Hinton and Williams extended this learning procedure to establish the back-propagation learning rule, called Generalized Delta Rule-GDR. Back-propagation has been the most popular and widely implemented of all neural network paradigms. It is based on a multi-layered feed forward topology with supervised learning. The propagation of error operates into two modes: (1) mapping; and (2) learning. In mapping mode, information flow forward through the network, from inputs to the outputs. In the

learning mode, the information flow alternates between forward and backward. A key element in the back-propagation paradigm is the existence of a hidden layer of nodes. The back-propagation procedure there is an intrinsic data flow. First, the inputs are propagated forward through the network to reach the output. The output error is computed as the difference between the desired output and the current system output. Then errors are propagated back through the network upto the first layer after which the delta rule can be applied to each network PE.

Smith (1993) summarized five ways in which the power of back-propagation can deliver significant benefits, as follows:

- (1) Using back-propagation may reduce the cost of building the model as it allows the user to substitute machine time.
- (2) Back-propagation may produce a better model if two conditions are met. First, the form of relationship between inputs and desired outputs is more complex than the form of function that is imposed on the model by conventional tool. Second, the sample is large enough in order to permit it to find the relationships underlying the noise in the data.
- (3) Using back-propagation provides assurance that the model is as good as it can be, since the cost of finding out or time required to know the complexity of the problem may be prohibitive.
- 4) Back-propagation provides an opportunity to build a single model with multiple outputs that is not possible for conventional techniques.
- 5) There are advanced form of back-propagation with capabilities that are not found in conventional methods.

The stepwise algorithm is narrated below:

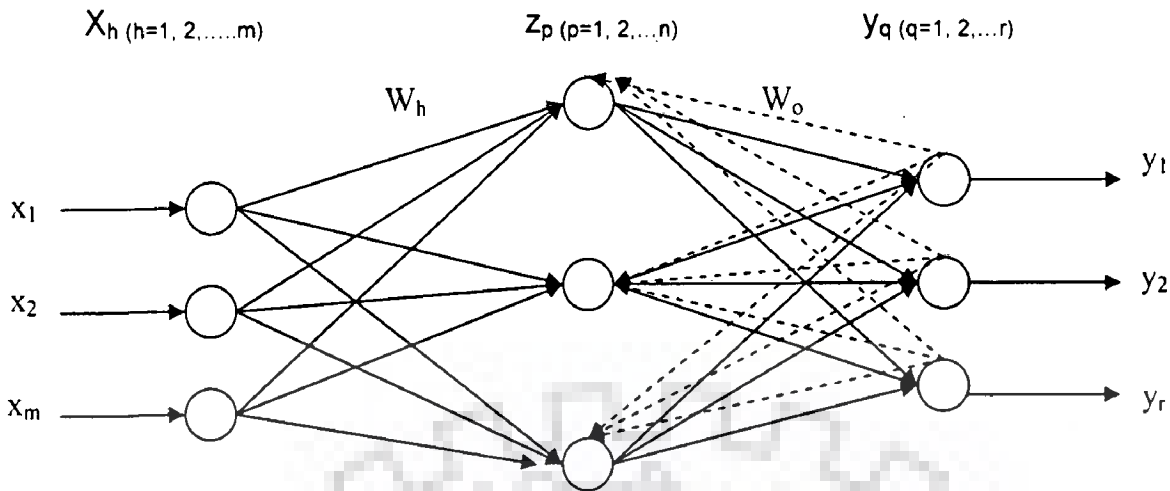


**Figure 2.17** Two layered back-propagation network (Umamahesh and Rao, 2001)

Back-propagation is a systematic method of training multilayer artificial neural networks. This learning algorithm is applied to multilayer feed forward network consisting of neurons with continuous differentiable activation functions. Such network associated with the back-propagation learning algorithm is called back-propagation networks.

Considering a two layer feed forward neural network, the network has  $m$  nodes in the input layer,  $n$  neurons in the hidden layer and  $r$  neurons in the output layer. The weight associated between the  $h^{\text{th}}$  input node and  $p^{\text{th}}$  hidden layer neuron is represented by  $W_h$ , while  $W_o$  represents the weights of the connection between  $p^{\text{th}}$  hidden layer neuron and  $q^{\text{th}}$  output neuron and also considering an input-output training pair  $(x,d)$ .

Given an input pattern  $x$ , a neuron  $p$  in the hidden layer receives a net input

$$net_p = \sum_{h=1}^m W_h x_h - b_i \quad (2.16)$$

Where  $b_i$  is the bias (certain minimum value) and gives an output of

$$Z_p = f(net_p) = f\left(\sum_{h=1}^m W_h x_h - b_i\right) \quad (2.17)$$

$f\left(\sum_{h=1}^m W_h x_h - b_i\right)$  is an activation function of neuron

The net input for a neuron q in the output layer is

$$netq = \sum_{p=1}^n W_o Z_p = \sum_{p=1}^n W_o f\left(\sum_{h=1}^m W_h x_h - b_i\right) \quad (2.18)$$

and it gives an output of  $y_q$  as

$$y_q = f(netq) = f\left(\sum_{p=1}^n W_o Z_p\right) = f\left(\sum_{p=1}^n W_o f\left(\sum_{h=1}^m W_h x_h - b_i\right)\right) \quad (2.19)$$

The error function for a given input-output pair is

$$\Delta E = \frac{1}{2} \sum_{q=1}^r (d_q - y_q)^2 \quad (2.20)$$

Where,  $d_q$  is an object output

The objective of the back-propagation algorithm is to adjust the weights of the network such that the error function is minimized.

$$\Delta W_o = -\eta \frac{\partial E}{\partial W_o} \quad (2.21)$$

Where,  $\eta$  is a positive number called learning rate, which determines the rate of learning. Using equations (2.18), (2.19), (2.20) and (2.21):

$$\begin{aligned} \Delta W_o &= -\eta \left[ \frac{\partial E}{\partial y_q} \right] \left[ \frac{\partial y_q}{\partial netq} \right] \left[ \frac{\partial netq}{\partial W_o} \right] \\ &= \eta \left( \sum_{q=1}^r (d_q - y_q) \right) (f'(netq)) (Z_p) \\ &= \eta \delta_{oq} Z_p \end{aligned} \quad (2.22)$$

Where  $\delta_{oq}$  is the error signal at q<sup>th</sup> node in output layer which is equal to

$$\begin{aligned}\delta_{\omega q} &= \frac{\partial E}{\partial(\text{net}q)} = -\left[\frac{\partial E}{\partial y_q}\right] \left[\frac{\partial y_q}{\partial(\text{net}q)}\right] \\ &= [d_q - y_q][f'(\text{net}q)]\end{aligned}\quad (2.23)$$

Similarly, the weight is updated from the input to hidden layer connection, the weight connecting neuron j in the input layer to neuron q in the hidden layer.

$$\begin{aligned}\Delta W_h &= -\eta \frac{\partial E}{\partial W_h} = -\eta \left[\frac{\partial E}{\partial \text{net}_p}\right] \left[\frac{\partial \text{net}_p}{\partial W_h}\right] \\ &= -\eta \left[\frac{\partial E}{\partial Z_p}\right] \left[\frac{\partial Z_p}{\partial \text{net}_p}\right] \left[\frac{\partial \text{net}_p}{\partial W_h}\right]\end{aligned}\quad (2.24)$$

From equation (2.20), the error term  $(d_q - y_q)$ ,  $q = 1, 2, \dots, r$  is a function of  $Z_p$ , i.e.

$$\begin{aligned}\Delta W_h &= -\eta \left[\frac{\partial E}{\partial \text{net}q} \frac{\partial \text{net}q}{\partial Z_p}\right] f'(\text{net}_p)x_h \\ &= +\eta \sum_{q=1}^r [(d_q - y_q)f'(\text{net}q)W_o] f'(\text{net}_p)x_h\end{aligned}\quad (2.25)$$

Using equation (2.18) to equation (2.21)

$$\begin{aligned}\Delta W_h &= \eta \sum_{q=1}^r [\delta_{\omega q} W_o] f'(\text{net}_p)x_h \\ &= \eta \delta_{np} x_h\end{aligned}\quad (2.26)$$

Where  $\delta_{np}$  is the error signal of neuron p in the hidden layer, i.e.

$$\begin{aligned}\delta_{np} &= \frac{\partial E}{\partial(\text{net}p)} = -\left[\frac{\partial E}{\partial Z_p}\right] \left[\frac{\partial Z_p}{\partial \text{net}_p}\right] \\ &= f'(\text{net}_p) \sum_{q=1}^r \delta_{\omega q} W_o\end{aligned}\quad (2.27)$$

In general with an arbitrary number of layers, the back-propagation update rule is in the form

$$\Delta W_{qh} = \eta \delta_q x_h = \eta \delta_{\text{output-}q} x_{\text{input-}h} \quad (2.28)$$

Where  $\delta_{\text{output-}q}$  and  $\delta_{\text{input-}h}$  refer to the two ends of the connection from neuron  $h$  to neuron  $q$ ,  $x_h$  is the proper input-end activation from a hidden neuron or an external input, and  $\delta_q$  is the error signal.

In case of activation function

$$y_h = \frac{1}{1 + e^{-u_h}} \quad (2.29)$$

Where  $u_h$  is the net activation internal activation level of neuron  $h$  and  $y_h$  is the output of the neuron. Then the error is

$$\begin{aligned} \delta_{oq} &= [d_q - y_q] [f'(netq)] \\ &= [d_q - y_q] y_q (1 - y_q) \end{aligned} \quad (2.30)$$

$$\delta_{ip} = Z_p (1 - Z_p) \sum_{q=1}^r \delta_{oq} W_{oq} \quad (2.31)$$

#### 2.17.11.1 Feed forward back-propagation network

The feed-forward network is also known as the error back-propagation network because of the method used in its training. The nodes are generally arranged in layers, starting from first input layer and ending at the final output layer. There can be several hidden layers with each layer having one or more nodes. Information propagation is in the forward direction from the input to the output side, and errors are propagated back in the other direction to change the weights to obtain a better performance. The neurons in one layer are connected to those in the next, but not to those in the same layer. Thus, the output of a node in one layer is only dependent on the input it receives from previous layers and the corresponding weights.

### **2.17.12 Criteria for Stopping Training**

There are two common criteria to stop training a network: (1) training cycles (epochs); and (2) desired errors. The other criterion is to limit the difference between desired output and output calculated by the network (89; 172). The training process may be brought to halt using either the worst error difference after complete presentation of all input-output patterns, or the root mean square error summed over all patterns. In practice, it is sometimes necessary to apply or compare both approaches to ensure the capability of the trained network in generalizing on the tested samples and application. The errors of tested samples are generally higher than the error of training sample as the network is trained to reduce the latter, not the former. However, the over-trained network would occasionally result in over-fitting. Over-fitting means the network can converge and yield a minimum or desired error in training samples but it cannot generalize well when validated with testing sample.

Weigend et al. (1991), Hergert et al. (1992) showed that the validation error decreases to a minimum for the simulations involving back propagation and then starts to increase even though the training error continues to decrease. This global minimum of the validation error curve, which is a function of the number of the hidden neurons in the ANN, determines the number of learning epochs and optimal step to stop the network.

### **2.17.13 Testing and Validation**

Testing is a phase to examine the performance of the network by using the derived weights. It is to measure the ability of network to classify the testing samples correctly (110). This set is not used during training and thus can be considered as consisting of new data entered by the user for neural network application. Then forecasting error is measured on each case and used as the estimation of network



quality. It is a part the input data set used only to test how well the neural network will perform on new data.

The cross-validation provides an appealing guiding principle (67). The use of cross-validation set is to determine the best number of hidden neurons, and when it is best to stop the training. The use of cross-validation set is appealing, particularly when a large neural network is to be designed with good generalization as goal (164).

#### **2.17.14 Strength of ANNs**

ANNs offer certain advantages over the traditional rule-based system, i.e. conventional programming and knowledge-based expert systems. ANNs are preferable because of the following reasons:

1. They are weighted connection and massively parallel processing with fault tolerance in the sense that their performance degrades gracefully under adverse operating conditions and they can automatically learn from experience. This is called internal representation (91).
2. They have the generalization capability to learn complex patterns of inputs and provide meaningful solutions to problems even when input data contain errors, or are incomplete, or are not presented during training. In other words, they have the ability to integrate information from multiple sources and incorporate new features without degrading prior learning (87; 66; 110; 50).
3. They are distribution free because no prior knowledge is needed about the statistical distribution of the classes in the data sources in order to apply the method for classification. This is an advantage over most statistical methods that

require modelling of data (87; 66; 178). Neural networks could avoid some of the shortcomings of the currently used statistically or empirically based techniques.

4. They take care of determining how much weight each data source should have in the classification, which remains a problem for statistical methods (87; 178). The non-linear learning and smooth interpolation capabilities give the neural network an edge over standard computers and rule-based systems for solving certain problems (90; 178).
5. They are able to recognize the relation between the input and output variables without knowing physical consideration.
6. They work well even when the training set contains noise and measurement errors. There is no need to make assumptions about the mathematical form of the relationship between input and output. Moreover, the ability to perform repeated simulations, thus allowing simulation tests and what-if-then scenario can be valuable aid in environmental planning and management.

#### ***2.17.15 The Problem of Explanation***

ANNs are unable to reason in a sequential or stepwise manner that results in precise conclusions. These restrictions could be critical when dealing with situations that demand exact answers and lucid justifications (66; 110). Due to the difficulty in explaining, the only way to test the system for consistency and reliability is to monitor the output (66; 157).

Back-propagation networks suffer from four main problems. The first problem is that network structuring is a versatile, intuitive, and highly solution-dependent trial-and-error task. The second is that the algorithm is slow in training, and convergence is very

sensitive to the initial set of weights. The third is that training can be trapped in local minima. The fourth is that the design of an optimum network configuration for a given problem is a non-guided or trial-and-error process that does not guarantee adequate generalization.

#### ***2.17.16 Applications of ANN Techniques in River Morphology***

A wide range of application of ANN techniques has been investigated in the field of river engineering. From more general point of view, AI techniques can be applied for prediction and simulation in river engineering. If significant variables are known, without knowing the exact relationships, ANN is suitable to perform a kind of function fitting by using multiple parameters on the existing information and predict the possible relationships in the coming future. This sort of problem includes water level and discharge relations, flow and sediment transport. Also, restoring of missing data in a time series can be considered as a kind of prediction.

### **2.18 FUZZY LOGIC SYSTEM**

Fuzzy set theory was developed by Zadeh (1965) to provide a mathematical tool for dealing with the concepts used in natural language. Fuzzy logic has an advantage over many statistical methods in that the performance of a fuzzy expert system is not dependent on the volume of historical data available. Since these expert systems produce a result based on logical linguistic rules, extreme data points in a small data set do not unduly influence these models. Because of these characteristics, fuzzy logic may be a more suitable method for forecasting than the current regression modelling techniques. The main dissimilarity between fuzzy logic system (FLS) and neural network

is that FLS uses heuristic knowledge to form rules and tunes these rules using sample data, whereas, NN forms "rules" based entirely on data.

Creation of a fuzzy expert system consists of four basic steps:

1. For each variable, whether an input variable or a result variable, a set of membership functions must be defined. A membership function defines the degree to which the value of a variable belongs to the group and is usually a linguistic term, such as high or low.
2. Statements or rules are defined that relate the membership functions of each variable to the result, normally through a series of IF-THEN statements. For example, one rule would be: IF the condition is low (linguistic term represented by a membership function) THEN the conclusion is low (linguistic term represented by a membership function).
3. The rules are mathematically evaluated and the results are combined. Each rule is evaluated through a process called implication, and the results of all of the rules are combined in a process called aggregation.
4. The resulting function is evaluated as a crisp number through a process called defuzzification. Subjective decisions are frequently required in fuzzy logic modelling, particularly in defining the membership functions for variables. In cases such as this, where large data sets are not available to define every potential occurrence scenario for the model, expert opinion is used to create logic.

### **2.18.1 Membership Functions**

Membership functions are the most subjective part of fuzzy logic modelling. Each variable must have membership functions, usually represented by linguistic terms, defined for the entire range of possible values.

The linguistic terms normally describe a concept related to the value of the variable, such as low, average and high. These linguistic membership functions define

the degree to which a particular numerical value of a variable fits the concept expressed by the linguistic term. The value ranges from zero to one.

Membership functions can take several shapes, depending on the philosophy behind the concept of the linguistic term. With fuzzy logic, membership functions typically overlap, making it possible for a value of a variable to have a membership in more than one linguistic term. The number, shape and range of the membership functions are key factors in the final numerical predictions provided by the fuzzy logic model. The transition from no membership to 100% membership may take any concave shape. The simplest representation is a straight line. If supported by data or specific knowledge of the subject, then the transition of the membership function can be related by complex equations.

### 2.18.2 Rule Definition

The fuzzy expert system consists of linguistic rules relating the membership functions of the input variables to the membership function of the output variable. A series of IF-THEN statements relates the input to the output. Operators, such as AND can be used to relate the input variables to each other to define the result as a combination of the input variables.

The AND operator is mathematically applied as an intersection operator by either the 'minimum' or 'product' function. Minimum is commonly used when the input data are independent of each other, and product is often applied if input variables are interdependent (137).

In a rule-based model, the relationship between input variables and the results are easily understood by simply reading the rule. Rules are influential in selecting the number of variables and membership functions to be modelled with fuzzy logic because

the model becomes exponentially more complex as the number of variables or membership functions increase. This is because a rule must be available for each possible combination of input variable membership functions and potential outcome membership functions. If a model consists of two input variables  $m$  defined by three membership functions  $n$ , then  $3^2$  rules are required to define all situations. For three input variables with three membership functions each, the number of rules increases to 27 ( $3^3$ ). The addition of unnecessary variables and membership functions would create a more complex model than necessarily required, and may lead to problems defining rules. Although relationships are easy to define for both the high and low extreme conditions, the intermediate rules are determined by examining the historical records. Therefore, although large data sets are not essential, it is desirable to have sufficient data points to define these rules adequately. For cases where there is insufficient data to dictate a rule, rules governing adjacent membership functions can be considered along with knowledge about the relationships. Some rules can be weighted to have more influence on the result than other rules, if there is physical evidence in the data to support a heavier weighting.

### **2.18.3 Implication and Aggregation**

Implication is a process that evaluates the portion of the membership function which is active for a particular rule. The minimum function defines the implication as follows: if a value of a variable belongs to a set to the degree, then the active set area can be considered to be all of the values in the membership function that belong to the membership function to an equal or lesser degree. In contrast, the product method of implication scales the entire membership function by the degree to which the variable belongs. Implication results in one set of values for each rule evaluated. The sets from

implication are combined into a single set in a process called 'aggregation'. If the sets from implication are summed together, the method of aggregation is called 'summation'. If aggregation of the sets occurs by combining the maximum values obtained for each output membership function after implication, the maximum method is used. No firm guidelines have been developed for applying various methods of implication and aggregation. Typically, a sensitivity analysis is performed to determine which methods perform best for a particular fuzzy logic model. More information on these processes is given by Klir et al. (1997).

#### **2.18.4 Defuzzification**

Defuzzification is the process by which a solution set is converted into a single crisp value. The fuzzy logic solution set is in the form of a function, relating the value of the result to the degree of membership. The entire range of possible solutions may be contained in the fuzzy solution set. Defuzzification is a process to extract an easily comprehensible answer from the set. The centre of gravity method is one of the most common of the defuzzification methods and consists of selecting the value corresponding to the centre of gravity for the solution set. The bisector method produces a value that will split the area of the solution set in half. Three other defuzzification methods focus on the maximum membership value attained by the solution set.

Frequently the maximum value of the solution set is a range of values rather than a point value. 'Smallest of maxima' selects the lowest value at which the highest membership value is attained. Similarly, 'middle of maxima' and 'largest of maxima' respectively select the middle value and the largest value at which the largest membership value occurs. The method of defuzzification normally is the most sensitive of the calculation parameters (137).

## 2.19 HYDROLOGIC ENGINEERING CENTER (HEC-6) SOFTWARE

### 2.19.1 Theoretical Basis for Hydraulic Calculations

The hydraulic parameters needed to calculate the sediment transport capacity are velocity, depth, width and slope - all of which come from water surface profile calculations. The one dimensional energy equation, shown below, is solved using the standard step algorithm and the above hydraulic parameters are calculated at each cross section for each successive discharge. Back-water computations proceed in the upstream direction for sub-critical flow, and in the downstream direction for supercritical flow (63). The data needed to perform these computations include: flow regime, starting elevation, discharge, Manning's roughness, cross-section geometry, and reach lengths. Figure 2.18 shows a representation of the terms in the energy equation.

$$WS_2 + \frac{\alpha_2 V_2^2}{2g} = WS_1 + \frac{\alpha_1 V_1^2}{2g} + h_e \quad (2.32)$$

Where,  $g$  = acceleration due to gravity,  $h_e$  = energy loss

$V_1, V_2$  = average velocities ( $\frac{\text{total discharge}}{\text{total flow area}}$ ) at ends of reach,  $WS_1, WS_2$  = water

surface elevations at ends of reach and  $\alpha_1, \alpha_2$  = Velocity distribution <sup>Coefficient</sup> for flow at ends of reach (Figure 2.18)

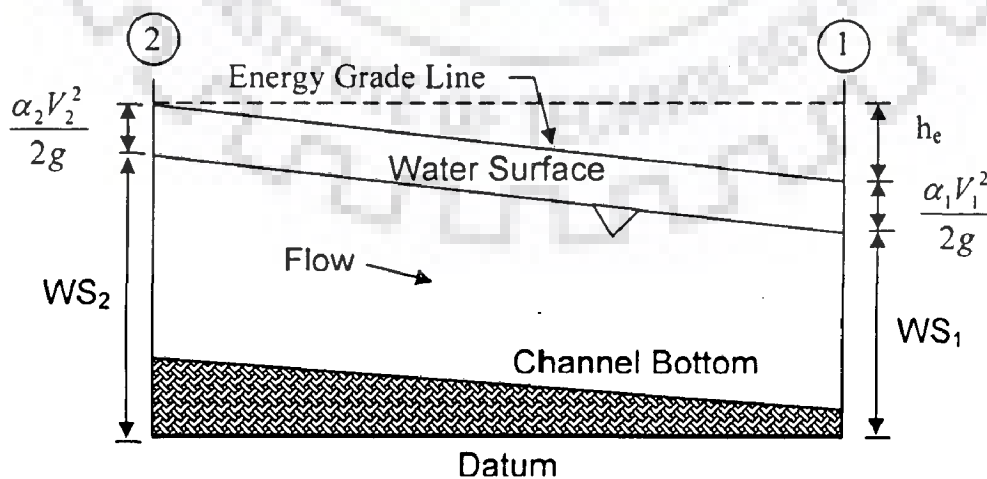


Figure 2.18 Representation of terms in energy equation



## 2.19.2 Hydraulic Losses

### 2.19.2.1 Friction losses

The energy loss term  $h_e$  in equation 2.33 is composed of friction loss  $h_f$  and form loss  $h_o$ . Only contraction and expansion losses are considered in the geometric form loss term.

$$h_e = h_f + h_o \quad (2.33)$$

To approximate the transverse distribution of flow of the river is divided into strips having similar hydraulic properties in the direction of flow. Each cross section is subdivided into portions that are referred to as subsections. Friction loss is calculated as shown below:

$$h_f = \left( \frac{Q}{K^1} \right)^2 \quad (2.34)$$

$$\text{Where, } K^1 = \sum_{j=1}^J \left[ \frac{1.49}{n_j} \right] \frac{\left( \frac{A_2 + A_1}{2} \right) \left[ \frac{R_2 + R_1}{2} \right]_j^{1/2}}{L_j^{1/2}} \quad (2.35)$$

$A_1, A_2 =$  downstream and upstream area, respectively of the cross sectional flow normal to the flow direction

$J =$  total number of subsections

$L_j =$  length of the  $j^{\text{th}}$  strip between subsections

$n =$  Manning's roughness coefficient

$Q =$  water discharge

$R_1, R_2 =$  down stream and upstream hydraulic radius

### 2.19.2.2 Other losses

Energy losses due to contractions and expansions are computed by the following equation:

$$h_0 = C_L \left| \frac{\alpha_2 V_2^2}{2g} - \frac{\alpha_1 V_1^2}{2g} \right| \quad (2.36)$$

Where,  $C_L$  = loss coefficient for contraction and expansion. If the quantity within the absolute value notation is negative, flow is contracting,  $C_L$  is the coefficient for contraction; if is positive, flow is expanding and  $C_L$  is the coefficient of expansion. In the standard step method for water surface profile computations, calculations proceed from the downstream to upstream based upon the reach's downstream boundary conditions and starting water surface elevation.

### 2.19.3 Theoretical Basis for Sediment Calculations

Each cross section represents a control volume. The control volume width is usually equal to the movable bed width and its depth extends from the water surface to top of bed rock or other geological control beneath the bed surface. In areas where no bed rock exists, an arbitrary model bottom or datum is assigned. The cross section uses end area concept. Since both mass continuity and energy should encompass the same space and since the averaging of two cross sections tend to smooth the numerical results, the shape of the control volume is deformed, as shown in Figure 2.19.

The quantity of sediment in the stream bed, using an average end area approximation, is

$$V_{sed} = B_0 \cdot Y_s \cdot \frac{L_u + L_d}{2} \quad (2.37)$$

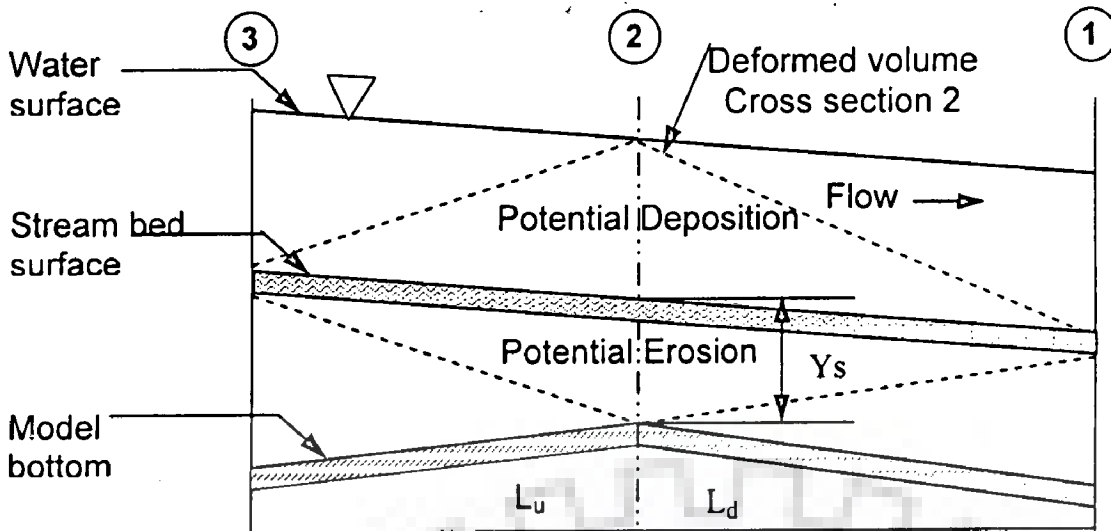


Figure 2.19 Deformed control volume for bed deposits

Where,  $B_0$  = width of the movable bed,  $L_u$ ,  $L_d$  = length of the upstream and downstream reach, respectively, used in control volume computation,  $V_{sed}$  = volume sediment in control volume, and  $Y_s$  = depth of sediment in control volume

For a water depth of  $D$ , the volume of water column is

$$V_i = B_0 \cdot D \cdot \frac{L_u + L_d}{2} \quad (2.38)$$

$B_0$  and  $D$  are hydraulic parameters width and depth, which are calculated by averaging over the same space used in solving the energy equation. The continuity assumes that initial sediment concentration is zero. The hydraulic parameters, bed material gradation and calculated transport capacity are assumed to be uniform throughout the control volume. HEC-6 assumes instantaneous diffusion of all grain size classes in a control volume basis.

The basis for simulating vertical movement of the bed is the continuity equation for sediment (the Exner equation):

$$\frac{dG}{dx} + B_0 \cdot \frac{dY_s}{d(DD)} = 0 \quad (2.39)$$

Where,  $B_0$  = width of movable bed,  $DD$  = duration of time step,  $G$  = sediment discharge,  $x$  = distance along channel, and  $Y_s$  = depth of sediment in control volume.

## 2.20 REVIEW OF SEDIMENT DISCHARGE PREDICTORS

A major hurdle, normally encountered in simulation studies of alluvial rivers can be identified to be availability of required data on sediment discharge. This difficulty can be appreciated, especially for large alluvial rivers in the context of considerable hazards involved in collection of sediment data during high floods. The inadequate measured sediment discharge data at different flow stages and different cross-sections is generally required to be made up by an appropriate sediment transport function for obtaining simulated values. For the models constituted in this work, several sediment discharge predictors are experimented, and Yang's 1973 method has been incorporated to yield the best possible result. A brief description of these predictors is given below:

### 2.20.1 Ackers and White Method

Based on Bagnold's stream power concept, Ackers and White (1973) applied the advantages of dimensional analysis technique, but used the physical arguments to express the mobility and transport rate of sediment in terms of some dimensionless parameters. They postulated that only a part of the shear stress on the channel bed is effective in causing the movement of coarse sediment, while in the case of fine sediment, suspended load movement predominates and the total shear stress is effective in causing the movement of sediment.

**Sediment Mobility:** Sediment mobility is described by the ratio of the appropriate shear stress on unit area of the bed to the immersed weight of a layer of grains. This mobility

number is denoted by  $F_{gr}$ , and a general definition is:

$$F_{gr} = \frac{V_*^n}{\sqrt{gD(s-1) \left[ \frac{\nu}{32 \log(\alpha d / D)} \right]^{(1-n)}}} \quad (2.40)$$

**Dimensionless Grain Diameter:** The dimensionless grain diameter is applicable to coarse, transitional and fine sediments, and is the cube of the ratio immersed weight to viscous forces. Thus

$$D_{gr} = D[g(s-1)/\nu]^{1/3} \quad (2.41)$$

Where,  $\nu$  = Kinematic viscosity of fluid

**Dimensionless sediment Transport function:** A general dimensionless sediment transport function can be expressed as

$$G_{gr} = f(F_{gr}, D_{gr}) \quad (2.42)$$

$$G_{gr} = C \left[ \frac{F_{gr}}{(A-1)} \right]^m \quad (2.43)$$

$$\text{Where, } G_{gr} = \frac{Xd}{sD} \left[ \frac{V_*}{V} \right]^n \quad (2.44)$$

Where, X=rate of sediment transport in terms of mass flow per unit mass flow rate.

c = Coefficient in sediment transport function

a = value of F at nominal initial motion

m = Exponent in sediment transport function

The parameters and the functional relationships used in equations 2.39 to 2.43 were determined by Ackers and White from flume experiments with sediment particle size greater than 0.04 mm and Froude number less than 0.8.

A, C, m and n can be obtained from the following relationships:

For the transition,  $1 < D_{gr} \leq 60$

$$n = 1.0 - 0.56 \log D_{gr}, a = \frac{0.23}{\text{sqrt}(D_{gr})} + 0.14, m = \frac{9.66}{D_{gr}} + 1.34$$

$$\text{Log } C = 2.86 \log D_{gr} - (\log D_{gr})^2 - 3.53$$

For coarse sediment,  $D_{gr} > 60$ ,  $n = 0$ ,  $a = 0.17$ ,  $m = 1.50$ ,  $c = 0.025$

### 2.20.2 Yang's Model (1973 & 1979)

Yang hypothesized that for a steady uniform flow total sediment concentration should be related to the rate of potential energy expenditure per unit weight of water, i.e., the unit stream power. The unit stream power can be expressed by the velocity and slope product. Yang's non-dimensional unit stream power equations can be expressed in the basic form of

$$\text{Log } C_t = M_2 + N_2 \log \left( \frac{U_s}{w_o} \right) \quad (2.45)$$

Where,  $C_t$  = total sediment concentration in parts per million by weight.

$U_s$  = unit stream power

$M_2, N_2$  = parameters related flow to and sediment characteristics.

$w_o$  = average fall velocity of sediment particles

### 2.20.3 Yang's Model of 1973

Non dimensional unit stream power equation proposed by Yang which includes criteria for incipient motion can be expressed:

$$\text{Log } C_t = 5.435 -$$

$$\frac{0.286 \log w d_{50}}{v} - \frac{0.457 \log V_c}{w_o} + \left( \frac{1.799 - 0.409 \log w d_{50}}{v} - \frac{0.314 \log V_c}{w_o} \right) \log \left( \frac{U_s}{w_o} - \log \frac{V_c S}{w_o} \right) \quad (2.46)$$

Where, the non-dimensional critical velocity required at incipient motion condition can be expressed as:

$$\frac{V_{cr}}{w} = \frac{2.5}{[\log(V.d_{50}/\nu) - 0.06]} + 0.66; 1.2 < V.d_{50}/\nu < 70 \quad (2.47)$$

$$\text{and } \frac{V_{CR}}{w} = 2.05; 70 \leq V.d_{50}/\nu \quad (2.48)$$

Where,  $V_{cr}$  = average flow velocity at incipient motion

#### 2.20.4 Yang's Model of 1979

Yang proposed another formulation without any criteria for incipient motion as below:

$$\log C_r = 5.165 - 0.153 \log w d_{50} / \nu - 0.297 \log \left( \frac{V_s}{w} \right) + \left( 1.780 - \frac{0.36 w d_{50}}{\nu} - \frac{0.48 \log V_s}{w} \right) \log \left( \frac{VS}{w} \right) \quad (2.49)$$

Where,  $\frac{VS}{w}$  = non dimensional unit stream power.

The non-dimensional parameters obtained by Yang from dimensional analysis, and the associated coefficients were determined from multiple regression analysis of 463 sets of laboratory data.

#### 2.20.5 Engelund and Hansen Model (1967)

Bagnold introduced the concept of stream power for the study of sediment transport. He defined stream power as the product of shear stress along the bed and the average flow velocity. Bagnold's stream power has the dimension of power per unit bed area. Engelund and Hansen applied the stream power concept and the similarity principle to obtain a sediment transport equation as given below:

$$f\theta = 0.1\theta^{5/2}, \quad \text{where, } f = \frac{2gsd}{\nu^2} \quad \& \quad \theta = \frac{\tau}{(\gamma_s - \gamma)d} \quad (2.50)$$

$$\phi = \frac{q_i}{\sqrt{((s-1)gd_{50}^3)}} \quad (2.51)$$

$$\tau_0 = \gamma Ds \quad (2.52)$$

Strictly speaking, equation 2.51 should be applied to those flows with dune beds in accordance with the similarity principle. However, Engelund and Hansen found that equation 2.51 can be applied to dune bed and upper flow regime with particle size greater than 0.15 mm without serious deviation from the theory.

### 2.20.6 Swamee and Ojha Formulations

Swamee and Ojha (1991) proposed empirical equations for bed load and suspended load transport rate of non-uniform sediments. They also derived equations for bed load and suspended load transport rate of uniform sediments.

#### Bed load Transport:

Swamee and Ojha (1991) plotted bed load transport data from Gilbert (1914), Costello (1974), Paris and Graf (1977) and Misri et al. (1984). These data cover a range of non dimensional grain shear stress  $\tau^*$  from 0.02 to 0.2 and bed load parameter  $\phi_B$  from  $10^{-6}$  to 0.2.

For  $\tau^* < 0.04$ ,  $\phi_B$  is expressed by the following relationship

$$\phi_B = \left[ \frac{\tau^*}{0.0947} \right]^9 \quad (2.53)$$

Where as for  $\tau^* \geq 0.15$ ,

$$\phi_B = \left[ \frac{\tau^*}{0.355} \right]^{1.6} \quad (2.54)$$

They combined equations 2.14 and 2.15 in such a way that the combination satisfactorily represent the data, such combination is

$$\phi_B = \left[ \frac{0.0947}{\tau^*} \right]^9 + \left[ \frac{0.355}{\tau^*} \right]^{1.6} \quad (2.55)$$



The conventional relation between the volumetric bed load transport per unit width of stream  $q_B$  is

$$\phi_B = \frac{q_B}{D_{65} \sqrt{((s-1)gD_{65})}} \quad (2.56)$$

The non dimensional grain shear stress is

$$\tau_*^- = \frac{R'S}{(s-1)D_{65}} \quad (2.57)$$

With Manning - Strickler's equation, hydraulic values corresponding to grain resistance,

$$R' = \left[ \frac{V_m D_{65}^{1/6}}{24 \sqrt{(s)}} \right]^{1.5} \quad (2.58)$$

**Suspended load transport:**

Based on the analysis of available data from Einstein et al., (1986), Swamee and Ojha obtained the following equation for suspended load transport rate:

$$\phi_s = \left[ \left[ \frac{0.567}{\tau_*^-} \right]^6 + \left[ \frac{0.547}{\tau_*^-} \right]^3 \right]^{-1} \quad (2.59)$$

Where,  $\phi_s$  = suspended load parameter

$$\phi_s = \frac{q_s}{D_{65} \sqrt{((s-1)gD_{65})}} \quad (2.60)$$

$q_B$  and  $q_s$  can be added to obtain the volumetric total load transport rate per unit width of the stream,  $q_t$ .

## 2.21 CONCLUDING REMARKS

This chapter has presented a review the literature of last 45 years, which indicated that braided rivers react to changes in flow stage. More quantitative data is needed for research on the processes involved during the flow stages. The apparent scale invariance of the braided pattern seems to have implications for the nature of the

main processes involved in shaping braided morphology, bar genesis and evolution. With advances in survey techniques, as data becomes more available on larger rivers, such as the Brahmaputra, the issue of morphological processes and their relationship to channel scale in braided systems can be addressed.

There still remains a great deal of uncertainty over the actual classification of the braided system. Another field yet to be fully explored by quantitative investigations is the mechanisms and processes of channel confluences and diffluences. It has been demonstrated by many authors that a proper understanding of the flow and sedimentary processes at channel junctions is fundamental to the braided river morphology (99; 31; 23; 8).

The problem of applying understanding of key morphological processes of braided channels has yet to be fully addressed (27). The apparent similarities of planform and cross-sectional characteristics require further investigation (27). The morphology of braided river systems has not been as extensively studied as single-channel rivers. The studies to-date that have been carried out to establish models and frameworks for understanding braided river behaviour have been mostly qualitative in nature. The lack of quantitative studies on morphology of braided rivers has impeded the development of the understanding of this complex environment. From this review of the literature, it is seen that there is a complete lack of studies on spatio-temporal morphological model of the braided rivers.

## DESCRIPTION OF STUDY AREA

---

### 3.1 INTRODUCTION

The Brahmaputra is a major international river covering a drainage basin of 580,000 km<sup>2</sup>, extending from 82°E to 97° 50' E longitudes and 25° 10' to 31° 30' N latitudes. The basin spans over an area of 293,000 km<sup>2</sup> (50.51%) in Tibet (China), 45,000 km<sup>2</sup> (7.75%) in Bhutan, 194,413 km<sup>2</sup> (33.52%) in India and 47,000 km<sup>2</sup> (8.1%) in Bangladesh. Its basin in India is shared by Arunachal Pradesh (41.88%), Assam (36.33%), Nagaland (5.57%), Meghalaya (6.10%), Sikkim (3.75%) and West Bengal (6.47%) (59). Originating in a great glacier mass at an altitude of 5,300 m just south of the lake Konggyu Tso in the Kailas range, about 63 km southeast of Mansarovar lake in southern Tibet at an elevation of 5300m, the Brahmaputra flows through China (Tibet), India and Bangladesh for a total distance of 2880 km, before emptying itself into the Bay of Bengal through a joint channel with the Ganga. It is known as the Tsangpo in Tibet (China), the Siang or Dihang in Arunachal Pradesh (India), the Brahmaputra in Assam (India) and the Jamuna, Padma, and Meghana in Bangladesh.

Before entering India, the river flows in a series of big cascades as it rounds the Namcha-Barwa peak. The river forms almost trough receiving the flows of its tributaries both from North and South. The river, with its Tibetan name Tsangpo in the uppermost reach, flows through southern Tibet for about 1,625 km eastward and parallel to tributaries, viz., the Nau Chhu, the Tsa Chhu, the Men Chhu, the Charta Tsangpo, the Raga Tsangpo, the Tong Chhu, the Shang Chhu, the Gya Chhu, the Giamda Chhu, the Po Tsangpo and the Chindru Chhu and the right bank tributaries, viz. the Kubi, the

Kyang, the Sakya Trom Chhu, the Rhe Chhu, the Rang Chhu, the Nyang Chhu, the Yarlang Chhu, and the Trulung Chhu join the river along its uppermost reach. At the extreme eastern end of its course in Tibet the Tsangpo suddenly enters a deep narrow gorge at Pe, where in the gorge section the river has a gradient ranging from about 4.3 to 16.8 m/km (Figure 3.1).

The river enters in India near Tuning in Arunachal Pradesh. After travelling for a distance of 278 km up to Kobo, it meets with two rivers the Dibang and the Lohit in Assam near Kobo. Below this confluence point, the river is known by the name of the Brahmaputra. It passes through Assam into Bangladesh and at last it meets with the Ganga near Goalundo in Bangladesh before joining the Bay of Bengal. Its total length is 2,880 km comprising of 1,625 km in Tibet, 918 km in India and 337 km in Bangladesh. It is also one of the most braided rivers in the world with width variation from 1.2 km at Pandu near Guwahati to about 18.13 km near Gumi few km distances downstream to this point.

Traversing through deep narrow gorges of the Himalayan terrain the Tsangpo takes a southward turn and enters Indian territory at an elevation of 660 m. The river then enters the State of Assam (India) taking two important tributaries the Dibang and the Lohit. At the exit of the gorge the slope of the river is only 0.27 m/km. At the head of the valley near Dibrugarh the river has a gradient of 0.09-0.17 m/km, which is further reduced to about 0.1 m/km near Pandu (Figure 3.1). The mighty Brahmaputra rolls down the Assam valley from east to west for a distance of 640 km up to Bangladesh border (Table 3.1).

**Table 3.1 The Brahmaputra river: Country and Indian state-wise break-up of basin area and channel length**

Country	Basin area (Km <sup>2</sup> )	Channel Length (Km)
1. Tibet (China)	293,000	1,625
2. Bhutan	45,000	-
3. India	194,413	918
(a) Arunachal Pradesh	81,424	278
(b) Assam	70,634	640
(c) Nagaland	10,803	-
(d) Meghalaya	11,667	-
(e) Sikkim	7,300	-
(f) West Bengal	12,585	-
4. Bangladesh	47,000	337

### 3.2 LONGITUDINAL SECTION OF THE BRAHMAPUTRA RIVER

The longitudinal section of the Brahmaputra river from its origin to the outfall point is depicted in Figure 3.1.

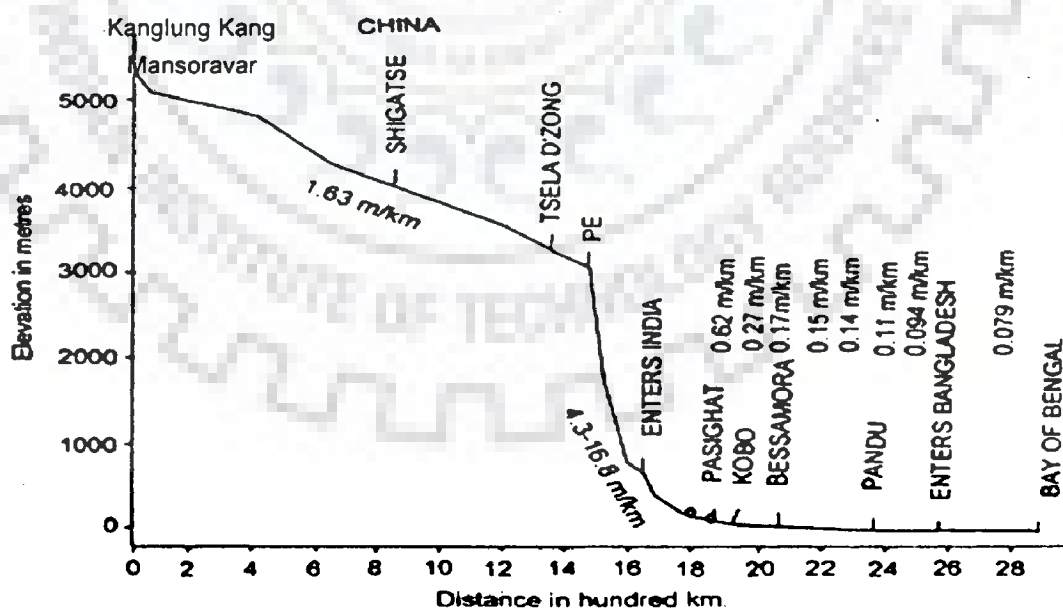


**Figure 3.1 Longitudinal profile of the Brahmaputra river (modified after WAPCOS, 1993)**

### 3.3 THE BRAHMAPUTRA BASIN

The Brahmaputra basin is confined by the great Himalayan ranges in the North and Northeast, Naga-Patkai hills in the East, and Mikir hills and Shillong plateau in the South. The Assam valley is the eastern continuation of the Indo-Gangetic plains of the Indian subcontinent valley. It is very narrow in the east and gradually expands to the west to nearly 80 km width, covering an area of about 5,62,704 km<sup>2</sup>. In this valley, the river itself occupies a width of 6 to 12 km in most places. The basin of the river extends from parts of Tibet, Nepal, Bangladesh, Northeast India and Bhutan. The state wise distribution within India and the country wise distribution of the basin are presented in Table 3.2.

The Indian part of the basin has a maximum east-west length of about 1,540 km and a maximum north-south width of about 682 km along 93° east longitude. The basin is characterized by large variations in relief slope, landforms, climate, vegetation and land use. The upper basin lying in Tibet (China) and in the eastern Himalayas of Arunachal Pradesh, Sikkim and Nagaland comprise mostly mountain ranges and narrow valleys and the channels are restricted within steep and narrow valleys in the mountains. In Assam and Meghalaya, the basin consists of hills, plateaus and plains covered by forests, tea gardens, agricultural lands and built-up areas. In West Bengal also, the basin covers hills and valleys dominated by forests, tea gardens, agricultural lands and built-up areas. The lower portion of the basin in Bangladesh consists largely of fertile plains and delta regions.

The Brahmaputra basin in India is most generously gifted with a fabulous water wealth that accounts for nearly 30% of the total water resources and about 40% of the

total hydropower potential of the country. However, so far the utilisation of this enormous water resources potential of the region is limited. For example, less than 5% of the existing hydropower potential, 10% of the irrigation potential and about 4% of the ground water potential have so far been harnessed.

The Brahmaputra river is characterized by high intensity flood which flows during the monsoon season, June through September, with an average annual flood discharge of 48,160 m<sup>3</sup>/sec (August, 1998 at Pancharatna). The highest flood discharge recorded in the Brahmaputra at Pandu (Assam) was of the order of 72,148 m<sup>3</sup>/sec (in year 1962), which had a recurrence interval of 100 years (173). The daily hydrograph of the river at Pandu exhibits drastic fluctuations in discharge during the monsoon season, whereas the time series of annual maximum flood events for the period 1955-2000 do not indicate any perceptible trend (59).

Analysis of 100-year rainfall records at Guwahati also does not show any distinct long term trend (59). However, there is a considerable variation in the spatio-temporal distribution of rainfall with marked seasonality. For example, precipitation varies from as low as 120 cm in parts of Nagaland to above 600 cm in the southern slopes of the Himalayas. A gradual increase in rainfall from the valley bottom towards the lower ranges of the Himalayas, followed by a decrease towards the higher ranges is evident from the observed records at Dibrugarh (285 cm) in the eastern part of the valley through Pasighat (507 cm) in the foothills to Tuting (274 cm) further up in the Himalayas. Monsoon rains from June to September accounts for 60-70% of the annual rainfall. These rains that contribute a large portion of the runoff in the Brahmaputra and its tributaries are primarily controlled by the position of a belt of depressions, called the monsoon trough, extending from northwest India to the head of the Bay of Bengal. In the

course of the north-south oscillations in summer, when this axis moves closer to the foothills of the Himalayas, heavy precipitation occurs in Assam and adjoining highlands. The severity of rainstorms occasionally reaches as high as 40 cm per day. The years 1998 and 2004 which saw extremely high floods in the region also recorded excessively high rainfall, especially in the upper basin areas. Rainfall recorded at Guwahati during the monsoon months in 1998, June through September, is 922 mm, while at Dibrugarh it is 2002 mm and Pasighat in Arunachal Pradesh 4,573 mm accounting for 60%, 67% and 75% of the annual rainfall respectively (59). During the flood season, all the districts in Arunachal Pradesh receive rainfall much above the normal rainfall. The intensity of rainfall recorded at Dibrugarh on June 28, 1998 is of the order of 17 mm/hr.

The Brahmaputra basin, especially its monsoon dominated wetter parts, is enormously rich in biotic resources with a great diversity of flora and fauna types marked by significant variations, both in vertical and horizontal distributions. The forest cover of the basin in India, as indicated by recent satellite surveys, is 144,922 km<sup>2</sup>, which accounts for 59% of the total geographical area (Myint and Hofer, 1997). In contrast to this, the total basin forest cover including the portion outside India accounts for only 14.07% of the total geographical area of the basin. The distribution of forest cover in different states lying within the basin in India is estimated as: Arunachal Pradesh (82.8%), Nagaland (68.9%), Meghalaya (63.53%), Sikkim (39.52%), West Bengal (21.4%) and Assam (20.56%) (Myint and Hofer, 1997). In fact, Arunachal Pradesh accounts for about 60% of the forest cover in the Indian part of the basin.

The vegetation changes from tropical evergreen and mixed deciduous forest in the Assam valley and the foothills, through temperate coniferous belts in the middle Himalayas to alpine meadows and steppes in the still higher ranges. There has been



considerable decline in the forest cover due to deforestation, land use conversion and land degradation in the basin. Shifting cultivation, involving traditional slash and burn technique of agriculture which is widely being practiced in the hills of northeast India, is a major cause of environmental degradation leading to deterioration of forest cover, loss of biodiversity, soil erosion, loss of soil fertility and crop yield, reduction in ground water recharge, increase in surface runoff, lowering of water table and acceleration in the rates of sedimentation in rivers and reservoirs downstream.

The Brahmaputra basin in northeast India provides a unique habitat for an exquisite variety of fauna, some of which belong to the most rare and endangered species. The floodplain of the Brahmaputra river in Assam is dotted with a large number of wetlands, numbering more than 3,500, which have great significance as unique habitats for exquisite varieties of flora and fauna and also as natural flood water retention basins. Degradation and destruction of these wetlands have considerable impact on the deteriorating flood hazard scenario in the state.

### **3.4 THE BRAHMAPUTRA RIVER SYSTEM**

The Brahmaputra river, termed as a moving ocean (173), is an antecedent snow-fed large Trans-Himalayan river which flows across the rising young Himalayan range. Considerable variations in width, gradient, discharge and channel pattern occur throughout its course. Geologically, the Brahmaputra is the youngest of the major rivers of the world and unique in many respects. It happens to be a major river for three countries, viz., China, India and Bangladesh. The river basin of the Brahmaputra is bounded on the north by the Kailas and Nyen- Chen-Tanghla ranges of mountains; on the east by the Salween river basin and the Patkai range running along the Indo-Myanmar border; on the south by the Nepal Himalayas, the Naga and Barail ranges and

the Meghalaya Plateau; and on the west by the Ganga river basin.

The maximum meridional extent of the basin is 1,540 km along 29°30' N latitude and maximum latitudinal extent is 780 km along 90° E longitude. The total length of the river is 2,880 km (Table 3.1). Several tributaries join the river all along its length. The average annual runoff of the Brahmaputra at Pasighat, Pandu and Bahadurabad in Bangladesh is 186,290,494,357 and 589,000 million cubic metre respectively. The monsoon flow of the Brahmaputra at Tesla Dzong in Tibet is 36.27% of the flow at Pasighat (173).

Throughout its course within India, the Brahmaputra is braided with some well defined nodal points where the river width is narrow and restricted within stable banks. All along its course in the valley, abandoned wetlands and back swamps are common. The river carries about 735 million metric tons of suspended sediment loads annually.

The Indian section of the Brahmaputra river receives innumerable tributaries flowing down the northern, north-eastern and southern hill ranges. The mighty Brahmaputra along with the well-knit network of its tributaries controls the geomorphic regime of the entire region, especially the Brahmaputra valley. In the north, the principal tributaries are the Subansiri, the Jia Bhareli, the Dhansiri, the Puthimari, the Pagladiya, the Manas and the Champamati. Amongst these, the Subansiri, the Jia Bhareli and the Manas are the Trans-Himalayan rivers. The principal south bank tributaries are the Burhi Dehing, the Disang, the Dikhow, the Dhansiri (south), the Kopili and the Krishnai. Hydrological characteristics of 18 important north bank tributaries and 10 important south bank tributaries are presented in Table 3.2.

It is observed that three Trans-Himalayan tributaries, the Subansiri, the Jia Bhareli and the Manas on the north have a basin more than 10,000 km<sup>2</sup>, i.e., only two south bank tributaries namely the Dhansiri and the Kopili form a basin area more than 10,000 km<sup>2</sup>. The Manas river combined with the Aie and the Beki rivers drains biggest area of 41,350 km<sup>2</sup>. The 442 km long Subansiri river and the 360 km long Burhi Dehing river are considered longest, respectively, among the north-bank and south bank tributaries (Water Year book, CWC, 2002). In terms of the average annual discharge, the Subansiri carries a discharge of 755,771 m<sup>3</sup>/sec, which ranks first among all the important tributaries. The Jia Bhareli and the Manas in the north carrying an average annual suspended sediment load of 2,013 ha.m and 2,166 ha.m, respectively, are the leading rivers in the case of sediment discharge (59). Of all the north and south bank tributaries, as many as fourteen have sediment yields in excess of 500 tons/ km<sup>2</sup>/year, the highest being 4,721 tons/km<sup>2</sup> /year.

### **3.5 THE TRIBUTARIES OF THE BRAHMAPUTRA RIVER**

In the past, the Dibang and the Lohit, two major rivers joined the Dihang a short distance upstream of Kobo to form the Brahmaputra. Now, the situation has undergone a radical change. Dibang and Lohit joined Dihang through another channel Dibru, developed through phenomenon river avulsion. Dibru is receiving major part of the discharge of Lohit for the last few years. The river receives numerous tributaries from both sides all along its course, thereby progressively growing in its size. Some of the tributaries are trans-Himalayan rivers with considerable discharges. In the north, the principal tributaries are the Subansiri, the Jia Bhareli, the Dhansiri (north), the Puthimari, the Pagladiya, the Manas, the Champamati. On the south bank the main tributaries are the Burhi Dehing, the Disang, the Dikhow, the Dhansiri (south) and the Kopili. The

Brahmaputra also has some important tributaries, like the Teesta, the Jaldhaka, the Torsa, the Kaljani and the Raidak flowing through North Bengal.

The important tributaries on both the north and the south bank of Brahmaputra are listed in Table 3.3 along with chainage in km of their present outfalls from Indo Bangladesh border. The position of the outfall changes whenever bank erosion takes place there. Besides these tributaries, there are many other small streams which drain directly into the river.

Certain fluvio-geomorphic features which are found in the Brahmaputra basin have a significant bearing on the characteristics of the north and south bank tributaries. The variations in environmental settings, including geology, geomorphology, physiography, relief, precipitation and soils of the two regions belonging to the north bank and south bank river basins bring about notable differences between these two groups of rivers. On the north, the rainfall is heavier and the hills are less stable and more liable to soil erosion and landslides. In consequence, the north bank tributaries carry larger silt charge. The characteristics of north bank and south bank tributaries (173) reveal the following points of differences -

### **3.5.1 The North Bank Tributaries**

- (i) The north bank tributaries have higher rainfall and pass through the Himalayan reaches with steep channel gradient.
- (ii) In case of northern tributaries, the long section of river course is in the hilly terrain while the small section is in the plains.
- (iii) The northern tributaries carry an enormous sediment load as compared to the southern tributaries. On an average, the sediment yield of the north-bank

tributaries is three times higher than that of the south bank tributaries coming out of the Naga, Mikir hills and the Meghalaya plateau (173).

- (iv) Due to steep slope and heavy sediment load, these streams are braided over major portion of their travel. These have shallow braided channels for a considerable distance from the foot of the hill and in some cases right up to the outfall.
- (v) The northern tributaries have generally coarse sandy beds with occasional gravel beds up to some distance from the foothills.
- (vi) These tributaries generally have flashy floods.
- (vii) The basins of all the north bank tributaries have hypsometric curves with a plateau indicating a relatively youthful stage in their development.
- (viii) The north bank tributaries show a general parallel drainage pattern.
- (ix) The northern tributaries have shallow braided channels.
- (x) The northern tributaries are characterized by frequent shifting of their channels during floods. As revealed by the study, the northern tributaries have peculiar channel shifting patterns. The Subansiri and all other eastern rivers shift their channels westward, while the rivers between the Pagladiya and Subansiri shift eastwards. Again from the Manas up to the river Sonkosh in the west, all the rivers migrate westward.

### **3.5.2 The South Bank Tributaries**

- (i) These tributaries have comparatively flatter gradient and deep meandering channels almost from the foot hills.
- (ii) The southern tributaries have beds and banks composed of fine alluvial soils.

- (iii) The southern tributaries have their long courses over the plains.
- (iv) These tributaries have comparatively less silt charge with finer fractions.
- (v) In contrary to the north bank basins, the basins of the tributaries from the south bank indicate much mature stage with hypsometric curves showing a continuously decreasing profile.
- (vi) The south bank tributaries while keeping the parallel drainage pattern, show signs of dendritic configuration.
- (vii) The southern tributaries change their courses less frequently.
- (viii) The southern ones have their meandering channels over the plains.

### 3.6 HYDROLOGICAL CHARACTERISTICS OF SOME MAJOR TRIBUTARIES

The hydrological characteristics such as basin area, length, average annual discharge, average annual suspended load and the sediment yield of some major tributaries are outlined in Table 3.2 (173).

**Table 3.2 Hydrological characteristics of some major tributaries**

Tributaries	Basin Area (Km <sup>2</sup> )	Length (Km)	Average annual discharge (m <sup>3</sup> /sec)	Average annual suspended load (ha. m)	Sediment yield (ton/ Km <sup>2</sup> /year)
<b>Northern Tributaries</b>					
1. Subansiri	28,000	442	755,771	992	959
2. Ranganadi	2,941	150	74,309	186	1,598
3. Burai	791	64	20,800	16	529
4. Bargang	550	42	16,000	27	1,749
5. Jia Bhareli	11,716	247	349,487	2013	4721
6. Gabhru	577	61	8450	11	520
7. Belsiri	751	110	9300	9	477

8. Dhansiri (North)	1,657	123	26,577	29	463
9. Noa Nadi	907	75	4450	6	166
10. Nanoi	860	105	10,281	5	228
11. Bamadi	739	112	5756	9	323
12. Puthimari	1,787	190	26,324	195	2,887
13. Pagladiya	1674	197	15201	27	1,883
14. Manas-Aie-Beki	41,350	215	307,947	2,166	1,581
15. Champamati	1,038	135	32,548	13	386
16. Gaurang	1379	98	22,263	26	506
17. Tipkai	1,364	108	61,786	31	598
18. Gadadhar	610	50	7,000	0.21	272
<b>Southern Tributaries</b>					
1. Burhi Dehing	8,730	360	1411,539	210	1,129
2. Disang	3,950	230	55,101	93	622
3. Dikhow	3,610	200	41,892	34	252
4. Jhanzi	1,130	108	8,797	16	366
5. Bhogdoi	920	160.	6072	15	639
6. Dhansiri (South)	10,242	352	68,746	147	379
7. Kopili	13,556	297	90,046	118	230
8. Kulsi	400	93	11,643	0.6	135
9. Krishnai	1,615	81	22,452	10	131
10. Jinari	594	60	7,783	3	96

**TABLE 3.3 Tributary distances measured from Indo-Bangladesh border  
(Along the upstream) (WAPCOS, 1993)**

Sl. No	North Bank Tributaries	Chainage in km.
1.	Simen	580
2.	Jiyadhol	540
3.	Subansiri	430
4.	Burai	392
5.	Bargang	382
6.	Jia Bhareli	338
7.	Gabhru	300
8.	Belsiri	280
9.	Dhansiri	270
10.	Noa Nadi	230
11.	Nanai Nadi	215
12.	Bar Nadi	205
13.	Puthimari	172
14.	Pagladiya	170
15.	Beki	115
16.	Manas	85
17.	Champamati	63
18.	Gaurang	43
19.	Tipkai	40
20.	Sankosh	0
Sl. No	South Bank Tributaries	Change in km
1.	Dibru	592
2.	Burhi Dehing	540
3.	Disang	515
4.	Dikhow	505
5.	Jhanzi	495
6.	Dhansiri (south)	420
7.	Kopili	220



8.	Kulsi	140
9.	Deosila	130
10.	Dudhnai	108
11.	Krishai	107
12.	Jinari	100
13.	Jinjiram	0

### 3.7 HYDROLOGIC AND PHYSIOGRAPHIC CHARACTERISTICS OF THE BRAHMAPUTRA RIVER

The hydraulic characteristics describing the average annual runoff of the Brahmaputra and its major tributaries are represented in Figure 3.2 a schematic diagram. The statistical details of the river are described below:

- |       |   |                         |
|-------|---|-------------------------|
| (a)   | Total basin area from its source to its confluence with Ganga at Goalundo in Bangladesh | 580,000 km <sup>2</sup> |
| (i)   | Basin area within Tibet   | 293,000 km <sup>2</sup> |
| (ii)  | Basin area in Bhutan and India  | 240,000 km <sup>2</sup> |
| (iii) | Basin area in Bangladesh  | 47,000 km <sup>2</sup>  |
| (b)   | Length from its source to outfall in Bay of Bengal                                      | 2,880 km                |
| (i)   | Length within Tibet   | 1,625 km                |
| (ii)  | Length within India   | 918 km                  |
| (iii) | Length within Bangladesh  | 337 km                  |
| (c)   | Gradient  |                         |
| (i)   | Reach within Tibet  | 1 in 385                |
| (ii)  | Reach between Indo-China border and Kobo in India                                       | 1 in 515                |
| (iii) | Reach between Kobo and Dhubri   | 1 in 6,990              |
| (iv)  | Reach within Bangladesh   |                         |
|       | First 60 km from Indian Border  | 1 in 11,340             |

Next 100 km stretch

1 in 12,360

Next 90 km stretch

1 in 37,700

(d) Observed discharge

(i) Maximum observed discharge at Pandu (on 23.8.1962) 72,727 m<sup>3</sup>/sec

(ii) Minimum observed discharge at Pandu (on 20.2.1968) 1,757 m<sup>3</sup>/sec

Average dry season discharge at Pandu 4,420 m<sup>3</sup>/sec

(e) Normal annual rainfall within basin ranges between 2,125 mm in Kamrup district of Assam and 4,142 mm in Tirap district of Arunachal Pradesh.

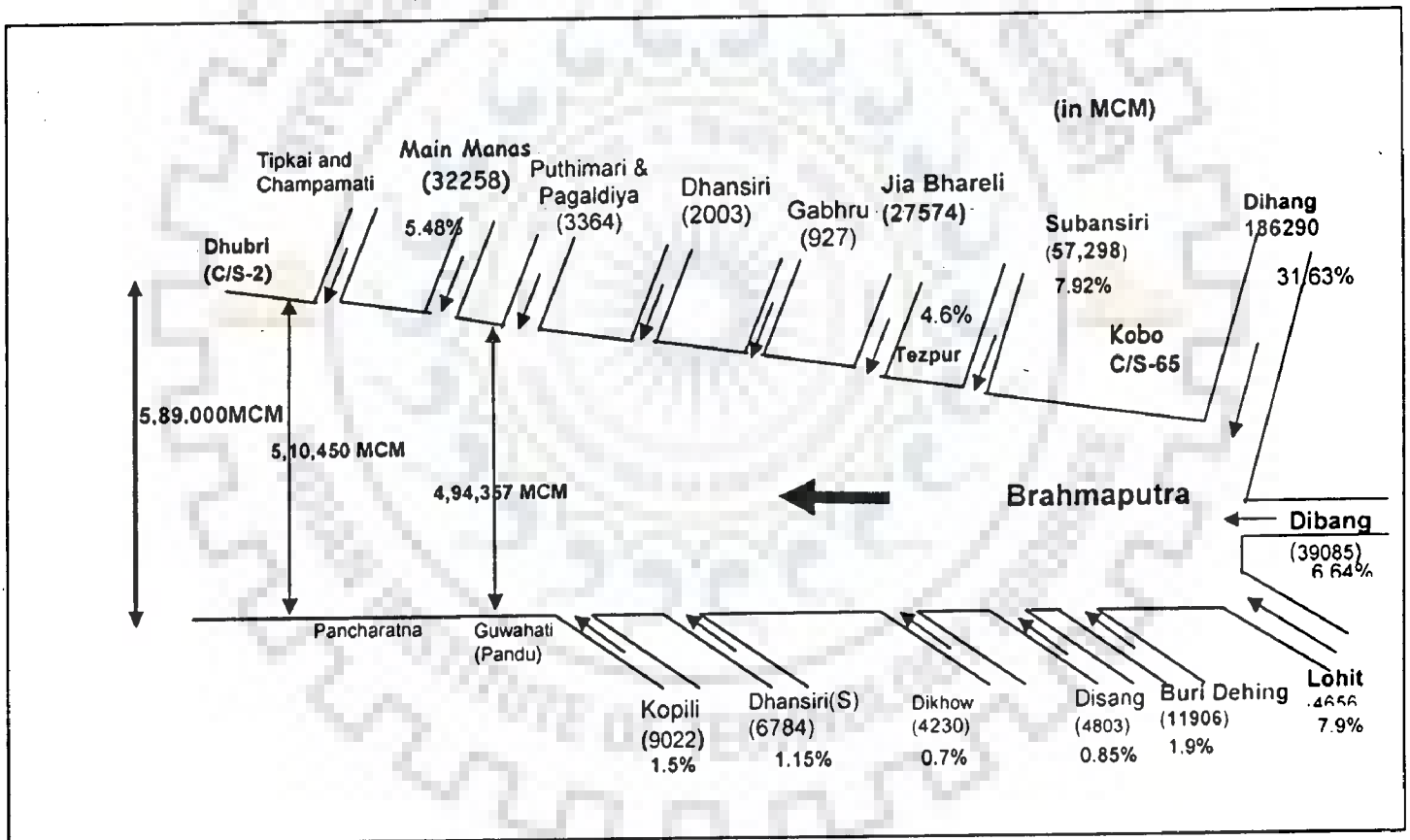


Figure 3.2 Average annual runoff of the Brahmaputra and its tributaries

### 3.8 GEOLOGY AND GEOMORPHOLOGY

The Brahmaputra basin in India, comprising of varying geologic and geomorphic characteristics, represents its peculiar physiographic make-up. The basin is bounded by the eastern Himalayas on the north and east, the Naga-Patkai ranges on the northeast and Meghalaya Plateau and Mikir hills on the south. The region can be geologically and tectonically divided into four major zones, viz. the Himalayan folded and Tertiary hills and mountains, the Naga-Patkai ranges, the Meghalaya Plateau and Mikir hills and the Brahmaputra valley in Assam.

The Himalayan zone comprises of three topographic units that rise progressively to the north. The lowermost ranges, called sub-Himalayas with an average elevation of 1,000 m, consist mainly of Tertiary sand stones, and are conspicuous by the presence of many raised, relatively young terraces (60). The middle Himalayas, having an average elevation of 4,000 m are underlain by lower Gondwana (Palaeozoic) deposits comprising shales, slates, and phyllites overlain by a thick horizon of basaltic rocks. The greater Himalayas with an average elevation of 6,000 m consist primarily of granites and gneisses (60). The Himalayan Mountains with their syntaxial N-E bends originated out of the Tethyan Geo-syncline (Wadia, 1968) and are essentially composed of loose sedimentary rocks. The sub Himalayas and the lower Himalayas are characterized by piedmont zones, low discontinuous ridges, low linear ridges, high rugged hills and upland valley depressions.

The Patkai-Naga ranges stand on the eastern and south-eastern border of the Brahmaputra valley in Assam. These ranges, with an average elevation of 1,000 m, are composed of Tertiary sediments and characterized by the presence of a large number of active faults. This zone consists of piedmont plains, anticlinal ridges and synclinal

valleys with terraced alluvial fills, undifferentiated sharp ridges and narrow valleys, upland valley depressions and plateau remnants. The Meghalaya plateau and the Mikir hills attaining an elevation ranging from 600 m to 1,800 m are made up primarily of gneisses and schist. This part, being a rigid mass, belongs to the Deccan plateau of the stable Indian peninsular block of Pre-Cambrian age. It is characterized by plateau remnants, inselbergs, deeply dissected uplands with faulted monoclines of Tertiary cover, denuded hills, basement controlled structural ridges covered with Tertiary rocks and upland valley depressions.

The Brahmaputra valley in Assam, on the other hand, is underlain by recent alluvium approximately 200-300 m thick, consisting of clay, silt, sand, and pebbles (57). The valley is developed over the fore deep in between the peninsular mass and the Tethyan geosynclines. The fore deep is characterized by some complicated tectonic features represents a series of faults and thrust extending in the NE-SW direction from the eastern margin of the Meghalaya plateau across the North Cachar Hills to Tirap District of Arunachal Pradesh. These thrusts are originated at the time of the late Himalayan-Patkai-Naga Hills orogeny and pushed the tertiary deposits into folds and faults. The fore deep is believed to be under the sea till the sub-recent period received deposits during all the periods of the tertiary and quaternary ages. The tertiary deposits consist mainly of sand stones, shale, grit, conglomerate and lime stones.

Towards the close of the Pleistocene period, alluvium began to be deposited in the form of sand, pebbles and gravels especially along the northern foothills of the Brahmaputra valley. These valley deposits of reddish brown sandy clay with some pockets of unasserted pebble, cobble, sand and silt have been identified as older alluvium. The tertiary beds of the valley are overlain by a thick layer of newer alluvium

composed of sand, silt and clay, which are being brought down from the rising Himalayas in the north, the Patkai Naga ranges in the east and south-east and the Meghalaya plateau in the south by numerous tributaries of the Brahmaputra. The characteristic geological and tectonic framework coupled with structural complexities has rendered the Brahmaputra basin geo-morphologically a most complicated one. A variety of landform under varied climatic conditions has formed over the geologic and tectonic base of the region. The peri-glacial, glacio-fluvial, and fluvial processes are dominantly operative in the basin at varying altitudes.

The higher elevations of the Himalayas experience peri-glacial and glacio-fluvial erosion and deposition. The bare relief of the sub-Himalayas and greater Himalayas suffer from immense sheet erosion owing to peri-glacial solifluction. The low hill ranges with hot and humid climate and heavy rainfall concentrated to a few months of the year experience solifluction, sheet erosion and landslides.

The incidence of landslides is high in the Himalayan foothills, where heavy rainfall, high seismicity and toe cutting of hill slopes by the streams are most frequent. Heavy rains often loosen soil and the soft rocks of the young Himalayan ranges. Rainwater percolates through joints, fractures, foliations, and pores of rocks and soils and finally makes them loose and heavy, which cause heavy slope failure. Fluvial processes are, on the other hand, significantly dominant on the valley bottoms and plains where alluvial deposition takes place due to erosion of the higher surface by rivers and flooding in the valleys. The erosional and depositional processes conspicuously intensified by copious rainfall and frequent seismic movements, however, play a dominant role in creating various fluvio-geomorphic environments in the basin.

### 3.9 BRIEF DESCRIPTION ON ORIGIN OF MAJULI ISLAND

Majuli, the world's largest river island is situated to the north of Jorhat and at the confluence of Subansiri river and Brahmaputra river. It is formed by bifurcation of the Brahmaputra into two branches, viz., the Kherkatia Suti or the Luit Suti on the north and the Brahmaputra (Dehing) on the south. Majuli is not a normal alluvial island formed by the Brahmaputra. It was a piece of land known as Majali, on the south bank of the Brahmaputra (Luhit), situated north of the tributary of the Dehing river (Burhi Dehing) till the year 1,750. An extreme flood of that year caused the Brahmaputra (Luit) to divert its course southwards on the east of Majali, thereby joining it with the Dehing river. Subsequently, the Brahmaputra diverted its main flow through the lower reach of the Dehing, and the land Majali in between the two rivers resulted in the island Majali, which is now called Majuli. The Tuni is the main river in Majuli island.

### 3.10 CHANNEL PROCESSES

The Brahmaputra river in India forms a complex river system characterized by the most dynamic and unique water and sediment transport pattern. The Brahmaputra is the fourth largest river in the world (60). The water yield from per unit basin area is among the highest of the major rivers of the world. The Jia Bhareli, a major tributary, carries a mean annual water discharge in the order of  $0.0891 \text{ m}^3/\text{sec}/\text{km}^2$  (Bora, 1990). As estimated by Goswami (1982), the Brahmaputra yields  $0.0306 \text{ m}^3/\text{sec}/\text{km}^2$  at Pandu. As regards sediment transport, the river has also set records in carrying large volumes of sediment. The high intensity of monsoon rains, easily erodible rocks, steep slopes, and high seismicity contribute a lot by rendering the river a heavily sediment-laden one. Thus, the Brahmaputra becomes one of the leading sediment carrying rivers of the

world. Amongst the large rivers of the world, it is second only to the Yellow river in China in the amount of sediment transport per unit of basin area (60).

At Pandu, the river carries an average suspended load of 402 million metric tons. A river with such gigantic water and sediment discharge magnitudes represents its most dynamic fluvial regime. Its large alluvial channel having a width of 6 to 10 km is, therefore, marked by intense braiding, rapid aggradation and drastic bank line changes. The Brahmaputra is a uniquely braided river of the world. Although braiding seems to be best developed in rivers flowing over glacier outwash plains or alluvial fans, perfect braiding is also found to occur in large alluvial rivers having low slope, such as the Brahmaputra in Assam (India) and Bangladesh or the Yellow River in China. The Assam section of the Brahmaputra River is in fact, highly braided and characterized by the presence of numerous lateral as well as mid channel bars and islands.

The high degree of braiding of the Brahmaputra channel near Dibrugarh and downstream of Guwahati is indicated by the calculated braiding indices of 5.3 and 6.7 respectively for the two reaches, following the method suggested by Brice (1964). A braiding Index of 4.8 for the entire Assam section of the river calculated on the basis of satellite data of 1993 also suggests a high degree of braiding of the Brahmaputra river.

The basin with varied terrain characteristics and being an integral part of the monsoonal regime of south-east Asia shows a marked spatial variation in the distribution of precipitation. The rainfall in the Teesta valley varies from 164 cm in the south to 395 cm in the north. The average annual rainfall in the lower Brahmaputra valley is 213 cm while the same in the north-eastern foothill belt is 414 cm. The basin as a whole has the average annual rainfall of 230 cm with a variability of 15-20%. The Himalayan sector receives 500 cm of rainfall per year, the lower ranges receiving more than the higher

areas (60). During the monsoon, months of May to October receive about 12% of the annual total.

In the sub-Himalayan belt soils with little depth developed over the Tertiary sand stones generally belong to red loam, laterite, and brown hill soil type with admixtures of cobbles and boulders. The greater part of the Brahmaputra valley is made up of new alluvium of recent deposition overlying Tertiary, Mesozoic and Archaean bedrocks. Along the piedmont zone, there occur some patches of older alluvium extending along the interfluves of the tributaries flowing from the Himalayan foothills. The soils of the Meghalaya plateau and the Mikir Hills in the south are of laterite and loamy silt and fine silt types.

In general, braiding in the Brahmaputra follows the mechanism of central bar type of braid formation. During high flow, a central bar is deposited in the channel and gradually the bar accretes vertically to the level of the floodplain. It also builds on the downstream end through deposition of bed load material due to the slack water occurring behind the bar. The bar growth causes a decrease in total cross-sectional area leading, thereby, to the instability of the channel. Lateral erosion then follows on one or both the banks. Through repetition of this process in the divided reach, a well developed braided reach with multiple sandbars and islands is produced.

In the Assam section of the river, the presence of such nodes of stable banks is found to effect the formation and location of the bars. There are nine nodal reaches of narrow constriction at various locations along the Brahmaputra, which are at Murkongselek (4.8 km), Disangmukh (5.10 km), downstream of Jhanjimukh (3.75), upstream of Dhansiri north (4.0 km), downstream of Dhansirimukh (4.4 km), upstream of Tezpur (3.6 km), Pandu, Guwahati (1.2 km), Sualkuchi (2.4 km) and Pancharatna (2.4



km). Since banks are relatively stable in these reaches, the river scours deeper to accommodate the flood discharge. The scoured debris is then deposited in the channel immediately downstream from the narrow section. As a result, the channel becomes wider and bars and islands are produced. Formation of bars causes reduction in cross sectional area and the river, therefore, cuts its banks laterally to accommodate the discharge. Thus, the downstream of the nodes intense braiding develops resulting in channel widening through continuous migration of both banks of the Brahmaputra.

As reported from the studies carried out on braided rivers of the world, the major factors thought to be responsible for braiding and bar formation are steep channel gradient, high erodibility of bank materials, great variability in discharge, overabundance of load, and aggradation of the channel bed. In case of the Brahmaputra river in Assam bar formation and channel division are owing to a combination of factors like high variability in discharge, excessive sediment transport, easily erodible bank materials and aggradation of the channel. Being the fourth largest river in the world with an average discharge of 19,830 m<sup>3</sup>/sec at its mouth (61), the Brahmaputra carries 82% of its annual flow at Pandu (Assam) only during the rainy season from May to October. The maximum and minimum mean monthly flows in the river during 1990-2002 are 48,160 m<sup>3</sup>/sec and 3,072 m<sup>3</sup>/sec, respectively. On an average, therefore, the maximum flow is more than fifteen times the minimum.

High variability in discharge of the river is mainly caused by seasonal rhythm of the monsoon and the freeze-thaw cycle of the Himalayan snow. As regards the pattern of sediment transport, the river has the record of carrying excessive sediment load which is believed to be one of the important factors responsible for braiding.

### 3.11 THE STUDY AREA

Considering the river flows, the gradients and the confluence of river tributaries, the study area has been divided into seven reaches (Figure 3.3). The reaches are described as under in Table 3.4.

**Table 3.4 Details of study reaches**

Reach	Cross section		Location		Distance (Km)
	From	To	From	To	
Reach-I	02	10	Fakiraganj (Dhubri)	Goalpara	65.28
Reach-II	11	20	Goalpara	Palasbari	89.76
Reach-III	21	30	Palasbari	Tongani	79.57
Reach-IV	31	40	Tongani	Behali	120.88
Reach-V	41	50	Behali	Jhanjimukh	107.60
Reach-VI	51	60	Jhanjimukh	Kahai Spur, Dibrugarh	98.44
Reach-VII	61	65	Kahai Spur, Dibrugarh	Dighaltarang (Kobo)	51.00

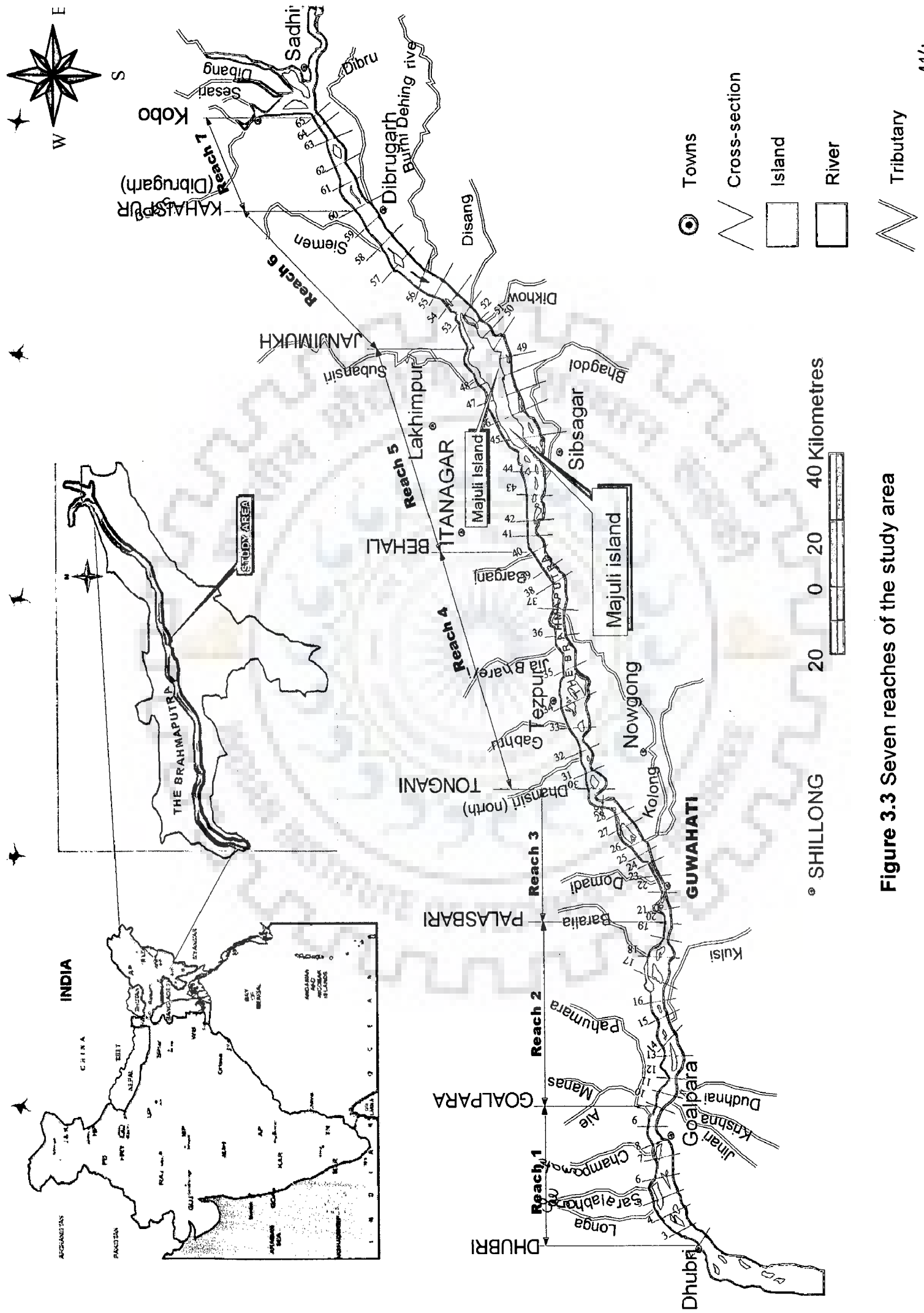


Figure 3.3 Seven reaches of the study area

## DEVELOPMENT OF SPATIO-TEMPORAL MORPHOLOGICAL MODEL

---

### 4.1 INTRODUCTION

The Brahmaputra is a snow-fed large Trans-Himalayan river with considerable variations in width, gradient, discharge and displays complex fluvial planform throughout its course. On a global level too, the river ranks fifth in terms of discharge, third in terms of sediment discharge, and eleventh in terms of drainage area (167). The river is also well known for its braiding characteristics (59; 135). The morphology of such a braided river system has not been as extensively studied as single-channel rivers. The studies that have previously been carried out to establish models and frameworks for understanding the morphological behaviour of this river were mostly qualitative in nature (118). The lack of quantitative studies on morphology of the river Brahmaputra has impeded the development of the understanding of its intricate channel processes.

The present research considers a stretch of approximately 622.73 km of the river Brahmaputra in India based on the data spanning from year 1990 to 2002. Figure 3.1 depicts the study area of the river stretch. The width of the river in this segment varies from 1.2 to 18.13 km within this stretch.

The Brahmaputra in India, particularly its valley in Assam Province, represents an acutely flood-prone region characterized by awesome hazards of flood and erosion that create an annual mayhem of devastations bringing untold miseries to the people and causing colossal loss and damage to public property and infrastructure. Institutional arrangement for flood forecasting adopted so far in the country, especially with regard to the Brahmaputra basin, needs to be revamped and reorganized, so that river

management activities are done more efficiently using state-of-the-art technology. Inadequacies in the monitoring network and lack of desired level of sophistication and standardization in data acquisition and processing techniques have been realized now by technologists, planners and administrators as improvements for proper river management. More efficient and wider dissemination of information in regard to river management is a matter of great urgency requiring focussed attention of concerned national governments and international agencies.

With the advent of satellites into space, a new vista opened to the resource survey planners as the space borne remote sensing offered unique feature to provide comprehensive and synoptic view of fairly large area at regular intervals. Coupled with ground information, satellite remote sensing is ideally suited tool for studying river morphology. The satellite based data maps could be used to a great advantage in monitoring the areas affected by floods and erosion in the absence of surveys conducted otherwise. In the present research, multi-date digital satellite data covering the study area have been used to extract information on river configuration on repetitive basis. The multi-date digital satellite data were integrated with the observed ground data available through published literature available in the form of maps, reports and field data.

Modelling of river influences on the fluvial morphology is inherently data intensive. Overall, demands on diverse data input and management have led to an increased awareness and use of remote sensing data and GIS techniques in studying river morphology. One particular challenge in morphological modelling is to capture and represent the complexity of a real world entity in sufficient detail to offer meaningful abstractions amenable to processing whilst maintaining its physical identity.

In this research, the use of neuromorphic techniques in conjunction with remote sensing and GIS has been investigated. It has been endeavoured to demonstrate that ANN models could be applied in real-time conditions to simulate morphological variability in the river Brahmaputra. This chapter provides the details of development of neuromorphic models and analytic techniques related to the Brahmaputra river morphology that are central to understanding its intricate behaviour.

## 4.2 DATA SOURCES AND DATA TYPES

Four types of data were used during the research work, namely:

- (a) Topographical maps
- (b) Digital satellite images
- (c) Collateral data (published)
- (d) Hydrographic and hydraulic data from surveys

### 4.2.1 Topographical Maps

For the purpose of preparation of base maps, 39 numbers of topographical maps of Survey of India (SOI) at the scale of 1:50,000 and 1:63,000 were used. The toposheets used have been enlisted in Table 4.1.

**Table 4.1 Survey of India (SOI) toposheets used in the study**

Sl. No	Toposheet No	Area	Lat/Long	Scale
1.	78 J/4	Goalpara	90° 00'X26° 15'	1:63,000
2.	78 J/7	Gaurang	90° 15'X26° 30'	1:63,000
3.	78 J/16	Dudhnai	90° 45'X26° 15'	1:63,000
4.	78 J/15	Manas	90° 45'X26° 30'	1:63,000
5.	78 J/11	Barpeta	90° 30'X26° 30'	1:63,000
6.	78 J/3	Sankosh	90° 00'X26° 00'	1:63,000
7.	78 J/8 & 78 K/3	Dhubri	90° 15'X26° 15'	1:63,000
8.	78N/11	Puthimari	91° 30'X26° 30'	1:50,000

9.	78N/16	Guwahati	91° 45'X26° 15'	1:63,000
10.	78N/15	Guwahati	91° 45'X26° 30'	1:63,000
11.	78N/3	Barpeta	91° 00'X26° 30'	1:63,000
12.	78N/7	Barpeta D/S	91° 15'X26° 30'	1:63,000
13.	78N/8	Barpeta U/S	91° 15'X26° 15'	1:63,000
14.	78N/4	Barpeta	91° 00'X26° 15'	1:63,000
15.	83 I/8	Sibsagar	94° 45'X27° 30'	1:63,000
16.	83 I/15	Dibrugarh	94° 45'X27° 30'	1:63,000
17.	83 I/11	Dihingmukh RF	94° 30'X27° 30'	1:63,000
18.	83M/6	Dihang	95° 15'X27° 45'	1:50,000
19.	83M10	RH of Dihang	95° 30'X27° 45'	1:50,000
20.	83M/14	Noa Dihing	95° 45'X27° 45'	1:50,000
21.	83M/13	Lohit	95° 45'X28° 00'	1:50,000
22.	83M/9	Dibang	95° 30'X28° 00'	1:50,000
23.	83M/2	Dibru RF	95° 00'X27° 45'	1:50,000
24.	83I/14	Siemen River	94° 45'X27° 45'	1:50,000
25.	83I/10	NEFR	94° 30'X27° 45'	1:50,000
26.	83F/10	Dhansiri (S)	93° 30'X26° 45'	1:50,000
27.	83F/2	Kaziranga	93° 00'X26° 45'	1:50,000
28.	83F/6	Tezpur	93° 15'X26° 45'	1:50,000
29.	83F/14	Dhansiri (N)	93° 45'X26° 45'	1:50,000
30.	83B/13	Jia Bhareli	92° 45'X27° 00'	1:50,000
31.	83J/1	Subansiri	94° 00'X27° 00'	1:63,000
32.	83J/2	Jorhat	94° 00'X26° 45'	1:63,000
33.	83B/10	Gabhru	92° 30'X26° 45'	1:63,000
34.	83B/2	Dhansiri(N)	92° 00'X26° 45'	1:63,000
35.	83B/6	Dhansiri	92° 15'X26° 45'	1:63,000
36.	83B/3	Noa Nadi	92° 00'X26° 30'	1:63,000
37.	83B/7	Mangladoi	92° 15'X26° 30'	1:63,000
38.	83B/14	Jia Bhareli	92° 45'X26° 45'	1:63,000
39.	83F/10	Dhansiri	93° 30'X26° 45'	1:63,000

#### 4.2.2 Digital Satellite Images

The satellite index maps of the river Brahmaputra as covered by the Indian Remote Sensing Satellite (IRS) 1A, 1C and 1D have been presented in Figure 4.1 and Figure 4.2 respectively. The satellite images presented in Table 4.2 were used to synthesise a map of cumulative stream bank erosion of the Brahmaputra for the period 1990 - 2002. Satellite scenes covering the study area were identified from the satellite pass index map of IRS. Dates of satellite passes over the area were selected from the orbital calendars available for the years under consideration. However, it could not be possible to procure the satellite data of monsoon period due to the presence of cloud cover for the period under study. In all, the digital satellite data comprising of 32 scenes of IRS Linear Imaging Self Scanner (LISS) I and LISS III for the years 1990, 1997, 2000 and 2002 were analysed. These sensors provide multi-spectral data in 4 bands, two in visible ( $0.52-0.59\mu\text{m}$ ) and ( $0.62-0.68\mu\text{m}$ ), one in near infrared (NIR  $0.77-0.86\mu\text{m}$ ) and one in shortwave infrared (SWIR  $1.55-1.70\mu\text{m}$ ) regions of the electromagnetic spectrum. The spatial resolution of LISS-I is 72.5 m and that of the LISS-III is 23.5 m. In addition, Radarsat satellite data ScanSAR Narrow Beam (SCNB) (C band, HH polarization and  $31$  to  $46^\circ$  incidence angle) of February, 2002 and Advanced Very High Resolution Radiometer (AVHRR) sensor data of National Oceanographic and Atmospheric Administration (NOAA) satellite of US Geological Survey having resolution of 1.1 km of July and August 2002 were used to study the flood scenario. This was selected for its large coverage (300 km swath) acceptable pixel spacing (25 m) and small volume of data. Digital Elevation Model (DEM) data of the year 2002 for the sub-basin was used to derive the drainage details of the area.



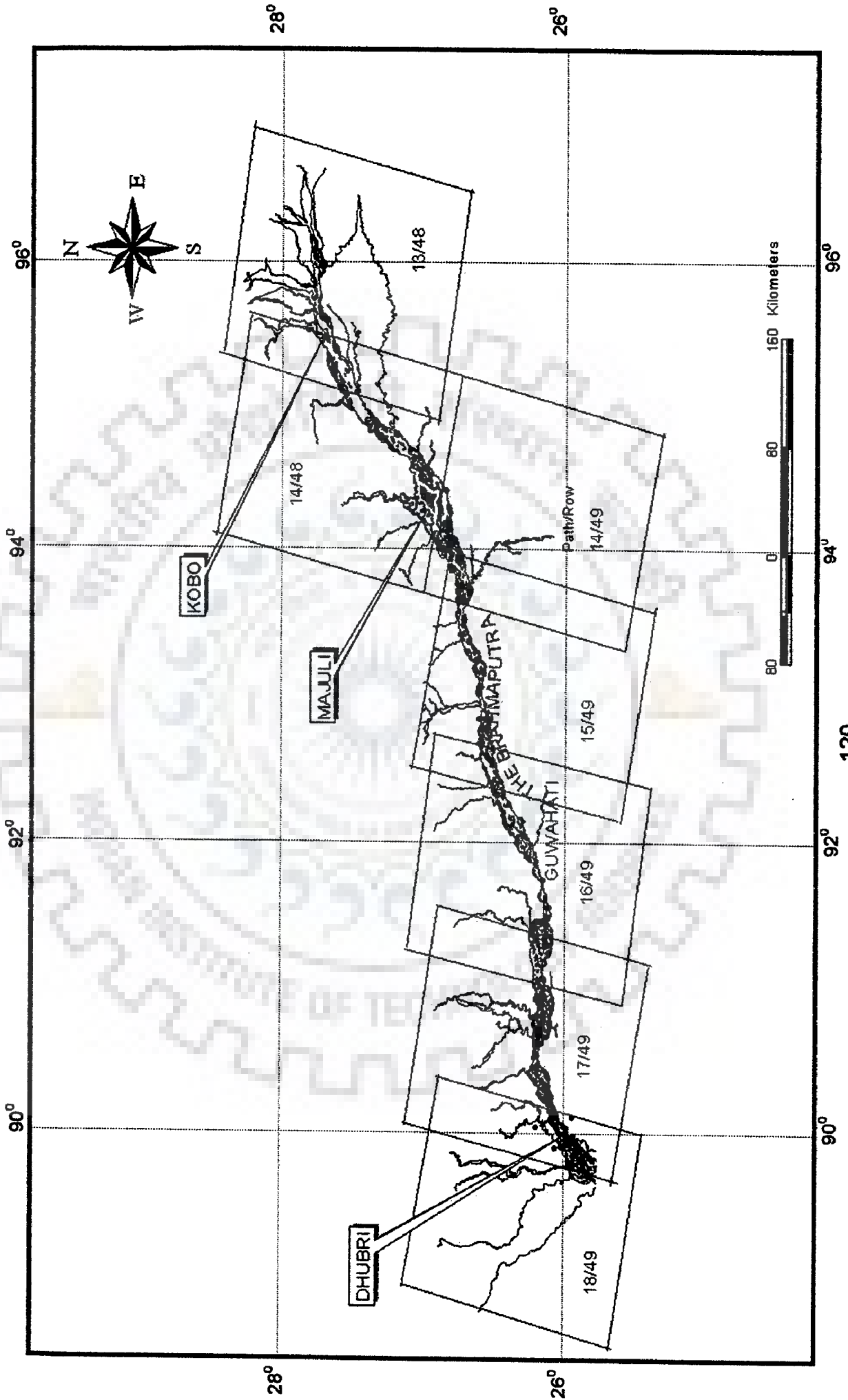
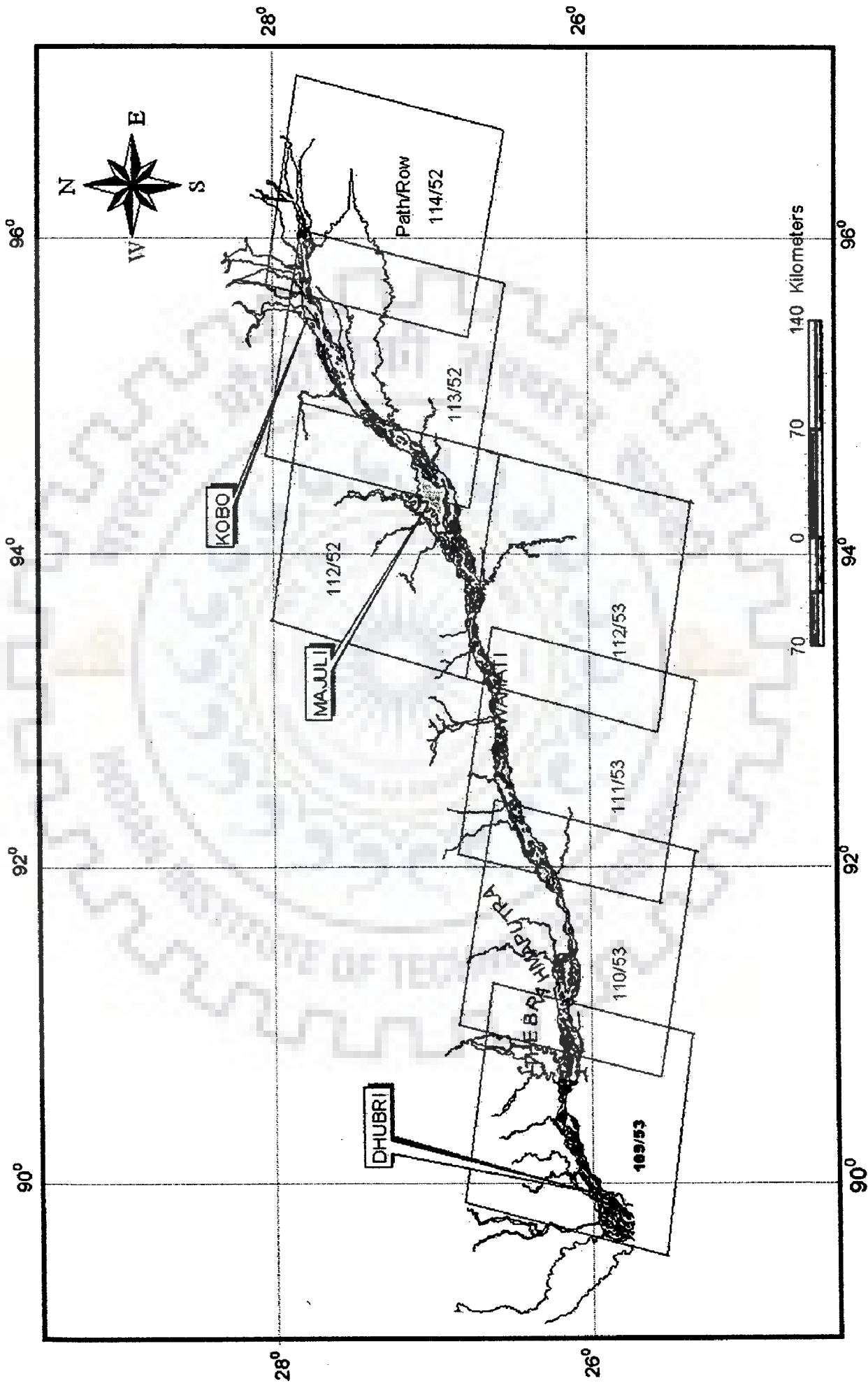


Figure 4.1 Index to IRS 1A coverage



121  
 Figure 4.2 Index to IRS 1C/1D coverage

### 4.2.3 Collateral Data (published)

Thematic maps and reports of Ministry of Water Resources, Government of India (Brahmaputra Atlases, Volume - I and Volume-II, 1986) providing static information on land use, flood inundation, embankment systems etc., over the Brahmaputra basin were referred to while carrying out the satellite data interpretation work. In addition, ground truth data were collected during the field visits of the area, which confirmed the interpretation. Bearing of cross-sections, latitude and longitude of tributaries and important bridges were collected from the Central Water Commission (CWC), Government of India, based on surveys conducted by them.

### 4.2.4 Observed Hydrographic and Hydraulic Data

#### 4.2.4.1 Hydrographic data

Morphometric data, like the reduced levels of the river cross-sections of post-monsoon period for the years 1957, 1971, 1977, 1981, 1988, 1993 and 1997 have been collected in respect of all the 64 pre-defined river cross-sections from the Brahmaputra Board, Government of India.

**Table 4.2 Digital satellite data used in this study**

Sl. No	Satellite	Sensor	Path	Row	Year
1	IRS-1A	LISS-I	18	49	1990
2	IRS-1A	LISS-I	17	49	1990
3	IRS-1A	LISS-I	16	49	1990
4	IRS-1A	LISS-I	15	49	1990
5	IRS-1A	LISS-I	14	49	1990
6	IRS-1A	LISS-I	14	48	1990
7	IRS-1A	LISS-I	13	48	1990
8	IRS-1C	LISS-III	109	53	1997
9	IRS-1C	LISS-III	110	53	1997
10	IRS-1C	LISS-III	111	53	1997
11	IRS-1C	LISS-III	112	53	1997
12	IRS-1C	LISS-III	112	52	1997

13	IRS-1C	LISS-III	113	53	1997
14	IRS-1C	LISS-III	113	52	1997
15	IRS-1C	LISS-III	114	52	1997
16	IRS-1C	LISS-III	109	53	2000
17	IRS-1C	LISS-III	110	53	2000
18	IRS-1C	LISS-III	111	53	2000
19	IRS-1C	LISS-III	112	53	2000
20	IRS-1C	LISS-III	112	52	2000
21	IRS-1C	LISS-III	113	53	2000
22	IRS-1C	LISS-III	113	52	2000
23	IRS-1C	LISS-III	114	52	2000
24	IRS-1C	LISS-III	114	52	2000
25	IRS-1C	LISS-III	114	53	2000
26	IRS-1D	LISS-III	109	53	2002
27	IRS-1D	LISS-III	110	53	2002
28	IRS-1D	LISS-III	111	53	2002
29	IRS-1D	LISS-III	112	53	2002
30	IRS-1D	LISS-III	113	53	2002
31	IRS-1D	LISS-III	113	52	2002
32	IRS-1D	LISS-III	114	52	2002
33	NOAA	AVHRR			2002
34	Radarsat	SCNB (C band, HH polarization and 31 to 46° incidence angle) Resolution 26mX 27m			2002

#### 4.2.4.2 *Discharge and stage data*

Discharge and stage data of the river Brahmaputra were collected for various cross-sections from Central Water Commission (CWC), Assam Flood Control Department and Brahmaputra Board. The length of data record was from year 1990 to 2002. Hourly and daily monsoon stage data were collected for Pancharatna and Pandu for the period from 1990 to 2002. The details of data collected have been tabulated in Table 4.3. Water Year Books in respect of 1999, 2000, 2001 and 2002 of the river Brahmaputra were collected from CWC.

**Table 4.3 Discharge and stage data**

Sl. No	Cross-section	Type of data	Duration/Year
1	Pancharatna	Average monthly water level v/s average monthly discharge	1990 - 2002
2	Pancharatna	Daily water level v/s discharge	Monsoon period (June to October) (1993 -2002)
3	Pancharatna	Hourly water level v/s discharge	(June to October) (1990 -2002)
4	Pandu	Average monthly water level v/s average monthly discharge	1990 - 2002
5	Pandu	Daily water level v/s discharge	(June to October) (1993 -2002)
6	Pandu	Hourly water level v/s discharge	(June to October) (1990 -2002)
7	Dhubri	Average monthly water level	(1990 -2002)
8	Dhubri	Daily water level	(June to October) (1999 -2003)
9	Bessamora	Daily water level v/s discharge	2000
10	Bessamora	Average monthly water level	1990 - 2002
11	Bhomoraguri	Daily water level	1997 - 2002
12	Palasbari C/S 20	Average monthly water level	1990 - 1999
13	Bhomoraguri C/S 26	Average monthly water level	1990-2002
14	Ganeshghat C/S 35	Average monthly water level	1997-2002
15	Tezpur C/S 36	Average monthly water level	1990 - 2002
16	C/S 38	Average monthly water level	1990 - 2002
17	C/S 40	Average monthly water level	1990 - 2002
18	C/S 47	Average monthly water level	1990 - 1992
19	Neamatighat C/S 49	Average monthly water level	1990 - 2002
20	C/S 52	Average monthly water level	1990 - 1992
21	Dibrugarh C/S 59	Average monthly water level	1990 - 1992

#### 4.2.4.3 Sediment data

Daily suspended sediment data in respect of Pancharatna and Pandu were collected for the years from 1990 to 2002. The ten days total and average monthly discharge ( $m^3/sec$ ) and monthly average suspended sediment yield of major tributaries, such as the Manas, the Jia Bhareli at Bhalukpong, the Subansiri at

Chouldhowaghat, the Dhansiri (N), the Dhansiri (south) at Golaghat the Kopili at Jagibhakatgaon, the Dikhow at Sibsagar (daily), and the Buri Dehing at Chenimari were collected for all the years from 1999 to 2002. Characteristic sediment particle size distribution at the cross-sections was collected from CWC. Tables 4.4 and 4.5 show the details of sediment data collected.

**Table 4.4 Sediment load data of the Brahmaputra**

SI. No	Cross-section	Type of data	Duration/Year
1.	Pancharatna	Average monthly discharge v/s sediment	1990 -2002
2.	Pandu	Average monthly discharge v/s sediment	1990 -2002

**Table 4.5 Discharge and sediment data of tributaries**

SI. No	Site	Type of data	Duration/Year
1	Buri Dehing	Average monthly discharge v/s sediment	1999 - 2002
2	Subansiri	Average monthly discharge v/s sediment	1999 - 2002
3	Kopili	Average monthly discharge v/s sediment	1999 - 2002
4	Dikhow	Average monthly discharge v/s sediment	1999 - 2002
5	Dhansiri (North)	Average monthly discharge v/s sediment	1999 - 2002
6	Dhansiri (South)	Average monthly discharge v/s sediment	1999 - 2002
7	Jia Bhareli	Average monthly discharge v/s sediment	1999 - 2002
8	Manas, Beki	Average monthly discharge	1999 - 2002
9	Puthimari	Average monthly discharge	1999 - 2002
10	Champamati	Average monthly discharge	1999 - 2002
11	Pagladiya	Average monthly discharge	1999 - 2002

### 4.3 PROCESSING OF HYDROGRAPHIC DATA

#### 4.3.1 Generation of Hydraulic/Hydrologic Data

The hydraulic data pertaining to discharge, stage and sediment load were compiled as per the requirement of Hydrologic Engineering Center (HEC-6) program devised by the US Corps of Engineers (May, 2004). All the data were converted to FPS system of units before simulation in the software. The generation of all the data were carried out in three phases, as the software has limitations of processing not more than 9 tributary flows and not more than 50 cross-sections at a time. Considering the observed data availability at Dhubri (cross-section 2), Pancharatna (cross-section 9), Pandu (cross-section 22) and Bessamara (cross-section 50), the data for all the 64 stations were generated in three phases, i.e. from cross-section 2 to 9 in first phase, cross-section 10 to 50 in second phase and cross-section 51 to 65 in third phase.

Few cross-sections were coded as a test reach first, prior to coding the entire problem. As movable stream bed profile calculations were much more sensitive to errors in boundary geometry than were fixed-bed water surface profile calculations, the geometry data were debugged. Sensitivity analysis was carried out in fixed-bed mode in HEC-6 before generating data in movable-bed mode. Appropriate values of Manning's  $n$  were determined from the actual observed data at some cross-sections and at other cross-sections, it was calibrated through trial and error by running the computer model several times in fixed-bed mode. This was needed to compare calculated water surface elevations with the observed water surface profiles and with established rating curves, and thus, allowed the adjustment and determination of the proper values to use for Manning's  $n$ . To check the model performance, three water discharges were selected as very low

flow, bank full flow and extremely high flow. The bank elevations were specified for each cross-section from the field data. The fraction of total load, which moved as clay, silt and as sand were calculated from the observed sediment data and subdivided into class intervals: very fine sand, fine sand, medium sand etc. Bed load of 10% (of suspended load) has been taken with the suspended load to calculate the total sediment load (60). Temperatures for the inflowing water discharge of all the corresponding months were taken into account while simulating the movable-bed. Average monthly water discharge, water level and sediment discharge at all the 64 cross-sections were calculated using movable-bed model in HEC-6 for all the months for all the 13 years from 1990 to 2002.

#### **4.3.2 Generation of Discharge and Stage Data**

The discharge at Pancharatna (cross-section 9), and Pandu (cross-section 22), Bhomoraguri (cross-section 36) and Bessamara (cross-section 50) and the stage data at 14 number of cross-sections were simulated as input and the discharges were generated at all 64 cross-sections. The average monthly discharges from the major tributaries were included in corresponding computer runs to have realistic data in the simulation.

#### **4.3.3 Generation of Sediment Data**

Conventional methods provide a reasonably robust estimate of the time and space averaged sediment load, even on large rivers like the Brahmaputra, provided the field conditions are appropriate for the method and some independent means of confirming the transport estimate available. While there are many formulae for the estimation of suspended sediment and bed load, none has been universally proved to be the best (73). They all apply more or less to a limited range of conditions and none reproduce the short-term



fluctuations in sediment transport rates found in reality. The modes of transport, the processes that disperse sediment within a river, and the factors that affect sediment supply all contribute to substantial spatial and temporal variation in the sediment load. Since, measuring the sediment load everywhere on the river continuously is impracticable, an approach has been attempted to reasonably estimate the total load of sediment with respect to time.

Transport potential was calculated at each cross section using hydraulic information yielded from the water surface profile calculation and the gradation of bed material. Sediment was routed downstream after the backwater computations were made for each successive discharge (time step). The theoretical basis for adjusting bed elevations for scour or deposition was provided by the continuity equation for sediment material or the Exner equation as described in Chapter 2, equation 2.38.

Before the sediment discharge data were generated in HEC-6, computer codes were developed for different sediment predictors, such as Acker's & White (1973), Yang's (1973 & 1979), Engelund & Hansen (1967) and Swamee & Ojha (1991) to test the suitability of a model for the river condition. It was found that among the available sediment transport equations in HEC-6, the unit stream power equation recommended by Yang (1973), simulated satisfactorily for the river. The sediment discharge predicted by various models was compared and shown in Table 4.6. As only at two cross-sections, namely Pancharatna and Pandu, sediment data were recorded, the sediment discharge was simulated at all the 64 sections using Yang's 1973 model in HEC-6 software, which introduced approximation of interpolation in the sediment data. The discrepancy ratio was used to indicate the goodness of fit between the computed and measured results.

**Table 4.6 Comparisons of sediment load by different sediment predictors (Pancharatna)**

Sediment predictors	Acker's & White (1973)	Engelund & Hansen (1967)	Yang's 1973	Yang's 1979	Swamee & Ojha (1991)	Observed sediment (June, 1990)
Sediment load (Tons/day)	564505.0	3067334.0	2259967.0	1550703.0	256256.0	2251005.0
Discrepancy ratio $R_i = Q_{ci}/Q_{mi}$	0.25	1.36	1.003	0.689	0.114	

#### 4.3.4 Normalisation of the Generated Data

As the observed data were not at identical points, the same were normalised in order to have a cohesive data base. A computer program was used (Programme 1, Annexure I) which had adopted Lagrangian interpolation moving window for computing the normalised value of  $x$  (distance) and  $y$  (discharge or stage) (154). The hydraulic data thus generated at pre-defined 64 cross-sections were normalised into 100 equi-spaced data points. Subsequently, in this chapter, cross-sections have been referred to as the 64 pre-defined spatial points and sections have been attributed to the 101 normalised spatial points.

#### 4.4 PROCESSING OF REMOTE SENSING DATA

Multi-date IRS-1A, 1C and 1D LISS III digital satellite data for the years 1990, 1997, 2000 and 2002 of the Brahmaputra river corridor were obtained for the study. These satellite images were procured for post-monsoon period (February), when cloud-free imagery was available and when water levels, vegetation cover and other ground conditions were relatively consistent, so that the morphological interpretations were not substantially affected. The study area covered the river Brahmaputra from Kobo at the upstream side to Dhubri at the downstream side which is 17.34 km from the Indian border with Bangladesh, for a

distance of 622.73 km. This area under study was represented by seven image frames merged into a single mosaic for each period. The images were analysed using the ERDAS IMAGINE 8.6 software for image processing & raster GIS analysis, and ARC/INFO for vector analysis. The steps comprised of -

- a. Data base geo-referencing
- b. Extraction of channel forms
- c. Preparation of NDVI layer
- d. Preparation of theme layers
- e. DEM preparation
- f. GIS analysis

The methodology adopted for remote sensing and GIS analysis has been shown in the flow chart (Figure 4.3).

#### **4.4.1 Data Base Geo-referencing**

In order to transform component images to the same co-ordinate system, 39 numbers of Survey of India (SOI) toposheets (Table 4.1) were converted into digital format and geo-referenced with twenty five or more Ground Control Points (GCPs) to form the master base map for registration of subsequent images.

The IRS images were geo-referenced by first projecting the data onto a plane, and then rotating and scaling to polyconic map projection system with respect to the geo-referenced topomap base. The geo-referencing was done using a second order affine transformation model with second order polynomial to create a geo-referenced image of pixel size 23.5m x 23.5m and 72.5m x 72.5m in case of LISS III and LISS I images respectively.

An *rmse* less than 0.5 pixel was obtained using the nearest neighbourhood re-sampling technique. Subsequently, other images were also co-registered with the geo-referenced images using image-to-image registration technique. Figure 4.4 shows the False Colour Composite (FCC) of the mosaic image frame of LISS III for the year 2000.

#### **4.4.2 Extraction of channel forms**

As is known, the incident energy in Near Infra-red (NIR) band striking on the water surface is highly absorbed; it appears blackish blue on the satellite imagery. In contrast to water, the land features absorb much less incident energy depending on land cover type, roughness, composition etc. This sharp contrast between land and water boundaries in NIR band makes the delineation of the river boundary from the land mass easier.

As the study reach was covered by seven image frames, these were merged into a single mosaic each for the years 1990, 1997, 2000 and 2002. The geo-referenced mosaic image frames of all the four years were used to delineate the active river segments, tributaries, islands and bars. The river braid belt was used to delineate the margins of the primary braided channel from each set of imageries and the channel patterns were digitized using ARC/INFO software to assess lateral movement between images for a spatial analysis of channel morphology over the period. On screen digitization of geo-referenced satellite data was carried out for the delineation of river boundaries.

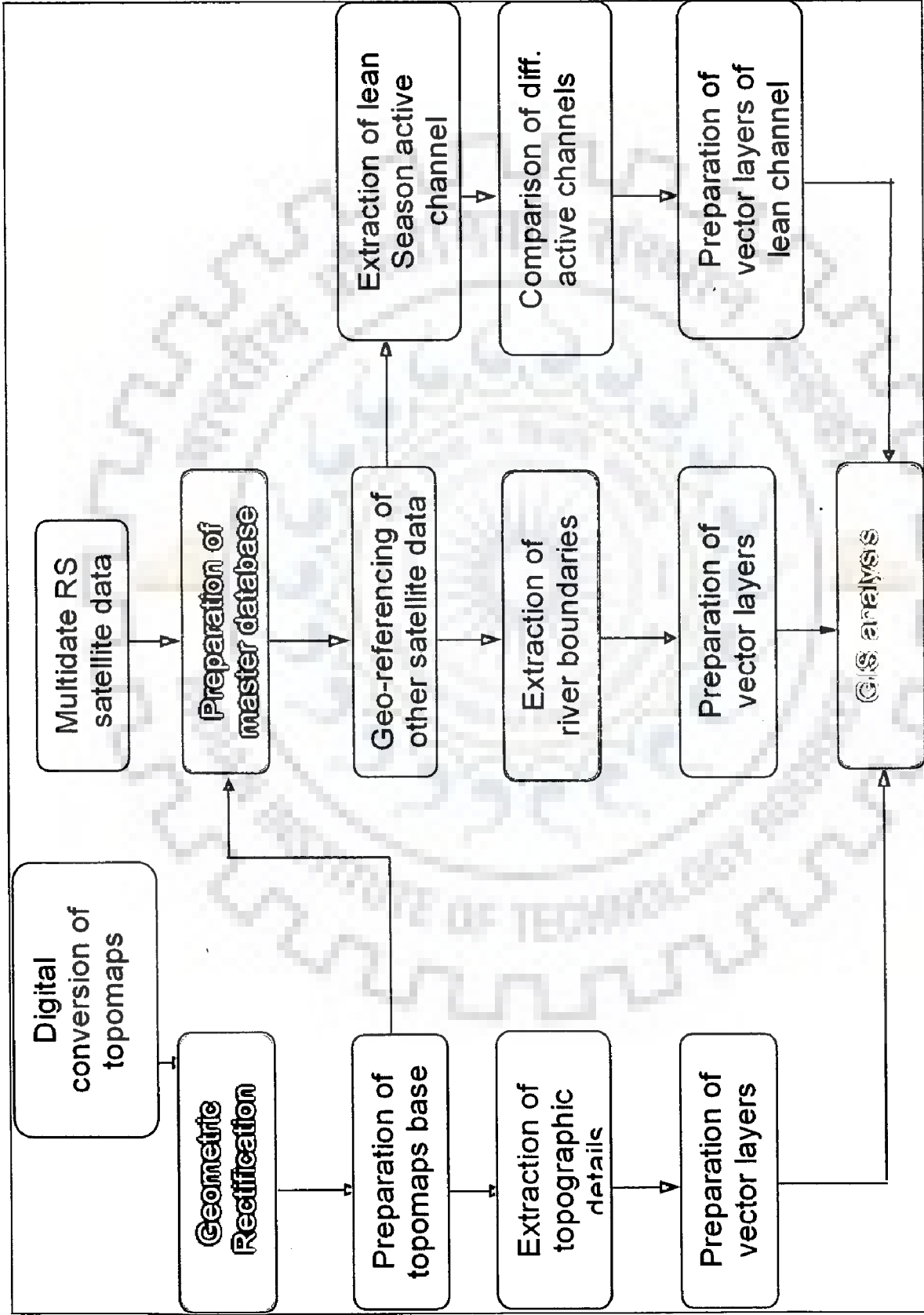


**Figure 4.3** Flow chart showing the methodology of image processing and GIS analysis

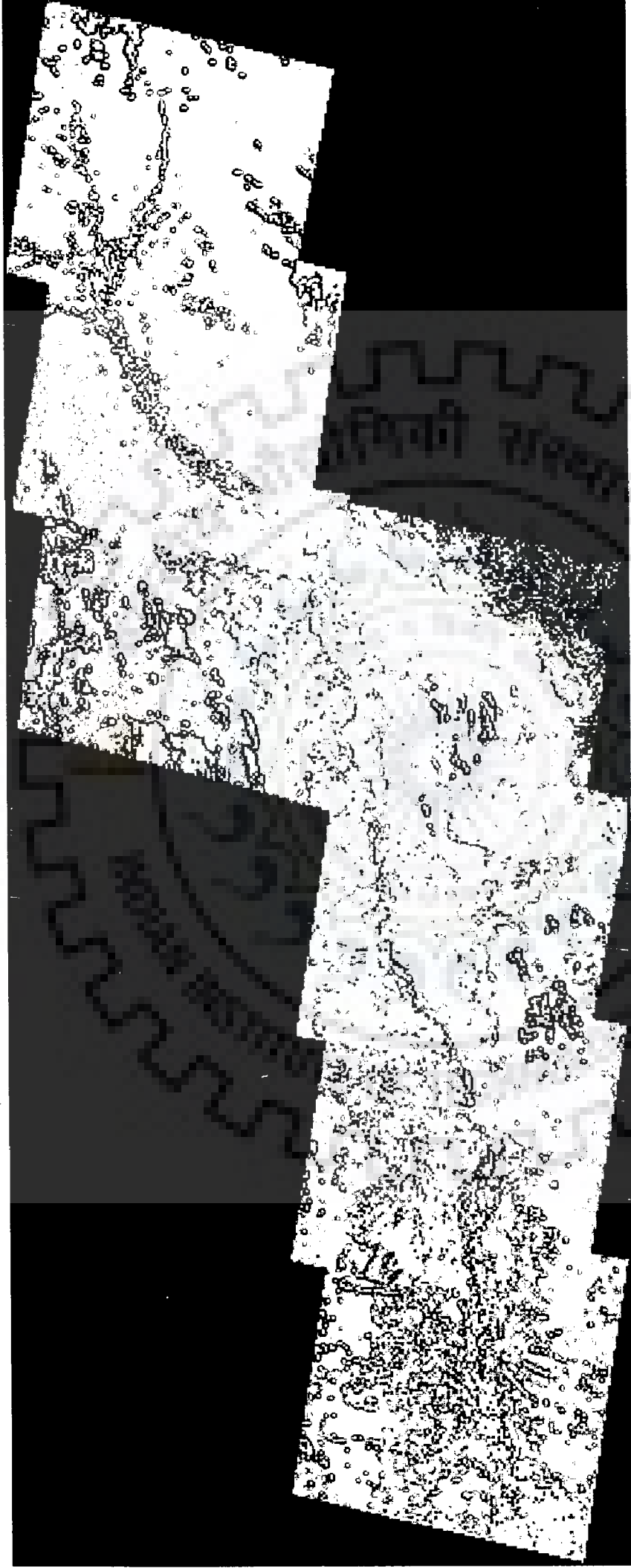


Figure 4.4 False Colour Composite (FCC) of the mosaic LISS III, 2000.

#### 4.4.3 Preparation of Normalized Difference Vegetation Index (NDVI) layer

The study area has been divided into seven reaches (Figure 3.3) as discussed in chapter 3, para 3.11. The mosaic image frames for all the years were prepared reach-wise and the variation in Normalised Difference Vegetation Indices (NDVI) for the Brahmaputra basin were found out reach-wise for different years to infer dominant trends in morphological variability response in the basin due to presence of vegetative cover in the flood-plain.

$$NDVI = \frac{(CH_2 - CH_1)}{(CH_2 + CH_1)} \quad (4.1)$$

Where, CH1 and CH2 are the spectral reflectance at near infrared and red wavelengths respectively. To highlight the vegetation classes, NDVI values were rescaled using the formula given below. The output generated gives the vegetation densities.

$$\text{Rescaled NDVI} = NDVI * 200 + 50 \quad (4.2)$$

The underlying principle for the analysis here is that presence of vegetative cover reduced the erosion and hence the transported silt load in stream flow was reduced. This was tested to provide new information and improved sensitivity to vegetation. As part of an effort to understand the pattern of the vegetation cover, the response of spectral vegetation indices to its temporal changes as well as their ability to discriminate among the major vegetation types encountered in the basin was studied. An assessment of the functional behaviour of this vegetation index with the sediment erosion was also made in this work. Such an investigation yielded a preliminary insight on the dominant trends over the Brahmaputra basin. Vegetation layers obtained by NDVI were density sliced to have four vegetation classes (Table 4.7). Figures 4.5 and 4.6 show the NDVI maps of the study area for the year 1997 and 2000. Figure 4.7 compares the NDVI images of the reach

number 1 in 1990 and 2002. Figures 4.8 to 4.10 present the trends of vegetation cover and sedimentation.

**Table 4.7 Classes in NDVI analysis**

<b>Vegetation category</b>	<b>class</b>
Very high vegetation	1
High vegetation	2
Medium vegetation	3
Less vegetation	4
Water	5
Sand bars/islands	6

#### **4.4.4 Preparation of Theme Layers**

The near static information on roads, rails, towns/villages were extracted from Radarsat satellite image of 2002 and Survey of India toposheets and stored in the form of different GIS layers in ARC/INFO format. The location of embankments prior to year 1990 has been derived from the Brahmaputra Atlas of Brahmaputra Board and transformed by digitization to ARC/INFO environment, which was used to carryout GIS analysis for river morphology for studying the protective structures on both banks. River morphology study was done by overlaying the river layers corresponding to different periods. Changes in river course, bank erosion, and adverse impingement on embankment and other river training works were detected from such analysis. The Figures 4.11 to 4.17 depict the planform view of the reaches showing embankments and their breach points by floods. The zones prone to severe damage by floods have also been marked on the figures.



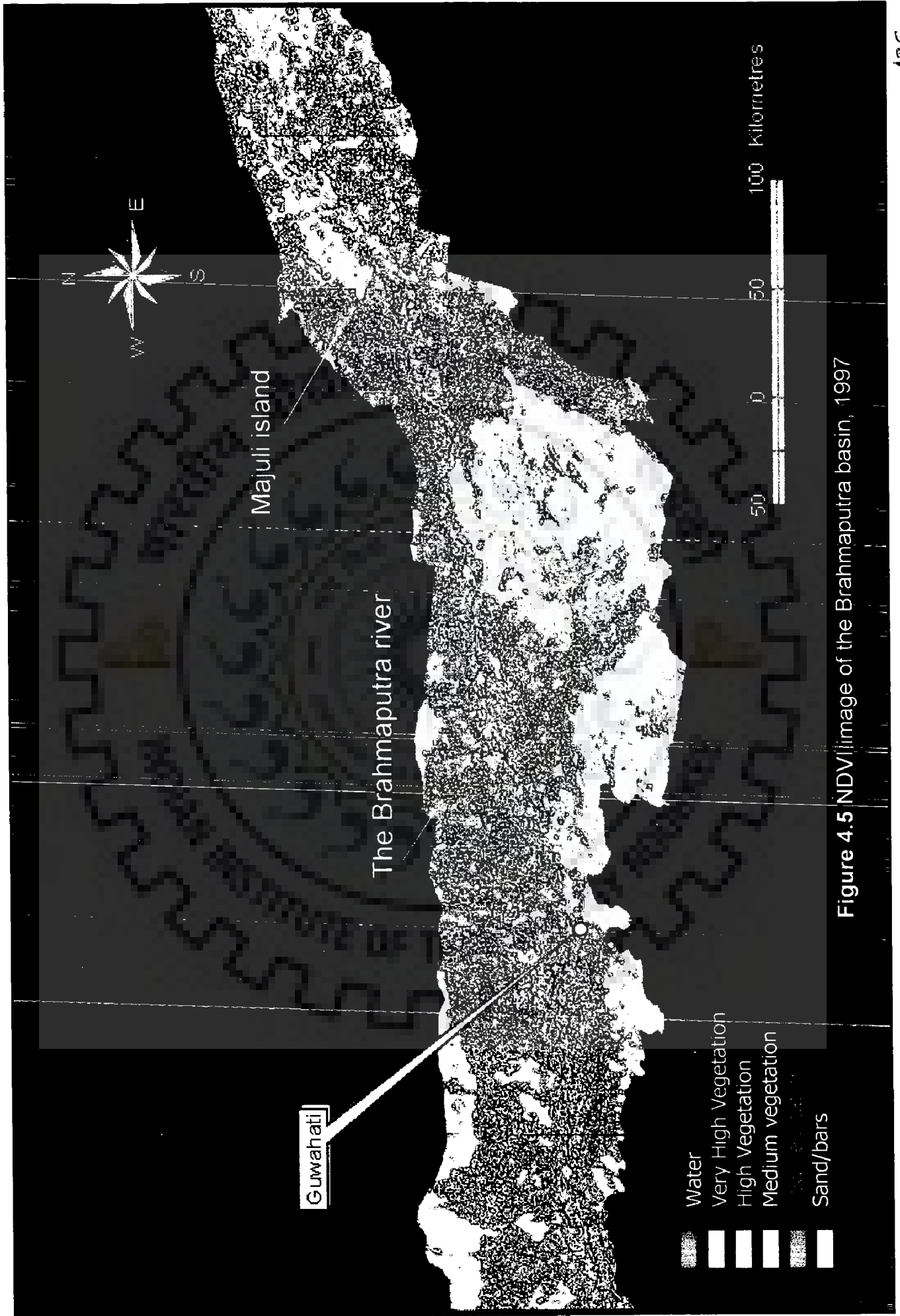


Figure 4.5 NDVI image of the Brahmaputra basin, 1997

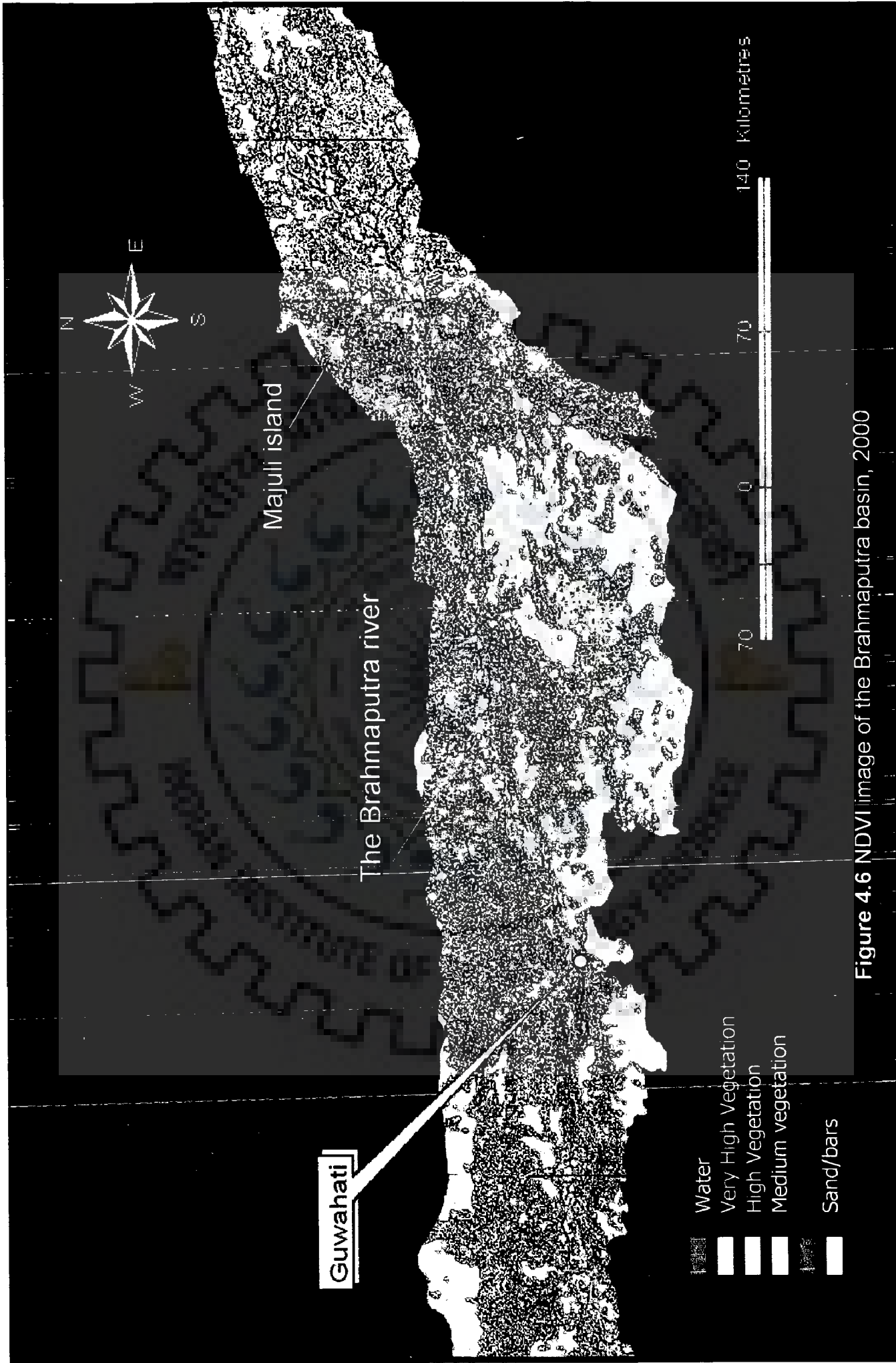


Figure 4.6 NDVI image of the Brahmaputra basin, 2000

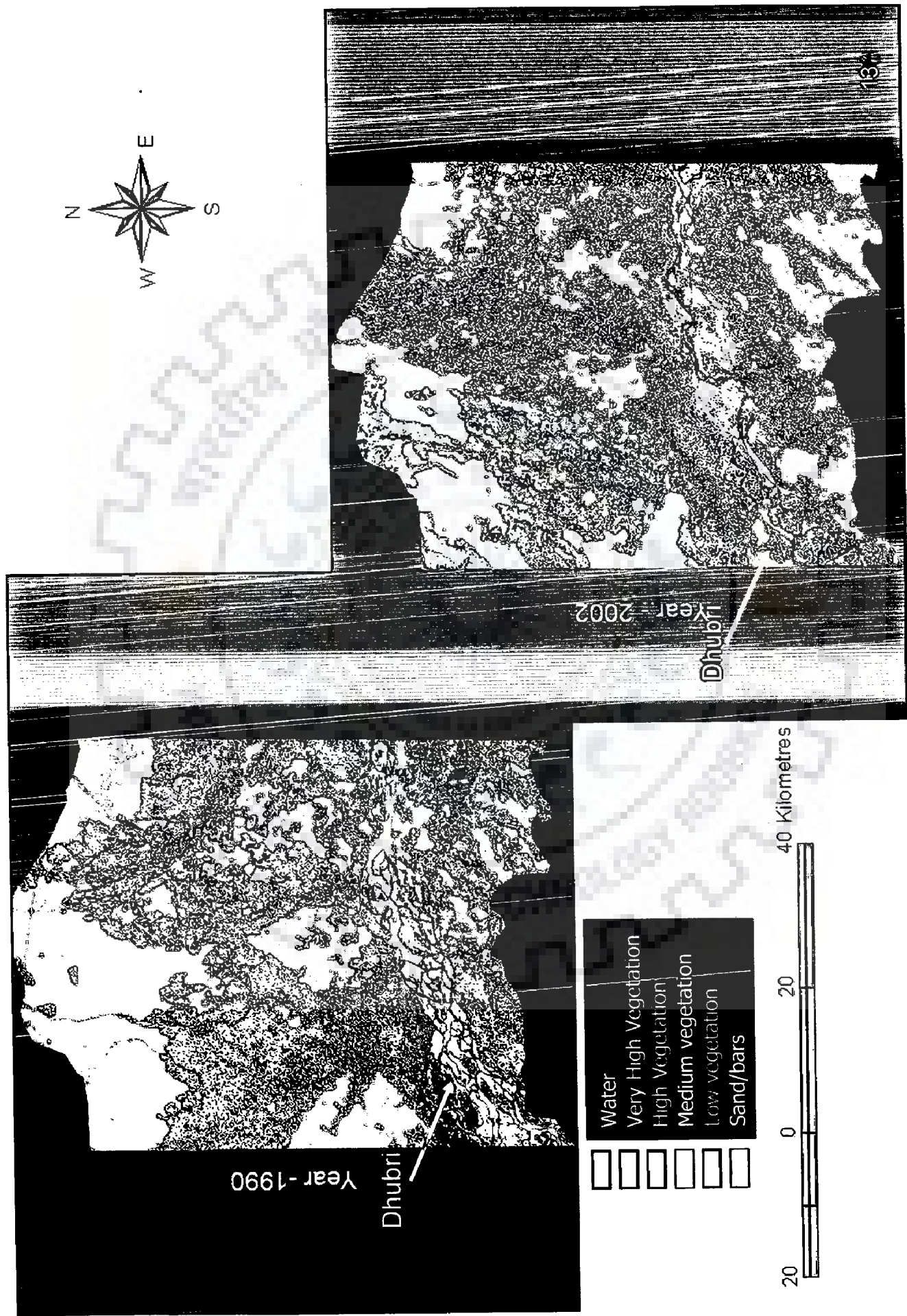


Figure 4.7 NDVI image of reach number 1 of the Brahmaputra basin

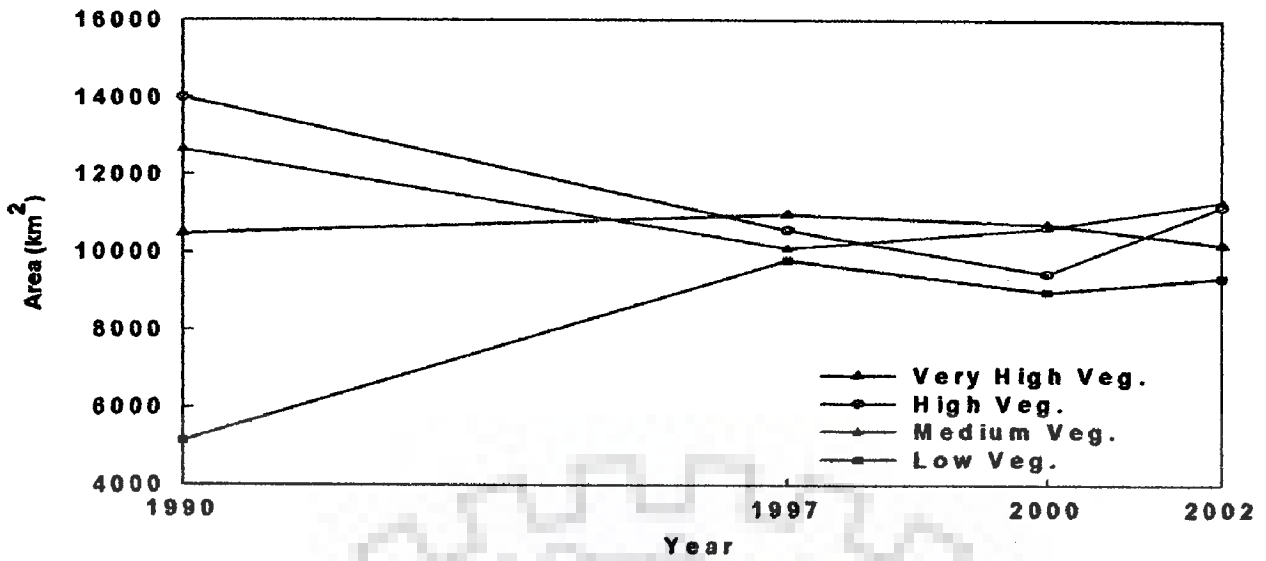


Figure 4.8 Trends of vegetation cover

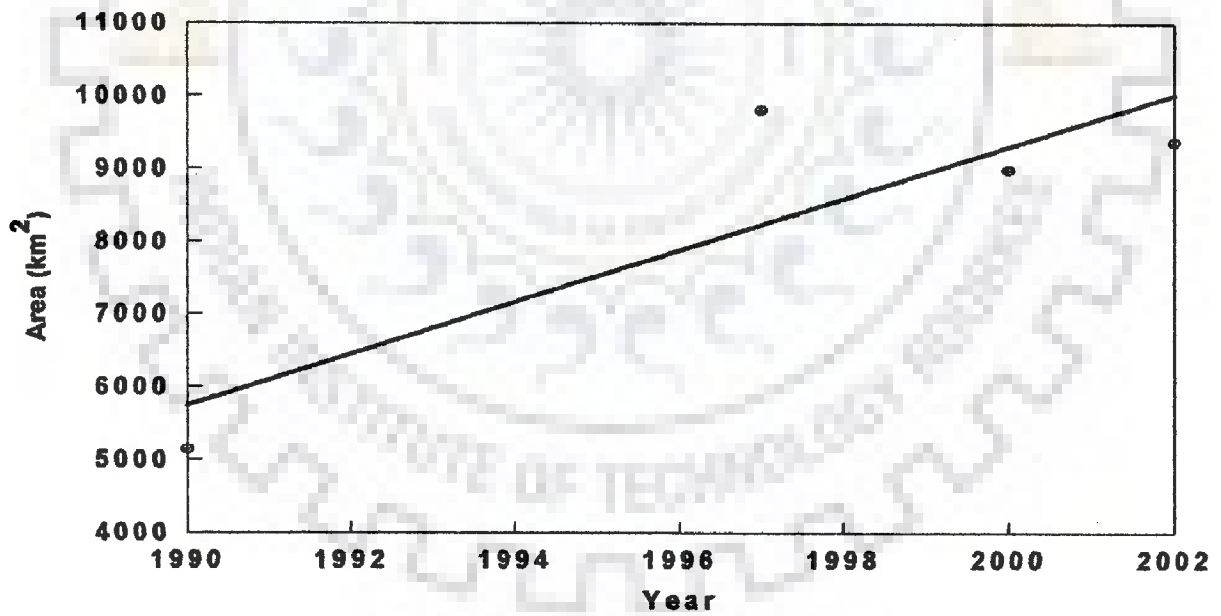


Figure 4.9 (a) Trends of low vegetation cover change in the basin

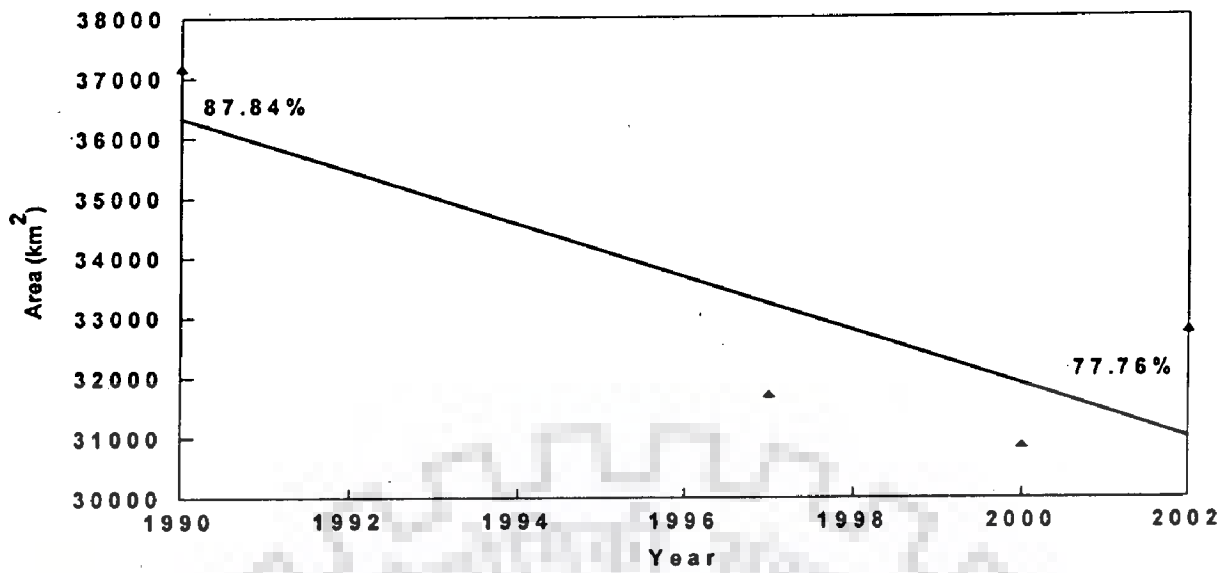


Figure 4.9 (b) Trends of high vegetation cover change in the basin

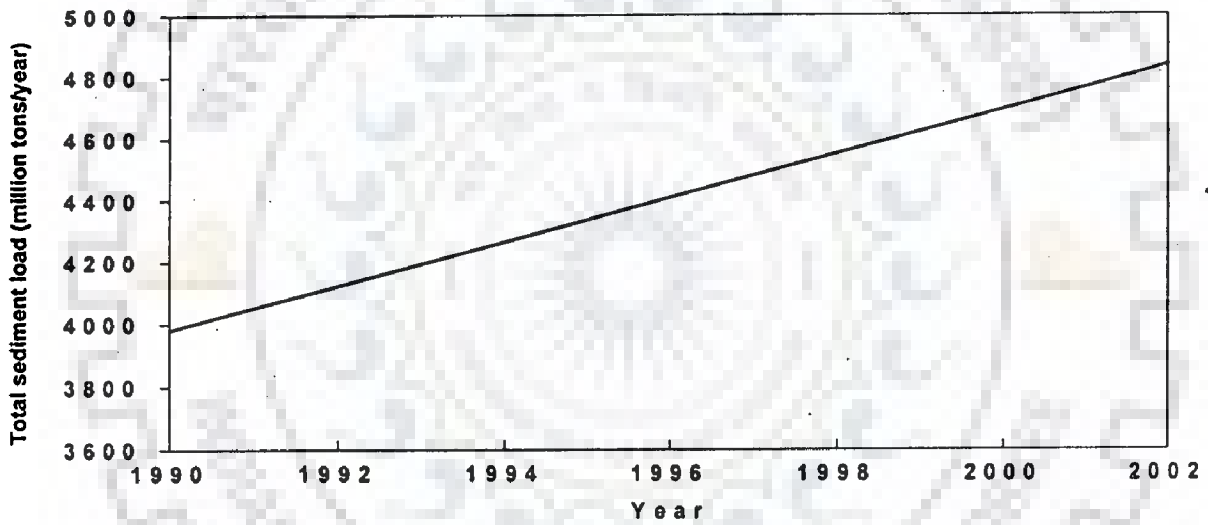
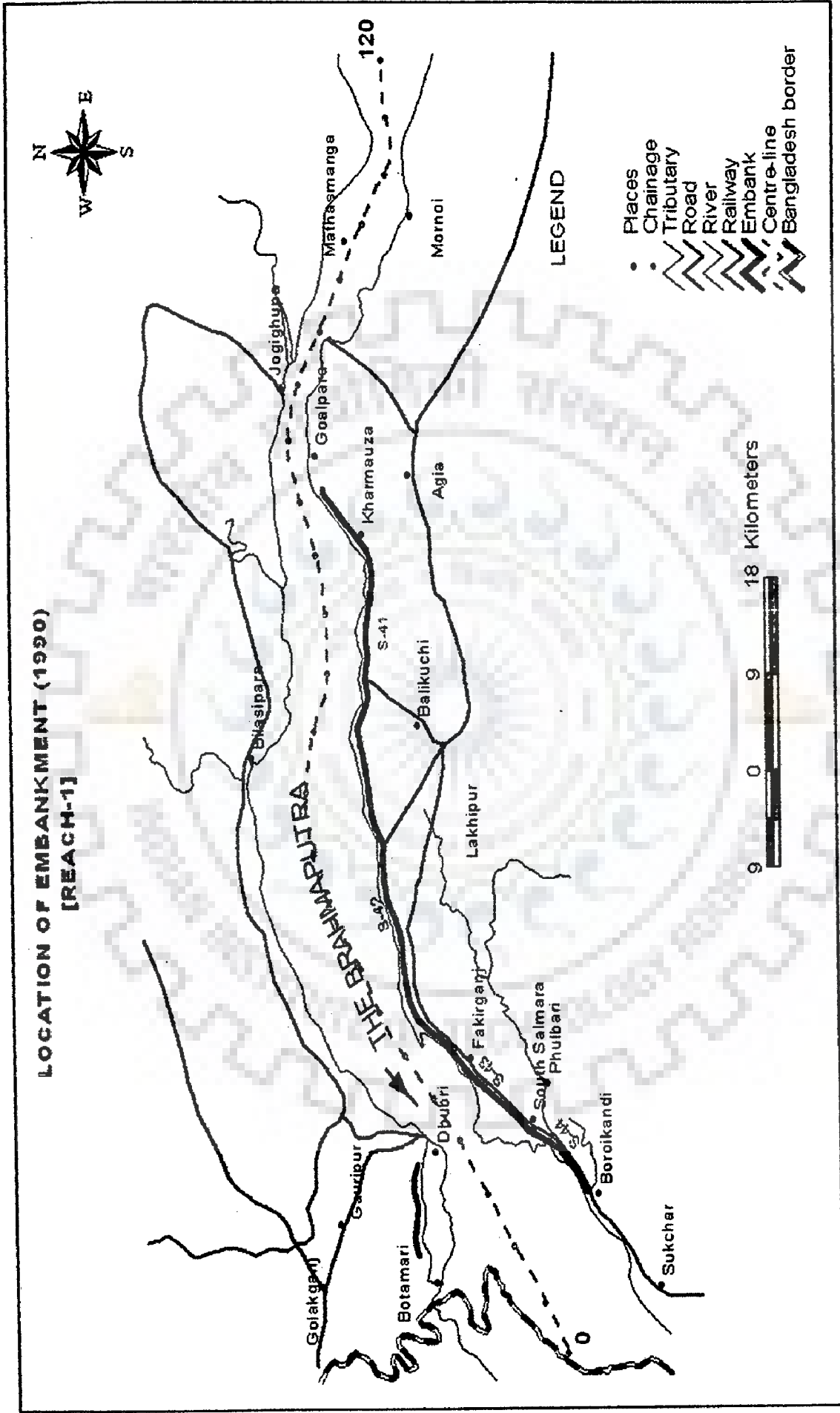
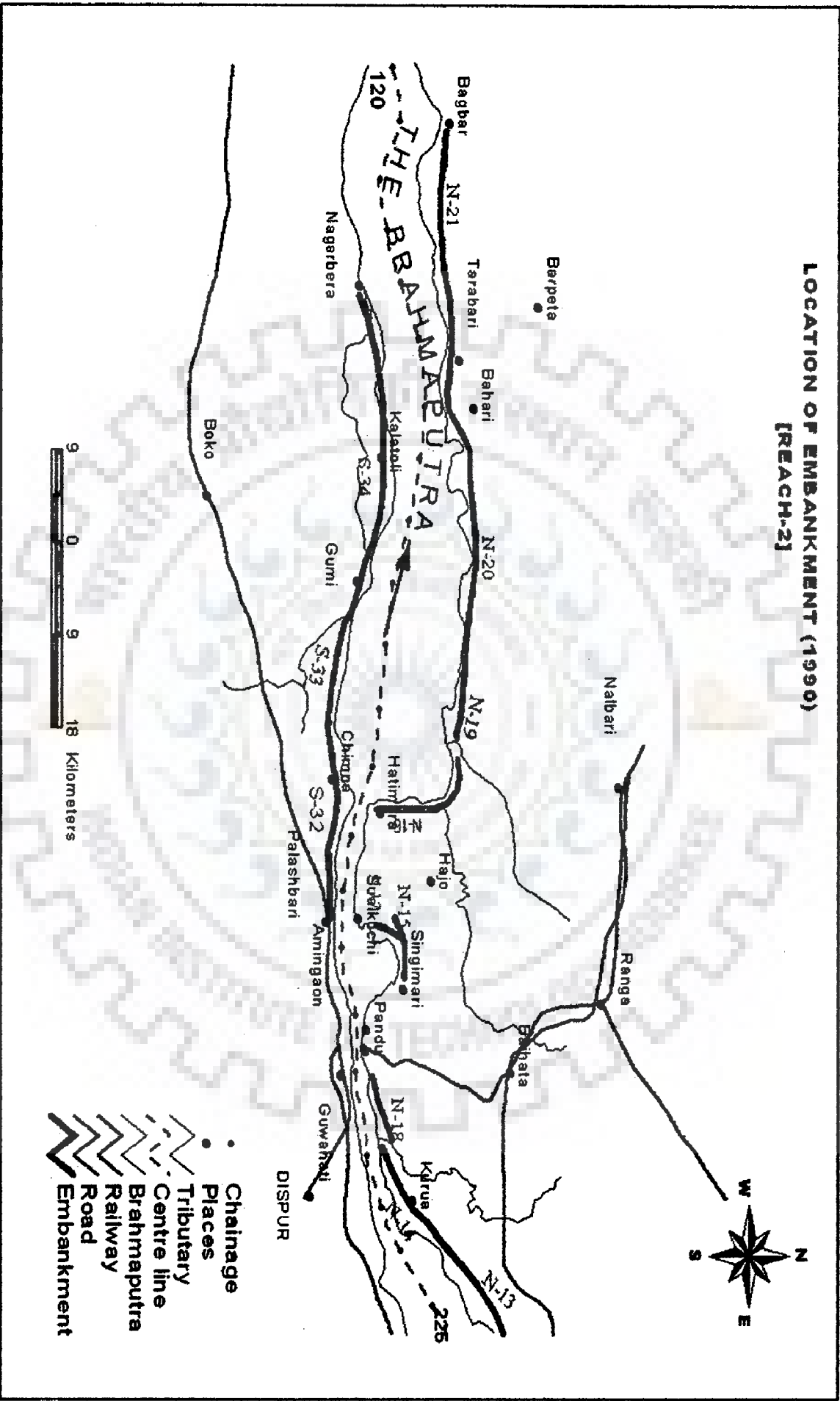


Figure 4.10 Trends of observed total sediment load at Pancharatna



**Figure 4.11** Planform & embankment locations in Reach I along the Brahmaputra, before 1990



**Figure 4.12** Planform & embankment locations in Reach II along the Brahmaputra, before 1990

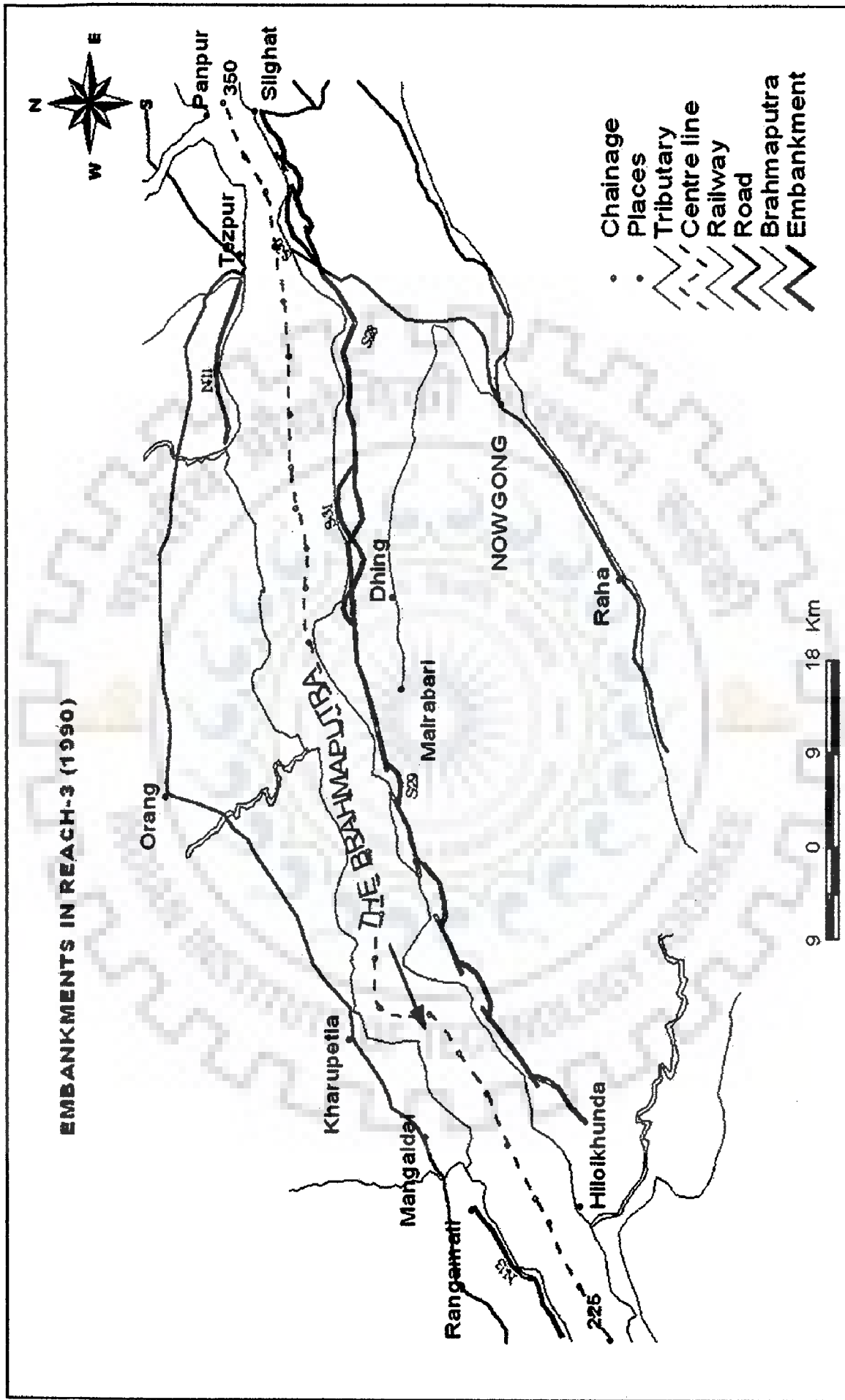


Figure 4.13 Planform & embankment locations in Reach III along the Brahmaputra, before 1990



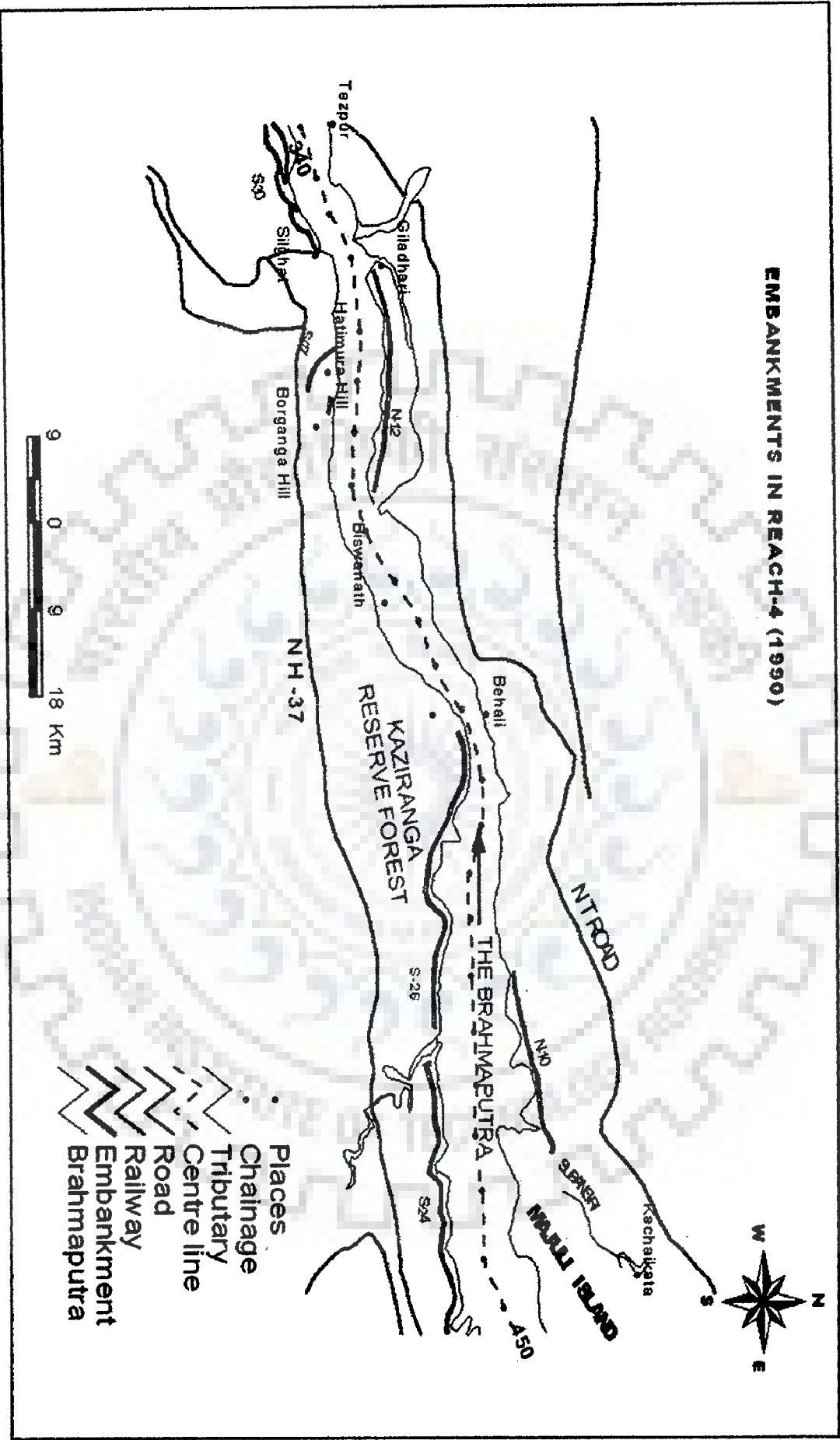


Figure 4.14 Platform & embankment locations in Reach IV along the Brahmaputra, before 1990

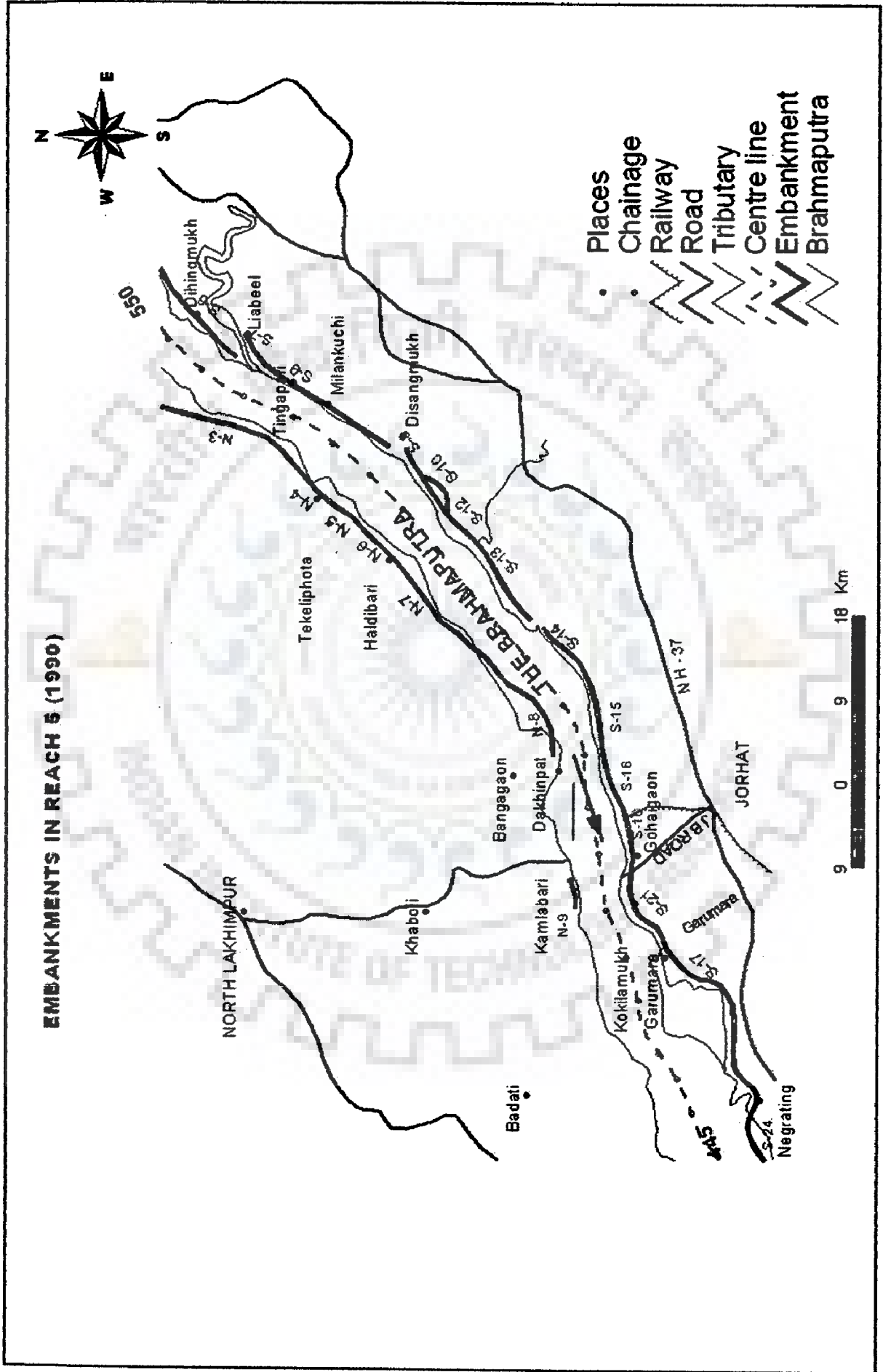


Figure 4.15 Planform & embankment locations in Reach V along the Brahmaputra, before 1990

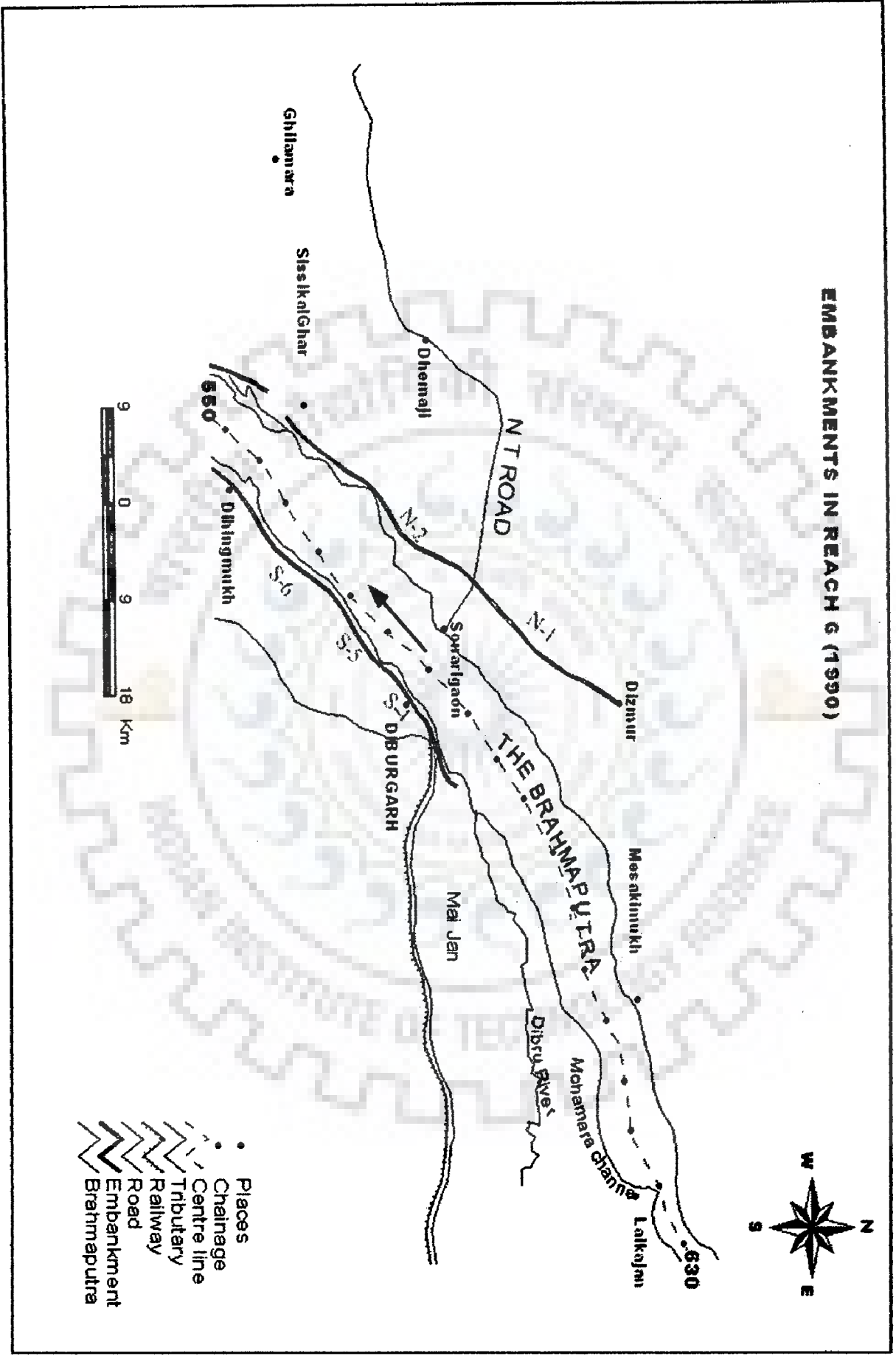


Figure 4.16 Platform & embankment locations in Reach VI along the Brahmaputra, before 1990

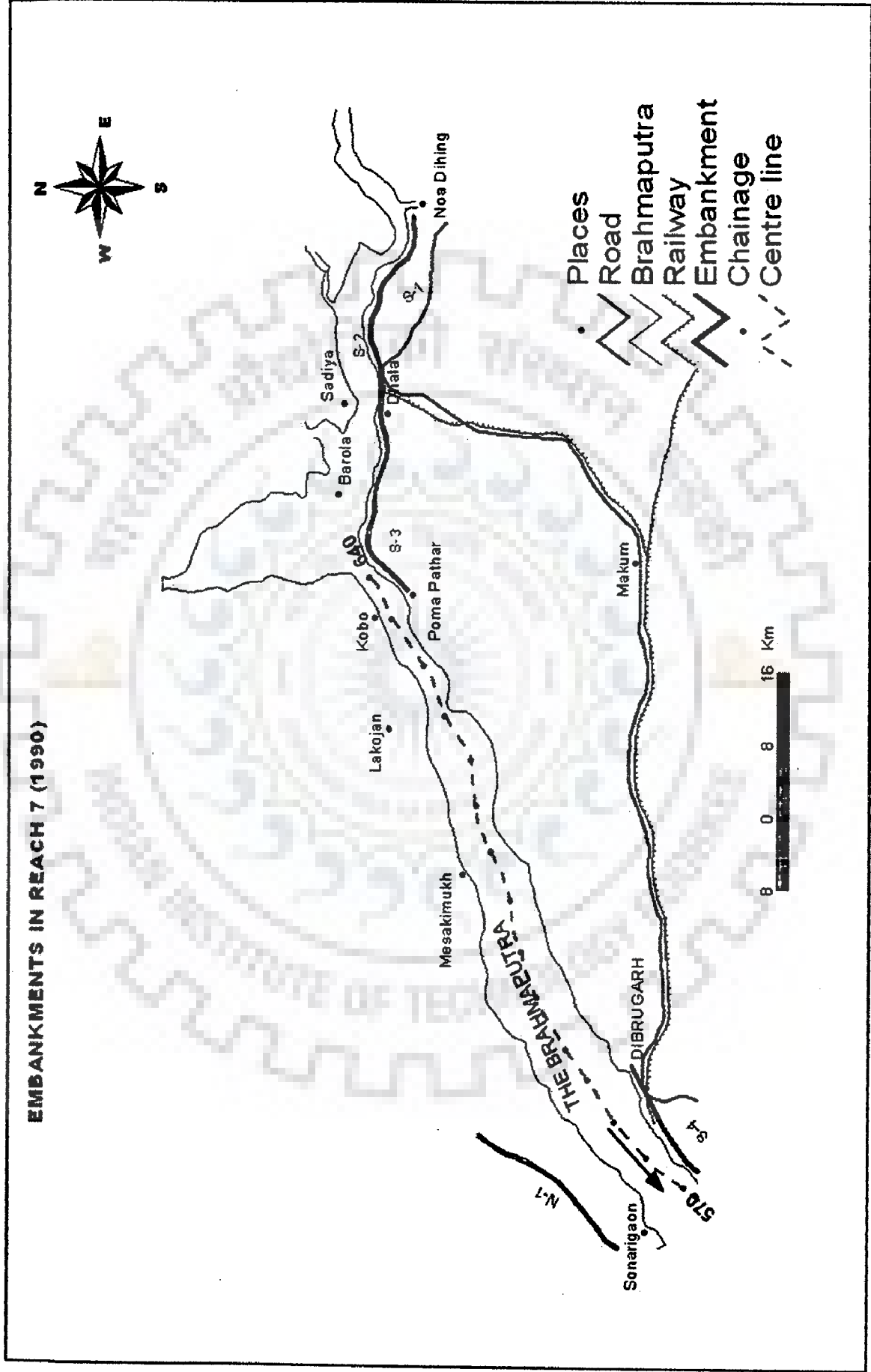


Figure 4.17 Planform & embankment locations in Reach VII along the Brahmaputra, before 1990

#### **4.4.5 Digital Elevation Model (DEM)**

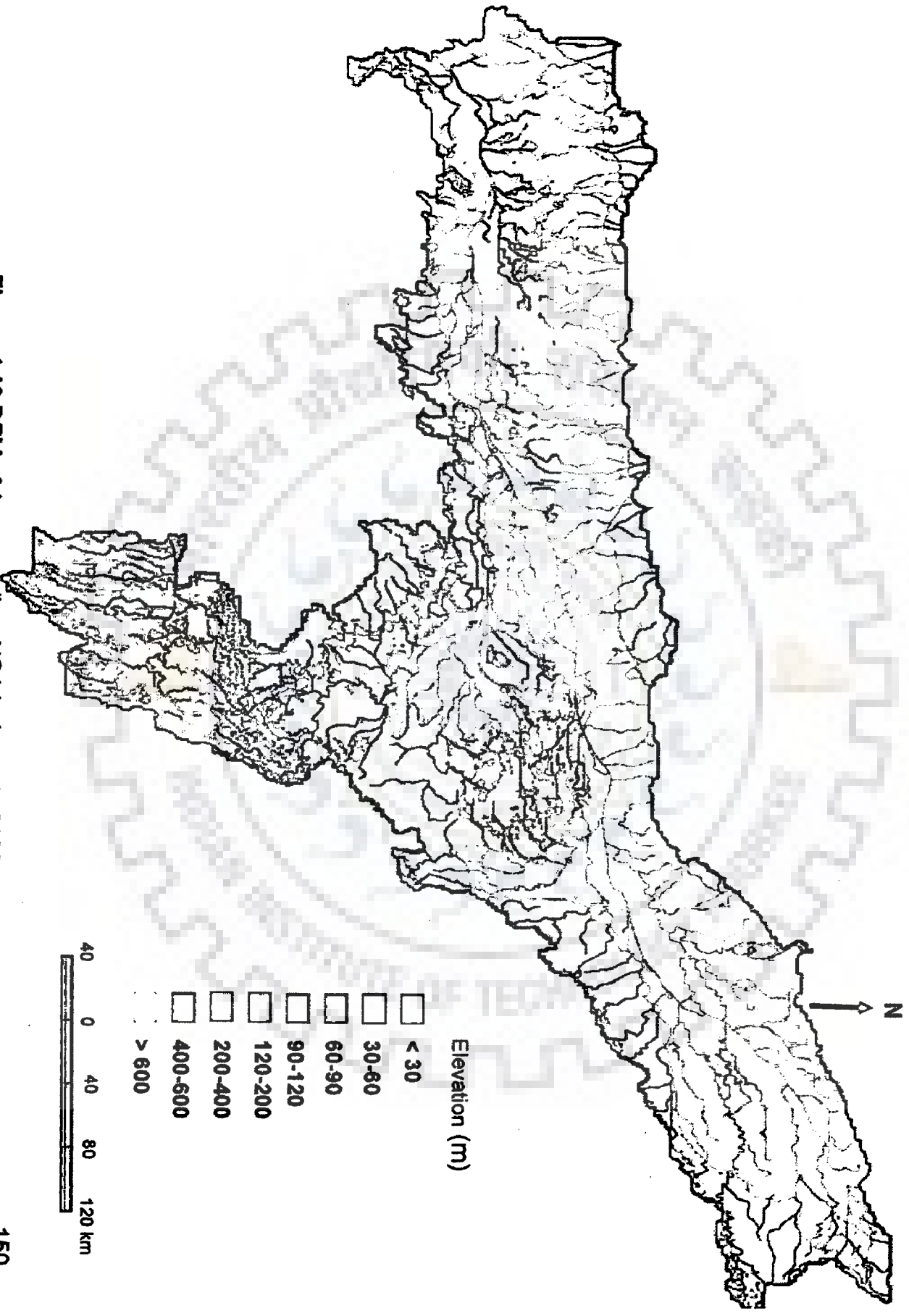
Digital satellite data provided by National Oceanographic & Atmospheric Administration (NOAA), AVHRR sensor having spatial resolution of 1.1 km for the year August, 2002 has been used for deriving the Digital Elevation Model (DEM) and shallow and deep flooding phenomena in the Brahmaputra valley. The DEM has been evolved by regular array of contour values referred to a common datum, which represents and appreciates the terrain relief. Figure 4.18 shows the FCC of NOAA data. The elevation range was divided into eight classes from 30m to over 600m. DEM map was prepared with drainages overlaid as shown in Figure 4.19. Figure 4.20 depicts the shallow and deep flooding map based on arbitrary classification of the Assam area into three classes.

#### **4.5 GIS ANALYSIS**

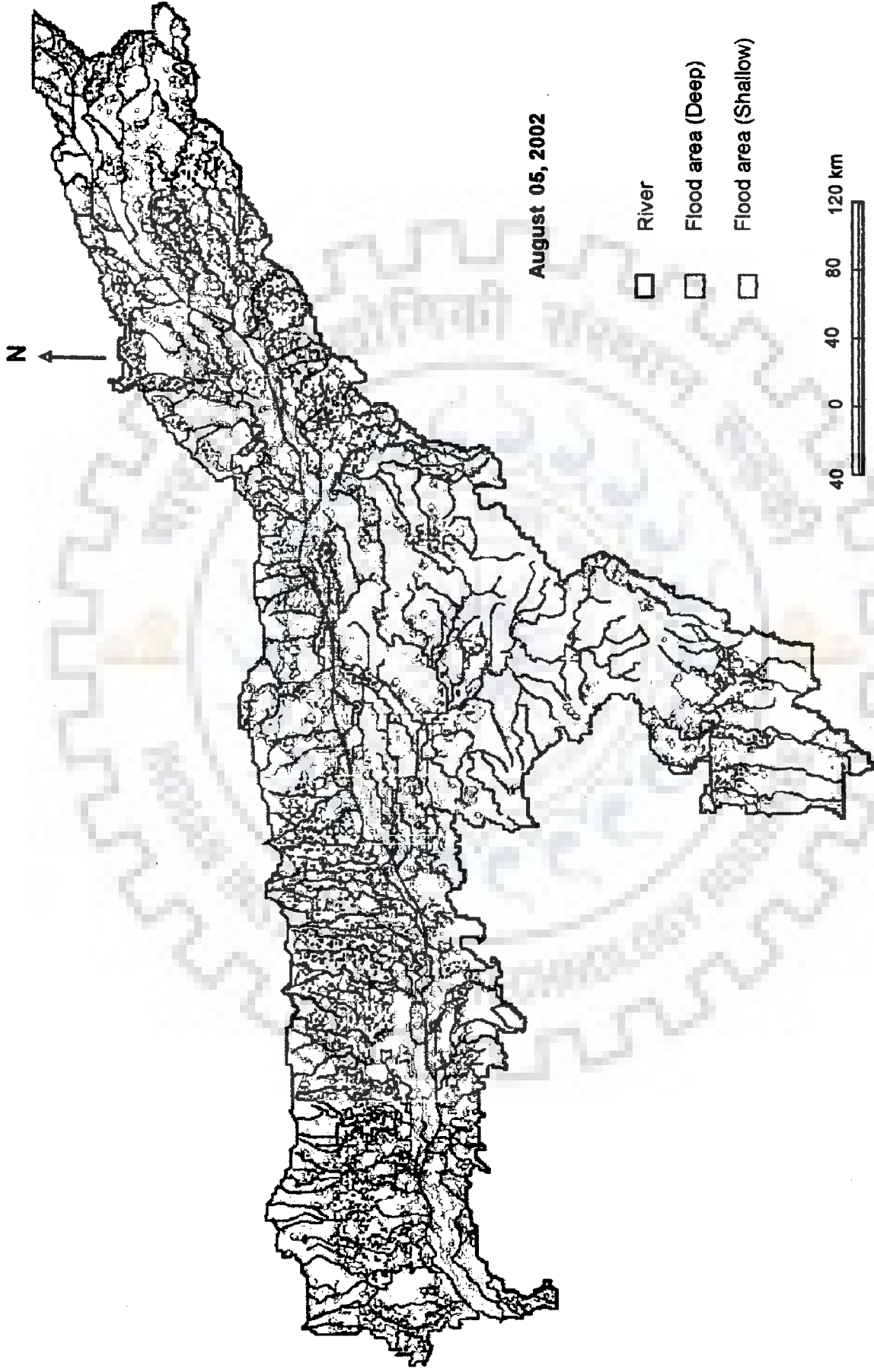
Some of the advantages of using a GIS are the convenience of data storage; the ease of statistical analysis and data manipulation, including quantification of error; and the flexibility of graphical display. The conceptual GIS for morphological study of river Brahmaputra includes map base creation, overlay preparation and analysis. In addition, dynamic information extracted from the analysis of satellite data for the lean season of 1990, 1997 and 2000 as well as active channel in February, 2002 were registered as GIS layers. A quantitative assessment of fluvial landform pattern with the aid of GIS was studied in this work. ANN models, later discussed, allowed prediction of spatial and temporal patterns of erosion and deposition on the floodplain and the creation and consumption of substrates for plants and animals. Such models could make predictions of bank erosion and deposition rates through time that correlate with the observed rates.



Figure 4.18 FCC image of NOAA, August , 2002



**Figure 4.19** DEM of Assam valley, NOAA, August, 2002



**Figure 4.20** Deep and shallow flooding map of Assam valley, NOAA, August , 2002



#### **4.5.1 Mapping of River Configuration Changes**

The river Brahmaputra changes the courses of its braided channels frequently after every flood wave, attacking different locations at different times. The river, which is under dynamic equilibrium with fluvial as well as seismotectonic processes, does not present stable river configuration. Channel forms of the river Brahmaputra could be the result of dissimilar causes, and because channel adjustments migrate over time and space and possibly affect previously undisturbed reaches, it was felt essential to properly identify and quantify the overall fluvial landform change and not just the local symptoms. Hence, it becomes necessary to understand the behaviour of the river and its latest configuration downstream, to plan and implement the river protection measures. It is equally important to monitor the existing flood control structures from time to time to avoid embankment breaches in view of frequent changes in river configuration due to varied flow conditions. Acquisition of timely and reliable information about the flooded areas, watershed areas, river behaviour and configurations becomes a necessity.

On superimposing non-flood season river channel boundaries of the years 1990, 1997, 2000 and 2002, it was found that due to floods, there were channel deviations at many locations from the river course of 1990, and whereas at some locations, the channel remained more or less within the normal water way - largely due to construction of embankments on both banks. The active channels were continuously changing direction from one bank to another. The river behaviour and the configurations along the river qualitatively and quantitatively were presented reach-wise in the following paragraphs.

## 4.5.2 River behaviour and Configurations from 1990 to 2002

### 4.5.2.1 Reach- I (From Fakirganj to Goalpara)

This reach has a length of 65.28 km. The average width of the river in this reach is 8.9 km. The minimum width is 1.25 km at Pancharatna. During flood, the river in this reach is one sheet of water from bank to bank and has a maximum width of 16.0 km at cross-section 7. The gradient of the river from Goalpara to Dhubri is 1 in 14,650. Tributaries Tipkai, Saralbhanga (Gaurang) and Champamati, which join the river from north, from their origins in the Bhutan Himalayas. The south bank tributaries of this reach are smaller compared to the north bank ones, because of the closeness of the Meghalaya Plateau on the south. Another notable river, the Jinjiram, drains its basin from this reach. It divides itself into two anabranches, one of which joins the river near Indo-Bangladesh border and the other meets the old Brahmaputra near Divanganj in Bangladesh.

The river Jinjiram has been under active avulsion process in this reach (Figure 4.21). It separated out at the south side from the Brahmaputra river near downstream side of cross-section 5 and joined with the main Brahmaputra at about 7.98 km downstream side of the Phulbari town. There was a sagging of the river loop towards north bank at cross-section 3 amounting to 6.5 km in the year 2002 as compared to the year 1990. At cross-section 5 and 8, the river width has widened by 0.56 km and 0.39 km respectively. The river width at Dhubri has increased by 0.95 km over 13 years. At cross-section 4 and 6, there was no significant change in width.

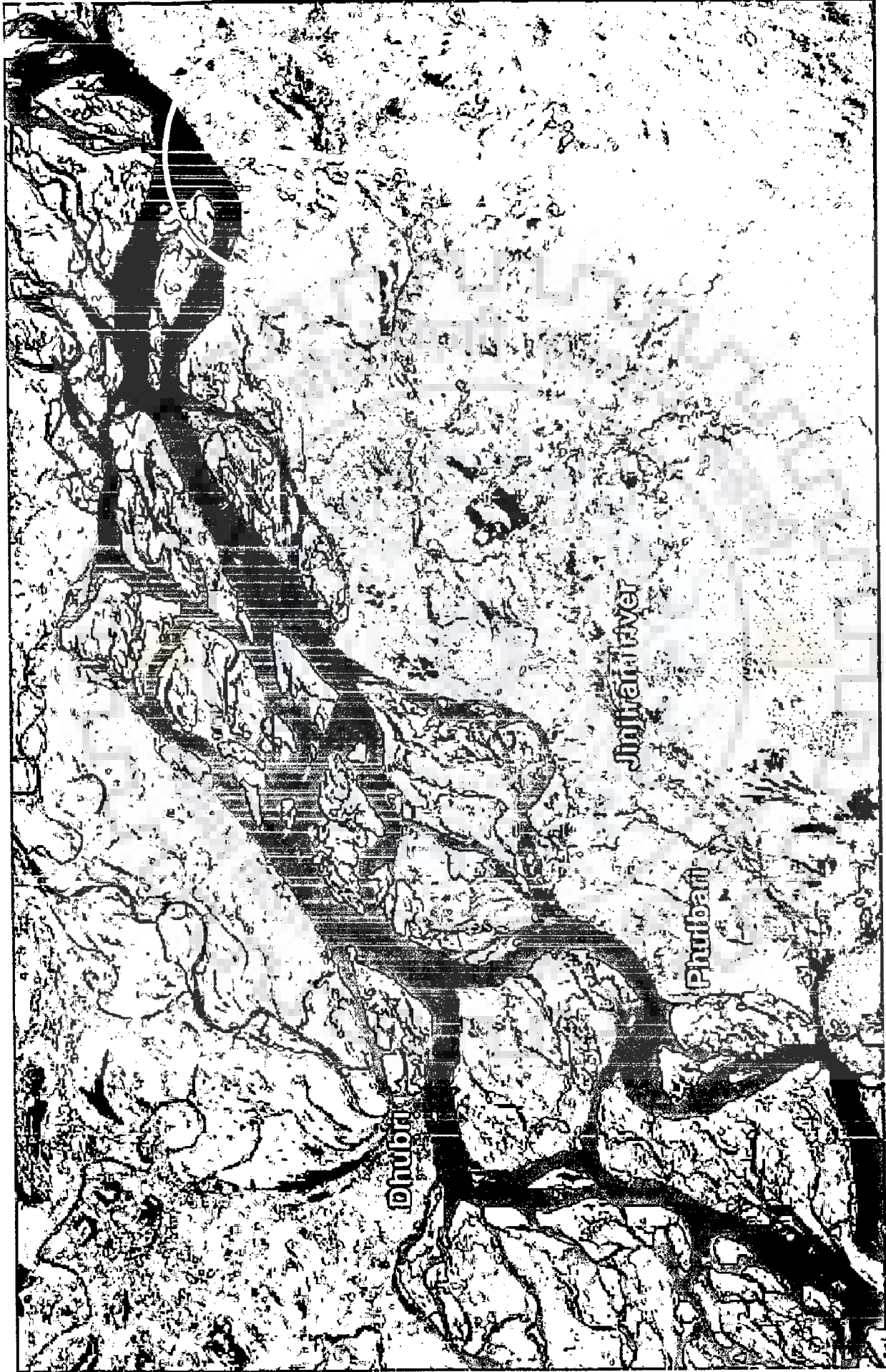


Figure 4.21 Avulsion by Jinjiram river near Dhubri, 2002

Figure 4.22 depicts the configuration of the river in this reach. The important townships of this reach are Goalpara on the south bank and Dhubri on the north. The river was navigable throughout the year in this reach.

The embanked reach is from Kharmuza, about 20 km downstream of Goalpara, upto Hazirhat located within the Goalpara and Dhubri districts. The embankments in this reach are (i) from Kharmuza to Balikuchi (length 19.80km) (ii) Balikuchi to Fakirganj to South Salmora (length 4.55 km) (iii) South Salmora to Baroikandi (length 4.55 km) and (iv) Baroikandi to Hazirhat (length 7.90 km). It was observed that the protection structures have been fairly stable against high floods, and at some sections breaches occurred due to recurring erosion.

#### **4.5.2.2      *Reach-II (From Goalpara to Palasbari)***

This reach has a length of 89.76 km. The average width of the river in this reach was 11.6 km. The gradient of the river from Pandu to Goalpara (115 km) was 1 in 8875. Bhutan Himalayan tributaries, viz., the Puthimari, Pagladiya, Manas Beki, Kujia join the river from north. There are also many important sub-tributaries in this reach. The Sessa and Borolia are two notable rivers, being tributaries of the Puthimari and Pagaldiya, respectively. A branch of the Pagaldiya, called the Buradia, has joined successively by the Mora Pagaldiya, Tihu, Kaldia, Pahumora and Palla. This unified flow meets the Beki, which is a branch of the River Manas. The Manas is the biggest tributary of this reach. It finds its origin as the Kuru Chu from a glacier in the northern slope of Mount Kula Kangri (28° 15' N, 90° 35' E) in Tibet. After flowing for 90 km through Tibet and 140 km through Bhutan it bifurcates near the Indian border to create the Beki. The Manas and the Beki flow individually for 112 km and 198 km respectively through the Assam Valley before meeting the Brahmaputra.

The Manas is known as the Kar in Bhutan, where it joined by its major tributary the Dongma. The Manas has a length of 375km and drains a basin of 38,176 km<sup>2</sup> with a maximum discharge of 7,641m<sup>3</sup>/sec. It contributes 5.48% of total discharge of the Brahmaputra. The Aie is the main tributary of the Manas in India. The tributaries of this south bank reach are the Khana, Kalmani, Kalbhog, Kulsī, Deosila, Habri, Krishnai and the Balbala (Jinari). The Kulsī and the Krishnai are two notable rivers in this reach. The Rani is the major tributary of the Kulsī and the Dudhnai that of the Krishnai.

The unchanged maximum width of the river was 18.13 km in 2002 at downstream side of Pandu at cross section 17 near Gumi and the minimum width of the river was 1.2 km at Pandu and has not changed its width over years due to constrictions by the underlying geological formation near Saraighat bridge. The Hatimura hill on north and Dakhala hills on south has held the river constricted by the rocky banks. The excess stream power carried by the river has been expended in widening its width at the alluvial banks near Chimpa. At section 15, just upstream of Nagarbera the river width has registered an increase of 1.28 km. At the south bank, there has been deposition of 2.2 km and at the north; the erosion was about 0.92 km wide. Figure 4.23 shows the FCC image of the fanning out portion at the downstream side of Guwahati. The length of mid-channel island inscribed by the river periphery near Gumi was about 18 km long and 4.90 km wide. Figure 4.24 depicts the temporal changes in the channel configurations of the reach.



Figure 4.22 River configurations in Reach I of the Brahmaputra



Figure 4.23 Radarsat image (FCC) at d/s of Guwahati

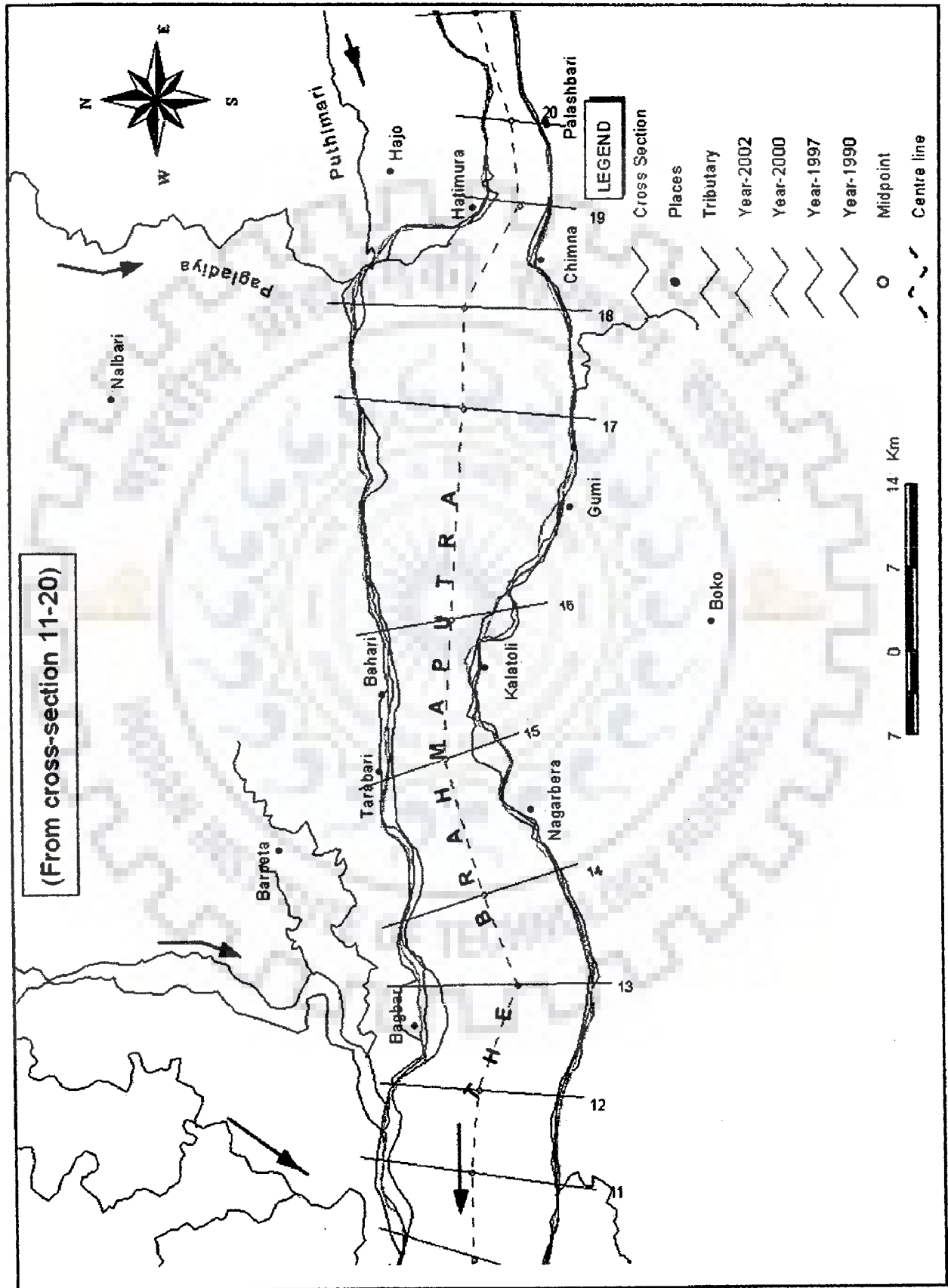


Figure 4.24 River configurations in Reach II of the Brahmaputra



#### **4.5.2.3 Reach-III (From Palasbari to Tongani)**

The reach was about 79.57 km in length. The average width of the river in this reach was 7.0 km. The river flows in this reach through alluvium with inselbergs at some places. The gradient of this river in this zone from Neamati to Pandu was 1 in 6571. The river has braided channel configuration except at Pandu where it was constricted into a single channel of 1.2 km width. This was the narrowest point in the entire reach. The river was navigable in this reach throughout the year and has the important townships of Guwahati on the south. On the north bank progressively from east are the Noanadi and from south, the big tributary of Kopili. Within the enclave of the Kolong and the Brahmaputra the Kadam, Leteri, Sonai, and Mora Sonai join the Brahmaputra. Beyond the outfall of the Kolong, two small rivers, the Amchang and the Bharalu join the Brahmaputra on the east of Guwahati city.

Figure 4.25 shows the river planform of the reach. Near Rangamati, the river has not changed its course and the flow was confined to the same channel as it was in 1990. But at Lahorighat (cross-section 27), the river has eroded the left bank by an amount of 2.64 km and at Kharupetia (cross-section 28), the river width has increased by 0.32 km. At cross-section 29, the river width has increased by 1.32 km. In 1997, the river at the above sections could not change much, but after 2000, the erosion at these sections has given the waterway to incise the flood plain. Other portions of the river did not register much change during the period from year 1990 to 2002.

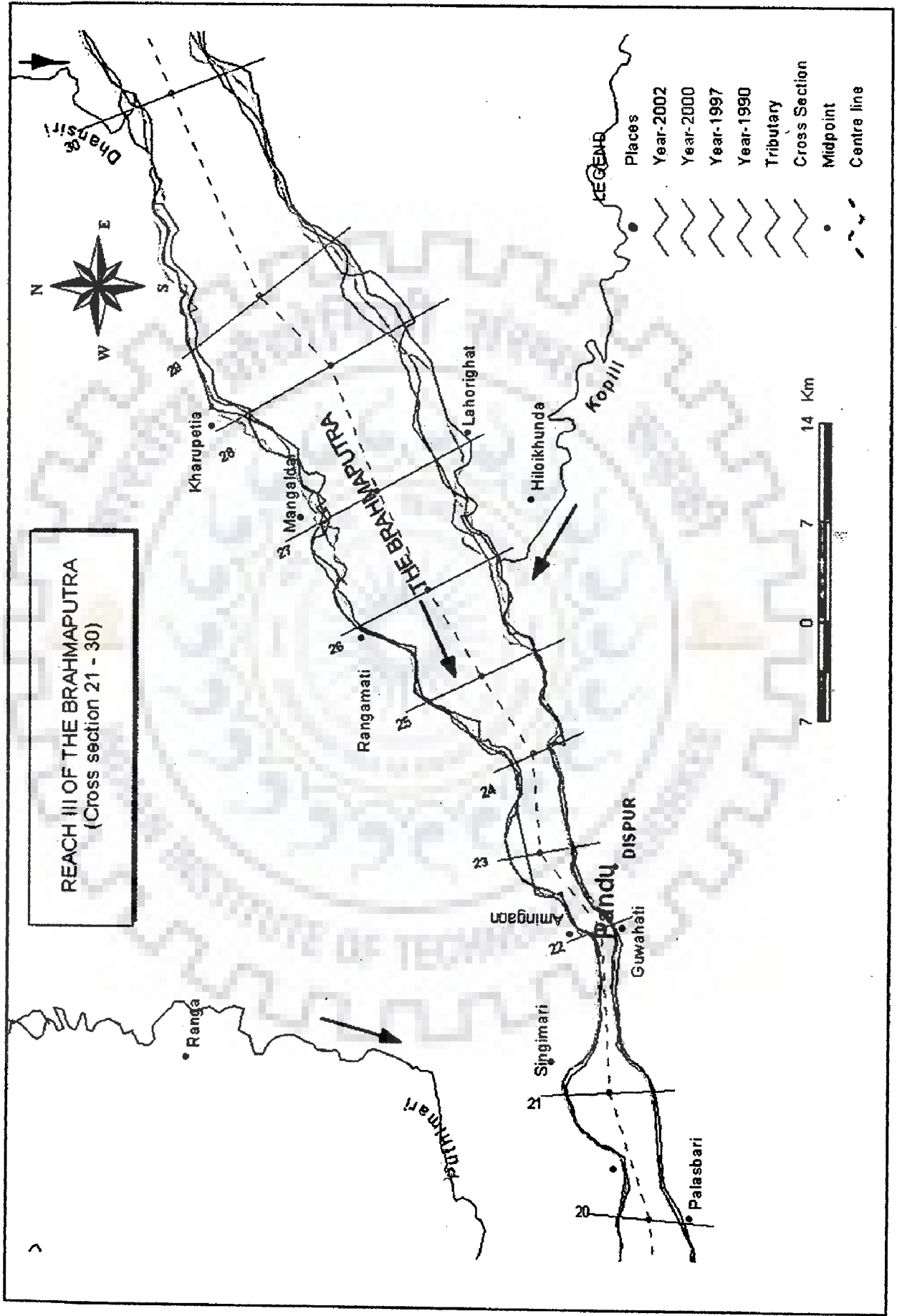


Figure 4.25 River configurations in Reach III of the Brahmaputra

#### **4.5.2.4 Reach-IV (From Tongani to Behali)**

This reach was about 120.88 km in length. The average width of the river in this reach was 7.0 km. The river was navigable in this reach throughout the year and has the important townships of Tezpur on its north bank and Nowgaon on the south. A great number of tributaries of various magnitudes meet the river along this reach. On the north bank, progressively from east are the Ghiladhari, Jia Bhareli, Gabhru, Belsiri, Panchnoi, Dhansiri (north), Borgang, Doipham, Mora Dhansiri, Dhansiri. The biggest amongst them is the Jia Bhareli, which is a snow-fed Trans-Himalayan river. It enters India as the Kameng river. It has a length of 264 km in India and drains a basin of 14,450 km<sup>2</sup>.

The Tenga and the Dikrai are the two principal tributaries of the Jia Bhareli. The Jia Bhareli contributes about 4.9% of total discharge of the Brahmaputra. On the south bank of this reach, the Brahmaputra is met by the Diphlu and Mora Diphlu and tiny Borghop from east. Thereafter, the river shoots off a branch called Kolong Suti near Kukurakata hill. The Kolong has now plugged at the upstream entry point and it does not depict any characteristics of the main braided river. On the contrary it is a perfectly meandering river. There is ample evidence to regard it as the lower reach of the Dhansiri, detached from the latter owing to erosion of the Brahmaputra. The Kolong has a length of 160 km, it receives small rivers, such as the Nanai, Misa, Diju, Haria and Digaru and also a big river, the Kopili.

As seen from the Radarsat satellite image in Figure 4.26, rock outcrops of the north side and Kamakhya hills on south near Silghat constricted the river passage into a narrow single channel of 1.2 km width and near the Kaliabhomora bridge, the river has increased its width to 2.7 km and could not open up further due to the presence of Agnigarh hills of Tezpur town in the north and an

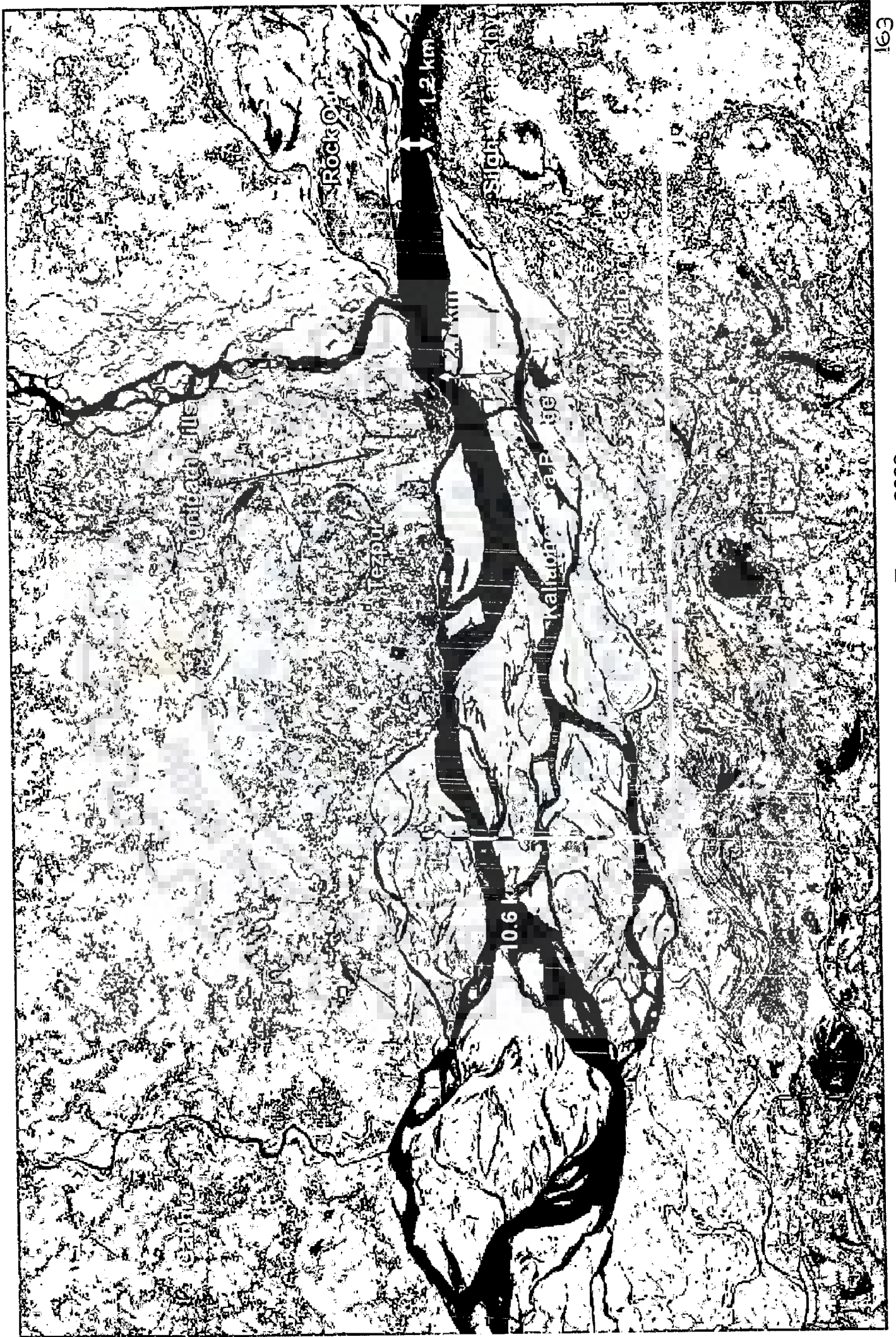


Figure 4. 26 Radersat image near Tezpur, 2002

embankment on the south near Koliabor area. In a distance of about 21 km, the river has fanned out to 10.6 km from 2.7 km at the bridge site, succinctly illustrating the stream power concept by dissipating the flow energy through channel widening. Figure 4.27 depicts the fluvial landform changes in this reach during the 13 years from 1990 to 2002. The Jia Bhareli has migrated towards west by 1.75 km just about 10 km upstream side from the confluence with the Brahmaputra. The river at cross-sections 33 and 34 has been sagged southward by 3.72 km and 2.88 km in 1997 and then maintained its course. The river was highly braided in this reach. Just upstream side of cross-section 36, the river channel course has been changing frequently since 1990.

#### **4.5.2.5      *Reach-V (From Behali to Jhanjimukh)***

This reach was about 107.60 km in length. The average width of the river in this reach was 8.7 km. The river has a braided channel with large channel bars. Here the river attains a width of about 15 km during flood period. The important townships are North Lakhimpur in the north and Sibsagar, Jorhat, and Golaghat on the South. The major north bank tributaries of the river in this part are the Jiadhol, and Subansiri; along with the latter a combined flow of the Ranga, Pabha, Meneha and Dikrong also meets the Brahmaputra. The Kachikata, Mora Dikrong and Pinchola are other smaller rivers of the north bank. On the south bank, the major tributaries such as the Disang, Dikhow, Jhanji and Dhansiri along with smaller ones like the Balama, Dorika and Kikila join the Brahmaputra in this reach. The Jiadhol is infamous for floods and frequent diversion of its channel. The perennially snow-fed Trans-Himalayan river Subansiri, which has been formed by the association of the Lokong Chu (Char Chu), Chayal Chu and Tsdri Chu in Tibet, is the largest tributary of the Brahmaputra. Gold was mined commercially from its

deposits till the recent past, hence it derived its name from gold. After traversing the Himalayas and passing through the Miri Hills, it enters the plains and flows through for 90 km before meeting the Brahmaputra. The Kamala, Ghagar and Sampara are its major tributaries in India. The total length of the river is 442 km. Draining an area of 37,700 km<sup>2</sup>, the Subansiri observed a maximum discharge of 18,799 m<sup>3</sup>/sec and minimum of 131 m<sup>3</sup>/sec during the study period. It contributes 7.92% of total yield of the Brahmaputra. From the satellite imageries of 1990 and 2002, it was observed that the river was shifting west ward.

The river Disang originated from the mount of Patkai Bum in Arunachal Pradesh and flowed 230 km. The Dikhow, the most famous holy river of ancient times as well as the Jhanji, both found their origins from the Naga Hills. The Yangmun and the Namdang are major tributaries of the Dikhow. Some small rivers, viz., the Teok, the Mudoijan, and the Kakojan all originating in the plains flow collectively through the Kokila to the Brahmaputra.

The Dhansiri (south) originates in the southwest corner of the Laishong Peak (1868 m) of the Baril range. Its major tributaries are the Diyung near the foothills and the Kaliani and Gelabil near its mouth. The Bhogdoi and the Kakodonga are two large tributaries flowing through the Gelabil to the Dhansiri. The Dhansiri has a length of 354 km and draining an area of 12,250 km<sup>2</sup>, it contributes 1.03% of the total discharge of the Brahmaputra.

The most remarkable feature of this reach is the Majuli island, which is the biggest river island of the world. Majuli, island (26°32'N to 27°10' N Lat.; 93° 30'E to 94° 35'E Long.), with mean height of 84.5m, is covered by the Survey of India toposheet nos. 83 F/5, F/6, F/9, F/13, I/4, I/8 and J/1. Over the past few decades, Majuli Island (Figure 4.28 (a)) lost considerable areas due to erosion. Its area was

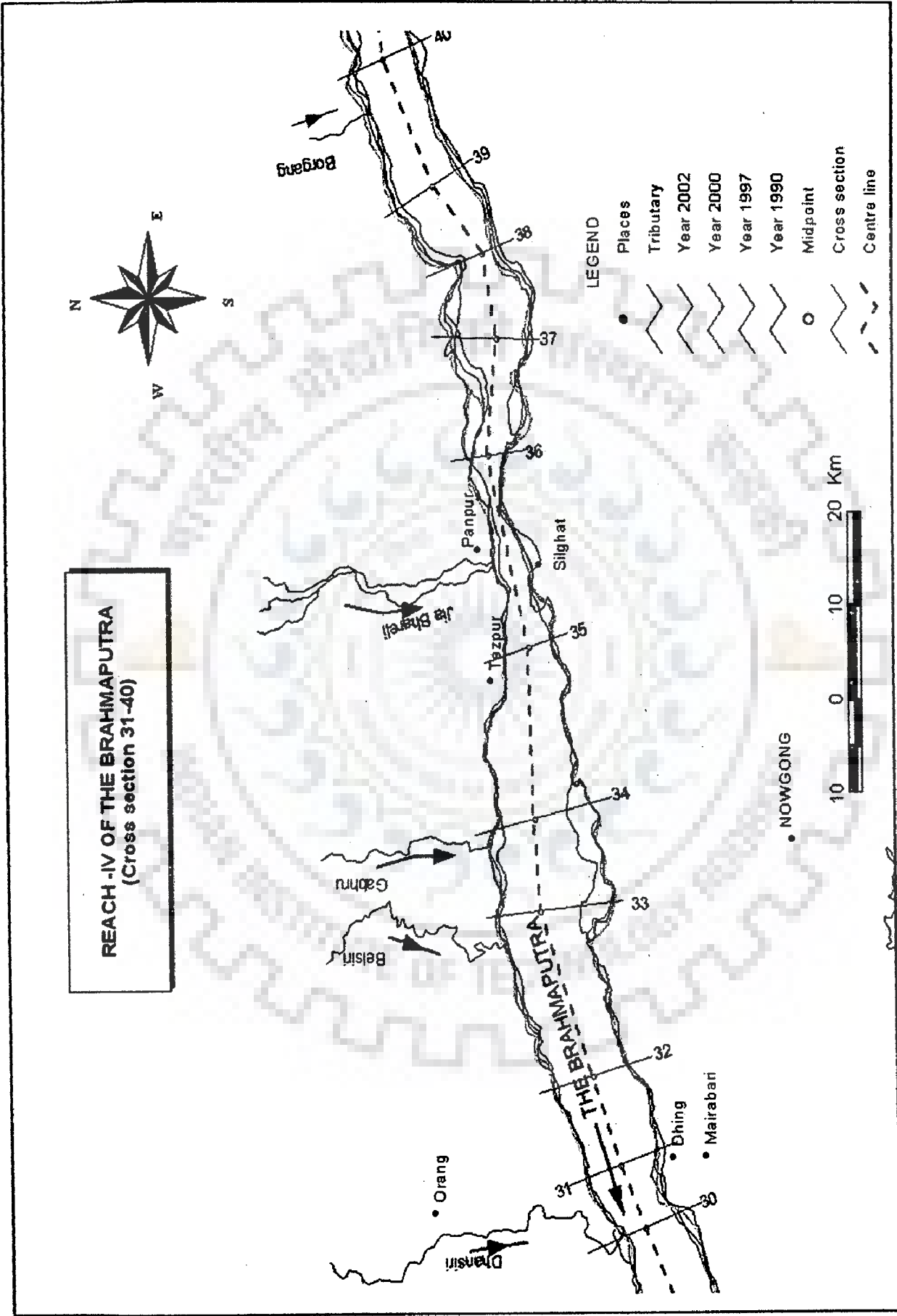


Figure 4.27 River configurations in Reach IV of the Brahmaputra

1,245 km<sup>2</sup> before 1950 (84), which has been reduced from 416.23 km<sup>2</sup> in 1990 to 376.93 km<sup>2</sup> in 2002. The erosion history of Majuli can be divided into two eras - before and after the 1950 earthquake. Before 1950, erosion was insignificant, but after 1950 especially from 1954 onwards, erosion in Majuli has taken a serious turn. In 1950, erosion protection measures are taken on south bank of the Brahmaputra in Kokilamukh area leaving the north bank. As a result of this, large scale erosion started in the downstream portion of Majuli. After the flood of 1990, the configuration of the river reach from Bessamara to Kamalabari changed considerably and an old dead channel named Chumoimari started developing rapidly on the Bessamara-Kamalabari side. The heavy discharge carried by Chumoimari channel led to severe bank erosion from Dakhinpat to Kamalabari, which ultimately resulted in breach of Dakhinpat-Kamalabari embankment in 1993 (Kaman et al., 2001). Large scale erosion also started in upstream portion upto Bessamara. The flow was re-orientated from a southwest to an almost southward channel heading at Hatisal Neamati and is a serious threat to erosion, which has been vividly portrayed in Figure 4.28(b). The presence of clayey soil in Bessamara prevented further erosion downstream upto Kamalabari.

Kaziranga Reserve Forest is another vital land mark in the reach, having abode for the one horned Rhinoceros about 240 km east of Guwahati. Figure 4.29 shows the Radarsat FCC of the area during February, 2002. It is of rough oval shape and has extent of about 45 km long and 15 km wide at its broadest point covering an area of about 430 km<sup>2</sup>. Its northern side is mighty Brahmaputra and on south, the Mora Diphlu river, which is close and almost parallel to National Highway (NH) 37. About 1.25 km in the west bank (u/s of Bar Bill) and 1.80 km (d/s of cross-section 40) in east bank (near Rangamati Bil) major erosion of the



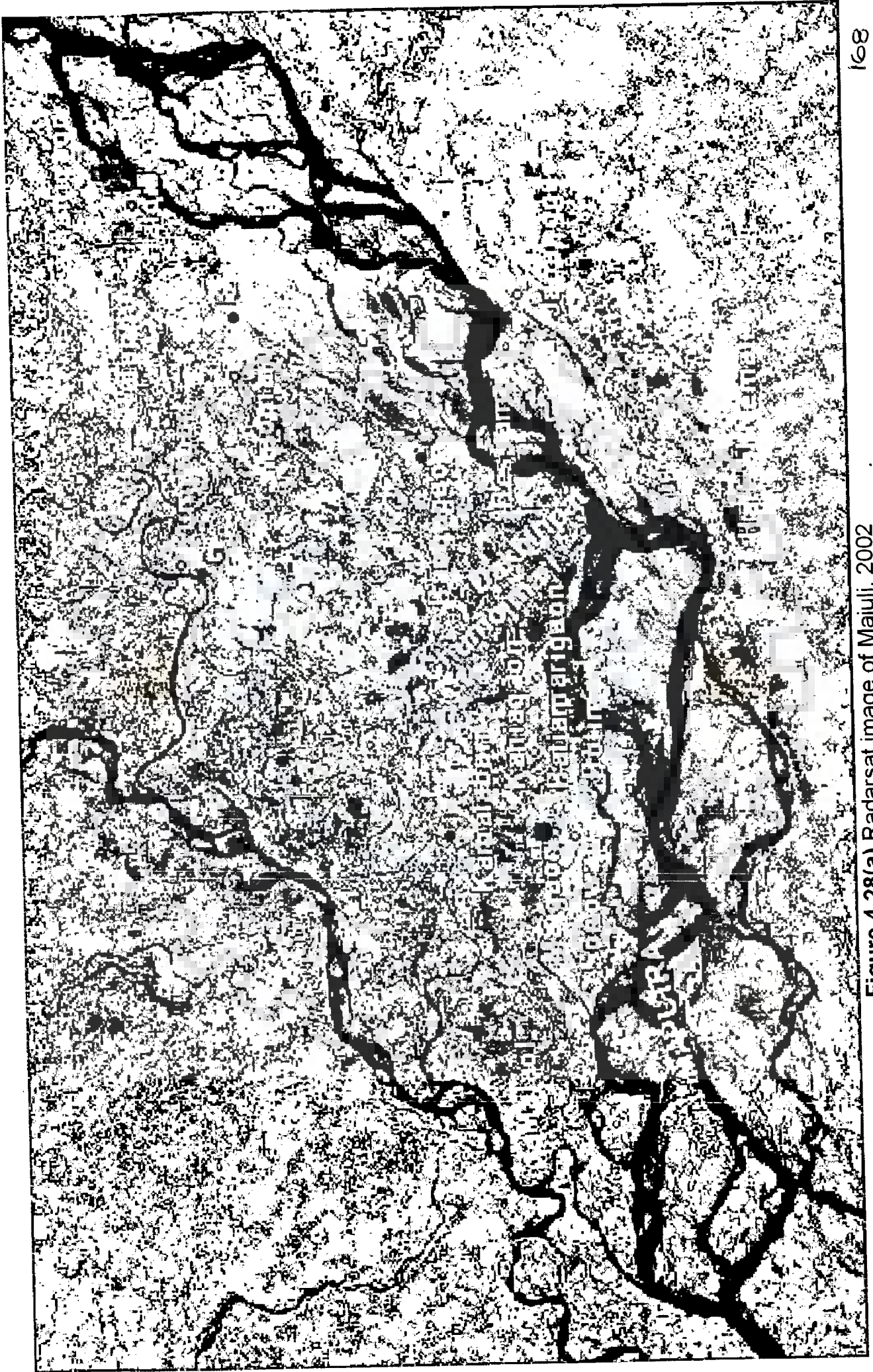


Figure 4.28(a) Radarsat image of Majuli, 2002

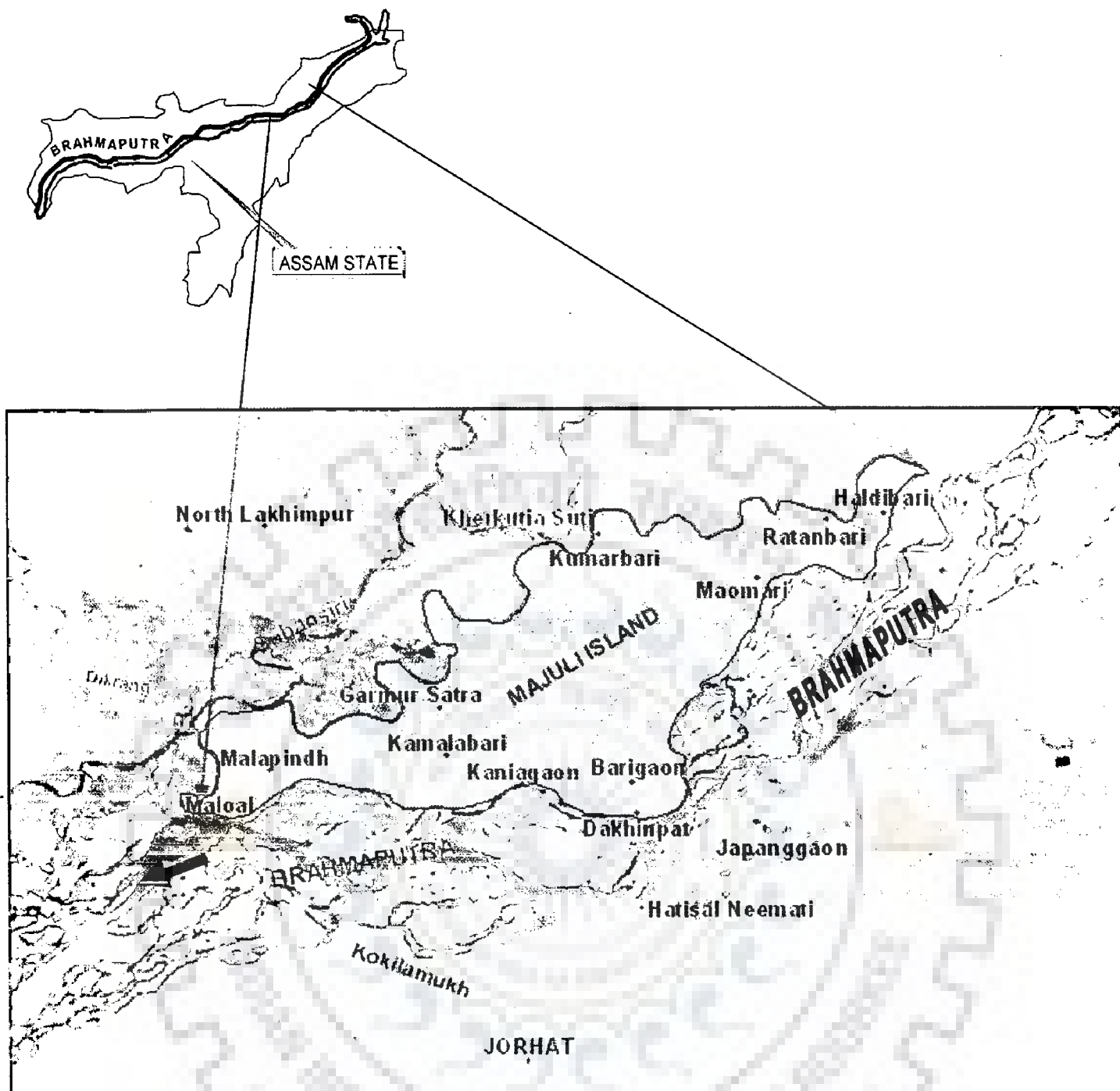


Figure 4.28(b) Location of Majuli, 1990



Figure 4.29 Radarsat image of Kaziranga Reserve Forest, 2002

Kaziranga National Park land has been noticed from the IRS LISS-III satellite imagery of 1990 and 2002 respectively. It was observed that the erosion was more predominant on the eastern as well as western side of the Park. In the mid portion, near Debeswari Chapori, there was bank retreat by an amount of 3.0 km. In other parts of the reach, the river has changed its course to some extent. The river is highly braided in this reach. Figure 4.30 pictorially depicts the stream bank migration of the banks of the Brahmaputra over 12 years from 1990 to 2002.

#### **4.5.2.6      *Reach-VI (From Jhanjimukh to Kahai Spur, Dibrugarh)***

This reach was only about 98.44 km in length. The average width of the river in this reach was 9.6 km and overall orientation has veered from northeast-southwest. Anabranch was dominant in this reach and showed a general progressive trend towards a more braided pattern. The river has a westerly course upto the outfall of the Dibru tributary and then it has a south-westerly course to a little beyond Dihingmukh. Its channel is braided, and there are many channel bars and islands. The river islands have their maximum and average lengths of 14.0 km and 3.75 km, respectively with average width of 2 km. The gradient of the river was 1 in 3,700 between Laikaghat to Dibrugarh and 1 in 5,595 from Dibrugarh to Neamati. The river was navigable throughout the reach and has the important townships of Tinsukia and Dibrugarh on its South bank. The river shoots off a distributary named Burhi Suti from its north side at about 14 km downstream of Laikaghat and it joins the main river 60 km downstream. The Sisi and Tangani are two rivers joining the Brahmaputra directly on its north bank. On the south bank it receives small rivers, such as the Laikajan, Mohmorajan, Dibru, Maijan and the biggest tributary of this reach, the Burhi Dehing. The Burhi Dehing was formed by the Namphuk, Namchik, Megantion, Khaikhe, Tirap, Digboi, Tingrai and Sessa.

It has a length of 360 km and the drainage basin of about 6,000 km<sup>2</sup> and contributes 1.87% of the total discharge of the Brahmaputra.

A characteristic feature of the river Brahmaputra in the Assam valley is the presence of distributaries (local name Suti). The Buri Suti, mentioned above, flows almost parallel to the Brahmaputra maintaining a distance of 3 to 5 km. Many small streams, viz., the Yagalong, Rayang, Je, Debing, Gali, Depi, Nate, Dikari, Narad, Somkhong, and Simen join this Suti progressively from the east. Moreover, on the way the Burhi Suti also shoots off three branches to meet the Brahmaputra; amongst them the Lakhmi Suti is the largest. All the tributaries feeding this Suti have their origins in the lowermost slope of the Arunachal Himalayas. In this area, the change in the courses of these rivers was very frequent resulting in interlacing of many streams and an intricate drainage network. Radical changes did not occur in river width in this portion of the river, but the change in fluvial pattern was excessively high thus culminating in severe braiding. Near cross-section 58, there was lateral shift of the river leftwards by 0.32 km. Figure 4.31 shows the reach and the river configuration during the study period from 1990 to 2002. Figure 4.32 shows the extent of braiding near Dibrugarh.

#### **4.5.2.7      *Reach-VII (From Kahai Spur, Dibrugarh to Dighaltarang (Kobo)***

This small reach was only about 51 km in length. The striking feature of this reach was the formation of a river avulsion near Saikhowa Reserve Forest, thus making the river sag southwards maximum by 10.54 km near cross-section 63. ~~LSSAT~~ satellite imagery of 2002 shows the avulsion in 2002 (Figure 4.33), which was absent in the year 1990. At cross-section 61 the river has encompassed loops to the north, thus incising the flood plain by 0.32 km. The river had retreated back in 1997 in these sections and again has regained the position by incision.

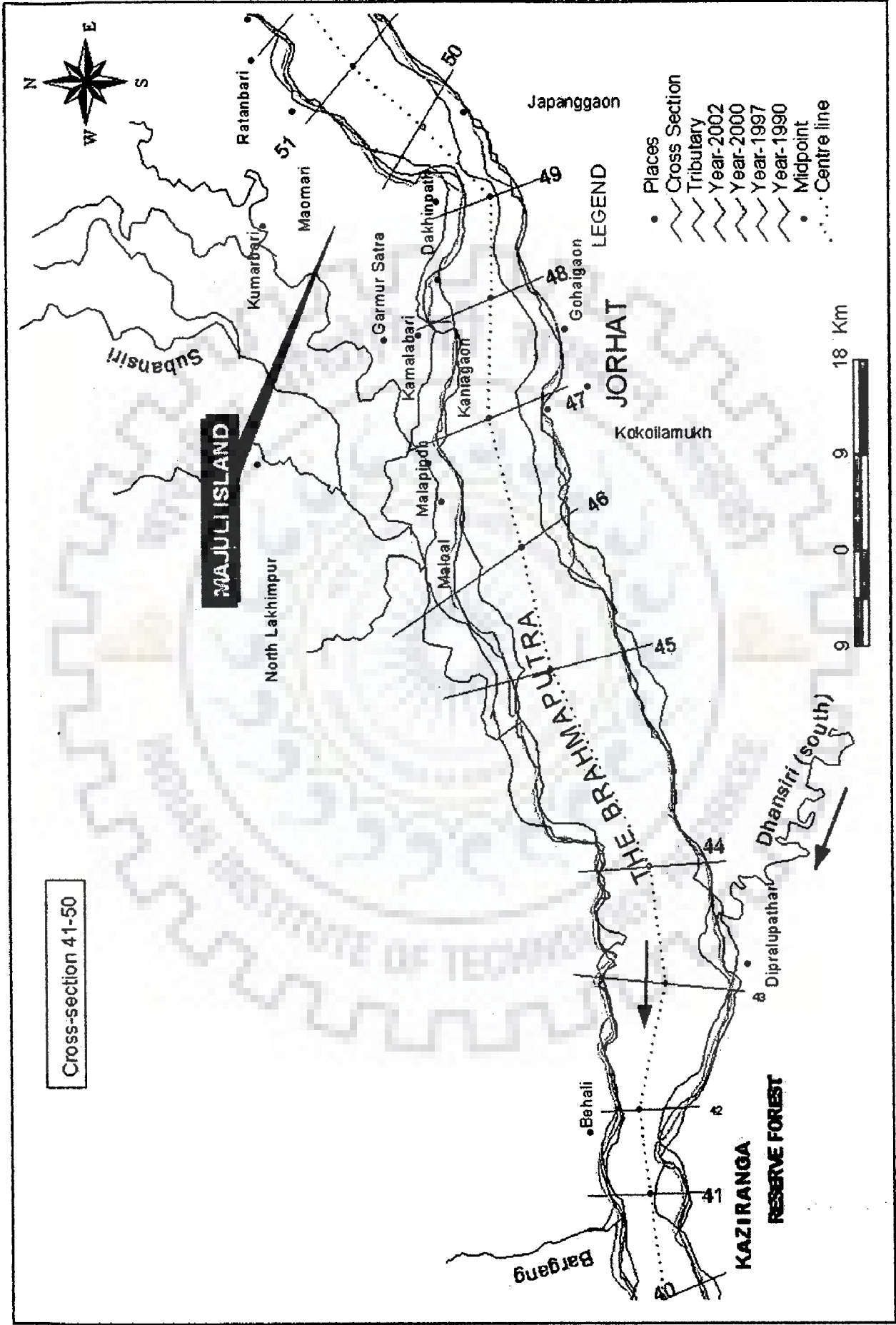


Figure 4.30 River configurations in Reach V of the Brahmaputra

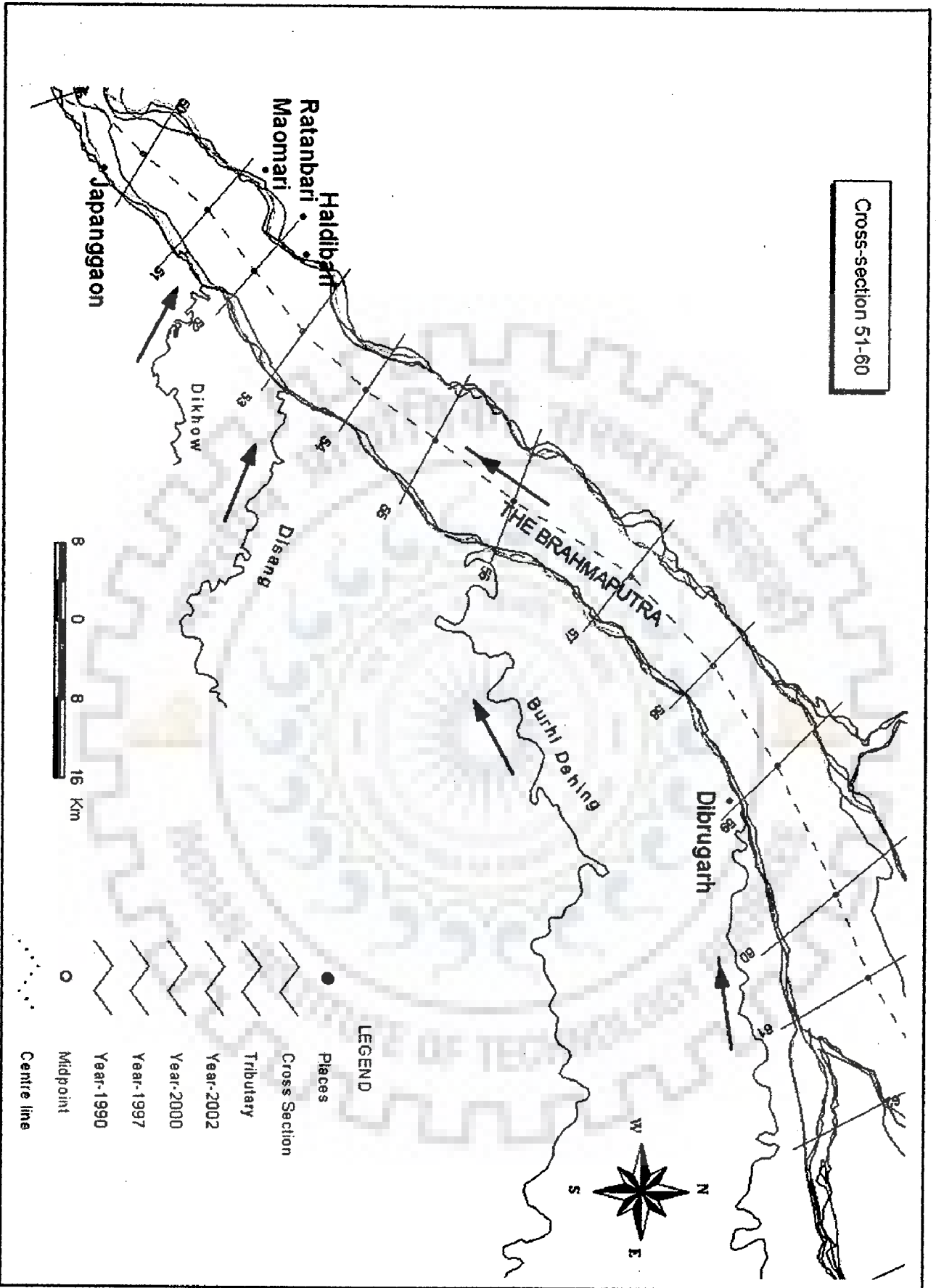


Figure 4.31 River configurations in Reach VI of the Brahmaputra



Figure 4.32 IRS ID, LISS III image showing braiding near Dibrugarh, 2002





Figure 4.33 IRS ID, LISS III image showing avulsion near Saikhowa, 2002

The river configuration in the reach that evolved during 1990 - 2002 was depicted in the Figure 4.34.

The sequential reconstruction of river positions in this reach suggests a gradual southward migration of the river downstream of the confluence of Noa Dihing river (Fig. 4.33) and has been constantly shifting and avulsing over relatively short time scales and is unstable. The amplitudes of the embayment in the right bank have increased. Planform stability is a culmination of profile in this portion and cross-sectional stability. The planform instability was closely linked with both floodplain and channel alterations. It was opined that significant changes of floodplain roughness could initiate planform instability, especially when channel roughness exceeded floodplain roughness, thus creating a preferential flow path across the floodplain and setting the stage for this channel avulsion.

#### **4.5.2.8 Tributaries**

The study revealed that most of the tributaries of the Brahmaputra have their catchment areas over high mountains. The tributaries of the alluvial valley of Assam have been divided into two categories. The tributaries joining from north rise in the Arunachal Himalayas and bring more sediment. As a result the north bank tributaries choke up their bed leading to diversion of channel, river capture, as well as channel bifurcation to modify their river systems more frequently. In contrary to this, the south bank tributaries have a lower rate of sediment yield and their drainage systems exhibit a more or less conservative nature. The north tributaries show parallel configuration and are braided, where as south tributaries show dendritic configuration. Superimposing the imageries of different years, it was seen that the Subansiri and all other eastern rivers shift westward. Rivers between the Pagladiya and Subansiri shift eastwards. From Manas upto Tipkai, all the rivers migrate westward. South tributaries show meandering pattern and are

less shifting. The shifting was due to alteration of direction of flow because of neck cut-off or progressive shifting of meander bends without neck cut-off.

#### 4.6 MONITORING OF EROSION

The analysis of multi-date satellite data revealed progressive encroachments by the river Brahmaputra during the period 1990-2002. The comparative study of the lateral river migration has been presented at Table 4.8.

##### 4.6.1 Erosion Status and Response

Integration of the bank extracted from the Radarsat (Figure 4.35) and IRS LISS III imagery with the field information depicts the status of erosion. The map presents the actual situation of the river bank prevailing during February 2002 vis-à-vis the land boundary. It could be seen that the average erosion has been to the extent of 0.47 km on north bank and 0.48 km south bank. Figure 4.36 presents graphically the stream bank migration of the river Brahmaputra.

**Table 4.8 Major points indicating the status of hazard of the river Brahmaputra**

Location of fluvial hazards (Cross-section)	River width (km) (1990)	River width (km) (2002)	Remarks/ Change in width (km)
Dhubri (2)	8.50	9.45	River width increased by 0.95
Pancharatna (9)	2.41	2.64	0.23
Pandu (22)	1.61	1.61	No change
Mangaldai (27)	9.33	11.67	Left bank eroded by 2.64
Cross-section 29	11.26	12.58	Width increased by 1.32
Tezpur (36)	4.09	4.62	Width increased by 0.53
Neamatighat (49)	5.68	4.69	The width reduced by 0.99
Hatisal Neamati (Majuli)			The channel may lead to avulsion
Dibugarh (59)	10.02	10.35	0.32
Cross-section 63	11.85	22.39	Avulsion of left anabranch to the tune of 10.54
Kobo (65)	16.72	23.48	6.76 (due to avulsion)

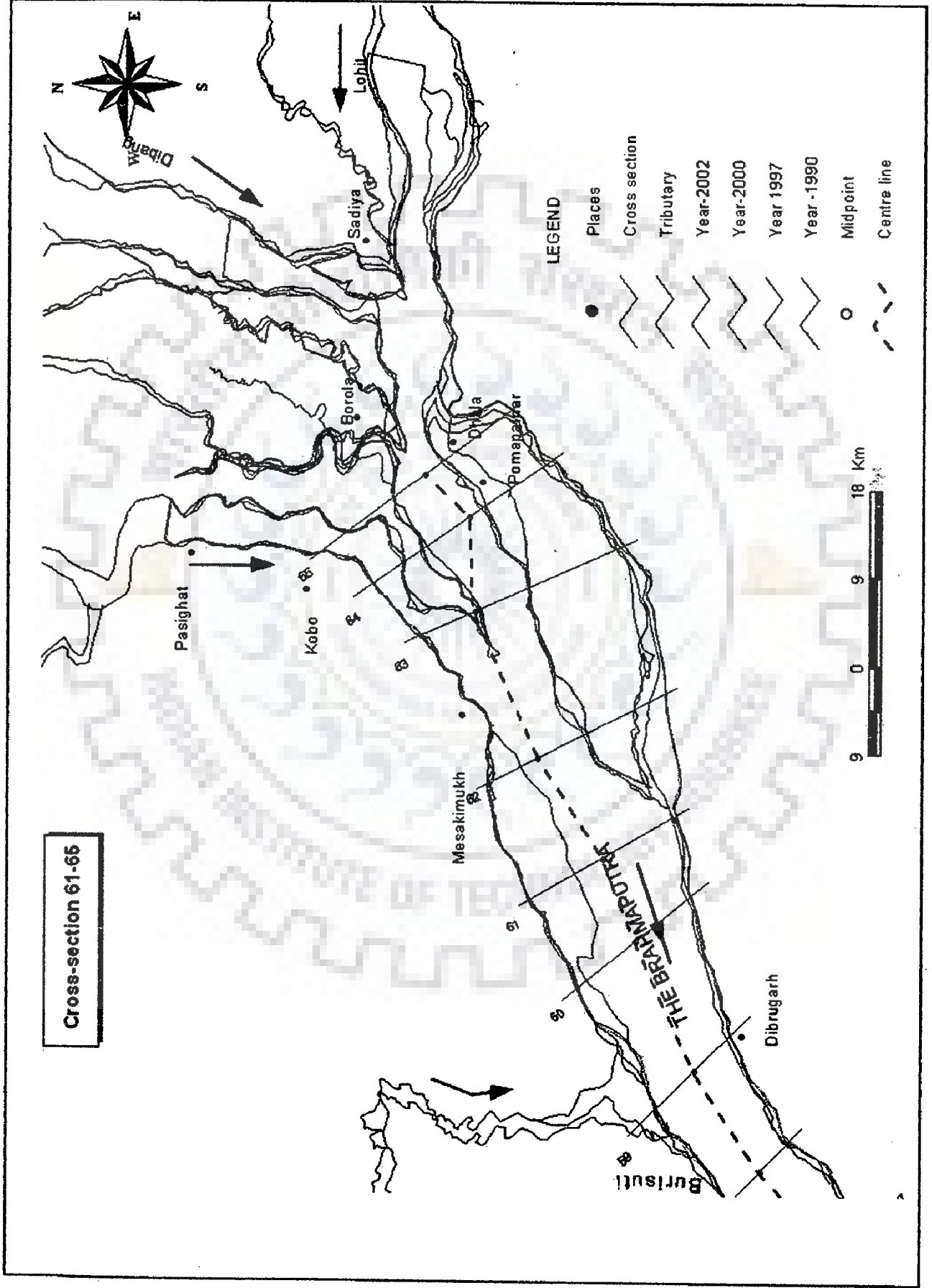


**Figure 4.34 River configurations in Reach VII of the Brahmaputra**

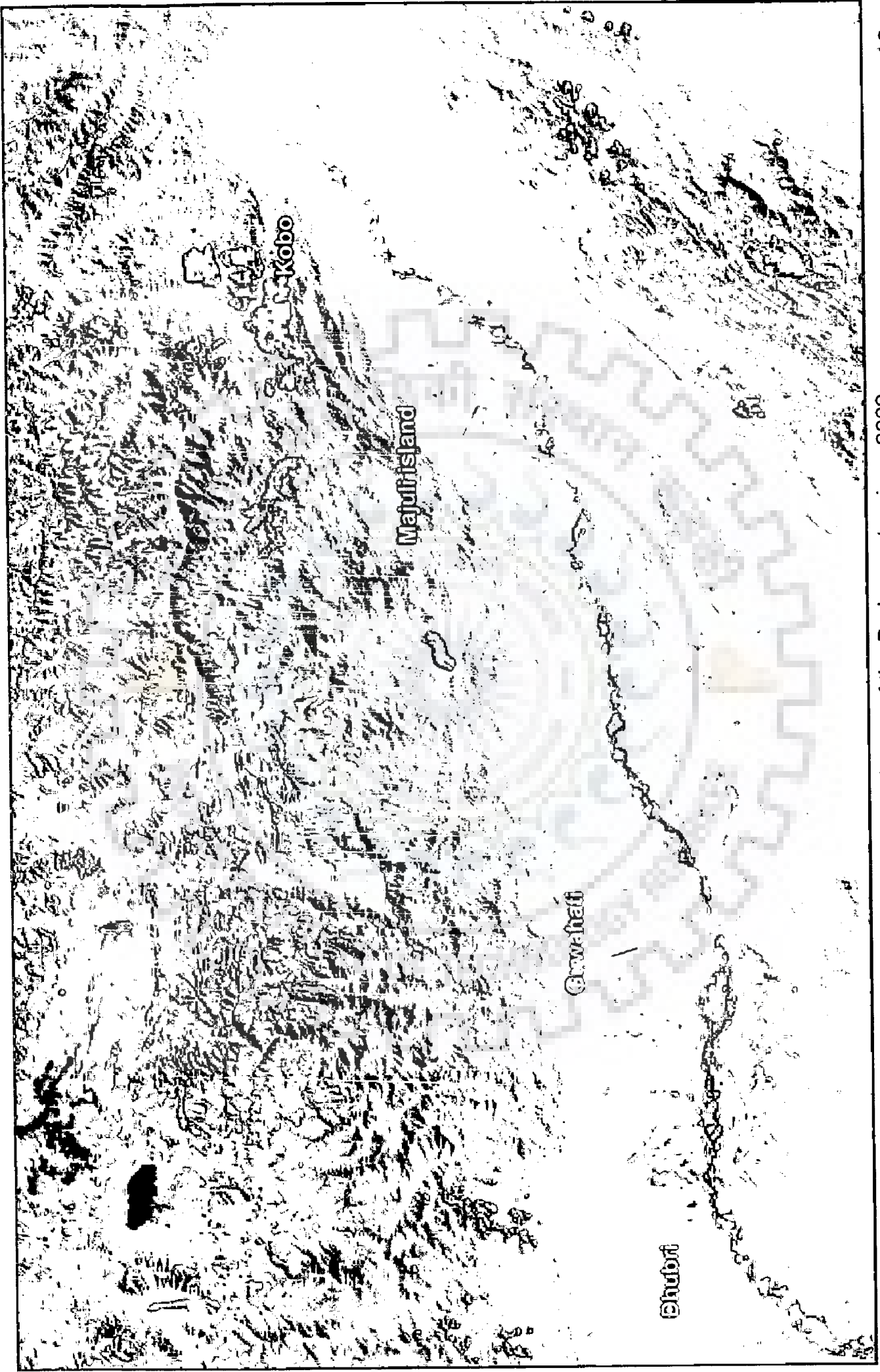


Figure 4.35 Radarsat image of the Brahmaputra river, 2002

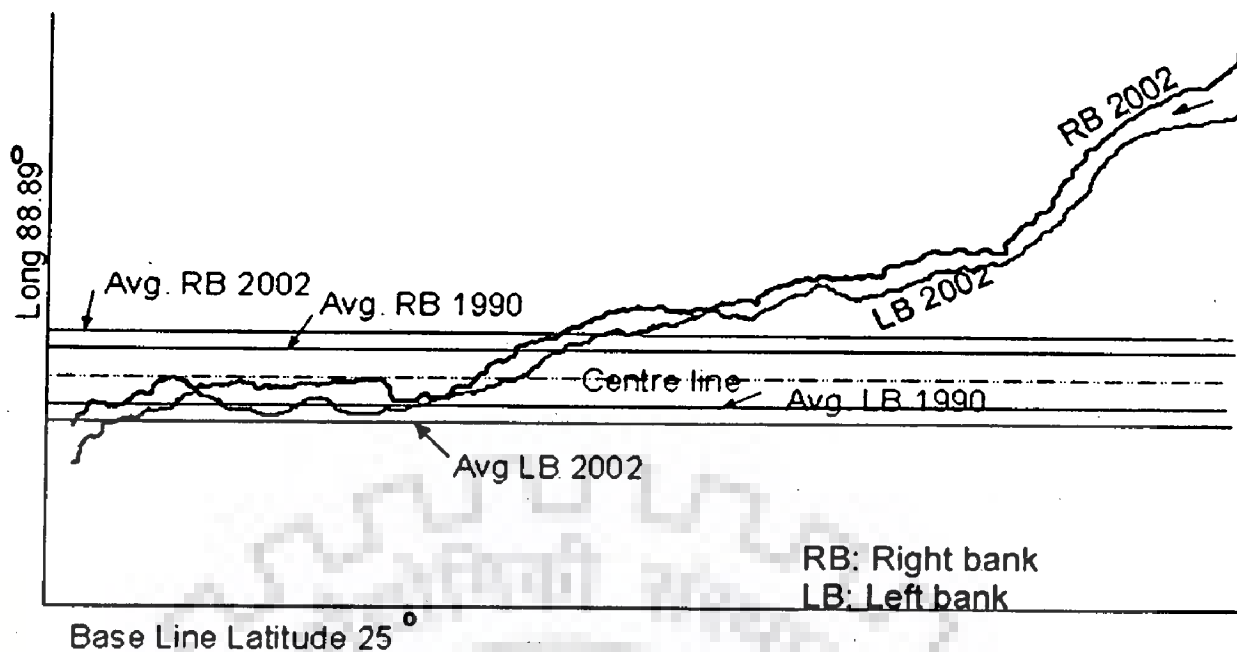


Figure 4.36 Stream bank migration of the river Brahmaputra

Analysis of satellite data of four different years supplemented by ground truth indicated that erosion effects of the river has increased the overall river area by 12.10% during the period from 1990 to 2002. It could be seen that the banks of the river Brahmaputra have been experiencing predominantly type-II and type-III type of erosion response spread over a large area as can be noted from Table 4.9. The general trend that emerged from the present research was that the river was suffering from moderate to considerable erosion affecting both its banks. The net flow area has registered an increase of 17.23% in 2002 as compared with 1990.

Table 4.9 Classes of erosional response (1990-2002)

Class	Erosional response	Criteria	Location
Type - I	Major erosional changes affecting large area	Area loss > 20 km <sup>2</sup>	Reach 1 and 7
Type - II	Moderate to considerable erosion affecting certain areas along bank line	5 km <sup>2</sup> < Area loss < 10 km <sup>2</sup>	Reach 4
Type - III	Minimum erosion with response only at isolated sites	Area loss < 5 km <sup>2</sup>	Reach 2, 3, 5 & 6

## **4.7 NEUROMORPHIC MODELLING**

Artificial neural network (ANN) models have been found to be useful and efficient particularly in problems for which the characteristics of the processes are difficult to be described fully using physical equations. The standard feed forward, back propagation artificial neural network architecture has been successfully applied to studies of rivers before. The use of neural methods seems adequate and in fact well chosen for morphological studies as shown by the results. ANN was better used when interrelations are complicated among several parameters, which statistics was inadequate to model. The study showed the ability of one of the sub-symbolic modelling techniques, namely ANN, in simulating morphological processes in the river with an acceptable demand on computing time and other resources.

### **4.7.1 Data Division**

The input data of all the models were divided into three sets: training, testing and a segment of the database has been deliberately left out in the model training and development phase for use later in model validation. Where the available data were large, the models have been further revalidated from a query data set. The training set was used to adjust the connection weights, whereas the testing set was used to check the performance of the model at various stages of training and to determine when to stop training to avoid over-fitting. The validation set was used to estimate the performance of the trained network in the deployed environment.

### **4.7.2 Selection of Input and Output Variables and Hidden Neuron**

This is one of the most important stages of neural network application because the accuracy of solution for most of the networks depends on the quality

and quantity of training data set. The ANN models have been constituted with feed forward back-propagation supervised training algorithm. The number of hidden neurons has been obtained after several runs of the network with different numbers of neuron initially with a single layer. Finally, the model architecture was selected. The procedure has been described in chapter 2, under para 2.17.8.

A systematic approach, *adaptive method of architecture determination* as suggested by Ghaboussi and Sidarta (1998) has been used to obtain automatically the optimal network architecture. This method suggested starting with an arbitrary, but small, number of nodes in the hidden layers. During training, and as the network approaches its capacity, new nodes were added to the hidden layers, and new connection weights were generated. Training was continued immediately after the new hidden nodes were added to allow the new connection weights to acquire the portion of the knowledge base, which was not stored in the old connection weights. For this process to be achieved, some training was carried out with the new modified connection weights only, while the old connection weights were frozen. Additional cycles of training were then carried out, where all the connection weights were allowed to change. The above steps were repeated and new hidden nodes were added as needed to the end of the training process, in which the appropriate network architecture was automatically determined for minimum *rmse*. The networks were trained using Neural Planner, Neural Power ver 2.5, NeuroSolutions 4.3 and Neuro-Intelligence software.

#### 4.7.3 Normalisation of the Data

It is mentioned that the sigmoidal function can take the values ranging in the (0, 1) domain, a normalisation of the values of the input variables were done. The standard procedure in neural network theory gives the normalisation equation used for this purpose.



$$SF = (SR_{\max} - SR_{\min}) / (X_{\max} - X_{\min}) \quad (4.3)$$

$$X_p = SR_{\min} + (X - X_{\min}) * SF \quad (4.4)$$

Where:  $X$  - actual value of a numeric column,  $X_{\min}$  - minimum actual value of the column,  $X_{\max}$  - maximum actual value of the column,  $SR_{\min}$  - lower scaling range limit,  $SR_{\max}$  - upper scaling range limit,  $SF$  - scaling factor and  $X_p$  - pre-processed value.

#### 4.7.4 Validation and Evaluation of Predictive Capability

The purpose of the model validation phase was to ensure that the model has the ability to generalize within the limits set by the training data in a robust fashion, rather than simply having memorized the input-output relationships that were contained in the training data. The validation process consisted of the analysis of errors, defined as the difference between observed and estimated values for each set of outputs (training, validation and test sets). A high value of *rmse* indicated a deficiency in generalization of the network due to a bad selection of the number of hidden neurons or a weak learning process. In order to evaluate the consistency of the input-output pairs the following strategy was adopted. First, the network was trained with all the pairs selected for the learning process. Then, some of the pairs were eliminated from the set and the network was trained with the rest of the pairs and the isolated pairs were used as the validation set.

Numerous goodness-of-fit statistical criteria have been proposed in the literature for evaluating the performance of the predictions resulting from both the training and the verification of the hydrological modelling results. In this research, only three of these were considered, namely *rmse*, coefficient of correlation and Nash - Sutcliffe coefficient (1970). The *rmse* can take any positive value but the closer it was to zero, the better the model performs. When the Nash value was

between 0 and 1, the forecast model did better than simply forecasting using  $y_0$ . The closer the Nash index was to one, the better. These performance criteria were used as basis of comparison to select the best model.

$$\text{RMSE} = \sqrt{\frac{1}{N} \sum_i^N (Y_o - Y_p)^2} \quad (4.5)$$

Nash-Sutcliffe coefficient is defined by

$$\text{Nash} = 1 - \frac{\sum_i^N (Y_o - Y_p)^2}{\sum_i^N (Y_o - \bar{Y}_o)^2} \quad (4.6)$$

Where,  $Y_o$  = Observed value  $i$ ;,  $Y_p$  = Predicted value  $i$ ;  $\bar{Y}_o$  = Mean observed value;

The coefficient of correlation is a measure that has been used here to determine the relative correlation and the goodness-of-fit between the predicted and observed data and was calculated as follows:

$$r = \frac{C_{y_j d_j}}{\sigma_{y_j} \sigma_{d_j}} \quad (4.7)$$

and

$$C_{y_j d_j} = \frac{1}{n-1} \sum_{j=1}^n (y_j - \bar{y})(d_j - \bar{d}) = \frac{1}{n-1} \left\{ \sum_{j=1}^n y_j d_j - \frac{\sum_{j=1}^n y_j \sum_{j=1}^n d_j}{n} \right\} \quad (4.8)$$

$$\sigma_{y_j} = \sqrt{\frac{\sum_{j=1}^n (y_j - \bar{y})^2}{n-1}} \quad (4.9)$$

$$\sigma_{d_j} = \sqrt{\frac{\sum_{j=1}^n (d_j - \bar{d})^2}{n-1}} \quad (4.10)$$

$$\bar{y} = \frac{\sum_{j=1}^n y_j}{n} \quad (4.11)$$

$$\bar{d} = \frac{\sum_{j=1}^n d_j}{n} \quad (4.12)$$

Where,  $y_j$  = model (predicted output),  $y_j = y_1, y_2, y_3 \dots y_n$ ;  $d_j$  = model (desired output),  $d_j = d_1, d_2, d_3 \dots d_n$ ;  $C_{y_j d_j}$  = Covariance between the model output ( $y_j$ ) and desired output ( $d_j$ );  $\sigma_{y_j}$  = standard deviation of the model predicted output  $y_j$ ,  $\sigma_{d_j}$  = standard deviation of the model predicted output  $d_j$ ,  $n$  = number of data,  $\bar{y}$  = mean of the model predicted output; and  $\bar{d}$  = mean of the desired output.

Smith (1986) suggested the following guide for values of  $r$  between 0.0 and 1.0;

- (i)  $|r| \geq 0.8$  strong correlation between two sets of variable
- (ii)  $0.2 < |r| \leq 0.8$  correlation exists between two sets of variable
- (iii)  $|r| \leq 0.2$  weak correlation exists between two sets of variable

In the present research, the neuromorphic modelling has been employed for the following in addition to development of fluvial landform indices:-

- I. MORPHOLOGICAL CHARACTERISTIC MODELS
  - a) Stream bank migration models
    - i. Predictive models
    - ii. What-if-then model
  - b) Hydrographic characteristic model
  - c) Fluvial landform indices
- II. FLOW CHARACTERISTIC MODELS
  - i. Predictive model
  - ii. What-if-then model
- III. Majuli island erosion model
- IV. Stage - discharge models
- V. Flood forecasting models

Table 4.10 shows the description of the models used in this study.

**Table 4.10 Description of neuromorphic models**

Models	Type of model	Description of model with input and output
M 1	Morphological characteristic models (Stream bank migration models) Predictive models	Stream bank co-ordinates from satellite data (left bank)
M 2		Stream bank co-ordinates from discharge data (right bank)
M 3		Stream bank co-ordinates from <del>Satellite</del> data (left bank)
M 4		Stream bank co-ordinates from discharge data (right bank)
M 5		Strip area (left bank) ( $\alpha_1 \dots \alpha_{100}$ )
M 6		Strip area (right bank) ( $\alpha_1 \dots \alpha_{100}$ )
M 7		Strip length (left bank) ( $\lambda_1 \dots \lambda_{100}$ )
M 8		Strip length (right bank) ( $\lambda_1 \dots \lambda_{100}$ )
M 9	What-if-then model	From flash flood (left bank) – stream bank co-ordinates
M 10		From flash flood (right bank)- stream bank co-ordinates
M 11	Hydrographic parameter model	Generation of reduced level {Chainage, Year} --- {reduced level}
M 12	Flow characteristic models (Predictive model)	{Year, Month, Q} --- {Qs <sub>1</sub> ..Qs <sub>100</sub> , WL <sub>1</sub> ..WL <sub>100</sub> }
M 13		{Year, Month, Qs} --- {Q <sub>1</sub> ..Q <sub>100</sub> , WL <sub>1</sub> ..WL <sub>100</sub> }
M 14		{Year, Month, WL} --- {Q <sub>1</sub> ..Q <sub>100</sub> , Qs <sub>1</sub> ..Qs <sub>100</sub> }
M 15	What-if-then model	{Q/Qs/WL} --- {Qs <sub>1</sub> ..Qs <sub>100</sub> , WL <sub>1</sub> ..WL <sub>100</sub> }
M 16	Majuli island erosion model	Year, month --- area of sectors
M 17	Stage-discharge ANN models	Stage - discharge (Dibrugarh)
M 18		Stage - discharge (Pancharatna)
M 19		Stage - discharge (Dhubri)
M 20	Stage-discharge Fuzzy models	Stage - discharge (Dibrugarh)
M 21		Stage - discharge (Pancharatna)

M 22		Stage - discharge (Dhubri)
M 23	Stage-discharge Neuro-fuzzy models	Stage - discharge (Dibrugarh)
M 24		Stage - discharge (Pancharatna)
M 25		Stage - discharge (Dhubri)
M 26	Flood forecasting models	Stage - stage (Pandur)
M 27		Stage - stage (Pancharatna)
M 28		Stage - stage (Dhubri)
M 29	Sediment concentration model	$(\psi, \varphi, \frac{w_0}{u_*}, S, \frac{h}{d_{50}}, F, R, \frac{h}{B}) - - - C_s$ (Pancharatna)

## 4.8 MORPHOLOGICAL CHARACTERISTICS

### 4.8.1 Stream Bank Migration Models

The derived data from satellite images of years 1990, 1997, 2000, 2002 have been analysed and the boundary of river banks were digitized for all the years. The length of arcs on the digitized boundaries of both the left and right banks for all the four years were found out using ARC/INFO software.

For modelling the stream bank migration, a base line of 25° N Latitude along x-axis and 89.88° E Longitude line along y-axis have been taken as permanent reference lines, so that they maintain their identity when the morphology is changed. For convenience, the river Brahmaputra was divided into 100 strips of equal base length of 5.363 km (Figure 4.37). An Arc Macro Language (AML) program was devised and run, which splits the arcs in 100 equal parts and 101 nodes were created. The co-ordinates of the nodes were found by ARC/INFO GIS. Accordingly, the area enclosed by each of the strips was found out. The lengths of 100 arcs for both the banks for all the four year data were computed as shown in Figure 4.38. The various models have been described in the following paragraphs.

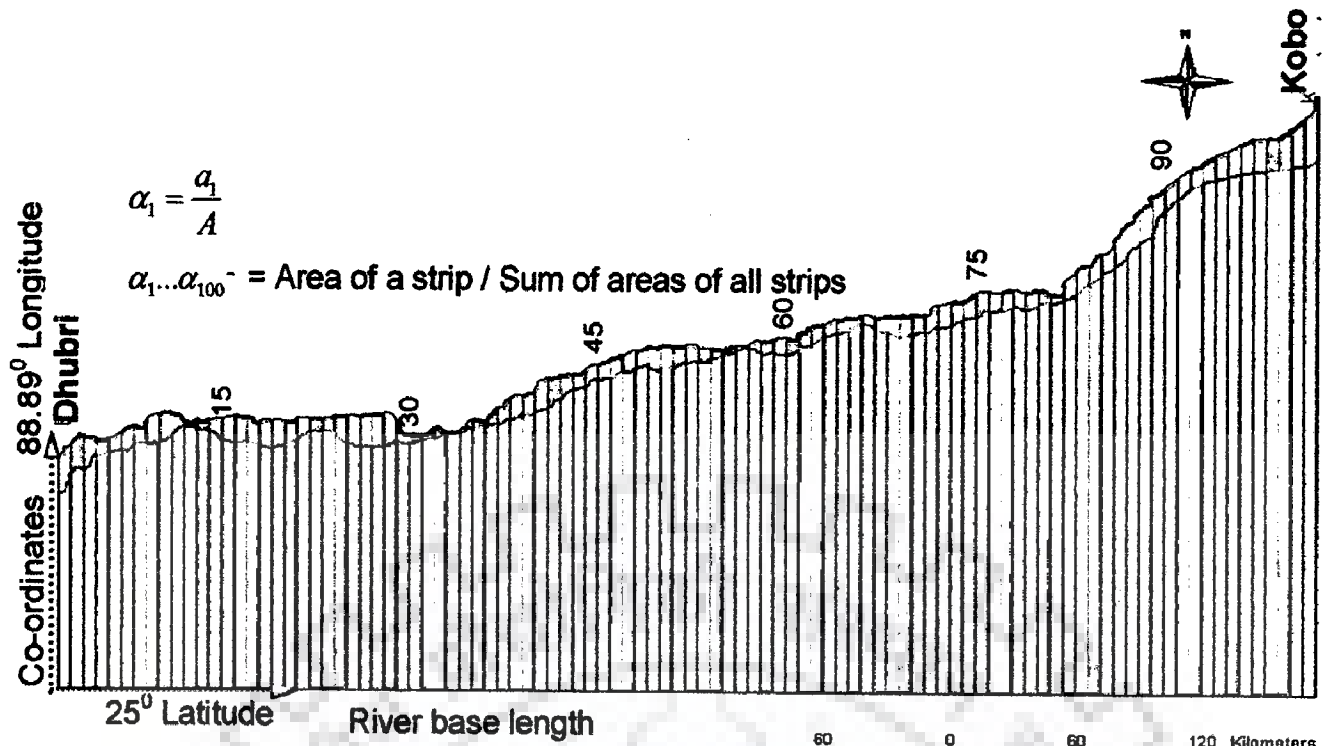


Figure 4.37 The Brahmaputra river divided into 100 equal strips

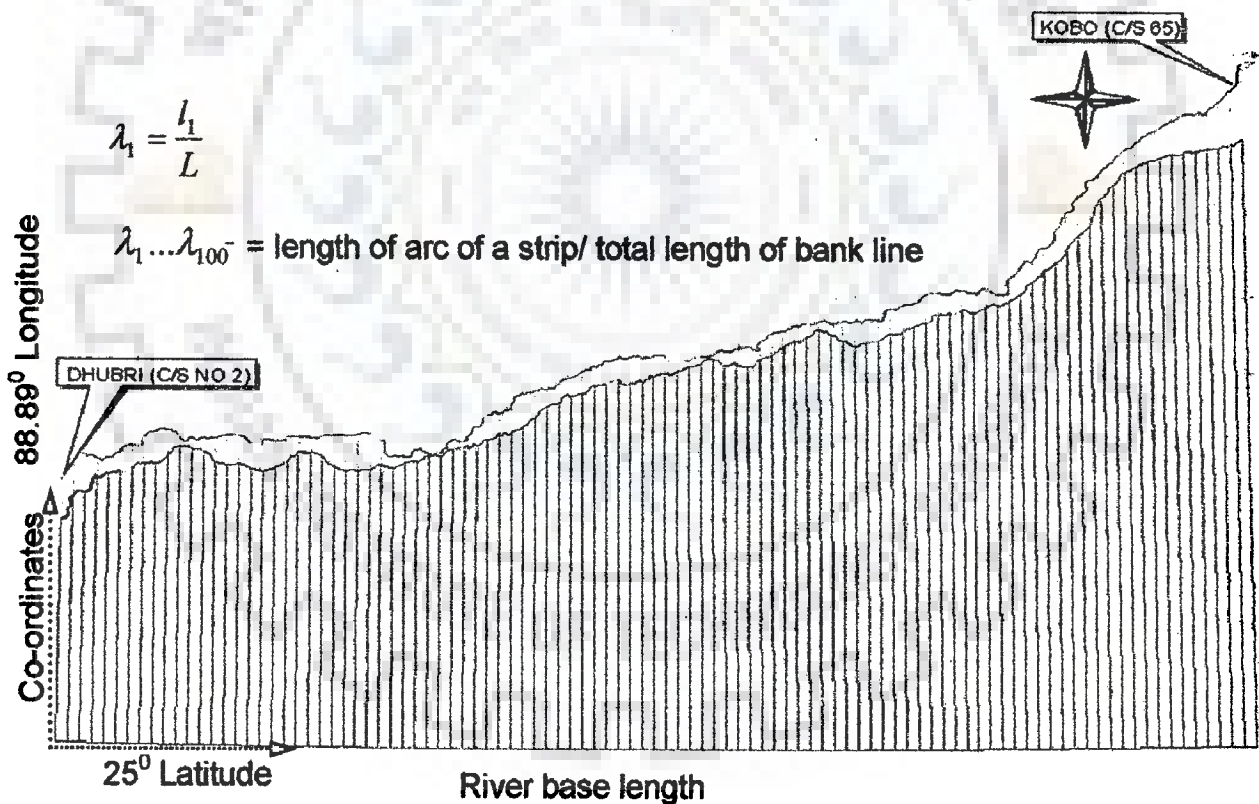


Figure 4.38 The Brahmaputra river divided into 100 arcs

#### 4.8.1.1 Model 1

The model 1 was constituted to simulate the left bank co-ordinates for any year from the known co-ordinates derived from satellite data for the years 1990,

1997, 2000 and 2002. The data of years 1990, 1997 and 2000 were divided into three sets: training (70%), testing (15%) and a segment of the database of year 2002 has been deliberately left out in the model training and development phase for use later in model validation (15%).

Figure 4.39 depicts the architecture of the spatio-temporal ANN model showing the input and output parameters. The model architecture was designated as (2 - 68 - 68 - 101), indicating two input neurons, two hidden layers with 68 neurons each and 101 output neurons. The ANN model was simulated with month and year as input and the left bank co-ordinates at 101 points as outputs. Month and year have been taken as input variables, as the parameters were to be calculated for different years and these form the independent variable. Table 4.11 shows the comparison of ANN predicted co-ordinates for 2006 with 2002 for the left bank.

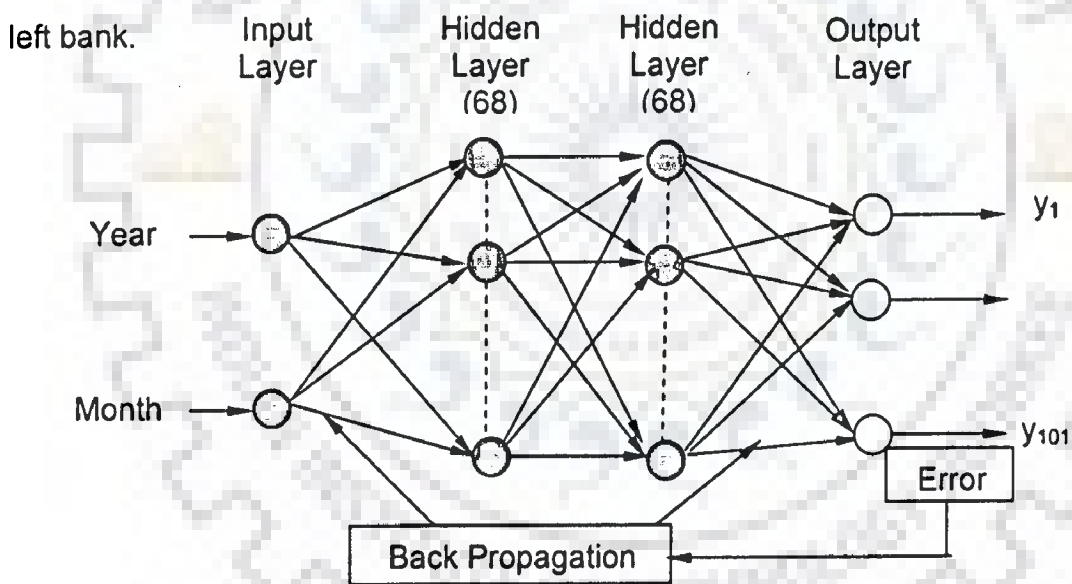


Figure 4.39 Architecture of the ANN Model 1

A computer code was developed using Fortran 90 for computing the *rmse* and Nash co-efficient (Annexure-I, Programme-9). In this model, an *rmse* error of 0.011 and Nash co-efficient of 0.9659 were obtained from the training and verification simulation. The iterations were 7270 and average correlation co-efficient "*r*" was 0.9998. Efficiency of this model was 96.59%. Figure 4.40 shows the plot of validation curve between observed data and ANN predicted data for left bank co-ordinates for the year 2002. Figure 4.41 shows the plot of difference of co-ordinates between the observed of 2002 and ANN predicted values of 2006.

**Table 4.11** Comparison of ANN predicted co-ordinates in metre from 25° Latitude for 2006 with 2002 (left bank) (Erosion-E, Deposition-D)

Co-ordinates	Year-2002	Year-2006	Remarks	Co-ordinates	Year-2002	Year-2006	Remarks
Y1	168390	168300	Phulbari (E)	Y52	244510	244510	
Y2	182290	182270		Y53	245420	245390	
Y3	183160	183140		Y54	247650	247640	
Y4	189710	189690		Y55	249630	249510	c/s 35-36 (E)
Y5	192010	192000		Y56	251720	251720	
Y6	194290	194280		Y57	248290	248330	
Y7	196530	196540		Y58	249240	249240	
Y8	197630	197640		Y59	248540	248550	
Y9	198010	198010		Y60	252850	252850	
Y10	202320	202330		Y61	254890	254890	
Y11	206660	206650		Y62	258890	258790	c/s 40-41 (E)
Y12	205590	205580		Y63	261710	261700	
Y13	202880	202870		Y64	263500	263500	
Y14	198570	198560		Y65	264380	264380	
Y15	197450	197460		Y66	265390	265390	
Y16	197300	197290		Y67	262170	262170	
Y17	195280	195280		Y68	259740	259740	
Y18	194320	194320		Y69	260430	260220	u/s of c/s 43 (E)
Y19	196210	196210		Y70	261920	261910	
Y20	199050	199050		Y71	265560	265560	



Y21	201040	201040		Y72	266280	266280	
Y22	203990	203990		Y73	269260	269150	
Y23	202150	202160		Y74	271300	271300	
Y24	197990	197990		Y75	274320	273950	u/s of 45 (E)
Y25	195120	195120		Y76	275680	275600	
Y26	195160	195160		Y77	276810	276790	
Y27	195780	195780		Y78	276030	276000	
Y28	197720	197720		Y79	277830	277770	
Y29	196780	196780		Y80	279850	279830	
Y30	198930	198940		Y81	283260	283140	u/s of c/s 49 (E)
Y31	199730	199740		Y82	285610	285600	
Y32	202530	202530		Y83	292050	292020	
Y33	202490	202490		Y84	298070	298060	
Y34	205840	205850		Y85	301310	301230	
Y35	206650	206650		Y86	309240	309250	
Y36	207920	207920		Y87	315250	315250	
Y37	210760	210700	c/s 25-26 (E)	Y88	320400	320400	
Y38	213420	213410		Y89	334200	334190	
Y39	214720	214680	c/s 28-29 (E)	Y90	340660	340640	
Y40	218970	218980		Y91	346860	346860	
Y41	222950	222910		Y92	350320	350320	
Y42	227630	227620		Y93	352990	352970	
Y43	230190	230210		Y94	354940	354940	
Y44	233760	233750		Y95	356650	356640	
Y45	234430	234430		Y96	357500	357490	
Y46	237830	237830		Y97	357700	357620	
Y47	239430	239430		Y98	359260	359200	
Y48	240450	240450		Y99	360530	360640	Between c/s 64-65 (D)
Y49	239700	239670		Y100	361960	362040	
Y50	240350	240400	c/s 34 (D)	Y101	365930	366060	
Y51	242900	242890					

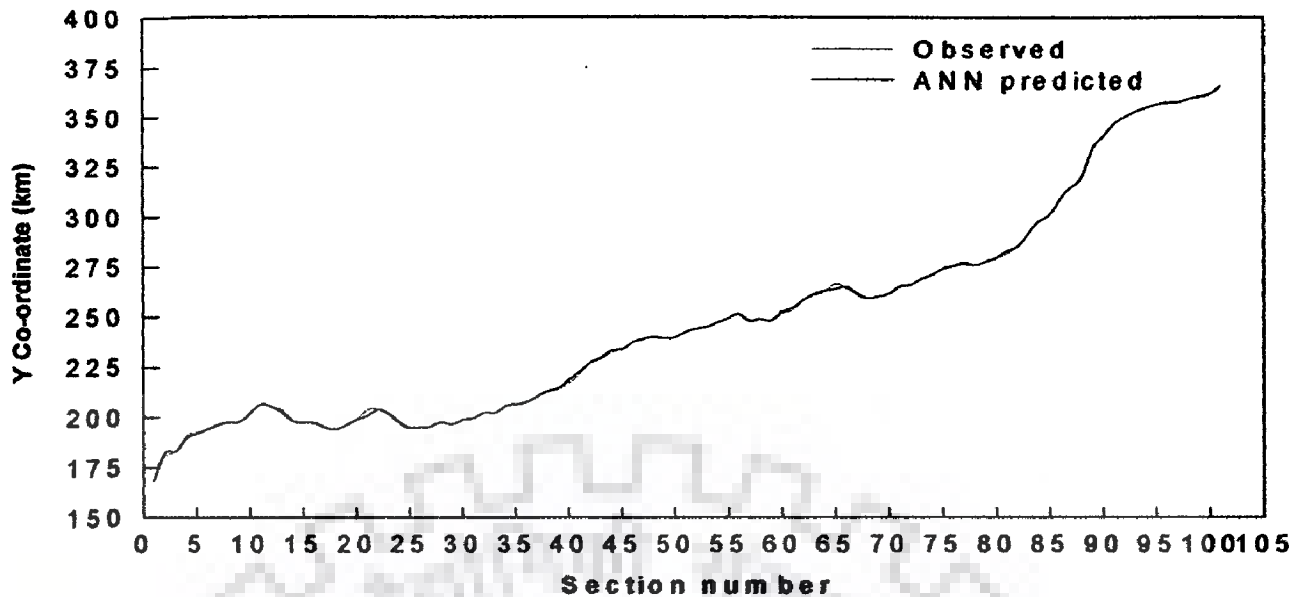


**Figure 4.40** Plot of observed and ANN predicted left bank co-ordinates (2002)

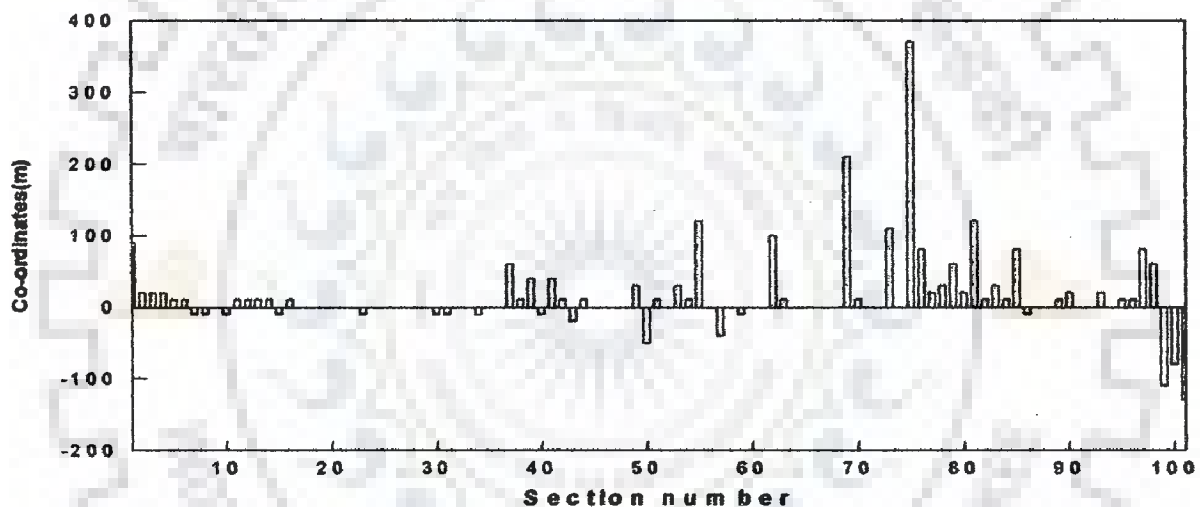


**Figure 4.41** Plot of probable changes of left bank co-ordinates in 2006 (ANN) with respect to 2002 (observed)

#### 4.8.1.2 Model 2

The model 2 was constituted to simulate the left bank co-ordinates for any year from the known discharges for the years 1990, 1997, 2000 and 2002. The data of years 1990, 1997 and 2000 were partitioned into training (80%), testing sets (20%), where a segment of the database of year 2002 has been left out for model validation. Back-propagation algorithm (BPA) has been used to train feed forward models (FFMs), in which the outputs were sent only to the immediate next layers.

The model architecture was designated as 103-105-101, indicating 103 input neurons, one hidden layer with 105 neurons each and 101 output neurons. The ANN model was simulated with month, year and discharge at 101 points as input and the left bank co-ordinates at 101 points as outputs. Month, year and discharge have been taken as input variables, as the left bank co-ordinates were to be calculated for different years and these form the independent variables. The data were normalised between values 0 and 1.

In this model, an *rmse* error of 0.0139 and Nash co-efficient of 0.9997 were obtained. The iterations were 25,000 and average correlation co-efficient ' *r* ' was 0.9999. Efficiency of this model was 99.97%. Figure 4.42 shows the plot of validation curve between observed data and ANN predicted data for left bank co-ordinates for the year 2002. Table 4.12 shows comparison of ANN predicted co-ordinates for 2006 with 2002 for the right bank.

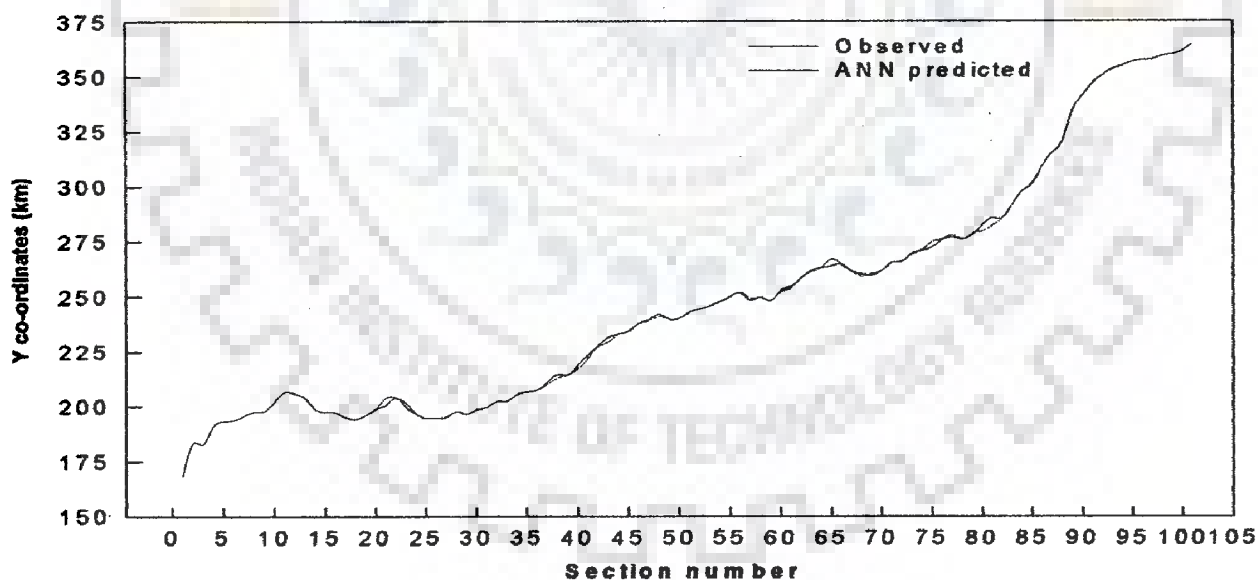


**Figure 4.42** Plot of observed and ANN predicted left bank co-ordinates (2002)

To cross-validate the predicted left bank co-ordinates, a computer programme was developed (Annexure-I, Programme 2) for spatio-temporal idealisation of river Brahmaputra. The computer programme for computing values

of shape function at different nodes has been used at any spatial point at any instant of time. The co-ordinates for the year 1996 computed from model 1, 2 and the computer programme were again cross-validated to re-check the accuracy of the models. Figure 4.43 presents the cross-validation check of the above data for the year 1996. It was observed from the plot that the curves from the two ANN models and the spatio-temporal programme have given desired results for all the prediction horizons. Figure 4.44 shows the plot of difference of co-ordinates between the observed of 2002 and ANN predicted values of 2006.

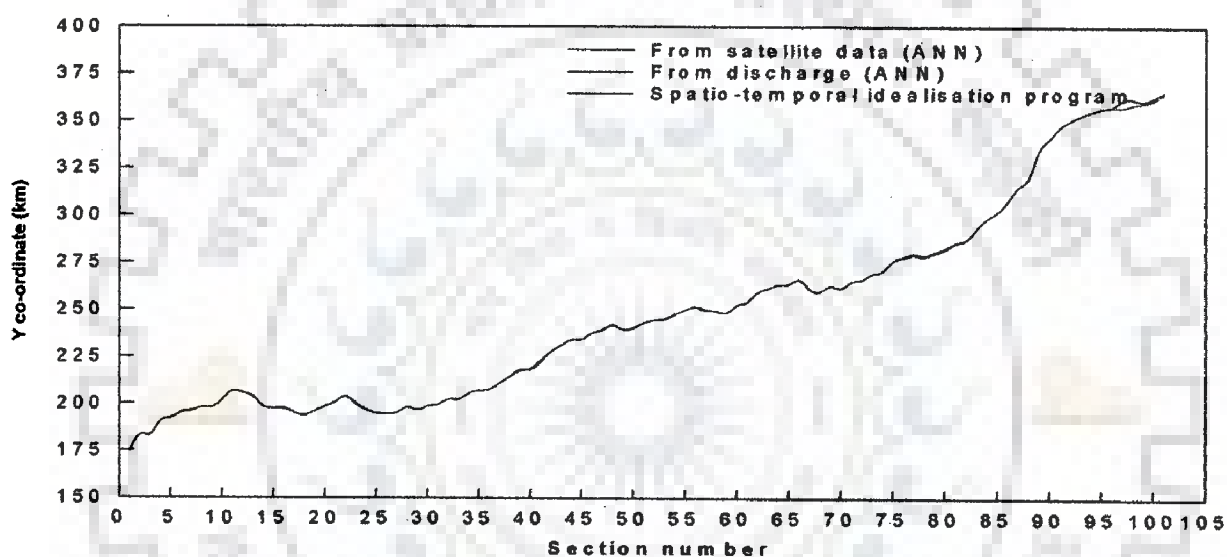


Figure 4.43 Plot of observed, ANN predicted and data computed from spatio-temporal idealisation programme for left bank co-ordinates (1996)

Table 4.12 Comparison of ANN predicted co-ordinates in metres for 2006 & 2002 (right bank) \*(Erosion-E, Deposition D)

Co-ordinates	Year-2002	Year-2006	Remarks	Co-ordinates	Year-2002	Year-2006	Remarks
Y1	190160	190000		Y52	252410	252290	
Y2	197120	196290	Dhubri(E)*	Y53	251580	251620	
Y3	202010	202080		Y54	251130	251150	
Y4	200550	200670		Y55	253080	253150	
Y5	200870	200960		Y56	253970	253770	
Y6	204250	204290		Y57	255870	256050	
Y7	207660	207690		Y58	257150	256490	c/s 37(D)
Y8	211600	212050	u/s of c/s 6 (E)	Y59	258520	258570	

Y9	214410	214520		Y60	260740	260090	c/s 38(D)
Y10	215060	215270	d/s of c/s 8(E)	Y61	264770	264490	
Y11	210960	210990		Y62	266490	266210	
Y12	211180	211250		Y63	269250	269020	
Y13	211120	211110		Y64	270170	269890	
Y14	211230	211310		Y65	271360	271090	
Y15	212810	212950		Y66	270300	270210	
Y16	212250	212280		Y67	271340	271300	
Y17	208720	208760		Y68	271480	271310	
Y18	209350	209430		Y69	272320	272220	
Y19	209560	209520		Y70	272250	272180	
Y20	211520	211330		Y71	278030	277780	c/s 44- 45(D)
Y21	211780	211870		Y72	279410	279260	
Y22	211150	211220		Y73	280670	280410	
Y23	212510	212550		Y74	285070	284600	c/s 46(D)
Y24	212800	212710		Y75	285980	285500	c/s 47(D)
Y25	212540	212120	d/s of c/s 17(D)	Y76	285560	285290	
Y26	213400	213380		Y77	287110	286920	
Y27	213870	213960		Y78	285970	285750	
Y28	210310	210640	d/s of c/s 19(E)	Y79	287740	287130	d/s of c/s 49(D)
Y29	202250	202250		Y80	285490	285340	
Y30	202090	202110		Y81	293250	293230	
Y31	205690	205660		Y82	299240	299110	
Y32	203810	203810		Y83	302200	302090	
Y33	204160	204140		Y84	308820	308670	
Y34	210400	210620	u/s of c/s 23(E)	Y85	317830	318220	d/s of c/s 55 (E)
Y35	210010	210010		Y86	326850	326890	
Y36	217380	217390		Y87	335130	335180	
Y37	223210	223250		Y88	343270	343730	c/s 58(E)
Y38	224290	224300		Y89	347850	347770	
Y39	228300	227980	c/s 28(E)	Y90	353050	353000	
Y40	234200	234250		Y91	358730	358750	
Y41	235890	235710		Y92	362780	362990	
Y42	236580	236560		Y93	366890	367020	

Y43	239690	239580		Y94	369670	369880	c/s 61(E)
Y44	242220	242180		Y95	373400	373690	
Y45	245390	245420		Y96	376570	377050	
Y46	248000	247910		Y97	376920	377080	
Y47	250490	250410		Y98	377960	377380	c/s 63(D)
Y48	252340	252080	d/s of c/s 33	Y99	383170	382830	c/s 64(D)
Y49	252910	252980		Y100	388750	388740	
Y50	252360	252200		Y101	402030	402020	
Y51	253350	253290					

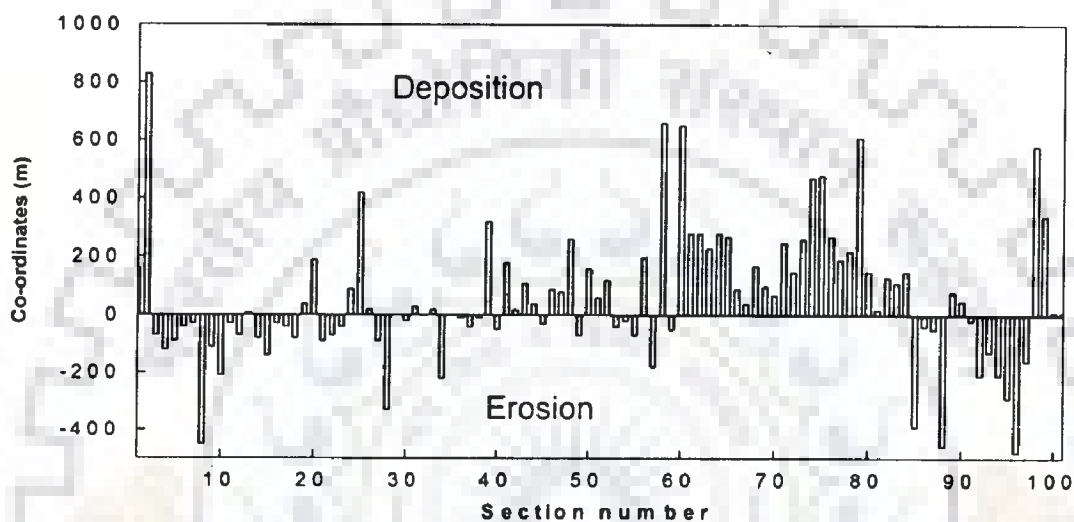


Figure 4.44 Plot of probable changes of right bank co-ordinates in 2006 (ANN) with respect to 2002 (observed)

#### 4.8.1.3 Model 3

Similar to model 1, model 3 (2 - 68 - 68 - 101) was constituted to simulate the right bank co-ordinates for any year from the known co-ordinates derived from satellite data for the years 1990, 1997, 2000 and 2002. The data of years 1990, 1997 and 2000 were partitioned into training (80%), testing sets (20%), whereas the database of year 2002 has been left out for model validation. Figure 4.39 depicts the architecture of the ANN model. The ANN model was simulated with month and year as input and the right bank co-ordinates at 101 points as outputs. The data were normalised between values 0 and 1.

#### 4.8.1.3.1 Validation and evaluation of predictive capability

An *rmse* of 0.0001 and Nash co-efficient of 0.9786 were obtained for this model. The iterations were 7270 and average correlation co-efficient "*r*" was 0.999. Efficiency of this model was 97.86%. Figure 4.45 shows the plot of validation curve between observed data and ANN predicted data for left bank co-ordinates for the year 2002.

#### 4.8.1.4 Model 4

The model 4 was constituted similar to model 2 with architecture 103-105-101 and back-propagation algorithm (BPA) used to simulate the right bank co-ordinates from the known discharges for the years 1990, 1997, 2000 and 2002. The data of years 1990, 1997 and 2000 were partitioned into training (80%), testing sets (20%), where the database of year 2002 was used for model validation. The data were normalised between values 0 and 1. The sigmoid function has been used as the activation function. The goodness-of-fit criteria, such as *rmse* and Nash coefficient for the result were 0.0397 and 0.9997 respectively. The iterations were 20,862 and average correlation co-efficient '*r*' was 0.9673. Efficiency of this model was 99.99%. Figure 4.46 shows the plot of validation curve between observed data and ANN predicted data for right bank co-ordinates for the year 2001.

The co-ordinates for the year 1996 computed from model 3, 4 and the spatio-temporal computer programme using shape function were revalidated to verify the accuracy of the models. Figure 4.47 presents the plot of the data for 1996. The model efficiency of all these models suggests that ANN rendered a good predicting capability.

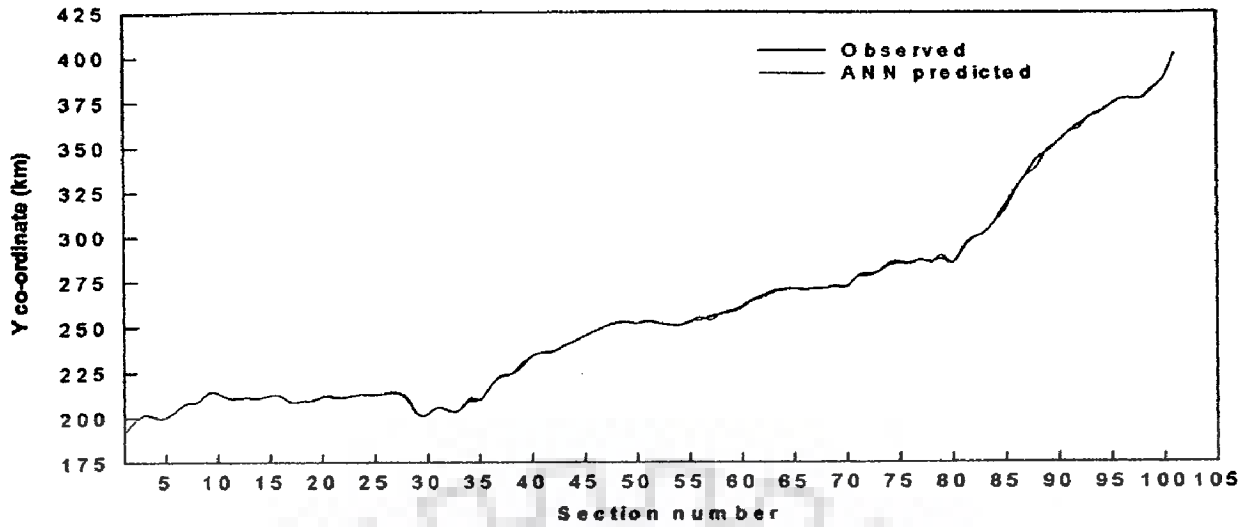


**Figure 4.45** Plot of observed and ANN predicted data for right bank co-ordinates (2002)

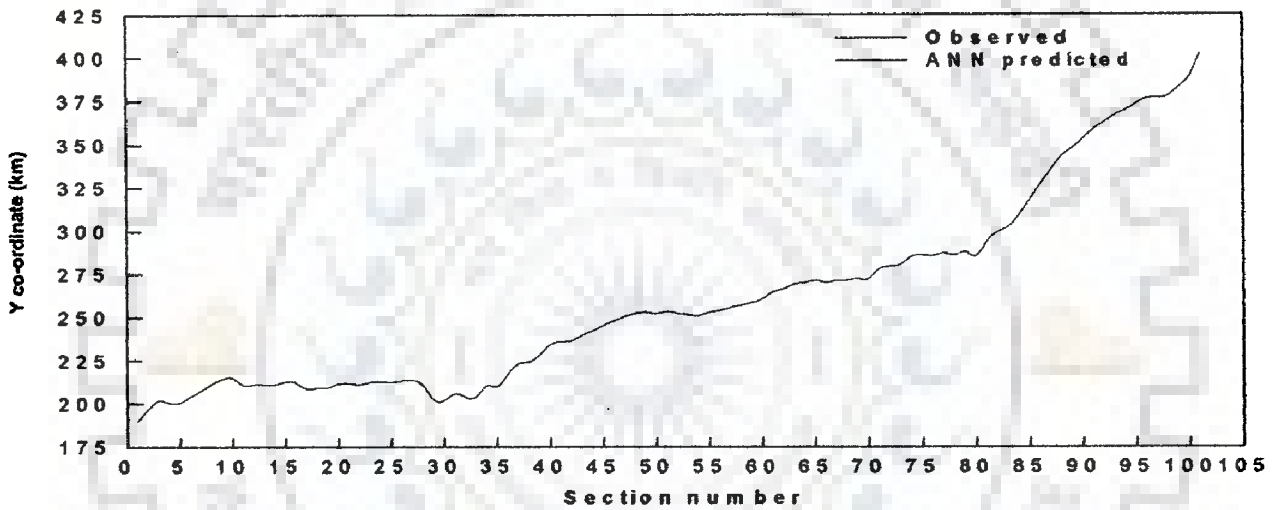


**Figure 4.46** Plot of observed, ANN predicted for right bank co-ordinates (2001)

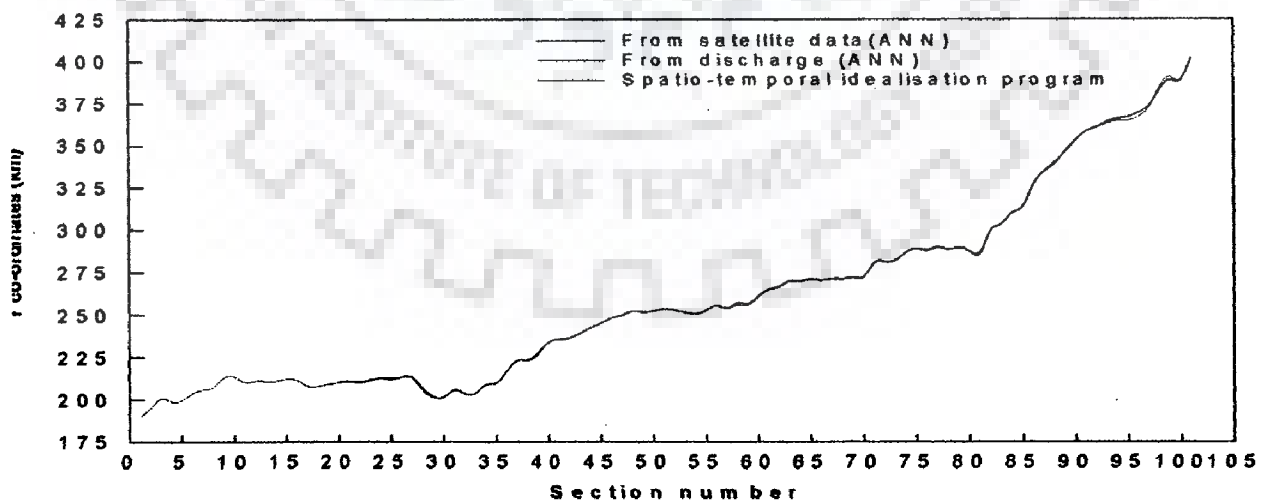


**Figure 4.47** Plot of observed, ANN predicted and data computed from spatio-temporal idealisation programme for right bank co-ordinates (1996)



**Table 4.13 Performance indicators of the models 1, 2, 3 and 4**

Items	Model 1	Model 2	Model 3	Model 4
<i>rmse</i>	0.011	0.0139	0.0001	0.0397
Nash coefficient	0.9659	0.9997	0.9786	0.9999
Correlation coefficient	0.9998	0.9999	0.999	0.9673
Iterations	7270	25000	7270	20862
Learning algorithm	Conjugate Gradient Descent	Conjugate Gradient Descent	Conjugate Gradient Descent	Conjugate Gradient Descent
Architecture	2-68-68-101	103-105-101	2-68-68-101	103-105-101

#### 4.8.1.5 Models 5, 6, 7 and 8

##### 4.8.1.5.1 Data preparation and selection of input and output variables

The ANN models 5, 6, 7 and 8 with architecture 2-75-100 have been constituted with supervised feed forward back-propagation method with first-order gradient descent learning algorithm with one hidden layer for prediction of erosion and deposition. The number of hidden neurons has been obtained after several runs of the network with different numbers of neuron using a systematic approach, *adaptive method of architecture determination*, as described earlier. The data were divided into three sets: training (70%), testing (15%) and validation (15%). Month and year has been used as input variables in the models 5, 6, 7 and 8. Two sets of dimensionless parameters  $\alpha_1, \dots, \alpha_{100}$  and  $\lambda_1, \dots, \lambda_{100}$  have been calculated for both the banks of the river for all the four years 1990, 1997, 2000 and 2002. The dimensionless parameters were defined as;

$$\alpha_1, \dots, \alpha_{100} = \text{Area of a strip} / \text{Sum of areas of all strips} \quad (4.13)$$

$$\lambda_1, \dots, \lambda_{100} = \text{length of arc of a strip} / \text{total length of bank line} \quad (4.14)$$

Model 5 and 6 used dimensionless parameters  $\alpha_1, \dots, \alpha_{100}$  as output training data for left and right banks respectively to calculate the variation in strip area. Similarly, models 7 and 8 used dimensionless parameters  $\lambda_1, \dots, \lambda_{100}$  for left and right banks respectively to assess the change in strip arc length. Figure 4.48 depicts architecture of the spatio-temporal ANN model showing the input and output parameters. The dimensionless parameters  $\alpha_1, \dots, \alpha_{100}$  and  $\lambda_1, \dots, \lambda_{100}$  fed into ANN models with month and year as input and the dimensionless parameters  $\alpha$  and  $\lambda$  as outputs.

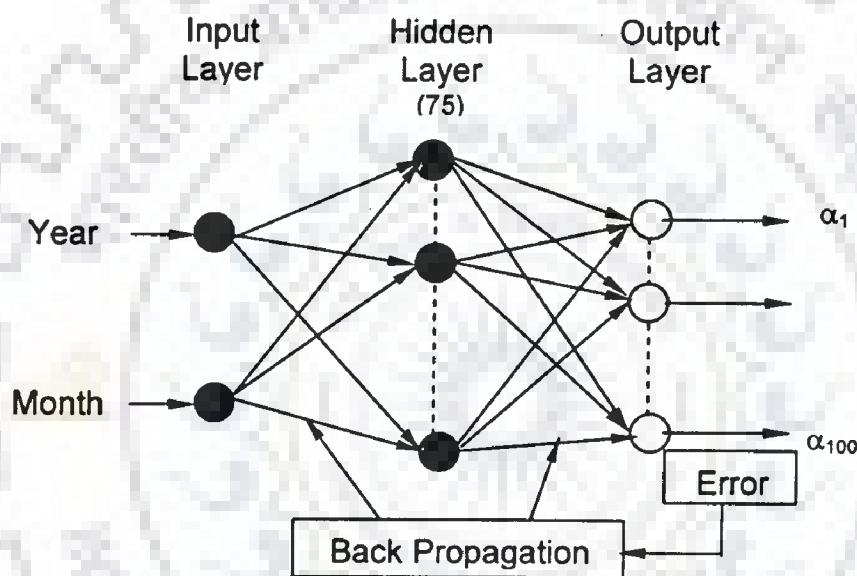
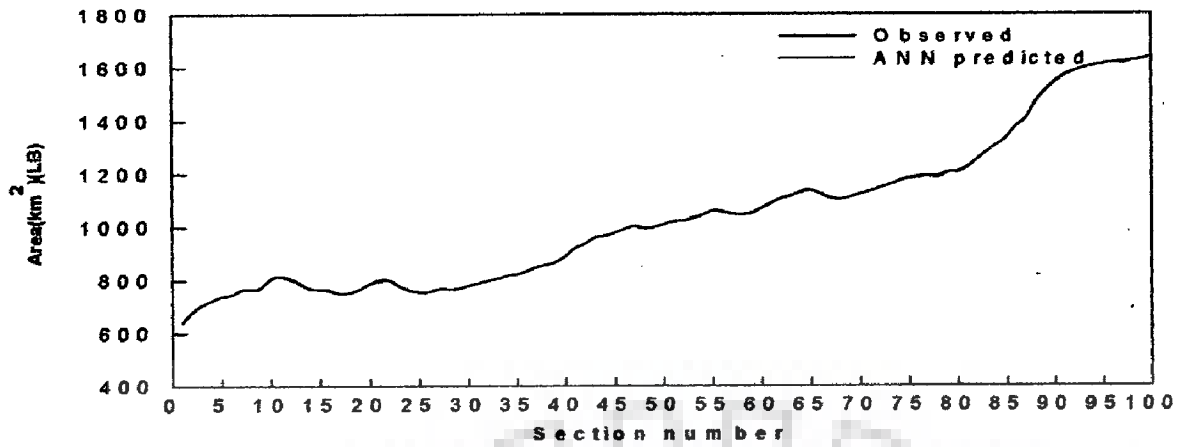


Figure 4.48 Architecture of ANN models 5, 6, 7 & 8

#### 4.8.1.5.2 Results and model validation

After the training phase of the models has been successfully accomplished, the performance of the trained models was validated. The approach that was adopted to achieve this was to test the performance of trained ANNs on an independent validation set, which has not been used as part of the training process. Figures 4.49 to 4.52 present the validation curves of the models.



**Figure 4.49** Plot of observed, ANN predicted area of strips for left bank (2002)

The coefficient of correlation  $r$ , the  $rmse$  and Nash coefficient were used to evaluate the prediction performance in respect of the ANN models 5, 6, 7 and 8 as shown in Table 4.14. Also, other training parameters were high lighted.

To provide a complete qualitative as well as quantitative assessment of erosion and deposition in different strips, the individual strips were analysed.

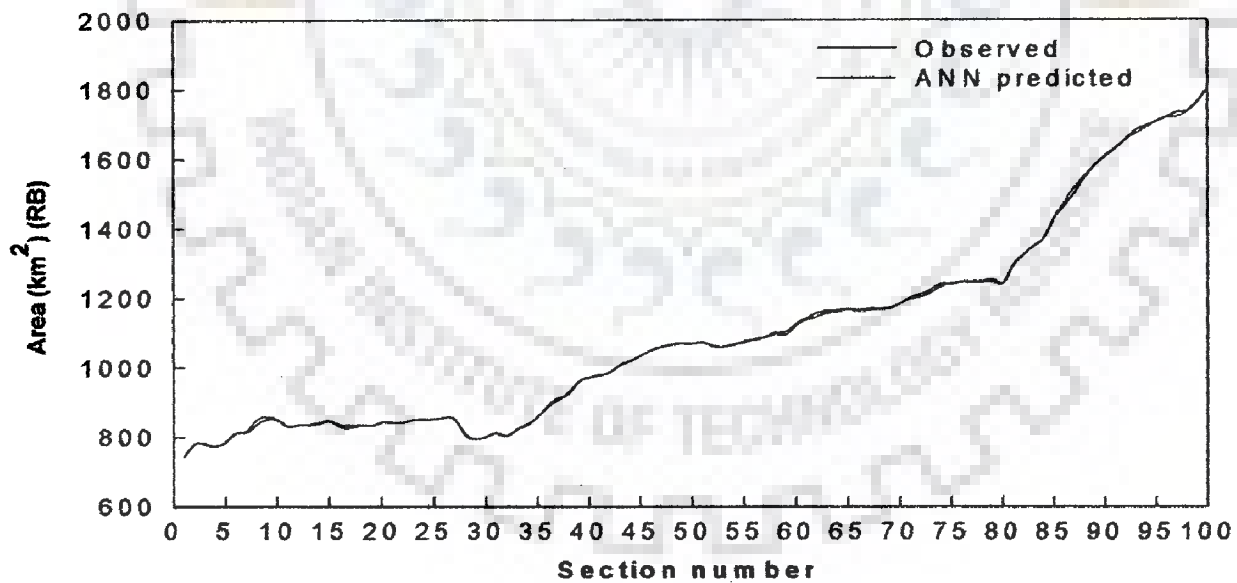


**Figure 4.50** Plot of observed, ANN predicted area of strips for right bank (2002)

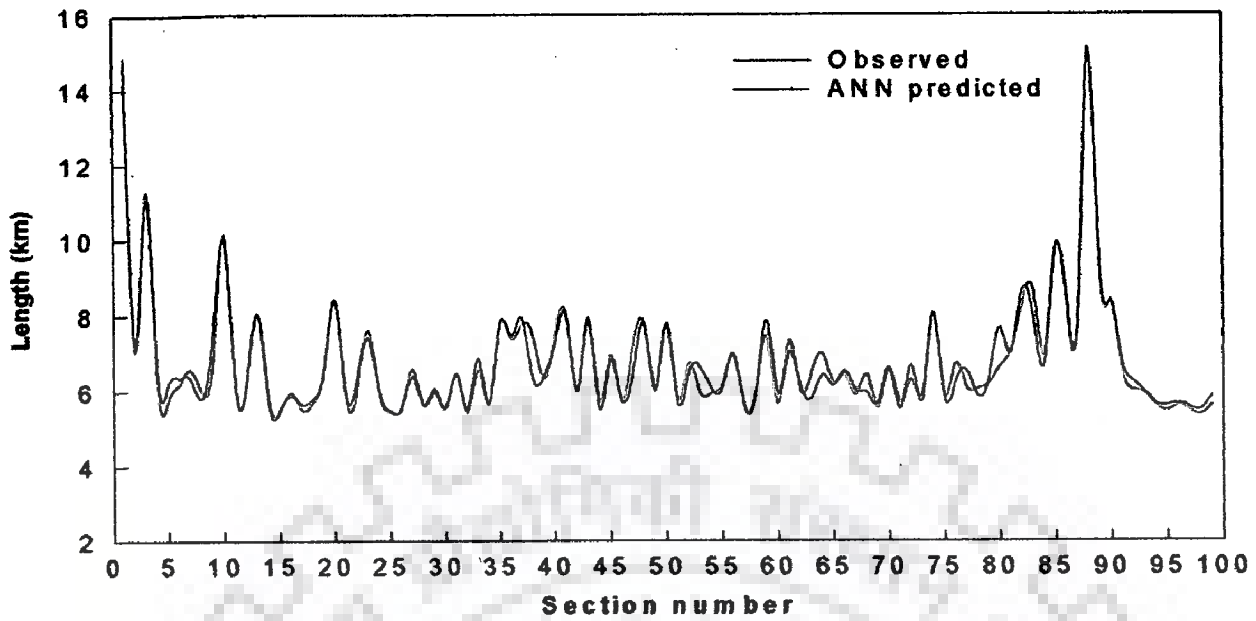


**Figure 4.51** Plot of observed, ANN predicted strip arc length for left bank (2002)

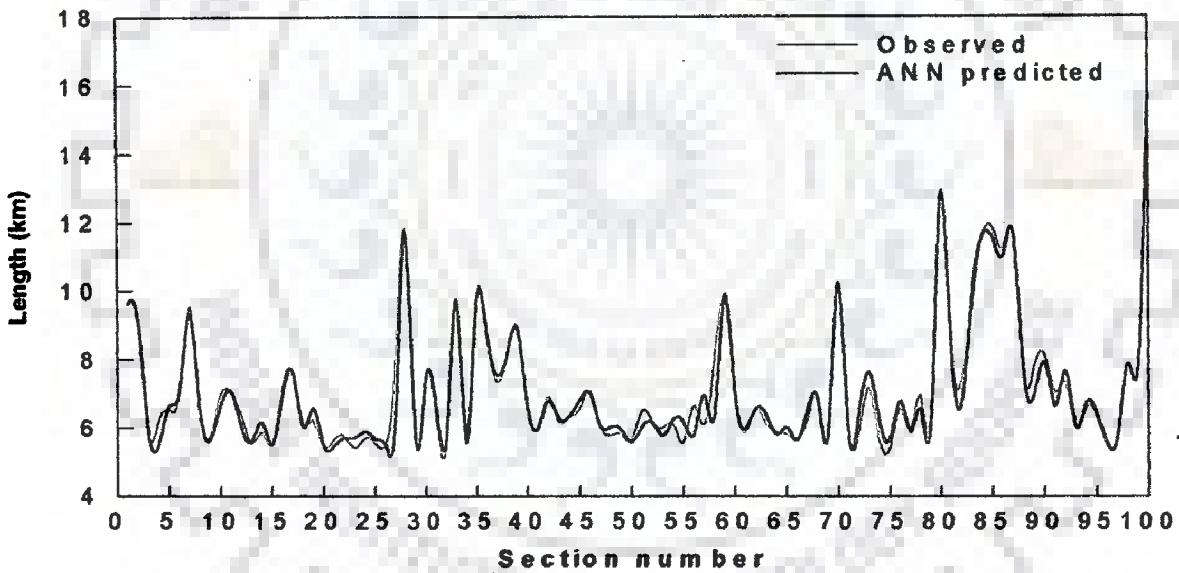


**Figure 4.52** Plot of observed, ANN predicted strip arc length for right bank (2002)

For example, considering left bank of the river, the  $i^{\text{th}}$  strip earlier having area  $a_1$  has increased to area  $a_2$  as shown in Figure 4.53, the increase in area as shown by hatched portion shows deposition. If there was a decrease in area, then there was erosion in the strip. The change in the arc length suggests the change in the bank boundary.

**Table 4.14 Performance indicators of the models 5, 6, 7 and 8**

Items	Model 5	Model 6	Model 7	Model 8
<i>rmse</i>	1.0234E-6	1.0291E-6	0.001	0.001
Nash coefficient	0.9748	0.9998	0.9520	0.8149
Correlation coefficient	0.9776	0.9981	0.9967	0.9867
Iterations	126809	141303	128233	74901
Learning algorithm	Conjugate Gradient Descent	Conjugate Gradient Descent	Conjugate Gradient Descent	Conjugate Gradient Descent
Architecture	2-75-100	2-75-100	2-75-100	2-75-100

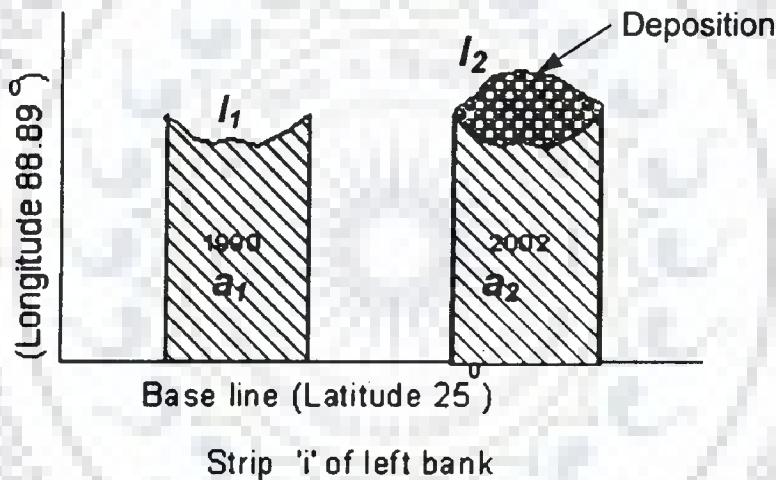


**Figure 4.53 Change in strip area and arc length**

To demonstrate the potential applicability of the models, a sample calculation with the result of the analysis was illustrated in Table 4.15. Using ANN, the dimensionless parameters were evaluated for all the years 1990 to 2002. For the years, 1991 and 2001, the comparison of erosion and deposition was made for all the 100 strips along the river Brahmaputra.

#### **4.8.1.6 Model 9 and 10 (Scenario analysis)**

As the river Brahmaputra is networked by many Trans-Himalayan tributaries, forecasting and warning of impending stages and lateral boundary spreads due to a flash flood assists in regulating outflows during low river flows for river management during non-seasonal flood. In such a situation, one may prefer not to expend the time and efforts required in developing and implementing a conceptual model or numerical model, but instead implement a simpler system theoretic model, such as ANN, which was better way forward. With a view to implementing this, a model predicting the scenario of flash flood was constituted with multilayered perceptron feed forward back-propagation architecture (103-75-101).

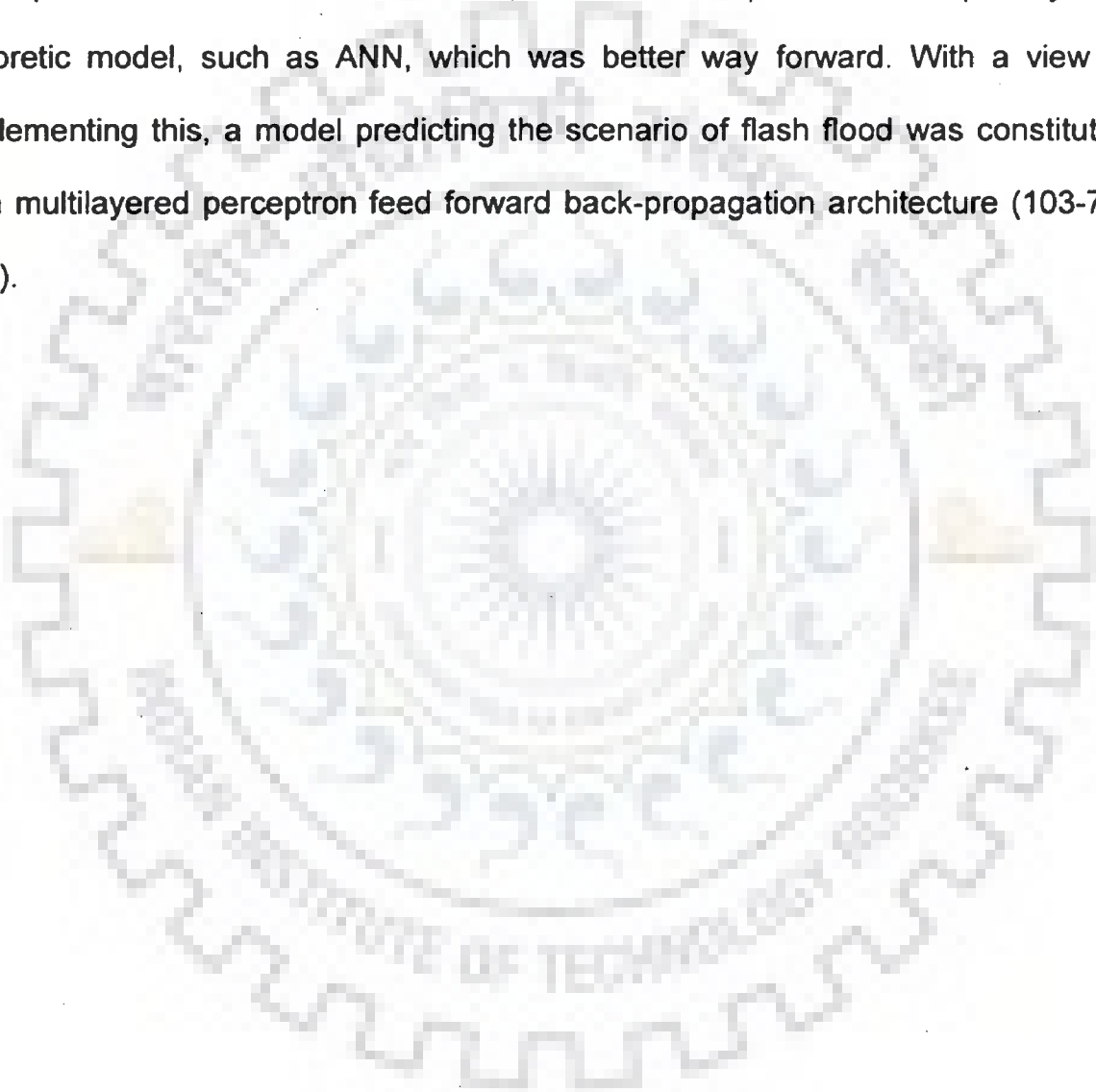


Table 4.15 Sample erosion and deposition pattern analysis for left bank

Year	2001	2001	1991	1991	1991	1991	2001	2001	2001	2001	2001	2001	2001	2001
Strip No	Dimension less param ( $\alpha_1, \dots, \alpha_{100}$ )	Area in km <sup>2</sup>	Dimensio n less param ( $\alpha_1, \dots, \alpha_{100}$ )	Area in km <sup>2</sup>	Dimension less param ( $\lambda_1, \dots, \lambda_{100}$ )	Bank arc length	Dimension less param ( $\lambda_1, \dots, \lambda_{100}$ )	Bank arc length (Km)	Increase/Decrease in area	Increase/Decrease in length	Erosion /Deposition			
1	0.006026	627.18	0.006310	657.09	0.0166365	33.17	0.0237238	47.54	-29.903	14.369	Erosion			
2	0.006540	680.66	0.006560	683.12	0.0094588	18.86	0.0101383	20.32	-2.461	1.456	Erosion			
3	0.006736	701.01	0.006830	711.24	0.0146479	29.21	0.016493	33.05	-10.228	3.844	Erosion			
4	0.006963	724.68	0.007000	728.94	0.0087914	17.53	0.009300	18.64	-4.261	1.106	Erosion			
5	0.007090	737.90	0.007130	742.48	0.009712	19.37	0.0086673	17.37	-4.576	-1.996	Erosion			
6	0.007152	744.38	0.007200	749.77	0.0085227	16.99	0.0093026	18.64	-5.389	1.648	Erosion			
7	0.007330	762.88	0.007325	762.79	0.0089158	17.78	0.009601	19.24	0.093	1.462	Deposition			
8	0.007349	764.86	0.007345	764.89	0.0084201	16.79	0.0087834	17.60	-0.031	0.812	Erosion			
9	0.007429	773.18	0.007411	771.71	0.0109563	21.85	0.010763	21.57	1.477	-0.278	Deposition			
10	0.007742	805.80	0.007743	806.33	0.011583	23.10	0.0144024	28.86	-0.533	5.766	Erosion			
11	0.007810	812.84	0.007800	812.28	0.0086253	17.20	0.0093027	18.64	0.555	1.444	Deposition			
12	0.007721	803.58	0.007718	803.67	0.01055	21.05	0.010220	20.48	-0.086	-0.564	Erosion			
13	0.007555	786.31	0.007532	784.30	0.01233	24.59	0.011738	23.52	2.005	-1.069	Deposition			

Year	2001	2001	1991	1991	1991	1991	2001	2001	2001		
Strip No	Dimension less param ( $\alpha_1, \alpha_{100}$ )	Area in km <sup>2</sup>	Dimension less param ( $\alpha_1, \alpha_{100}$ )	Area in km <sup>2</sup>	Dimension less param ( $\lambda_1, \lambda_{100}$ )	Bank arc length	Dimension less param ( $\lambda_1, \lambda_{100}$ )	Bank arc length (Km)	Increase/Decrease in area	Increase/Decrease in length	Erosion /Deposition
14	0.007376	767.64	0.007346	765.00	0.00825	16.45	0.008369	16.77	2.644	0.324	Deposition
15	0.007347	764.68	0.007340	764.38	0.00805	16.06	0.008083	16.20	0.300	0.137	Deposition
16	0.007306	760.34	0.007273	757.37	0.00872	17.39	0.008654	17.34	2.973	-0.044	Deposition
17	0.007211	750.48	0.007172	746.85	0.00855	17.05	0.008198	16.43	3.630	-0.623	Deposition
18	0.007235	753.03	0.007192	748.93	0.00854	17.04	0.008521	17.08	4.098	0.039	Deposition
19	0.007361	766.06	0.007326	762.92	0.00933	18.61	0.009675	19.39	3.147	0.779	Deposition
20	0.007556	786.45	0.007520	783.06	0.01078	21.49	0.011105	22.26	3.395	0.769	Deposition
21	0.007670	798.31	0.007621	793.62	0.00972	19.39	0.009244	18.52	4.686	-0.863	Deposition
22	0.007676	798.84	0.007582	789.57	0.01175	23.42	0.009139	18.31	9.275	-5.108	Deposition
23	0.007467	777.17	0.007433	774.02	0.01079	21.51	0.011027	22.10	3.155	0.585	Deposition
24	0.007312	761.01	0.007280	758.10	0.00831	16.57	0.009080	18.20	2.915	1.622	Deposition
25	0.007231	752.96	0.007250	754.57	0.00810	16.16	0.008038	16.11	-1.610	-0.050	Erosion
26	0.007260	755.64	0.007238	753.67	0.00807	16.08	0.008201	16.43	1.966	0.352	Deposition
27	0.007358	765.78	0.007338	764.09	0.01012	20.18	0.009452	18.94	1.698	-1.235	Deposition



Year	2001	2001	1991	1991	1991	1991	2001	2001	2001	2001	
Strip No	Dimension less param ( $\alpha_1, \alpha_{100}$ )	Area in km <sup>2</sup>	Dimension less param ( $\alpha_1, \alpha_{100}$ )	Area in km <sup>2</sup>	Dimension less param ( $\lambda_1, \lambda_{100}$ )	Bank arc length	Dimension less param ( $\lambda_1, \lambda_{100}$ )	Bank arc length (Km)	Increase/Decrease in area	Increase/Decrease in length	Erosion/Deposition
28	0.007355	765.44	0.007349	765.26	0.00855	17.04	0.008268	16.57	0.177	-0.474	Deposition
29	0.007380	768.10	0.007361	766.55	0.00861	17.16	0.008890	17.82	1.551	0.655	Deposition
30	0.007485	779.04	0.007453	776.07	0.00818	16.32	0.008170	16.37	2.966	0.056	Deposition
31	0.007570	787.88	0.007542	785.38	0.00945	18.85	0.009540	19.12	2.498	0.266	Deposition
32	0.007660	797.26	0.007631	794.62	0.00808	16.12	0.008067	16.17	2.638	0.051	Deposition
33	0.007745	806.12	0.007721	804.03	0.00974	19.42	0.009960	19.96	2.088	0.535	Deposition
34	0.007850	817.02	0.007822	814.51	0.00823	16.41	0.008340	16.71	2.510	0.301	Deposition
35	0.007900	822.22	0.007873	819.80	0.00929	18.53	0.009743	19.52	2.421	0.992	Deposition
36	0.008015	834.18	0.007981	831.07	0.01031	20.55	0.010909	21.86	3.110	1.311	Deposition
37	0.008154	848.69	0.008117	845.24	0.00997	19.87	0.011040	22.12	3.452	2.252	Deposition
38	0.008243	857.88	0.008305	864.79	0.01008	20.11	0.009818	19.68	-6.904	-0.431	Erosion
39	0.008354	869.45	0.008420	876.80	0.00857	17.09	0.010600	21.24	-7.343	4.154	Erosion
40	0.008579	892.86	0.008530	888.25	0.01423	28.37	0.010706	21.46	4.613	-6.917	Erosion

Year	2001		1991		1991		1991		2001		Increase/ Decrease in length	Erosion /Deposition
	Strip No	Dimension less param ( $\alpha_1, \dots, \alpha_{100}$ )	Area in km <sup>2</sup>	Dimensio n less param ( $\alpha_1, \dots, \alpha_{100}$ )	Area in km <sup>2</sup>	Dimensi on less param ( $\lambda_1, \dots, \lambda_{100}$ )	Bank arc length	Dimensio n less param ( $\lambda_1, \dots, \lambda_{100}$ )	Bank arc length (Km)	Increase/ Decrease in area		
41	0.008860	922.12	0.008845	921.11	0.01055	21.05	0.011490	23.03	1.010	1.979	Deposition	
42	0.009010	937.70	0.009014	938.65	0.01007	20.07	0.008989	18.01	-0.948	-2.058	Deposition	
43	0.009229	960.56	0.009212	959.29	0.00942	18.79	0.011691	23.43	1.279	4.642	Deposition	
44	0.009283	966.15	0.009271	965.43	0.00810	16.15	0.008272	16.58	0.724	0.426	Deposition	
45	0.009400	978.35	0.009370	975.79	0.00992	19.77	0.010130	20.30	2.563	0.529	Deposition	
46	0.009530	991.85	0.009522	991.52	0.00882	17.59	0.008412	16.86	0.334	-0.728	Erosion	
47	0.009630	1002.28	0.009601	999.83	0.00945	18.85	0.009952	19.94	2.443	1.096	Deposition	
48	0.009556	994.56	0.009664	1006.40	0.00992	19.78	0.010215	20.47	-11.846	0.689	Deposition	
49	0.009606	999.79	0.009678	1007.79	0.01059	21.12	0.008856	17.75	-7.996	-3.375	Erosion	
50	0.009694	1008.91	0.009757	1016.01	0.00849	16.93	0.011286	22.62	-7.108	5.683	Deposition	
51	0.009795	1019.47	0.009771	1017.50	0.00828	16.52	0.008433	16.90	1.974	0.382	Deposition	
52	0.009825	1022.60	0.009801	1020.65	0.00920	18.34	0.009715	19.47	1.949	1.126	Deposition	
53	0.009924	1032.90	0.009890	1029.87	0.01384	27.60	0.009255	18.55	3.024	-9.054	Erosion	

Year	2001	2001	1991	1991	1991	1991	1991	2001	2001	2001	2001	2001	2001	2001
Strip No	Dimension less param ( $\alpha_1, \alpha_{100}$ )	Area in km <sup>2</sup>	Dimension less param ( $\alpha_1, \alpha_{100}$ )	Area in km <sup>2</sup>	Dimension less param ( $\lambda_1, \lambda_{100}$ )	Bank arc length	Dimension less param ( $\lambda_1, \lambda_{100}$ )	Bank arc length (Km)	Increase/Decrease in area	Increase/Decrease in length	Erosion/Deposition			
54	0.010045	1045.46	0.009986	1039.85	0.00942	18.79	0.008874	17.78	5.609	-1.006	Deposition			
55	0.010180	1059.55	0.010142	1056.17	0.00990	19.75	0.008982	18.00	3.382	-1.745	Deposition			
56	0.010141	1055.44	0.010138	1055.69	0.01223	24.39	0.010361	20.76	-0.245	-3.626	Erosion			
57	0.010073	1048.34	0.010096	1051.33	0.00857	17.09	0.010042	20.12	-2.991	3.036	Deposition			
58	0.010001	1041.46	0.010048	1045.72	0.00934	18.63	0.008743	17.52	-4.263	-1.111	Erosion			
59	0.010110	1052.18	0.010026	1044.04	0.01109	22.12	0.011403	22.85	8.140	0.736	Deposition			
60	0.010282	1070.15	0.010223	1064.60	0.00844	16.83	0.008584	17.20	5.548	0.376	Deposition			
61	0.010469	1089.61	0.010395	1082.47	0.01104	22.01	0.010410	20.86	7.147	-1.153	Deposition			
62	0.010635	1106.84	0.010583	1102.07	0.00906	18.07	0.008913	17.86	4.772	-0.211	Deposition			
63	0.010726	1116.32	0.010710	1115.25	0.00897	17.89	0.008825	17.69	1.075	-0.209	Deposition			
64	0.010809	1125.57	0.010869	1131.09	0.00857	17.09	0.009852	19.74	5.521	2.649	Erosion			
65	0.010916	1136.12	0.010843	1129.16	0.00960	19.14	0.010598	21.24	6.965	2.097	Deposition			
66	0.010780	1121.92	0.010833	1128.07	0.01048	20.90	0.009514	19.07	-6.148	-1.831	Erosion			
67	0.010643	1107.71	0.010653	1109.31	0.00867	17.29	0.008794	17.62	-1.605	0.335	Erosion			

Year	2001	2001	1991	1991	1991	1991	1991	2001	2001	2001	2001	2001	2001
Strip No	Dimension less param ( $\alpha_1, \alpha_{100}$ )	Area in km <sup>2</sup>	Dimension less param ( $\alpha_1, \alpha_{100}$ )	Area in km <sup>2</sup>	Dimension less param ( $\lambda_1, \dots, \lambda_{100}$ )	Bank arc length	Dimension less param ( $\lambda_1, \dots, \lambda_{100}$ )	Bank arc length (Km)	Increase/Decrease in area	Increase/Decrease in length	Erosion /Deposition		
68	0.010611	1104.39	0.010564	1100.10	0.00864	17.22	0.009219	18.48	4.294	1.251	Deposition		
69	0.010677	1111.21	0.010645	1108.49	0.01017	20.29	0.008245	16.52	2.716	-3.762	Erosion		
70	0.010788	1122.76	0.010764	1120.95	0.00961	19.15	0.009760	19.56	1.802	0.404	Deposition		
71	0.010886	1132.96	0.010845	1129.34	0.00807	16.09	0.008262	16.56	3.619	0.471	Deposition		
72	0.011007	1145.58	0.010897	1134.79	0.00903	18.01	0.009701	19.44	10.792	1.431	Deposition		
73	0.011120	1157.37	0.011028	1148.37	0.01042	20.77	0.008517	17.07	9.000	-3.701	Erosion		
74	0.011255	1171.41	0.011160	1162.19	0.00921	18.37	0.010880	21.80	9.223	3.429	Deposition		
75	0.011378	1184.14	0.011350	1181.92	0.01057	21.07	0.008614	17.26	2.220	-3.807	Erosion		
76	0.011411	1187.66	0.011409	1188.07	0.00839	16.72	0.009519	19.08	-0.416	2.356	Deposition		
77	0.011463	1193.04	0.011461	1193.46	0.00948	18.90	0.009397	18.83	-0.426	-0.067	Erosion		
78	0.011439	1190.48	0.011425	1189.70	0.00861	17.17	0.008781	17.60	0.785	0.426	Deposition		
79	0.011587	1205.93	0.011576	1205.45	0.00910	18.14	0.009182	18.40	0.478	0.258	Deposition		
80	0.011623	1209.73	0.011601	1208.08	0.00885	17.65	0.010781	21.60	1.645	3.951	Deposition		
81	0.011798	1227.92	0.011763	1224.97	0.01107	22.08	0.009418	18.87	2.945	-3.210	Erosion		

Year	2001	2001	1991	1991	1991	1991	1991	2001	2001	2001	2001	2001	2001	2001	2001
Strip No	Dimension less param ( $\alpha_1, \dots, \alpha_{100}$ )	Area in km <sup>2</sup>	Dimension less param ( $\alpha_1, \dots, \alpha_{100}$ )	Area in km <sup>2</sup>	Dimension less param ( $\lambda_1, \dots, \lambda_{100}$ )	Bank arc length	Dimension less param ( $\lambda_1, \dots, \lambda_{100}$ )	Bank arc length (Km)	Increase/Decrease in area	Increase/Decrease in length	Erosion /Deposition				
82	0.012062	1255.34	0.012012	1250.86	0.01201	23.96	0.012565	25.18	4.484	1.224	Deposition				
83	0.012296	1280.47	0.012333	1283.53	0.01432	28.56	0.012442	24.93	-3.064	-3.629	Erosion				
84	0.012585	1309.84	0.012561	1308.03	0.00902	17.99	0.010034	20.11	1.811	2.119	Deposition				
85	0.012817	1333.96	0.012775	1330.28	0.01424	28.39	0.014290	28.64	3.679	0.243	Deposition				
86	0.013193	1373.81	0.013230	1376.96	0.01274	25.40	0.012365	24.78	-3.148	-0.624	Erosion				
87	0.013515	1406.59	0.013475	1403.16	0.01120	22.34	0.011528	23.10	3.431	0.767	Deposition				
88	0.014084	1465.79	0.014014	1459.39	0.02275	45.35	0.023594	47.28	6.396	1.929	Deposition				
89	0.014501	1509.23	0.014467	1506.49	0.01277	25.46	0.013366	26.78	2.743	1.330	Deposition				
90	0.014826	1543.07	0.014772	1538.27	0.01267	25.27	0.012318	24.68	4.805	-0.585	Deposition				
91	0.015071	1568.56	0.015016	1563.68	0.00974	19.43	0.009762	19.56	4.874	0.135	Deposition				
92	0.015225	1584.57	0.015184	1581.19	0.00893	17.80	0.009000	18.04	3.378	0.235	Deposition				
93	0.015330	1595.53	0.015283	1591.52	0.00846	16.87	0.008726	17.49	4.004	0.620	Deposition				
94	0.015415	1604.38	0.015382	1601.79	0.00823	16.42	0.008325	16.68	2.593	0.265	Deposition				
95	0.015452	1609.11	0.015475	1610.62	0.00813	16.20	0.008138	16.31	-1.513	0.105	Erosion				

Year	2001	2001	1991	1991	1991	1991	1991	2001	2001	2001	2001	2001	2001	2001	2001
Strip No	Dimension less param $(\alpha_1, \alpha_{100})$	Area in km <sup>2</sup>	Dimension less param $(\alpha_1, \alpha_{100})$	Area in km <sup>2</sup>	Dimension less param $(\lambda_1, \lambda_{100})$	Bank arc length	Dimension less param $(\lambda_1, \lambda_{100})$	Bank arc length (Km)	Increase/Decrease in area	Increase/Decrease in length	Erosion /Deposition				
96	0.015529	1616.25	0.015598	1624.32	0.01299	25.90	0.008263	16.56	-8.066	-9.337	Erosion				
97	0.015552	1618.57	0.015918	1657.64	0.01001	19.96	0.008098	16.23	-39.068	-3.729	Erosion				
98	0.015600	1623.63	0.016001	1666.29	0.00986	19.66	0.007983	16.00	-42.658	-3.665	Erosion				
99	0.015654	1629.24	0.016143	1681.03	0.00865	17.24	0.008382	16.80	-51.792	-0.442	Erosion				
100	0.015734	1637.56	0.016252	1692.43	0.00973	19.41	0.010448	20.94	-54.874	1.528	Deposition				

Month and year along with river flow at 101 points were simulated as input with incremental extrapolation to achieve the output as co-ordinates at 101 spatial points on the river right and left bank in Model 9 and 10 respectively. Flash flood of magnitude  $45,000 \text{ m}^3/\text{sec}$  was injected in the month of March at the confluence point (section 53) of Jia Bhareli - a flashy north side tributary of the river Brahmaputra with the main river and simulation was carried out in steps gradually increasing the flash flood flow from  $30,000 \text{ m}^3/\text{sec}$ . Figure 4.54 demonstrates the generalization ability of such approach to predict a scenario, when compared with the average monthly flow of March, 2002.

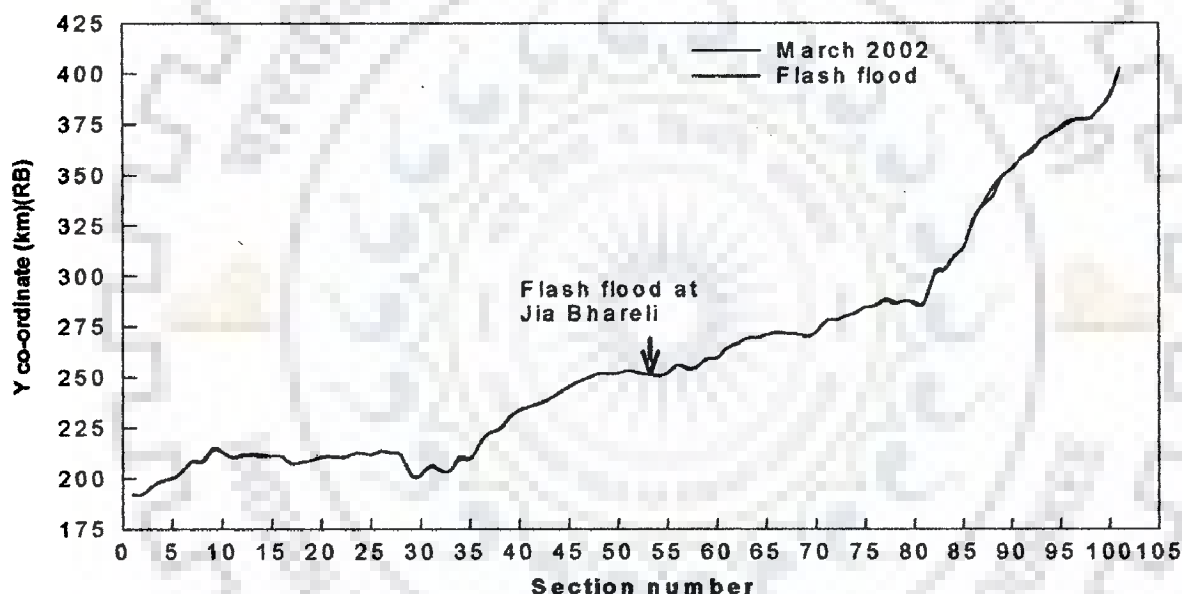


**Figure 4.54** Plot of right bank migration due to flash flood at Jia Bhareli-section 53

## 4.8.2 Hydrographic Models

### 4.8.2.1 Model 11

Measurement of cross-sections of a large braided river like the Brahmaputra is probably the most difficult task involving of huge amount of time and money. The reduced level data of the cross-sections provide the needed information for a number of uses, including active channel width and depth, wetted perimeter, bank height and

angle, elevation and extent of floodplain and adjacent terraces. Derived attributes for the active channel include cross-sectional area, average depth, hydraulic radius, and width to depth ratio. These values can be combined with longitudinal and hydraulic data to calculate channel velocity and discharge at various stages, stream power, shear stress, and other parameters that begin to quantify channel processes.

Adjustment of cross-sectional form is primarily effected by bank erosion and lateral channel migration, channel widening or narrowing, which represents a dominant means of channel response and affects the entire fluvial system in spatial and temporal scale. ANN prediction of cross-sectional form has been modelled at which the measurement variance is minimised.

The ANN architecture used was a four-layer perceptron (2-20-20-52) feed forward neural network. This type of the neural network was trained for 5000 iterations with the back-propagation algorithm. Figure 4.55 shows the plot of observed and predicted data for the year 1997 in respect of Pancharatna (cross-section 9). The goodness-of-fit criteria, such as *rmse* and Nash coefficient for the results were 1.292 and 0.9989 respectively. The efficiency of the model was 99.89%.

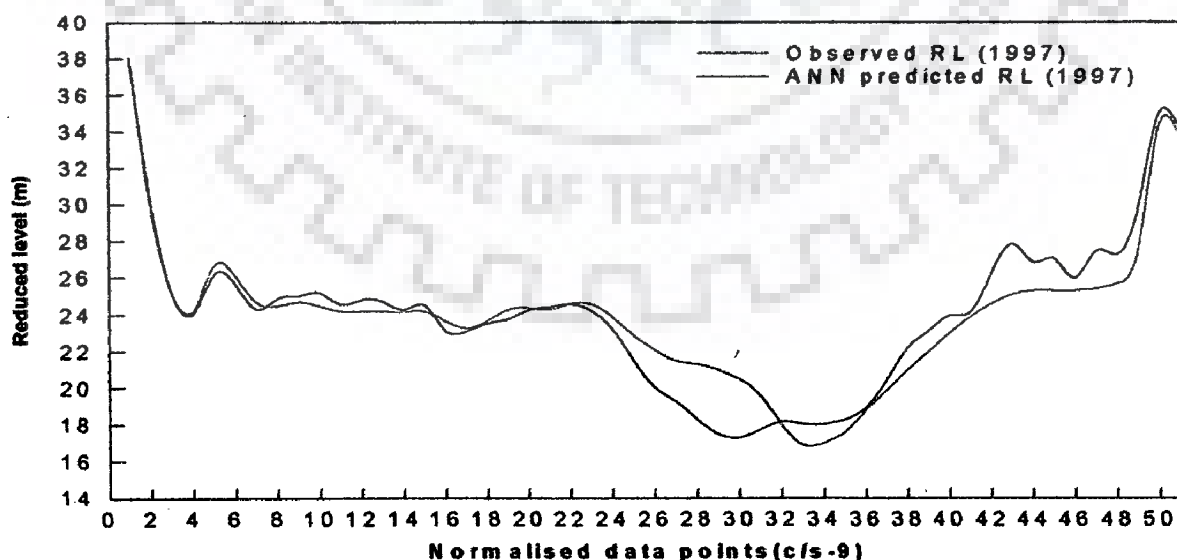


Figure 4.55 Plot of observed and predicted reduced level data for Pancharatna



## **4.9 FLOW CHARACTERISTIC MODELS**

### **4.9.1 Predictive Models**

The behaviour of the Brahmaputra is highly unpredictable and erratic as it shifts its course very abruptly during monsoon causing erosion and deposition at various locations. The maximum discharge passed during the study period was about 48,160m<sup>3</sup>/sec (at Pancharatna in August, 1998). The width of the river varied from 1.20 to 18.13 km and barring few nodal points it has highly braided planform. Discharge at monsoon period submerged large area in the plains of the Brahmaputra valley. Therefore, a systematic study of total river dynamics has been attempted at for effective river basin management.

#### **4.9.1.1 Model 12, 13 and 14**

Flow characteristic prediction models were constituted to demonstrate the applicability of the ANN approach in developing effective nonlinear flow characteristic models of the river stage, flow and sediment discharge at pre-defined 101 sections without the need to explicitly represent the internal hydrologic structure of the river Brahmaputra. The models were formulated for three segments, e.g. normalised sections 1 to 35, 41 to 70 and 62 to 101 and combined together for the entire stretch. The ANN models thus developed have been validated with the observed data of the river Brahmaputra and are expected to reasonably predict the fluvio-morphological variability, such as discharge, stage and sediment flow at discrete points with respects to space and time. The average monthly discharges, stages and sediment discharges have been predicted in three different neuromorphic models. For each neuromorphic model, the data were split up into three parts; one for model training (70%), one for cross validation (15%) (to prevent model over training), and another for testing (15%) the performance of the model. In order to keep the simplicity of model structure, the

number of hidden layers for the neural architecture was chosen as one after several trials.

The performance analysis was represented by statistical goodness-of-fit measures, including rmse (*rmse*), Nash coefficient and correlation coefficient, which significantly support the gainful use of the ANN model. The salient details of the input, output and performance analyses in respect of the models 12, 13 and 14 have been illustrated in a tabular form in Table 4.16. A database was developed using 13 years data (from 1990 to 2002) of average river flow, stages and sediment discharges from 101 sections for the monsoon period (June to October).

ANN architecture used was a three-layer perceptron feed-forward back-propagation method with conjugate gradient descent learning algorithm. The data of June to October, 2001, a separate set has been used for query for validation purpose. The observed and the ANN predicted stages (August, 2001) and sediment discharges (June, 2001) validated for Model 12 have been plotted in Figures 4.56 and 4.57 respectively. The observed and the ANN predicted water discharges (June, 2001) and stages (Sept, 2001) for 101 points validated for Model 13 and plotted in Figures 4.58 and 4.59 respectively. The stages thus predicted from the model 12 and 13 were again re-validated as depicted in Figure 4.60 to recheck the accuracy of the models. Figure 4.61 and 4.62 demonstrate the validation curves of water discharges and sediment discharges in respect of Model 14.

The sediment models show a poorer performances compared to water discharge, stage as the observed data are measured at only two points, i.e. at Pandu and Pancharatna on the Brahmaputra and at other points the data have been generated using Hydrologic Engineering Centre (HEC)-6 movable bed model developed by US Army Corps of Engineers. As could be seen from the graphs, the models proved their

capability in predicting the data, especially the stage data, which showed a high correlation of the observed and predicted data.

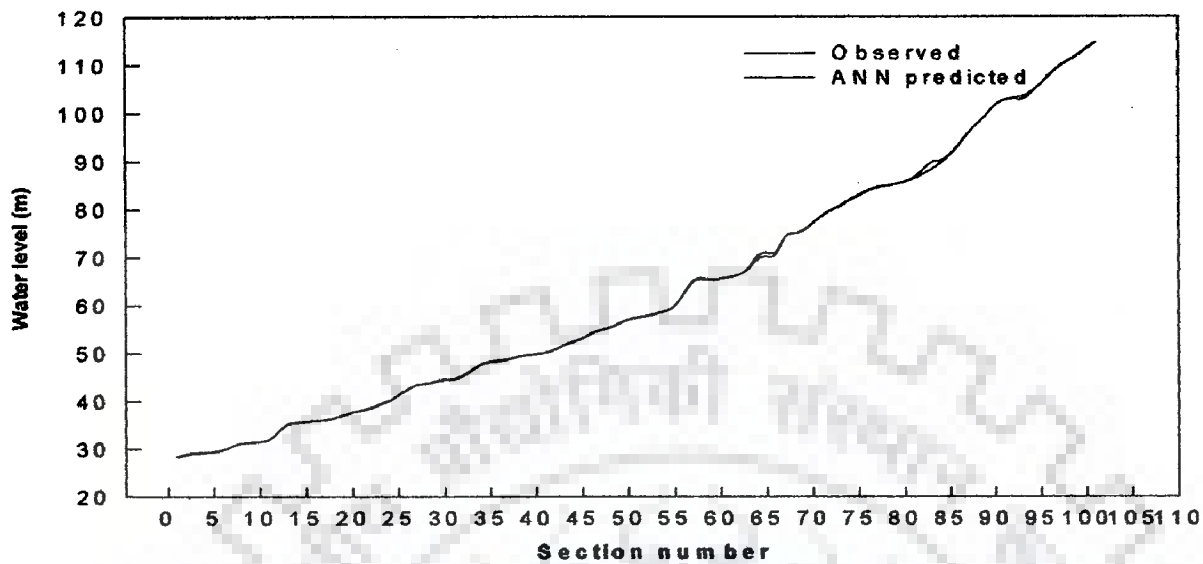
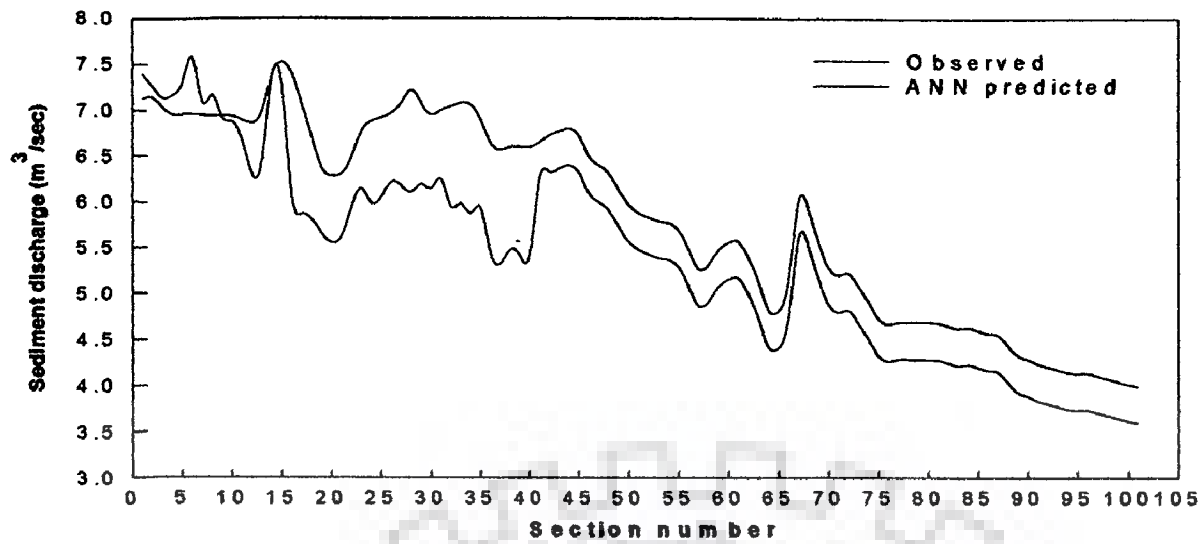


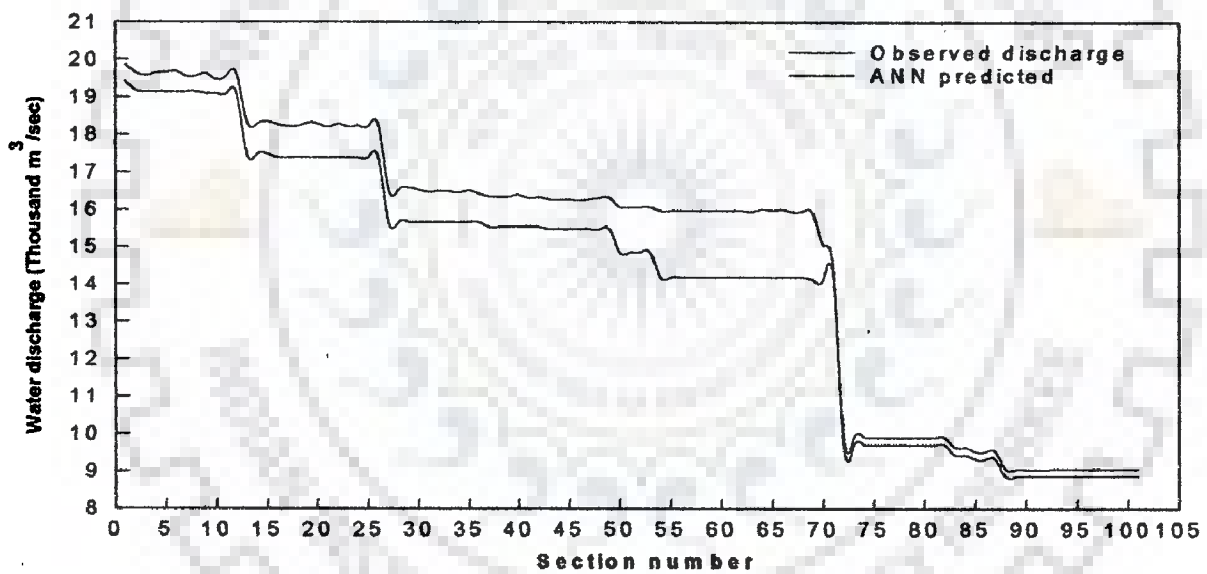
Figure 4.56 Observed v/s ANN predicted water levels for August, 2001 (Model 12)

Table 4.16 Performance analyses for observed and ANN predicted data for Models 12, 13 and 14

	Input	Output	<i>rmse</i>	Nash Coefficient
Model 12	Discharge (Q)	Sediment (Qs) &	0.590	0.7029
		Water level (WL)	0.271	0.9999
Model 13	Sediment (Qs)	Discharge (Q) &	0.835	0.9738
		Water level (WL)	0.228	0.999
Model 14	Water level (WL)	Discharge (Q) &	0.382	0.988
		Sediment (Qs)	1.60	0.487



**Figure 4.57** Observed v/s ANN predicted sediment discharges, July, 2001 (Model 12)



**Figure 4.58** Observed v/s ANN predicted discharge for June, 2001 (Model 13)

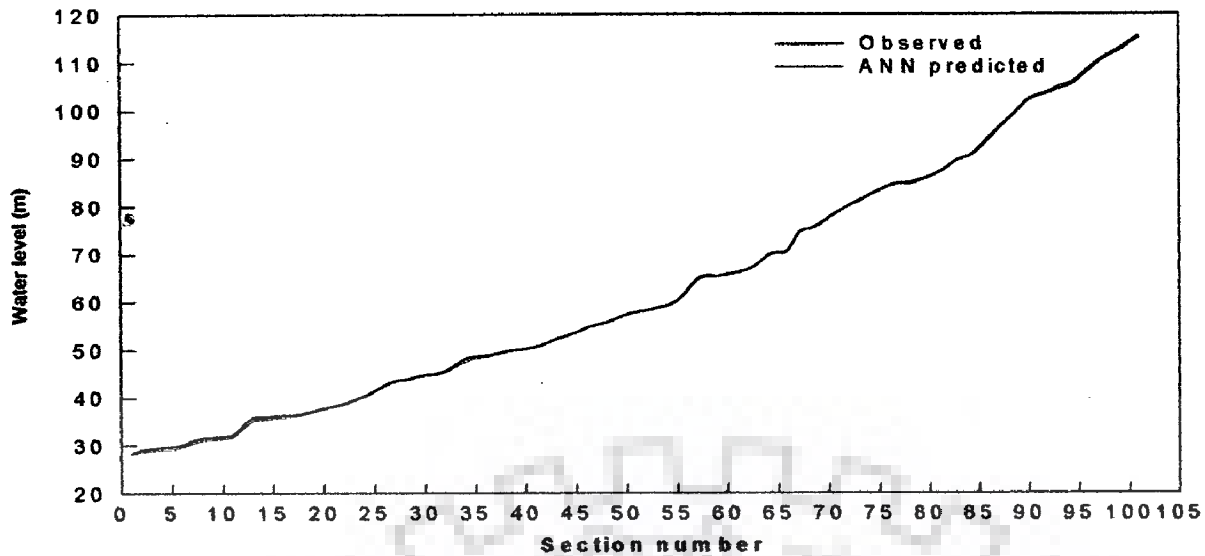


**Figure 4.59** Observed v/s ANN predicted water level for Sept, 2001 (Model 13)

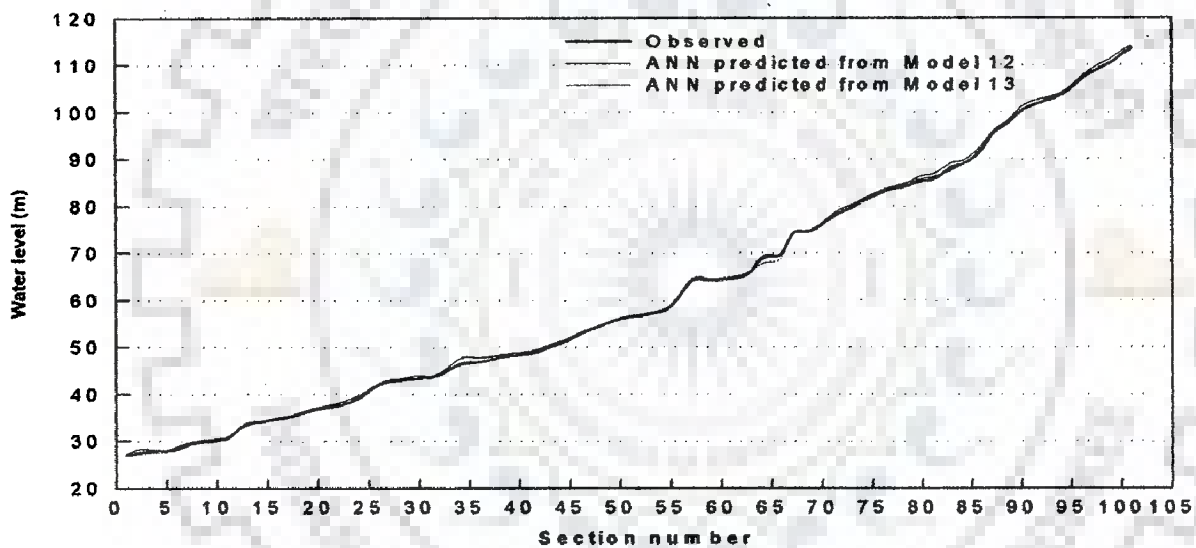


**Figure 4.60** Plot of observed v/s ANN predicted water levels from Model 12 & 13 for Sept, 2001

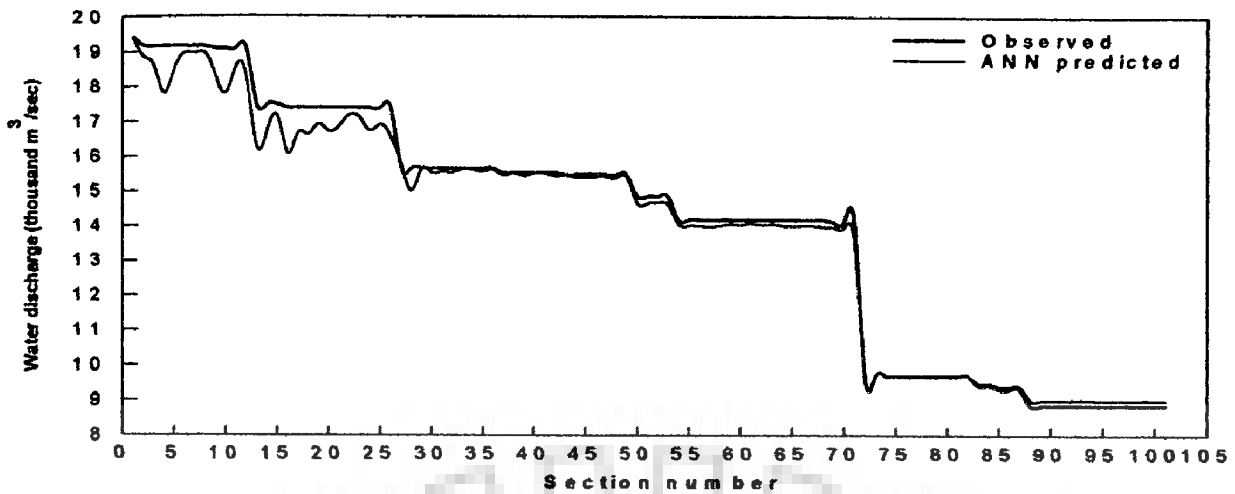


**Figure 4.61** Plot of observed v/s ANN predicted discharge from Model 14 for June, 2001

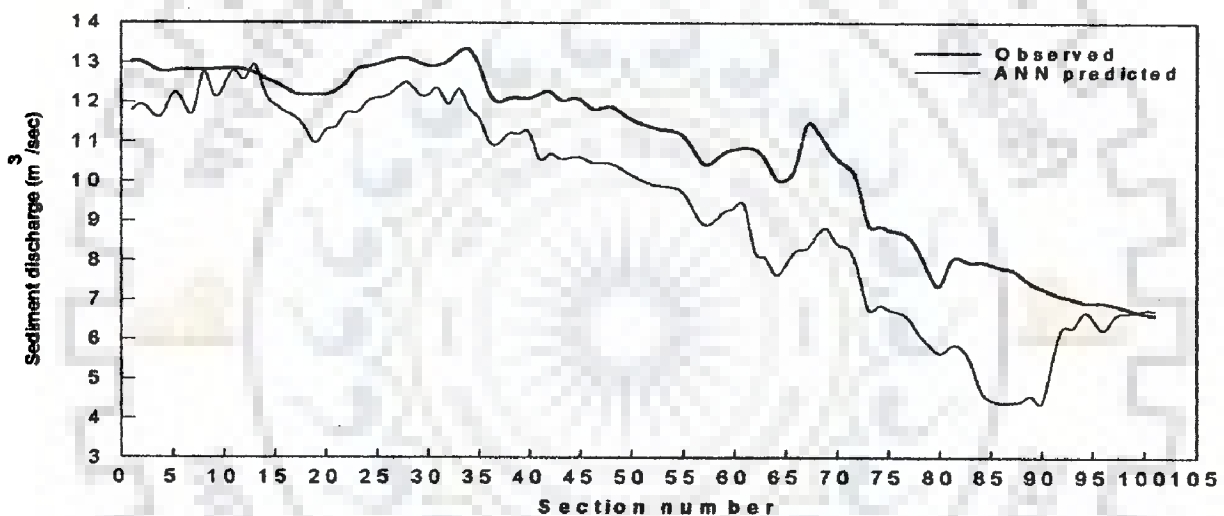


**Figure 4.62** Plot of observed v/s ANN predicted sediment discharge from Model 14 for August, 2001

## 4.9.2 What-if-then Model

### 4.9.2.1 Model 15 (Composite model for missing & imperfect data)

The composite model was constituted to reasonably predict the fluvio-morphological variability, such as discharge, stage and sediment flow at discrete points with respects to space and time, when some particular data were imperfectly presented or missing. The models were formulated for four segments, e.g. normalised sections 1 to 25, 26 to 50, 51 to 75 and 76 to 101 and results were fused together for the entire stretch. The performance analysis was represented by quantity numbers,

including *rmse*, Nash coefficient and correlation coefficient. The model efficiencies were 98.9% and 50.29% in respect of observed and ANN predicted stage and sediment discharges respectively. The *rmse* values for the models were 0.14 and 1.68 respectively, which showed the reliability of the forecasted values. Figures 4.63 and 4.64 demonstrate the validation curves of water levels and sediment discharges for October, 2001 in respect of Model 15.

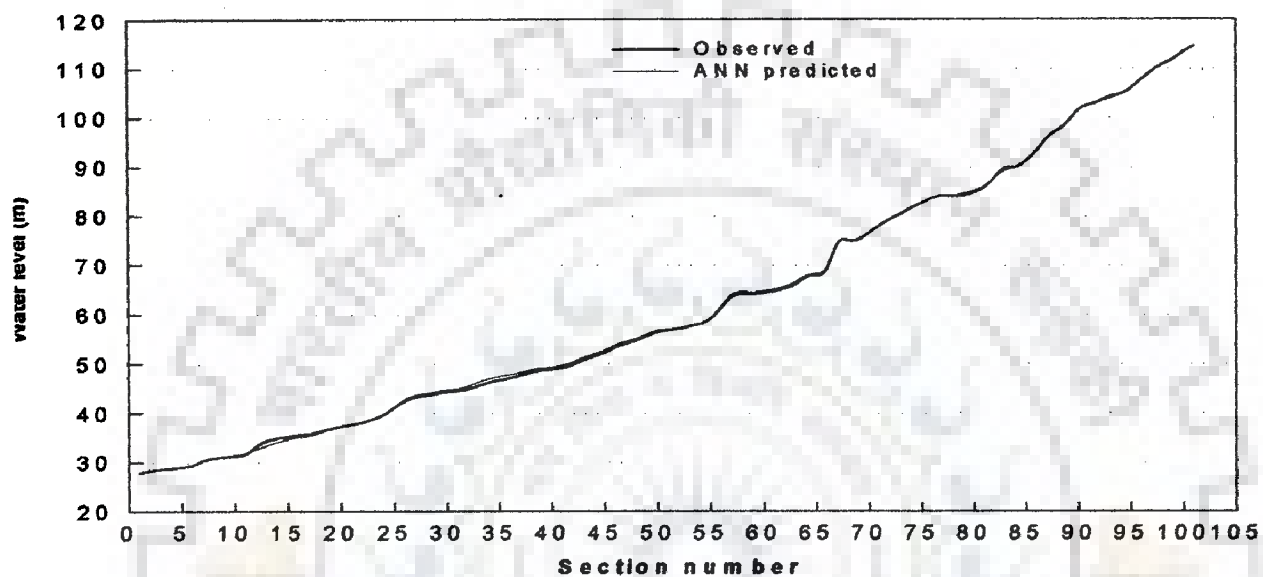


**Figure 4.63** Plot of observed v/s ANN predicted water levels for October, 2001

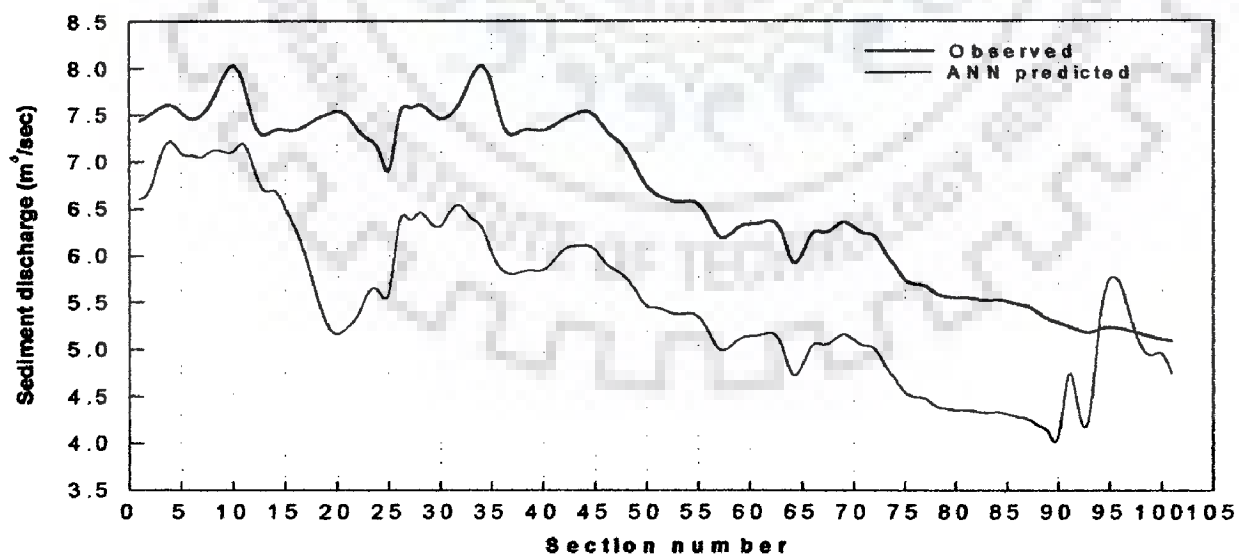


**Figure 4.64** Plot of observed v/s ANN predicted sediment discharge for October, 2001

The sediment model show a poorer performances compared to water discharge, stage as the observed data are measured at only two points, i.e. at Pandu and Pancharatna on the Brahmaputra and at other points the data have been generated using HEC-6 movable bed model.

#### **4.10 MAJULI RIVER ISLAND EROSION MODEL**

##### **4.10.1 GIS analysis**

Majuli island, the largest river island of the world was demarcated from each set of imageries and the area of the island was determined for the years 1990, 1997, 2000 and 2002 using ARC/INFO GIS software. A permanent point having latitude  $27^{\circ} 16'$  and longitude  $94^{\circ} 25'$ , nearly at the centre of the island was chosen as centre point of an imaginary circle circumscribing the island. The circle was divided into eight equal sectors radially, as shown in Figure 4.65. For all the four years, 1990, 1997, 2000 and 2002, the same process was repeated. The area bounded by each radially enclosed sector was calculated for all the years using Arc View 3.2 software. Figure 4.66 depicts the superimposed island area for all the years 1990, 1997, 2000 and 2002. Figure 4.67 shows the variation of areas in different years graphically.

Table 4.17 shows the year wise area variation of the sectors and the loss of area with respect to the base year 1990. It indicates that the year 1997 has registered a loss of area of 4.94% and loss of 9.44% in year 2002. The sector wise loss of area in the island was depicted graphically in Figure 4.68.

##### **4.10.2 Erosion process of the island**

The Majuli river island is facing severe bank erosion by both the rivers, the Brahmaputra and the Subansiri, during flood season every year. The erosion was more conspicuous from the southern side of the island, caused by the Brahmaputra. During the south-west monsoon season, a large part of the island was inundated by the spill waters of the Subansiri and the Brahmaputra rivers, when they were in high spate.



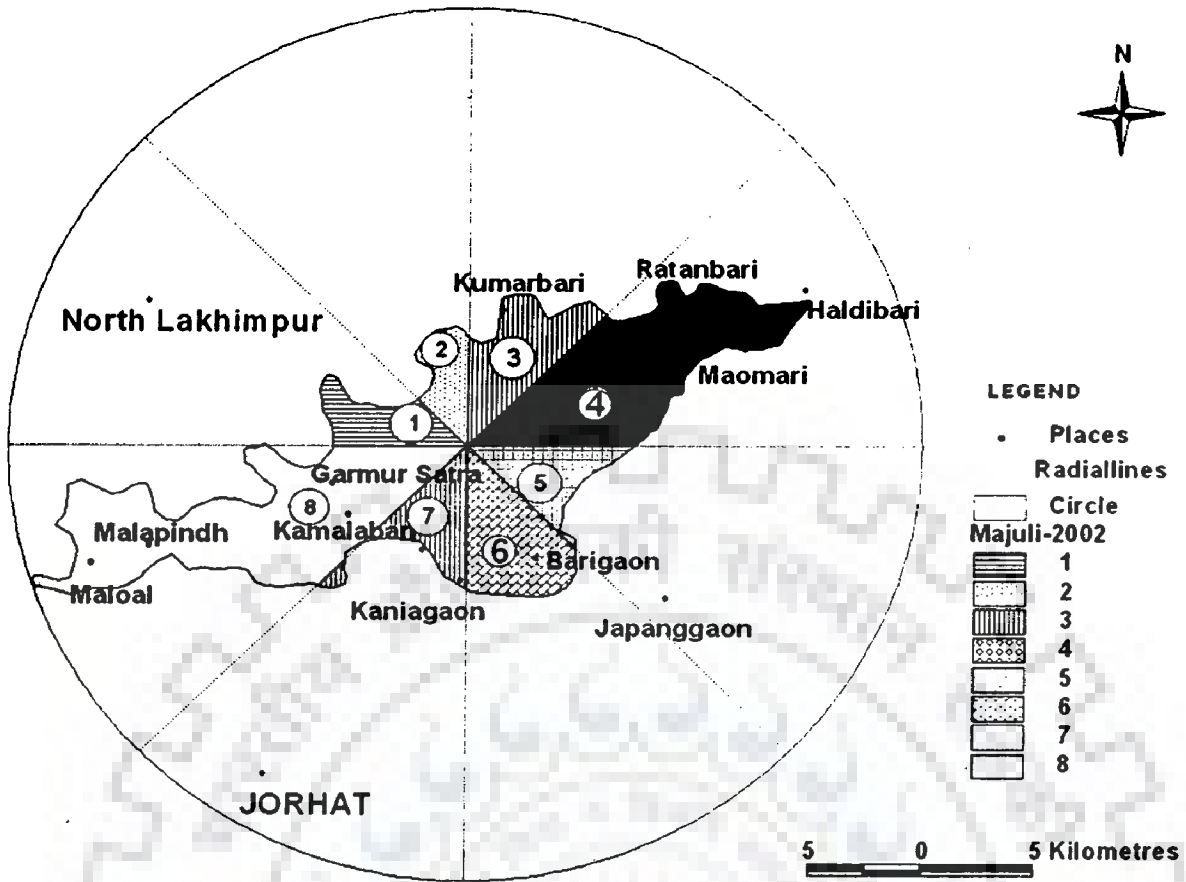


Figure 4.65 Eight sectors of Majuli island, 2002

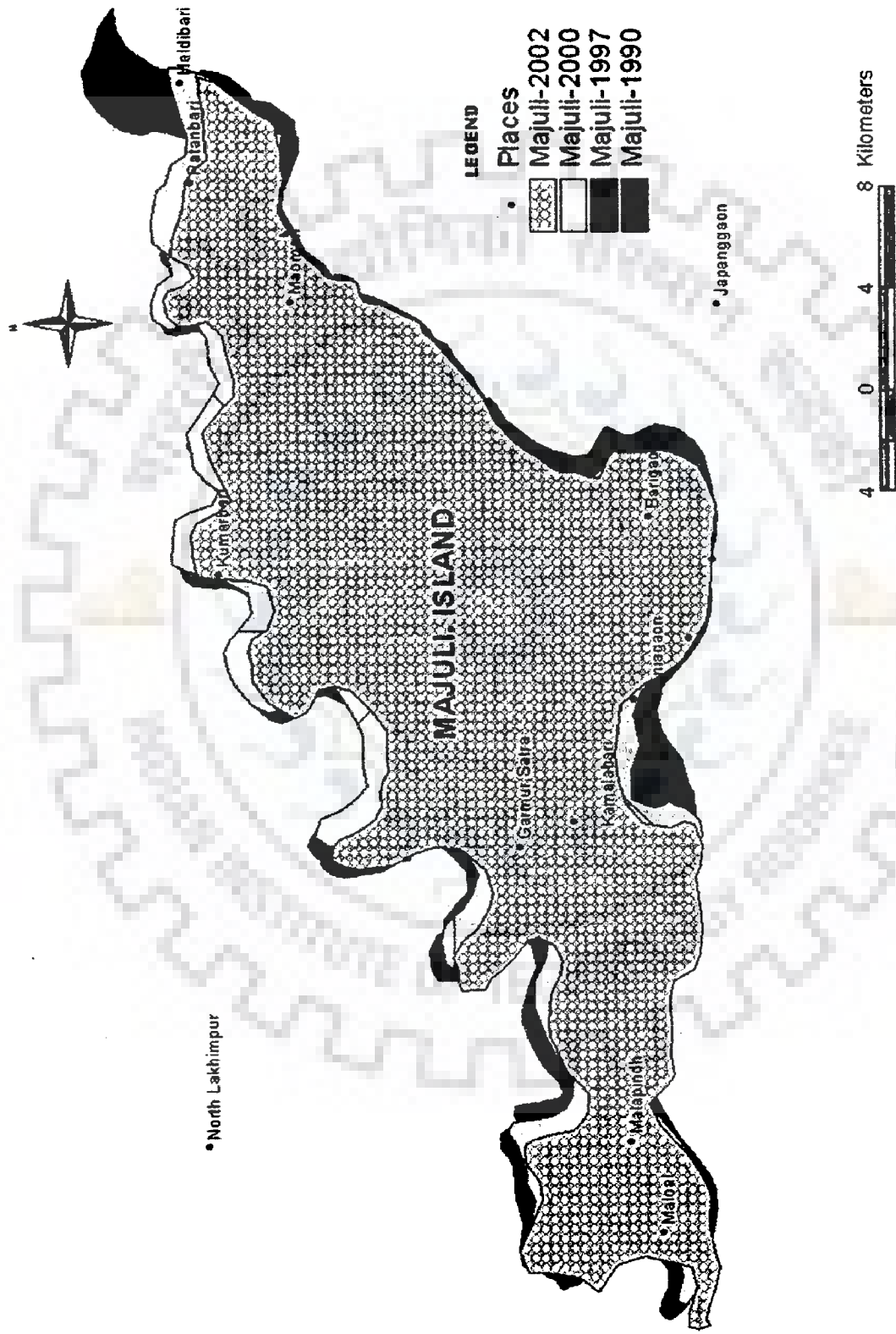


Figure 4.66 Superimposed areas of Majuli in different years

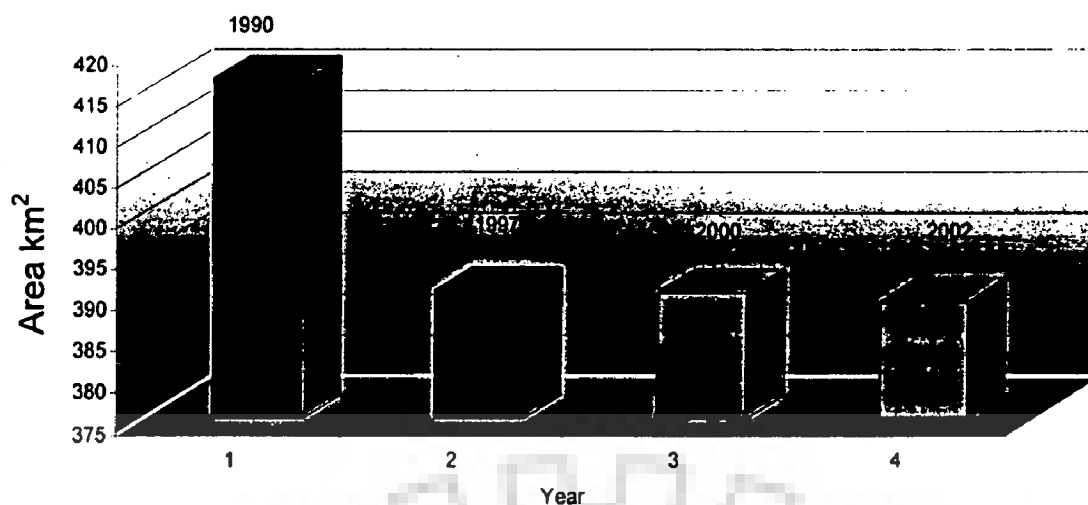
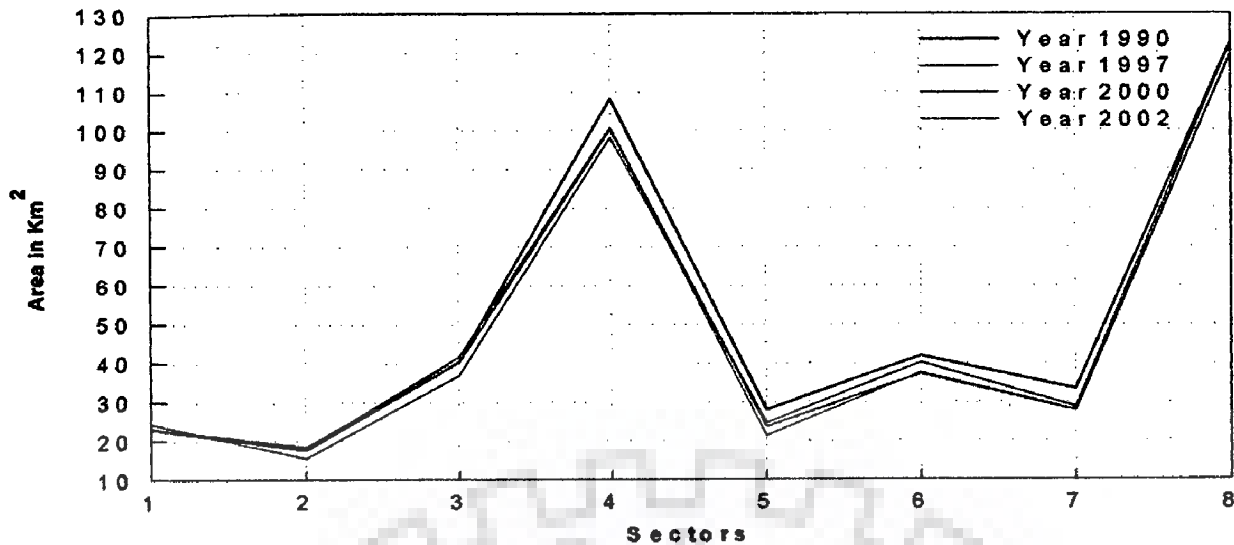


Figure 4.67 Area of Majuli island in different years

Table 4.17 Sector and year wise area of Majuli island

Year	Sect 1	Sect 2	Sect 3	Sect 4	Sect 5	Sect 6	Sect 7	Sect 8	Total area
	Area (Km <sup>2</sup> )	Area (Km <sup>2</sup> )	Area (Km <sup>2</sup> )	Area (Km <sup>2</sup> )	Area (Km <sup>2</sup> )	Area (Km <sup>2</sup> )	Area (Km <sup>2</sup> )	Area (Km <sup>2</sup> )	Area (Km <sup>2</sup> )
1990	23.166	18.399	40.581	108.145	27.966	41.835	33.353	122.781	416.23
1997	24.305	15.533	36.881	98.144	24.464	40.143	28.737	122.043	390.25
2000	23.089	18.008	41.706	100.627	21.323	37.515	27.981	119.840	390.09
2002	20.643	15.948	35.765	95.073	24.598	40.301	25.041	119.571	376.93
% loss of area w.r.t 1990	0.89%	4.49%	0.90%	7.34%	15.62%	11.18%	16.81%	2.61%	9.44%

Vast areas remain under sheet of flood water with an average depth of 2 to 3 m over a period of 10 to 15 days. This badly hits the economy of the island being agriculturally dominated. According to the 1971 Census of India, the geographical area of the island was 924.60 km<sup>2</sup>, as against its earlier area of 1245 km<sup>2</sup> during 1950, reported in revenue record. The land area of the Majuli island within the two arms of Brahmaputra river, as revealed from 2002 LISS III imagery was 376.93 km<sup>2</sup>.



**Figure 4.68** Variation of sector wise area of Majuli

Moreover, a comparison of the satellite images of 1990 and 2002 shows that the area has decreased by 39.30 km<sup>2</sup> in a period of 12 years. As per the 1991 Census of India, the island has 244 villages, out of which 35 villages have been eroded by the two rivers. Already since 1991, 35 villages have been washed away (Indian Express, 23<sup>rd</sup> July, 2004). Studies show that 15-20 years from now Majuli may be totally submerged in water. The flood ravages them every year robbing the inhabitants of their basic requirements of life. Struggle for survival continues unabated.

As floods in the Brahmaputra are accompanied by disastrous erosion of banks it is a common sight at the Majuli island to witness 30 to 40 m strip being eroded away within a few hours during the flood. The Figure 4.69 depicts an example of the wreaking havoc, as a strip of landmass separates out from the bank. In a study (1996), commissioned by the Brahmaputra Board, maps of river configuration and areas affected by bank erosion, performance of the embankments and their breaches in Majuli island were prepared using multi-date satellite data for the years - 1987, 1988, 1992, 1993, 1994.

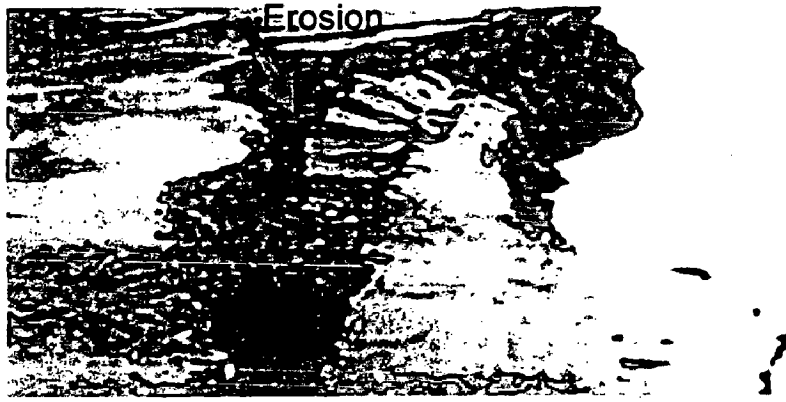


**Figure 4.69** Typical landmass slide (Indian Express, 23<sup>rd</sup> July, 2004)

The total loss of land in the island during 1969 -1994 has been estimated to be 50.27 km<sup>2</sup> (11).

The causes of erosion in the river island Majuli may be attributed to vortex generation due to uneven deposition, faulty land use, large scale deforestation and frequent earthquakes of various magnitudes. In order to combat erosion of the island, nothing substantial has been done except construction of embankments, which has been useful for temporary flood protection purpose only. Most of the embankments have been facing severe erosion due to erosive currents of flood water. Erosion has been continuing at an alarming rate despite the presence of embankments. Different Government and Non-Government organisations, such as Flood Control Department, River Research Station, Brahmaputra board, AVARD-NE (Association of Voluntary Agencies for Rural Development - North East) etc., are taking some measures. The various structural and non-structural measures taken by AVARD-NE have been found to be most effective from Botimari to Sonowal. Table 4.18 shows the categories of bank erosion in Majuli, as studied by Ministry of Water Resources, Government of India in 2002.

**Table 4.18 Categories of bank erosion in Majuli island (Figure 4.28(a))**

<b>Erosion Category</b>	<b>Criteria</b>	<b>Location</b>
A. Major erosion affecting large area	loss of land >10 km <sup>2</sup>	A-Kathanigaon, Ujanigajeragaon, Sounal Kacharigaon
B. Moderate erosion affecting certain areas along bank line	loss of land between 1 to 10 km <sup>2</sup> .	B-Lachangaon, C-Kumargaon, Barmari E-Kaniagaon, Batiamari gaon F-Khoraparagaon, Kumarbari
C. Minimum erosion at isolated sites	Loss of land < 1 km <sup>2</sup>	D-Salmaragaon, Bessamora, Mirigaon H-Chitadarchapari I-Chitadashchapari J- Borbari K- Kaibartgaon

\*(Source- Ministry of Water Resources, December, 2002)

#### **4.10.2.1 Model 16**

##### **4.10.2.1.1 Neural network modelling for future trend prediction of Majuli**

ANN has been potentially used to explore the future trend of the erosion activities taking into account the past foot-prints of the river behaviour. Figure 4.70 shows the structure of the used network. Multilayer perceptron architecture with gradient descent learning algorithm has been used to train the neural network training. For this experiment, the data were split up into three parts; one for model training, one for cross validation (to prevent model over training), and another for testing the performance of the model.

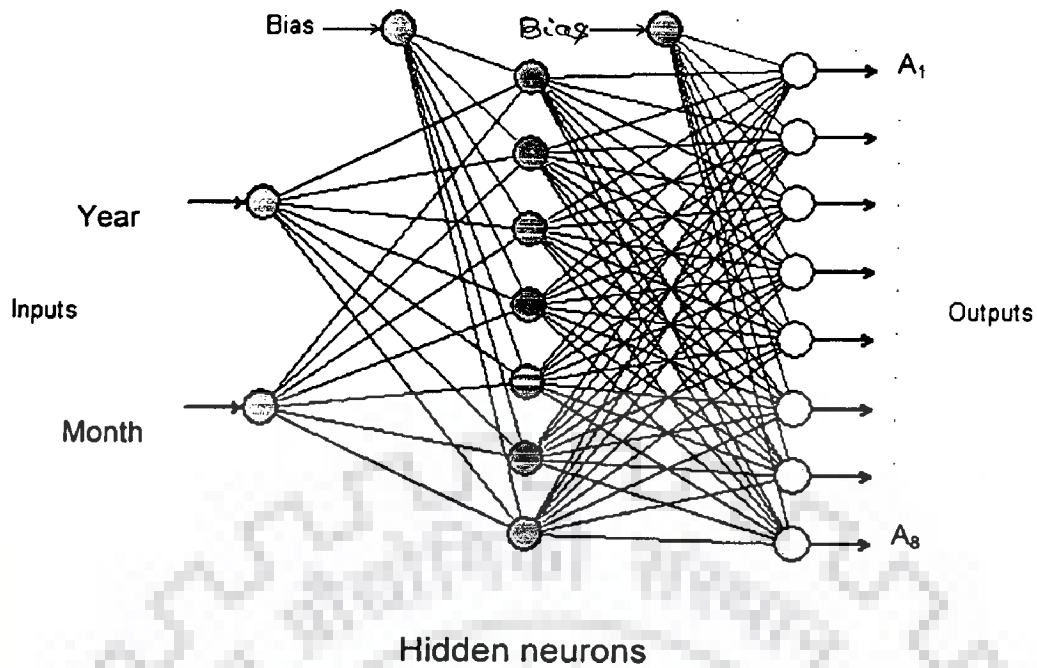


Figure 4.70 Architecture of neural net of model 16

The result of the neural network modelling was encouraging. The data of 2002 has been tested for the performance of the network. The actual and ANN predicted area of the island have been graphically represented in Figure 4.71. Figure 4.72 shows the plot of *rmse* versus number of iterations. The sigmoid function has been used as the activation function. The goodness-of-fit criteria, such as *rmse* and Nash coefficient for the results were 0.0001 and 0.998 respectively. The erosion of the sectors has been predicted for 2004 as shown in Table 4.19. It could be seen that the sector 5, 6 and sector 7 were decaying more as compared to other sectors.

Table 4.19 ANN predicted values of sector areas for 2004

Year	Area in km <sup>2</sup>							
	Sect 1	Sect 2	Sect 3	Sect 4	Sect 5	Sect 6	Sect 7	Sect 8
2004 (ANN)	22.951	17.639	35.075	94.010	23.250	37.102	27.679	119.536

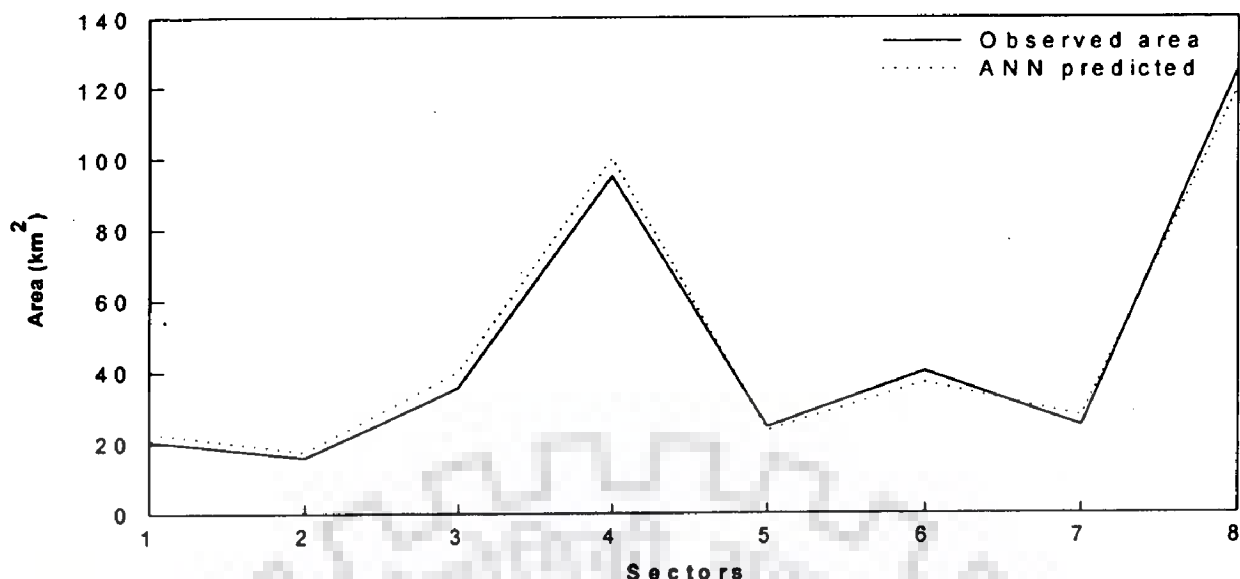


Figure 4.71 Observed and ANN predicted area, 2002

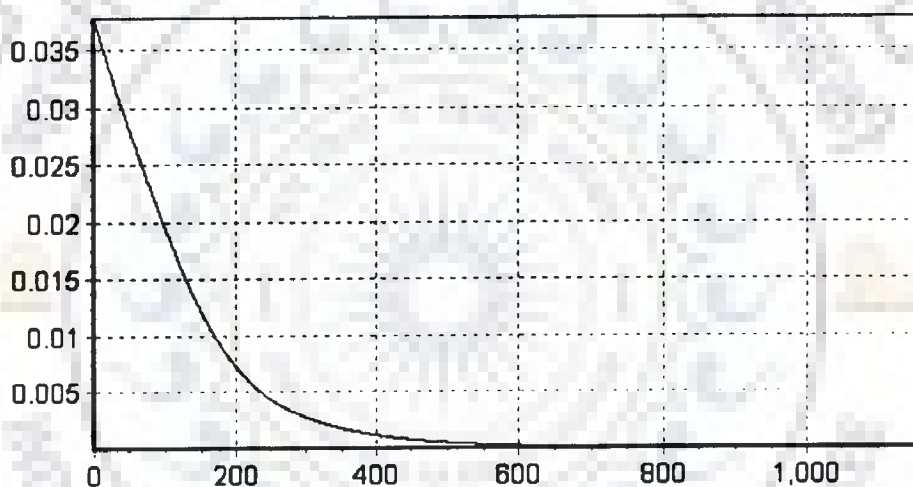


Figure 4.72 Plot of root mean square error v/s iterations

#### 4.10.2.1.2 Ground truth verification

Ground observations on the overall erosion activity around Majuli island exhibited two types of features. The bowl-shaped shear failure activated by the flow of sediments was more common around Gajeragaon, the easternmost corner of the island. During the high flood of the river, water was forced into the massive sand bodies, providing additional support to the bank materials, which acted as a continuous system. However, with the fall in water level, the pressure diminished



rapidly and water from the pore spaces of sand bodies tended to flow to the main channel. This flow of water from the sand bodies has caused liquefaction of sediments and the bank materials have been subjected to different degrees of flow. This type of failure was more common around Kumargaon, Batiamarinagar and Bessamora. However, around Salmora, where the bank material comprised of mainly cohesive clay material, the slope was almost  $90^\circ$  causing significant over-steepening, which triggered towards initiation of bank failure.

Moreover, the cohesive clay material on the other hand, produced a comparatively stable land mass that was not prone to erosion and thereby helped to generate a nodal point. The nodal point, in turn, also offered significant resistance to the connected flow regime. As the bank materials were relatively stable in this area, the river scours deeper to accommodate the flood discharge, thereby increasing the suspended load of the river temporarily. Below the nodal point, the river tended to be wide, thereby, facilitating formation of bars. Here, the current velocities diminished when large quantities of sediments were deposited and mid-channel bars were formed. Once formed, the bars or chars locally decreased the cross-sectional area and they cut the bank laterally to maintain a proper cross-sectional area that was in equilibrium with discharge. This possibly is the explanation about the enhanced rate of erosion activity around Neamatighat and Kamalabari which has already taken a large proportion of the land area.

#### **4.11 ANN-BASED STAGE & DISCHARGE RATING CURVES AT DIBRUGARH, PANCHARATNA AND DHUBRI**

Stage and discharge are time-dependent phenomena and very often these exhibit random fluctuations, their relationship is not always unique. The parameters,

stage and discharge describe processes that develop in time. Historical data are used in determining the properties of the time series. For obvious reasons, the longer the series, the better are the estimates of parameters describing the processes. Discharge can not be measured directly. It is functionally dependent upon river geometry as well as upon flow conditions prevailing at the desired time. However, water-surface elevation, i.e. stage can be measured directly. If functional relationship between stage and discharge at some location in a river can be established, then discharge can be estimated from it. Mathematically this can be described as follows:

$$\text{as } h = h(t) \quad (4.15) \text{ and } Q = Q(h), \quad (4.16)$$

$$\text{so, } Q = Q[h(t)] = Q(t) \quad (4.17)$$

Where, stage, discharge and time are expressed as  $h$ ,  $Q$  and  $t$  respectively.

Frequency of observation depends on the rate of change of surface-water level. If  $dh/dQ$  is very small, observations can be taken at long intervals, may be once in a day. If  $dh/dQ$  is very high, suggesting quick changes in surface-water level, frequency intervals for stage observations should be as minimum as possible. The functional relationship between stage and discharge was obtained at Dibrugarh, Pancharatna and Dhubri using ANN, as smooth and continuous curves with reasonable degree of sensitivity.

#### 4.11.1 Model 17, 18 and 19

The models 17, 18 and 19 were developed with 1-4-1 architecture with feed-forward back-propagation method with conjugate gradient descent learning algorithm. The 120 data patterns spanning for a period of 13 years (1990-2002) have been used

to train and as a reference to test the performance of the networks. 28 to 36 data patterns have been used to validate the efficiency of the models.

#### 4.11.2 Validation of Models

The model developed on the basis of observed data for a time span of 10 years, has been validated using similar data of 3 years. The discharge hydrograph as estimated from the models 17, 18 and 19 was plotted in Figures 4.73, 4.74 and 4.75 along with the measured discharge hydrograph. It was observed that the estimated discharge, most of the times, remained within reasonable proximity of the measured data. Model output was also separated as per the slope of the stage i.e. one with the rising stage cases and the other with the falling stage cases. No significant difference in behaviour of the two groups was discernible. Figure 4.76, 4.77 and 4.78 depict the validation of the target and output model during training of network of models. Table 4.20, 4.21 and 4.22 show the performance indicators for the models for Dibrugarh, Pancharatna and Dhubri respectively. Table 4.23 outlines the statistical measures of goodness-of-fit of the three models.

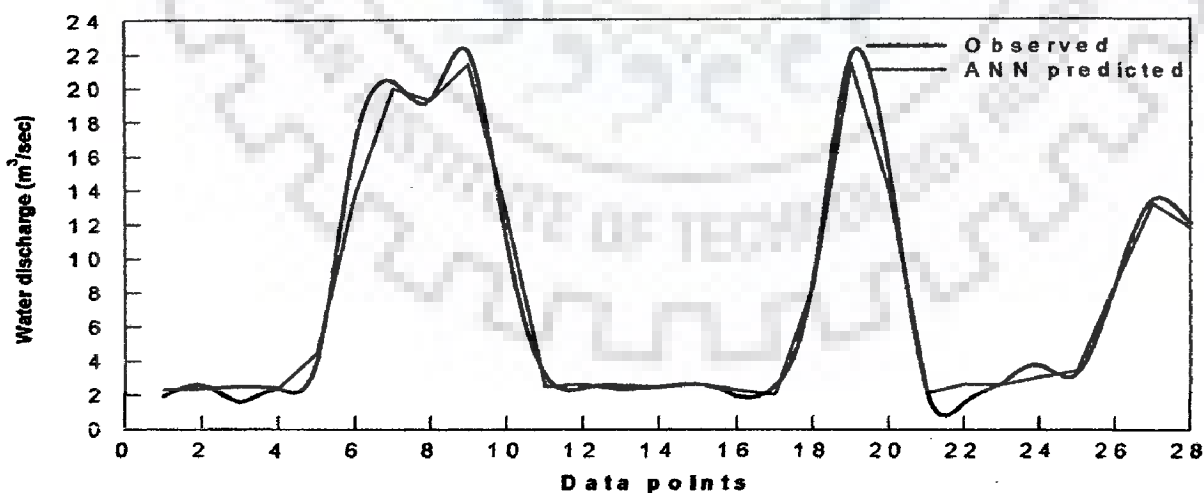


Figure 4.73 Validation of output of model 17 (Dibrugarh)

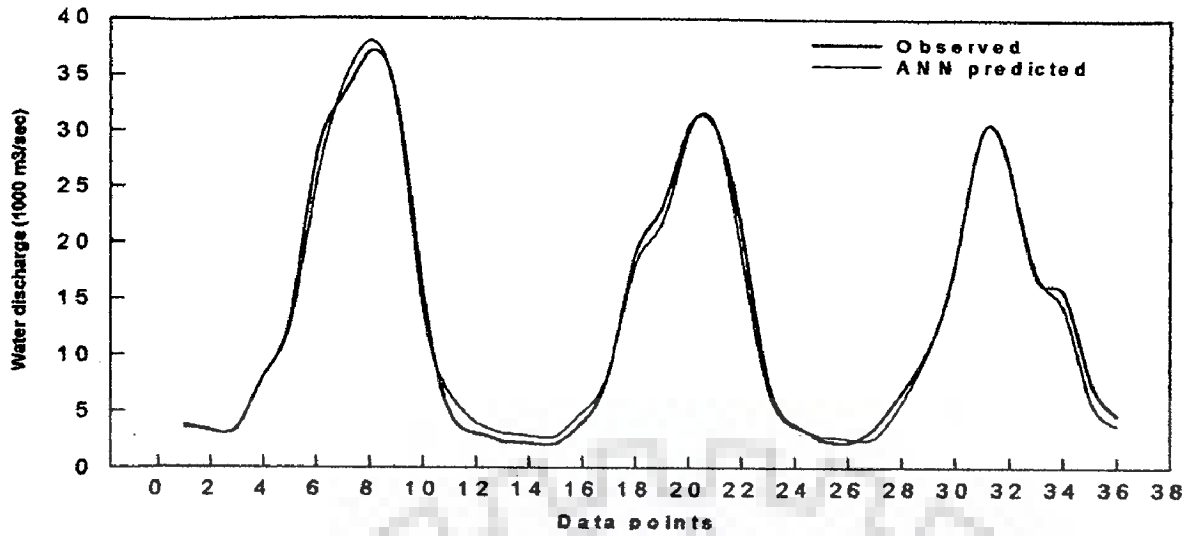


Figure 4.74 Validation of output of model 18 (Pancharatna)

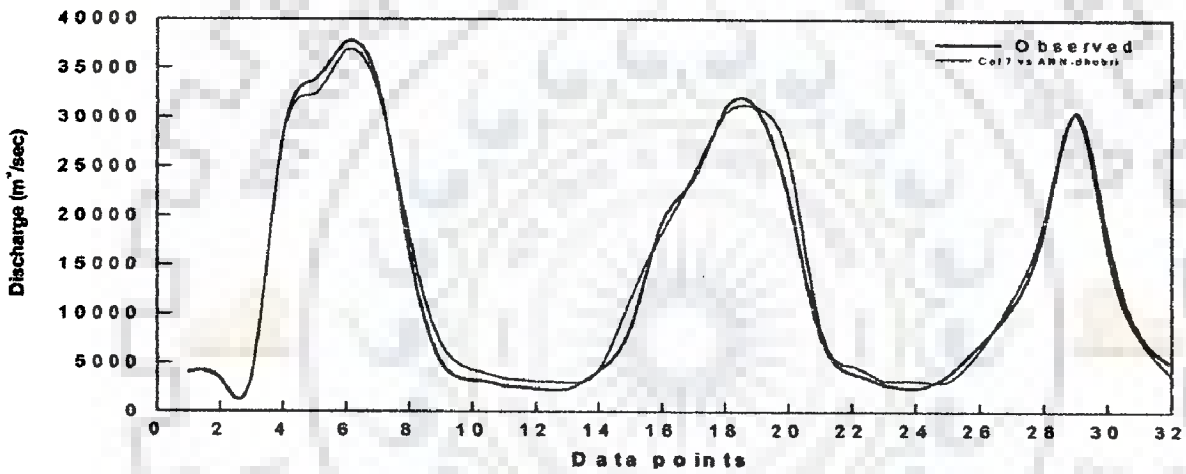


Figure 4.75 Validation of output model 19 (Dhubri)

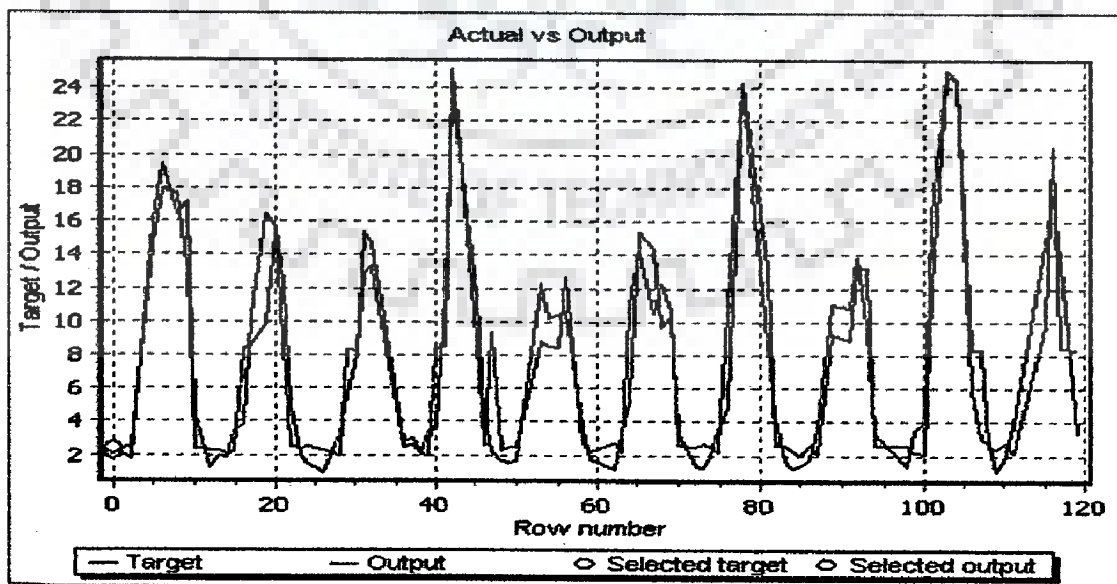


Figure 4.76 Plot of target and output data in model 17 training (Dibrugarh)

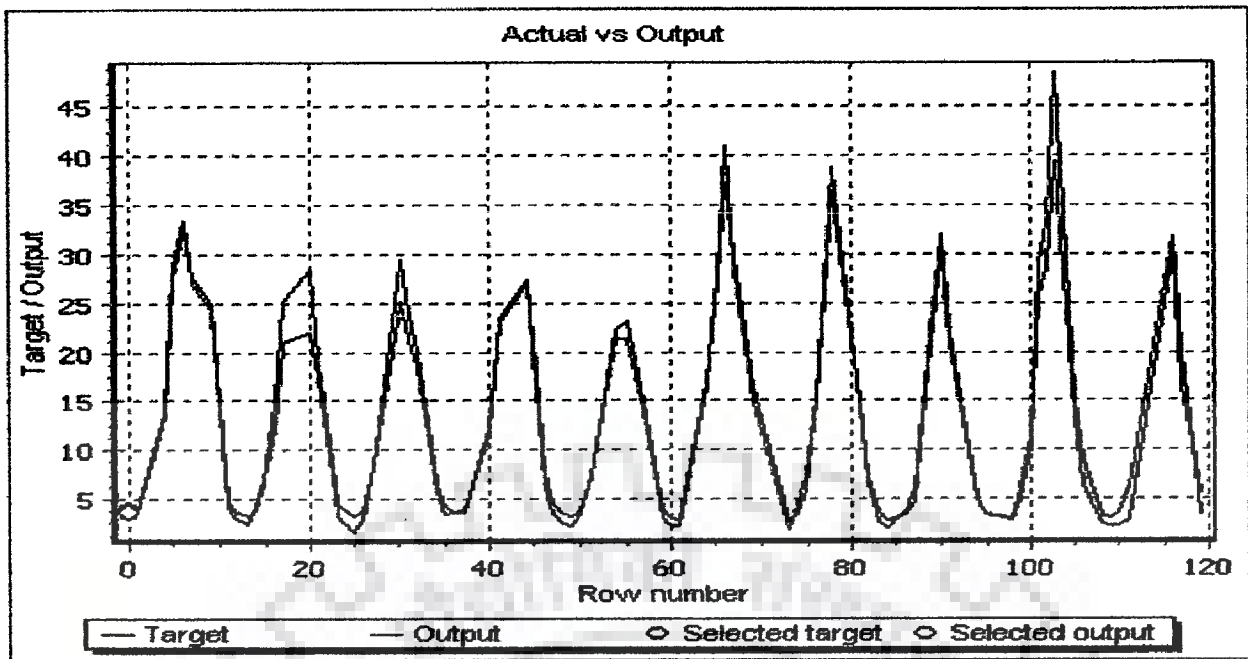


Figure 4.77 Plot of target and output data in model 18 training (Pancharatna)

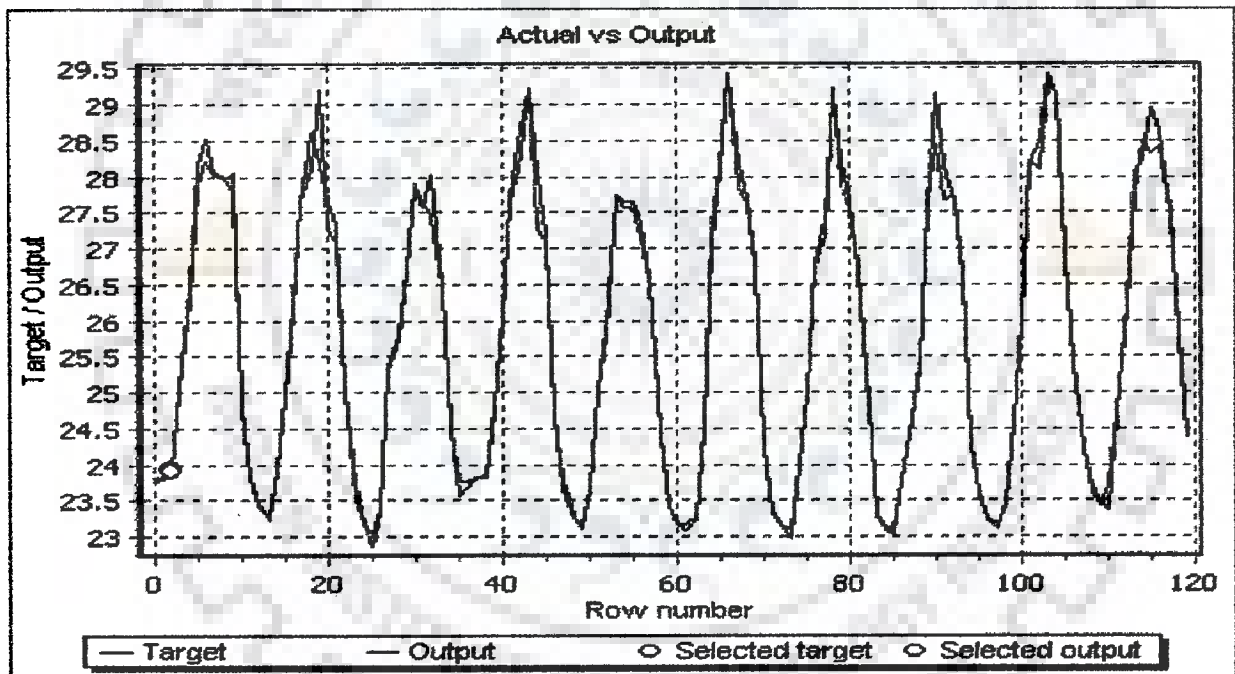


Figure 4.78 Plot of target and output data in model 19 training (Dhubri)

Table 4.20 Performance indicators for Model 17 (Dibrugarh)

Training	Target	Output	Absolute Error	Absolute Relative Error
Mean	7.324	7.308	1.932	0.460
Std Dev	6.461	6.070	1.650	0.501
Min	0.929	1.958	0.026	0.004
Max	25.025	25.152	7.150	3.327

C	0.92			
R <sup>2</sup>	0.82			
<b>Validation</b>				
Mean	10.195	10.636	1.824	0.480
Std Dev	7.462	6.314	2.346	1.014
Min	1.243	1.960	0.166	0.008
Max	25.360	25.152	9.102	4.444
C	0.92			
R <sup>2</sup>	0.77			
<b>Testing</b>				
Mean	7.016	7.075	3.268	0.689
Std Dev	6.655	5.257	2.880	0.661
Min	1.449	1.956	0.482	0.073
Max	20.551	18.887	8.723	2.222
C	0.75			
R <sup>2</sup>	0.31			

C = Correlation coefficient, R<sup>2</sup> = statistical ratio that compares model forecasting accuracy with accuracy of the simplest model that just use mean of all target values as the forecast for all records, AE = Absolute Error = (Target value - desired value), ARE = Absolute Relative Error = (Target value - desired value)/(Target value)

**Table 4.21 Performance indicators for Model 18 (Pancharatna)**

Training	Target	Output	Absolute Error	Absolute Relative Error
Mean	13.236	13.219	1.389	0.163
Std Dev	11.102	10.631	1.444	0.160
Min	1.629	2.224	0.016	0.002
Max	48.460	39.384	9.076	1.000
C	0.983			
R <sup>2</sup>	0.964			
<b>Validation</b>				
Mean	11.868	11.698	1.082	0.175
Std Dev	11.462	11.209	0.926	0.171
Min	2.097	2.544	0.010	0.000
Max	39.545	36.271	3.418	0.640
C	0.992			
R <sup>2</sup>	0.983			
<b>Testing</b>				
Mean	17.985	18.143	1.802	0.126
Std Dev	11.360	11.305	2.114	0.099
Min	2.012	2.615	0.007	0.000
Max	39.137	34.179	8.037	0.300

**Table 4.22 Performance indicators for Model 17 (Dhubri)**

Training	Target	Output	Absolute Error	Absolute Relative Error
Mean	25.886	25.888	0.139	0.005
Std Dev	2.078	2.063	0.189	0.007
Min	22.982	23.102	0.000	0.000
Max	29.421	29.421	0.999	0.034
C	0.993			
R <sup>2</sup>	0.987			
<b>Validation</b>				
Mean	25.605	25.655	0.098	0.004
Std Dev	1.965	1.994	0.129	0.005
Min	23.171	23.186	0.003	0.000
Max	29.223	29.236	0.503	0.018
C	0.997			
R <sup>2</sup>	0.993			
<b>Testing</b>				
Mean	25.334	25.353	0.079	0.003
Std Dev	1.549	1.565	0.059	0.002
Min	22.866	23.047	0.011	0.000
Max	28.140	28.078	0.212	0.008
C	0.998			
R <sup>2</sup>	0.996			

**Table 4.23 Statistical measures of goodness-of-fit for models**

	Model 17 (Dibrugarh)	Model 18 (Pancharatna)	Model 19 (Dhubri)
<i>rmse</i>	0.816	0.945	1.258
Nash Coefficient	0.9864	0.9927	0.9849

## 4.12 FUZZY AND NEURO FUZZY MODELS

### 4.12.1 Models 20, 21, 22, 23, 24 and 25

Fuzzy variables have been used through models 20, 21 and 22, as the relationships between cause and effect (variable and results) were vague. This was done to organize knowledge that was expressed 'linguistically' into a formal analysis and was not dependent on the volume of data available. Since these expert systems produce a result based on logical linguistic rules, extreme data points in a small data

set do not unduly influence these models. Because of these characteristics, fuzzy logic application has been made to evaluate the stage-discharge relationship.

#### 4.12.2 Fuzzy Expert System Design

Linguistic terms were chosen to describe the input variable stage and the results (Figure 4.79). Further refinement of the models could not be achieved by adding extra membership functions. Nine Gaussian membership functions were used. Applying a similar method of data classification, membership functions were determined for the output variable discharge.

#### 4.12.3 Rule Definition

Five years of average monthly data i.e. from 1998 to 2002 and expert knowledge were used to create a rule base for the fuzzy logic model. Rules were defined for both the high and low extreme conditions, with regard to actual occurrences, because of the physical nature of the relationships. Since, there were nine membership functions for each input variable; the minimum rule base of 17 rules was created. For each data point, all rules were evaluated.

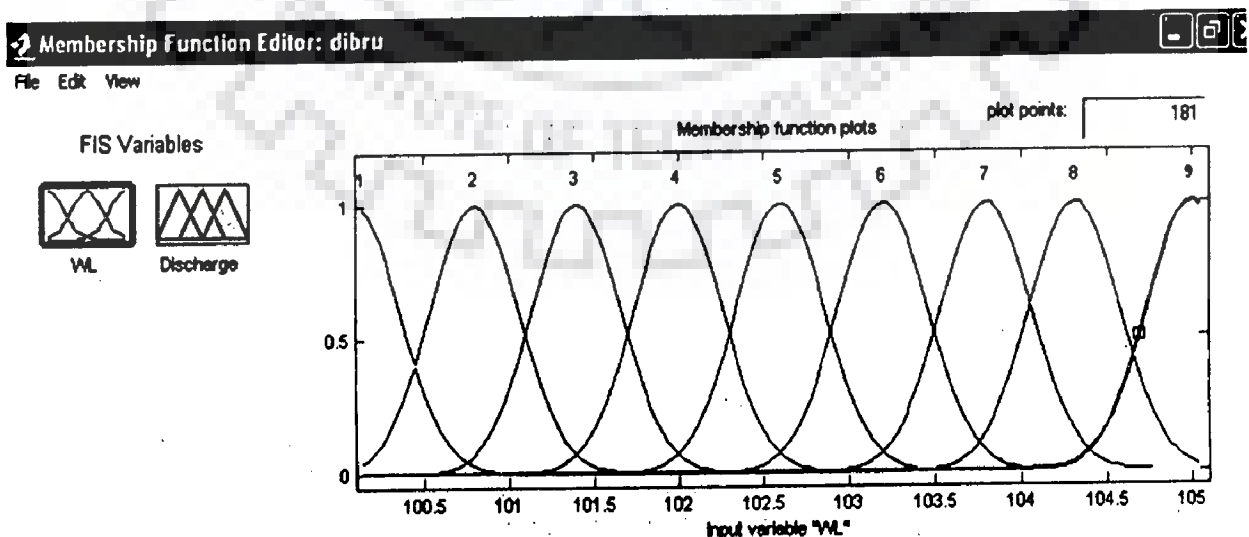


Figure 4.79 Gaussian membership functions for the input and output variable



#### **4.12.4 Model Construction**

The platform selected for the fuzzy logic expert system was MATLAB (Version 6.5) and MATLAB'S Fuzzy Logic Toolbox (Version 2.1.1). The variables were combined into rules using the concept of 'AND'. The fuzzy operator 'minimum' was applied as the 'AND' function to combine the variables. No weightings were applied, which means no rule was emphasized as more important in respect to estimating the discharge. Implication was performed with the minimum function, and aggregation was performed with the maximum function. The centre of gravity method was applied as a means of defuzzification of the output membership functions to determine a crisp set (Figure 4.80). Based on this structure, a baseline model fuzzy logic expert system for stage-discharge relationship was constructed for the three stations, namely, Dibrugarh, Pancharatna and Dhubri. Alternate functions for the expert system were investigated through sensitivity analysis.

#### **4.12.5 Sensitivity Analysis**

A sensitivity analysis was performed for the fuzzy logic operator AND, and for the methods of implication, aggregation and defuzzification. The results of changing a single operator or method while the rest of the model was held constant were compared with the results from the baseline model. The results were evaluated on the basis of correct linguistic matches. Based on this sensitivity analysis, the AND operator 'minimum' and the implication method 'minimum' were found to perform better than the product method. The fuzzy logic and ANN models were evaluated based on their ability to predict the discharge. Figure 4.81 presents the rule viewer for Pancharatna (model 21).

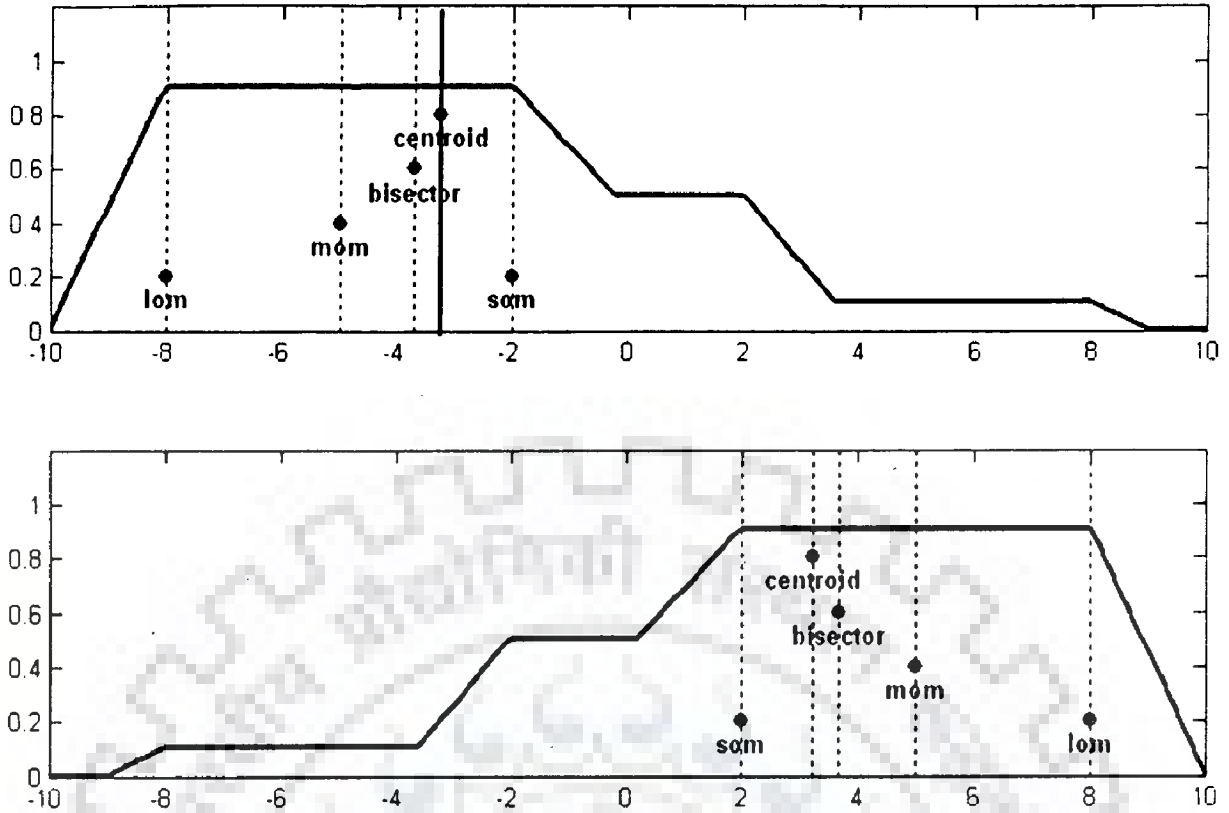


Figure 4.80 Defuzzification methods

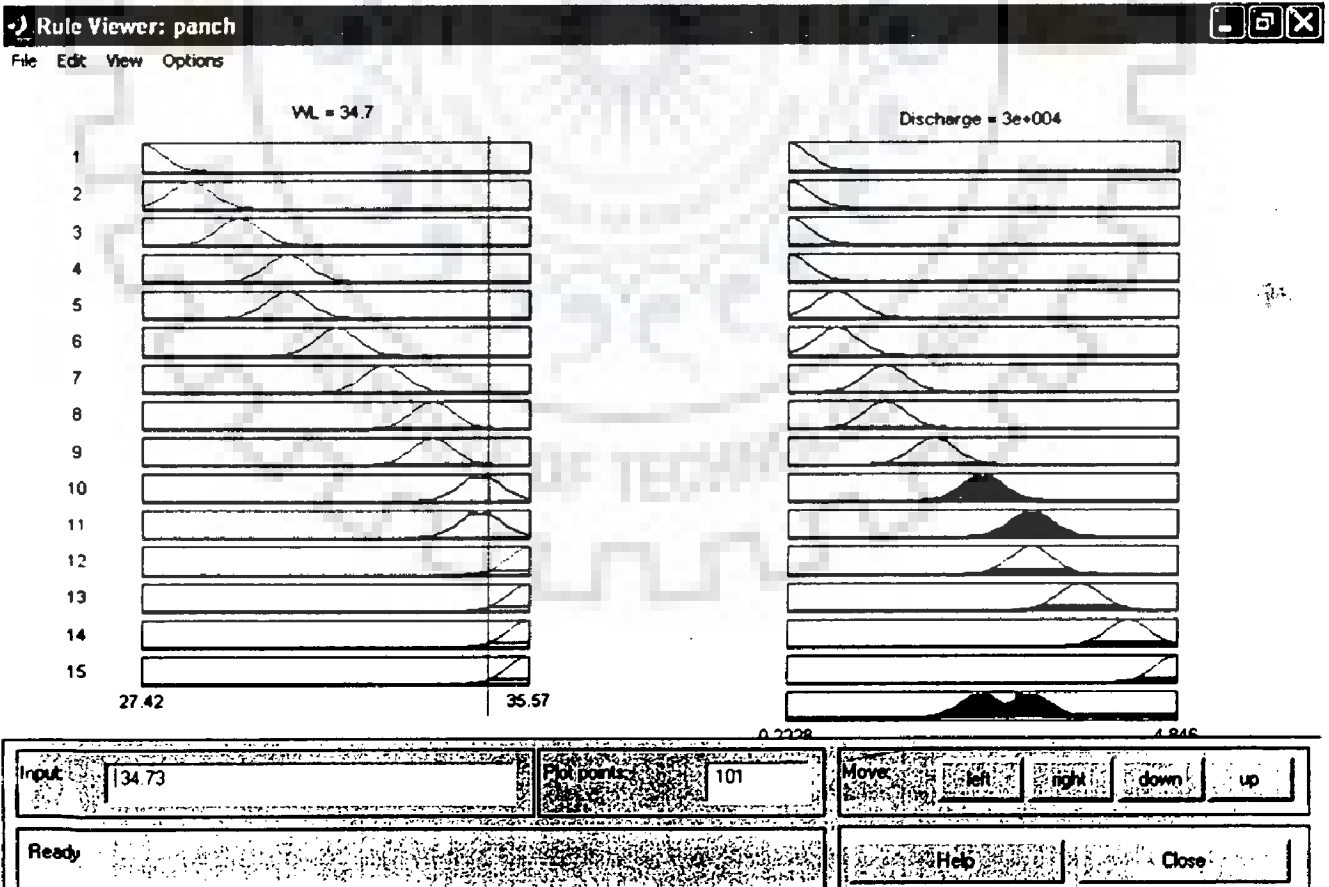


Figure 4.81 Rule viewer of model 21 (Pancharatna)

### 4.13 ANFIS (ADAPTIVE NEURO-FUZZY INFERENCE SYSTEM) MODELS

The hybrid system of learning has been attempted at combining ANN and fuzzy logic for developing the stage-discharge relationship to achieve a faster rate of convergence by controlling the learning rate parameter with fuzzy rules as shown in Figure 4.82. The objective was to get a minimizer, which has a low computing time and a large convergence domain. This learning ability was achieved by presenting a training set of different examples to the network and using learning algorithm, which changes the weights in such a way that the network reproduces a correct output with the correct input values. The main dissimilarity between fuzzy logic system (FLS) and neural network was that FLS used heuristic knowledge to form rules and tunes these rules using sample data, whereas NN forms "rules" based entirely on data. Sugeno type ANFIS has been used. Gaussian membership functions has been used with 50 rule bases, because of their low computational requirements and as it has the important properties of smooth mapping, universal approximation, normal distributions can be approximated well by this type of functions. Figure 4.83 shows architecture of the neuro-fuzzy models 23, 24 and 25.

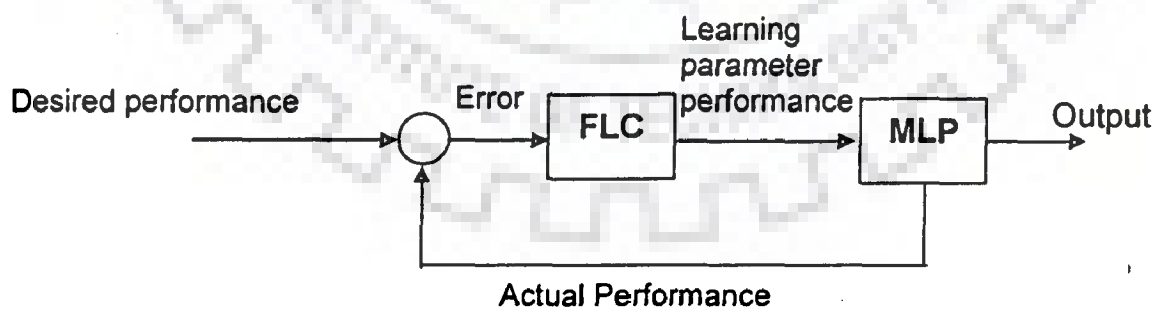


Figure 4.82 Learning rate control by fuzzy logic. FLC is fuzzy logic controller MLP is multilayer perceptron

### 4.13.1 Validation and Comparison of Results

The ANN, fuzzy and neuro-fuzzy models, thus developed, were validated and compared with the 36 observed data points. Figure 4.84 depicts the plot of output and target data in respect of Pancharatna. The Figures 4.85, 4.86 and 4.87 present the comparison of all the models in respect of Dibrugarh, Pancharatna and Dhubri respectively. However, the ANN models were found to be clearly superior to fuzzy expert systems, based on their ability to predict, except for Dhubri, where the neuro-fuzzy model and the ANN model give similar results.

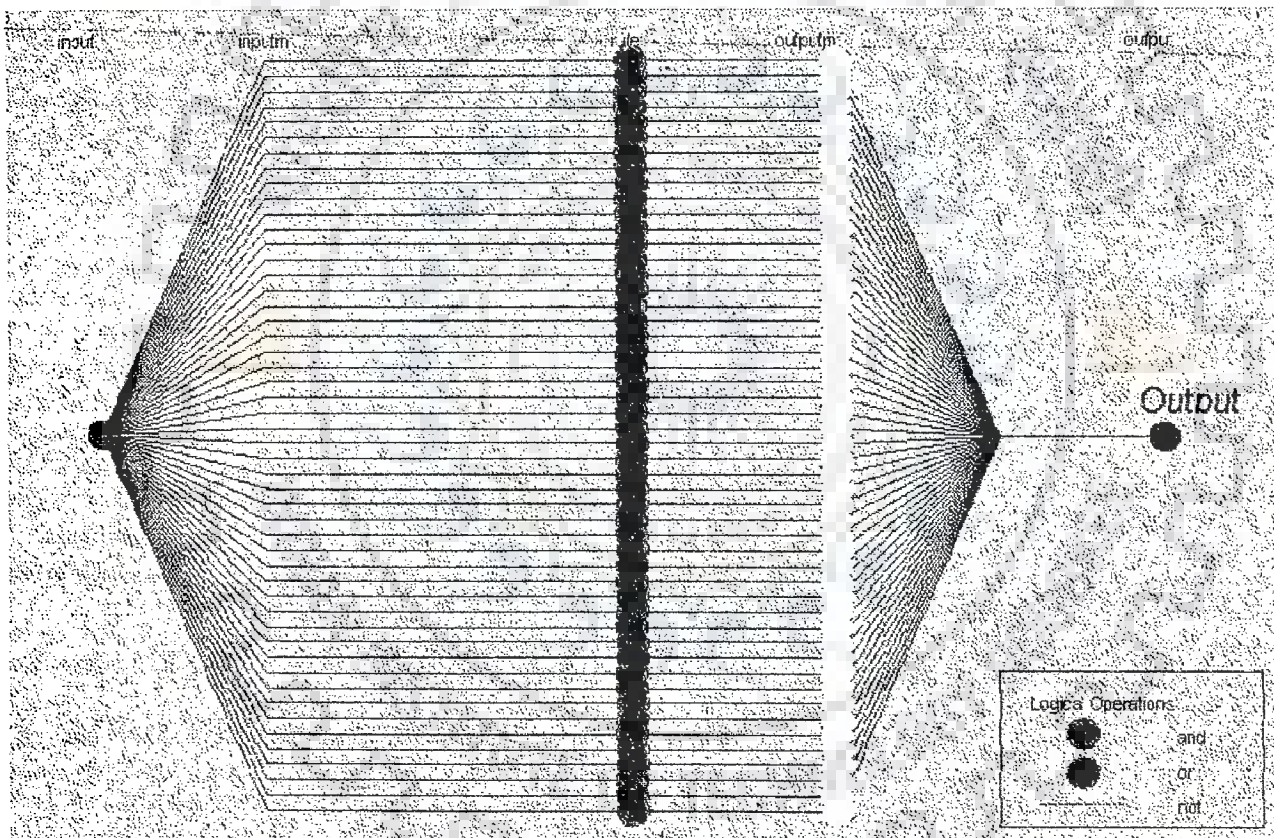


Figure 4.83 Architecture of the neuro-fuzzy models

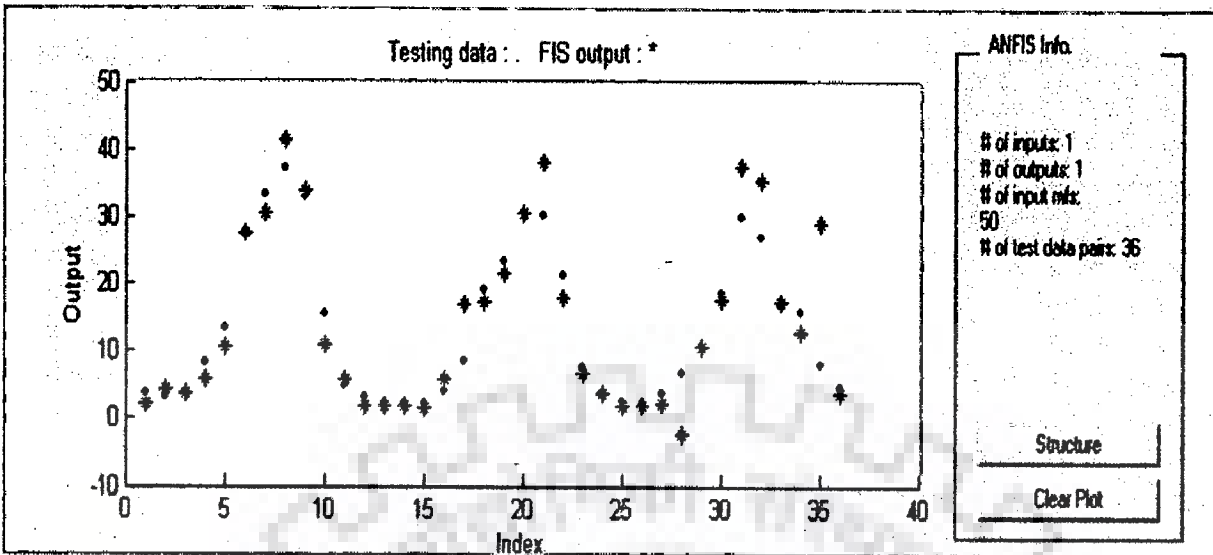


Figure 4.84 Plot of target and out put data of the ANFIS model 24

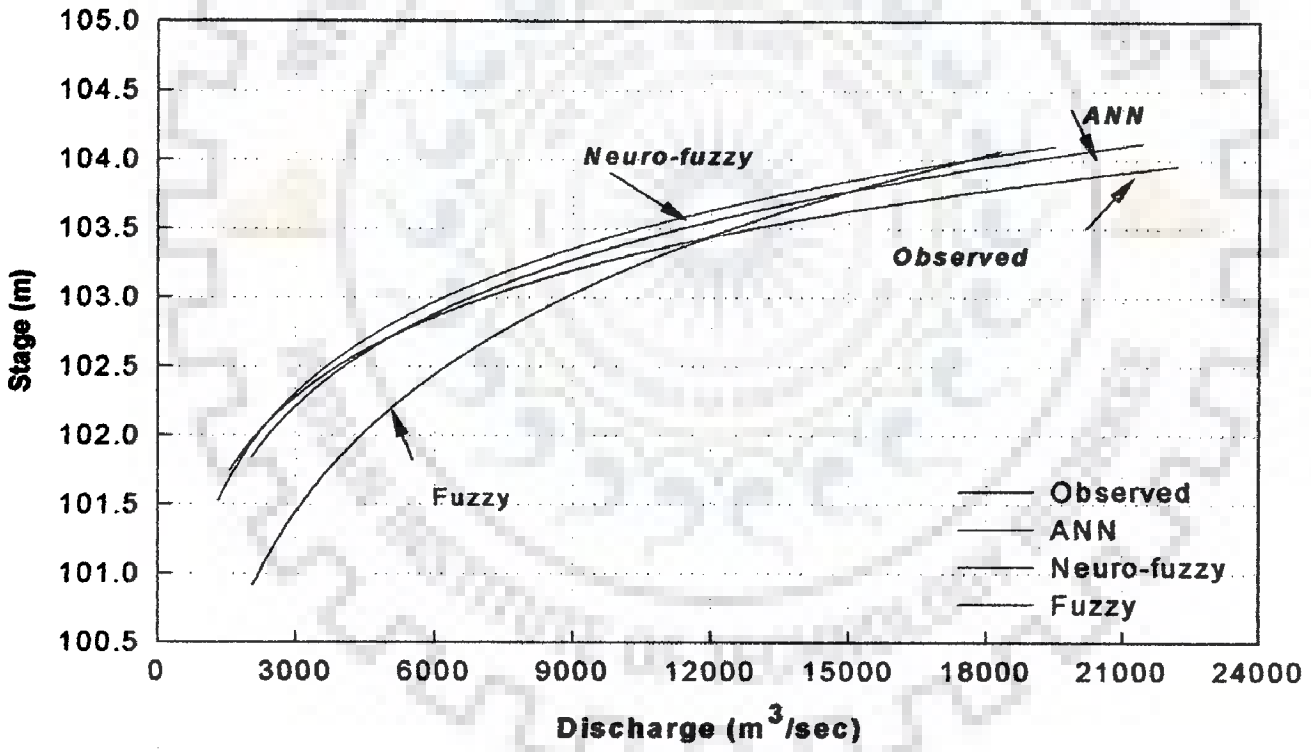


Figure 4.85 Validation and comparison of models 17, 20, 23 and observed data (Dibrugarh)

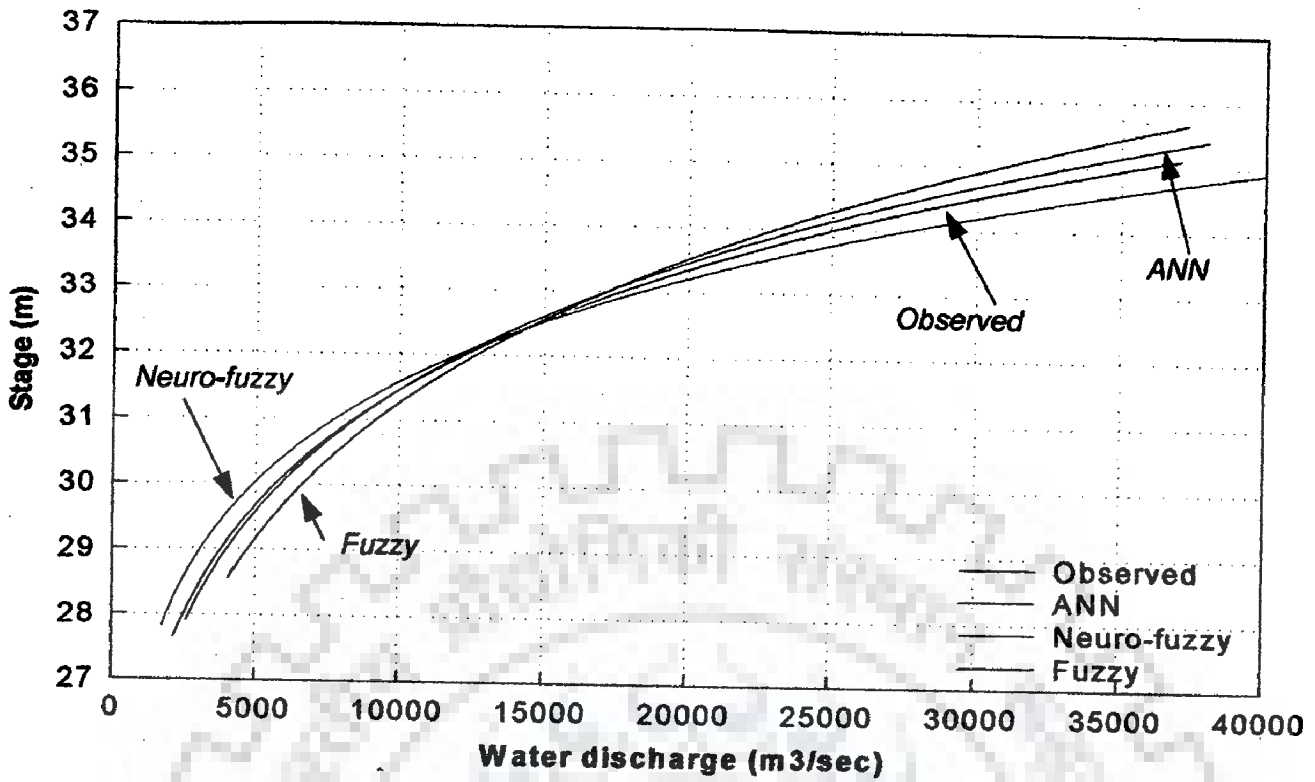


Figure 4.86 Validation and comparison of models 18, 21, 24 and observed data (Pancharatna)

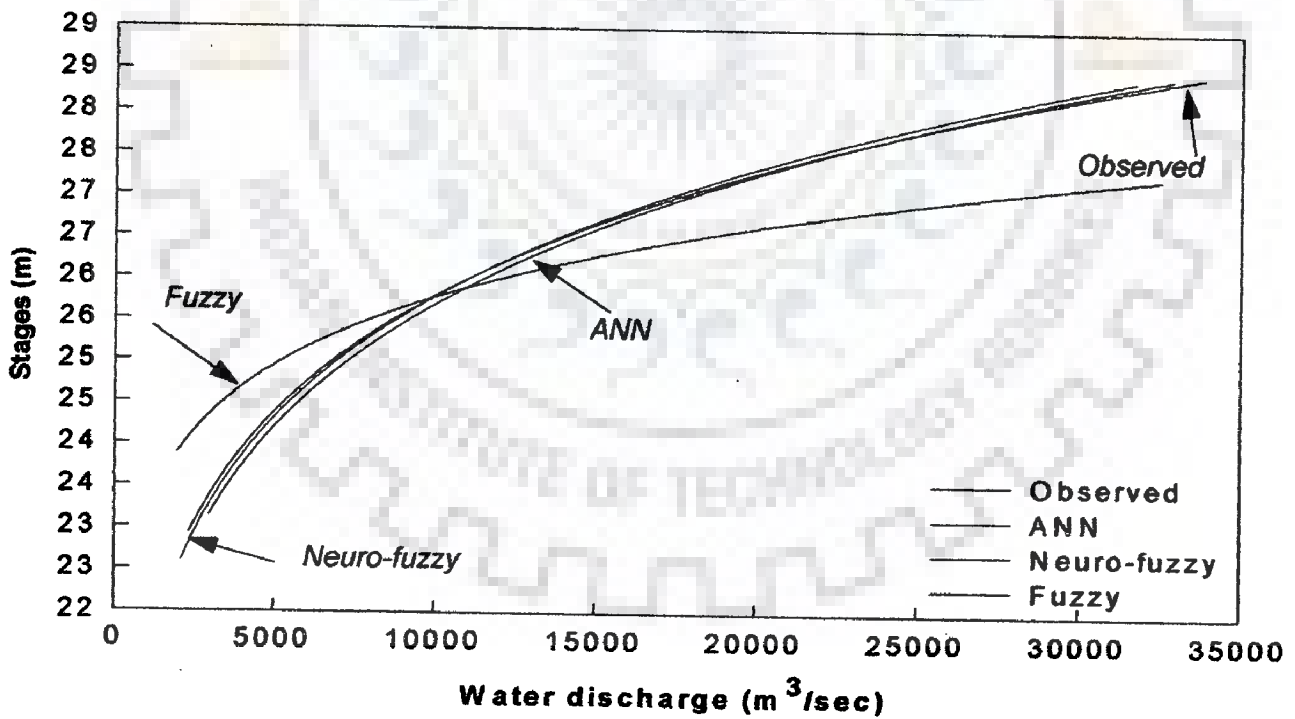


Figure 4.87 Validation and comparison of models 19, 22, 25 and observed data (Dhubri)

## 4.14 REAL-TIME FLOOD FORECASTING

### 4.14.1 Models 26, 27 and 28

#### 4.14.1.1 Input and output data

As presented in Figure 4.88, three gauging sites namely, Pandu, Pancharatna and Dhubri have been selected with distances of 0, 115 and 180 kilometres from the subject reference site Pandu gauging station respectively. A total of 103 data patterns, covering the period from May 15 to October 15, 2002 have been used to train the network, i.e., to determine the optimal set of weights. To prepare the data for ANN, and to determine the time lag of the peak stages, the observed stage hydrographs were plotted and the travel times were determined. For each neuromorphic model, the data were split up into three parts; training (70%), 15% of data have been applied to validate the efficiency and 15% of the data were used as a reference to test the performance of the three models as a predictor of the river stage with a lead time of one day ahead. 50 sets of data patterns were used to forecast the daily stages at all the above sites. The variables which have served as the input have been shown in Table 4.24. Similarly, 103 data patterns each for the years 2000 and 2002 were used to forecast the daily stages of the river at Pancharatna, Pandu and Dhubri.

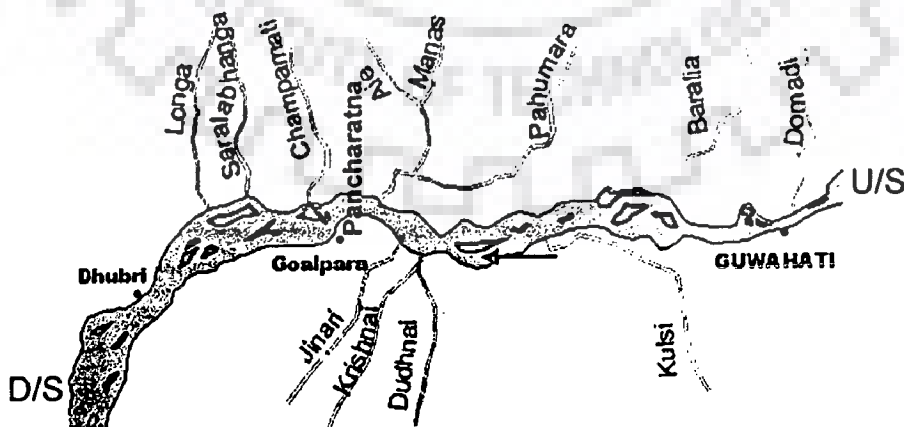


Figure 4.88 Plan of the study reach showing the gauging stations Pandu, Pancharatna and Dhubri

**Table 4.24 Network input and output data of three stations**

Station	Input data	Desired output data	Travel time
Pandu (Model 17)	(t) <sup>th</sup> day stages (Pandu) (t-1) <sup>th</sup> day stages (Pandu)	(t+1) <sup>th</sup> day Stages (Pandu)	
Pancharatna (Model 18)	(t) <sup>th</sup> day stages (Pandu) (t) <sup>th</sup> day stages (Pancharatna)	(t+1) <sup>th</sup> day Stages (Pancharatna)	1 day (from Pandu)
Dhubri (Model 19)	(t-1) <sup>th</sup> day stages (Pandu) (t) <sup>th</sup> day stages (Pancharatna) (t) <sup>th</sup> day stages (Dhubri)	(t+1) <sup>th</sup> day Stages (Dhubri)	1 day (from Pancharatna)

#### 4.14.1.2 Network setup and adjustment

The vital concern of the ANN set up was to determine the appropriate number of neurons in each layer to model efficiently the phenomena under study. The procedure suggested by Weigend et al. (1991), Hergert et al. (1992), who showed that for the simulations involving back propagation, the validation error decreases to a minimum then starts to increase even though the training error continues to decrease. This global minimum of the validation error curve, which was a function of the number of the hidden neurons in the ANN, determines the number of learning epochs and optimal step to stop the network. Conjugate gradient descent algorithm has been resorted to train the networks. Hidden layer neurons were determined by the exhaustive search method keeping in view the fitness criteria, as R-square value to maximum. The R-square is the statistical ratio that compares model forecasting accuracy with accuracy of the simplest model that just use mean of all target values as the forecast for all records. The data were normalised between values 0 and 1.

The forecasted stage of day (t+1),  $S_{t+1}$ , was dependant on the variables as listed in Table 4.24. The configuration chosen for the ANN models has been shown in Figure 4.89, where the bias inputs have the effect of lowering or



increasing the net result of the activation function. The activation used was the sigmoidal function, which has the purpose of limiting the permissible amplitude range of the output values to some finite value. The characteristics of the stage data at Pandu, Pancharatna and Dhubri have been depicted in Figure 4.90.

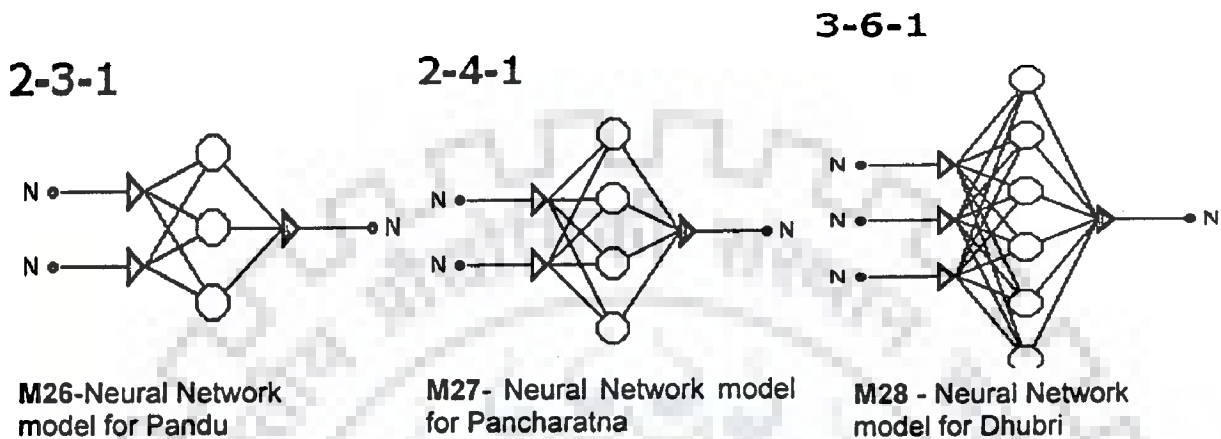


Figure 4.89 Architecture of the ANN models 26, 27 and 28

#### 4.14.1.3 Validation of results

The daily stages at Pandu, Pancharatna and Dhubri have been predicted in three different neuromorphic models referred to as model M26 to M28. The model efficiencies of the M26, M27 and M28 were 93% & 98.3%, 96.3% & 95.8%, 89% & 96.6% for the year 2002 and 2000 respectively. The *rmse* for all the three models were 0.14 & 0.104, 0.12 & 0.16 and 0.17 & 0.10 for the year 2002 and 2000 respectively. The performance indicator and results obtained during the training and validation period of the ANN have been summarised in Table 4.25(a) to Table 4.27(b), which show the reliability of the forecasted values for one day ahead. Moreover, the  $R^2$ , correlation coefficient and the plots in Figure 4.91, Figure 4.92 and Figure 4.93 of the observed versus ANN forecasted values vividly portray visual appreciation of the models. A simple recursive algorithm may be used to obtain forecasts for successive lead times. Tables 4.28 to 4.30 show the real-time observed

and ANN forecasted values of the stages at Pandu, Pancharatna and Dhubri respectively.

Conventional forecasting models require a great deal of detailed data, e.g. topographical maps, river networks and characteristics, soil characteristics, rainfall and runoff data. Often, these data were not available which posed a great difficulty in model calibration. In addition, a sufficiently long lead time for forecasting was required to take the necessary flood evacuation measures. In the case of dissemination of flood information and other flood evacuation measures, the computational speed of the models used are of absolute importance. Conventional models are not ideal for real-time forecasting due to the large amount of detailed information they require, and the associated long computation time.

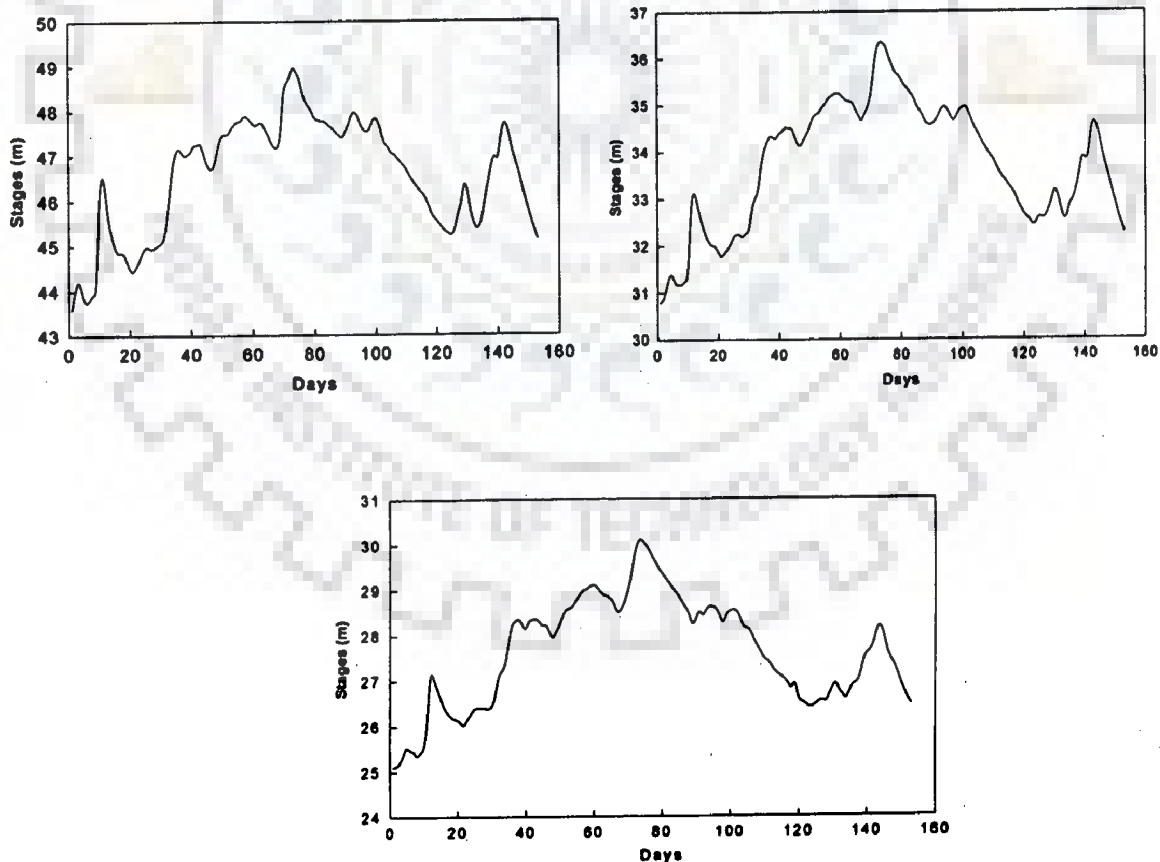


**Figure 4.90** Characteristics of stage data at Pandu, Pancharatna and Dhubri (May-Oct, 2002)

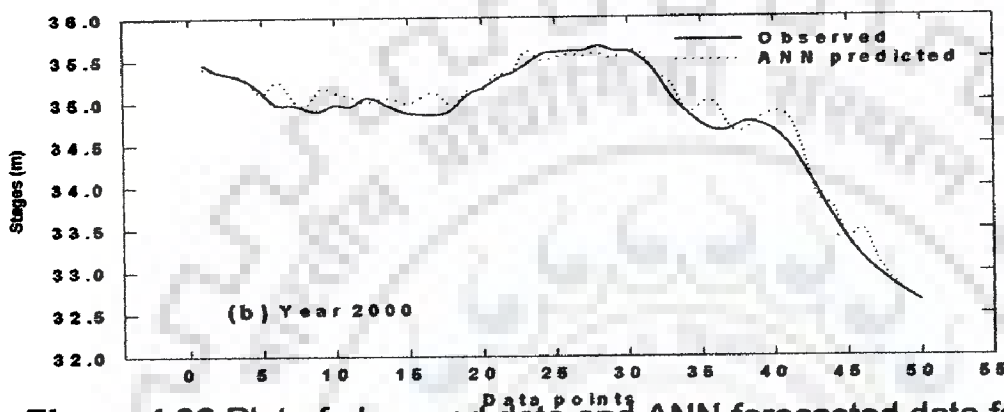
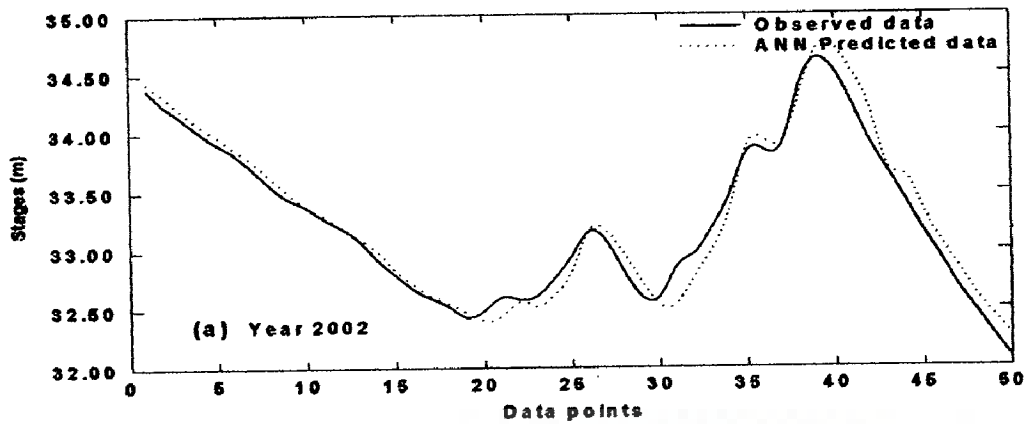


**Figure 4.92** Plot of observed data and ANN forecasted data for Pancharatna

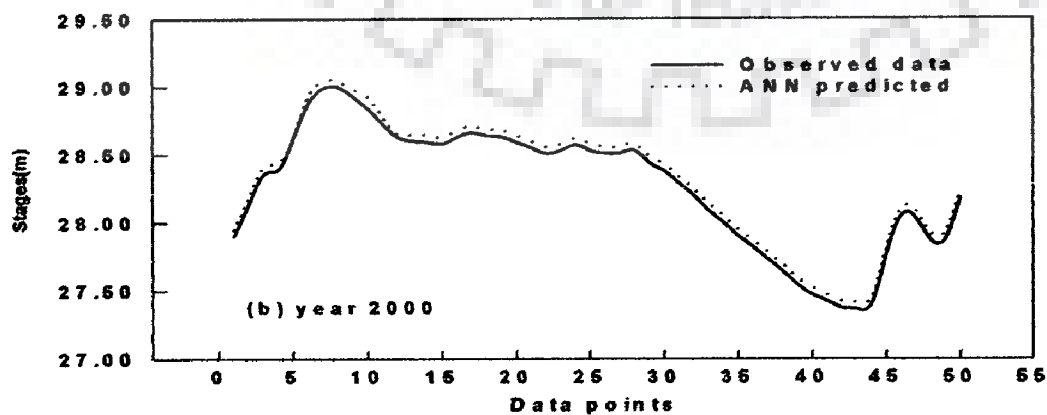
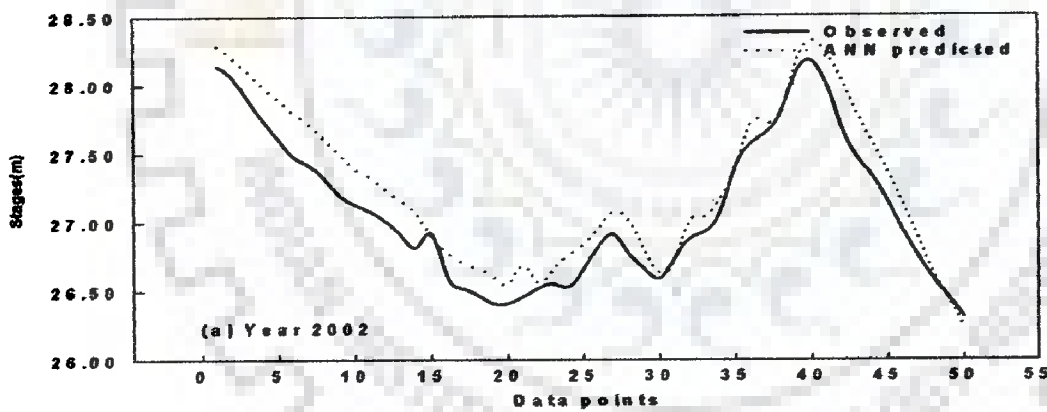


**Figure 4.93** Plot of observed data and ANN forecasted data for Dhubri

**Table 4.28 Observed and ANN forecasted stages at Pandu**

Date	(t+1) <sup>th</sup> day Obs. Stage(m) (Pandu)	(t+1) <sup>th</sup> day ANN output	Date	(t+1) <sup>th</sup> day Obs. Stage(m) (Pandu)	(t+1) <sup>th</sup> day ANN output
27-Aug-02	47.06	47.13	21-Sep-02	46.23	46.27
28-Aug-02	47.01	46.97	22-Sep-02	45.82	46.23
29-Aug-02	46.93	47.00	23-Sep-02	45.52	45.22
30-Aug-02	46.86	46.90	24-Sep-02	45.37	45.11
31-Aug-02	46.78	46.84	25-Sep-02	45.42	45.24
01-Sep-02	46.68	46.76	26-Sep-02	45.67	45.64
02-Sep-02	46.55	46.65	27-Sep-02	46.10	46.14
03-Sep-02	46.45	46.49	28-Sep-02	46.47	46.64
04-Sep-02	46.34	46.42	29-Sep-02	46.81	46.89
05-Sep-02	46.25	46.32	30-Sep-02	46.96	46.91
06-Sep-02	46.17	46.25	01-Oct-02	46.94	47.13
07-Sep-02	46.08	46.20	02-Oct-02	47.39	46.96
08-Sep-02	45.94	46.08	03-Oct-02	47.70	47.71
09-Sep-02	45.77	45.89	04-Oct-02	47.64	47.91
10-Sep-02	45.63	45.64	05-Oct-02	47.35	47.59
11-Sep-02	45.55	45.53	06-Oct-02	47.04	47.07
12-Sep-02	45.46	45.58	07-Oct-02	46.81	46.73
13-Sep-02	45.37	45.45	08-Oct-02	46.58	46.54
14-Sep-02	45.30	45.34	09-Oct-02	46.28	46.38
15-Sep-02	45.25	45.31	10-Oct-02	46.03	45.96
16-Sep-02	45.23	45.30	11-Oct-02	45.78	45.76
17-Sep-02	45.37	45.32	12-Oct-02	45.54	45.52
18-Sep-02	45.68	45.72	13-Oct-02	45.32	45.26
19-Sep-02	45.93	46.21	14-Oct-02	45.12	45.05
20-Sep-02	46.33	46.37	15-Oct-02	44.95	44.87

**Table 4.29 Observed and ANN forecasted stages at Pancharatna**

Date	(t+1) <sup>th</sup> day Obs. Stage(m) (Pancharatna)	(t+1) <sup>th</sup> day ANN output	Date	(t+1) <sup>th</sup> day Obs. Stage(m) (Pancharatna)	(t+1) <sup>th</sup> day ANN output
27-Aug-02	34.38	34.43	21-Sep-02	33.16	33.17
28-Aug-02	34.24	34.32	22-Sep-02	33.07	33.16
29-Aug-02	34.13	34.19	23-Sep-02	32.81	32.96

30-Aug-02	34.01	34.07	24-Sep-02	32.60	32.72
31-Aug-02	33.91	33.97	25-Sep-02	32.60	32.53
01-Sep-02	33.82	33.86	26-Sep-02	32.86	32.54
02-Sep-02	33.69	33.76	27-Sep-02	32.97	32.77
03-Sep-02	33.55	33.62	28-Sep-02	33.19	33.00
04-Sep-02	33.44	33.49	29-Sep-02	33.47	33.34
05-Sep-02	33.37	33.37	30-Sep-02	33.83	33.88
06-Sep-02	33.27	33.29	01-Oct-02	33.84	33.93
07-Sep-02	33.19	33.19	02-Oct-02	33.90	33.92
08-Sep-02	33.08	33.10	03-Oct-02	34.40	34.32
09-Sep-02	32.92	32.99	04-Oct-02	34.62	34.71
10-Sep-02	32.79	32.83	05-Oct-02	34.51	34.72
11-Sep-02	32.67	32.71	06-Oct-02	34.23	34.50
12-Sep-02	32.59	32.61	07-Oct-02	33.91	34.19
13-Sep-02	32.52	32.54	08-Oct-02	33.66	33.70
14-Sep-02	32.43	32.47	09-Oct-02	33.41	33.62
15-Sep-02	32.49	32.40	10-Oct-02	33.15	33.33
16-Sep-02	32.60	32.44	11-Oct-02	32.92	33.06
17-Sep-02	32.58	32.56	12-Oct-02	32.67	32.84
18-Sep-02	32.61	32.52	13-Oct-02	32.47	32.61
19-Sep-02	32.76	32.62	14-Oct-02	32.26	32.43
20-Sep-02	32.95	32.82	15-Oct-02	32.07	32.26

**Table 4.30 Observed and ANN forecasted stages at Dhubri**

Date	(t+1) <sup>th</sup> day Obs. Stage(m) (Dhubri)	(t+1) <sup>th</sup> day ANN output	Date	(t+1) <sup>th</sup> day Obs. Stage(m) (Dhubri)	(t+1) <sup>th</sup> day ANN output
27-Aug-02	28.14	28.24	21-Sep-02	26.83	26.97
28-Aug-02	28.06	28.14	22-Sep-02	26.91	27.11
29-Aug-02	27.90	28.03	23-Sep-02	26.77	27.03
30-Aug-02	27.75	27.93	24-Sep-02	26.66	26.85
31-Aug-02	27.61	27.83	25-Sep-02	26.59	26.68
01-Sep-02	27.48	27.75	26-Sep-02	26.74	26.71
02-Sep-02	27.42	27.68	27-Sep-02	26.88	26.95
03-Sep-02	27.32	27.56	28-Sep-02	26.93	27.02
04-Sep-02	27.20	27.45	29-Sep-02	27.08	27.17
05-Sep-02	27.13	27.36	30-Sep-02	27.40	27.39
06-Sep-02	27.08	27.31	01-Oct-02	27.57	27.68

07-Sep-02	27.01	27.23	02-Oct-02	27.65	27.67
08-Sep-02	26.91	27.16	03-Oct-02	27.80	27.73
09-Sep-02	26.82	27.07	04-Oct-02	28.09	28.14
10-Sep-02	26.92	26.93	05-Oct-02	28.17	28.30
11-Sep-02	26.61	26.82	06-Oct-02	28.00	28.21
12-Sep-02	26.52	26.74	07-Oct-02	27.68	27.98
13-Sep-02	26.47	26.68	08-Oct-02	27.47	27.72
14-Sep-02	26.41	26.62	09-Oct-02	27.33	27.52
15-Sep-02	26.41	26.55	10-Oct-02	27.15	27.31
16-Sep-02	26.46	26.62	11-Oct-02	26.94	27.10
17-Sep-02	26.52	26.73	12-Oct-02	26.75	26.92
18-Sep-02	26.55	26.71	13-Oct-02	26.59	26.71
19-Sep-02	26.53	26.72	14-Oct-02	26.45	26.56
20-Sep-02	26.66	26.82	15-Oct-02	26.31	26.39

#### 4.15 NEURAL NETWORK IN PREDICTION OF SEDIMENT LOAD CONCENTRATION

An ANN model was developed in this work to estimate the sediment discharge of the river Brahmaputra in terms of sediment concentration at Pancharatna. The selection of water and sediment variables used in the model was based on the prior knowledge of the conventional analyses, based on the dynamic laws of flow and sediment transport. Selecting an appropriate neural network structure and providing field data to that network for training purpose were addressed by using a constructive back-propagation with conjugate gradient descent learning algorithm. The model parameters, as well as fluvial variables, were extensively investigated in order to get accurate results.

##### 4.15.1 Selecting Sediment Discharge Parameters

The most pertinent variables in river hydraulics are the water discharge per unit width  $q$ , the water depth  $h$ , the longitudinal slope  $S$ , the bed shear stress  $\tau$ , the sediment discharge per unit width  $q_s$ , the particle's median diameter  $d_{50}$ , the

sediment and fluid density  $\rho_s$  and  $\rho$ , the kinematic viscosity  $\nu$ , the acceleration due to gravity  $g$ , and the particle's fall velocity  $w_0$ . For natural sand  $\rho_s$  and  $\rho$  are constants. The parameter  $C_s$  is equal to  $q_t/q$ , and the parameter  $\tau$  can be represented in terms of shear velocity  $u_* = (ghS)^{1/2}$ . These parameters have been presented in dimensionless forms in several previous studies. Table 4.31 shows the summary of most effective dimensionless parameters, which are commonly used for investigating the sediment discharge problem. Engelund and Hansen (1967) applied the stream power concept and similarity principle to obtain their sediment transport equation. This equation relates the sediment concentration with the dimensionless tractive shear stress  $\psi = hS/(G_s-1)d_{50}$ , where  $G_s$  = sediment specific gravity, and the  $u_m S$  represents the unit stream power or the rate of energy expenditure per unit weight of water, where  $u_m$  = flow mean velocity. Based on the stream power concept, Ackers and White (1973) presented general dimensionless sediment transport function by applying the dimensional analysis. The variables used in their formula are the dimensionless grain diameter  $d_g = d_{50} [g(G_s-1)/\nu^2]^{1/3}$ , the velocity ratio  $\phi = \frac{u_m}{u_*}$ , depth scale ratio  $d_{50}/h$ , tractive shear stress  $c$ , and  $u_m/u_*$ , where  $u_*$  is the grain shear velocity. Also, based on stream power concept, Yang (1973) used the  $\pi$  theorem to develop his formula for determining total sediment concentration. The relevant variables are the particle Reynolds number  $w_0 d_{50}/\nu$ , the mobility number  $u/w_0$ , dimensionless unit stream power  $u_m S/w_0$ , and dimensionless critical unit stream power  $u_m S/w_{0c}$ . Brownlie (1981) expressed the mean sediment concentration in terms of several variables including the grain Froude number  $F_g = u_m / [(G_s-1)gd_{50}]^{1/2}$ , critical shear stress  $\psi_c$ , the longitudinal slope  $S$ , the depth ratio  $h/d_{50}$ , and the geometric

standard deviation of grain size  $\sigma_g$ . Shen and Hung (1972) used regression analysis to develop their formula. The only used dominant parameter was  $(u_m S^{0.57}/W_0^{0.32})^{0.00750189}$ , which contains the same elements of unit stream power variable. Laursen (1958) developed a functional relationship between flow condition and the sediment discharge. The effective variables in his expression are the specific weight of water  $\gamma_w$ , the water depth ratio  $d_{50}/h$ , the mobility number  $u/W_0$ , and the dimensionless grain tractive force  $\tau'/\tau_c$ , where  $\tau'$  = shear stress due to grains and  $\tau_c$  is the critical shear stress.

Reviewing the presented conventional sediment discharge equations helped in selecting the dominant parameters. In the present model, it was designed to use the fundamental as well as measurable parameters in order to avoid using any empirical formula, which may affect the accuracy of results. The final developed equation for total load concentration yielded

$$C_s = f\left(\psi, \phi, \frac{w_0}{u_*}, S, \frac{h}{d_{50}}, F, R, \frac{h}{B}\right) \quad (4.18)$$

Where,  $F = \frac{u_m}{(gh)^{1/2}}$  is the Froude number,  $R = u \cdot d_{50}/\nu$  is the Reynold's number and  $h/B$  is width scale ratio.

**Table 4.31 Total load discharge approaches and relevant variables**

Sediment concentration formula	Dependant variable	Independent variable
Engelund & Hansen (1967)	C <sub>s</sub>	$G_s/(G_s-1), u_m S/[(G_s-1)gd_{50}]^{1/2}, \psi$
Ackers & White (1973)		$d_g, d_{50}/h, u_m/u', \phi$
Yang (1973, 1979, 1996)		$w_0 d_{50}/\nu, u_m S/W_0, u_c S/W_0$
Brownlie (1981)		$u_m/[(G_s-1)gd_{50}]^{1/2}, S, h/d_{50}, \psi_c, \sigma_g$
Shen and Hung (1972)		$u_m S^{0.57}/W_0^{0.32})^{0.00750189}$
Laursen (1958)		$\gamma_w, d_{50}/h, \tau'/\tau_c, u/W_0$



#### 4.15.2 Training the Network and Verification of Results

Total 50 data patterns, covering the monsoon period (June to October) from year 1990 to 1999 have been used to train the network, i.e., to determine the optimal set of weights. For each neuromorphic model, the data were split up in to three parts; one for model training (70%), one for cross validation (to prevent model over training), and another for testing the performance of the model. 15 data sets covering the monsoon period (June to October) from year 2000 to 2002 were used for verification. To prepare the data for ANN, and to determine the time lag of the peak stages, the stage hydrographs were plotted and the travel times were noted. 15% of data have been applied to validate the efficiency of the ANN and 15% of the data were used as a reference to test the performance of the model. The ranges of used variables have been summarized in Table 4.32. The network (8 -12 -1) was set up with the eight parameters of Eqn. (4.18) as the input pattern, and the sediment concentration  $C_s$  as the output pattern. In other words, the input layer contains eight neurons, while the output layer contains one and hidden layer with 12 neurons. Between the two layers, there was another hidden layer that contains a suitable number of neurons (under investigation). The network was trained with the 50 data sets. The best fit of the obtained and given data for concentration has been shown in Figure 4.94, where the number of neurons in the hidden layer was 12. Figure 4.95 shows the verification between measured and estimated values for new patterns. The *rmse*, Nash-Shutcliffe and the correlation coefficients between the observed and the ANN predicted values of the model were found to be 0.152, 0.62 and 0.988 respectively.

**Table 4.32 Range of data used in learning and verification of sediment concentration model**

Variables	Range	Variables	Range
Tractive shear stress $\psi$	4.31 - 5.71	Froude number Fr	0.07 - 0.17
Velocity ratio $\phi$	0.06 - 0.14	Reynold's number R.	13.63 - 15.59
Suspension parameter $w_0/u_*$	0.31 - 0.34	width scale ratio h/B	0.0014 - 0.0019
Longitudinal Slope S	0.000084 - 0.000089	Sediment concentration $C_s$	323 - 1719
Water depth ratio $h/d_{50}$	80942 - 105942		

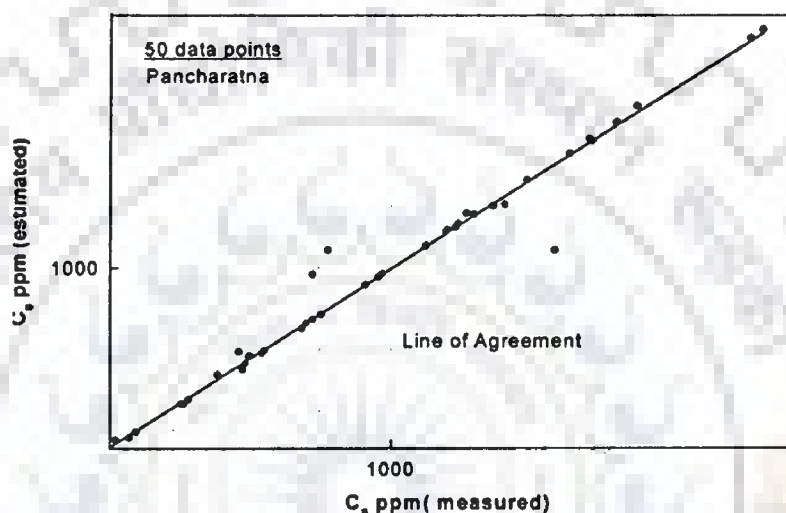


**Figure 4.94 Comparison between measured and estimated concentration**

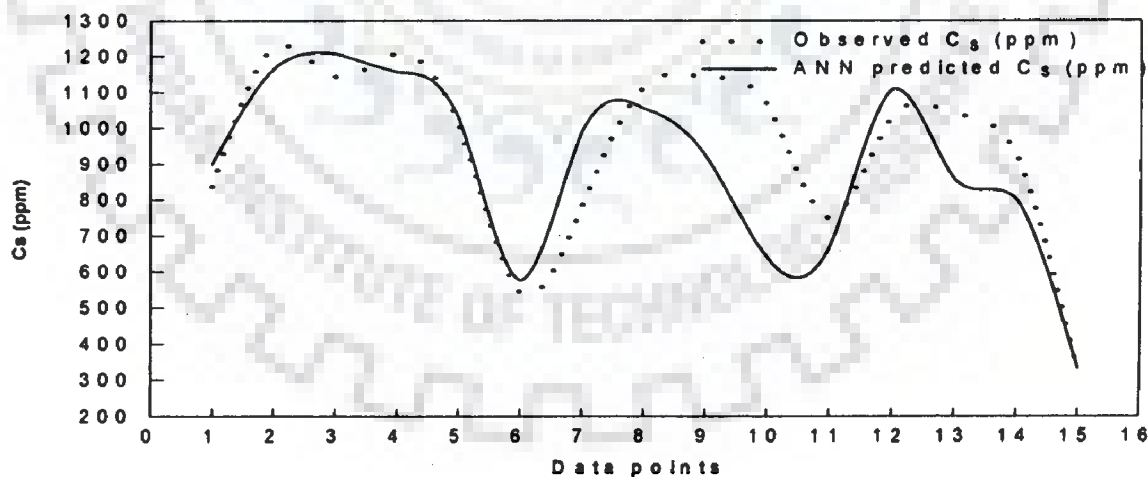


**Figure 4.95 Validation of observed and ANN predicted concentration**

### 4.15.3 Calibration of Flow and Sediment Parameters

The variables presented in Eqn. (4.18) were assumed to be the most effective parameters on the dynamics of sediments. However, a sensitivity analysis was

recommended to investigate the effect of each parameter on the model results. Some parameters may have no significant effect on results. On the other hand, existence of other parameters may confuse the training process of the network.

Trial runs made with the help of software examined the sensitivity of the provided parameters. The first run was carried out with the eight input parameters of Eqn. (4.18). Then, each parameter was eliminated by turn from the group. An error analysis was conducted for determining the accuracy in each case. As a result, two parameters were eliminated without sacrificing accuracy: the velocity ratio  $\phi$  and the longitudinal slope  $S$ .

The functional form of the new group yields

$$C_s = f\left(\psi, \frac{w_0}{u_*}, \frac{h}{d_{50}}, F, R_*\right) \quad (4.19)$$

The mean of the discrepancy ratio between obtained and measured values was 0.961 and the standard deviation for the mean was 0.156.

## 4.16 APPRAISAL OF PLANFORM MORPHOLOGICAL CHANGES

### 4.16.1 Stream Bank Migration

The average northing for right bank line of the Brahmaputra river moved about 0.47 km to the north between 1990 and 2002, while that for the left moved about 0.48 km to the south. The river has avulsed just upstream side of the Dibrugarh town and excised areas of floodplain to create new bars. The magnitude of monsoon flood, especially during 1997-2000, had accelerated bank erosion, particularly along the right bank. Left bank movement occurred mainly through rapid erosion in the embayment next to braid bars, while right bank movement involved looping, both through embayment erosion and capture of floodplain.

#### **4.16.2 River Width**

The river mean width has increased from 7.99 km to 8.94 km in the total length of the river, where as the minimum width at Pandu was slightly constricted due to the presence of hard geological formations. The maximum width has not registered any significant change and was 18.13 km just downstream side of Pandu at cross section 17 near Gumi. Thus, the mean width has increased much more than the minimum and maximum width. The spatial and temporal records of river width were examined under the study to identify the occurrence and persistence of any narrow points or reaches that could indicate the existence of 'nodes' or 'nodal reaches'. The study findings suggested that both morpho-dynamically controlled nodal reaches were present at Pancharatna, Pandu and Tezpur.

#### **4.16.3 Within-bank Morpho-dynamics**

The study further revealed that the total river area within the stream bank has increased by 12.10% between 1990 and 2002 due to erosion process causing channel widening. Figures 4.96 and 4.97 show the erosion of the bank of the river Brahmaputra at u/s of Dibru and view at Dibru Reserve Forest. Expansion of the river has taken place primarily through flood plain erosion and excision coupled with bar or island growth. Trends of expansion showed no sign of slacking and the expansion process appears to continue. The planform within the braid-belt displayed a wide range of morphological features of varying scales and geometrics. There was a persistence of islands at relatively-fixed geographical locations, as well as a persistence of major convergent flow features at particular geographical locations for

over one decade, providing further evidence of the existence of 'nodal reaches' in the braiding pattern of the river.

#### 4.16.4 River Braiding

The degree of braiding of individual reaches fluctuates in the short-term due to morphological response to the magnitude and duration of monsoon runoff events. It was found that the overall degree of braiding to have increased slightly until the year 2000, after which it had slowed down showing the decrease until 2002. The detailed discussion on braiding has been dealt in Chapter 5.



**Figure 4.96** Erosion at u/s of Dibru Reserve Forest

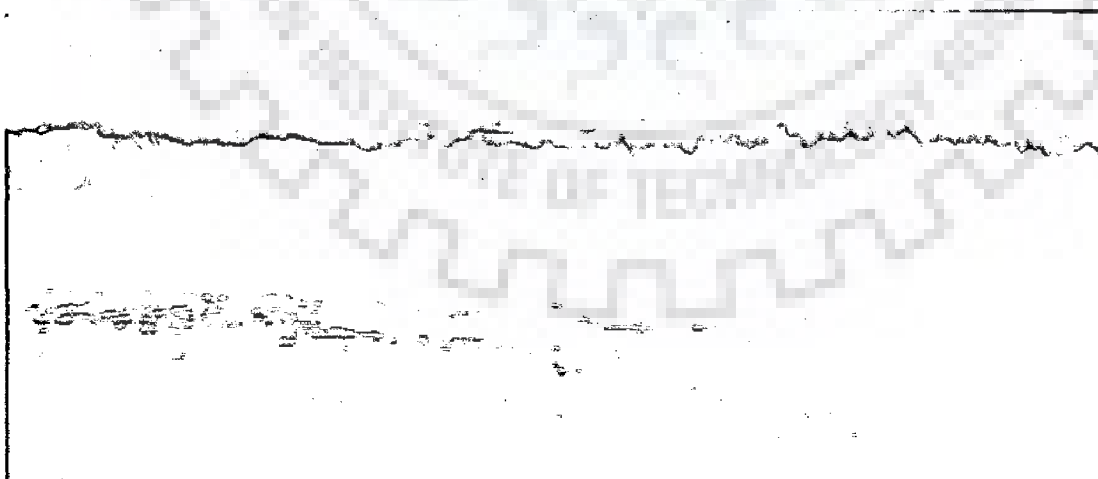


**Figure 4.97** A view of erosion at Dibru Reserve Forest

#### **4.17 ANALYSIS OF EROSION COUPLED WITH GROUND TRUTH**

Along the Brahmaputra, bank materials are rarely homogeneous in composition, and result in uneven bank slumping. This causes the flow to take a different path changing the orientation of the stream-bank. Ground observations along the stretch under study also revealed that at some localities older alluvium protruding into the river offers significant resistance to the flow regime and causes changes in hydraulic conditions. The finely divided bank material and the constant change in flow direction produce severe bank caving along the river. When the flow approaches the bank at an angle, severe under-cutting takes place resulting in slumping of sediments. Slumps are more common along banks composed of clayey-silt. Quite often, the highly saturated clayey-silt liquefies and tends to flow towards the channel. As the materials flow, the overlying, less-saturated bank sediments tend to slump along well-defined shear planes. Thus, there appears to be two prominent types of slumping, which cause the stream-bank to recede; undercutting during the flood stage and the flow of highly saturated sediments during the falling stage. However, the intensity of slumping was more acute after the flood stage. The accumulated water level during the flood stage provides additional support to the bank material as the pore spaces of the loosely bound bank materials are occupied by water and act as a continuous system. With the fall in water level, the support diminishes abruptly, and the bank materials are subjected to different degrees and nature of failure.

The ground truth survey along a reach of the Brahmaputra river channel around Neamatighat, Majuli and Kaziranga areas provided ample evidence on the severity of bank failure. In some localities, stratified fine sand, quite massive channel sands and silts underlie the silty-clay of the natural levee deposits. During high stage

of the river, water was forced into the strata, raising pore pressure in the strata. As the water level in the river falls rapidly and the pressure against channel wall was lessened, water moves from the formation back into the river. This causes a lateral flow of sands and silts into the channel, resulting in sub-aqueous failure. This normally produces a bowl-shaped shear failure in the overlying cohesive natural levee deposits. This type of bank failure could be seen near Neamatighat (Figure 4.98) and in some localities around Majuli and Kaziranga. These types of failure with semi-circular outlines of different magnitude area abundant along the Brahmaputra river channel within the studied reach. The mechanisms involved and responsible for riverbank erosion at Neamatighat, Majuli and Kaziranga are basically related to liquefaction enhanced by the heterogeneous bank materials, over-steepening and associated sub-aerial processes of weathering and weakening in relation to soil moisture content.

Areas upstream of Neamatighat (between spur no 5 and 8), and some waterlogged areas developed near the bank of the river, are probably related with the construction of flood embankment. These water bodies have no direct outlets to the river. Thus, as the water level in the river recedes, water from these areas moves through permeable levee materials and oozes out along the bank of the river. This type of phenomenon also causes failure of bank materials during the post-flood period (Figure 4.99). Another type of failure noticed that occurred in the upper bank and natural levee materials were clearly related to the sub-aqueous flow.

Because of the braided nature of the river channel and constant migration of the river, many abandoned channels intersect the stream-bank. This gives rise to a zone of well-sorted silt and fine sand localized in the abandoned channel fill. During

rising and flood stage, the sand and silt become highly saturated. The rapid drop in water level in the channel results in rapid withdrawal of water from these sediments. The highly saturated sediments liquefy and flow towards the channel. As the materials flow, the overlying less-saturated bank sediments tend to shear along well-defined planes. This type of failure was conspicuous in the western tip of Majuli Island and also upstream of Neamatighat (Figure 4.100 and 4.101) and near Dibru Reserve Forest. Shear failure was one of the most effective causes of bank line recession of the Brahmaputra. Majority of the failures occurred as a result of the current undermining of the natural levee deposits, due to which large blocks of natural levee sediments are shearing-off and tilting into the river.

The other major cause of shear failure was over-steepening of the bank materials as thalweg of the channel hug banks. In localities where bank materials are slightly cohesive, shear failure of the bank results in a rotated step-like structure leading from the top of the bank to the water edge. Most of the shear planes diminish in the slope as they penetrate into sub-surfaces, and as a result the blocks are tilted land-ward by rotation. In some areas around Salmora in Majuli Island and in some localities in Kaziranga, such types of over-hangs were observed.





**Figure 4.98** Erosion due to bowl shaped failure, d/s Neamatighat

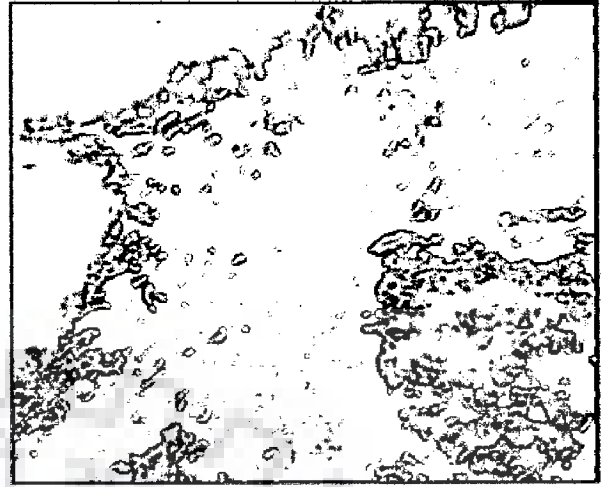


**Figure 4.99** Flow failure triggered by adjacent waterlogged areas, d/s Neamatighat

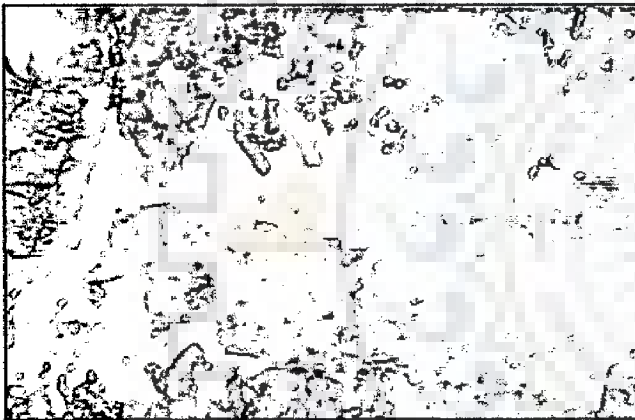


**Figure 4.100** Shear failure of bank near spur no 2 Neamatighat

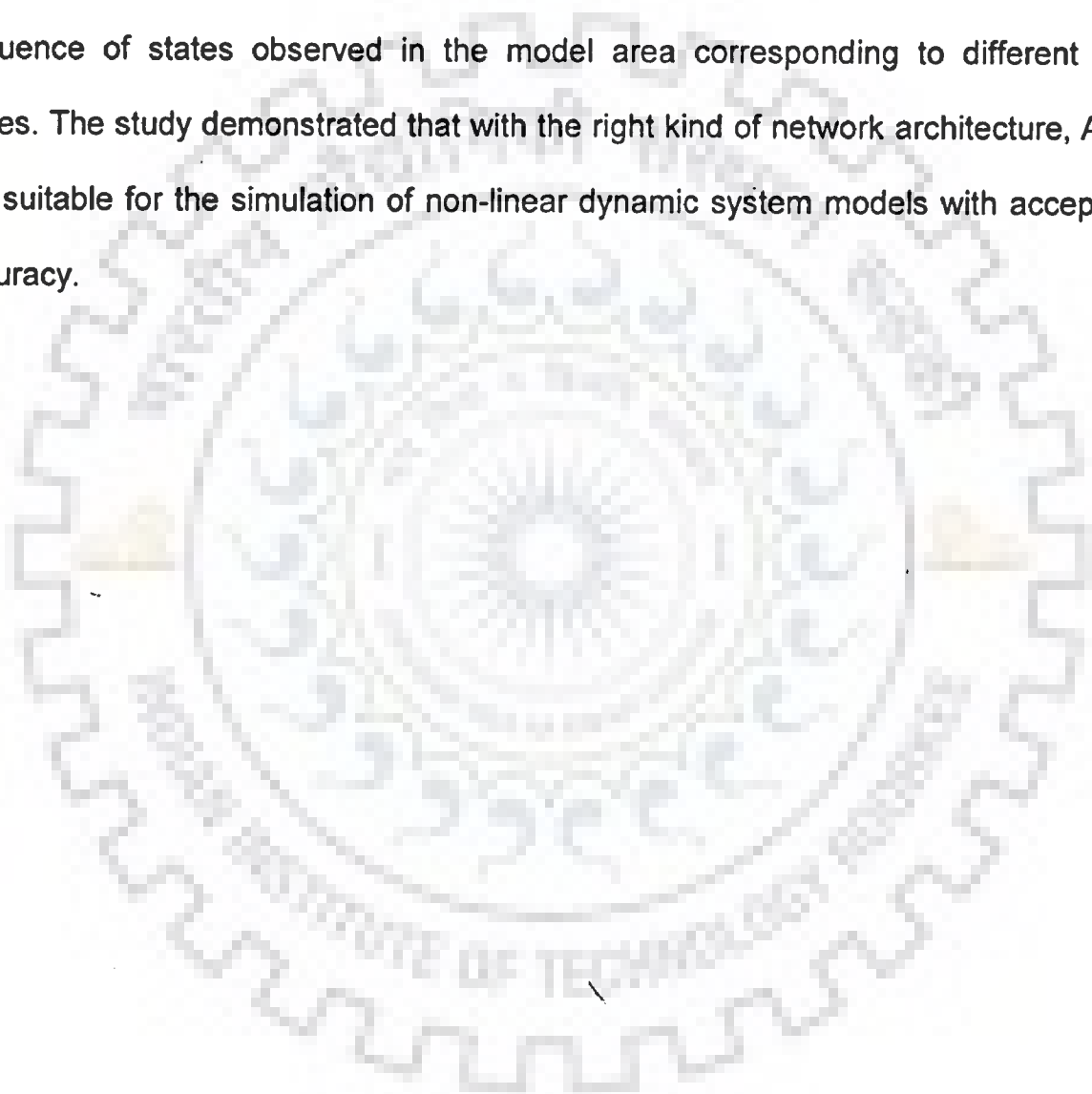


**Figure 4.101** Shear failure of bank near spur no 5 Neamatighat

#### **4.18 CONCLUDING REMARKS**

In this chapter, an in-depth investigation has been made to gain an insight into the behaviour of the Brahmaputra river system for hydrological and morphological changes. The morphological changes during the period 1990-2002 revealed that the morphology of the river evolved markedly in response to the imposed flow and sediment regimes. Several ANN models have been developed, which took into

account constraints on fluvial landform change, hydrographic changes and hydraulic characteristics. ANN, which is a relatively new approach, found to have gainful applications for various fluvial attributes of a large braided river, like the Brahmaputra. The study outcomes have indicated the potential use of ANN and fuzzy techniques for prediction and flood forecasting. The results of this study showed that ANNs could be used to encapsulate site-specific knowledge and data to reproduce the temporal sequence of states observed in the model area corresponding to different input series. The study demonstrated that with the right kind of network architecture, ANNs are suitable for the simulation of non-linear dynamic system models with acceptable accuracy.



## FLUVIAL LANDFORM INDICATORS

---

### 5.1 GENERAL

Fluvial landforms are those features produced by the action of running water in the terrestrial environment, whereas the fluvial geomorphic processes are natural phenomena that produce, maintain and change fluvial landforms. The channel pattern or landform of a reach of an alluvial river reflects the hydrodynamics of flow within the channel and the associated processes of sediment transfer and energy dissipation. Channel patterns form a continuum in response to varying energy conditions, ranging from straight to meandering or braided forms. Generally, braiding is favoured by high energy fluvial environments with steeper gradients, large and variable discharges, dominant bed load transport and non-cohesive banks lacking stabilization by vegetation (134). The secondary flow component also contributes to the growth of channel deformations (13).

Fluvial landform indicators have been used in this work for a quantitative description to assess the extent or severity of braiding in a stream. It is well recognised that bed topography and planform geometry is the result of complex interaction of fluid flow with the channel boundaries and sediment transport. For an unstable channel, the channel deformation controls the development of or braid. Modelling the channel deformations in an unstable state is quite complex. Investigators (22; 115) have preferred to use braiding indicators as a means of studying the braiding characteristics of alluvial streams for a quantitative measure.

There is an imperative need to formulate appropriate parameters to describe the

braiding phenomenon and fluvial landform pattern in quantitative terms on a more rational basis. It is necessary to mention here that braided rivers like the Brahmaputra are hydraulically less efficient and the formation of braid bars plays an important role in the modification of the energy losses due to friction. With a view to incorporating the effect of the above hydraulic variables, fluvial landform index and at-a-station hydraulic geometry indices were developed during this work, making conjunctive use of field and remote sensing data. A reasonable quantitative estimate could be made from the developed indices to provide a better understanding of the braiding pattern of the river Brahmaputra.

## 5.2 EXISTING BRAIDING INDICATORS

Several studies have presented the discrimination between straight, meandering, and braided streams on the basis of discharge and channel slope. Lane (1957) suggested the following criterion for the occurrence of braiding:

$$S > 0.004 (Q_m)^{-0.25} \quad (5.1)$$

Where,  $Q_m$  = mean annual discharge; and  $S$  = channel slope.

Using bank full discharge ( $Q_b$ ), Leopold and Wolman in 1957 (134) proposed the following relationship for braiding to occur, which also predicts braids at higher slopes and discharges:

$$S > 0.013 Q_b^{-0.44} \quad (5.2)$$

Antropovskiy (1972), however, developed the following criterion for the occurrence of braiding:

$$S > 1.4Q_b^{-1} \quad (5.3)$$

Leopold and Wolman (1957) also indicated that braided and meandering streams can be separated using the relationship:

$$S = 0.06 Q^{0.44} \quad (5.4)$$

Where, S = channel slope; and Q = water discharge. Thus, for the streams studied, higher slopes for given discharges tended to favour braided pattern rather than meandering.

These indicators have been criticised by Schumm and Khan (1972) as none of these recognizes the importance of sediment transport. There is higher power expenditure rate in braided streams, a conclusion reinforced by Schumm and Khan's (1972) flume experiments. However, none of these investigators recognised the control of channel pattern by sedimentology. Since, bed material transport and bar formation was necessary in both meander and braid development processes, the threshold between the patterns related to bed load.

Henderson (1961) re-analysed Leopold and Wolman's data to derive the following expression including  $d_{50}$ , median grain size (mm):

$$S > 0.002 d_{50}^{1.15} Q_b^{-0.46} \quad (5.5)$$

According to equation (5.5), a higher threshold slope is necessary for braiding in coarse bed materials. Bank material resistance affects rate of channel migration and should also influence the threshold, although its effect may be difficult to quantify and also be non-linear since greater stream power is required to erode clays and cobbles than sands.

Parker's stability analysis (1976) indirectly illustrates the effects of bank material resistance by defining the meander - braid threshold as

$$S/F_r = D/B \quad (5.6)$$

Where,  $D$  = mean depth of the flow;  $B$  = width of the stream, and  $F_r$  = Froude number, which may be expressed in terms of discharge and bank silt-clay percentage, as suggested by Schumm (134). Meandering occurs for  $S/F_r \leq D/B$ , braiding occurs for  $S/F_r \geq D/B$ , and transition occurs in between  $S/F_r \approx D/B$ .

Ferguson (1981) suggested Eqn. 5.7 for braiding to occur, this predicts steeper threshold slopes for braiding in channels with resistant silty banks.

$$S > 0.0028 (Q_b)^{-0.34} B_c^{0.90} \quad (5.7)$$

Where,  $B_c$  = percentage of silty clay content in the bank material.

Measures of the degree of braiding generally fall into two categories: (i) the mean number of active channels or braid bars per transect across the channel belt; and (ii) the ratio of sum of channel lengths in a reach to a measure of reach length (total sinuosity). The sinuosity,  $P$  is thalweg length / valley length.

Smith (1970) illustrated the measurement of cross-section bed relief index (BRI), measured by:

$$\text{Bed Relief Index (BRI)} = \frac{2 \left[ \sum_{i=1}^n T_i - \sum_{i=1}^n t_i \right] \pm \sum_{i=1}^n T_{ei}}{B_L} \quad (5.8)$$

where,  $T_i$  = height maxima between hollows;  $t_i$  = minima between peaks;  $B_L$  = transect length; and  $T_e$  = end heights.

Sharma (1995) proposed Flow Geometry Index (FGI), Plan Form Index (PFI) and cross-slope ratio for identifying the degree of braiding of highly braided river. The PFI, FGI and cross- slope formulae have are as below:

$$\text{Plan Form Index (PFI)} = \frac{\frac{W}{B} \times 100}{N} \quad (5.9)$$

$$\text{Flow Geometry Index (FGI)} = \left[ \frac{\sum d_i x_i}{WxD} \right] \times N \quad (5.10)$$

$$\text{Cross-slope} = \frac{\frac{B_L}{2}}{(\text{Bank level} - \text{Av. bed level})} \quad (5.11)$$

Where, W = flow top width; B = overall width of the channel; B<sub>L</sub> = Transect length across river width; N = numbers of braided channel; d<sub>i</sub> and x<sub>i</sub> are depth and top lateral distance of submerged sub-channel; and D = hydraulic mean depth.

Other indices proposed in the literature are as in the Table 5.1.

**Table 5.1 Different types of indices**

Authors	Indices
Ashmore (1991a)	Mean number of active channels per transect Mean number of active channel links in braided network
Brice (1960, 1964)	Braiding Index = $\frac{2(\text{Sum of lengths of bars or islands in a reach})}{\text{Centre line reach length}}$
Engelund and Skovgaard (1973), Parker (1976), Fujita (1989)	Mode = Number of rows of alternate bars (and sinuous flow paths) = 2 times the number of braid bars and number of side (points) bars per transect.
Friend and Sinha (Bristow & Best, 1993)	Braid channel ratio = $\frac{\text{Sum of mid - channel lengths of all channels in reach}}{\text{Length of mid - line of widest channel}}$
Hong and Davies (1979)	Total sinuosity = $\frac{\text{Length of channel segments}}{\text{Channel belt length}}$ Number of braids or channels in cross –section
Howard, Keetch and Vincent (1970)	Average number anabranches bisected by several transects perpendicular to flow direction
Mosley (1981)	Braiding index = $\frac{\text{Total length of bankful channels}}{\text{Distance along main channel}}$
Richards (1982) Robertson - Rintoul and Richards (1993)	Total sinuosity = $\frac{\text{Total active channel length}}{\text{Valley length}}$
Rust (1978a)	Number of braids per mean curved channel wave length = (mode – 1)

Sharma (1995)	Plan form index = $T/B * 100/N$
	Flow geometry index = $\left[ \frac{\sum d_i x_i}{WxD} \right] \times N$
	Cross slope index = $\frac{B_L}{2}$ (Bank level - Av. bed level)

### 5.2.1 Topological Analysis of the Brahmaputra River

The analysis of the planform changes of the Brahmaputra was carried out employing IRS 1C/D LISS-III digital satellite data comprising of 32 scenes for the years 1990, 1997, 2000 and 2002. The entire river from Dhubri (Chainage 17.34 km) to Kobo (Chainage 640.07 km) was divided in to 13 blocks, e.g., C/S 2-5 as block one, c/s 5-10 as block two and so on. Since a braided channel was characterised by (i) channel segments (anabranches),(ii) nodes where segments branched or joined, and (iii) islands enclosed by segments, their network could be studied by using topological theory as suggested by Howard et al (1970) and Orme and Krumbein (1972). Accordingly, the following topological parameters for various blocks have been measured for different years from the satellite images. Figure 5.1 shows a typical definition sketch of the different parameters.

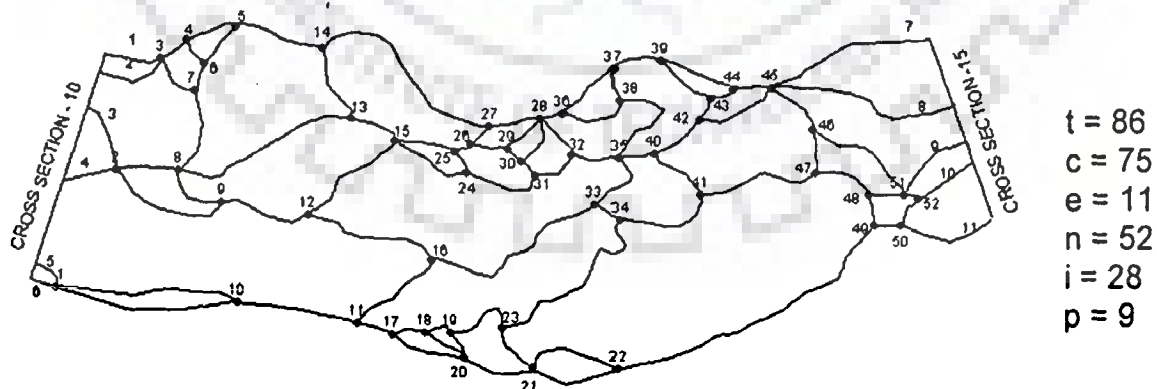


Figure 5.1 A typical definition sketch of the topological parameters (February, 1990)



where,  $t$  = total number of segments, including segments lying entirely within the block and those bisected by the lines bounding the block,  $e$  = total number of bisected segments,  $c$  = total number of entire segments,  $i$  = total number of unbisected islands,  $p$  = total number of islands bisected by the bounding lines and  $n$  = total number of nodes.

In addition, as suggested by Howard et al (1970), topological indices  $\alpha$ ,  $\beta$  and  $\gamma$  describing the degree of connection between the nodes on a graph have been determined. These are defined as follows-

$$\text{Alpha } (\alpha) \text{ Index} = \frac{t - (n + e) + 1}{2(n + e) - 5} \quad (5.12)$$

$$\text{Beta } (\beta) \text{ Index} = \frac{t}{n + e} \quad (5.13)$$

$$\text{Gamma } (\gamma) \text{ Index} = \frac{t}{3(n + e - 2)} \quad (5.14)$$

The alpha ( $\alpha$ ) index is the ratio of the observed number of islands to the greatest possible number of islands for a given number of nodes. The higher the alpha index, more the network is connected. A simple network will have a value of 0, while a value of 1 indicates a completely connected network.

The beta ( $\beta$ ) index measures the level of connectivity, and is expressed by the relationship between the number of links ( $t$ ) over the number of nodes ( $n$ ). More complex networks have a value greater than 1. In a network with a fixed number of nodes, the higher the number of segments, the higher the number of channels possible in the river network. Complex networks have a high value of beta.

The gamma ( $\gamma$ ) index is the ratio of the observed number of channel segments to the greatest possible number of segments for a given number of nodes (Berge, 1962).

The value of gamma is between 0 and 1 where a value of 1 indicates a completely connected network and would be extremely unlikely in reality.

### 5.3 INTERPRETATION OF THE TOPOLOGICAL INDICES

Variations of different topological parameters and indices with time in different blocks have been shown in Figures 5.2 to 5.9. The indices and parameters as plotted, indicate that the degree of braiding of individual reaches fluctuates in the short-term due to morphological response to the magnitude and duration of monsoon runoff events. The following observations are evident from these figures:

- (i) For the years under consideration, variables  $t$ ,  $c$ ,  $i$ ,  $e$  and  $n$  showed distinct decrease in values in blocks 5, 10 and 11. The lowest trend was marked in block 5. On the contrary, block 4, 7, 9 and 12 showed increase in their values. The indices  $\alpha$ ,  $\beta$  and  $\gamma$  were characterised by approximately similar decrease in values in blocks 5, 9 and 11.
- (ii) Comparison of trends for the different years indicated that  $t$ ,  $c$ ,  $n$  and  $i$  values increased in the upstream direction for block 2 for the years 1990, 1997, 2000 and 2002 and this trend was gradual for the year 2002. Probably, the trend has been decelerated after the construction of the Naranarayan Bridge at Pancharatna, at cross section 9, which was pronounced for these blocks. Similar trend has been observed at block 8, which may be due to the presence of Kaliabhomara Bridge near Tezpur.
- (iii) It was noted that the decrease in values in block 13 of  $t$ ,  $c$ ,  $n$  and  $i$  for the years 1990, 2000 and 2002 showed the intensity of non-braiding tendency.

The braiding intensity was high in blocks 4, 7, 9 and 12, indicating that the island formations were more in these reaches.

- (iv) The study of  $\alpha$ ,  $\beta$  and  $\gamma$  indices over the entire stretch revealed that their values in blocks 2 and 4 were very low as compared to other blocks.

An increase in the values of the parameters and indices discussed above, suggested an increase in intensity of braiding, while a decrease in their values indicated a tendency towards non-braiding. Another reason for low values of these indices in blocks 5, 8 and 9 may be attributed due to the existence of the hills on the sides of the river, thereby restricting the flow and constraining of the formation of more channels.

The average values of  $\alpha$ ,  $\beta$  and  $\gamma$  indices for the entire stretch were found to be 0.222, 1.401 and 0.487 for the year 2000 and 0.215, 1.390 and 0.482 for 1990 respectively. The years 1990, 1997 and 2002 showed less channelization of the planform as compared to the year 2000.

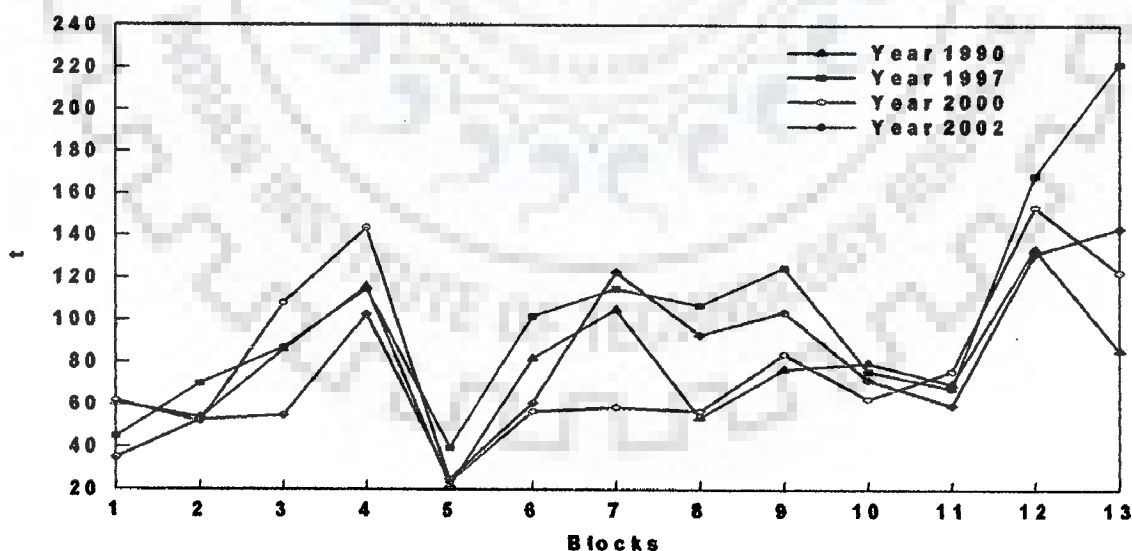


Figure 5.2 Variation of  $t$  in different blocks

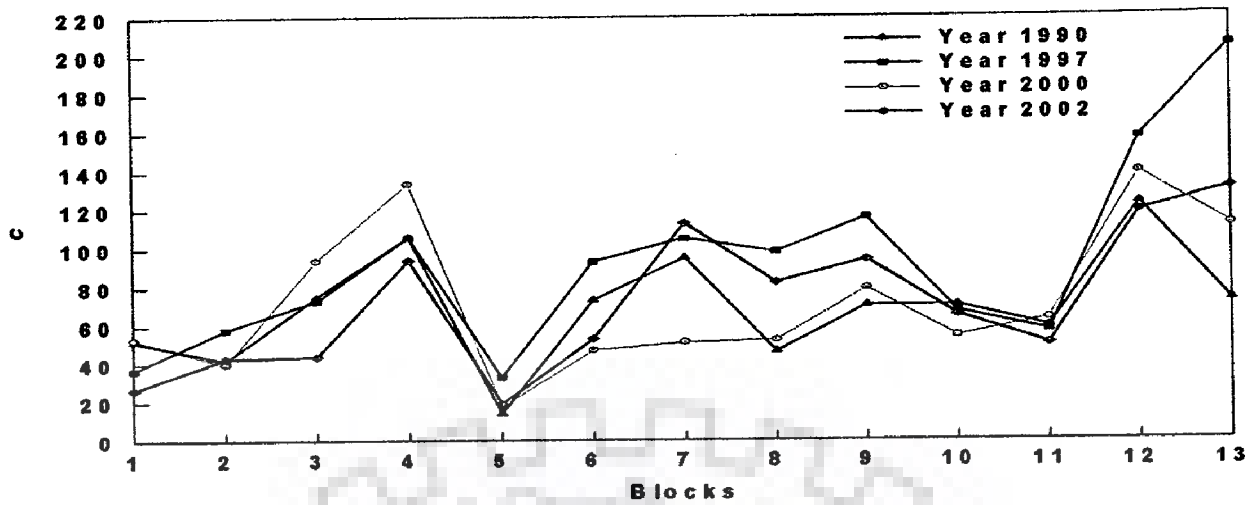


Figure 5.3 Variation of  $c$  in different blocks

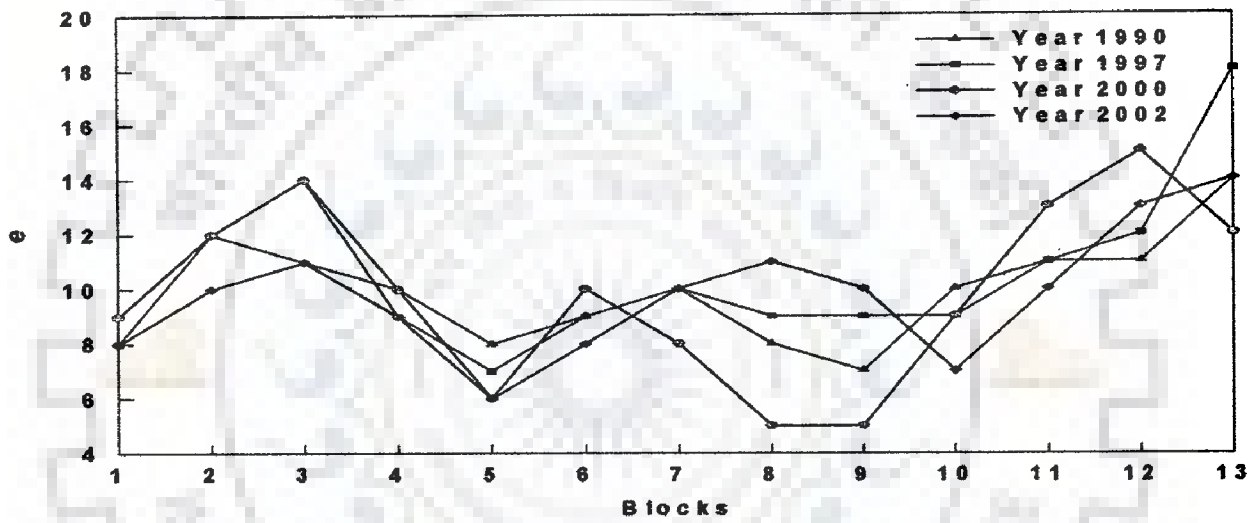


Figure 5.4 Variation of  $e$  in different blocks

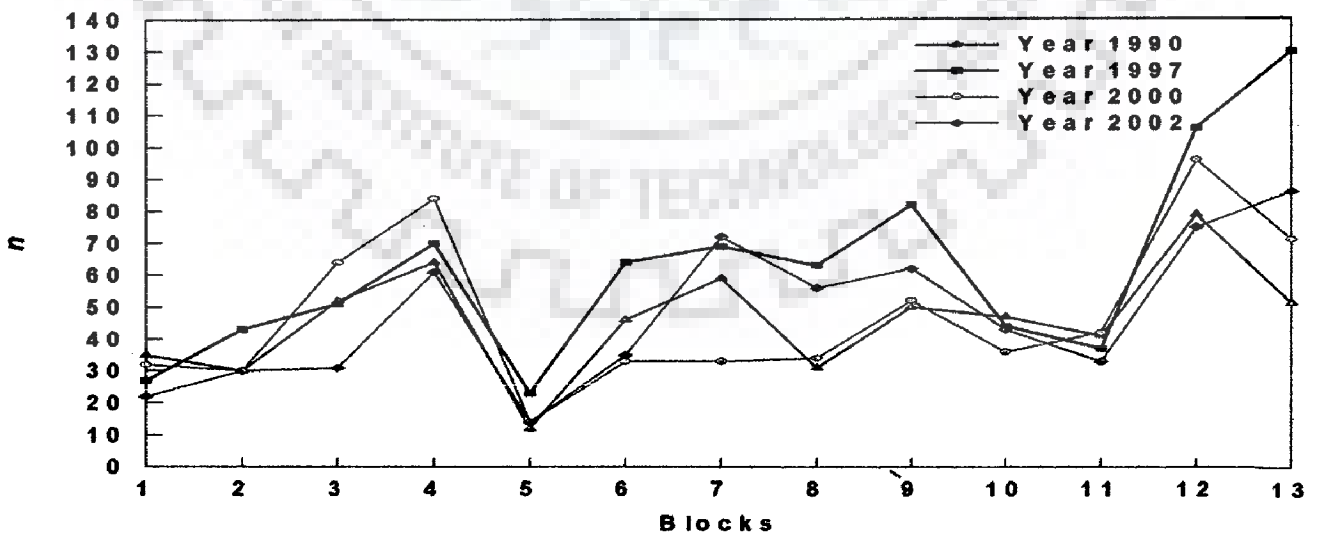


Figure 5.5 Variation of  $n$  in different blocks

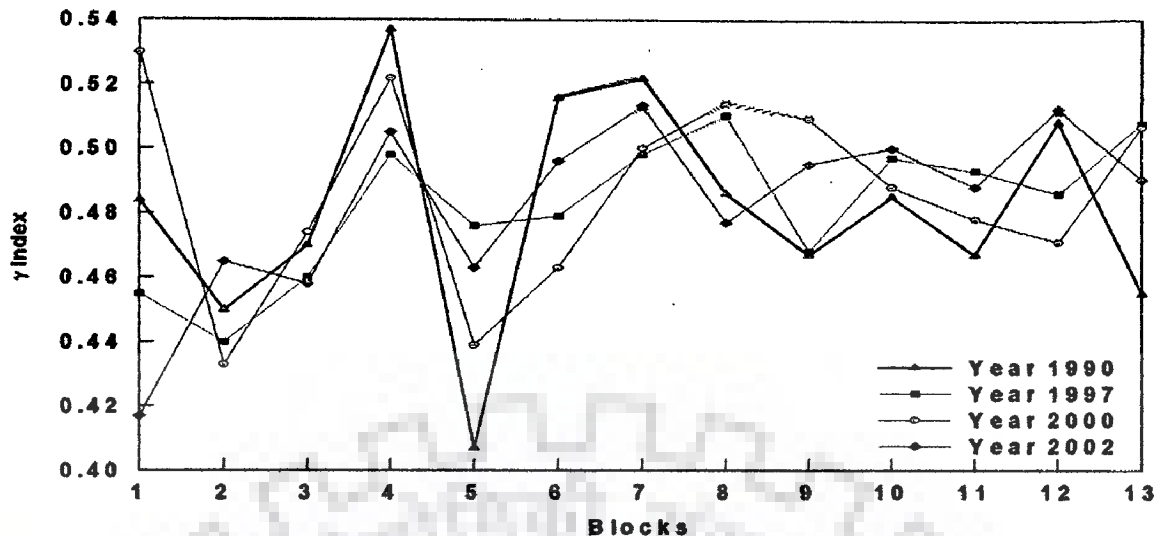


Figure 5.9 Variation of gamma index in different blocks

## 5.4 FORMULATION OF FLUVIAL LANDFORM INDICES

### 5.4.1 Hydraulic Geometry

The hydraulic geometry refers to the interrelationship among water discharge, sediment discharge, river width, depth, velocity, and planform for the river. At a river cross-section, the width  $B$ , mean depth  $D$ , mean velocity  $V$ , and suspended sediment load  $Q_s$  change with discharge. Formulae for these relationships have been given as power functions of the discharge by Leopold and Maddock (1953):

$$B = C_a Q^a, D = C_b Q^b, V = C_c Q^c, Q_s = C_d Q^d = 6E-05 Q^{1.7035} \text{ (for Pancharatna)}$$

$C_a$ ,  $C_b$ ,  $C_c$  and  $C_d$  are numerical constants. Since  $Q = BDV$ , it follows that  $C_a C_b C_c = 1$  and  $a + b + c = 1$ .

At Pancharatna the suspended sediment relationship with water discharge has been plotted in Figure 5.10, which indicated an exponent value of 1.70, thus the sediment load at this point increased faster than the discharge, i.e., the exponent  $d$  is greater than unity. Values of  $d$  typically lied in the range 1 -3, although the variation of  $Q_s$  with  $Q$  could vary considerably from one occasion to the other. It was noted that the goodness-of-fit implied by the  $Q_s$  Versus  $Q$  relationship was spurious. It was more

appropriate to determine the regression of sediment concentration versus water discharge for Pancharatna as shown in Figure 5.11.

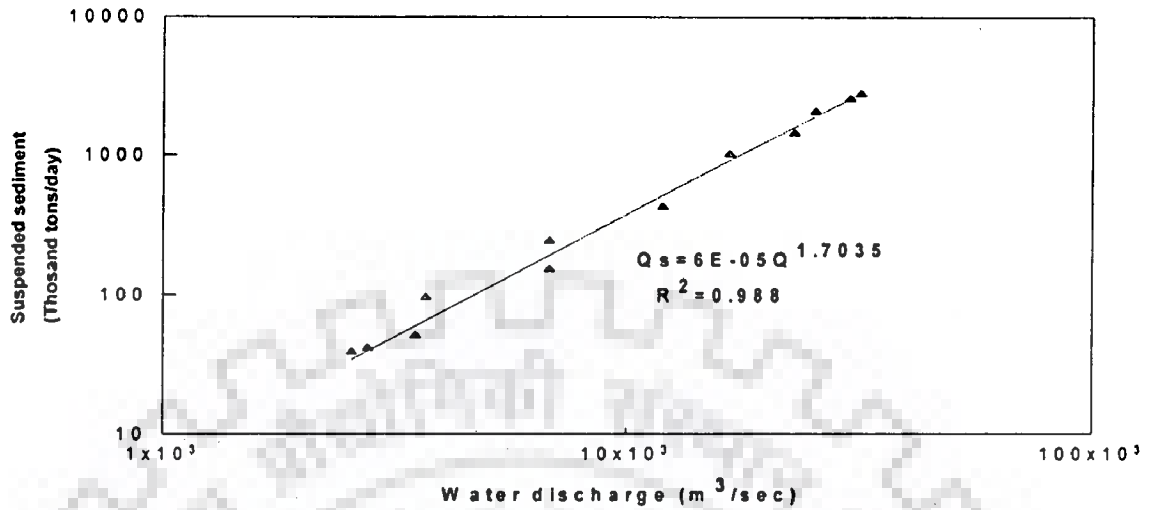


Figure 5.10 Suspended sediment in relation to water discharge for the Brahmaputra at Pancharatna

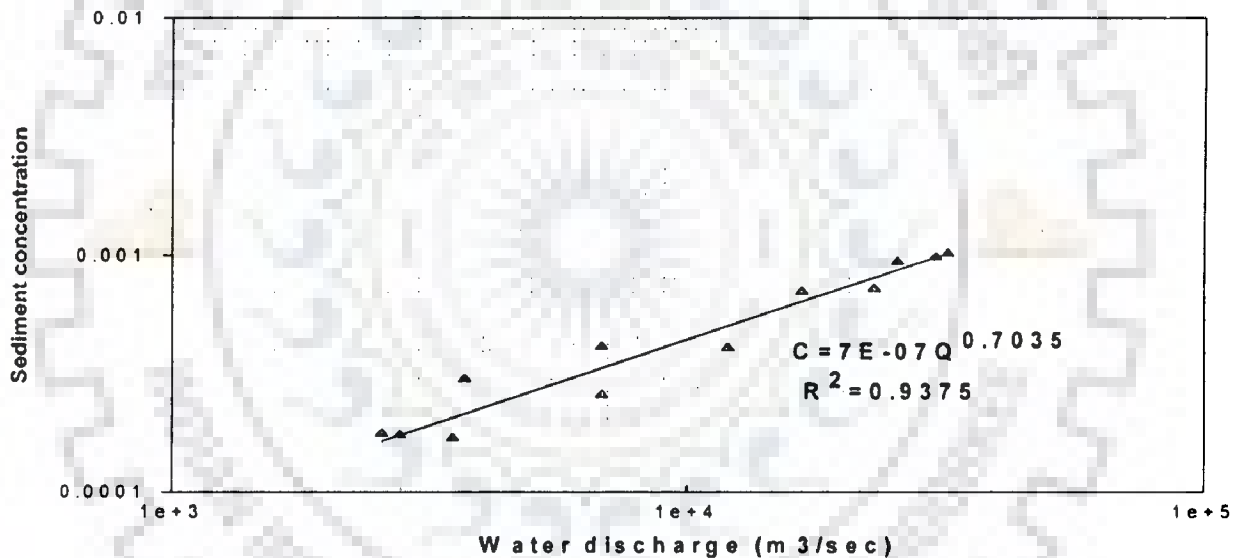


Figure 5.11 Sediment concentration in relation to water discharge for the Brahmaputra at Pancharatna

#### 5.4.2 Hydraulic Geometry Index

The existing braid indicators, like bed relief index, braid intensity and sinuosity were not adequate to properly describe the braiding phenomenon quantitatively as well as qualitatively in terms of key variables, controlling the geometry of a reach like the discharge  $Q$ , bed material size  $d_{50}$  (which influences the resistance), the water surface slope  $S$ , the hydraulic radius  $R$ . There are four degrees of freedom of the river reach like

width, depth, mean velocity and the hydraulic roughness (97). Hey (1978) suggested that they had nine degrees of freedom may allow adjustment to  $w$ ,  $d$ ,  $v$ ,  $d_{max}$ , sinuosity  $P$ , meander arc wave length  $\lambda$ , slope  $S$ , wave length  $l$  and amplitude of bed form  $h$ , which reflect the rate of sediment transport and influence the form resistance of the bed. Cross-section shape is not specified by  $d$ ,  $w$  alone, as for example rectangular and semi circular channels could have the same width and depth but different maximum depths. As the Brahmaputra was a braided river, (i) thus the later variables such as  $\lambda$ ,  $P$  were not considered, (ii) bed form parameters  $i$  and  $h$  were not included as sediment concentration  $C$  ( $Q_T/Q$ ), and (iii)  $d_{50}$  was incorporated to take care of the sediment transport and the form resistance. With the sediment load and discharge imposed, the sediment concentration (load per unit discharge) became an independent variable. Channel forms adjusted to maintain this concentration on the minimum possible gradient, which implied minimum rate of energy loss at constant discharge. Hydraulic radius,  $R$  was included in the proposed model, as this determines the hydraulic efficiency of the channel form.

A model was constituted to formulate the Hydraulic Geometry Index (HGI), and the variables have been presented in a tabular form in Table 5.2. The values of  $t$ ,  $c$ ,  $e$ ,  $i$ ,  $n$ ,  $\alpha$ ,  $\beta$  and  $\gamma$  indices for all the blocks have been shown in Table 5.3.

**Table 5.2 Model variables for Hydraulic Geometry Index**

Independent variables	Degrees of freedom (DOF)	Hydraulic Geometry Index (HGI)
Discharge, $Q$	Mean depth, $d$	$HGI = \frac{Q_T S_w R}{Q d_{50}} \times 100$
Bed material size $d_{50}$ ,	Width, $w$	
Water surface slope, $S$	Mean flow velocity, $v$	
Sediment load, $QT$	Hydraulic Radius, $R$	

$$\text{Hydraulic Geometry Index} = \frac{Q_T S_W R}{Q d_{50}} \times 100 \quad (5.15)$$

Where, Q = Water discharge in m<sup>3</sup>/sec, Q<sub>T</sub> = Sediment discharge in m<sup>3</sup>/sec

R = Hydraulic mean radius, S<sub>w</sub> = Water surface slope

d<sub>50</sub> = Median size of the sediment particles

### 5.4.3 Fluvial Landform Index

Quantitative analysis of channel processes and formation of islands, were given a due weightage in this study as huge volume of collected field data in conjunction with remote sensing digital data could make the estimates of fluvial landform changes a usable, reliable model. Analysis of remotely sensed data has been made to measure the temporal changes quantitatively in fluvial landforms. The Fluvial Landform Index (FLI) has been developed in this research to account for the planform of the Brahmaputra. The equation developed for FLI has been given below:

$$i) \text{ Fluvial Landform Index (FLI)} = \frac{\text{Area of islands in a transect}}{(\text{Area of gross river} - \text{Area of islands in the transect})} \quad (5.16)$$

## 5.5 THRESHOLDS OF THE INDICES

The parameters discussed above yielded a profound influence on the intensity of braiding. Thus, after a critical analysis of the trends of the variation of  $\alpha$ ,  $\beta$  and  $\gamma$  indices in the entire reach of the Brahmaputra river, the following thresholds were identified to provide a classification of the braiding phenomena as well as to make them useful for practical applications subsequently. Table 5.5 presents the threshold values for the Alpha Index ( $\alpha$ ), Beta Index ( $\beta$ ), Gamma Index ( $\gamma$ ), Fluvial Landform Index (FLI), Hydraulic Geometry Index (HGI) and Form Ratio for the Brahmaputra river. The



Hydraulic Geometry Indices, thus developed, were compared for braiding with the  $\alpha$ ,  $\beta$ ,  $\gamma$  indices for the same blocks under study, and has been shown in Table 5.6.

**Table 5.3 Values of Alpha ( $\alpha$ ), Beta ( $\beta$ ) and Gamma ( $\gamma$ ) Index for different years for the Brahmaputra river (Howard et al. 1970)**

Block No	Year	<i>t</i>	<i>e</i>	<i>n</i>	<i>i</i>	<i>c</i>	Alpha Index	Beta Index	Gamma Index
1	1990	61	9	35	19	52	0.217	1.386	0.484
	1997	45	8	27	14	37	0.169	1.286	0.455
	2000	62	9	32	22	53	0.286	1.512	0.530
	2002	35	8	22	9	27	0.109	1.167	0.417
2	1990	54	12	30	14	42	0.165	1.286	0.450
	1997	70	12	43	21	58	0.152	1.273	0.440
	2000	52	12	30	15	40	0.139	1.238	0.433
	2002	53	10	30	14	43	0.187	1.325	0.465
3	1990	86	11	52	28	75	0.198	1.365	0.470
	1997	87	14	51	25	73	0.184	1.338	0.460
	2000	108	14	64	36	94	0.205	1.385	0.474
	2002	55	11	31	15	44	0.177	1.310	0.458
4	1990	116	10	64	44	106	0.301	1.568	0.537
	1997	115	9	70	38	106	0.242	1.456	0.498
	2000	144	10	84	53	134	0.279	1.532	0.522
	2002	103	9	61	36	94	0.252	1.471	0.505
5	1990	22	8	12	5	14	0.086	1.100	0.407

	1997	40	7	23	12	33	0.200	1.333	0.476
	2000	24	6	14	6	18	0.143	1.200	0.444
	2002	25	6	14	6	19	0.171	1.250	0.463
6	1990	82	9	46	28	73	0.267	1.491	0.516
	1997	102	9	64	32	93	0.213	1.397	0.479
	2000	57	10	33	16	47	0.185	1.326	0.463
	2002	61	8	35	20	53	0.235	1.419	0.496
7	1990	105	10	59	36	95	0.278	1.522	0.522
	1997	115	10	69	37	105	0.242	1.456	0.498
	2000	59	8	33	19	51	0.247	1.439	0.504
	2002	123	10	72	41	113	0.264	1.500	0.513
8	1990	54	8	31	18	46	0.219	1.385	0.486
	1997	107	9	63	36	98	0.259	1.486	0.510
	2000	57	5	34	21	52	0.260	1.462	0.514
	2002	93	11	56	28	82	0.209	1.388	0.477
9	1990	77	7	50	32	70	0.193	1.351	0.467
	1997	125	9	82	43	116	0.198	1.374	0.468
	2000	84	5	52	30	79	0.257	1.474	0.509
	2002	104	10	62	34	94	0.237	1.444	0.495
10	1990	80	10	47	27	70	0.220	1.404	0.485
	1997	76	9	44	26	67	0.238	1.434	0.497
	2000	63	9	36	20	54	0.224	1.400	0.488
	2002	72	7	43	25	65	0.242	1.440	0.500

11	1990	70	11	41	20	59	0.192	1.346	0.467
	1997	68	11	37	22	57	0.231	1.417	0.493
	2000	76	13	42	24	63	0.210	1.382	0.478
	2002	60	10	33	18	50	0.222	1.395	0.488
12	1990	134	11	79	45	123	0.257	1.489	0.508
	1997	169	12	106	59	157	0.225	1.432	0.486
	2000	154	15	96	55	139	0.203	1.387	0.471
	2002	132	13	75	48	119	0.263	1.500	0.512
13	1990	86	14	51	24	72	0.176	1.323	0.455
	1997	222	18	130	75	204	0.258	1.500	0.507
	2000	123	12	71	41	111	0.255	1.482	0.506
	2002	144	14	86	45	130	0.231	1.440	0.490

**Table 5.4 Fluvial Landform Index (FLI) for different years**

Reach	1990	1997	2000	2002
1	1.104	0.224	0.168	0.192
2	0.703	0.384	0.353	0.236
3	0.291	0.293	0.252	0.129
4	0.381	0.297	0.445	0.358
5	0.317	1.012	0.354	0.427
6	0.158	0.200	0.208	0.242
7	0.285	0.766	0.900	1.013

**Table 5.5 Thresholds for the indices for the Brahmaputra river**

Braiding Intensity	Alpha Index ( $\alpha$ )	Beta Index ( $\beta$ )	Gamma Index ( $\gamma$ )	Fluvial Landform Index (FLI)	Hydraulic Geometry Index (HGI)	Form Ratio (B/D)
Less Braided (LB)	< 0.15	< 1.25	< 0.44	< 0.30	< 0.08	< 500
Moderately Braided (MB)	0.15 - 0.20	1.25 - 1.38	0.44 - 0.47	0.30 - 0.40	0.08 - 0.16	500 - 1000
Highly Braided (HB)	0.20 - 0.25	1.38 - 1.46	0.47 - 0.50	0.40 - 0.50	0.16 - 0.22	1000 - 4000
Very Highly Braided (VHB)	> 0.25	> 1.46	> 0.50	> 0.50	> 0.22	> 4000

**Table 5.6 Comparison of Hydraulic Geometry Index, Alpha Index, Beta Index and Gamma Index (Year - 2002)**

Block No	Hydraulic Geometry Index (HGI)	Braiding Intensity as per HGI	Alpha Index ( $\alpha$ )	Beta Index ( $\beta$ )	Gamma Index ( $\gamma$ )	Braiding Intensity
1	0.053	LB	0.109	1.167	0.417	LB
2	0.156	MB	0.187	1.325	0.465	MB
3	0.100	MB	0.177	1.310	0.458	MB
4	0.312	VHB	0.252	1.471	0.505	VHB
5	0.157	MB	0.171	1.250	0.463	MB
6	0.185	HB	0.235	1.419	0.496	HB
7	0.225	VHB	0.264	1.500	0.513	VHB
8	0.215	HB	0.209	1.388	0.477	HB
9	0.162	HB	0.237	1.444	0.495	HB
10	0.166	HB	0.242	1.440	0.500	HB

11	0.181	HB	0.222	1.395	0.488	HB
12	0.184	HB	0.263	1.500	0.512	VHB
13	0.190	HB	0.231	1.440	0.490	HB

## 5.6 DETERMINATION OF FUNCTIONAL RELATIONSHIP

On the basis of the modelling study, it was envisaged to determine the functional relationships for the fluvial landform indicators defined in section 5.4, to study their variation as well as to make them useful for practical applications subsequently. Towards this end, plots were prepared and best fit lines have been drawn for obtaining the functional relationship for the indices.

$$\text{HGI} = 0.00004 (B/D) + 0.05 \quad (5.17)$$

$$\text{HGI} = 6.388 (S_w)^{0.4147} \quad (5.18)$$

$$S_f/F_r = 0.0024 (B/D)^{-0.1234} \quad (5.19)$$

Where, HGI= Hydraulic Geometry Index

$\frac{B}{D}$  = Form Ratio = Overall width/ Average depth

$S_w$ =Water surface slope,  $Fr$  = Froude number =  $\frac{V}{\sqrt{gD}}$  and  $\frac{S_f}{F_r}$  = Energy slope

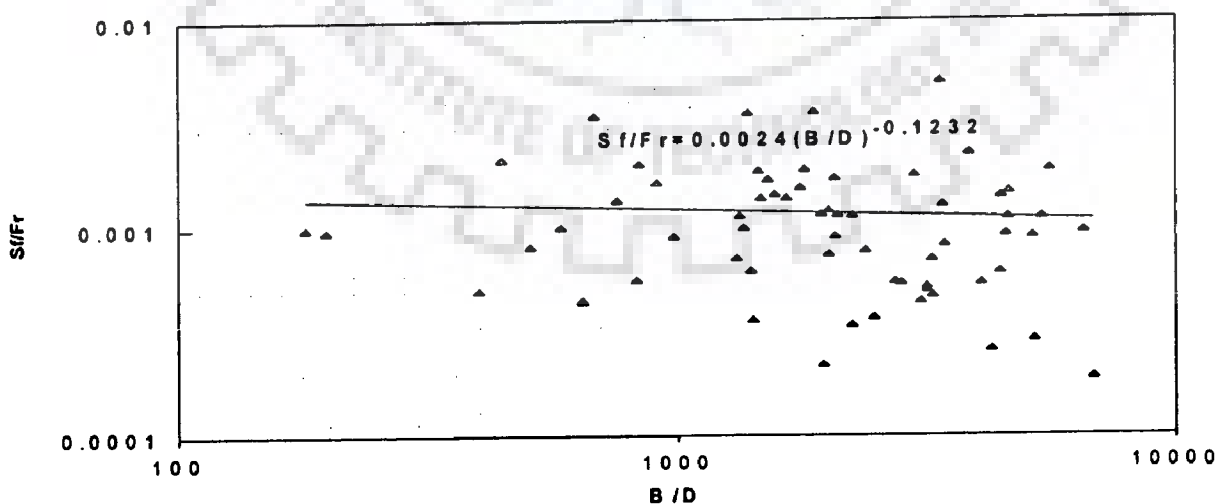


Figure 5.12 Plot of energy slope  $S_f/F_r$  and  $B/D$

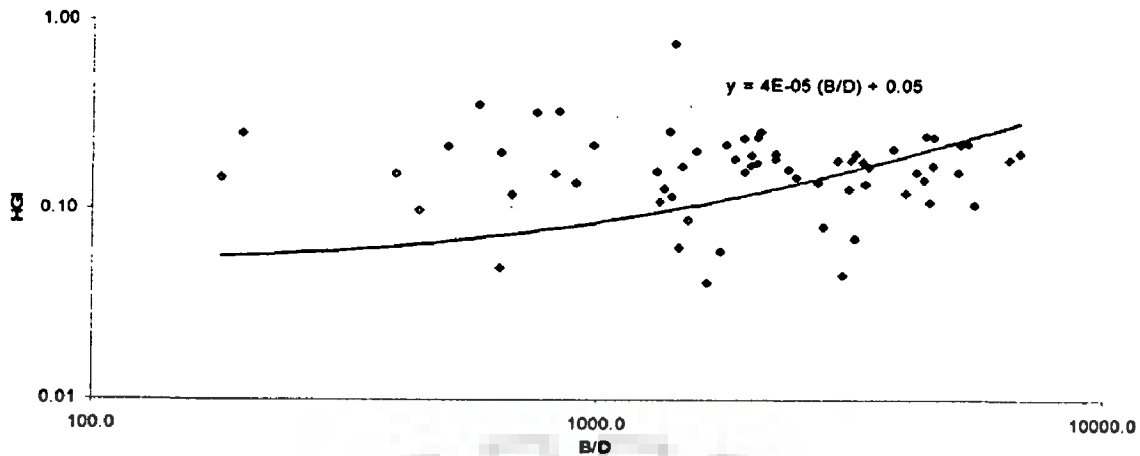


Figure 5.13 Plot of HGI and B/D

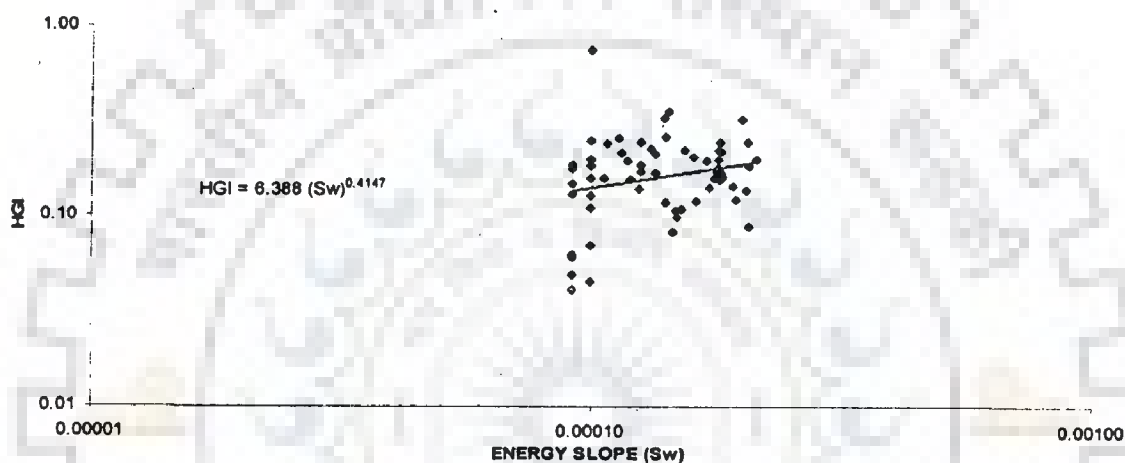


Figure 5.14 Plot of HGI and energy slope  $\frac{S_f}{F_r}$

In the Figure 5.12, energy slope and Froude Number have been plotted against width to depth ratio for field data of July 2002, according to Richardson and Thorne, (2001). The plot showed that an increase in the form ratio indicated a decrease in  $\frac{S_f}{F_r}$ , which indicated that the braided pattern was conducive for the dissipation of energy due to boundary friction resulting in more width, thus low velocity. The graphical plot of HGI and the Form Ratio for the river Brahmaputra in Figure 5.13 showed an increasing trend of both, as one takes an uptrend, thereby registering an increasing level of braiding, as could be seen from the threshold limits at Table 5.5. Similar plot was drawn in Figure 5.14 between the energy slope and HGI, which depicted an increasing trend of both the

values, as one increased. These plots clearly demonstrated the rationality of the HGI formulated in this work, and conformed to the actual physical situation of the phenomenon of braiding.

Agreement between topological indices  $\alpha$ ,  $\beta$  and  $\gamma$  (81) for the year 2002 and the HGI has been studied, which indicated a very good agreement between these, except for block 12, where there was a slight variation which might possibly be due to erroneous field data. The detailed branching of the segments and the variation of the topological indices  $\alpha$ ,  $\beta$  and  $\gamma$  have been shown for some reaches of the Brahmaputra river for the years 1990, 1997, 2000 and 2002 in Figures 5.15(a) to (h).

## 5.7 CONCLUDING REMARKS

This chapter has primarily sought to study different indicators for their performance evaluation as fluvial landform indicators. Many a time, these do not show any consistent or discernible trend with the B/D ratio. This raises a doubt over their use as a fluvial landform indicator. In this respect, use of two fluvial landform indicators has been also explored in this work. It was found that the indices proposed by Howard et al. (1970) worked well for well-defined topological patterns. However, it was difficult to interpret these indices for complicated topological patterns such as encountered in a braided stream channel. The present study has indicated the promising use of the topological indices in being able to predict channel change, qualitatively. It was evident that the portions of the river (blocks 4, 6 and 10 to 12) were the locus of the maximum sedimentation zones, whereas the portions comprising blocks 2 and 5 were marked as the low sedimentation rates. With a view to explicitly reflecting the influence of the hydraulic variables on channel formation or deformation process, FLI and HGI were

evolved for desired appraisal of degree and intensity of braiding appropriately, making conjunctive use of field and remote sensing data. The newly developed indices FLI and HGI rationally classified the degree as well as intensity of braiding for the Brahmaputra by accounting for the pertinent fluvial variables. These indices objectively modulated the effect of plan-form changes on channel migration, island formation and braiding and exert significant effect on river morphology.







Figure 5.6 Variation of  $i$  in different blocks

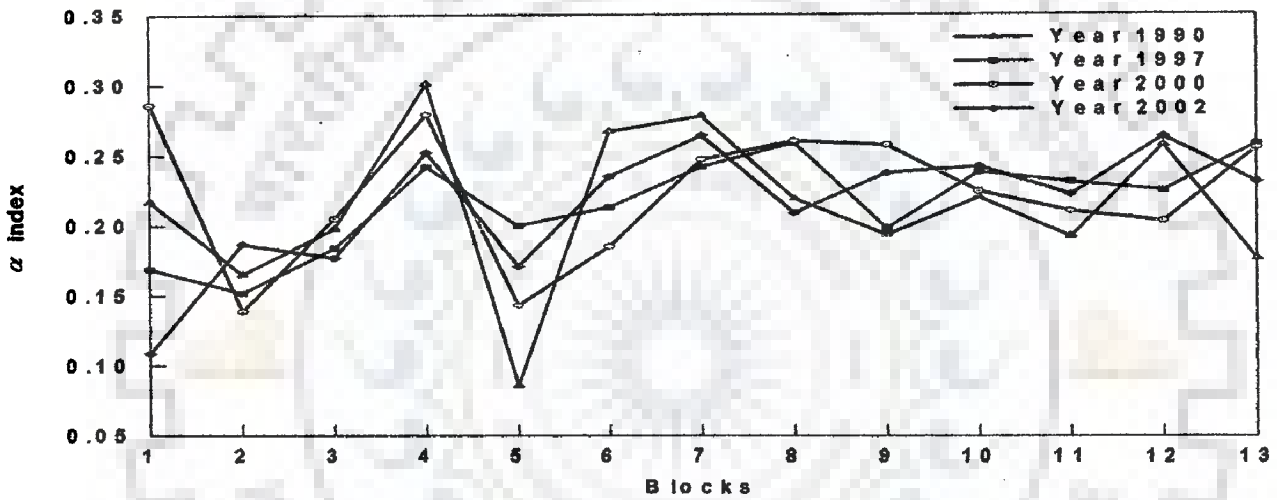


Figure 5.7 Variation of alpha index in different blocks

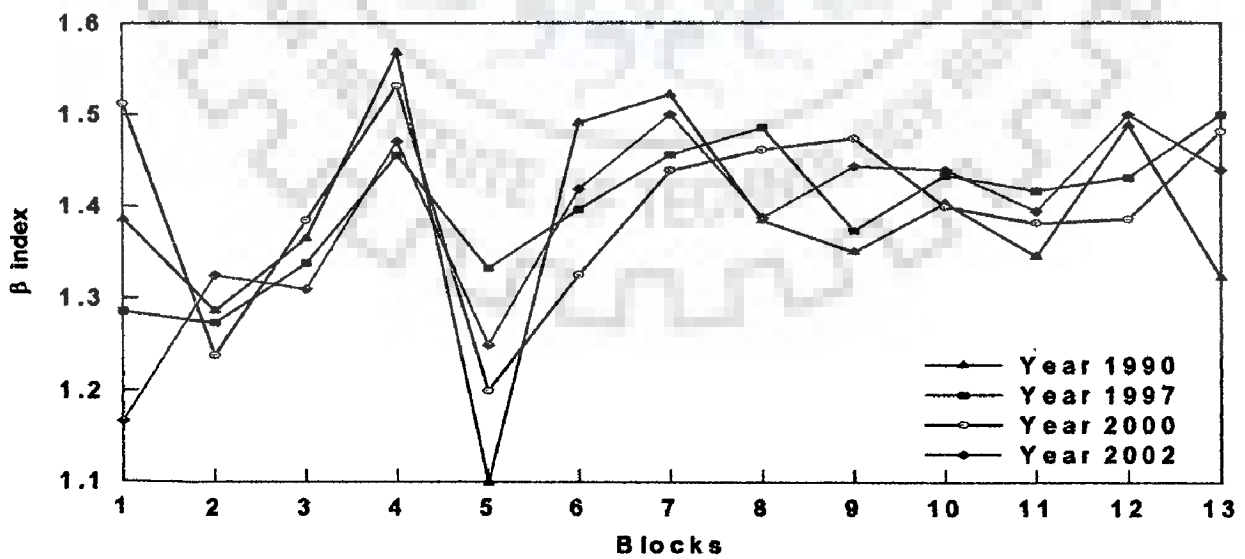
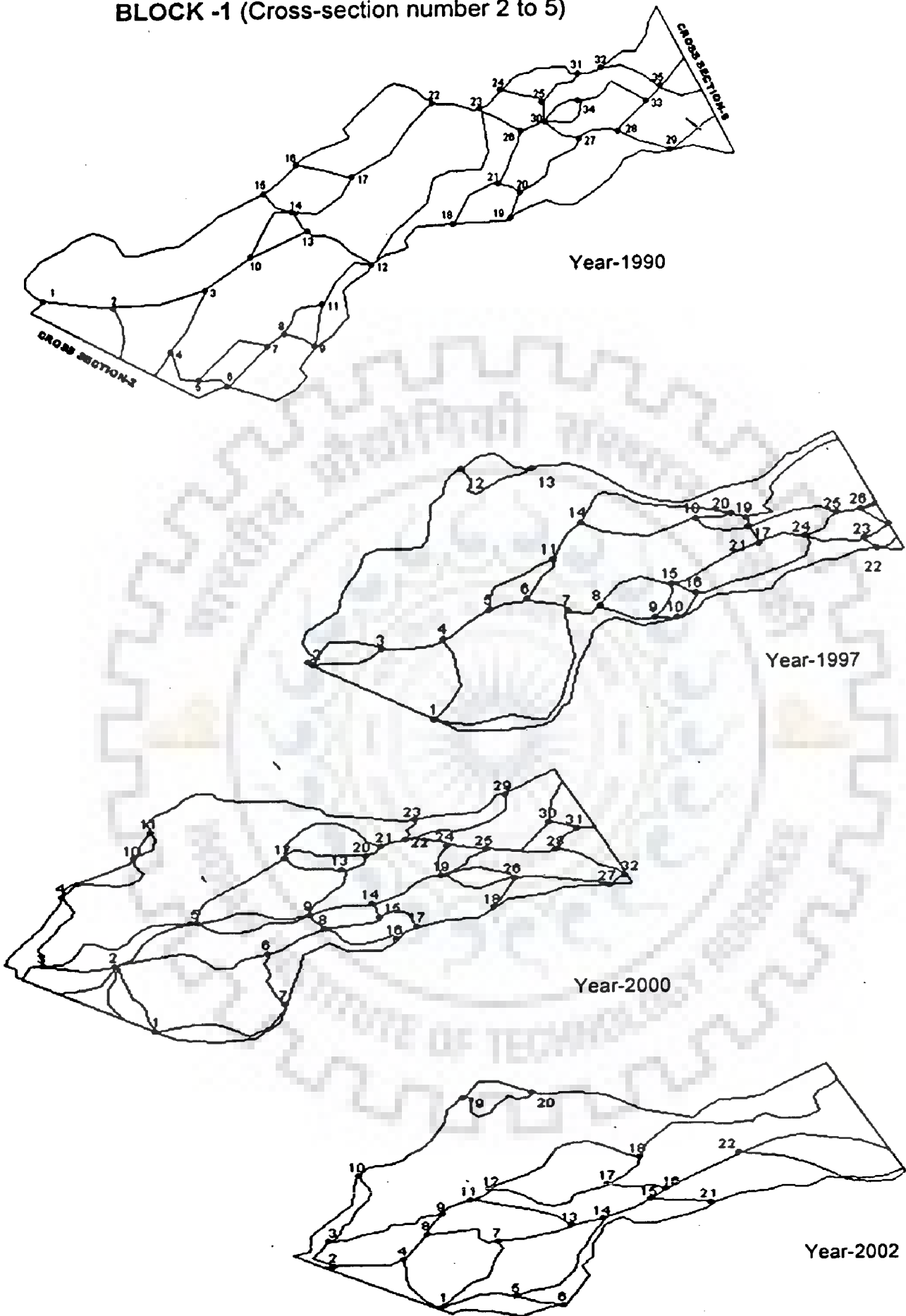


Figure 5.8 Variation of beta index in different blocks

**BLOCK -1 (Cross-section number 2 to 5)**



**Figure 5.15 (a) Topologic condition of block-1**

**BLOCK -2 (Cross-section number 5 to 10)**

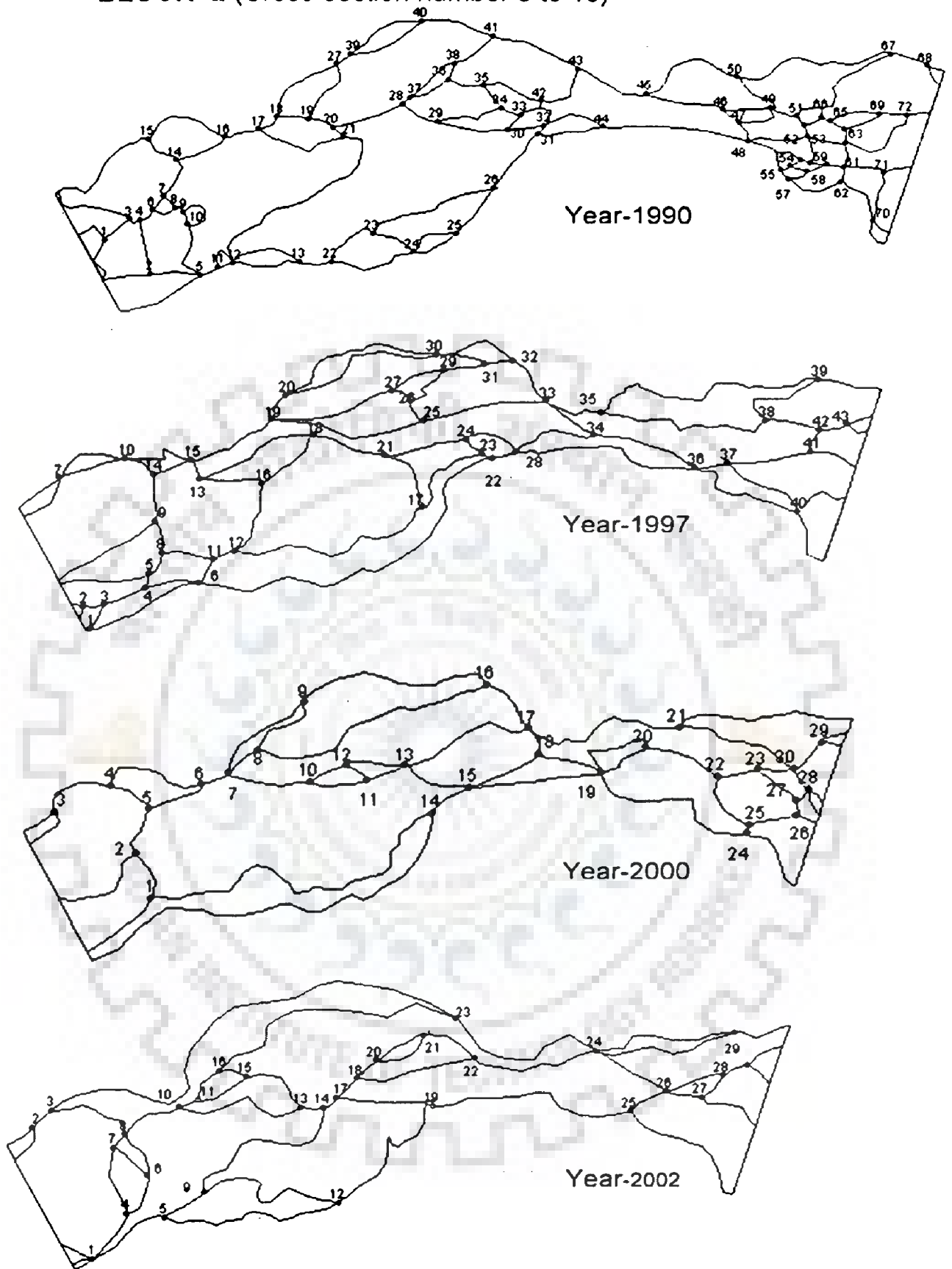


**Figure 5.15 (b) Topologic condition of block-2**

**BLOCK -3 (Cross-section number 10 to 15)**

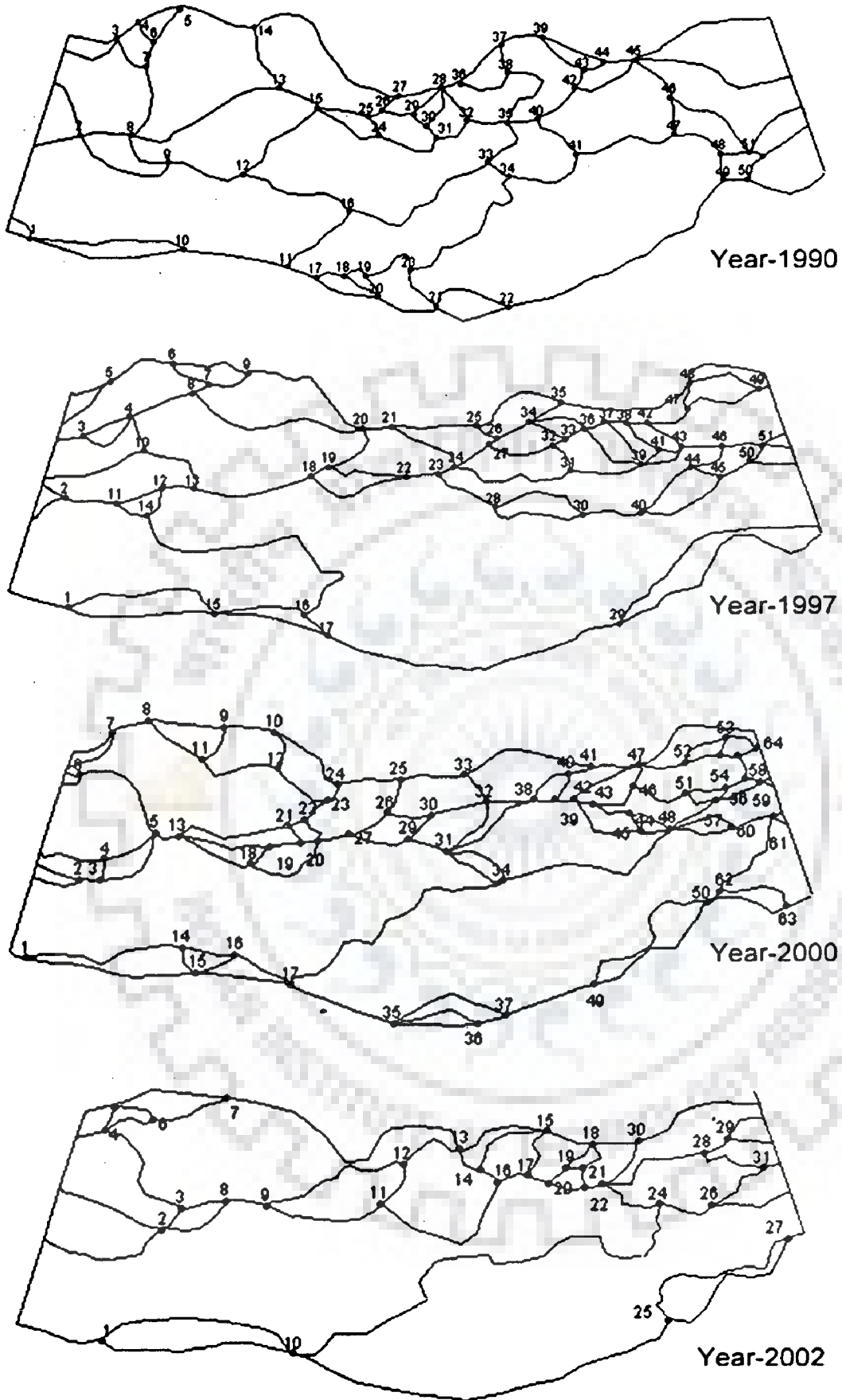


**Figure 5.15 (c) Topologic condition of block-3**

**BLOCK 4 (Cross-section number 15 to 20)**

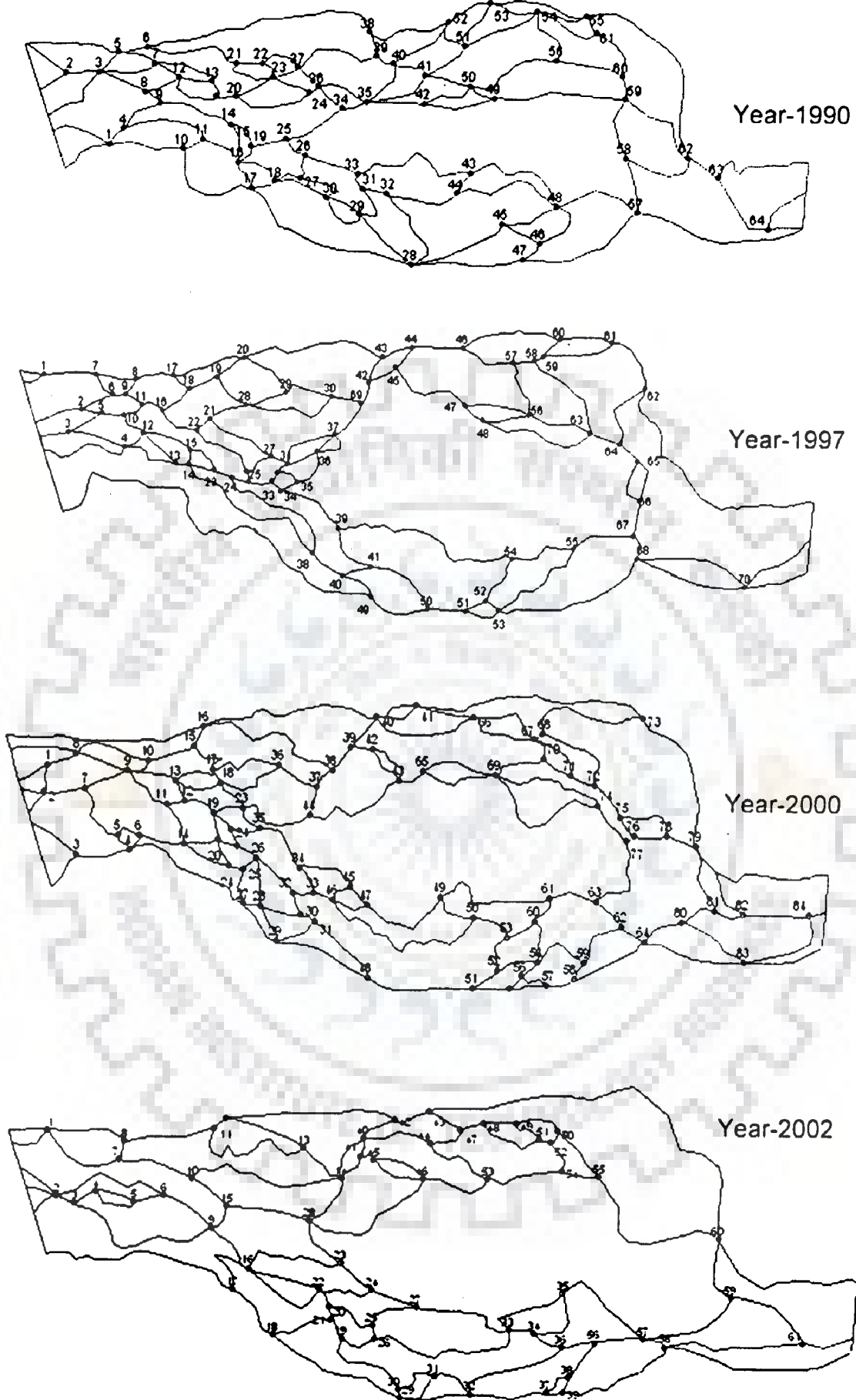


**Figure 5.15 (d) Topologic condition of block-4**

**BLOCK 5 (Cross-section number 20 to 25)**

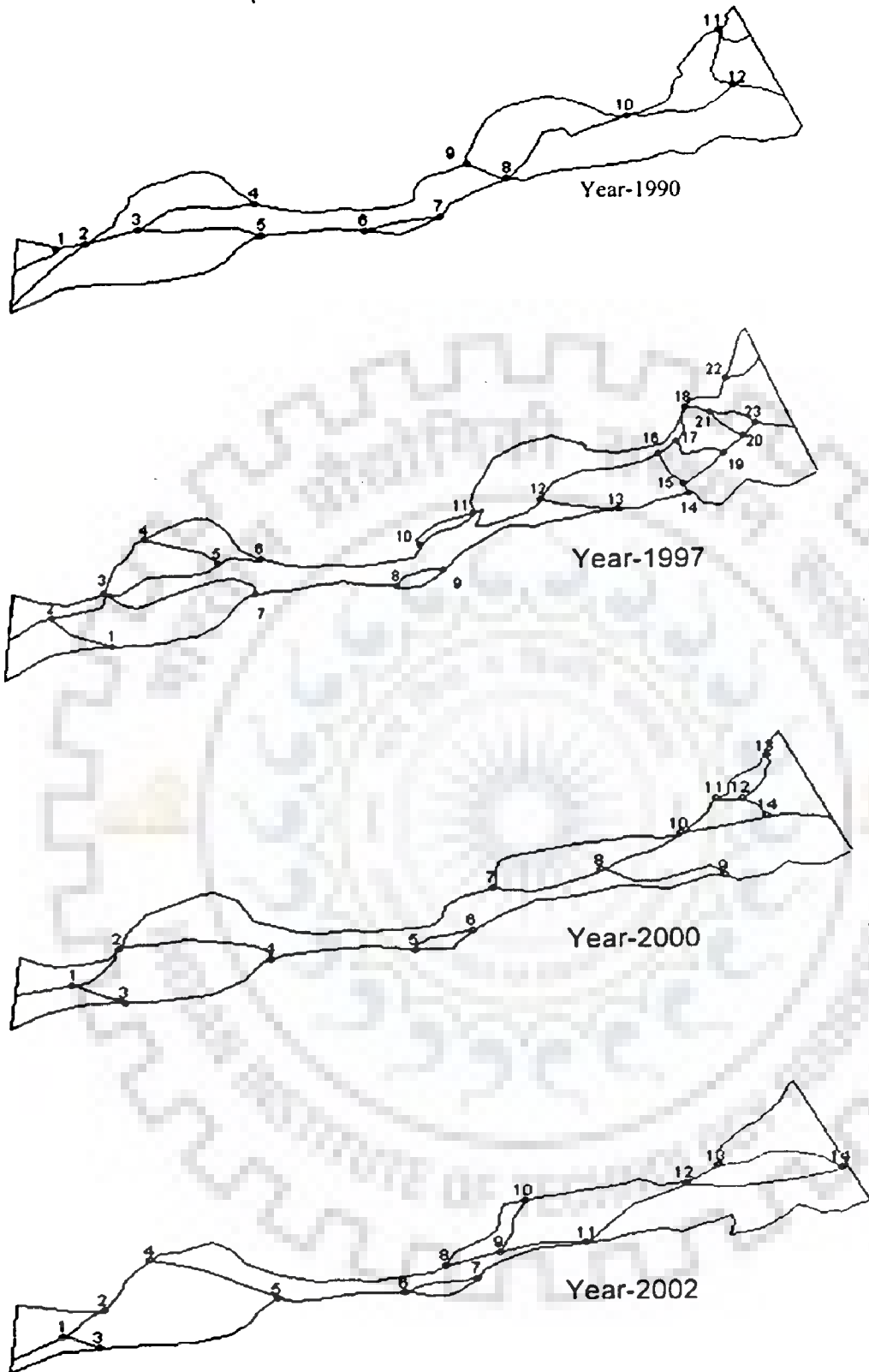


**Figure 5.15(e) Topologic condition of block-5**

BLOCK - 6 (Cross-section number 25 to 30)

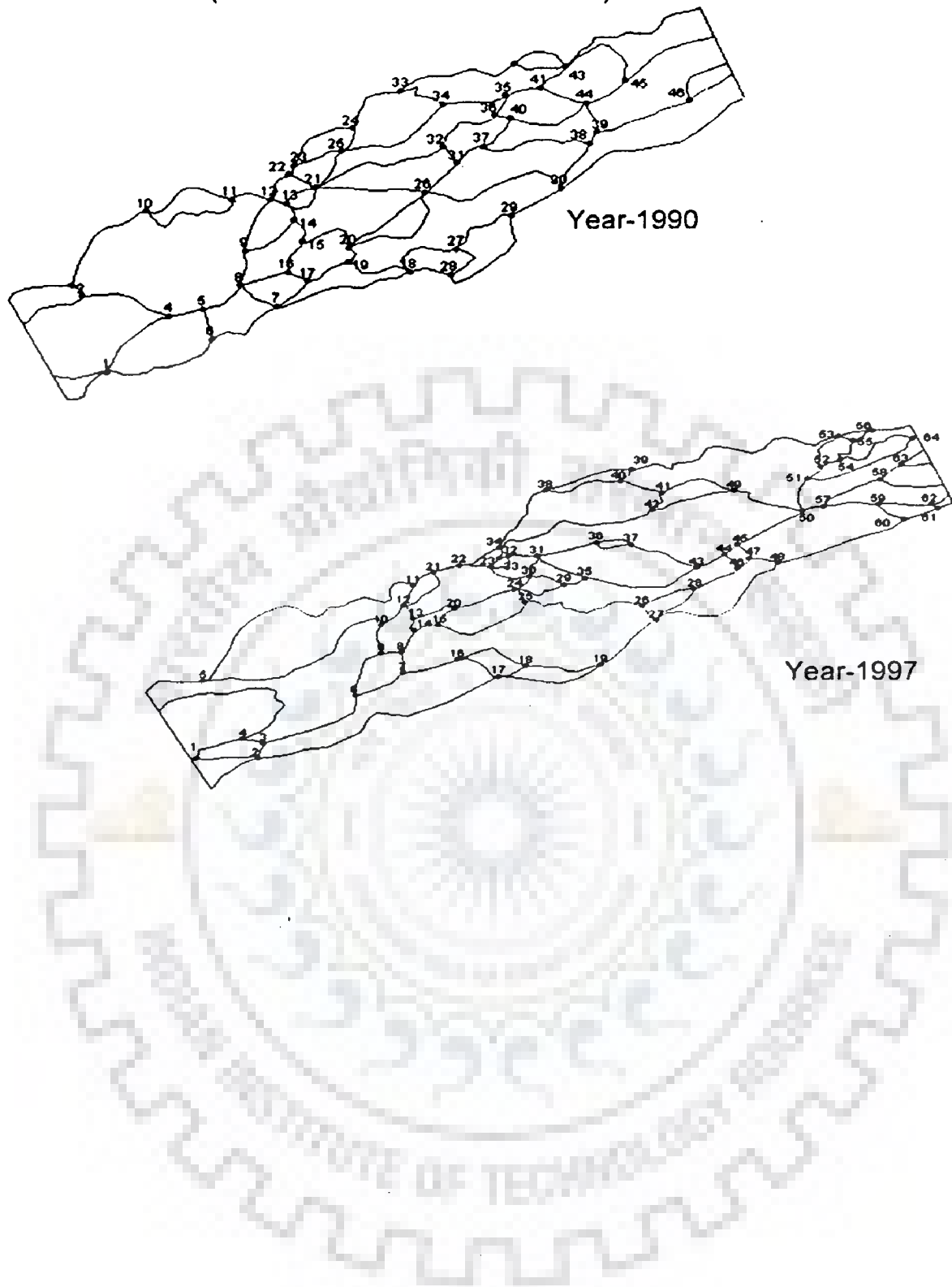
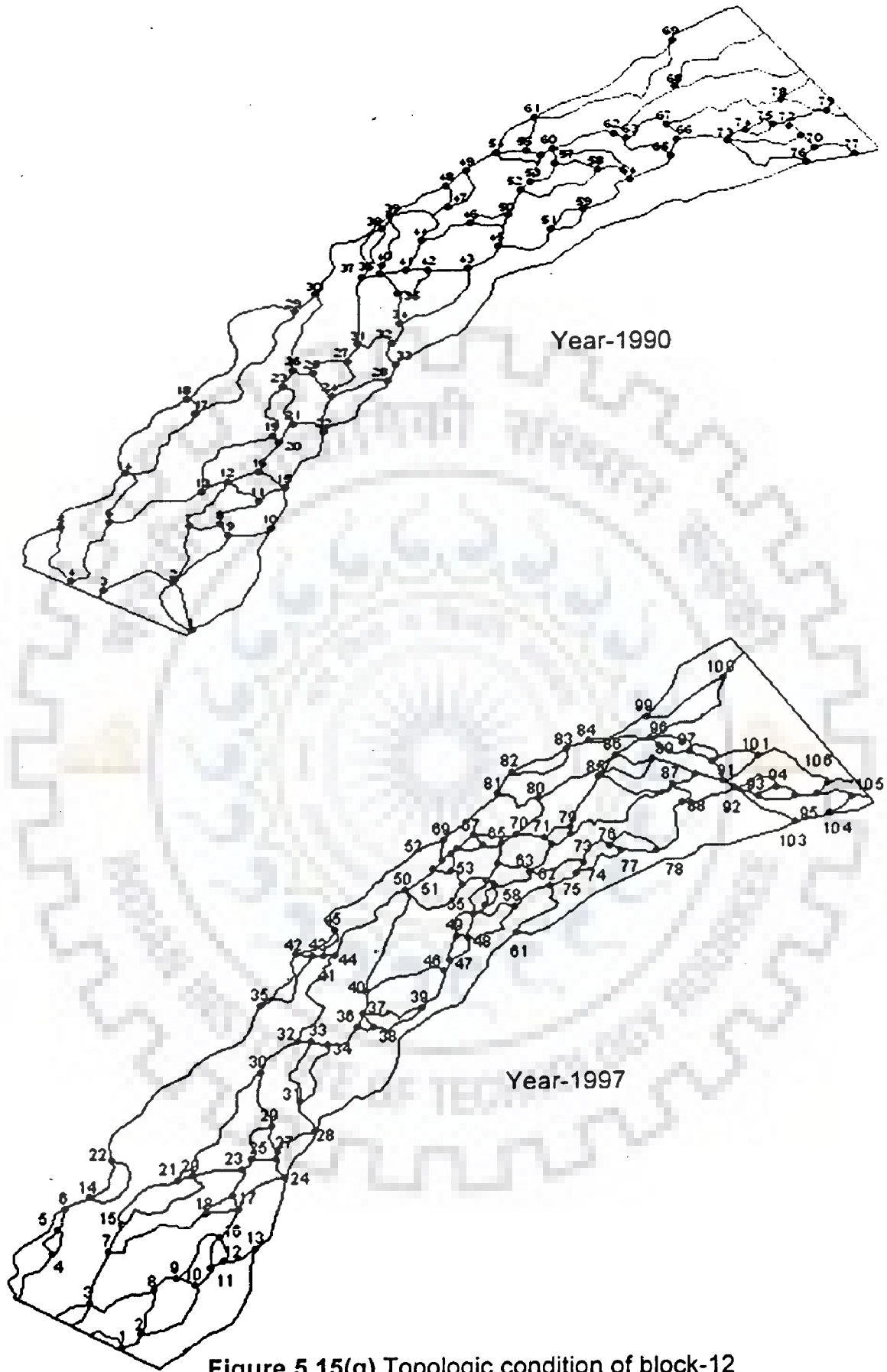


Figure 5.15(f) Topologic condition of block-6

**BLOCK -12 (Cross-section number 55 to 60)**



**Figure 5.15(g) Topologic condition of block-12**



BLOCK -12 (Cross-section number 55 to 60)

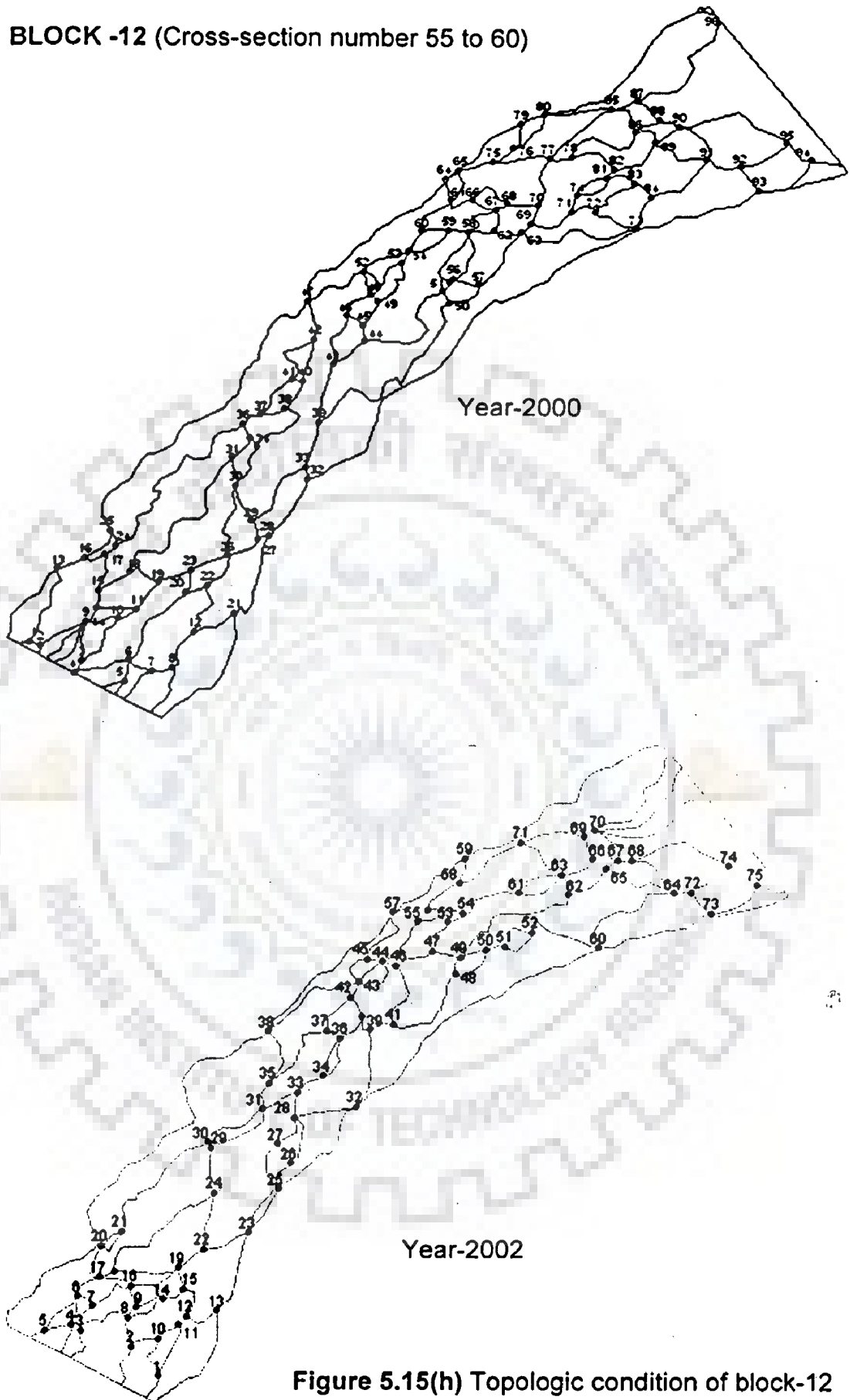
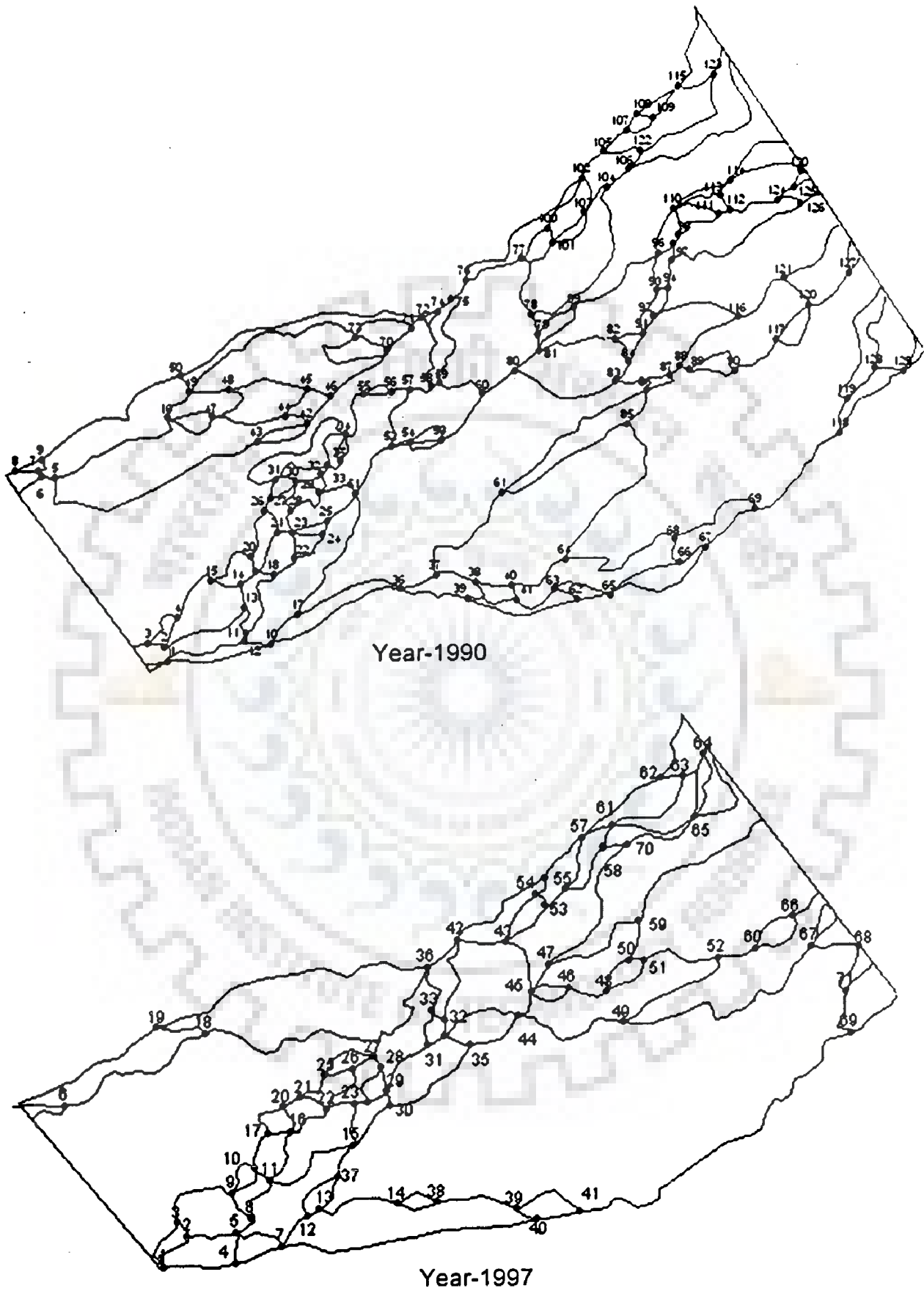


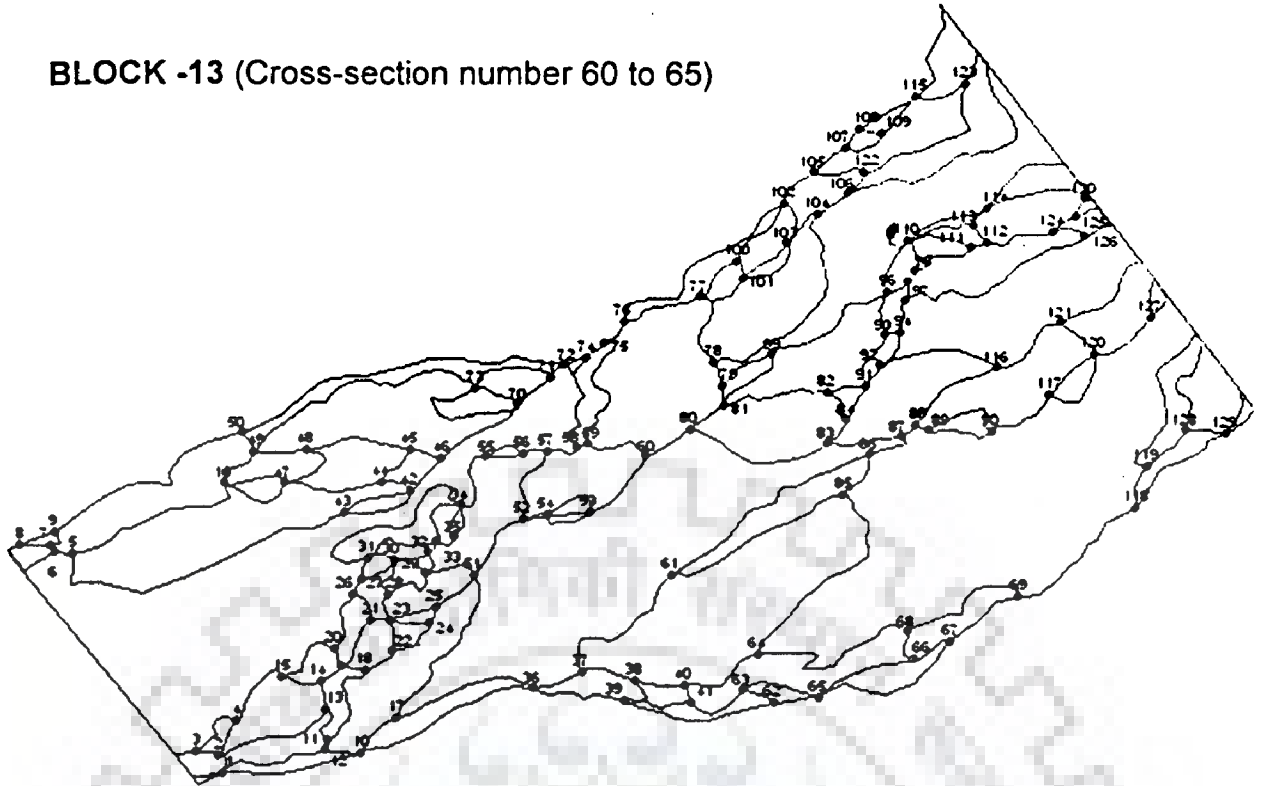
Figure 5.15(h) Topologic condition of block-12

**BLOCK -13 (Cross-section number 60 to 65)**

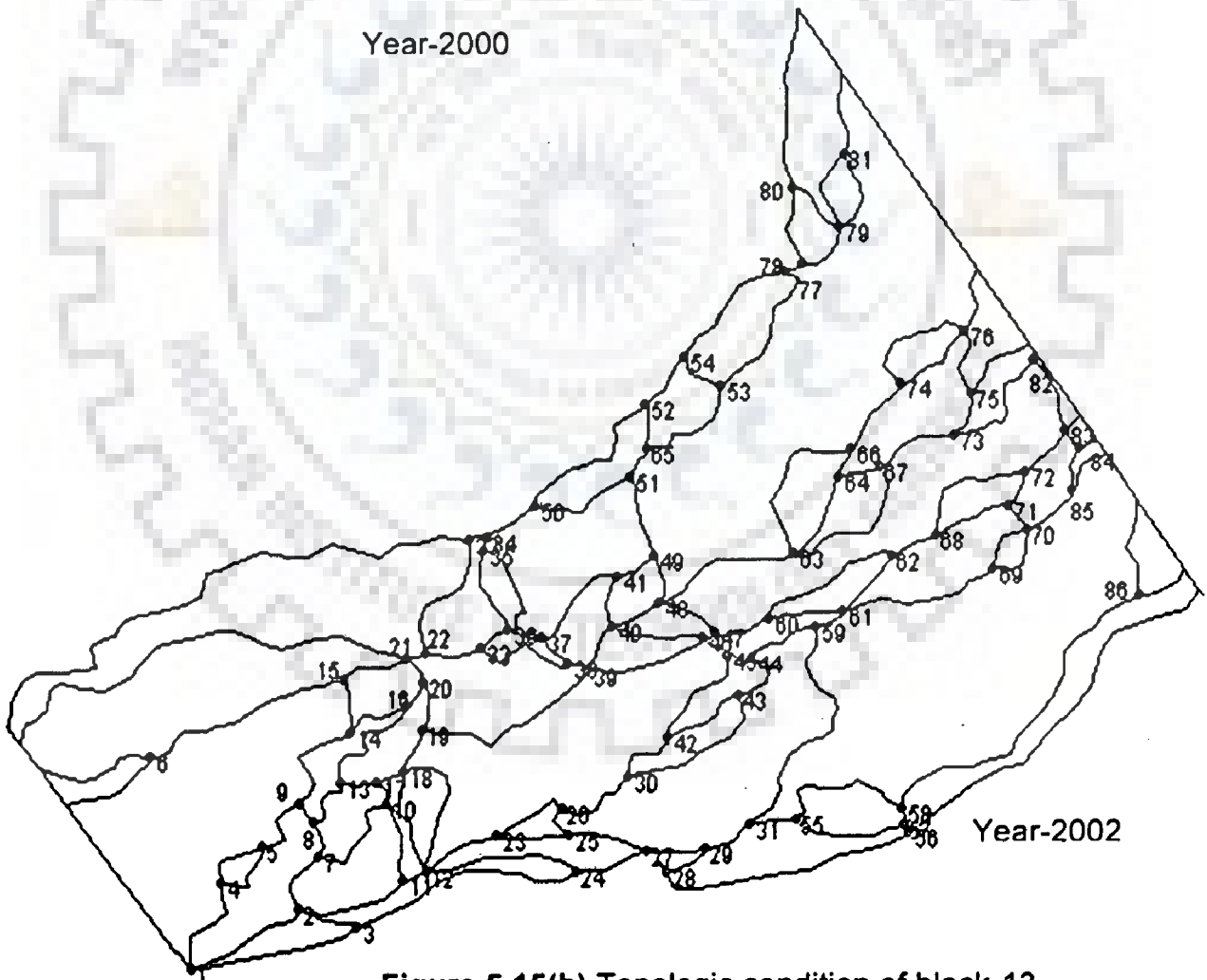


**Figure 5.15(g) Topologic condition of block-13**

**BLOCK -13 (Cross-section number 60 to 65)**



Year-2000



Year-2002

**Figure 5.15(h) Topologic condition of block-13**

**RESULTS AND DISCUSSIONS****6.1 CHANGES IN THE BRAHMAPUTRA RIVER CONFIGURATION**

The hydrologic processes of the river Brahmaputra exhibit a high degree of temporal and spatial variability, and are further complicated by issues of nonlinearity of the physical processes, conflicting spatial and temporal scale, and uncertainty in parameter estimates. The neuromorphic models in conjunction with remote sensing and GIS technique are capable of extracting the functional relationship between the inputs and the outputs of fluvial morphological processes, without the physics of the problem being explicitly provided. It is also possible to map from one multivariable space to another from the set of data representing river morphology. The use of reliable field data coupled with ground truth verification has seen to it that the ANN models truly represent the fluvial process. The results obtained for changes in the Brahmaputra river configuration have been summarized below reachwise:

***Reach I***

There was a sagging of the river loop towards north bank at cross-section 3, amounting to 6.5 km in the year 2002 as compared to the year 1990. The river width at Dhubri (c/s 2) has increased by 0.95 km over 12 years. The construction of retirement and anti-erosion measures were required just upstream of Salmora on south face as the Jinjiram fell into the main river causing erosion. The tributary Jinjiram was under active avulsion process (Figure 4.21), and it separated out along at the south of the river near downstream side of cross-section 5 and joined with the main Brahmaputra at about 7.98 km downstream of the Phulbari town. Due to this, there is a possibility of river flooding in the flood-plain due to avulsion.

## ***Reach II***

The maximum width of the river was 18.13 km in 2002 at cross-section 17 near Gumi (Figure 4.23) and has not been changed over years due to constrictions by the geological formations near Saraighat bridge. The excess stream power carried by the river has been expended in widening its width near Chimpa (Figure 4.23).

## ***Reach III***

At Lahorighat (cross-section 27), the river has eroded the left bank by an amount of 2.64 km. At cross-section 29, the river has fanned out by 1.32 km by erosion. The erosion at these sections has enabled the waterway to incise in the flood plain (Figure 4.25).

## ***Reach IV***

The rock outcrops projecting along the north bank as well as along the south near Kamakhya hills (Silghat) constricted the river passage into a narrow single channel of 1.2 km width. This waterway constriction has been expanding its width to 2.7 km near the Kaliabhomora bridge (Figure 4.26 & Figure 4.27) and could not open up further due to the presence of Agnigarh hills of Tezpur town in the north and an embankment on the south near Koliabor area. In a distance of about 21 km, the river has fanned out to 10.6 km from 2.7 km at the bridge site, indicating the operation of stream power concept by dissipating the flow energy through channel widening (Figure 4.26).

## ***Reach V***

The configuration of the river from Bessamara to Kamalabari has changed considerably and an old dead channel named Chumoimari started developing rapidly on the Bessamara-Kamalabari side (Figure 4.28 (a)). The heavy swirling current flows

carried by Chumoimari channel led to severe bank erosion from Dakhinpat to Kamalabari, which ultimately resulted in breach of Dakhinpat-Kamalabari embankment (Figure 4.28 (a)). The presence of clayey soil in Bessamara impeded further erosion in the stream bank downstream upto Kamalabari. The deep river channel at Hatisal Neamati was steeply eroding with direct southward orientation, which was indicative of an approaching danger of probable river avulsion in future.

About 1.25 km in the west bank (u/s of Bar Bil) and 1.80 km (d/s of cross-section 40) in east bank (near Rangamati Bil), major erosion of the Kaziranga National Park land could be noticed from the IRS LISS-III satellite imagery of 1990 and 2002 respectively. Moreover, the area around Kaziranga National Park has also witnessed major erosion activity near Sohola Bil up to Diphlumukh. Significantly, the banks on both sides of the Brahmaputra from Orang Reserve Forest to Haloukonda Bil are subjected to significant erosion. It was observed that the erosion was more predominant on the eastern as well as western side of the Park. Notably, in the mid-portion near Debeswari Chapori (u/s of Naobhangi Bil) (Figure 4.29), there was bank retreat by an amount of 3.0 km during the study period. Short term measures comprising of permeable temporary structures constructed in-situ for immediate protection of the bank from river attack using local materials and local artisans may be provided to protect the vulnerable areas of the Kaziranga National Park from continuous erosion.

### ***Reach VI***

The variation in river width was not so severe in this portion of the river, but the variability of the fluvial landform characteristics pattern was excessively high thus culminating in intense braiding. This reach was very highly braided near Dibrugarh

(Figure 4.32) as could be discerned from the values of topological indices vide Table 5.3. The braid islands have their maximum and average lengths of 14.0 km and 3.75 km, respectively having average width of the order of 2 km.

### ***Reach VII***

The notable feature of this reach was the formation of a river channel avulsion near Saikhowa Reserve Forest, thus making the river sagging southwards by a maximum of 10.54 km near cross-section 63. Radarsat satellite imagery showed the development of avulsion in 2002 (Figure 4.33), which was absent in the year 1990. At cross-section 61, the river has encompassed loops to the north, thus incising the flood plain by 0.32 km.

### ***Tributaries***

It could be seen that the Subansiri and all other eastern rivers shifted westward, while rivers between Pagladiya and Subansiri shifted eastwards. From Manas up to Tipkai, all the rivers migrated westward. South tributaries showed meandering pattern and have shifted slightly. The north bank tributaries choke up their bed leading to diversion of channel, river capture as well as channel bifurcation to modify their river systems more frequently. In contrast to this, the south bank tributaries have a lower rate of sediment yield and their drainage systems exhibited a more or less conservative nature.

## **6.2 DISCUSSION ON DEVELOPMENT OF CHANNEL AVULSION IN THE BRAHMAPUTRA - THE RATIONALE**

As could be seen from the analysis of river configuration in chapter 4, under para 4.5, the planform of river Brahmaputra was in a state of constant flux and has developed severe fluvial hazards in the form of channel avulsions near Dhubri (Figure 4.21) and

near Saikhowa Reserve Forest (Figure 4.33) in course of relatively short time scales. Hydrological characteristics, sedimentological adjustments and geotectonics of the river have together played an important role in triggering the avulsions. An avulsion normally occurs when the magnitude of the triggering mechanism exceeds the geomorphic threshold (148). The avulsion near Saikhowa Reserve Forest occurred due to increase in slope of potential avulsion course and decrease in slope of the existing channel, thereby increasing the discharge in this left anabranch significantly. This was again the manifestation of the increased flow in this anabranch due to slow abandonment of the right anabranch.

Significant changes of floodplain roughness initiated planform instability, especially when channel roughness exceeded floodplain roughness. Thus, a preferential flow path has been created across the floodplain at the d/s of Dhubri, setting the stage for a progressive channel avulsion (Figure 4.21). The shift in the river course has caused a stage reduction in the upstream reaches. The new avulsed channels were shorter than their precursors, and had a greater gradient. Thus, the flow velocity was higher and stages, for the same discharges, were lower. The sediment-laden flow built up its channel by depositing sediment in the low velocity areas and scouring sediments in the high velocity areas. During this evolutionary process, seasonal variations of the discharge and sediment deposition in the area have resulted in a high frequency of mouth migration. Planform instability was closely linked with both floodplain and channel alterations.



### **6.3 INFERENCE ON DOMINANT CHANGE IN SEDIMENT LOAD**

The salient morphological features of the Brahmaputra were shaped by fluvial processes of the process of erosion, transport and deposition of sediment that were fundamental to the hydraulic geometry of the channel. The rationale behind high yield of sediment in the river could be attributed to the erosion process due to loss of vegetative cover, growth of urbanisation, encroachment of flood plain by the incising river. Also, prevalence of shifting 'Jhum' cultivation in the region caused heavy soil erosion in the hills, silting of river beds and floods in the plains. The multi-spectral vegetation index like NDVI has been tested to provide new information and improved sensitivity to vegetative cover. As part of an effort to understand the pattern of the vegetative cover, the response of spectral vegetation indices to such temporal changes as well as their ability to discriminate among the major vegetation types encountered in the basin, was studied. An assessment of the functional behaviour of this index with the sediment erosion has also been attempted in this investigation. Such an investigation yielded a preliminary insight on the dominant trends over the Brahmaputra basin. The reach-wise study of NDVI vividly portrayed that the loss of vegetative cover in the basin is about 10% (Figure 4.7 to 4.11) and the increase in sediment load at Pancharatna (cross-section 9), which was near the downstream end of the basin was found to be about 12%. The outcome of the investigation was a pointer to the relationship between loss of vegetative cover with river sediment load.

### **6.4 CHANGES IN FLUVIAL PLANFORM**

Adjustment processes that affected fluvial system of the Brahmaputra include channel degradation and aggradation, lateral river migration, widening or narrowing,

avulsion, and changes in the quantity and character of the sediment load at spatial and temporal scale. Erosion in the river has increased the overall river area by 12.10% during the study period from 1990 to 2002. The net flow area has registered an increase of 17.23% in 2002, as compared with 1990. It was observed that the banks of the river Brahmaputra experienced predominantly type-II (moderate to considerable erosion affecting certain areas along bank line) and type-III (minimum erosion with response only at isolated sites) over a large area. The braided Brahmaputra river channel exhibited a differential rate of erosion and deposition.

The average northing for right bank of the Brahmaputra river moved about 0.47 km to the north between 1990 and 2002, while that for the left moved about 0.48 km to the south (Figure 4.36). Left bank movement occurred mainly through rapid erosion in the embayment next to braid bars, while right bank movement involved looping, both through embayment erosion and incision of floodplain.

During the study period, the river mean width has increased from 7.99 km to 8.94 km in a total length of the river Brahmaputra. The maximum width of 18.13 km just downstream side of Pandu at cross section 17 near Gumi has not registered any significant change (Figure 4.23) perhaps because of bank protection system on both banks. The mean width has registered an increase much more than the minimum and maximum widths. The spatial and temporal records indicated the existence of 'nodes' or 'nodal reaches'. The study findings suggested that morpho-dynamically controlled nodal reaches were present at Pancharatna, Pandu and Tezpur (Table 4.8).

Expansion of the river had taken place primarily through floodplain erosion and excision in consonance with bar or island growth. Trends of expansion showed no sign of slackening and the expansion process appears to remain unabated.

DEM data provided by NOAA (Figures 4.19 and 4.20) have been used for backdrop information, as ERDAS raster grids. Shallow and deep flooding phenomena have been inferred the extent and pattern of flooding at different altitudes of the Brahmaputra valley after drainage pattern are overlay.

## **6.5 NEUROMORPHIC MODELLING**

For each neuromorphic model, the data were split up into three parts; namely model training (70%), cross-validation (15%) (to prevent model over training), and testing (15%) the performance of the model. Furthermore to revalidate the models, a separate set has been used as query set. In order to keep the simplicity of model structure, the number of hidden layer for the neural architecture was chosen as one after several trials. The performance analysis was represented by three statistical goodness-of-fit measures, including *rmse*, Nash-Sutcliffe coefficient (1970) and correlation coefficient, which significantly supported the gainful use of the ANN model. The *rmse* could take any positive value, but the model performs better if it was close to zero. When the Nash value was between 0 and 1, model forecasted better. If the Nash index was closer to one, better results were obtained. These performance criteria were used as basis of comparison to select the best model.

### **6.5.1 Stream Bank Migration Models**

Month, year and discharge have been taken as input variables, and the left bank co-ordinates which were calculated for different years form the independent variable. To

cross validate the predicted left bank co-ordinates, a computer programme was developed (Annexure-I, Programme-2) for spatio-temporal idealisation of river Brahmaputra. Computer programme for computing the values of shape function at different nodes has been used spatially and temporally. The co-ordinates for the year 1996 computed from models 1 & 2 and the above mentioned computer program were again cross validated to compute the accuracy of the models. Figure 4.43 presents the cross validation check of the above data for the year 1996. It was observed from the plot (Figure 4.43) that the curves from the two models and the spatio-temporal programme have given desired results for all the prediction horizons. The model efficiency of all these models suggested that ANN rendered a good predicting capability.

A comparison of ANN predicted co-ordinates for right bank for year 2006 and observed co-ordinates for year 2002 has been made to visualise the likely changes in streambank migration, and to provide a complete qualitative as well as quantitative assessment of erosion and deposition in individual 100 strips (Figures 4.37 and 4.38) along the Brahmaputra. Table 4.15 illustrates a sample calculation of the erosion and deposition in the 100 individual strips.

In order to have an idea of the lateral spreading of water, an attempt has been made to implement a simpler system ANN model. This demonstrated a better way to analyse the scenario due to a flash flood in Jia Bhareli tributary.

### **6.5.2 Hydrographic Models**

ANN prediction of cross-sectional channel geometry was attempted in this work which would enable measurement variance and would eliminate difficulties in surveying the cross-sections. The observed reduced levels at Pancharatna have been verified with

the ANN simulated ones (Figure 4.55). The goodness-of-fit criteria, such as *rmse* and Nash-Shutcliff coefficient for the model were found to be 1.292 and 0.9989 respectively. This range of error has been set as this gave a realistic estimate of the output. The efficiency of the model was found to be 99.89%.

### **6.5.3 Flow Characteristics Models**

Flow characteristic prediction models were designed to demonstrate the applicability of ANN approach in developing effective nonlinear flow characteristic models of river stage, flow and sediment discharge at pre-defined 101 sections. The prediction of average monthly stages yielded good results as the efficiencies were 99.9% in the models 12 and 13 (Figure 4.56) and that for the discharge were 97.38% and 98.8% in models 13 and 14 respectively (Figures 4.58 and 4.61).

The sediment models showed a poorer performance compared to water discharge and stage as the observed data were measured at only two points, i.e. at Pandu and Pancharatna, while at other points the data have been generated using Hydrologic Engineering Center (HEC)-6 movable bed model, developed by US Army Corps of Engineers (2004).

### **6.5.4 Composite Model for Missing and Imperfect Data**

A composite model has been constituted to reasonably predict the fluvio-morphological variability, such as discharge, stage and sediment flow at discrete points with respect to space and time, when some particular data were imperfectly presented or missing. The model efficiencies were found to be 98.9% and 50.29% in respect of observed and ANN predicted stage and sediment discharges respectively (Figures 4.63

and 4.64). The *rmse* values for the models were 0.14 and 1.68 respectively, which showed the reliability of the forecasted values.

## 6.6 MAJULI RIVER ISLAND EROSION MODEL

The area of the Majuli river island has been found to be 416.23 km<sup>2</sup> in 1990 to 376.93 km<sup>2</sup> in 2002, and evidently it has decreased by 39.30 km<sup>2</sup> over a period of 12 years from (Table 4.17). The study has revealed that the loss of land area of Majuli island was 4.94% in 1997 and 9.44% in year 2002 as compared to the area in 1990. The activity of erosion was much more pronounced near Jorhat-Majuli area, and continues for 50 km upto Kumargaon.

Ground observations on the overall erosion activity around Majuli island exhibited two types of features. The bowl-shaped shear failure (Figure 4.98) activated by the flow of sediments was more common around Gajeragaon, the easternmost corner of the island. During the high flood of the river, water was forced into the massive sand bodies, providing additional support to the bank materials, which acted as a continuous system. However with the fall in water level, the pressure diminished rapidly and water from the pore spaces of sand bodies tended to flow to the main channel. This flow of water from the sand bodies has caused liquefaction of sediments, and the bank materials have been subjected to different degrees of flow. This type of failure was more common around Kumargaon, Batiamarinagar and Bessamara. However, around Salmora, where the bank material comprises of mainly cohesive clay material, the bank slope was almost 90° causing significant over-steepening, which triggered towards initiation of bank failure.

Moreover the cohesive clay material on the other hand, produced a comparatively stable land mass that was not prone to erosion and thereby generated a nodal point. The nodal point, in turn, also offered significant resistance to the connected flow regime. As the bank materials were relatively stable in this area, the river scoured deeper to accommodate the flood discharge, thereby increasing the suspended load of the river temporarily. Therefore, below the nodal point, the river tends to be wide, thereby facilitating formation of bars. Here, the current velocities diminished when large quantities of sediments were deposited and mid-channel bars or chars were formed. Once formed, the chars locally decreased the cross-sectional area and cut the bank laterally to maintain a proper cross-sectional area that was in equilibrium with discharge. This might be the appropriate explanation about the enhanced rate of erosion activity around Hatisal Neamati, Kamalabari and Kaziranga, which has already taken a large proportion of land area.

## **6.7 STAGE AND DISCHARGE RATING CURVES**

The hybrid system of learning has also been constructed combining ANN and fuzzy logic (Figures 4.85, 4.86 & 4.87) for developing the stage-discharge relationship to achieve a faster rate of convergence by controlling the learning rate parameter with fuzzy rules. This could interpret linguistic assessment of flow levels. When prediction results were compared with the measured data, prediction accuracy level was comparable with that from the data driven neural network approach. However, the ANN models were found to be clearly superior to fuzzy expert systems, based on their ability to predict, except for Dhubri, where the neuro-fuzzy model and the ANN model gave at par results. The efficiencies of the ANN models 17 (Dibrugarh), 18 (Pancharatna) and 19 (Dhubri) were found to be 98.6%, 99.27% and 98.49% respectively.

## 6.8 REAL-TIME FLOOD FORECASTING

The daily stages at Pandu, Pancharatna and Dhubri have been predicted in three different neuromorphic models, referred to as model M 26 to M 28. This would help in event of measurement failure in any of the gauging stations during the critical flow level, by interpreting assessment of flow levels and as a desirable advance warning forecasting tool. The efficiencies of the models 26, 27 and 28 were 93%, 96.3% and 89% respectively, which indicated that model 27 (for Pancharatna) performed the best. The *rmse* for the three models were 0.14, 0.12 and 0.17 respectively. Moreover, correlation coefficient, the  $R^2$  (Figures 4.91, 4.92 and 4.93) of the observed and ANN forecasted values suggested satisfactory performance of the models.

## 6.9 PREDICTION OF SEDIMENT LOAD CONCENTRATION

A sediment concentration ANN model was constituted to estimate the natural sediment discharge of the river Brahmaputra in terms of sediment concentration at Pancharatna using water and sediment variables based on the dynamic laws of flow and sediment (Figures 4.94 and 4.95). The variables used to predict were tractive shear stress  $\psi$ , velocity ratio  $\phi$ , longitudinal slope  $S$ , suspension parameter  $w_0/u_*$ , water depth ratio  $h/d_{50}$ , Froude number  $Fr$ , Reynold's number  $R_*$ , width scale ratio  $h/B$ . The mean of the discrepancy ratio between obtained and measured values was 0.961 and the standard deviation for the mean was 0.156. The model efficiency was 62%.

## 6.10 TOPOLOGICAL ANALYSIS OF THE RIVER BRAHMAPUTRA

The topological indices and parameters, as suggested by Howard et al. (1970) and Orme and Krumbein (1972), are characterised by anabranches, nodes and islands. This showed that the degree of braiding of individual reaches fluctuate in the short-term



due to morphological response to the magnitude and duration of monsoon runoff events. The following revealing observations have been made from the results of the topological analysis:

- (i) For all the years under study, variables  $t$ ,  $c$ ,  $e$ ,  $n$  and  $i$  showed distinct decrease in values in blocks 5, 10 and 11 (Figures 5.2 - 5.6). The lowest trend was marked in block 5. In contrary, blocks 4, 7, 9 and 12 showed increase in their values. The indices  $\alpha$ ,  $\beta$  and  $\gamma$  were characterised by approximately similar decrease in values in blocks 5, 9 and 11 (Figures 5.7 - 5.9).
- (ii) Comparison of trends for the different years indicated that  $t$ ,  $c$ ,  $n$  and  $i$  values increased in the upstream direction for block 2 for the years 1990, 1997, 2000 and 2002, and this trend was gradual for the year 2002 (Figures 5.2 - 5.6). Probably, the trend has been decelerated after the construction of the Narnarayan Bridge at Pancharatna, at cross-section 9, which was pronounced for these blocks. Similar trend has been observed at block 8, which may be due to the presence of Kaliabhomara Bridge near Tezpur.
- (iii) It was noted that the decrease in values in block 13 of  $t$ ,  $c$ ,  $n$  and  $i$  for the years 1990, 2000 and 2002 showed the intensity of non-braiding tendency. The braiding intensity was high in blocks 4, 7, 9 and 12, indicating that the island formations were more in these reaches.
- (iv) The study of  $\alpha$ ,  $\beta$  and  $\gamma$  indices over the entire stretch revealed that their values in blocks 2 and 4 were very low as compared to the other blocks (Figures 5.7 - 5.9).

The average values of  $\alpha$ ,  $\beta$  and  $\gamma$  indices for the entire stretch were found to be 0.222, 1.401 and 0.487 for the year 2000 and 0.215, 1.390 and 0.482 for 1990 respectively.

## 6.11 FORMULATION OF NEW FLUVIAL LANDFORM INDICES

The four degrees of freedom of the river reach, namely width, depth, mean velocity and the hydraulic roughness, as per Langbein (1964a), and the nine degrees of freedom i.e.  $w$ ,  $d$ ,  $v$ ,  $d_{max}$ , sinuosity  $P$ , meander arc wave length  $\lambda$ , slope  $S$ , wavelength  $\ell$  (reflects the rate of sediment transport) and amplitude of bed form  $h$  (influences the form resistance of the bed), as suggested by Hey (1978), are critically examined. Cross section shape is not specified by  $d$  and  $w$  alone, as for example rectangular and semi circular channels could have the same width and depth but different maximum depths. As the river Brahmaputra was a highly braided river, (i) thus the later variables, such as  $\lambda$ ,  $P$  were not considered, (ii) bed form parameters  $i$  and  $h$  were not included as sediment concentration  $C$  ( $Q_T/Q$ ), and (iii)  $d_{50}$  were incorporated to take care of the sediment transport and the form resistance. The sediment concentration was an independent variable. Channel forms adjusted to maintain this concentration on the minimum possible gradient, which implied minimum rate of energy loss at constant discharge. Hydraulic radius,  $R$  was included in the proposed model, as this determines the hydraulic efficiency of the channel form. To measure the temporal changes quantitatively in fluvial landforms, real time areal data were analysed and the Fluvial Landform Index (FLI) was developed to account for the planform of the Brahmaputra river. The indices were narrated in Eqns. 5.15 and 5.16.

### 6.11.1 Thresholding of the Indices

After a critical analysis of the trends of the variation of  $\alpha$ ,  $\beta$  and  $\gamma$  indices in the entire reach of the Brahmaputra river, the thresholds have been developed to provide a classification of the braiding phenomena as well as to make them useful for practical applications subsequently. The thresholds of  $\alpha$ ,  $\beta$  and  $\gamma$  indices and HGI and FLI were in consensus with each other. Comparison between topological indices  $\alpha$ ,  $\beta$  and  $\gamma$  for the year 2002 and the Hydraulic Geometry Index (HGI), indicated a very good agreement between these, except for block 12, where there was a slight variation, which might possibly be due to erroneous field data.

### 6.11.2 Functional Relationship of HGI with B/D Ratio and Energy Slope

From the functional relationship amongst the HGI,  $B/D$ ,  $S_w$  and  $S_f/F_R$  using field data of July 2002, it could be seen that as the form ratio increases, the energy slope ( $S_f/F_R$ ) decreases and HGI increases. This indicated that the braided pattern was conducive for the dissipation of energy due to boundary friction resulting in more width, thus low velocity, thereby indicating an increase in braiding (Figure 5.12). The graphical plot of HGI and the Form Ratio for the river Brahmaputra in Figure 5.13 portrays an increasing trend of both, as one takes an uptrend, thereby registering an increasing level of braiding, as could also be seen from the threshold limits at Table 5.5. Similar plot between the energy slope and HGI (Figure 5.14) depicts an increasing trend of both the values. These plots clearly demonstrated the rationality of the HGI formulated in this work, and conform to the actual physical situation of the phenomenon of braiding.

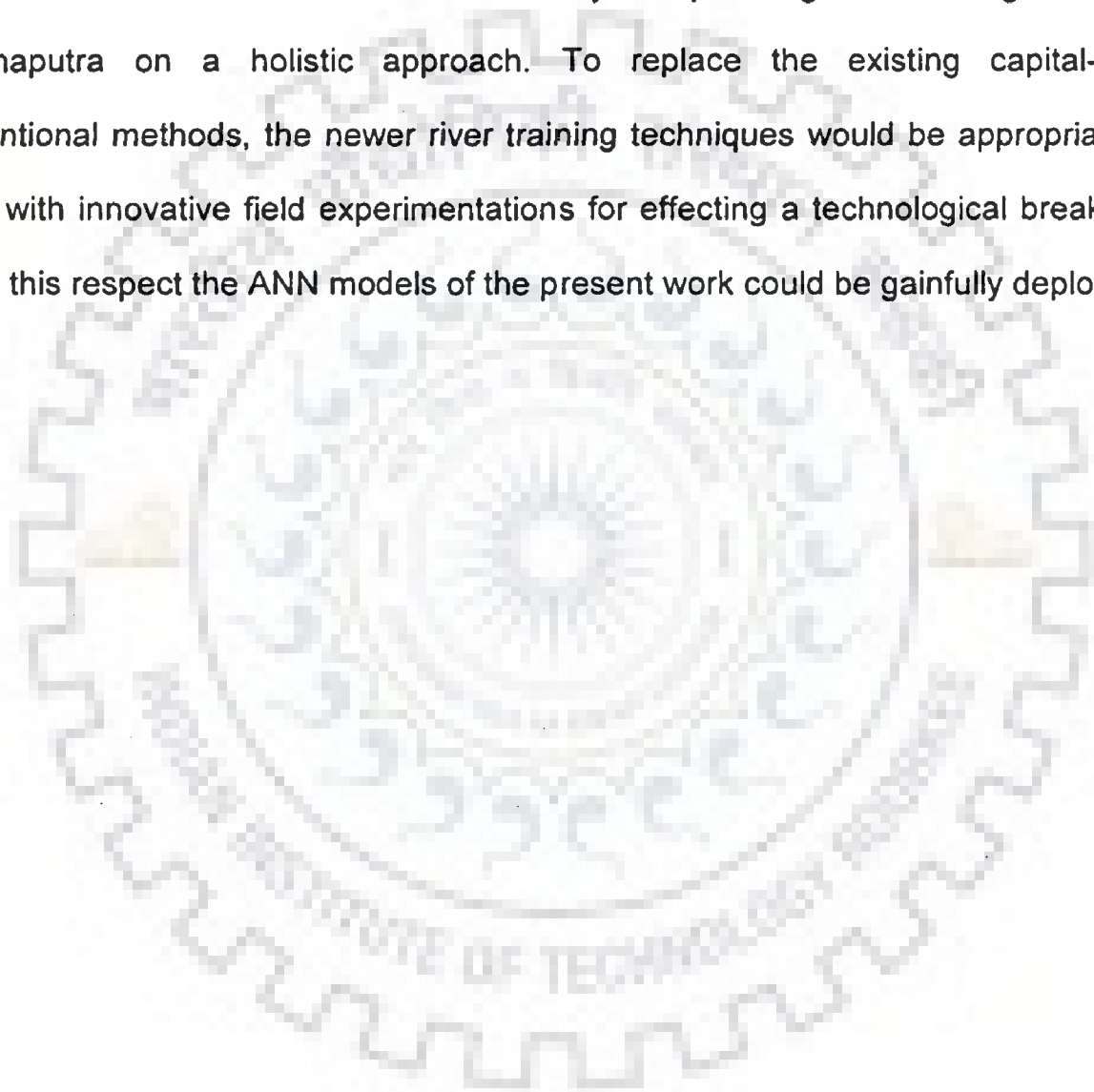
## 6.12 CONCLUDING REMARKS

Emerging latest technique of ANN has been deployed in the present research for modelling erosion, channel migration, flow levels and other variability of the Brahmaputra with very encouraging results, meriting further work. The morphological changes during the period 1990-2002 revealed that the morphology of the river evolved markedly in response to the imposed flow and sediment regime. The study also demonstrated two significant results: (i) the suitability of an NN for simulation and prediction of all the vital hydrological variability with high accuracy at a fraction of the computational time required by the conventional models; and (ii) a technique for detecting less sensitive input neurons in an effort to reduce the unnecessary data collection and operational cost.

The flow regime of the Brahmaputra responds to the seasonal rhythms of the monsoon and freeze-thaw cycle of the Himalayan snow. Likewise prediction of future morphological changes depends on anticipating cyclical variation in approach flow, orientation. For problem solving of the Brahmaputra, for the planners and administrators require a comprehensive understanding of the morphology of the river, and a better knowledge of hydrodynamic processes that are active in watersheds through the application of neuromorphic models, and these have been focused in this research. ANN models developed in this research can be updated to obtain better results by presenting new training examples to ANNs as new data become available.

Unless urgent remedial steps are formulated making use of these models, the basin would have to endure a much enlarged flood plain with higher flood levels, great loss of prime land to stream-bank erosion, severe drainage congestion, recurrent urban

flood events and flood devastation of agriculture. It could be inferred from the study that the Brahmaputra would become very wide, shallow and highly braided, requiring very tall embankments to prevent flooding. A plan for control of erosion would be evolved based on the projection of the past trend through neuromorphic modelling as carried out in the present research. To manage the river using these ANN models, newer cost-effective measures need to be considered seriously for planning and management of the Brahmaputra on a holistic approach. To replace the existing capital-intensive conventional methods, the newer river training techniques would be appropriately fine-tuned with innovative field experimentations for effecting a technological break-through and in this respect the ANN models of the present work could be gainfully deployed.



## CONCLUSIONS AND SCOPE FOR FUTURE WORK

---

The development of reliable functional relationships binding the fluvial phenomena associated with morphological changes in a large braided stream, like the Brahmaputra, continues in quest of an ideal solution. It has been endeavoured in this work to develop neuromorphic models in conjunction with satellite remote sensing to circumvent the difficulty in huge data processing. Satellite remote sensing technology with multi-band and multi-date satellite imageries offered considerable benefit in being able to acquire synoptic and an authentic source of information and has been used in this present research for mapping and monitoring of the river Brahmaputra. Use of Geographic Information System (GIS) eased the data storage, statistical analysis, data manipulation (including quantification of error) and the flexibility of graphical display.

Based on the present research on the river Brahmaputra, the following conclusions have emerged:

1. The morphological changes during the period 1990-2002 have revealed that there has been a marked evolution of the morphology of the river Brahmaputra in response to the imposed flow and sediment regime. Adjustment processes that affected fluvial system of the river include channel erosion and accretion, lateral river migration, widening or narrowing, avulsion and changes in the flow and sediment load in spatial and temporal scales.
2. In general, left bank movement of the river occurred mainly through rapid erosion of the embayments, while right bank movement involved looping, both through embayment erosion and incision of floodplain. The right bank of the river moved

about 0.47 km on an average, to the north between the years 1990 and 2002, while the left, moved about 0.48 km to the south.

3. The study revealed that the erosion process of the river significantly widened the channel. Erosion activity has increased the overall river area by 12.10% during the period from 1990 to 2002. The net flow area has registered an increase of 17.23% in 2002 as compared to year 1990 taken as datum due to erosional activity.
4. The ANN models developed in this work are capable of predicting river stage, water flow and sediment discharge at discrete points with respect to space and time without explicitly representing the internal hydrologic structure of the river. The prediction of average monthly stage yielded good results as the efficiencies were 99.9% for the models 12 and 13. The efficiencies for the models 13 and 14 pertaining to discharges were 97.3% and 98.8% respectively. The efficiencies of the composite model 15 were 98.9% (stage) and 50.29% (sediment discharge) in respect of observed and ANN predicted stage and sediment discharges respectively.
5. A very significant outcome of the present research is that the ANN model could perform superior to fuzzy and neuro-fuzzy models. This was apparent from the stage-discharge relationship models for Dibrugarh, Pancharatna and Dhubri sites. Based on their ability to predict, the ANN models 17 (Dibrugarh), 18 (Pancharatna) and 19 (Dhubri) were found to be clearly superior to fuzzy expert system models 20 (Dibrugarh), 21 (Pancharatna) and 22 (Dhubri), except for Dhubri, where the neuro-fuzzy model 25 and the ANN model 19 gave similar results. The efficiencies of the ANN models 17, 18 and 19 were 98.6%, 99.27% and 98.49% respectively.

6. As a relatively new approach, ANN modelling technique could be seen in this research to be a highly suitable flow prediction tool yielding a high degree of water-level prediction accuracy at Pandu, Pancharatna and Dhubri for one-lead-day. This could be seen from the models 26 (Pandu), 27 (Pancharatna) and 28 (Dhubri) with efficiencies 93%, 96.3% and 89% respectively.
7. The research contributed the development of ANN models capable of predicting reduced levels of the river cross-sections. Derived attributes from this could quantify channel processes, along with the longitudinal and hydraulic data. The observed reduced levels at Pancharatna have been verified with the ANN simulated ones, and the efficiency of the hydrographic model was 99.89%. The goodness-of-fit criteria, such as *rmse* and Nash coefficient for the result were 1.292 and 0.9989 respectively.
8. The area of the Majuli river island has evidently decreased by 39.30 km<sup>2</sup> over a period of 12 years from 416.23 km<sup>2</sup> in 1990 to 376.93 km<sup>2</sup> in 2002 (Table 4.17). The study has revealed that the loss of land area has been 4.94% in 1997 and 9.44% in year 2002 as compared to the area of Majuli island in the year 1990. After the flood of 1990, the configuration of the river reach from Bessamora to Kamalabari changed considerably and an old dead channel named Chumoimari started developing rapidly on the Bessamora - Kamalabari side. The heavy discharge carried by Chumoimari channel led to severe bank erosion from Dakhinpat to Kamalabari. A deep channel is heading south at 90<sup>0</sup> near Hatisal Neamati causing severe erosion, and it is expected that this may trigger severe fluvial hazard avulsion. Ground observations on the overall erosion activity around Majuli island exhibited two types of features, i.e. (i) bowl-shaped shear failure,



which is more common around Gajeragaon, the easternmost corner of the island, and (ii) liquefaction failure at Kumargaon, Batiamarinagar and Bessamara.

9. This research has yielded the promising use of the topological indices in being able to predict channel change and braid characteristics. The average values of  $\alpha$ ,  $\beta$  and  $\gamma$  indices for the entire stretch were found to be 0.222, 1.401 and 0.487 for the year 2000 and 0.215, 1.390 and 0.482 for 1990 respectively.
10. To formulate appropriate parameters to describe the braiding phenomenon and fluvial landform pattern in quantitative and qualitative terms on a more logical basis, two new braid indicators namely HGI and FLI have been developed in this work. It could be analysed that these indices rationally classify the degree as well as intensity of braiding for the Brahmaputra. The HGI value is 0.312 for reach 4 indicating very high braiding. The performance evaluation of the newly developed HGI with topological indices, like the alpha ( $\alpha$ ), beta ( $\beta$ ) and gamma ( $\gamma$ ) with respect to intensity of braiding clearly demonstrated the usefulness and relevance for applying these indices in the Brahmaputra for a quantitative measure of the fluvial landform.
11. On the basis of a critical analysis of the trends of the variation of HGI, FLI, form ratio,  $\alpha$ ,  $\beta$  and  $\gamma$  indices in the study area of the river Brahmaputra, the thresholds were determined for all the aforesaid indices to provide an objective basis for classification of the braiding phenomenon as well as to make them useful for practical applications subsequently. As HGI increased, the form ratio increased, the energy slope ( $S_f/F_R$ ) decreased, which indicated that the braided pattern was conducive for the dissipation of energy due to boundary friction resulting in more width, thus low velocity, thereby indicating an increase in braiding.

12. One of the vital finding of the investigation was a pointer to the close relationship between losses of vegetative cover with river sediment load. The multi-spectral vegetation index like the NDVI has been tested to provide new information and improved sensitivity. The analysis has brought that loss of 10% vegetation cover contributed to 12% increase in the sediment load at Pancharatna (cross-section 9) of the river. Considering the relevance of flood inundation on river morphology, Digital Elevation Model (DEM), shallow and deep flooding phenomena in the Brahmaputra valley have been derived from NOAA satellite digital data to infer the flooding pattern of the basin.
13. An ANN model for sediment concentration was constituted to estimate the sediment discharge of the river Brahmaputra. This model has been developed in terms of sediment concentration at Pancharatna using water and sediment variables based on the dynamic laws of flow and sediment. The variables used for the model were tractive shear stress  $\psi$ , velocity ratio  $\phi$ , longitudinal slope  $S$ , suspension parameter  $w_0/u_*$ , water depth ratio  $h/d_{50}$ , Froude number  $Fr$ , Reynold's number  $R$ , width scale ratio  $h/B$ . The mean of the discrepancy ratio between obtained and measured values was 0.961 and the standard deviation for the mean was 0.156. The model efficiency was 62%.
14. The present investigation showed that the mean width of the river has increased much more than the minimum and maximum width. The river mean width has increased from 7.99 km to 8.94 km in the study reach of the river Brahmaputra. There was no radical change in the maximum width of 18.13 km at cross-section 17 near Gumi.

## SCOPE FOR FUTURE WORK

There still remains a great deal of uncertainty over the actual classification of the braided system. Ecological consequences and aquatic biodiversity due to adjustments in channel pattern and planform changes need to be explored. Another field yet to be fully explored by quantitative investigations is the mechanisms and processes of channel confluences and diffluences. ANNs can always be updated to obtain better results by presenting new training examples to ANNs as new data become available. Formulating solutions to the problems of the Brahmaputra for the planners and administrators require a comprehensive understanding of the morphology of the river, and a better knowledge of hydrodynamic processes that are active through the application of neuromorphic models.



## BIBLIOGRAPHY

---

1. Ackers, P. and White, W. R., (1973), "Sediment Transport: New Approach and Analysis", *Journal of the Hydraulics Division, Proceedings of the ASCE*, Vol. 99, No. HY 11, pp. 2041-2060.
2. Adeli, H., (1992), Computer-aided engineering in the 1990's. *The International Journal of Construction Information Technology*, Proc. Paper, 1, pp. 1-10.
3. Anderson, D., Hines, E.L., Arthur, S.J., and Eiap, E.L., (1993): Application of Artificial Neural Networks to Prediction of Minor Axis Steel Connections. In: Topping, B.H.V., and Khan, A.I., Editors, *Neural Networks and Combinatorial Optimization in Civil and Structural Engineering*, Civil-Comp Press: pp. 31-37.
4. Antropovskiy, V.I., (1972), Critical Relations of Type of Channel Processes, *Soviet Hydrology*, Vol. 11, pp. 371-381.
5. Ashmore, P.E. and Parker, G., (1983), "Confluence Scour in Coarse Braided Streams", *Water Resources Research*, Vol. 19, pp.392-402.
6. Ashmore, P.E., (1991<sup>(a)</sup>), "How do Gravel Bed Rivers Braid", *Canadian Journal of Earth Sciences*, Vol.28, pp. 326-341.
7. Ashmore, P.E., (1991<sup>(b)</sup>), "Channel Morphology and Bed load Pulses in Braided, Gravel-bed Streams", *Geografiska Annaler*, Vol.73A, pp.37-52.
8. Ashworth, P.J., (1996), "Mild-Channel Bar Growth and its Relationship to Local Flow Strength and Direction", *Earth Surface. Processes Landforms*, Vol. 21, pp.103-124.
9. Ashworth, P.J., Ferguson, R. and Powell, M., (1992) "Bed load Transport and Sorting in Braided Channels", In: Bill, P., Hey, R.D., Thorne, C.R. and Tacconi, P., (Eds.) 'Dynamics of gravel bed rivers'. Wiley and Sons, pp. 497-513.
10. Bagnold, R. A, (1960a), 'Sediment discharge and stream power: a preliminary announcement', Circular, United States Geological Survey, pp. 421.
11. Bank erosion at Majuli island (1996), A study based on multi temporal satellite data, Space Application Centre, (ISRO), Ahmedabad and Brahmaputra Board, Guwahati.
12. Bastarache, D., El-Jabi, N. and Clair, T.A., (1997), "Predicting conductivity and acidity for small streams using neural network", *Canadian J. of Civil Eng*, 24(5), pp. 1030-1039.

13. Bathurst, J.C., and Thorne C.R. and Hey, R. D., (1979), "Secondary Flow and Stress at River Bends", Journal of the Hydraulics Divisions Proceedings of the American Society of Civil Engineers, Vol. 105, No. HY10, pp.1278-1295.
14. Berge, Claude, (1962), Theory of graphs and its applications, John Wiley, New York.
15. Berke, L. and Hajela, P., (1991), "Application of neural networks in structural optimization", NATO/AGARD Advanced Study Institute, 23 (I-II), 731-745.
16. Best, J.L. and Roy, A.G., (1991), "Mixing-Layer Distortion at the Confluence of Channels of Different Depth", Nature, Vol. 350, pp. 411-413.
17. Best, J.L., (1988), "Sediment Transport and Bed Morphology at River Channel Confluences." Sedimentology, Vol.35, pp.481-498.
18. Bhattacharya, B., and Solomatine, D.P., (2000) Application of artificial neural network in stage-discharge relationship, Proc. of the 4th Hydroinformatics Conf., Iowa, USA.
19. Brahmaputra Board, Ministry of Water Resources, Govt of India,(1986), Atlas of Brahmaputra Basin, Volume I.
20. Brahmaputra Board, Ministry of Water Resources, Govt. of India, (1986), Atlas of Brahmaputra Basin, Volume II.
21. Brice, J.C., (1960), "Index for Description of Channel Braiding", Bulletin of the Geological Society of America, Vol.71, and pp.1833.
22. Brice, J.C., (1964),"Channel Patterns and Terraces of the Loup Rivers in Nebraska", U.S Geological Survey professional paper, 422-D.
23. Bridge, J.S, (1993), "The interaction between channel geometry, water flow, sediment transport and deposition in braided rivers", In: Best, J. L, and Bristow, C.S, eds. Braided rivers, Special Publication no. 75, Geological Survey of London, pp. 13-63.
24. Bridge, J.S., Smith, N.D., Trent, F., Gabel, S.L. and Bernstein, P., (1986), "Sedimentology and Morphology of a Low Sinuosity River, Calamus River Nebraska Sand Hills", Sedimentology Vol. 33, pp.851-870.
25. Bristow C.S and Best J.L., (1993), "Braided rivers perspective and problems", Geological Survey, London Special Publication, Pub No-75, pp. 1-11.

26. Bristow, C.S (1987a), "Brahmaputra River: Channel Migration and Deposition." In: Ethridge, F.G., Flores, R.M. and Harvey, M.D., (Eds.) Recent development of Sedimentology. Soc. of Eco. Pale. and Mine. Special. Publication. Vol.39, pp. 63-74.
27. Bristow, C.S. and Best, J.L (1993), "Braided Rivers: Perspectives and Problems." A chapter in 'Braided rivers by Best, J. L. and Bristow, C.S., (Eds. 1993), Geological Society, London, Special. Publication, No. 75. pp. 1-11.
28. Bristow, C.S., (1987b), "Sedimentology of large braided rivers ancient and modern", Ph.D. thesis, University of Leeds, U.K.
29. Bristow, C.S., (1993), 'Sedimentary structures exposed in bar tops in the Brahmaputra river, Bangladesh', A chapter in 'Braided Rivers' by (Eds. Bristow, C.S. and Best, J .L, Geological Society Spl. Pub.No.75, pp.277-289.
30. Brownlie, W. R. (1981). "Prediction of flow depth and sediment discharge in open channels." Rep.No. KH-R-43B, Lab. of Hyd. Res., California Institute of Technology, Pasadena, Calif.
31. Carson, M.A., (1984), "The Meandering - Braided River Threshold: A Reappraisal", Journal of Hydrology, Vol. 73, pp.315-334.
32. Clair, T.A., and Ehrman, J.M., (1998)" Using neural networks to assess the influence of changing seasonal climates in modifying discharge, dissolved organic carbon, and nitrogen export in eastern Canadian rivers." Water Resources Research, 34(3), pp. 447-455.
33. Coleman, J.M (1969), "Brahmaputra river channel process and sedimentation", Sedimentary Geology, Vol.3, pp.129-239.
34. Cook, D.J., Dickinson, W.T. and Rudra, R.P., (1985) GAMES - The Guelph model for evaluating the effects of agricultural management systems on erosion and sedimentation: User's Manual. Technical Report No. 126-71, School of Eng., University of Guelph, Guelph, Ontario.
35. Daniel, T.M., (1991), "Neural networks - Applications in hydrology and water resources engineering." Int. Hydrology and Water Resources Symposium, Perth, 2-4 October, 791-802.
36. Dastorani, M.T. and Wright., N.G., (2002), Artificial neural network based real-time river flow prediction, Hydroinformatics, Proc. of 5<sup>th</sup> Int. Conf., Cardiff, UK.

37. Datta, B. and Singh V. P., (2004), Hydrology, The Brahmaputra Basin Water Resources, Kluwer Academic Publication, The Netherlands, pp. 139-195
38. Dawson, C.W., and Wilby, R.L., (1998), An artificial neural network approach to rainfall-runoff modelling, Hydrological Sciences Journal 48 (1), pp. 47-66.
39. De Villars, J. and Barnard, E., (1993) "Back propagation neural nets with one and two hidden layers", IEEE Trans, Neural News, 4(1), pp. 136-141.
40. Doeglas, C.S., (1967), Structure of sedimentary deposits of braided rivers, Sedimentology, 1, pp. 167-90.
41. Elazouni A.M., Nosair I.A., Mohieldin Y.A., and Mohamed A.G., (1997), Estimating Resource Requirements at Conceptual Design Stage Using Neural Networks, Journal of Computing in Civil Engineering, ASCE, Proc. Paper 11485, 11, 4: pp. 217-223.
42. Elliot, J.G, Gellis, A.C, and Aby, S.B (1999), Evolution of arroyos: Incised channels of the South Western US, In: Darby, S.E and Simon, A., eds., Incised River Channels, Chichester, England, Wiley and Sons. pp. 153-185.
43. Engelund, F. and Hansen, E., (1967) "A Monograph on Sediment Transport in Alluvial Streams", Teknish Forlag, Technical Press, Copenhagen, Denmark, pp. 62.
44. Engelund, F. and Skovgaard, O., (1973), "On the Origin of Meandering and Braiding in Alluvial Streams" Journal of Fluid Mechanics, Vol.57, Part 2, pp.289-302.
45. Falvey, H.T., and Schleiss, A, (2002), Assessment of turbulent jet impingement on rocky riverbeds : the particular properties of a near-prototype physical model study, Int. Conf. On Fluvial Hydraulics, Erik Bollaert, Switzerland
46. Ferguson, R.I (1981), "Channel Form and Channel Changes", In: 'British Rivers' by Lewin, J., (Editor), Allen and Unwin, London, pp.90-125.
47. Ferguson, R.I (1987), Hydraulic and sedimentary controls of channel pattern, In: Richards, K., eds. River Channels, Environment and process, Basil: Blackwell, pp. 129-158.
48. Ferguson, R.I., (1993), "Understanding Braiding Processes in Gravel-Bed Rivers: Progress and Unsolved Problems", In: Best, J.L. and Bristow, C.S., (eds), Braided rivers, Geological Society, London, Special. Publication 75, pp.73-88.

49. Flood, I. and Kartam, N., (1994a), Neural Network in Civil Engineering-I: Principles and Understanding. Journal of Computing in Civil Engineering ASCE, Proc. Paper No. 5789, 8, 2: 131-148.
50. Flood, I. and Kartam, N., (1994b), Neural Network in Civil Engineering-II: System and Application. Journal of Computing in Civil Engineering, ASCE, Proc. Paper No. 5790, 8, 2: 149-162.
51. Friend, P.F. and Sinha, R., (1993), "Braiding and Meandering Parameters", A chapter in 'Braided Rivers' by Best, J. L. and Bristow, C.S., (eds. 1993), Geological Society, London, Special Publication. No.75, pp.105-111.
52. Fujita, Y., (1989), "Bar and Channel Formation in Braided Streams", In: Ikeda, S. and Parker, G., (eds) River Meandering, American Geophysical Union, Water Resources Monographs, Vol.12, pp. 417-462.
53. Garde, R.J. and Ranga Raju, K.G., (1985), "Mechanics of Sediment Transportation and Alluvial Stream Problems", Wiley Eastern Ltd, 2<sup>nd</sup> eds., New Delhi.
54. Garde, R.J., Pande, P.K., Ranga Raju, K.G., Asawa, G.L., Srivastava, R., Kothyari, U.C., (1990), Mathematical modelling of the morphological changes in the river Kosi, Technical Report, Univ. of Roorkee, India.
55. Garrison, R I, (1977), Meander Migration: Equilibrium and change in river Channel changes, in river channel changes edited by Gregory, K.J John Wiley and Sons, New York.
56. Geological Survey of India (1981), Misc. Publication, 46, 141.
57. Geological Survey of India publication (1974), Bulletin Series B.
58. Ghaboussi, J., and Sidarta, D. E. (1998). "New nested adaptive neural networks (NANN) for constitutive modeling." J. Computers and Geotechnics, 22(1), 29-52.
59. Goswami, D.C. and Das, P.J., (2000), Report on some characteristics of high flow and low flow in the Brahmaputra river, India, Guwahati University.
60. Goswami, D.C., (1985), Brahmaputra River, Assam, India: Physiography, Basin Denudation, and Channel Aggradation, Water Resources Research, V-21, pp. 959-978.
61. Goswami, D.C., (1992), Zonal Planning in Water, In: Planning for Northeastern and Eastern Zone, Adisheshiah, M.S.(ed.), Lancer Publications, New Delhi, pp. 9-22.



62. Goswami, D.C., (1998), Fluvial regime and Flood Hydrology of the Brahmaputra River Assam, In: Kale V. S., (ed.) Flood studies in India, Geol. Soc. India, Memoir 41, pp. 53-75.
63. Guidelines for the calibration and application of computer programme HEC-6, (2004), US Army Corps of Engineers, Training doc. No 13.
64. Gupta, N.C., Prakash, B and Singhal B.B.S., (1980) Topological changes with time in the plan form of the Kosi river in north Bihar and Nepal, Proceedings of International Workshop on Alluvial River Problems, Roorkee.
65. Hall, M.J. and Minns, (1993) A.W., Rainfall-runoff modelling as a problem in artificial intelligence: experience with a neural network. In: Proc. BHS 4th National Hydrology Symposium, Cardiff, pp. 5.51-5.57.
66. Hawley, D.D., Johnson, J.D., and Raina, D., (1993), Artificial Neural Systems; A New Tool for Financial Decision-making. In: Trippi, R.R., and Turban, E., Editors. Neural Networks in Finance and Investing, Probus Publishing: 27-46.
67. Haykin, S., (2001), Neural Networks, Wiley and Sons, pp. 2-10, 213.
68. Hazarika, M. K. and Honda, K., (1999), Estimation of Soil Erosion Using Remote Sensing and GIS, Its Valuation and Economic Implication on Agricultural Production, 10<sup>th</sup> Int. Soil Conservation Organization Meeting, Purdue University, pp. 1090-1093.
69. Henderson, F.M., (1961), "Stability of Alluvial Channels, "Journal of the Hydraulics Division, Proceedings of the ASCE, Vol. 87, pp.109-138.
70. Hergert, F., Finnoff, W., Zimmermann, H.G,(1992). "A comparison of weight elimination methods for reducing complexity in neural networks", Proc. Int. Joint Conf. on Neural Networks, III, 980-987, IEEE, New York.
71. Hey, R.D., (1978) Determinate hydraulic geometry of river channels, Journal of Hyd. Divn, 104(Hy6), 869-885.
72. Hickin, E.J and Nansen,G.C.,(1975), The character of channel migration on the Britten river, North East British Columbia, Canada, Bulletin of Geological Society, America, Vol.86.
73. Hicks, D.M, and Gomez, B., (2003) Sediment Transport, In: Kondolf, G.M and Piegay, H, eds: Tools in Fluvial Geomorphology, Wiley, pp.425-453.
74. Hinton, G.E., (1992) How Neural Networks Learn from Experience. Scientific American. Vol. 267 No. 3, pp. 145-151.

75. Holmes, Pat, Baldock, Tom (1999). "Seepage effects of sediment transport by waves and currents" In: Elsevier 26th International Conference on Coastal Engineering, Copenhagen Denmark, Vol. 3, pp. 3601-3614.
76. Honda, K., (2004) Genetic algorithm for assimilating remotely sensed evapotranspiration data using a soil-water-atmosphere-plant model. FOSS/GRASS, International Organizing Committee.
77. Honda, K., Samarakoon, L., Ishibashi, A., (1998), Erosion control engineering and geoinformatics; river planform change and sediment yield estimation in a watershed of Siwalik, Nepal. In: R. B. Singh et al. (ed) Space Informatics for sustainable development. Oxford & IBH Publishing Co. Pvt. Ltd., New Delhi. pp. 63-70.
78. Honda, K., Samarakoon, L., Ishibashi, A., Mabuchi, Y. and Miyajima, S., (1996), Remote sensing and GIS technologies for denudation estimation in Siwalik watershed of Nepal. Prof. 17<sup>th</sup> Asian Conf. on Remote Sensing, Colombo, Sri Lanka, pp. B21-B26.
79. Hong, L. B. and Davies, T.R.H., (1979), "A Study of Streams Braiding", Geological Society of America Bulletin, Vol. 79, pp.391-394.
80. Hornik, K., Stinchcombe, M and White, H., (1989)" Multilayer feed forward networks are universal approximators, Neural Networks, 2(5), 359-366.
81. Howard, A.D., Keeth, M.E. and Vincent, L.C., (1970), "Topological and Geometrical Properties of Braided Streams", Water Resources Research, Vol.6, pp. 1674-1688.
82. Hsu, K. L., Gupta, H. V., and Sorooshian, S. (1995). "Artificial neural network modeling of the rainfall-runoff process." Water Resources Res., 31(10), pp. 2517-2530.
83. Hussain, (1992), Investigation of morphological changes of Brahmaputra river- Dhubri to Tezpur using satellite data, M.E. Dissertation, WRDTC (Univ of Roorkee).
84. Kaman, B. and Sarma, A.K, (2001), Mathematical model for erosion study in the braided channel of Majuli isalnd, National seminar on water and land management including CAD for socio economic upliftment of NE region, 22-23<sup>rd</sup> November, Guwahati.

85. Karayiannis, N.B. and Venetsanopoulos, A.N., (1993), *Artificial Neural Networks: Learning Algorithms, Performance Evaluation and Applications*. Kluwer Academic Publishers, Boston.
86. Karunanithi, N., Grenney, W.J., and Whitley, D (1994), Neural networks for river flow prediction, *Journal of Computational Civil Eng*, 8(2), pp. 201-220.
87. Karunasekera, H.N.D., (1992). *Neural Network Structure Generation for the Classification of Remotely Sensed Data Using Simulated Annealing*, M.Eng Thesis, Asian Institute of Technology, Bangkok.
88. Kellerhals, R., Church, M, and Bray, D.I, (1976), Classification and analysis of river processes, *Journal of Hydraulics Division, ASCE*, 102, 813-829.
89. Khan, A.I., Topping, B.H.V., and Bahreininejad, A., (1993), Parallel Training of Neural Networks for Finite Element Mesh Generation. In: Topping, B.H.V., and Khan, A.I., Editors. *Neural Networks and Combinatorial Optimization in Civil and Structural Engineering*, Civil-Comp Press: 81-94.
90. Kimoto, T., Asakawa, K., Yoda, M., and Takeoka, M., (1993). Stock Market Prediction System with Modular Neural Networks. In: Trippi, R.R., and Turban, E., Editors. *Neural Networks in Finance and Investing*, Probus Publishing: 343-356.
91. Kireetoh, S., (1995), *Neural Networks Technology*, Engineering Institute of Thailand, Proc.: EE371-EE384.
92. Klir, G.J, St Clair UH, Yuan B., (1997). *Fuzzy Set Theory Foundations and Applications*. Prentice Hall: New Jersey; 245.
93. Knighton, A.D, and Nanson, G.C (1993), Anastomosis and the continuum of channel pattern, *Earth surface processes and landforms* 18; 613-625.
94. Kohonen, T., (1988), An introduction to neural computing, *Neural Networks Vol-1*, pp. 3-16.
95. Krumbein, W. C. and Orme, A. R, (1972), Field Mapping and Computer Simulation of Braided Stream Networks, *Bulletin of Geological Society of America*, Vol 83.
96. Lane, E.W., (1957), "A study of the shape of channels formed by the natural streams flowing in erodible material", U.S Army Corps Engg. Div., Missouri River, M.R.D. Sediment. Ser. No. 9, pp.106.
97. Langbein, W.B., <sup>(1964)</sup> Geometry of river channels, ~~1964~~ Journal of Hydraulic Divn, ASCE, 90(Hy2), Proc Paper 3846, pp. 301-312.

98. Laursen, E. M., (1958). "The total sediment load of streams." J. Hydraulics. Div., ASCE, 54(1), pp.1-36.
99. Leopold, L. B. and Wolman, M.G., (1957a), "River channel patterns: Braided, meandering and straight", United States, Geological Survey Professional Paper 282-B, pp.35-85.
100. Leopold, L. B. and Wolman, M.G., (1957b), 'River channel patterns', Chapter in 'Rivers and River Terraces', by (ed. Dury, G.H.), published by Macmillan and Co. Ltd., London, pp.197-237.
101. Leopold, L.B. and Wolman, M.G. and Miller, J.P., (1964), "Fluvial Processes in Geomorphology", San Francisco, W.H. Freeman.
102. Lillesand, T. M. and Kiefer, R. W., (1992), Remote Sensing and Image interpretation, John Wiley, New York.
103. Lippmann, R.P., (1988), An Introduction to Computing with Neural Nets, In: Vemuri, V., Editor, Artificial Neural Networks; Theoretical Concepts, The Computer Society: 36-54.
104. Maddock, T., (1973), "A Role of Sediment Transport in Alluvial Channels", Journal of Hydraulics Division, ASCE, Vol. 99, No.HY11, pp.1915-1931.
105. Maier, H. R., and Dandy, G. C. (2000). "Neural networks for the prediction and forecasting of water resources variables: A review of modelling issues and applications." Environmental Modelling & Software, 15(2000), 101-124.
106. Masters, T. (1993). Practical neural network recipes in C++, Academic Press, San Diego, California.
107. Mazumder, S.K., (2001), "Training of River Ganga near Farakka Barrage", Proc. of National Conference on Hydraulics and Water Resources, HYDRO 2001, Org. by ISH & CW&PRS, Pune.
108. Mazumder, S.K.,(1988), "Effectiveness of impervious type groins in river bank protection with particular reference to river Kosi in India", Int. conf. on hydraulics of floods and flood control.
109. McCulloch, W.S., Pitts, W., (1943), A logical calculus of the ideas immanent in nervous activity, Bulletin Math. Biosphys. Vol. 5, pp. 115- 133.
110. Medsker, L., Turban, E., and Trippi, R.R., (1993), Neural Network Fundamentals for Financial Analysis. In: Trippi, R.R., and Turban, E., Editors. Neural Networks in Finance and Investing, Probus Publishing: pp. 3-26.

111. Mehra P. & Wah W.W., (1992), Artificial Neural Networks: Concepts and Theory. Los Alamitos, CA: IEEE Computer Society.
112. Miall, A.D., (1977), "A Review of the Braided River Depositional Environment", Earth Science Reviews, Vol.13, pp.1-62.
113. Minns, A.W., and Hall, M.J., (1996), Artificial neural networks as rainfall-runoff models, Hydrological Sciences Journal 41 (3), pp. 399-418.
114. Mosely, M. P., (1976), An experimental study of channel confluences, Journal of Geology, 84, pp. 535-562.
115. Mosley, M. P., (1981), "Semi-Determinate Hydraulic Geometry of River Channel. South Island New Zealand", Earth Surface Processes and Landforms, Vol.6 pp.127-137.
116. Mosley, M.P., (1982a), "Scour Depths in Branch Channel Confluences, Ohio River, Orago, New Zealand", Transactions, the Institutions of Professional Engineers, New Zealand Vol.9, pp. 17-24.
117. Mosley, M.P., (1982b), "Analysis of the Effect of Changing Discharge on Channel Morphology and Insteam Uses in a Braided River, Oahu river, New Zealand", Water Resources Research, Vol.8, pp. 800-812.
118. Murray, A.B, and Paola, C, (1994), A cellular model of braided rivers, nature 371, pp. 54-57.
119. Muttiah, R.S, Srinivasan, R., and Allen, P.M., (1997). "Prediction of the two year peak stream discharges using neural networks." Journal of American Water Res. Association, 33(3), 625-630.
120. Nagesh K. D., Raju, K S, and Satish, T, (2004), "River flow forecasting using recurrent neural network", Water Resources Management, 18, 143-161, Kluwer Publishers.
121. Nalluri, C. and F. Spalivieso, (1998) Suspended sediment transport in rigid boundary channels at limit deposition. Journal of Water Science Technology, 37 (1), pp. 147-154.
122. Nash, J.E. and Sutcliffe, J.V., (1970) River flow forecasting through conceptual models, part-1- A discussion of principles. Journal of Hydrology, 10(3), 282-290.
123. NeuroDimensions, (2001) NeuroSolutions, www.nd.com.
124. Oak, R.A, (1998), Note on prediction of bank erosion using satellite imageries-A case study, CWPRS, Pune.

125. Ota, J. J., Nalluri, C., Dettmer, P. H. C., and Medeiros, P. A. (2003). "Sediment transport over fixed plane beds." XV Brazilian Symp. of Water Resources, ABRH (Brazilian Society of Water Resources), Curitiba, Brazil (in Portuguese).
126. Pandey, A.D., (2004), Erosion model using ANN, Personal communication.
127. Parker, G., (1976), "On the Cause and Characteristic Scales of Meandering and Braiding in Rivers", *Journal of Fluid Mechanics*, Vol. 76, pp.459-480.
128. Prandtl, L, (1952), *Essentials of fluid dynamics*, London, Blackie and Sons
129. Press Trust of India Report, (1995), *The Sentinel*, 7<sup>th</sup> July, pp. 3.
130. Rajsekharan, S. and G. A Vijayalakshmi Pai (1996), *Neural networks, fuzzy logic and genetic algorithm*, Prentice Hall of India, pp. 34-86.
131. Raman, H., and Sunilkumar, N. (1995). "Multivariate modeling of water resources time series using artificial neural networks." *Hydrological Sci. J.*, 40(2), pp. 145-163.
132. Ramos, D.A. & Holmes, P. (1997). Modelling of river/coastal interaction. *Proc 4th Int. Conf on Coastal and Port Engineering in Developing Countries*, Am. Soc. Civil Eng. Vol 1, pp 341-353.
133. Report on the silting of reservoirs, Ministry of Water Resources, Government of India, December, 2002.
134. Richards K., (Ed.1982), "Rivers: Forms and Process in Alluvial Channels", Published by Methuen and Co. Ltd., London.
135. Richardson, W.R. and Thorne, C.R., (2001), "Multiple Thread Flow and Channel Bifurcation in a Braided River: Brahmaputra-Jamuna River", *Bangladesh: Geomorphology*, Vol. 38, No., (3-4), pp.185-196.
136. Robertson-Rintoul, M.S.E. and Richards, K.S., (1993), "Braided-Channel Pattern and Palaeohydrology using an index of total sinuosity", A chapter in 'Braided rivers' by Best, J. L. and Bristow, C.S., (Eds. 1993), Geological Society, London, Special. Publication, No. 75. pp. 113-118.
137. Robinson, Fayek A, Sun Z., (2001). A fuzzy expert system for design performance prediction and evaluation. *Canadian Journal of Civil Eng.* 28: pp. 1-25.
138. Rogers, J.L., and Lamarsh, W.J., (1992), Application of a Neural Network to Simulate Analysis in An Optimization Process. *Artificial Intelligence in Design*, Proc. Paper: Kluwer Academic Publishers: pp. 739-754.

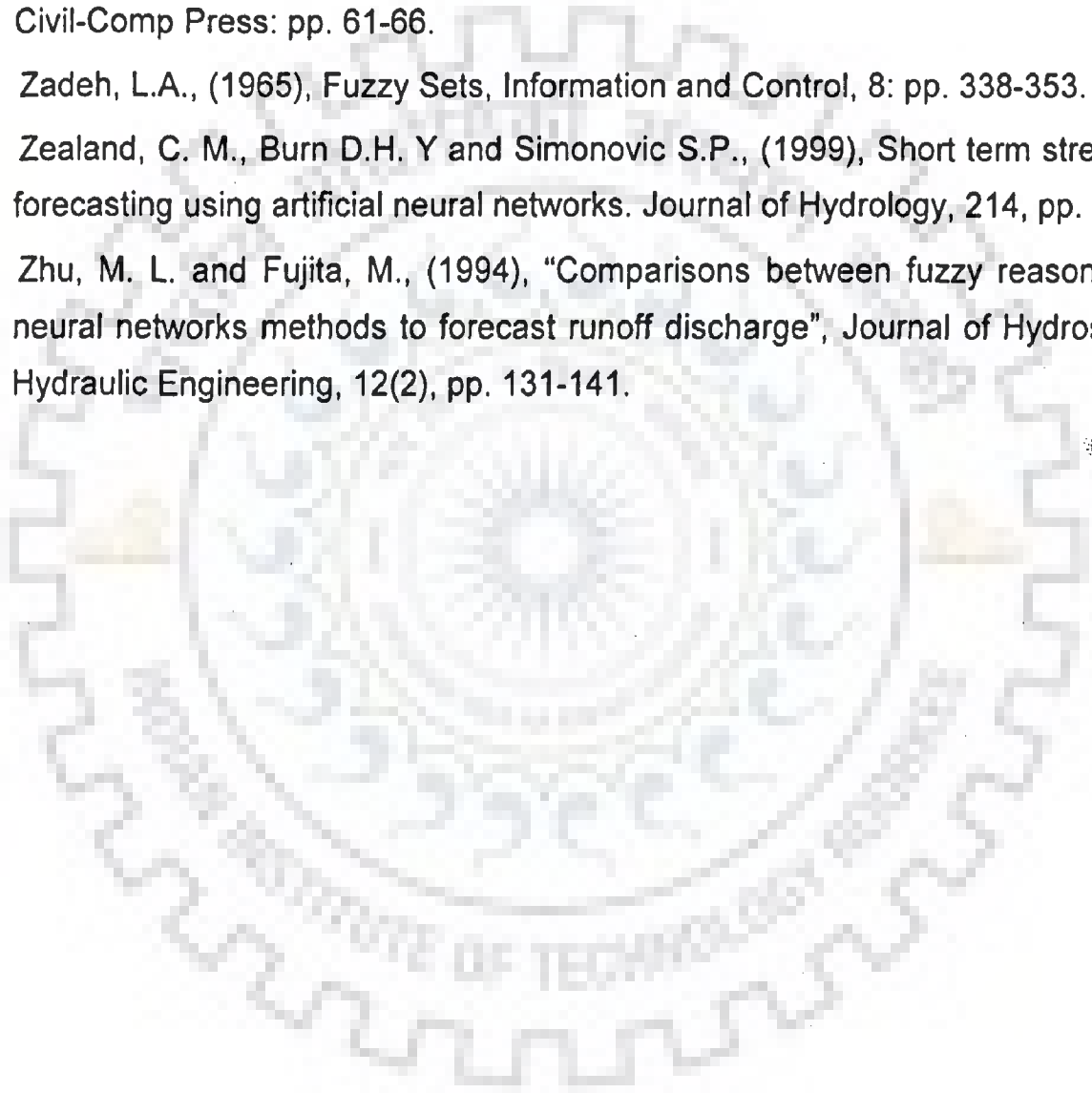
139. Rosenblatt, F., (1958), "Remarks on some non parametric estimates of a density function", *Annals of mathematical statistics*, vol-27, pp.832-837.
140. Rudra, R.P. and W.T. Dickinson, (1985). Soil erosion and fluvial sediment research at Guelph, Seminar delivered to researchers at the USDA National Soil Erosion Laboratory, W. Lafayette, Indiana.
141. Rumelhart, D. E., Hinton. G. E., and Williams, R. J., (1986)<sup>(cy)</sup>. "Learning internal representation by error propagation." *Parallel Distributed Processing*, D. E. Rumelhart and J. L. McClelland, eds., MIT Press, Cambridge.
142. Rumelhart, D.E., Hinton, G.E, and Williams, R.J, (1986~~a~~), Learning representations in back-propagation errors, *Nature (London)*, vol. 323, pp 533-536.
143. Rust, B.R., (1978a), "A Classification of Alluvial Channel Systems", In: Miall, A.D., (Ed) *Fluvial Sedimentology*, Canadian Society of Petroleum Geologists Memoirs, Vol. 5, pp. 187-198.
144. Rust, B.R., (1978b), "Depositional Models for Braided Alluvium", In: Miall, A.D., (Ed) *Fluvial Sedimentology*, Canadian Society of Petroleum Geologists Memoirs, Vol. 5, pp. 605-626.
145. Sarma A. K., (2004), *The Brahmaputra Basin Water Resources*, published by Kluwer Academic Publishers, The Netherlands pp. 261-273.
146. Schleiss, A, (2002), Scour formulae and their applicability to coarse gravel alpine rivers, *Int. Conf. on Fluvial Hydraulics*, Erik Bollaert, Switzerland
147. Schumm, S.A. and Khan, H.R., (1972), "Experimental Study of Channel Patterns", *Geological Society of America Bulletin*, Vol. 83, pp.1755-1770.
148. Schumm, S.A., (1977), *The fluvial system*, Chichester, UK, John Wiley and Sons, pp. 338.
149. Sen, D.J. and Garg, N.K., (2004), Efficient algorithm for gradually varied flows in channel networks, *Journal of Irrigation and Drainage*, ASCE, Vol 130,5, pp. 351-357.
150. Sharma Nayan (1995), "Modelling of braided alluvial channels", Ph.D thesis, WRDTC, University of Roorkee, Roorkee, India
151. Shen, H. W., and Hung, C. S. (1972). "An engineering approach to total bed material load by regression analysis." *Proc., Sedimentation Symposium*, Chap. 14, pp. 14.1-14.7.

152. Simon, A and Castro Janie, (2003) Measurement of alluvial channel form, In: Kondolf, G.M and Piegay, H, eds: Tools in Fluvial Geomorphology, Wiley, pp.289-321.
153. Singh V. P. and Fiorentino, M. (1992), "Entropy and Energy Dissipation in Water Resources", (Eds), Kluwer Academic Publishers P. O. Box 17, 3300 A. A. Dordrecht, The Netherlands.
154. Singh, G.P., (1995), Spatio-temporal idealization of Brahmaputra river, ME dissertation, University of Roorkee, Roorkee.
155. Smith, D.G. and Smith N.D, (1980), Sedimentation in anastomosed river systems; examples from alluvial valleys near Banff, Alberta, Journal of Sedimentary Petrology, 50(1), 157-164.
156. Smith, J. and Eli, R.M., (1995), "Neural network models of rainfall runoff process", Journal of Water Resources Planning & Management, 121(6), 499-508.
157. Smith, M., (1993), Neural Networks for statistical modelling, New York: Van Nostrand Reinhold.
158. Smith, N.D., (1970), "The Braided Stream Depositional Environment", Comparison of the Platte river with some Silurian Clastic Rocks, North central Appalachians, Geological Society of America Bulletin, Vol.81, pp. 2993-3014.
159. Smith, N.D., (1974), "Sedimentology and Bar Formation in the Upper Kicking Horse River, A Braided Out Wash Stream", Journal of Geology, Vol.82, pp. 205-223.
160. Soemardi, B.W., (1996), Fuzzy Neural Network Models for Construction Group Decision Making, In: Lye, H.K, Sang, C.Y., and Adeli, H., Editors. Computing & Information Tech. for Architecture, Eng. & Construction, Proc.: pp. 333-340.
161. Solomatine, D.P., (2002), Applications of data-driven modeling and machine learning in control of water resources. In: Computational Intelligence in Control, M. Mohammadian, R. A. Sarker and X.Yao (eds). Idea Group Publishing, Hershey, USA.
162. Soni, V., Ghosh, S.K. and Govil, S.K.,(2003) GIS for Site Suitability in Urban Planning, Geospatial Today, Vol. 2, Issue 1, pp. 37-38.
163. Srivastava, R. and Contractor, D.N., (1992). Discussion of "Bed-load and suspended-load transport of non-uniform sediments". Journal of Hydraulic Engineering, American Society of Civil Engineers, 118(6), pp. 948-949.



164. Stone, M., (1974), Cross validatory choice and assessment of statistical predictions, *Journal of the Royal Statistical Society*, Vol. B-36, pp. 111-133.
165. Swamee, P.K., and Ojha, C.S.P., (1991). "Bed Load and Suspended Load Transport of Non-Uniform Sediments", *Journal of Hydraulic Engineering*, ASCE, Vol.117, No.6, 774-787.
166. Thirumalaiah, K., and Deo, M. C. (1998). "River stage forecasting using artificial neural networks." *J. Hydrologic Eng.*, ASCE, 3(1), pp. 26–32.
167. Thorne, C.R., Russel, A.P.G. and Alam, M.K., (1993), "Planform Pattern and Channel Evolution of the Brahmaputra River, Bangladesh", A chapter in 'Braided Rivers' by Best, J. L. and Bristow, C.S., (eds.1993), Geological. Society London, Special Publication, No.75, pp.257-276.
168. Tokar, A. S., and Johnson, P. A. (1999). "Rainfall-runoff modeling using artificial neural networks." *J. Hydrologic Eng.*, ASCE, 4(3), pp. 232-239.
169. Tou, J. T, and Gonzalez, R C.,(1974), *Pattern Recognition Principles*, Addison-Wesley, Reading, Massachusetts.
170. Umamahesh, N. V. and Rao, Kameswara, (2001). Short term national training programme on Artificial Neural Network Application in Civil Engineering, Warangal, India.
171. Ural, D.N., and Saka, H, (1998), "Liquefaction assessment by neural networks", *Electronic J.Geotech Engg.*, <http://geotech.civen.okstate.edu/ejge/ppr9803/index.html>
172. Vaziri, M., (1996), Predicting the Air Pollution for Tehran Using Artificial Neural Networks. In: Lye, H.K, Sang, C.Y., and Adeli, H., Editors. *Computing & Information Technology for Architecture, Engineering & Construction*, Proc. pp. 385-390.
173. WAPCOS, (1993), *Morphological studies of river Brahmaputra*, New Delhi.
174. Weigend, A.S., Rumelhart, E, and Hubberman, B.A, (1991)"Generalizability by weight elimination with applications to forecasting." *Advances in neural information processing systems*", 3,875-882.
175. Wen, C. C. and Lee, C.S., (1998), "A neural network approach to multi objective optimization for water quality management in a river basin", *WRR*, 34(3), pp. 427-436.

176. William, T.P., (1993), Neural Networks to Predict Construction Cost Indexes. In: Topping, B.H.V., and Khan, A.I., Editors, Neural Networks and Combinatorial Optimization in Civil and Structural Engineering, Civil-Comp Press: pp. 47-52.
177. Williams, P.F and Rust, B.R, (1969) The sedimentology of a braided river, Journal of Sedimentary Petrology, 39, 649-79.
178. Wu, X., and Lim, S.Y., (1993), Prediction of Maximum Scour Depth at Spur Dikes with Adaptive Neural Networks. In: Topping, B.H.V., and Khan, A.I., Editors, Neural Networks and Combinatorial Optimization in Civil and Structural Eng., Civil-Comp Press: pp. 61-66.
179. Zadeh, L.A., (1965), Fuzzy Sets, Information and Control, 8: pp. 338-353.
180. Zealand, C. M., Burn D.H. Y and Simonovic S.P., (1999), Short term stream flow forecasting using artificial neural networks. Journal of Hydrology, 214, pp. 32-48.
181. Zhu, M. L. and Fujita, M., (1994), "Comparisons between fuzzy reasoning and neural networks methods to forecast runoff discharge", Journal of Hydroscience, Hydraulic Engineering, 12(2), pp. 131-141.



## PROGRAM -1

```

*****
!* PROGRAM - FOR NORMALISATION OF DATA AT EACH CROSS-SECTION
*****
!
! #Normalisation of observed data into equi-spaced data at desired number
! of points#
!
! x,y = Measured co-ordinates of the cross-section
! xs = Scaled values for interval -1 and 1
! xx, yy = Normalised values of x,y
! m = Number of years for which data are available
! n = Number of locations where x-sections have been measured
! norm = Number of normalised data points for each cross-section
! ninput = Number of points input
! nw = Number of points in interpolating window
! = 2 for linear interpolation
! = 3 for parabolic interpolation
! = 4 for cubic interpolation
*****
!
! use PORTLIB
! dimension x(250),y(250),xx(110,10)
! dimension xs(250),yy(110,10),ny(6)
! data nw/3/
! data ny/1990,1991,1992,1993,1994,1995/
! character*40 head
! character*9 fdat,ndat
! character(9) TODAY
! call date (TODAY)
! write(3,*) TODAY
! write(3,*) DATE()
! write(*,500)
! format(1X,///30X,*** WELCOME TO THE PROGRAM***)
! write(*,'(///)')
! pause 'Press any key to continue'
! write(*,'(///)')
! write(*,510)
! format(T10,'Normalise the measured data into 100&
! equispaced data points')
! write(*,'(///)')
! pause 'Press any key to continue'
! write(*,'(///)')
! write(*,8)
! format(' NAME OF THE OUTPUT FILE IS "ndat"')
! write(*,'(///)')
! *****
! INPUT DATA
! *****
!
! open(unit=1,file='normal.dat')
! read(1,*)m,n,norm
! do 300 ii=2,n
! call fnames(ii,fdat,ndat)

```

```

open(unit=2,file='fdat')
open(unit=3,file='ndat')
read(2,'(a)',end=1000) head
read(2,*) chain
!
write(*,*) head
write(3,7) head
7
format(t10,50a)
do 30 k=1,m
read(2,'(a)',end=1000)head
do 100 i=1,250
j=i
read(2,*,err=2,end=2)x(i),y(i)
write(*,*)x(i),y(i)
100
continue
2
ninput=j-1
!
TRANSFORM TO LIMITS BETWEEN -1 AND +1
x1=x(1)
x2=x(ninput)
tw=x2-x1
do 20 i=1,ninput
20
xs(i)=(2.*x(i)-(x1+x2))/(x2-x1)
!
continue
INTRPOLATE THE POLYNOMIAL AT NORMALIZED VALUES OF X
call interp(ninput,norm,nw,xs,y,tw,k,xx,yy)
backspace 1
30
continue
1000
write(3,*)chain,'(Chainage in Km)'
!
write(*,*)chain
!
write(3,60)(ny(i),i=1,m)
!
write(*,60)(ny(i),i=1,m)
do 50 i=1,norm
!
write(3,70)(xx(i,j),yy(i,j),j=1,m)
!
write(*,70)(xx(i,j),yy(i,j),j=1,m)
50
continue
!300
continue
70
format(f7.1,1x,f10.1,5(1x,f10.1,1x,f10.1))
60
format(3X,'Year ',6(i4,10x))
stop
end
!
*****
!
subroutine interp(ninput,norm,nw,xs,y,tw,k,xx,yy)
*****
!
LAGRANGIAN interpolation using moving window
!
for computing normalised value of x & y
!
!
dimension xs(250),y(250),xx(110,10),yy(110,10)
delx=2./float(norm)
nwm=int(float(nw)/2.+0.999999)
ns=1
ne=ns+nw-1
nwmid=ns+nwm
do 10 l=1,norm

```

```

xxx=-1.0+float(l-1)*delx
c=0.0
if(ne.lt.ninput)then
15  if(xxx.gt.xs(nwmid))then
      ns=ns+1
      ne=ns+nw-1
      nwmid=ns+nwm
      go to 15
    endif
  endif

      do 35 i=ns,ne
        axi=xs(i)
        p=1.0
          do 21 j=ns,ne
            if(i.eq.j)go to 21
            axj=xs(j)
            a=(xxx-axj)/(axi-axj)
            p=p*a
21          continue
          b=p*y(i)
          c=b+c
35        continue
        yy(l,k)=c
        xx(l,k)=(xxx*tw+tw)/2.
10      continue
      return
    end

! *****
!  subroutine fnames(ii,fdat,ndat)
! *****
!  subroutine to generate additional file names
character*15 fdat,ndat
open(unit=10,file='name.fil',status='new')
if(ii.lt.10)then
write(10,25)ii
write(10,26)ii
else
write(10,27)ii
write(10,28)ii
endif
25  format('cs0',i1,'.dat')
26  format('ns0',i1,'.dat')
27  format('cs',i2,'.dat')
28  format('ns',i2,'.dat')
close(unit=10)
open(unit=10,file='name.fil',status='old')
read(10,16)fdat
read(10,16)ndat
16  format(8a)
write(*,*)fdat,ndat
return
end

```

```
*****
|
|               END OF PROGRAM
|
|*****
```

**PROGRAM -2**

```
*****
|
|   * SPATIO-TEMPORAL IDEALISATION OF BRAHMAPUTRA RIVER *
|
|*****
```

```
WRITE(*,5001)
5001  FORMAT(1X,///30X,'W E L C O M E',//35X,'TO',//27X,&
'INTERACTIVE PROGRAM',/,35x,'ON',/, &
9X,'SPATIO-TEMPORAL IDEALISATION OF TYPICAL BANKLINE',&
/,21x,'OF LARGE BRAIDED ALLUVIAL RIVER',///,18X,'THE PROGRAM &
IS USEFUL FOR SIMULATING',//, &
9X,'THE RIVER CROSS-SECTION WITH RESPECT TO SPACE & TIME')
write(*,'(///)')
pause 'Press any key to continue'
write(*,'(///)')
write(*,5003)
5003  format(28x,'TO USE THIS MODEL',//14x,'FIRST NORMALISE THE &
MEASURED DATA INTO 101 EQUISPACED DATA POINTS',//, &
2x,' AND STORE THE SAME IN "nsm.dat" FILES', &
//7x,'THIS HAS TO BE DONE WITH THE HELP OF THE PROGRAM "NORMAL.F"',&
//10x,'USING MEASURED CROSS-SECTIONAL DATA IN FILE "csm.dat"',&
//6x,'THE FILE "nsm.dat" WILL FUNCTION AS DATA FILE FOR THE MODEL')
write(*,'(///)')
pause 'press any key to continue'
write(*,'(///)')
CALL FILE
write(*,8)
8  format(' NAME OF YOUR OUTPUT FILE IS "BANKLINE.OUT"')
write(*,'(///)')
STOP
END
```

```
*****
|
|               subroutine file
|
|*****
```

```
WRITE(*,9)
9  format(' GIVE YOUR OPTION HERE  ')
WRITE(*,'(///)')
WRITE(*,7)
7  format(' YOUR OPTION SHOULD BE  ')
WRITE(*,'(//)')
WRITE(*,5002)
5002  FORMAT(10x,' 1 IF THE CROSS -SECTION IS TO BE GENERATED &
AT',//18x,'SAME LOCATION AS THAT OF MEASUREMENT LOCATION',//29x,' &
(WITH RESPECT TO TIME)',///,13x,'2 IF THE CROSS-SECTION &
IS TO BE GENERATED AT',//,15x,'ANY LOCATION WITHIN THE REACH UNDER &
CONSIDERATION',//26x,'(WITH RESPECT TO SPACE AND TIME)')
write(*,'(///)')
read(*,*)noptn
if(noptn.eq.1)then
call temporal
```

```

        go to 912
        else if(noptn.eq.2)then
        write(*,'(///)')
        write(*,11)
11      format(10x,'Give the number of cross-sections to be used in',&
//,25x,'generating the profile ( 2 to 8)')
        write(*,'(///)')
        read(*,*)nx
        call spatial(noptn,nx)
        if (noptn.eq.1)call temporal
        go to 912
        end if
911     write(*,14)
14     format(10x,'Please exercise your option and run again')
912     return
        end
!
!      *      MAIN SUBROUTINE TEMPORAL
!      subroutine temporal
!
!      *****
!      * MODEL FOR TEMPORAL GENERATION OF RIVER BANK LINE
!      *****
!
!      generation of bankline with respect to time
!      implicit real*8 (a-h,o-z)
!      dimension x(110,10),y(110,10),sft(10)
!      dimension xx(110),yy(110),ny(10)
!      character*50 head
!      character*12 ndat
!
!      nyy =year for which Bankline is required
!      ny  =year in which data has been measured
!      n   =number of normalised data points
!      sft =shape fuction in temporal direction
!      x,y =normalised x&y co-ordinate
!      data n/101/
!      call fname(ndat)
!      open(unit=1,file=ndat)
!      open(unit=2,file='bankline.out')
!      read(1,'(a)')head
!      read(1,*)chain
!      read(1,*)(ny(i),i=1,4)
!      do 10 i=1,n
!      read(1,*)(x(i,j),y(i,j),j=1,4)
10     continue
!      write(*,'(///)')
!      write(*,11)
11     format(10x,'GIVE THE YEAR IN WHICH BANK LINE IS REQUIRED')
!      write(*,'(///)')
!      read(*,*)nyy
!      call sftemp(nyy,ny,sft)
!      write(*,*)(sft(i),i=1,4)
!      computation of coordinates of simulated profile
!      do 105 i=1,n

```

```

        xx(i)=0.
        yy(i)=0.
    do 106 j=1,4
        xx(i)=xx(i)+sft(j)*x(i,j)
        yy(i)=yy(i)+sft(j)*y(i,j)
106   continue
105   continue
    write(2,20)head
20   format(7x,50a)
    write(*,*)head
    write(2,12)chain
12   format(8x,'Brahmaputra =',f8.3)
    write(*,12)chain
    write(2,120)nyy
    write(*,120)nyy
120  format(12x,'YEAR ',i4)
    write(2,13)
13   format(40('*'))
    write(*,13)
    do 122 i=1,n
        write(2,123)xx(i),yy(i)
        write(*,123)xx(i),yy(i)
122  continue
123  format(5x,f9.2,5x,f9.4)
    write(2,14)
    write(*,14)
14   format(40('*'))
    return
    end
!
! *****
! SUBROUTINE FOR COMPUTING VALUES OF SHAPE FUNCTION
! AT DIFFERENT NODES
! *****
!
    subroutine sftemp(nyy,ny,sft)
    implicit real*8 (a-h,o-z)
    dimension ny(10),sft(10)
    do 111 i=1,4
        aa=1.
        anyi=ny(i)
        do 112 j=1,4
            if(i.eq.j)go to 112
            anyj=ny(j)
            a=(nyy-anyj)/(anyi-anyj)
            aa=aa*a
112  continue
        sft(i)=aa
111  continue
!   write(*,*)nyy,(ny(i),i=1,5),(sft(i),i=1,5)
    return
    end
! *****

```



```

!      SUBROUTINE FOR GENERATING NECESSARY FILES
!      *****
      subroutine fname(ndat)
      implicit real*8 (a-h,o-z)
!      subroutine to generate additional file names
      character*12 ndat
      open(unit=10,file='names.fil')
      write(*,'(///)')
      write(*,30)
30     format(8x,'GIVE FILE No. >>',//)
      write(*,31)
31     format(10x,'SUCH AS 06 or 20 etc.')
      write(*,'(///)')
      read(*,*)ncross
      if(ncross.lt.10)then
      write(10,15)ncross
      else
      write(10,17)ncross
      end if
15     format('ns0',i1,'.dat')
17     format('ns',i2,'.dat')
      close(unit=10)
      open(unit=10,file='names.fil',status='old')
      read(10,16)ndat
16     format(8a)
      write(*,*)ndat
      return
      end
!*****
!      MAIN SUBROUTINE SPATIAL
      subroutine spatial(noptn,nx)
!*****
!      * SPATIO-TEMPORAL GENERATION OF RIVER CROSS-SECTION *
!      *****
!      PROGRAM FOR GENERATING bank line (SPATIAL GENERATION)
!      xchain= chainage in km at which cross-section is to be
!      generated
!      n      = number of normalised data points
!      sfs    = shape function in spatial direction
!      sft    = shape function in temporal direction
!      along  = chainage in km at which observed data are available
!      x & y  = normalised co-ordinates of measured cross-section
!      year   = year in which banklines were measured
!      xx&yy = computed co-ordinates of simulated profile
!      *****
      implicit real*8 (a-h,o-z)
      dimension along(65),x(10,110,10),y(10,110,10),xx(110),yy(110)
      dimension nyear(10,10),chain(10),sfs(10),sft(10),xi(110,10),&
      yi(110,10)
      CHARACTER*50 head
      CHARACTER*12 ndat1,ndat2,ndat3,ndat4,ndat5,ndat6,ndat7,ndat8
      DATA n/101/

```

```

DATA along/0.,17.34,28.05,38.25,46.92,56.61,66.30,73.44,82.62, &
92.82,100.98,109.65,119.85,128.01,137.70,146.37,156.06,167.28, &
175.95,182.58,189.21,197.37,206.55,213.18,218.79,224.91,234.60,&
241.23,251.95,262.15,272.35,284.08,296.83,310.10,325.91,341.21,&
352.94,365.18,371.81,383.03,389.66,398.33,412.09,423.31,439.63,&
453.91,465.13,474.82,483.49,490.63,498.80,505.94,513.08,522.77,&
531.95,541.13,558.98,570.20,579.38,589.07,601.82,613.04,626.30,&
634.46,640.07/
write(*,'(////)')
write(*,40)
40 format(10x,'CHAINAGE AT WHICH CS IS TO BE GENERATED',&
//,28x,'CHAINAGE IN KM. ')
write(*,'(////)')
read(*,*)xchain

! co-relating chainage with cross-section number

do 200 i=1,75
if(xchain.gt.along(i))then
if(xchain.lt.along(i+1))go to 202
else
if(xchain.eq.along(i))then
noptn=1
return
endif
endif
200 continue
202 nfile=i

! identification of cross-sections which are on the
! upstream side and on the downstream side of the
! given chainage

call filgen(nfile,nx,ndat1,ndat2,ndat3,ndat4,ndat5,ndat6,&
ndat7,ndat8)
open(unit=21,file=ndat1)
open(unit=22,file=ndat2)
open(unit=23,file=ndat3)
open(unit=24,file=ndat4)
open(unit=25,file=ndat5)
open(unit=26,file=ndat6)
open(unit=27,file=ndat7)
open(unit=28,file=ndat8)
open(unit=7,file='bankline.out')

! data reading from different files

do 205 nr=1,nx
nread=20+nr
read(nread,'(a)')head
read(nread,*)chain(nr)
read(nread,*)(nyear(nr,j),j=1,4)

```

```

do 206 i=1,n
read(nread,*)(x(nr,i,j),y(nr,i,j),j=1,4)
206 continue
205 continue
call sfspace(xchain,chain,nx,sfs)
! write(*,*)(sfs(i),i=1,nx)
! interpolation of co-ordinates in spatial direction

do 211 j=1,4
do 210 i=1,n
xi(i,j)=0.
yi(i,j)=0.
do 212 k=1,nx
xi(i,j)=xi(i,j)+sfs(k)*x(k,i,j)
yi(i,j)=yi(i,j)+sfs(k)*y(k,i,j)
212 continue
210 continue
211 continue
write(*,'(////)')
write(*,42)
42 format(10x,'YEAR FOR WHICH BANK LINE IS TO BE GENERATED >>')
write(*,'(////)')
read(*,*)myear
call shape(myear,nyear,sft)
! write(*,*)(sft(i),i=1,5)
! interpolation of co-ordinates in temporal direction
do 218 i=1,n
xx(i)=0.
yy(i)=0.
do 219 j=1,4
xx(i)=xx(i)+sft(j)*xi(i,j)
yy(i)=yy(i)+sft(j)*yi(i,j)
219 continue
218 continue
write(7,43)
write(*,43)
43 format(7x,'GENERATED BANKLINE ')
write(7,44)xchain
44 format(9x,'PROFILE=',f8.3)
write(*,44)xchain
write(7,120)myear
write(*,120)myear
120 format(12x,'YEAR ',i4)
write(7,45)
write(*,45)
45 format(40('*'))
do 122 i=1,n
write(7,123)xx(i),yy(i)
write(*,123)xx(i),yy(i)
122 continue
123 format(5x,f9.2,5x,f8.3)
write(7,46)

```

```

46  write(*,46)
    format(40('='))
    return
    end

! *****
! SUBROUTINE FOR COMPUTING VALUES OF SHAPE FUNCTION
!   AT DIFFERENT NODES IN SPATIAL DIRECTION
! *****
subroutine sfspace(xchain,chain,nx,sfs)
implicit real*8 (a-h,o-z)
dimension chain(10),sfs(10)
do 207 i=1,nx
aa=1.
chaini=chain(i)
do 208 j=1,nx
if(i.eq.j)go to 208
chainj=chain(j)
a=(xchain-chainj)/(chaini-chainj)
aa=aa*a
208  continue
sfs(i)=aa
207  continue
return
end

! *****
! SUBROUTINE FOR COMPUTING VALUES OF SHAPE FUNCTION
!   AT DIFFERENT NODES IN TEMPORAL DIRECTION
! *****
subroutine shape(myear,nyear,sft)
implicit real*8 (a-h,o-z)
dimension nyear(10,10),sft(10)
do 111 i=1,4
aa=1.
anyi=nyear(1,i)
do 112 j=1,4
if(i.eq.j)go to 112
anyj=nyear(1,j)
a=(myear-anyj)/(anyi-anyj)
aa=aa*a
112  continue
sft(i)=aa
111  continue
return
end

! *****
! SUBROUTINE TO GENERATE ADDITIONAL FILE NAMES
! *****
subroutine filgen(nfile,nx,ndat1,ndat2,ndat3,ndat4,ndat5,&
ndat6,ndat7,ndat8)
implicit real*8 (a-h,o-z)
CHARACTER*12 ndat1,ndat2,ndat3,ndat4,ndat5,ndat6,ndat7,ndat8

```

```

open(unit=13,file='name.fil')
nxx=nx/2+1
if(nfile.lt.nxx) go to 56
go to 57
56 nfile=nxx
go to 61
57 nxy=nx/2
nyy=65-nxy
if(nfile.gt.nyy) go to 59
go to 61
59 nfile=nyy
61 i1bf=nfile
i1af=nfile+1
i2af=nfile+2
i2bf=nfile-1
i3af=nfile+3
i3bf=nfile-2
i4af=nfile+4
i4bf=nfile-3
if(i1bf.lt.10)then
    write(13,28)i1bf
else
    write(13,27)i1bf
endif
if(i1af.lt.10)then
    write(13,28)i1af
else
    write(13,27)i1af
endif
if(i2af.lt.10)then
    write(13,28)i2af
else
    write(13,27)i2af
endif
if(i2bf.lt.10)then
    write(13,28)i2bf
else
    write(13,27)i2bf
endif
if(i3af.lt.10)then
    write(13,28)i3af
else
    write(13,27)i3af
endif
if(i3bf.lt.10)then
    write(13,28)i3bf
else
    write(13,27)i3bf
endif
if(i4af.lt.10)then
    write(13,28)i4af
else

```

```

                write(13,27)i4af
endif
if(i4bf.lt.10)then
                write(13,28)i4bf
            else
                write(13,27)i4bf
endif
27  format('ns',i2,'.dat')
28  format('ns0',i1,'.dat')
    close(unit=13)
    open(unit=13,file='name.fil',status='old')
    read(13,29)ndat1
    read(13,29)ndat2
    read(13,29)ndat3
    read(13,29)ndat4
    read(13,29)ndat5
    read(13,29)ndat6
    read(13,29)ndat7
    read(13,29)ndat8
29  format(8a)
    write(*,*)ndat1,ndat2,ndat3,ndat4,ndat5,ndat6,ndat7,ndat8
    return
end

```

```

*****
!           END OF PROGRAM
*****

```

### PROGRAM -3

```

*****
!
!   Computation of sediment load by Ackers and White model
!   d50=particle size of which 50% is finer in meter
!   sg=specific gravity of sediment particle
!   g=acceleration due to gravity in meter/sec. /sec.
!   v=mean flow velocity in meter/sec.
!   d=depth of flow in meter
!   visc=kinematic viscosity in square meter/sec. .
!   s=water surface slope
!   vstar=shear velocity in meter/sec
!   dgr=dimensionless particle size
!   n=number of observation
!   a=value of f at nominal initial motion
!   am=exponent in sediment transport function
!   c=coeff. in sediment transport function
!   fgr=sediment mobility number
!   ggr=dimensionless sediment transport rate
!   x=sediment transport concentration by volume ppm
!   an=transition exponent depending on sediment size
!   q=water discharge in cubic meter/sec.
!   Ct=sediment Conc.in ppm.
!   xtt=Total sediment transport in tons/day
*****

```

```

program Ackers_White
dimension s(100),v(100),d50(100),xt(100),q(100),d(100),&
dgr(100),vstar(100),c1(100),c2(100),c3(100),c4(100),fgr(100),&
Ct(100),xxt(100),ggr1(100),ggr(100)
write(*,1)
1 write(*,1)
format(1x, //30x, '** Welcome to the Program**')
write(*, '(//)')
pause '                                press enter to continue'
write(*, '(//)')
write(*, 2)
2 format(t31, 'ACKERS AND WHITE SEDIMENT PREDICTOR METHOD')
write(*, '(//)')
pause '                                press enter to continue'
write(*, '(//)')
write(*, 3)
3 format(' Name of the output file is "acw.out"')
write(*, '(//)')

open(unit=1, file='acw.dat')
open(unit=2, file='acw.out')

!*****
! Data Input
!*****
Read(1,*) n
do 10 i=1,n
10 read(1,*)d(i),s(i),d50(i),q(i),v(i)
continue
g=9.81
sg=2.65
visc=0.909*10.0**(-6)
raww=1000.0
gamaw=9810.0
gamas=25996.50
do 20 i=1,n

vstar(i)=sqrt(g*d(i)*s(i))
dgr(i)=d50(i)*(g*1.65/visc**2)**(1./3.)

if((dgr(i) .le. 60.0) .and. (dgr(i) .gt. 1.0))then
c1(i)=1.0-0.56*log10(dgr(i))
c3(i)=0.23/sqrt(dgr(i))+0.14
c4(i)=9.66/dgr(i)+1.34
c2(i)=10.0**(2.86*log10(dgr(i))-(alog10(dgr(i))))**2-3.53)
else
c1(i)=0.0
c3(i)=0.17
c4(i)=1.50
c2(i)=0.025
endif
! fgr(i)=vstar(i)**an(i)*(v(i)/(32.*alog10(10.0*d(i)/&
fgr(i)=vstar(i)*(v(i)/(sqrt(32.*alog10(10.0*d(i)/d50(i))))))**&
(1.-c1(i))/sqrt(g*d50(i)*1.65)

```

```

!      ggr=c*(fgr/(a-1.))**am
      ggr1(i)=c2(i)*(fgr(i)/c3(i)-1.0)
      if (ggr1(i) .le. 0.)then
        ggr(i)=(-ggr1(i))**c4(i)
      else
        ggr(i)=ggr1(i)**c4(i)
      endif
      Ct(i)=ggr(i)*sg*d50(i)*(v(i)/vstar(i))**c1(i)/d(i)
      xt(i)=Ct(i)*10.0**(6)
!      xt(i)=Ct(i)*q(i)
      xtt(i)=2.65*g*86400.0*xt(i)*q(i)
20     continue
      write(2,400)
      write(2,*)'Sediment Discharge by Ackers and White Method'
      write(2,400)
400    format(1x,70('='))
      write(2,410)
      write(2,*)'INPUT DATA'
      write(2,410)
410    format(1x,70('='))
      write(2,420)
420    format(/1x,70('='))
      do 25 i=1,n
25     write(2,26)d(i),s(i),d50(i),q(i),v(i)
26     format(1x,3(f10.2,1x),1x,f10.2,1x,f8.3)
      write(2,430)
430    format(/1x,70('='))
      write(2,*)' Shear      Sediment  Discharge  Sediment'
      write(2,*)' Velocity  Mobility  in         transport'
      write(2,*)'(m2/sec)  Number   (m3/s)    (t/day)'
      write(2,430)
      do 30 i=1,n
30     write(2,31)vstar(i),fgr(i),q(i),xtt(i)
      continue
31     format(f8.2,1x,f10.4,3x,f10.2,3x,f10.1)
      write(2,430)
      close(1)
      close(2)
      stop
      end

```

#### PROGRAM - 4

```

!*****
!*  Programme for sediment discharge by Engelund and Hansen,s approach
!*  r(i)      =hydraulic radius in meter
!*  s(i)      =water surface slope
!*  d50(i)    =particle size in meter
!*  v(i)      =mean flow velocity in meter/sec.
!*  t0(i)     =initial shear stress in newton/meter/meter
!*  tstar(i)  =correction coefficient
!*  f(i)      =grain friction factor
!*  phit(i)   =total load parameter
!*  sqt(i)    =total load transport rate in newton/meter/meter

```



```

!* t=width of the flow
!* ss =specific gravity of particle
!* qtt =Total sediment load in tons/day
|*****
program Eng_Hansen
  dimension r(100),s(100),d50(100),v(100),t(100),qt(100),to(100), &
    tstar(100),f(100),phit(100),sqt(100),qtt(100)
    write(*,1)
1   format(1x, //30x, '*** Welcome to the Program***')
    write(*, '(//)')
    pause '          press enter to continue'
    write(*, '(//)')
    write(*, 2)
2   format(t31, 'ENGELUND & HANSEN SEDIMENT PREDICTOR METHOD')
    write(*, '(//)')
    pause '          press enter to continue'
    write(*, '(//)')
    write(*, 3)
3   format(' Name of the output file is "eng.out"')
    write(*, '(//)')

    open(unit=1, file='eng.dat')
    open(unit=2, file='eng.out')

|*****
!   DATA INPUT
|*****
    read(1,*)n
    do 100 i=1,n
      read(1,*)r(i),s(i),d50(i),v(i),t(i)
100  continue

      g=9.81
      !   pnu=0.909*10.0**(-6)
      gamaw=9810.0
      gamas=25996.50
      ss=2.65

      write(2,200)
      write(2,*)'***Sediment Discharge by Engelund & Hansen Method***'
      write(2,200)
200  format(1x,70('-'))
      do 300 i=1,n
        to(i)=gamaw*r(i)*s(i)
        tstar(i)=to(i)/((gamas-gamaw)*d50(i))
        f(i)=2.0*g*s(i)*r(i)/v(i)**2
        phit(i)=0.1*tstar(i)**2.5/f(i)
        sqt(i)=phit(i)*gamas*sqrt((ss-1.0)*g*(d50(i)**3))
        qt(i)=sqt(i)*t(i)
        qtt(i)=qtt(i)*86400.0/9810.0
300  continue
      write(2,400)
      write(2,*)'INPUT DATA'
      write(2,400)

```

```

400      format(1x,70('*'))
do 500 i=1,n
500  write(2,*)r(i),s(i),d50(i),v(i)
      write(2,530)
530      format(/1x,70('='))
      write(2,*)'Initial Correction Grain fric. Total load Total-load&
      total load'
      write(2,*)'shr.strs. coefficient factor parameter transport &
      in Tons/day'
      write(2,*)'(N/m2)          rate

      write(2,530)
      do 600 i=1,n
      write(2,601)t(i),tstar(i),f(i),phit(i),sqt(i),qtt(i)
600  continue
601  format(2x,3(f8.4,1x),5x,f8.4,3x,f10.2,5x,f12.1)
      write(2,530)
      close(1)
      close(2)
      stop
end
|*****
!      End of file
|*****

```

#### PROGRAM -5

```

|*****
!      Sediment load calculation by P.K Swamee et.al model
!      v(i)=mean flow velocity in meter/sec.;
!      d65(i)=grain size of which 65% is finer
!      s(i)=water surface slope;
!      ss=specific gravity of sediment;
!      g=acceleration due to gravity;
!      t(i)=top width of the water surface;
!      r1(i)=grain hydraulic radius;
!      tstrl(i)=grain shear stress;
!      phib(i)=sediment factor for bed load;
!      sqb(i)=bed load transport rate in cubic meter/sec./meter;
!      qb(i)=bed load transport rate in cubic meter/sec.;
!      phis(i)=sediment factor for suspended load;
!      sqs(i)=suspended load transport rate in cubic meter/sec./meter;
!      qs(i)=suspended load transport rate in cubic meter/sec.;
|*****

      program PKS_Ojha
      dimension s(100),t(100),v(100),d65(100),r1(100),sqb(100),phib(100),&
      qb(100),qs(100),qt(100),t1(100),phis(100),sqs(100),qtpd(100)
      write(*,1)
1      format(1x,//30x,'** W e l c o m e **')
      write(*,'(//)')
      pause 'press enter to continue'
      write(*,'(//)')
      write(*,2)

```

```

2      format(t31,'PKSWAMEE & OJHA SEDIMENT PREDICTOR METHOD')
      write(*,'(/)')
      pause 'press enter to continue'
      write(*,'(//)')
          write(*,3)
3      format(' Name of the output file is "pks.out"')
      write(*,'(//)')
          open(unit=1, file='pks.dat')
          open(unit=2, file='pks.out')
|*****|
|      Data Input
|*****|
      Read(1,*) n
          do 10 i=1,n
10         read(1,*)t(i),s(i),d65(i),v(i)
          continue
          write(2,400)
          write(2,*)'INPUT DATA'
          write(2,400)
400         format(1x,70('*'))
          do 500 i=1,n
500         write(2,*)t(i),s(i),d65(i),v(i)
          write(2,530)
530         format(/1x,70('='))
          g=9.81
          ss=2.65
          raww=1000.0
          gamaw=9810.0
          gamas=25996.50
          do 20 i=1,n
              r1(i)=((v(i)*d65(i)**(1.0/6.0))/(24.0*sqrt(s(i))))**1.5
              t1(i)=r1(i)*s(i)/((ss-1.0)*d65(i))
                  phib(i)=((0.0947/t1(i))**9+(0.355/t1(i))**1.6)**(-1.)
                  sqb(i)=phib(i)*d65(i)*sqrt((ss-1.0)*g*d65(i))
                  qb(i)=sqb(i)*t(i)
                  phis(i)=((0.567/t1(i))**6+(0.547/t1(i))**3)**(-1.)
                  sqs(i)=phis(i)*d65(i)*sqrt((ss-1.0)*g*d65(i))
                  qs(i)=sqs(i)*t(i)
                  qt(i)=qb(i)+qs(i)
                  qtpd(i)=qt(i)*86400.0*gamas/1000.0
20         continue
          write(2,*)'total   SuspendedBed load Sed factor Sed factor Tot load'
          write(2,*)'sed.load sediment Bed laod susp. laod T/day'
          write(2,*)'(m3/s) (m3/s) '
          do 30 i=1,n
30         write(2,525)qt(i),qs(i),qb(i),phib(i),phis(i),qtpd(i)
525         format(f10.3,3x,f8.2,1x,f8.3,1x,f10.4,3x,f8.2,2x,f10.0)
          write(2,540)
540         format(/1x,70('='))
          write(2,540)
          close(1)
          close(2)

```

stop  
end

```
*****  
!*      End of File  
*****
```

## PROGRAM -6

```
*****  
! Programme for computation of sediment discharge by Yang 1973,1979  
! n      =number of observations  
! d50(i) =particle size in meter  
! visc   =kinetic viscosity in m2/sec.  
! v(i)   =mean flow in meter/sec.  
! s(i)   =water surface slope  
! d(i)   =mean depth of flow in meter  
! g      =acceleration due to gravity in meter/sec/sec  
! gamas  =specific weight of particle in newton/cubic meter  
! gamaw  =specific weight of water in newton/cubic meter  
! raw    =density of water in kg/cubic meter  
! re(i)  =fall velocity Reynolds number  
! w(i)   =terminal fall velocity of the particle in meter/sec.  
! ustar(i) =avg. shear velocity in meter/sec.  
! vcr    =critical average water velocity at incipient motion in meter/sec  
! vcr/w(i) =v1(i)=the dimensionless critical velocity  
! ct(i)  =total sediment concentration in ppm  
! are    =assumed Reynold number  
! cre(i) =computed Reynold number  
! q(i)   =water discharge;  
! ct73m  =total sed.dis. in cubic meter/sec  
! ct79m  =total sed. dis. in cubic meter/sec.;  
*****  
program yang_sediment  
dimension d50(100),v(100),s(100),d(100), re(100),&  
w(100),ustar(100),u1(100),v1(100),cd(100),cre(100),diff(100),&  
ct73(100),ct79(100),alct73(100),alct79(100),q(100),ct73m(100),&  
ct79m(100),tpd73(100), tpd79(100)  
1      write(*,1)  
      format(1x,//30x,'** Welcome to the Program**')  
      write(*,'(//)')  
      pause '                          Press enter to continue'  
      write(*,'(//)')  
2      write(*,2)  
      format(t31,'YANG-73 & YANG-79 SEDIMENT PREDICTOR METHOD')  
      write(*,'(/)')  
      pause '                          Press enter to continue'  
      write(*,'(//)')  
3      write(*,3)  
      format(' Name of the output file is "yang.out"')  
      write(*,'(//)')  
      open(unit=1,file='yang.dat')  
      open(unit=2,file='yang.out')
```

! Input data

!\*\*\*\*\*

```
g=9.81
pnu=1.00*10.0**(-6)
gamaw=9810.0
gamas=25996.50
raww=1000.0
ss=2.65
visc=pnu*raww

read(1,*)n
do 10 i=1,n
10 read(1,*)q(i), d(i),v(i),s(i),d50(i)
    are=0.1
    write(2,21)
    write(2,*)'A. INPUT DATA'
    write(2,21)
21     format(1x,70('='))
    do 22 i=1,n
22     write(2,*)d50(i),v(i),s(i),d(i),q(i)
    do 15 i=1,n
15     re(i)=are
        i=1
20 cd(i)=24.0/re(i)+3.0/sqrt(re(i))+0.34
    write(2,*)re(i),cd(i),are

        w(i)=sqrt(4.0/(3.0*cd(i)*raww)*(gamas-gamaw)*d50(i))
        cre(i)=w(i)*d50(i)/pnu
        diff(i)=abs(re(i)-cre(i))
        if(diff(i).gt.0.0001)then
            re(i)=cre(i)
            go to 20
        else
            if(cre(i).lt.0.7)then
                w(i)=(gamas-gamaw)*d50(i)**2/(18.*visc)
            endif
            i=i+1
            if(i.le.n)go to 20
        endif
        do 25 i=1,n
            ustar(i)=sqrt(g*d(i)*s(i))
            u1(i)=ustar(i)*d50(i)/pnu
            if(u1(i) .gt. 1.2 .and. u1(i) .lt. 70.0)then
                v1(i)=0.66+2.5/(alog10(u1(i))-0.06)
            else
                v1(i)=2.05
            endif
25         continue
        do 40 i=1,n
            alct73(i)=5.435-0.286*alog10(w(i)*d50(i)/visc)-0.457*&
                alog10(ustar(i)/w(i))+(1.799-0.409*(w(i)*d50(i)/visc)&
                -0.314*alog10(ustar(i)/w(i)))*alog10(v(i)*s(i)/w(i)-v1(i)*s(i))
30         ct73(i)=10.0**alct73(i)
```

```

ct73m(i)=3.774e-07*q(i)*ct73(i)

alct79(i)=5.165-0.153*log10(w(i)*d50(i)/visc)-0.297* &
alog10(ustar(i)/w(i))+(1.780-0.36*(w(i)*d50(i)/visc)&
-0.486*log10(ustar(i)/w(i)))*alog10(v(i)*s(i)/w(i))
35 ct79(i)=10.0**alct79(i)
ct79m(i)=3.774e-07*q(i)*ct79(i)
tpd73(i)=ct73(i)*86400.0*2650.0*10.0e-06
tpd79(i)=ct79(i)*86400.0*2650.0*10.0e-06

40 continue

write(2,400)
write(2,*)'B. Sediment Discharge by Yang73 and Yang79 Method'
write(2,400)
400 format(1x,70('='))
write(2,430)
430 format(/1x,70('='))
write(2,*)'C/S ct73(i) ct73m(i) ct79(i), ct79m(i),tpd73(i),tpd79(i)'
write(2,431)
431 format(/1x,70('='))
do 445 i=1,n
write(2,440)(i+1),ct73(i),ct73m(i),ct79(i),ct79m(i),tpd73(i),tpd79(i)
440 format(i2,f8.2,2x,f6.2,f8.2,f8.2,2x,2f12.0)
445 continue
close(1)
close(2)
stop
end

|*****
! END OF PROGRAM
|*****

PROGRAM. 7
! COMPUTATION of GEOMETRY OF A RIVER CROSS SECTION
! Area =Area of Cross section
! Perim=Wetted perimeter
! R=hyd radius
! d=depth of flow in meter
! x= Abscissa co-ordinate along a C/S
! y= y ordinate along a C/S
|*****

use portlib
Dimension x(250),y(250),daa(250),dpp(250)
character(9) TODAY
call date (TODAY)
open(unit=1,file='data.dat')
open(unit=2,file='data.out')

write(2,*) TODAY
write(*,1)
1 format(1x,//30x,'** Welcome to the Program**')

```

```

write(*,'(//)')
    pause '                                press enter to continue'
    write(*,'(//)')
    write(*,2)
2    format(t31,'GEOMETRY OF A RIVER CROSS SECTION')
    write(*,'(//)')
    pause '                                press enter to continue'
    write(*,'(//)')
        write(*,3)
3    format(' Name of the output file is "data.out"')
    write(*,'(//)')
        write(2,50)
40    format(/8x,'OUTPUT'/8x,5('~*~')/)
write(2,50)
50    format(/1x,70('='))
    write(2,*)' Area of CS Wetted          Hyd Radius '
    write(2,*)' Cross Section Perimeter '
    write(2,*)'(m2) (meter) (meter)'
    write(2,50)
    area=0.0
    perim=0.0
!*****
! Data Input
!*****
    Read(1,*) n,wl
    do 10 i=1,n
        read(1,*)x(i)
10    continue
    do 11 i=1,n
        read(1,*)y(i)
11    continue
!*****
! Logic Formation
!*****
    nm1=n-1
do 30 i=1,nm1
    if(y(i+1).ge.wl.and.y(i).ge.wl) go to 30
    if(y(i+1).lt.wl.and.y(i).gt.wl)then
        x(i)=x(i)+(x(i+1)-x(i))/(y(i+1)-y(i))*(wl-y(i))
        y(i)=wl
    endif
    if(y(i+1).gt.wl.and.y(i).lt.wl)then
        x(i+1)=x(i)+(x(i+1)-x(i))/(y(i+1)-y(i))*(wl-y(i))
        y(i+1)=wl
    endif
    da=abs(2.0*wl-y(i+1)-y(i))/2.0
    daa(i)=da*(x(i+1)-x(i))
    dpp(i)=sqrt((x(i+1)-x(i))**2+(y(i+1)-y(i))**2)
    Area=area+daa(i)
    Perim=perim+dpp(i)
30    continue
    Radius=Area/perim

```

```

Write(2,60) Area, Perim, Radius
60 format(4x,f10.2,2x,f12.3,2x,f8.2)
close(1)
close(2)
stop
end

```

```

|*****
!      End of Program
|*****

```

### PROGRAM 8

```

% PROGRAM FOR ANN SIMULATION FOR THE BRAHMAPUTRA RIVER
% ANY NO.OF INPUT PATTERN WITH INPUT LAYER,
% HIDDEN LAYER AND OUTPUT LAYER
% *****TRAINING*****

```

```

clc
clear all
close all

```

```

j = 1;
k = 2;
disp('PROGRAMME FOR ANN SIMULATION FOR THE BRAHMAPUTRA')
disp('*****')
disp('The date is')
disp(date)
disp('-*-*-*-*-*-*-*-*-*-*-*-*-*-*-*-*')
m = input('How many inputs in the input layer:');
n = input('How many neurons in the hidden layer:');
r = input('How many neurons in the output layer:');
it = input('Number of iterations to be performed:');
patt= importdata('training.txt'); % Importing training file
No_pat = size(patt,1);
pl1 = patt(:,1);
pl3= patt(:,2);
pl4 = patt(:,3);
pl6 = patt(:,4);
pl7 = patt(:,5);
pl8 = patt(:,6);
% Normalisation
IP=[pl1';pl3';pl4';pl6';pl7';pl8'];
xmax=max(IP);
xxmax=max(xmax);
X=IP/xxmax;

upst=patt(:,7);
mmax=max(upst);
upst1=upst/mmax;
TD=[upst1'];

alpha = 1.0;
for h = 1:m
    for p = 1:n

```



```

        eta(h,p,j)= .4;
    end
end

for p = 1:n
    for q = 1:r
        eta(p,q,k)= .4;
    end
end

XX=2*rand(m,n)-1;
YY=2*rand(n,r)-1;

for h = 1:m
    for p = 1:n
        wh(h,p)= XX(h,p);
    end
end

for p = 1:n
    for q = 1:r
        wo(p,q)= YY(p,q);
    end
end

sse_goal=1e-5;

% MAIN PROGRAMME
title('GRAPH FOR ERROR IN ANN');
xlabel('no of iterations');
ylabel('sum sq.error');
hold on;

for No_it = 1:it

    for i = 1:No_pat

        for q = 1:r
            T(q) = TD(q,i);
        end

        for h = 1:m
            x(h,i) = X(h,i);
        end

        for p = 1:n
            l1 = 0.0;
            for h = 1:m
                l1 = l1 + (wh(h,p)*x(h,i));
            end
            l(p,j) = l1;
            phi(p,j) = 1.0/(1.0+exp(-alpa*l(p,j)));
        end
    end
end

```

```

end

for q = 1:r
    l1 = 0.0;
    for p = 1:n
        l1 = l1+(wo(p,q)*phi(p,j));
    end
    l(q,k) = l1;
    phi(q,k) = 1.0/(1.0+exp(-alpha*l(q,k)));
end

for q = 1:r
    e(q) = (T(q)-phi(q,k))^2;
end

for q = 1:r
    for p = 1:n
        deltaw(p,q,k) = eta(p,q,k)*(2*(T(q)-phi(q,k)))*(alpha*phi(q,k)*(1-phi(q,k)))*phi(p,j);
        wo(p,q) = wo(p,q) + deltaw(p,q,k);
    end
end
for p = 1:n
    for h = 1:m
        dwhpj = 0.0;
        for q = 1:r
            dwhpj = dwhpj + (eta(h,p,j)*(2*(T(q)-phi(q,k)))*(alpha*phi(q,k)*(1-phi(q,k)))*wo(p,q)*(alpha*phi(p,j)*(1-phi(p,j)))*x(h,i));
        end
        deltaw(h,p,j) = dwhpj;

        wh(h,p) = wh(h,p)+deltaw(h,p,j);
    end
end

for q = 1:r          %Global error matrix formation
    E(q,i) = e(q);
end

for q = 1:r          %Global weight between hidden & output layer

    for p = 1:n
        Wk(p,q,i) = wo(p,q);
    end
end

for p = 1:n          %Global weight between input & hidden layer

    for h = 1:m
        Wj(h,p,i) = wh(h,p);
    end
end

```

```

end
ep=sum(e(q));
end

    sse(No_it)=sum(sum(ep));
    if (sse(No_it)<sse_goal)
    break;
    end

plot(No_it,sse(No_it),'g*-');

end

disp('Error(row indicates No. of output & column indicates No. of patterns');
E(1:r,1:No_pat)
disp('Weight vector (column wise) matrix between input layer & hidden layer');
Wj(1:m,1:n,1:No_pat)
disp('Weight vector matrix between hidden layer & output layer');
Wk(1:n,1:r,1:No_pat)

fp2 = fopen('out1.txt', 'w+');
for h = 1:m
    for p = 1:n
        fprintf(fp2,'%f ',Wj(h,p,No_pat));
    end
    fprintf(fp2, '\n');
end
fclose(fp2);
fp3 = fopen('out2.txt', 'w+');
for p = 1:n
    for q = 1:r
        fprintf(fp3,'%f', Wk(p,q,No_pat));
    end
    fprintf(fp3, '\n');
end
fclose(fp3);

disp('Training is over');

WIH=Wj(:, :, No_pat);
WHO=Wk(:, :, No_pat);

disp('Trained outputs of Target values of the Network');

disp('----Target----- OUTPUT OF NNET-----');

for i=1:No_pat

    for p = 1:n
        for h = 1:m
            x1(h,i) = X(h,i);
            l1 = 0.0;

```

```

    l1 = l1 + (WIH(h,p)*x1(h,i));
    end
    l(p,j) = l1;
    phi(p,j) = 1.0/(1.0+exp(-alpha*l(p,j)));
    end

for q = 1:r          %Output calculation of the phi & l for the output layer
    l1 = 0.0;
    for p = 1:n
        l1 = l1+(phi(p,j)*WHO(p,q));
    end
    l(q,k) = l1;
    phi(q,k) = 1.0/(1.0+exp(-alpha*l(q,k)));
end

for q = 1:r
    y(i) = phi(q,k)*mmax;

end
end

[upst,y']

% End of the programme

PROGRAM. -8
% PROGRAMME FOR ANN SIMULATION FOR THE BRAHMAPUTRA RIVER
% ANY NO.OF INPUT PATTERN WITH INPUT LAYER,
% HIDDEN LAYER AND OUTPUT LAYER
% *****TESTING*****
clc
clear all
close all

j=1;
k=2;

W = importdata('testing.txt'); % IMPORTING TESTING FILE
vd1 = W(:,1);
vd2 = W(:,2);
vd3 = W(:,3);
vd4 = W(:,4);
vd5 = W(:,5);
vd6 = W(:,6);

fm=[vd1';vd2';vd3';vd4';vd5';vd6'];
maxcycle = size(fm,2);
opmax=max(fm);

Wh = importdata('out1.txt');
Wo = importdata('out2.txt');
m =size(Wh,1);

```

```

n =size(Wh,2);
r =size(Wo,2);

X=fm/oppmax;
alpa=1.0;

disp('Training is over');

for b = 1:maxcycle

    for h = 1:m
        x1(b,h) = X(h,b);
    end

    for p = 1:n          %Output calculation of the phi & I for hidden layer
        I = 0.0;
        for h = 1:m
            I = I + (x1(b,h)*Wh(h,p));
        end
        I(p) = I;
        phi(p) = 1.0/(1.0+exp(-alpa*I(p)));
    end
    for q = 1:r          %Output calculation of the phi & I for the output layer
        II = 0.0;
        for p = 1:n
            II = II+(phi(p)*Wo(p,q));
        end
        II(q) = II;
        phii(q) = 1.0/(1.0+exp(-alpa*II(q)));
        y1(b) = phii(q)*op1max;
    end
end %end of b

A=[y1']
% END OF PROGRAMME

% PROGRAM FOR ANN SIMULATION FOR THE BRAHMAPUTRA RIVER
% ANY NO.OF INPUT PATTERN WITH INPUT LAYER,
% HIDDEN LAYER AND OUTPUT LAYER
% *****VALIDATION*****

clc
clear all
close all

j=1;
k=2;

W = importdata('validation.txt'); % IMPORTING VALIDATION FILE
vd1 = W(:,1);
vd2 = W(:,2);
vd3 = W(:,3);
vd4 = W(:,4);
vd5 = W(:,5);

```

```

vd6 = W(:,6);
vd7 = W(:,7);
fm=[vd1';vd2';vd3';vd4';vd5';vd6'];
maxcycle = size(fm,2);
opmax=max(fm);
oppmax=max(opmax);
op1max=max(vd7);
Wh = importdata('out1.txt');
Wo = importdata('out2.txt');
m =size(Wh,1);
n =size(Wh,2);
r =size(Wo,2);
X=fm/oppmax;
alpa=1.0;
disp('Training is over');
for b = 1:maxcycle
    for h = 1:m
        x1(b,h) = X(h,b);
    end
    for p = 1:n          %Output calculation of the phi & I for hidden layer
        I = 0.0;
        for h = 1:m
            I = I + (x1(b,h)*Wh(h,p));
        end
        I(p) = I;
        phi(p) = 1.0/(1.0+exp(-alpa*I(p)));
    end
    for q = 1:r          %Output calculation of the phi & I for the output layer
        II = 0.0;
        for p = 1:n
            II = II+(phi(p)*Wo(p,q));
        end
        II(q) = II;
        phii(q) = 1.0/(1.0+exp(-alpa*II(q)));
        y1(b) = phii(q)*op1max;
    end
end %end of b
A=[vd7,y1']
ssqerr=0;
for i=1:maxcycle
    T(i) = vd7(i);
    OP(i)= y1(i);
    e = (T(i)-OP(i))^2;
    %summ(i)=sum(e);
    ssqerr=ssqerr+sum(e);
end
disp('sumsquare error is');
ssqerr
% END OF PROGRAMME

```

## PROGRAM\_9

!\*\*\*\*\*Program On RMSE & Nash-Sutcliffe coefficient\*\*\*\*\*

```

!      Computation of RMSE & Nash-Sutcliffe coefficient
!      N=Total no of data
!      Qo=Observed data
!      Qp=Predicted data
!*****

```

```

      use portlib
      Dimension Qo(250),Qp(250)
      character(9) TODAY
      call date (TODAY)
      open(unit=1,file='Rmse.dat')
      open(unit=2,file='Rmse.out')

      write(2,*) TODAY
      write(*,1)
1      format(1x,//30x,'** Welcome to the Program**')
      write(*,'(//)')
      pause '                                press enter to continue'
      write(*,'(//)')
      write(*,2)
2      format(t31,'Nash Coefficient')
      write(*,'(//)')
      pause '                                press enter to continue'
      write(*,'(//)')
      write(*,3)
3      format(' Name of the output file is "data.out"')
      write(*,'(//)')

      read(1,*) n, avQo
      read(1,*)(Qo(i),i=1,n)
      read(1,*)(Qp(j),j=1,n)

      t1=0.0
      t2=0.0
      do 20 i=1,n
          t1=t1+(Qo(i)-Qp(i))**2
          t2=t2+(Qo(i)-avQo)**2
20      continue
      CNash=1.0-(t1/t2)
      Rmse=sqrt(t1/float(n))

      write(2,49)
49      format(/8x,'OUTPUT'/8x,5('~*~')/)
      write(2,50)
50      format(/1x,70('='))
      write(2,57) CNash,rmse
57      format(5x,'Model Efficiency=',f9.4,5x,'RMSE=',f9.3)
      close(1)
      close(2)
      stop
      end

```

**PAPERS PUBLISHED/ACCEPTED/COMMUNICATED FOR PUBLICATION**

---

1. Use of remote sensing and ANN in assessment of erosion activities in Majuli-the world's largest river island, International Journal of Remote Sensing, Dandee, UK. (Accepted)
2. Application of artificial neural network for daily river stage forecast in the Brahmaputra river, Water and Energy International Journal, CBIP, New Delhi. (Accepted)
3. Monitoring fluvial hazard from space: A case study from Brahmaputra river plains, International Journal of Geoinformatics, Bangkok, Thailand. (Communicated)
4. Stage-discharge relationship for the river Brahmaputra with neuromorphic approach, International Journal of Hydraulic Research, Canada. (Communicated)
5. Use of neural network in prediction of sediment load concentration in the river Brahmaputra, International Journal of Sediment Research, Beijing, China. (Communicated)
6. Flood plain modelling of the river Brahmaputra, Journal of International Association of Hydraulics (IAHR). (Communicated)
7. Exploratory Use of Artificial Neural Network and Remote Sensing for Management of Bank Erosion of the Brahmaputra, proc. 4<sup>th</sup> IWMI-Tata Annual Partners Research Meet at Anand, Feb. 24-26, 2005, pp. 49.
8. Spatio-Temporal Modeling of Hydrological Variability for the river Brahmaputra using Artificial Neural Network, proc. International Symposium on Role of Water Sciences in Transboundary River Basin Management, Ubon Ratchathani, Thailand, March 10-12, 2005.
9. Problems and prospects in use of ANN in spatio-temporal morphological modelling of a large braided river, Int. Conf. on Environment and Simulation, IASTED, November, 2004, USA.
10. Development and performance of certain landform indicators in the Brahmaputra river, Journal of ISH, Pune. (Accepted)
11. Topological indices for study of spatio-temporal changes in the plan-form of the Brahmaputra river, Journal of IWRS, 2004. (Communicated)
12. Morphological study of the river Brahmaputra using remote sensing and GIS technique, Indian Journal of Remote Sensing, Dehradun, India. (Communicated)



13. Flood management through ANN-based spatio-temporal morphological model - A potential approach for the Brahmaputra, National Workshop, Guwahati.
14. Flood Management through Structural and Non-Structural Measures, proc. Workshop on Flood and Drought Management, CBIP, New Delhi, Sept. 16-17, 2004, pp. FM 108-119.
15. Monitoring of morphological changes of Indian rivers through ANN based spatio-temporal model-An Approach, National Seminar on silting of rivers in India, February, 12-13, 2004, New Delhi.
16. Evolution of the Morphology of the River Brahmaputra due to Vegetative Cover Changes, Water and Energy International Journal, CBIP, New Delhi. (Communicated)
17. Evaluation of sediment predictors and application of HEC-6 in total load estimation for the river Brahmaputra, ISH, Pune. (Communicated)
18. Morphology of the river Brahmaputra - A case study, Current Science. (Communicated)

relationship between parameters are not easily discernible, because the physics of the complex phenomena of formation of braided channels. Fuzzy logic system has been used in developing stage-discharge relationships, which deals with explicit knowledge that could be explained and understood. Comparison of the stage-discharge relationships yielded by ANN, fuzzy, neuro-fuzzy was made with the observed stage-discharge data of the river.

## **5. VALIDATION OF RESULTS**

The available data sets for all the models were randomly partitioned into training sets and a test set. The training set was further partitioned into two disjointed subsets; (i) estimation set, used to select the model; (ii) validation set, used to validate the model. Some portion of data was withheld for validation. To assess the validity of the models, all the ANN generated outputs were compared with the observed data of the river Brahmaputra. The goodness-of-fit of statistical criteria like root mean square error (*rmse*), Nash-Sutcliffe coefficients were evaluated for each model. The efficiency has also been tested for each model.

## **6. SALIENT CONTRIBUTIONS OF THE PRESENT RESEARCH**

This research endeavour encompasses the development of a number of ANN-based spatio-temporal morphological models of the river resulting in significant findings, important observations and the right provoking predictions as briefly narrated below:

### **Stream bank migration models**

The stream bank migration ANN models, so developed, have simulated the desired information on erosion and deposition patterns, stream bank migration at discrete points with respect to space and time. What-if-then ANN models have also been developed to

### **Prediction of sediment load concentration**

A sediment concentration ANN model was constituted to estimate the natural sediment discharge of the river in terms of sediment concentration at Pancharatna using water and sediment variables based on the dynamic laws of flow and sediment.

### **Planform morphology**

The variation in Normalised Difference Vegetation Indices (NDVI) for the Assam part of Brahmaputra basin were found out reach-wise, for different years to infer dominant trends in morphological variability response in the basin due to presence of vegetative cover in the flood-plain. Furthermore, digital satellite data of NOAA for the year 2002 have been used for deriving the Digital Elevation Model (DEM) and shallow and deep flooding phenomena in the valley.

The average northing for right bank line of the Brahmaputra river moved about 0.47 km to the north between 1990 and 2002, while that for the left moved about 0.48 km to the south. The river has avulsed just upstream side of the Dibrugarh town and excised areas of floodplain to create new bars. The river mean width has increased from 7.99 km to 8.94 km in the study reach. The study further revealed that the total area within the stream banks increased by 12.10% between 1990 and 2002 due to erosion process causing channel widening. Expansion of the river had taken place primarily through floodplain erosion and excision coupled with bar or island growth.

For morphological processes fraught with great deal of uncertainty in temporal and spatial variability, displaying nonlinearity of physical phenomena, ANNs could be seen to have provided fairly rational answers by mapping pertinent functional relationships of river behaviour. The signal contribution that emerged from the present study focuses on use of neuromorphic techniques for gainful planning and management of intricate river systems like the Brahmaputra.

relationship between parameters are not easily discernible, because the physics of the complex phenomena of formation of braided channels. Fuzzy logic system has been used in developing stage-discharge relationships, which deals with explicit knowledge that could be explained and understood. Comparison of the stage-discharge relationships yielded by ANN, fuzzy, neuro-fuzzy was made with the observed stage-discharge data of the river.

## 5. VALIDATION OF RESULTS

The available data sets for all the models were randomly partitioned into training sets and a test set. The training set was further partitioned into two disjointed subsets; (i) estimation set, used to select the model; (ii) validation set, used to validate the model. Some portion of data was withheld for validation. To assess the validity of the models, all the ANN generated outputs were compared with the observed data of the river Brahmaputra. The goodness-of-fit of statistical criteria like root mean square error (*rmse*), Nash-Sutcliffe coefficients were evaluated for each model. The efficiency has also been tested for each model.

## 6. SALIENT CONTRIBUTIONS OF THE PRESENT RESEARCH

This research endeavour encompasses the development of a number of ANN-based spatio-temporal morphological models of the river resulting in significant findings, important observations and the right provoking predictions as briefly narrated below:

### **Stream bank migration models**

The stream bank migration ANN models, so developed, have simulated the desired information on erosion and deposition patterns, stream bank migration at discrete points with respect to space and time. What-if-then ANN models have also been developed to

predict the scenario of the river pertaining to lateral migration, if a flash flood was impinged at the confluence of the tributary with the main stem of the river Brahmaputra.

### **Flow characteristic models**

The ANN models developed have simulated the river flow characteristic variables, which profoundly influenced morphological variability, such as discharge, water level, sediment at discrete points of river cross section with respect to space and time. The stage-discharge relationship models evolved for important stations at Dibrugarh, Pandu and Pancharatna of the river Brahmaputra have been used to predict the discharge at these points for a given stage. Real-time one-day-ahead stage forecasts at three stations, namely Pandu, Pancharatna and Dhubri have been made through another set of neuromorphic models.

### **Hydrographic characteristic models**

The research contributed the development of ANN models capable of predicting reduced levels of the river cross-sections profile in the past, present and the future to investigate the morphological changes of the river Brahmaputra from spatial as well as temporal standpoints.

### **Erosion model for Majuli island**

The erosion process in Majuli island of the Brahmaputra, the world's largest river island, has also been investigated deploying remote sensing and ANN techniques. The area of the Majuli river island has evidently decreased by 39.30 km<sup>2</sup> over a period of 12 years from 416.23 km<sup>2</sup> in 1990 to 376.93 km<sup>2</sup> in 2002. The study has revealed that the loss of land area has been 4.94% in 1997 and 9.44% in year 2002 with reference to the area of Majuli island in the year 1990.

## Evolution of new fluvial landform indicators

For appraisal of degree and intensity of braiding appropriately by duly reflecting the influence of pertinent hydraulic variables, fluvial landform index (FLI) and hydraulic geometry index (HGI) were evolved in this work making conjunctive use of field and remote sensing data. The empirical topological indices alpha ( $\alpha$ ), beta ( $\beta$ ) and gamma ( $\gamma$ ) have been found out block-wise for the river, for different years to investigate the braiding pattern.

The performance evaluation of the newly developed HGI with topological indices with respect to intensity of braiding clearly demonstrated the usefulness and relevance for applying these indices in the Brahmaputra for a measure of the fluvial landform. The newly developed indices FLI and HGI were designed to rationally classify the degree as well as intensity of braiding for the Brahmaputra by accounting for the pertinent fluvial variables. These indices logically reflected the effect of planform changes on channel migration, island formation and resultant braiding, which wielded significant influence on river morphology.

Furthermore, on the basis of a critical analysis of the trends of the variation of HGI, FLI, form ratio,  $\alpha$ ,  $\beta$  and  $\gamma$  indices in the study area of the river Brahmaputra, the thresholds were determined for all the aforesaid indices to provide an objective basis for classification of the braiding phenomenon as well as to make them useful for practical applications subsequently. Generalised functional relationships of the HGI with form ratio and energy slope were also worked out.

### **Prediction of sediment load concentration**

A sediment concentration ANN model was constituted to estimate the natural sediment discharge of the river in terms of sediment concentration at Pancharatna using water and sediment variables based on the dynamic laws of flow and sediment.

### **Planform morphology**

The variation in Normalised Difference Vegetation Indices (NDVI) for the Assam part of Brahmaputra basin were found out reach-wise, for different years to infer dominant trends in morphological variability response in the basin due to presence of vegetative cover in the flood-plain. Furthermore, digital satellite data of NOAA for the year 2002 have been used for deriving the Digital Elevation Model (DEM) and shallow and deep flooding phenomena in the valley.

The average northing for right bank line of the Brahmaputra river moved about 0.47 km to the north between 1990 and 2002, while that for the left moved about 0.48 km to the south. The river has avulsed just upstream side of the Dibrugarh town and excised areas of floodplain to create new bars. The river mean width has increased from 7.99 km to 8.94 km in the study reach. The study further revealed that the total area within the stream banks increased by 12.10% between 1990 and 2002 due to erosion process causing channel widening. Expansion of the river had taken place primarily through floodplain erosion and excision coupled with bar or island growth.

For morphological processes fraught with great deal of uncertainty in temporal and spatial variability, displaying nonlinearity of physical phenomena, ANNs could be seen to have provided fairly rational answers by mapping pertinent functional relationships of river behaviour. The signal contribution that emerged from the present study focuses on use of neuromorphic techniques for gainful planning and management of intricate river systems like the Brahmaputra.

and ANN forecasted values of the stages at Pandu, Pancharatna and Dhubri respectively.

Conventional forecasting models require a great deal of detailed data, e.g. topographical maps, river networks and characteristics, soil characteristics, rainfall and runoff data. Often, these data were not available which posed a great difficulty in model calibration. In addition, a sufficiently long lead time for forecasting was required to take the necessary flood evacuation measures. In the case of dissemination of flood information and other flood evacuation measures, the computational speed of the models used are of absolute importance. Conventional models are not ideal for real-time forecasting due to the large amount of detailed information they require, and the associated long computation time.

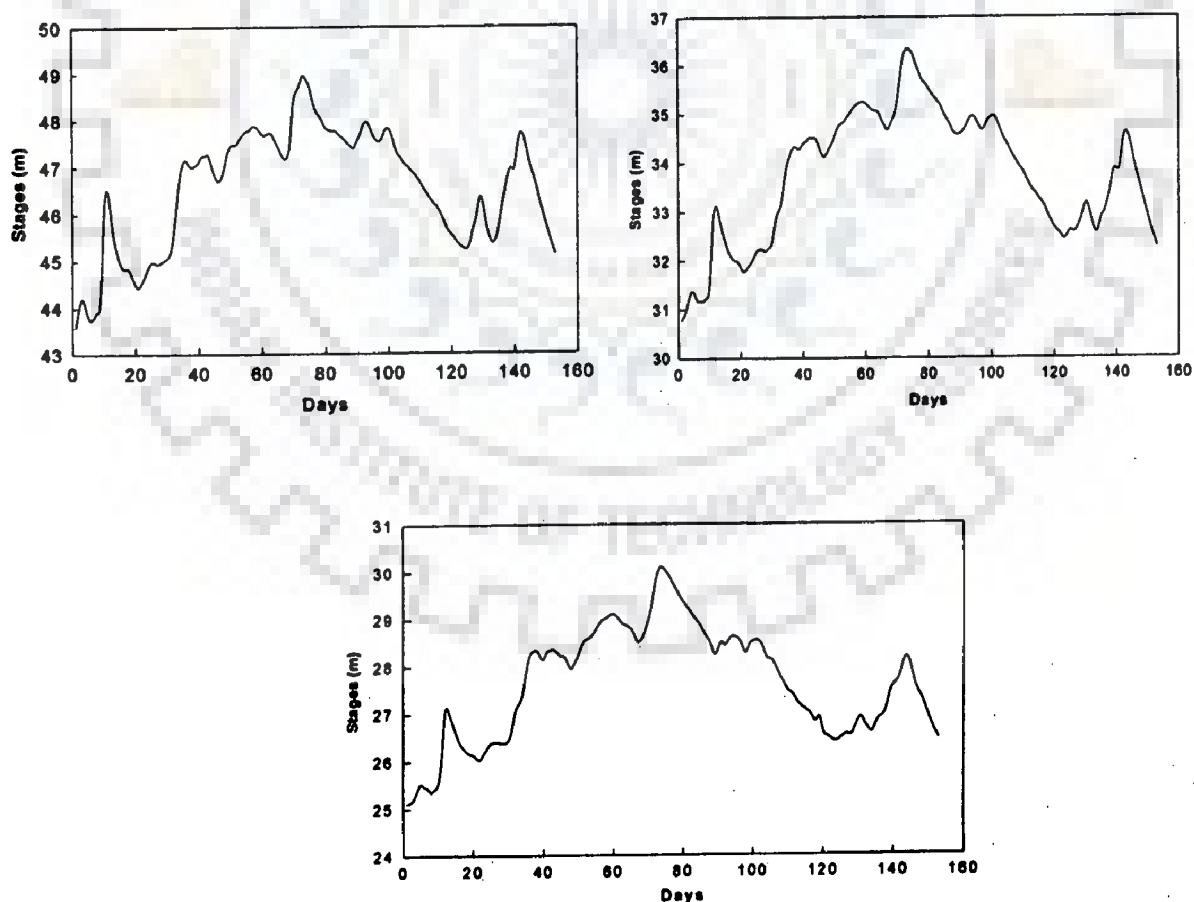


**Figure 4.90** Characteristics of stage data at Pandu, Pancharatna and Dhubri (May-Oct, 2002)



The possibility of measurement failure in any of the gauging stations Pandu, Pancharatna and Dhubri during the critical flow level requires prediction tools, which can interpret assessment of flow levels and as a desirable advance warning forecasting tool. Hence, ANN models prove to be ideal in forecasting river stages.

**Table 4.25(a) Performance indices based on data from test set at Pandu**

*rmse* = 0.14 (2002), 0.104 (2000)  
Nash-Sutcliffe Coefficient = 0.93 (2002), 0.983 (2000)

	Training		Validation		Testing		Model efficiency	
	Year 2002	Year 2000	Year 2002	Year 2000	Year 2002	Year 2000	Year 2002	Year 2000
Correlation Coefficient	0.99	0.991	0.984	0.994	0.985	0.980	93%	98.3%
R <sup>2</sup>	0.98	0.982	0.963	0.985	0.967	0.958		

**Table 4.25(b) Statistical parameters for Model 26 (Pandur)**

		Training		Validation			Testing		
		Target	Output		Target	Output		Target	Output
Year 2002	Mean	46.66	46.66	Mean	46.93	46.99	Mean	46.94	46.92
	SD	1.40	1.38	SD	1.32	1.28	SD	1.41	1.35
Year 2000	Mean	46.848	46.851	Mean	46.878	46.848	Mean	46.983	47.035
	SD	1.259	1.242	SD	1.167	1.121	SD	1.121	1.118

**Table 4.26(a) Performance indices based on data from test set at Pancharatna**

*rmse* = 0.12 (2002), 0.16 (2000)  
Nash-Sutcliffe Coefficient = 0.963 (2002), 0.958 (2000)

	Training		Validation		Testing		Model efficiency	
	Year 2002	Year 2000	Year 2002	Year 2000	Year 2002	Year 2000	Year 2002	Year 2000
Correlation Coefficient	0.995	0.989	0.995	0.992	0.995	0.988	96.3%	95.89%
R <sup>2</sup>	0.99	0.978	0.998	0.978	0.994	0.973		

**Table 4.26(b) Statistical parameters for Model 27 (Pancharatna)**

		Training		Validation			Testing		
		Target	Output		Target	Output		Target	Output
Year 2002	Mean	33.75	33.75	Mean	33.77	33.77	Mean	33.80	33.78
	SD	1.297	1.29	SD	1.29	1.29	SD	1.31	1.30
Year 2000	Mean	34.273	34.287	Mean	34.482	34.490	Mean	34.363	34.374
	SD	1.422	1.389	SD	1.467	1.372	SD	1.497	1.428

**Table 4.27(a) Performance indices based on data from test set at Dhubri**

*rmse* =0.17 (2002), 0.10 (2000)

Nash Sutcliffe Coefficient =0.89 (2002), 0.968 (2000)

	Training		Validation		Testing		Model efficiency	
	Year 2002	Year 2000	Year 2002	Year 2000	Year 2002	Year 2000		
Correlation Coefficient	0.997	0.995	0.995	0.994	0.996	0.990	89%	96.6%
R <sup>2</sup>	0.995	0.991	0.99	0.973	0.993	0.976		

**Table 4.27(b) Statistical parameters for Model 28 (Dhubri)**

		Training		Validation			Testing		
		Target	Output		Target	Output		Target	Output
Year 2002	Mean	27.83	27.83	Mean	28.09	28.10	Mean	28.08	28.06
	SD	1.34	1.34	SD	1.20	1.19	SD	1.15	1.153
Year 2000	Mean	27.97	27.97	Mean	28.229	28.159	Mean	28.156	28.101
	SD	1.254	1.242	SD	1.103	1.083	SD	0.993	0.985

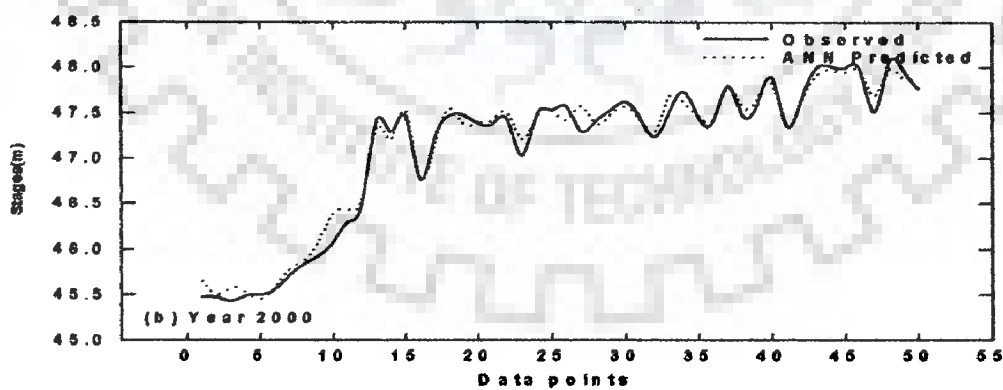
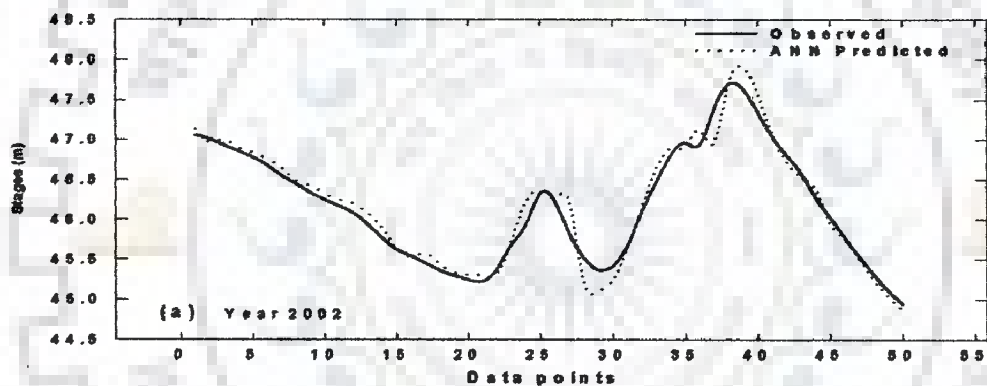


**Figure 4.91 Plot of observed data and ANN forecasted data for Pandu**

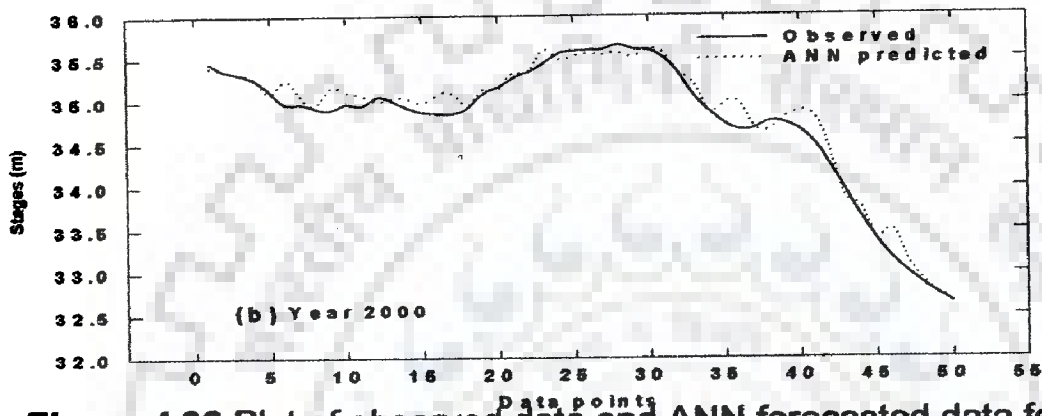
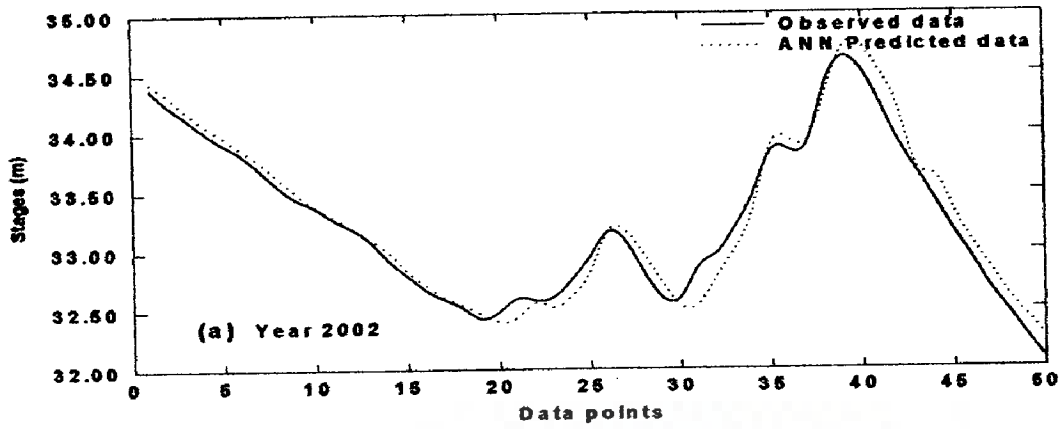


**Figure 4.92** Plot of observed data and ANN forecasted data for Pancharatna

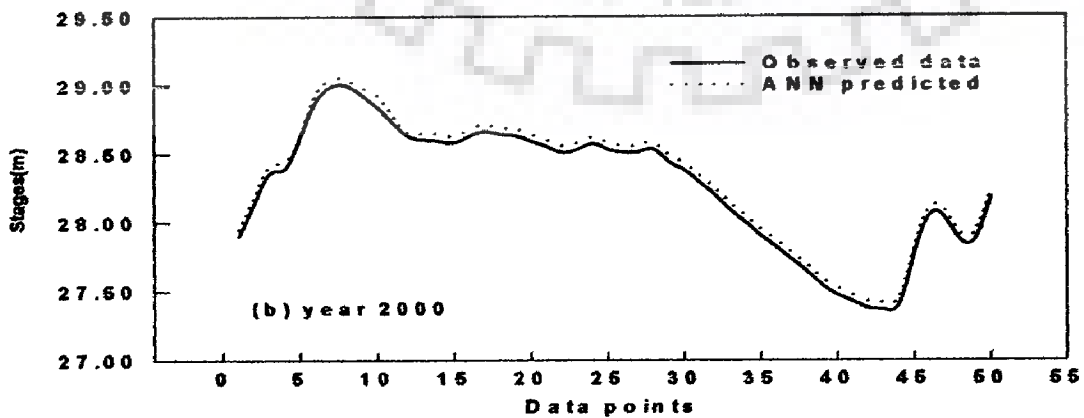
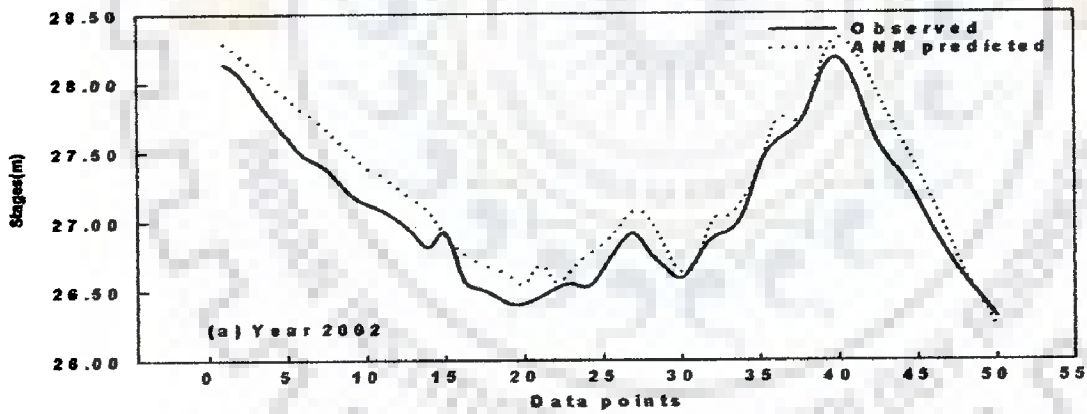


**Figure 4.93** Plot of observed data and ANN forecasted data for Dhubri